

Lawrence Berkeley National Laboratory

Recent Work

Title

MATERIALS AND MOLECULAR RESEARCH DIVISION. ANNUAL REPORT 1983

Permalink

<https://escholarship.org/uc/item/7sk7q4q7>

Author

Lawrence Berkeley National Laboratory

Publication Date

1984-07-01

LBL-16680 c.2
UC-13

RECEIVED
LAWRENCE
BERKELEY LABORATORY

SEP 10 1984

LIBRARY AND
DOCUMENTS SECTION

MATERIALS AND MOLECULAR RESEARCH DIVISION

Annual Report 1983

July 1984

TWO-WEEK LOAN COPY

*This is a Library Circulating Copy
which may be borrowed for two weeks.*

Lawrence Berkeley Laboratory
University of California
Berkeley, California 94720

DISCLAIMER

This document was prepared as an account of work sponsored by the United States Government. While this document is believed to contain correct information, neither the United States Government nor any agency thereof, nor the Regents of the University of California, nor any of their employees, makes any warranty, express or implied, or assumes any legal responsibility for the accuracy, completeness, or usefulness of any information, apparatus, product, or process disclosed, or represents that its use would not infringe privately owned rights. Reference herein to any specific commercial product, process, or service by its trade name, trademark, manufacturer, or otherwise, does not necessarily constitute or imply its endorsement, recommendation, or favoring by the United States Government or any agency thereof, or the Regents of the University of California. The views and opinions of authors expressed herein do not necessarily state or reflect those of the United States Government or any agency thereof or the Regents of the University of California.

MATERIALS AND MOLECULAR
RESEARCH DIVISION

Annual Report 1983

July 1984

Alan W. Searcy, Division Head
Rolf H. Muller, Asst. Division Head for Research
Conway V. Peterson, Asst. Division Head for Administration

Lawrence Berkeley Laboratory
University of California
Berkeley, California 94720

Materials
Sciences

Chemical
Sciences

Nuclear
Sciences

Fossil
Energy

Energy
Storage
Systems

Magnetic
Fusion Energy

Health and
Environmental Sciences

Work for
Others

Appendices

Contents

GENERAL INTRODUCTION

<i>Alan W. Searcy</i>	xi
-----------------------------	----

MATERIALS SCIENCES

Metallurgy and Ceramics

Structure of Materials

Structure and Properties of Transformation Interfaces

<i>Ronald Gronsky, Investigator</i>	1
---	---

Microstructure, Properties, and Alloy Design: Inorganic Materials

<i>Gareth Thomas, Investigator</i>	5
--	---

Solid-State Phase Transformation Mechanisms

<i>Kenneth H. Westmacott, Investigator</i>	17
--	----

National Center for Electron Microscopy

<i>Gareth Thomas, Ronald Gronsky, and Kenneth H. Westmacott, Investigators</i>	21
--	----

In Situ Investigations of Gas-Solid Reactions by Electron Microscopy

<i>James W. Evans, Investigator</i>	31
---	----

Local Atomic Configurations in Solid Solutions

<i>Didier de Fontaine, Investigator</i>	36
---	----

Mechanical Properties

Theoretical Problems in Alloy Design

<i>John W. Morris, Jr., Investigator</i>	39
--	----

Mechanical Properties of Ceramics

<i>Anthony G. Evans, Investigator</i>	44
---	----

Environmentally Affected Crack Growth in Engineering Materials

<i>Robert O. Ritchie, Investigator</i>	49
--	----

Physical Properties

Interfaces and Ceramic Microstructures

<i>Joseph A. Pask, Investigator</i>	55
---	----

High-Temperature Reactions

<i>Alan W. Searcy, Investigator</i>	58
---	----

Structure-Property Relationships in Semiconductor Materials

<i>Jack Washburn, Investigator</i>	62
--	----

Chemical Properties and Processing of Refractory Ceramics

<i>Lutgard C. De Jonghe, Investigator</i>	66
---	----

Structure and Electrical Properties of Composite Materials

<i>Robert H. Bragg, Investigator</i>	69
--	----

High-Temperature Oxidation and Corrosion of Materials	
<i>John Stringer, Acting Investigator*</i>	73
Ceramic Interfaces	
<i>Andreas M. Glaeser, Investigator</i>	75
Engineering Materials	
Abrasive, Erosive, and Sliding Wear of Materials	
<i>Iain Finnie, Investigator</i>	77
Erosion of Brittle Solids	
<i>Anthony G. Evans, Investigator</i>	79
Solid-State Physics	
Experimental Research	
Far-Infrared Spectroscopy	
<i>Paul L. Richards, Investigator</i>	82
Experimental Solid-State Physics and Quantum Electronics	
<i>Yuan R. Shen, Investigator</i>	87
Excitations in Solids	
<i>Carson D. Jeffries, Investigator</i>	91
Time-Resolved Spectroscopies in Solids	
<i>Peter Y. Yu, Investigator</i>	95
Superconductivity, Superconducting Devices, and 1/f Noise	
<i>John Clarke, Investigator</i>	97
Theoretical Research	
Theoretical Studies of the Electronic Properties of Solid Surfaces	
<i>Leo M. Falicov, Investigator</i>	102
Theoretical Solid-State Physics	
<i>Marvin L. Cohen, Investigator</i>	105
Materials Chemistry	
Chemical Structure	
Low-Temperature Properties of Materials	
<i>Norman E. Phillips, Investigator</i>	109
Electrochemical Processes	
<i>Charles W. Tobias, Investigator</i>	112
High-Temperature and Surface Chemistry	
High-Temperature Thermodynamics	
<i>Leo Brewer, Investigator</i>	115
Chemistry and Materials Problems in Energy Production Technologies	
<i>Donald R. Olander, Investigator</i>	118

*Affiliation: Electric Power Research Institute, Palo Alto, California.

Plasma-Enhanced Deposition of Thin Films <i>Dennis W. Hess, Investigator</i>	121
Electrochemical Phase Boundaries <i>Rolf H. Muller, Investigator</i>	122
Solid-State and Surface Reactions <i>Gabor A. Somorjai, Investigator</i>	125
Nuclear Magnetic Resonance <i>Alexander Pines, Investigator</i>	137

CHEMICAL SCIENCES

Fundamental Interactions

Photochemical and Radiation Sciences

Photon-Assisted Surface Reactions, Materials, and Mechanisms <i>Gabor A. Somorjai, Investigator</i>	143
Photochemistry of Materials in the Stratosphere <i>Harold S. Johnston, Investigator</i>	145

Chemical Physics

Energy Transfer and Structural Studies of Molecules on Surfaces <i>Charles B. Harris, Investigator</i>	148
Selective Photochemistry <i>C. Bradley Moore, Investigator</i>	151
Physical Chemistry with Emphasis on Thermodynamic Properties <i>Kenneth S. Pitzer, Investigator</i>	154
Molecular Interactions <i>William A. Lester, Jr., Investigator</i>	158
Spectroscopy and Structures of Reactive Intermediates <i>Richard J. Saykally, Investigator</i>	163
Theory of Atomic and Molecular Collision Processes <i>William H. Miller, Investigator</i>	167
Photoelectron Spectroscopy <i>David A. Shirley, Investigator</i>	171
Crossed Molecular Beams <i>Yuan T. Lee, Investigator</i>	179
Potential-Energy Surfaces for Chemical Reactions <i>Henry F. Schaefer III, Investigator</i>	185

Processes and Techniques

Chemical Energy

Formation of Oxyacids of Sulfur from SO ₂ <i>Robert E. Connick, Investigator</i>	197
--	-----

Catalytic Hydrogenation of CO <i>Gabor A. Somorjai and Alexis T. Bell, Investigators</i>	199
Organometallic Chemistry of Coal Conversion <i>K. Peter Vollhardt, Investigator</i>	203
Synthetic and Physical Chemistry <i>William L. Jolly, Investigator</i>	206
Chemistry and Morphology of Coal Liquefaction <i>Heinz Heinemann, Investigator, with Alexis T. Bell, R.H. Fish, and Gabor A. Somorjai, Investigators</i>	210
(Joint funding; see Fossil Energy Section)	
Electrochemical Systems <i>John Newman, Investigator</i>	211
Surface Chemistry — Application of Coordination Principles <i>Earl L. Muetterties, Investigator</i>	214
High-Energy Oxidizers and Delocalized-Electron Solids <i>Neil Bartlett, Investigator</i>	217
Transition-Metal-Catalyzed Conversion of CO, NO, H ₂ , and Organic Molecules to Fuels and Petrochemicals <i>Robert G. Bergman, Investigator</i>	220
Chemical Engineering Sciences	
High-Pressure Phase Equilibria in Hydrocarbon-water (Brine) Systems <i>John M. Prausnitz, Investigator</i>	226

NUCLEAR SCIENCES

Low-Energy Nuclear Sciences

Heavy-Element Chemistry

Actinide Chemistry

<i>Norman M. Edelstein, Richard A. Andersen, Neil Bartlett, John G. Conway, Kenneth N. Raymond, Glenn T. Seaborg, Andrew Streitwieser, Jr., David H. Templeton, and Alan Zalkin, Investigators</i>	231
--	-----

FOSSIL ENERGY

A Review of Unsolved Problems of Pressing Importance in Fluid Mechanics Affected Erosion <i>Joseph A.C. Humphrey, Investigator</i>	245
Electrode Surface Chemistry <i>Phillip N. Ross, Investigator</i>	247
Studies of Materials Erosion in Coal Conversion and Utilization Systems <i>Alan V. Levy, Investigator</i>	251

Chemistry and Morphology of Coal Liquefaction <i>Heinz Heinemann, Investigator, with Alexis T. Bell, R.H. Fish, and Gabor A. Somorjai, Investigators</i>	256
(Joint funding with Chemical Sciences)	

Materials Characterization in Fossil-Fuel Combustion Products <i>Donald H. Boone and Alan V. Levy, Investigators</i>	259
---	-----

ENERGY STORAGE SYSTEMS

Electrochemical Energy Storage

*James W. Evans, Rolf H. Muller, John Newman,
Philip N. Ross, and Charles W. Tobias, Investigators*

Surface Morphology of Metals in Electrodeposition <i>Charles W. Tobias, Investigator</i>	261
Metal Couples in Nonaqueous Electrolytes <i>Charles W. Tobias, Investigator</i>	263
Engineering Analysis of Electrolytic Gas Evolution <i>Charles W. Tobias, Investigator</i>	264
Surface Layers on Battery Materials <i>Rolf H. Muller, Investigator</i>	266
Electrode Kinetics and Electrocatalysis <i>Philip N. Ross, Investigator</i>	268
Electrical and Electrochemical Behavior of Particulate Electrodes <i>James W. Evans, Investigator</i>	271
Electrochemical Properties of Solid Electrolytes <i>Lutgard C. De Jonghe, Investigator</i>	272
Analysis and Simulation of Electrochemical Systems <i>John Newman, Investigator</i>	274

MAGNETIC FUSION ENERGY

Structural Materials and Weldments for High-Field Superconducting Magnets <i>John W. Morris, Jr., Investigator</i>	279
---	-----

HEALTH AND ENVIRONMENTAL SCIENCES

Semiconductor Materials and Devices <i>Eugene E. Haller, Investigator</i>	283
--	-----

WORK FOR OTHERS

National Aeronautics and Space Administration Theoretical Studies of Formyl Radical Formation in Selected Combustion Processes <i>William A. Lester, Jr., Investigator</i>	289
---	-----

Office of Naval Research	
Structure and Performance of Al ₂ O ₃ Scales Formed on Aluminides Containing Noble Metal	
<i>Donald H. Boone and Alan V. Levy, Investigators</i>	290
Quantum Monte Carlo for Molecular Studies	
<i>William A. Lester, Jr., Investigator</i>	291
Electron-Phonon Coupling and the Properties of Thin Films and Inhomogeneous Superconductors	
<i>Vladimir Z. Kresin, Investigator</i>	292
Electric Power Research Institute	
Inhibitive Salts for Reducing High-Temperature Oxidation and Spallation	
<i>John Stringer, Acting Investigator*</i>	294
Reaction Mechanism of the Oxidation of Bisulfite Ion by Oxygen	
<i>Robert E. Connick, Investigator</i>	295

APPENDICES

Appendix A. Division Personnel	297
Appendix B. Division Committees	313
Appendix C. List of Divisional Seminars	314
Appendix D. List of Investigators	322

*Affiliation: Electric Power Research Institute, Palo Alto, California.

GENERAL INTRODUCTION

MMRD personnel and other friends throughout the world were saddened by the illness in the Fall of 1983 and death on January 12, 1984, of Earl L. Muetterties. Dr. Muetterties, an MMRD investigator and a Professor of Chemistry at the University of California Berkeley, was informed in November that he had been named 1984 recipient of the Kirkwood Award, one of the greatest honors accorded to U.S. chemists.

The following awards and honors were accorded to other MMRD investigators in 1983:

- Two MMRD investigators, Carson D. Jeffries and Gabor A. Somorjai, were named fellows of the American Academy of Arts and Sciences.
- Three MMRD investigators — Leo Falicov, Carson Jeffries, and Gareth Thomas — were elected members of the National Academy of Sciences.
- Three MMRD investigators received awards in the 1983 DOE/Basic Energy Sciences Materials Sciences Competition. They were: Y. Ron Shen, outstanding scientific accomplishment in solid-state physics, for "Surface Nonlinear Optics as a Novel Surface Probe"; Alexander Pines, outstanding scientific accomplishment in materials chemistry, for "Multiple Quantum Spectroscopy"; and Donald R. Olander, sustained outstanding research in materials chemistry, for "Research on High-temperature Behavior of Nuclear Fuel Element Materials."
- Neil Bartlett was awarded the William H. Nichols Medal by the New York Chapter of the American Chemical Society (ACS) in recognition of his work in synthesis.
- Alexis T. Bell received the 1983 American Institute of Chemical Engineers Professional Progress Award in recognition of outstanding progress in chemical engineering.
- Robert G. Bergman was honored as a Miller Research Professor, University of California Berkeley, for 1982-1983.
- Leo Brewer received the Hume-Rothery Award from The Metallurgical Society of The American Institute of Mining, Metallurgical, and Petroleum Engineers (AIME) in recognition of his contribution to the science and understanding of chemical bonding in metals and alloys (now called the Engle-Brewer theory).
- John Clarke won a 1982-1983 Distinguished Teaching Award at the University of California Berkeley.
- Nigel Croft, a visiting Harkness Fellow from England working with Robert O. Ritchie, was awarded the Brunton Medal and Premium from the University of Sheffield for his Ph.D. thesis.
- Anthony G. Evans was honored as Van Horne Distinguished Lecturer, Case Western Reserve University, and as Clyde Distinguished Professor, University of Utah.
- James Evans was awarded the 1984 Mathewson Gold Medal of The Metallurgical Society of AIME. He also received the 1983 Extractive Metallurgy Science Award of AIME.
- Iain Finnie was elected as an Honorary Member of the American Society of Mechanical Engineers.
- George Gibson, a senior student with Carson D. Jeffries, received a \$2,000 scholarship from the Achievement Rewards for College Scientists Foundation.
- Ronald Gronsky was awarded the Burton Medal for 1983 by the Electron Microscopy Society of America in recognition of outstanding research accomplishments by a young scientist. He also received the First Place Blue Ribbon (with his graduate student James Howe) for the Transmission Electron Microscopy Class at the 1983 International Metallographic Exhibit for his entry, "A High-resolution Electron Microscopy Study of Interfacial Structure of Precipitate Plates in an Al-15 wt% Ag Alloy."
- Charles B. Harris was honored as a Miller Research Professor, University of California Berkeley, for 1984-1985.
- James M. Howe, a graduate student with Ronald Gronsky, won a Presidential Scholarship to present a paper at the 41st Annual Meeting of the Electron Microscopy Society of America. He also shared the First Place Blue Ribbon with Dr. Gronsky in the Transmission Electron Microscopy Class at

the 1983 International Metallographic Exhibit.

- Carson D. Jeffries was awarded a Miller Research Professorship, University of California Berkeley, for 1983-1984.
- Harold S. Johnston received the Tyler Ecology-Energy Prize for 1983 for his scientific breakthroughs in atmospheric chemistry. He was also awarded the Certificate of Commendation by the Federal Aviation Administration for his research in better understanding the effects of aircraft exhaust emissions on the upper atmosphere.
- Carl M. Lampert received a Fulbright Award to lecture in Yugoslavia for the International Seminar on Scientific Aspects of Solar Energy Conversion Technology.
- Yuan T. Lee was awarded the Harrison Howe Award for his outstanding work in the area of molecular-beam chemistry by the Rochester Section of ACS. He was also the 3M Lecturer, Department of Chemistry, University of Minnesota; FMC Lecturer, Department of Chemistry, Princeton University; Frontier Lecturer, Department of Chemistry, Texas A&M University; and the Sherman Fairchild Distinguished Scholar, California Institute of Technology.
- William A. Lester, Jr., received the Catholic University of America Alumni Award in Science for 1983.
- William H. Miller was elected a Fellow of the American Association for the Advancement of Science.
- Alexander Pines received an Alexander von Humboldt Senior U.S. Scientist Award, was elected Chairman of the Gordon Conference on Magnetic Resonance, and was named Trumbell Lecturer, Yale University.
- John M. Prausnitz was awarded an honorary Doctor of Engineering degree from the University of L'Aquila, Italy, and was elected to Corresponding Membership, Verein Deutscher Ingenieure (Dusseldorf).
- Robert O. Ritchie was elected a Fellow of the Institution of Metallurgists, London, UK, and received an Alco Foundation Fellowship.
- Henry F. Schaefer III received the 1983 Leo Hendrick Baekeland Award by the ACS in recognition of his accomplishments in pure chemistry.
- Glenn T. Seaborg received his 49th honorary Doctor of Science degree, conferred by the University of Pennsylvania.

- Subramanian Suresh, a postdoctoral fellow with Robert Ritchie, received the Robert Lansing Hardy Gold Medal from The Metallurgical Society of AIME.
- Charles W. Tobias was elected a member of the National Academy of Engineering and received the 1983 Alpha Chi Sigma Award of the American Institute of Chemical Engineers in recognition of outstanding recent accomplishments by an individual in fundamental or applied research in chemical engineering.
- K. Peter Vollhardt was awarded the Adolf Windaus Medallion of the German Chemical Society for outstanding achievement in steroid research. He was also plenary lecturer in four national and international meetings (workshops), invited special lecturer at the ACS Corpus Christi Section in Texas, and the John E. Mahler lecturer at the University of Texas at Austin.
- Gina Whitney, graduate student with Charles W. Tobias, was named one of six outstanding teaching assistants for 1982-1983 in the Department of Chemical Engineering, University of California Berkeley.

MMRD's staff at the end of 1983 consisted of 9 staff senior scientists, 49 University of California Berkeley faculty investigators, 29 staff scientists, 218 postdoctorals and other temporary scientific personnel, 427 graduate students (including guest students), and a support staff of 32 administrative and clerical personnel, for a total of 764. During the calendar year 338 journal articles and LBL reports were published by MMRD members. Students associated with MMRD received 14 M.S. and 47 Ph.D. degrees.

The National Center for Electron Microscopy (NCEM) was formally dedicated on September 30, 1983. Director David A. Shirley, UC Berkeley Chancellor Ira M. Heyman, and Dr. Richard H. Kropschot, Associate Director for Basic Energy Sciences of the Office of Energy Research, DOE, each spoke briefly. Professor Gareth Thomas, Scientific Director of the Center, introduced the keynote speakers. Professor J. A. Cowley, Galvin Professor of Physics and Director of the facility for High-resolution Electron Microscopy of Arizona State University, spoke on "High-resolution Electron Microscopy in America," and Professor H. Hashimoto of Osaka University and President of the International Federation of Societies for Electron Microscopy spoke on "The Impact of Electron Microscopy on Materials Sciences." Activities of

NCEM are reported in a section of this Annual Report.

The MMRD Annual Review of 1983 programs was held on February 6-7, 1984. George W. Parshall, E.I. Du Pont de Nemours & Co., served as chairman of the review committee. Other members were Richard Bradt, Chairman of the Department of Materials Science and Engineering, University of Washington; James Phillips, Bell Laboratories; William Chupka, Department of Chemistry, Yale University; Robert Madix, Department of Chemical Engineering, Stanford University; and Robert Mehrabian, Dean of the College of Engineering, University of California at Santa Barbara.

A review of programs supported by Chemical Sciences was held on February 27-29, 1984. The

outside reviewers were Henry Taube, Department of Chemistry, Stanford University; Gerd Rosenblatt, Los Alamos Scientific Laboratory; and James L. Kinsey, Chemistry Department, Massachusetts Institute of Technology, who served as chairman.

As of July 1, 1984, I will have served four and one-quarter years as Division Head. I have asked LBL Director David A. Shirley to replace me on that date so that I can take sabbatical leave in 1984-1985 to concentrate on research. It has been a very great honor to head this extraordinarily vital and successful research unit. I am grateful to Dave Shirley for giving me the opportunity to do so, and I am grateful to the MMRD support, scientific, and administrative staff, who have made the experience a pleasure.

Alan W. Searcy

Materials
Sciences

METALLURGY AND CERAMICS

STRUCTURE OF MATERIALS

Structure and Properties of Transformation Interfaces*

Ronald Gronsky, Investigator

INTRODUCTION

Transformation interfaces include homophase boundaries, heterophase boundaries, and free surfaces at which solid-state reactions are either initiated or propagated. The goal of this research is to determine the atomic configurations of such interfaces and to establish the relationship between their detailed structure and interfacial properties (mobility, diffusivity, conductivity, and ductility), because these properties strongly influence, if not completely dominate, the overall performance of materials.

Experiments are carried out chiefly by transmission electron microscopy, including energy-dispersive x-ray and electron-energy-loss spectroscopies. Results are correlated with theoretical predictions of interfacial structure and high-spatial-resolution image simulations.

1. Atomic Mechanisms of Precipitate-plate Growth in the Al-Ag System — I. Conventional Transmission Electron Microscopy (Publication 7)

J.M. Howe, R. Gronsky, and H.I. Aaronson[†]

The detailed interfacial structure of γ' precipitates in an Al/15-wt%-Ag alloy has been studied by conventional transmission electron microscopy. Contrast analysis indicates that there is a strong tendency for single $1/6 \langle 112 \rangle$ Shockley partial dislocations on the precipitate faces to interact, forming multiple-unit ledges that display the contrast behavior of $1/2 \langle 110 \rangle$ dislocations (see Figure 1-1). In addition, both the edges of these precipitates and the ledges on the edges comprise the same partial dislocations stacked vertically or slightly behind one another. All three variants of Shockley partials have been observed on the same $\{111\}$ faces of precipitates, and all interfaces of the precipitates display a strong preference for low-energy $\langle 110 \rangle$ configurations. A model is proposed to explain the preferred migration of the edges of precipitates by a ledge mechanism.

[†]Department of Metallurgy and Materials Science, Carnegie-Mellon University, Pittsburgh, Pennsylvania 15213.

*This work was supported by the Director, Office of Energy Research, Office of Basic Energy Sciences, Materials Sciences Division of the U.S. Department of Energy under Contract No. DE-AC03-76SF00098.

2. Atomic Mechanisms of Precipitate-plate Growth in the Al-Ag System — II. High-resolution Transmission Electron Microscopy (Publication 8)

J.M. Howe, R. Gronsky, and H.I. Aaronson†

High-resolution transmission electron microscopy was used to study the interfacial structure of γ' precipitates in an Al/15-wt%-Ag alloy aged at 350°C. These studies show the following results: (1) All ledges are multiples of two $\{111\}$ planes high. This observation supports the theory (and conventional transmission electron-microscopy observations) that plate thickening occurs by the passage of Shockley partial dislocations on alternate $\{111\}$ planes. (2) Most ledges are more than just two planes high, indicating a strong tendency toward diffusional interaction (see Figure 2-1). (3) The terraces between ledges are atomically flat, and ledges are uniformly stepped down from the center to the edges of isolated precipip-

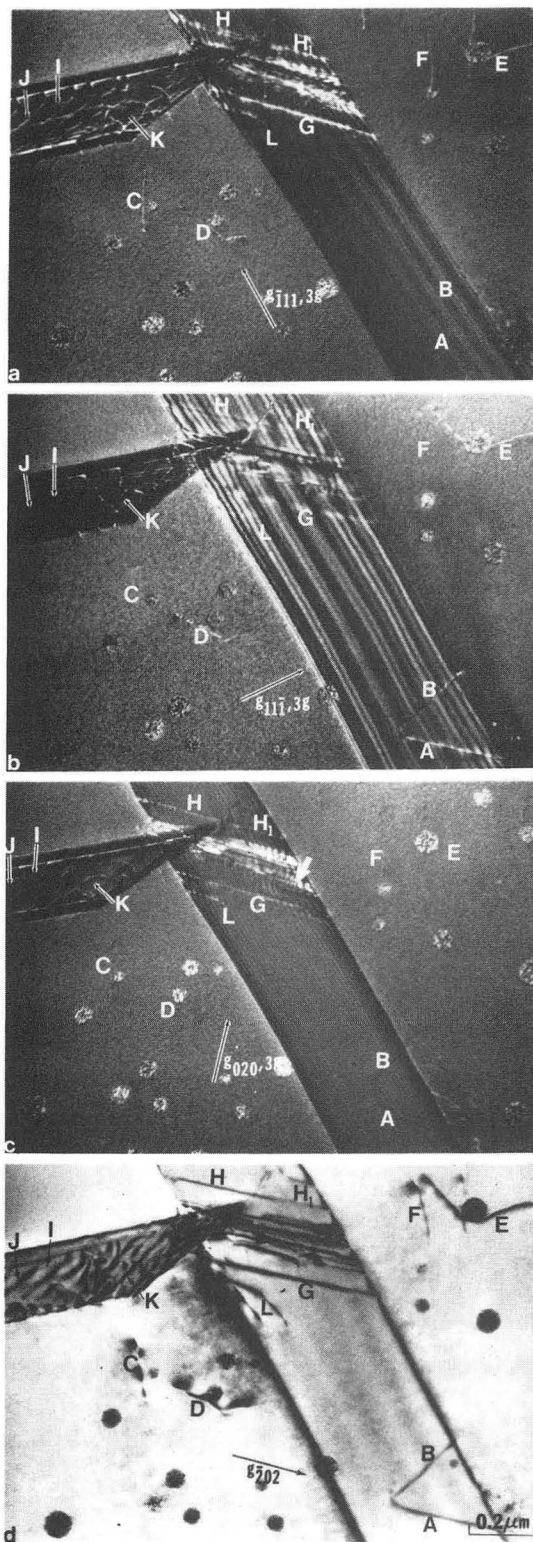


Figure 1-1. Contrast-analysis experiments showing multiple ledges and $1/2 \langle 110 \rangle$ Burgers-vector dislocations at the interfaces of γ' precipitates in an Al/15-wt%-Ag alloy. The lettered defects are identified by the variation in their visibility for these four different diffraction conditions. (XBB 837-6709)

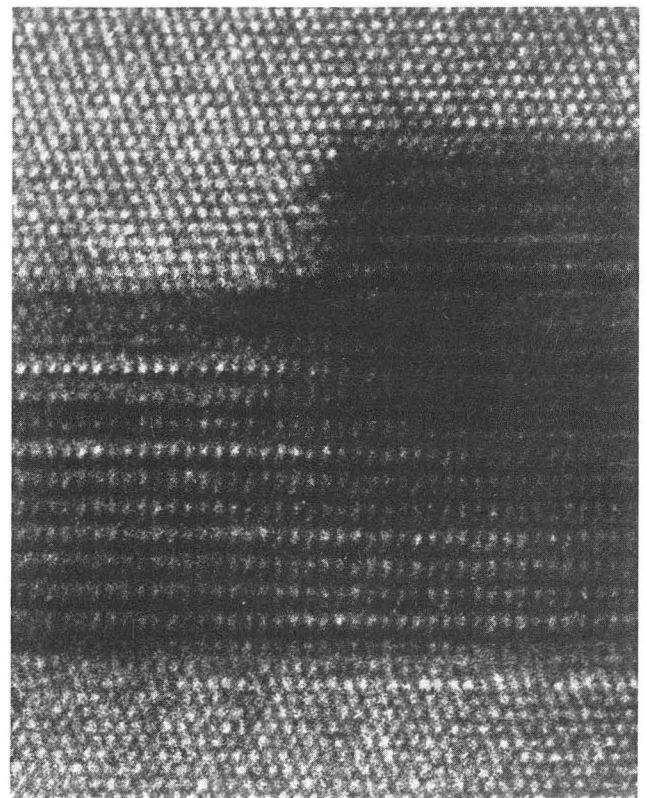


Figure 2-1. Lattice-resolution image of a large ledge (dark step at center top) in the interface between a γ' precipitate and its matrix in an Al/15-wt%-Ag specimen. The ledge height is twelve $\{111\}$ planes of the matrix phase and tends to follow a $\{111\}$ trace. (XBB 830-10305)

itates, as predicted by the general theory of precipitate morphology. (4) The $\{111\}$ planes are continuous across the edges or ledges, indicating that they are largely coherent and not disordered, the assumption made in most kinetic analyses. (5) The edges of precipitate plates appear to be composed of similar two-plane ledges arranged vertically above one another and hence may grow by the same mechanism of atomic attachment as ledges on the faces. Furthermore, examination of incipient γ' precipitates indicates that their aspect ratios may deviate from the predicted equilibrium value almost immediately, probably due to the ledge mechanism of growth. (6) An atomic model of a γ' precipitate was used to verify the high-resolution images obtained and to illustrate possible growth processes of the ledges.

[†]Department of Metallurgy and Materials Science, Carnegie-Mellon University, Pittsburgh, Pennsylvania 15213.

3. High-resolution Electron-microscopy Studies of the Native Oxide on Silicon (Publication 12)

J.H. Mazur, R. Gronsky, and J. Washburn

High-resolution electron microscopy (HREM) studies of cross-sectional specimens have shown that the thickness of the native oxide on silicon is 20 ± 3 Å, independent of surface orientation (see Figure 3-1). This result has confirmed the value 21 ± 4 Å determined by ellipsometry, assuming a stoichiometric SiO_2 native oxide. Previous reports of a nonstoichiometric transition layer between Si and SiO_2 containing more than $10^{15}/\text{cm}^2$ Si atoms have been alternatively explained by the observed morphological features of the Si- SiO_2 interface.

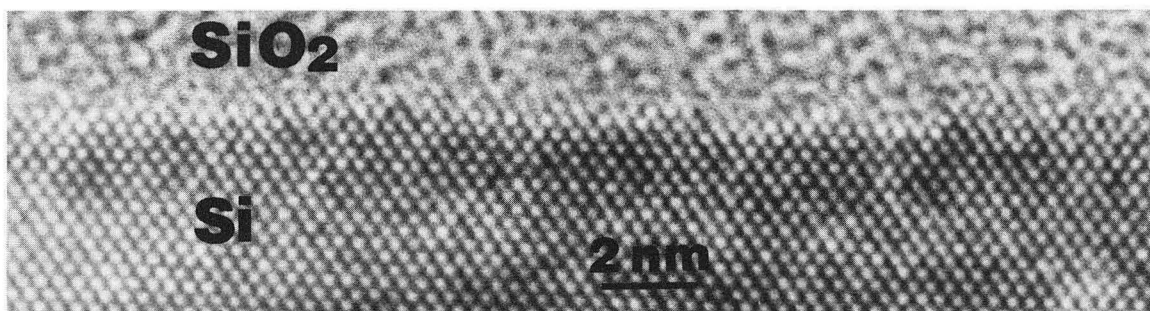


Figure 3-1. High-resolution image of a 20-Å thick native oxide on a surface 2° off the (111) plane. (XBB 833-2311)

4. Work in Progress

Atomic-resolution imaging of grain boundaries in metals (Cu, Nb) and dislocations in semiconductors (Si, GaAs) is currently under way. Image-simulation studies have been used to identify the appropriate experimental conditions needed for this work, where attention has been given to the influence of impurity segregation on contrast detail. The eventual goal of this research is to identify the atomistics of segregation to internal interfaces in these solids.

1983 PUBLICATIONS AND REPORTS

Refereed Journals

1. E.A. Kamenetzky and R. Gronsky, "The Mechanisms of Accommodation of Deformation at Grain Boundaries in BBC Materials," *Res. Mechanica* **8**, 185 (1983); LBL-14702.
2. J.M. Howe, "Relief Etching Technique for Scanning and Transmission Electron Microscopy Characterization of Submicron Precipitates in Aluminum Alloys," *Metallography* **16**, 275 (1983); LBL-15278.
3. J.M. Howe, "A HREM Study of the Interfacial Structure of γ' Precipitate Plates in an Al/15-wt%-Ag Alloy," in *Proc. 41st Ann. Meeting Electron Microsc. Soc. Amer.*, G.W. Bailey, Ed., San Francisco Press, p. 283, (1983); LBL-15550.
4. T.D. Sands, "Degradation Mechanisms of $\text{Cu}_{2-x}\text{S}/\text{CdS}$ Solar Cells as Revealed by High Resolution Electron Microscopy," in *Proc. 41st Ann. Meeting Electron Microsc. Soc. Amer.*,

G.W. Bailey, Ed., San Francisco Press, p. 104, 1983; LBL-15536.

5. J.H. Mazur, "High-resolution Imaging of Oxidized Stepped Silicon Surfaces," in *Proc. 41st Ann. Meeting Electron Microsc. Soc. Amer.*, G.W. Bailey, Ed., San Francisco Press, p. 106, (1983); LBL-15592.

LBL Reports

6. J.M. Howe (M.S. Thesis), "Atomic Mechanisms of Precipitate Plate Growth," LBL-15933.
7. J.M. Howe, R. Gronsky, and H.I. Aaronson, "Atomic Mechanisms of Precipitate Plate Growth in the Al-Ag System — I. Conventional Transmission Electron Microscopy," LBL-16503.
8. J.M. Howe, R. Gronsky, and H.I. Aaronson, "Atomic Mechanisms of Precipitate Plate Growth in the Al-Ag System — II. High-resolution Transmission Electron Microscopy," LBL-16504.
9. T.D. Sands, J. Washburn, and R. Gronsky, "High-resolution Study of the Relationship between Misfit Accommodation and Growth of $\text{Cu}_{2-x}\text{S}/\text{CdS}$ in CdS," LBL-16774.
10. T.D. Sands, D.K. Sadana, R. Gronsky, and J. Washburn, "High-resolution Structural Characterization of the Amorphous-crystalline Interface in Se^+ -implanted GaAs," LBL-17035.
11. T.D. Sands, R. Gronsky, and J. Washburn, "Characterization of Single-crystal $\text{Cu}_2\text{S}/\text{CdS}$ Heterojunctions by High-resolution Electron Microscopy," LBL-17141.

Other Publications

12. J.H. Mazur, R. Gronsky, and J. Washburn, "High-resolution Electron Microscopy Studies of Native Oxide on Silicon," in *Inst. Phys. Conf. Ser. No. 67: Section 2*, 1983, p. 77; LBL-16272.

13. J. Howe, M. Sarikaya, and R. Gronsky, "Chemical and Structural Analysis of γ' Precipitates in Al-Ag Alloys by EDS and CBED," in *Proc. Western Regional Meeting Electron Microscopists*, Asilomar, California, 1983, p. 7; LBL-15836A.

14. E.A. Kamenetzky and R. Gronsky, "The Structure of Grain Boundaries: Models and Microscopy," in *Proc. Western Regional Meeting Electron Microscopists*, Asilomar, California, 1983, p. 9.

Invited Talks

15. R. Gronsky, "Atoms at Interfaces: Direct Imaging by Electron Microscopy," Exxon Research and Engineering, Corporate Research Science Laboratories, Linden, New Jersey, February 14, 1983.
16. R. Gronsky, "Atomic Resolution Imaging of Grain Boundaries in Metals," JEOL Seminar on Electron Microscopy in Materials Science, Kaiser Center for Technology, Pleasanton, California, February 15-16, 1983.
17. R. Gronsky, "The Microscopy of Electronic Materials," Electrical Engineering and Computer Science Department, University of California Berkeley, March 4, 1983.
18. R. Gronsky, "Direct Imaging of Surfaces and Interfaces," DOE Panel on Coatings and Surface Modifications, Lawrence Berkeley Laboratory, August 25, 1983.
19. R. Gronsky, "Characterization of the Solid State at High Spatial Resolution," Condensed Matter Physics Seminar, Department of Physics, University of California Berkeley, October 19, 1983.
20. R. Gronsky, "Characterization of Defects in Semiconductors by Electron Microscope Methods," Electronic Materials Seminar, Department of Materials Science and Mineral Engineering, University of California Berkeley, October 27, 1983.

Microstructure, Properties, and Alloy Design: Inorganic Materials

Gareth Thomas, Investigator

INTRODUCTION

This research is concerned with the relationships between microstructure and properties, the control of properties through characterization and control of structure, and the application of principles of strengthening and phase transformations to alloy design for mechanical (including wear) and magnetic property improvements, especially energy and material conservation. Systems under investigation include ferrous alloys, dual-phase steels, rare-earth and Co-free alloys, and ceramics. Quantitative analyses of structure are made by electron microscopy, spectroscopy and diffraction, and high-voltage atomic-resolution electron microscopy. The research is divided into three sections: (1) alloy design, microstructure, and properties; (2) phase transformation in steels; and (3) magnetic-materials research.

ALLOY DESIGN, MICROSTRUCTURE, AND PROPERTIES

1. Design of Strong, Ductile, Duplex Low-alloy Steel (Publication 10)

G. Thomas

Strength, toughness, and ductility are undoubtedly the most important properties specified for structural steels unless the application involves aggressive environments. However, an increase in the ductility is achieved at the expense of the strength, and vice versa.

This paper summarizes current alloy design programs which use two-phase steel to optimize the properties listed above by using the principle of composites. The size, distribution, shape, and

volume fraction of the second phase critically control the mechanical behavior of the dual-phase systems. As a consequence, these structures offer a degree of metallurgical flexibility that is absent in single-phase structures and precipitation-strengthened systems for attaining optimum sets of mechanical properties.

Examples are presented of martensite-austenite (~ 2-5%) mixtures designed for optimum combinations of high strength, toughness, and wear properties in medium-carbon steel (e.g., for mining and agricultural applications), and martensite-ferrite (~ 80%) structures for high strength, good formability, and improved low-temperature ductility in low-carbon steels.

2. Retained Austenite and Tempered-martensite Embrittlement in Medium-carbon Steels (Publication 5)

M. Sarikaya, A.K. Jhingan, and G. Thomas

Electron microscopy, diffraction and microanalysis, x-ray diffraction, and Auger spectroscopy have been used to study quenched and tempered 0.3%-carbon low-alloy steels. Some *in situ* fracture studies were also carried out in a high-voltage electron microscope. Tempered-martensite embrittlement (TME) is shown to arise primarily as a microstructural constraint associated with decomposition of interlath-retained austenite into M_3C films upon tempering in the range of 250 to 400°C (see Figures 2-1 and 2-2). In addition, intralath Widmanstätten Fe_3C forms from epsilon carbide. The fracture is transgranular with respect to prior austenite. The situation is analogous to that in upper bainite. This TME failure is different from temper embrittlement (TE), which occurs at higher tempering temperature (approximately 500°C) and is not a microstructural effect. Rather, it is due to impurities (principally sulfur in the present work) segregating along prior austenite grain boundaries, thus leading to intergranular fracture along those boundaries. Both failures can occur in the same steels, depending on the tempering conditions.

*This work was supported by the Director, Office of Energy Research, Office of Basic Energy Sciences, Materials Sciences Division of the U.S. Department of Energy under Contract No. DE-AC03-76SF00098.

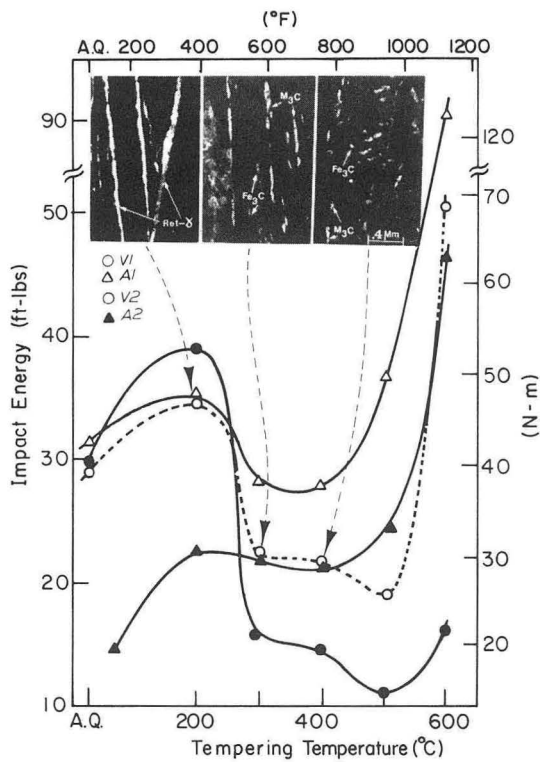


Figure 2-1. Impact energy (Charpy V-notch energy) vs tempering temperature. The curves reveal both TME and TE regions (1-hour tempering). Inset micrographs of B1 alloy show the corresponding dark-field images: (left) retained austenite, (center) interlath carbides, (right) spheroidized intralath and interlath carbides in 2%-Mn alloy. Values for the air-melted alloys of the same compositions are also plotted for comparison. (XBB 821-4)

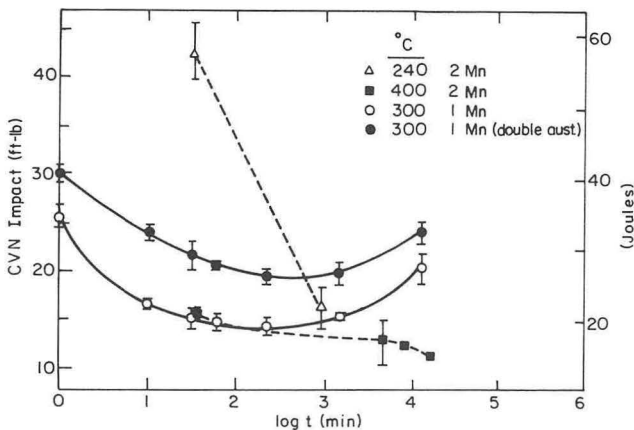


Figure 2-2. Charpy V-notch energy vs tempering time for isothermal heat treatments. The drastic drop in the Charpy values of 2%-Mn alloy after 240°C tempering for 16 hours is due to TME. Further decrease in fracture energy of this alloy occurs after long tempering at 400°C; this decrease is attributed to TE. On the other hand, prolonged heating in 1%-Mn alloys increases the impact value due to recovery and lower original retained austenite content. (XBL 824-5548)

3. Medium-carbon-steel Alloy Design for Wear Applications (Publications 1 and 12)

W.J. Salesky and G. Thomas

The fracture characteristics of steels are strongly influenced by martensitic substructure, retained austenite stability, and morphology. Attractive strength-toughness properties have been attained with Fe-Cr-C-Mn alloys. These alloys, when tested under sliding-wear conditions, also exhibit wear resistance that compares favorably with that of commercial wear-resistant alloys. The most significant finding is an apparently strong correlation between sliding-wear resistance and retained austenite, which in turn appears to correlate with Charpy-impact properties. Little correlation was observed between hardness and wear resistance for the experimental steels.

4. Development of Experimental Duplex Ferrite-bainite Steel for Line Pipe (Publication 7)

N.J. Kim and G. Thomas

An investigation has been made to develop a simple duplex steel for line-pipe applications. Controlled rolling of an Fe/1.5Mn/0.06C alloy followed by direct quenching produced a duplex ferrite-bainite structure in which the coarse upper bainite regions were uniformly distributed within a fine-grained ferrite matrix. The microstructure and mechanical properties of this duplex structure were strongly influenced by the processing variables. Decreasing the finish-rolling temperature improved both tensile and impact properties. This improvement was due mainly to a refinement of the ferrite grain size. There was an abrupt increase in the yield strength and a small increase in the ductile-brittle transition temperature as a result of cold working (pipe-forming) because of the steel's continuous yielding behavior and the high initial work-hardening rate. The mechanical properties attained in this duplex steel are attractive for low-temperature line-pipe applications.

5. Fatigue Resistance and Microstructure of Experimental Dual-phase Fe/2Si/0.1C Steel (Publication 23)

V.B. Dutta, S. Suresh, G. Thomas, and R.O. Ritchie

The fatigue behavior of an experimental dual-phase Fe/2Si/0.1C steel has been examined as a function of constituent morphology with the objective of developing ferritic-martensitic microstructures with optimum strength and fatigue-crack-propagation resistance. Microstructures containing fine globular or coarse martensite within a coarse-grained ferritic matrix were found to show the highest fatigue-threshold stress-intensity-range ΔK_0 values reported to date (to our knowledge). They certainly showed the highest combination of strength and ΔK_0 for steels (ΔK_0 values above $19 \text{ MPa}\sqrt{\text{m}}$ with yield strengths over 600 MPa). Such unusually high

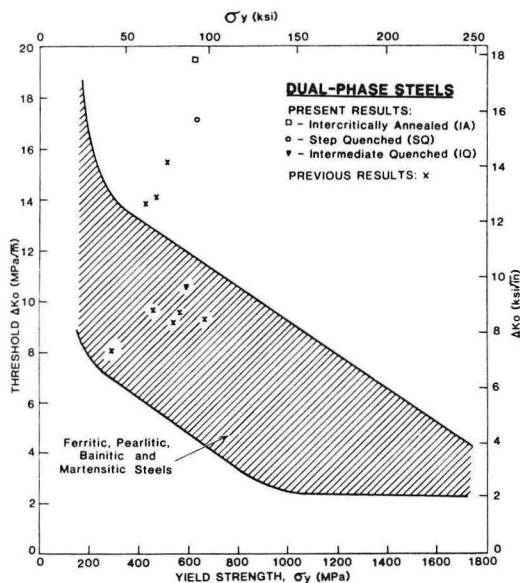


Figure 5-1. Variation of fatigue threshold stress intensity range ΔK_0 at $R \sim 0$ with yield strength for ferrous alloys, highlighting the usually high-strength and fatigue-threshold properties of dual-phase steels. (XBL 838-10895)

crack-growth resistance is attributed primarily to a meandering crack-path morphology, which promotes slower crack-extension rates from crack deflection and roughness-induced crack-closure mechanisms (see Figure 5-1).

PHASE TRANSFORMATIONS IN STEELS

6. Lath Structures in Medium-carbon Steels (Publication 22)

M. Sarikaya, H. Tokushige, and G. Thomas

The morphology and crystallography of lath structures in experimental medium-carbon structural steels quenched to martensite ($M_s \sim 300^\circ\text{C}$), or isothermally transformed (at 360°C) to bainite, have been investigated by transmission electron microscopy (TEM) techniques. The structures are very similar except for carbide morphologies. The microstructure in the as-quenched condition consists of heavily dislocated martensite laths belonging to different variants of $\{111\}_A$; each specific variant forms a packet. Retained austenite is always present in the form of thin films ($\sim 100\text{--}200 \text{ \AA}$) at the lath (except twin-related laths) and packet boundaries.

Bainitic-ferrite laths containing unidirectional carbides are less uniform than martensite laths, but they also form packets (see Figure 6-1). Although retained-austenite films are also present after short aging times (10 min), these films are transformed into elongated carbides at longer isothermal holding times (1 hr). The carbides, both within the laths and at the lath boundaries, obey variants of Isaichev-orientation relationships (see Figure 6-2).

Microdiffraction analyses showed the orientation relationships between austenite and martensite or bainite. These relationships vary from the Kurdjumov-Sachs and Mishiyama-Wassermann, clustering mostly about the Greninger-Troiano in both cases.

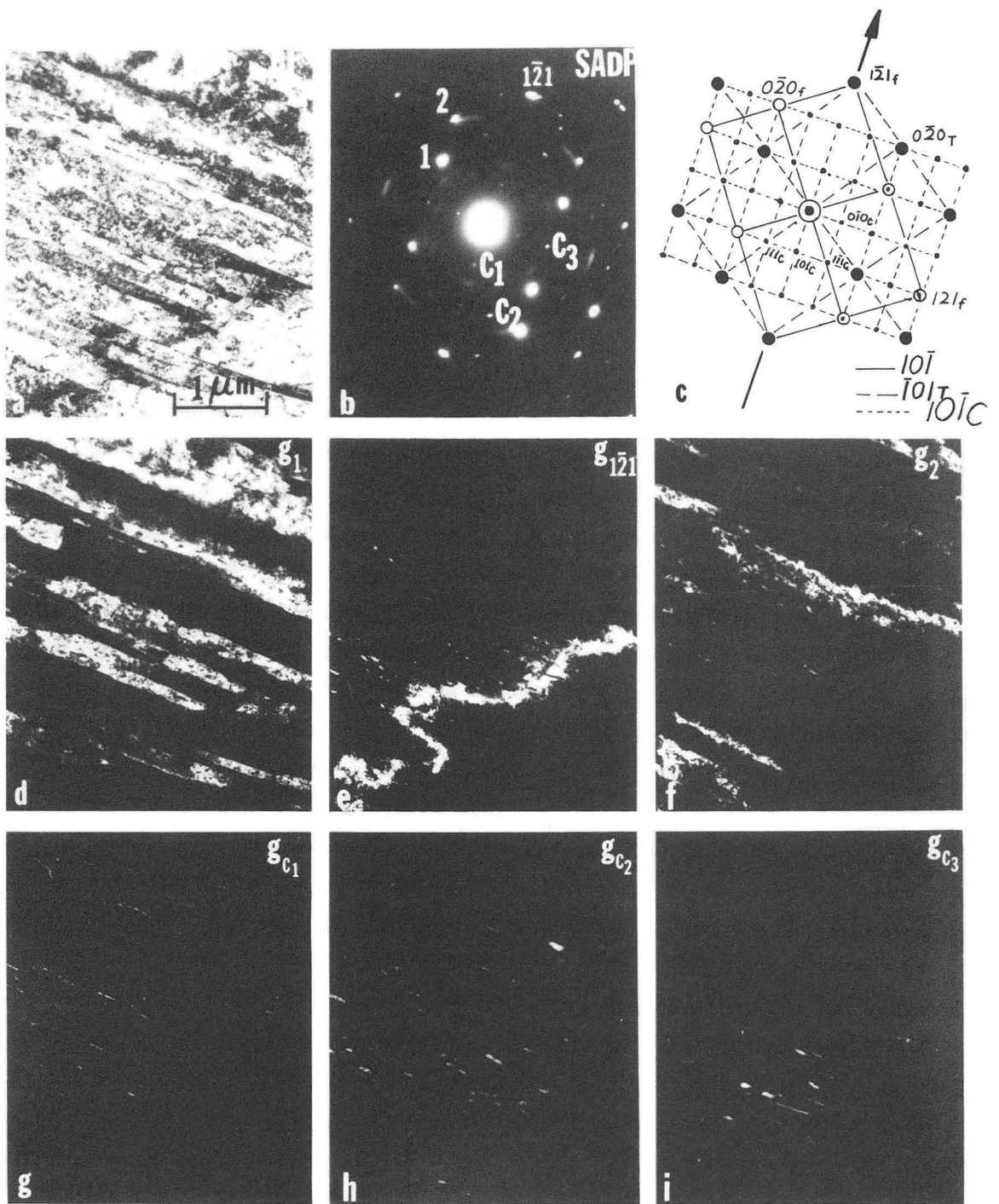


Figure 6-1. TEM micrograph of 0.3%-C sample after isothermal holding at 360°C for 1 hour. (a) Bright field, (b) selected area diffraction, (c) indexed pattern, (d-f) dark field from respective reflections. (XBB 827-6673A)

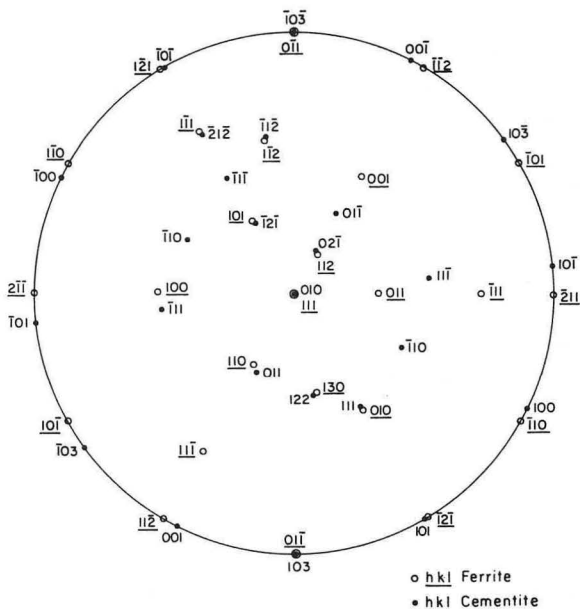
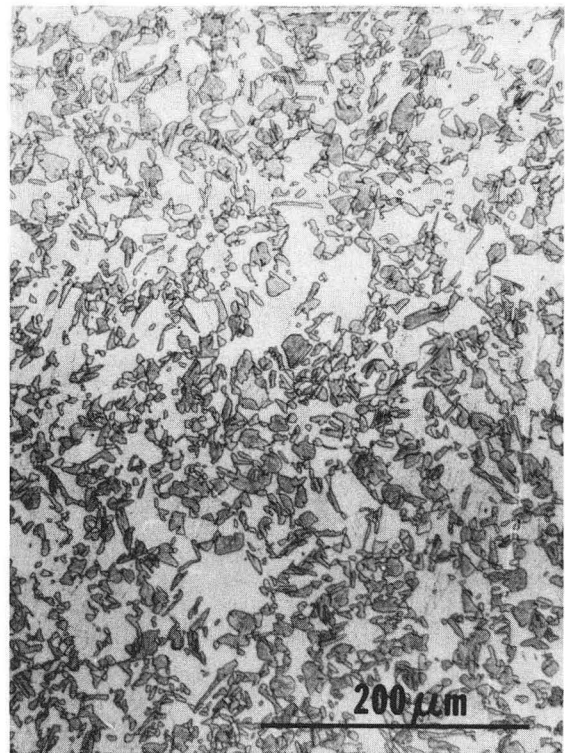


Figure 6-2. Stereographic representation of Isaichev orientation relationship between carbides and ferrite. (XBL 831-5159)



7. Design of High-strength Dual-phase Steel Wire (Publication 25)

J. Ahn, A. Nakagawa, and G. Thomas

A new process has been developed to make high-strength cold-formed wire from simple low-carbon ($\sim 0.1\%$ C) steels using a composite microstructure of ferrite and martensite (dual-phase steel) rather than the conventional high-carbon pearlitic wire.

Dual-phase steel was selected because of its pronounced strain-hardening rate and superior formability. These properties permit dual-phase steel to be drawn to large strains and high strengths without intermediate treatments, resulting in a reduction in the complexity of the operation as well as a reduction of production costs and energy consumption. Both the alloy composition of dual-phase steel and its processing are generally simple and can be varied to produce a wide range of structural and mechanical properties to fit specific applications.

Experimental results have shown that dual-phase steel can be drawn to 97% reduction in area (see Figure 7-1) for a strength level of $\sim 280\text{--}300$ ksi (1930–2070 MPa) or drawn to 99.8% reduction in area for strength levels of about 400 ksi (2760 MPa). Potential applications for dual-phase wire include bead and tire cord, wire rope, and prestressed concrete (see Figure 7-2).

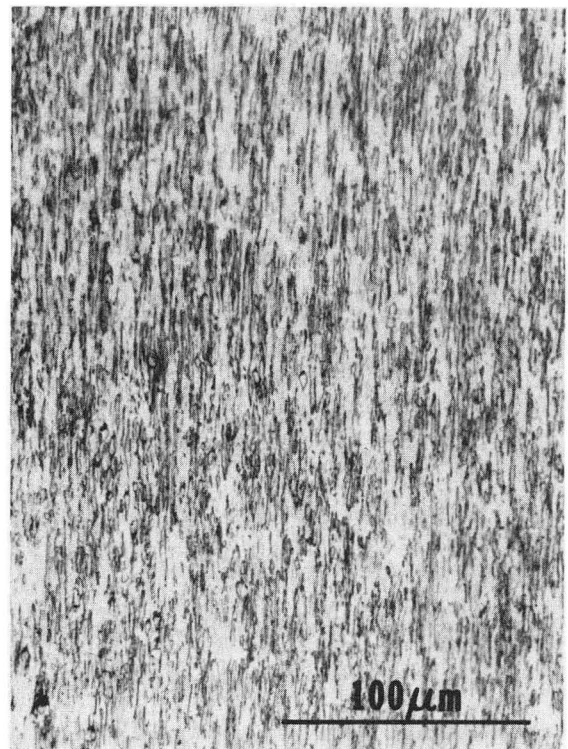


Figure 7-1. Scanning electron micrograph showing the ferrite-martensite structure before (top) and after (bottom) 99% reduction in area. Notice the excellent flow and alignment of both phases and no decohesion at the interfaces. Fe/2Si/0.08C. (XBB 8111-10279)

Dual-Phase Steel Wire

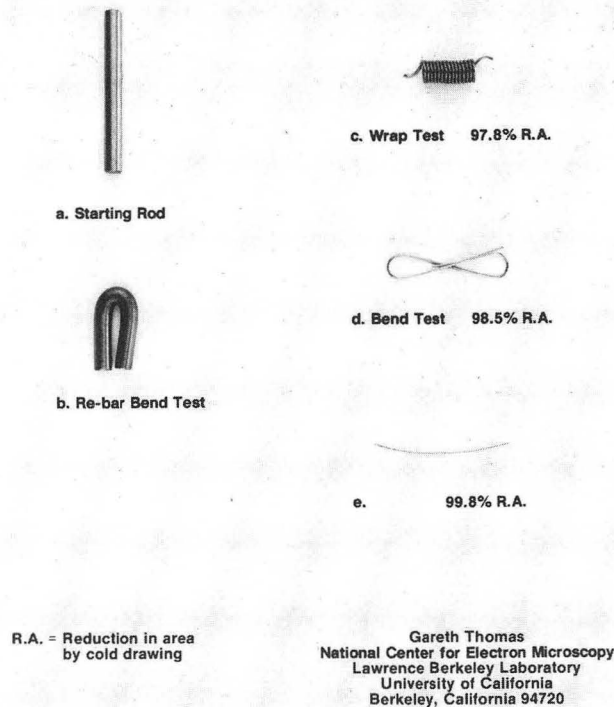


Figure 7-2. Photographs showing some examples of rod and wire characteristics obtainable in cold-formed dual-phase ferrite-martensite steels (carbon content 0.1% or less).
(XBB 830-10150)

8. Microstructure, Mechanical Properties, and Two-body Abrasive-wear Resistance of an Ultrahigh-strength Steel Based on Fe/3Cr/C (Publication 36)

Y. Yoon and G. Thomas

An ultrahigh-strength steel for structural and abrasive applications has been designed based on Fe/3Cr/C, and its structure-property relationships have been established. The microstructure has been characterized as dislocated lath martensite containing fine carbides and surrounded by a thin film of retained austenite. This microstructure results in an excellent combination of mechanical properties and

abrasion resistance. These properties are attractive in comparison to many commercial abrasive alloys. It has also been shown that the abrasion resistance depends mainly on the hardness of the steel.

Tempered martensite embrittlement occurs in the tempering-temperature range of 300 to 400°C and has been confirmed to be coincident with the decomposition of interlath-retained austenite into stringers of coarse cementite. Epsilon-carbon has been found in both the as-quenched condition and the 200°C-tempered condition. The most likely sites for the formation of the cementite are shown to be the ϵ -carbide interfaces with the matrix. As the cementite grows, the ϵ -carbon particles gradually disappear.

MAGNETIC MATERIALS RESEARCH

Characterization of the microstructures of hard and soft magnets has been emphasized, with the overall objective of designing new and superior magnet alloys.

9. Microstructure and Magnetic Properties of Mn-Zn Ferrite (Publication 33)

I-Nan Lin, R.K. Mishra, and G. Thomas

Grain boundaries in the Mn-Zn ferrites have been characterized, and their effects on magnetic and electrical properties have been investigated. In addition, controlled-atmosphere annealing has been performed on high-permeability ferrite to improve the electrical resistivity of the bulk materials.

The grain-boundary phases act as insulating layers for electrical conduction and also act as barriers to magnetic-domain wall motion. But the overall effect of adding Ca is not beneficial. The controlled-atmosphere annealing drastically improved the apparent resistivity of the sintered Mn-Zn ferrites through the reduction of the ferrous-ion content. The magnetic permeability, unfortunately, degrades as a result of annealing (see Figure 9-1), due to oxidation. A stringent control of the oxygen partial pressure during sintering is necessary to raise the intrinsic electric resistivity.

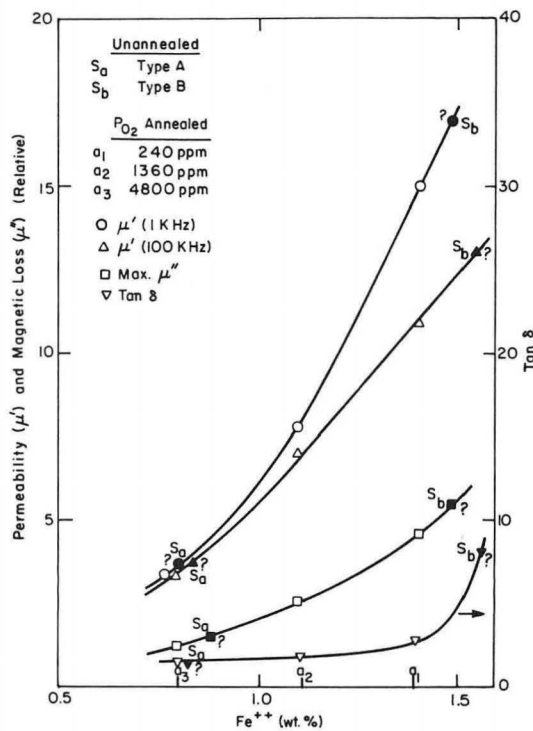


Figure 9-1. Fe²⁺ dependence on magnetic permeability (at 1 KHz and 100 KHz), maximum magnetic loss, and tan δ (at 6 MHz) of the same specimens. The magnetic properties decrease with the ferrous (Fe₂₊) ion content. (XBL 8212-6937)

10. Phase Transformations and the Development of Magnetic Coercivity in Samarium-cobalt-based Permanent Magnet Alloys (Publication 29)

Llewlyn Kay Rabenberg, R.K. Mishra, and G. Thomas

An experimental investigation of the microstructures of precipitation-hardening samarium-cobalt-based magnets has been undertaken in order to determine the nature of the microstructural features critical to high intrinsic coercivity in these alloys. In alloys aged near peak coercivity, three microstructural features are commonly observed. The bulk of the material consists of a modulated structure of twinned rhombohedral Sm₂(CoCuFeZr)₁₇ (the 2:17 phase), with thin layers of hexagonal Sm(CoCuFeZr)₅ (the 1:5 phase) developed on the six crystallographically equivalent pyramid planes. A Zr-rich phase having a structure related to that of SmCo₃ forms as a thin coherent plate on the basal planes of the modulated structure. The modulated structure results from precipitation

of the 1:5 phase from a supersaturated solution in the 2:17 phase; this precipitation reaction occurs concurrently with an allotropic transformation of the parent 2:17 phase. In order to develop the coercivity, a low-temperature aging process must be performed to allow Cu and Fe to partition into the 1:5 and 2:17 phases, respectively (see Figure 10-1). Thus a microstructure consisting of a continuous coherent two-phase dispersion with maximal chemical differentiation between the two phases is desirable for the best Sm-Co magnets.

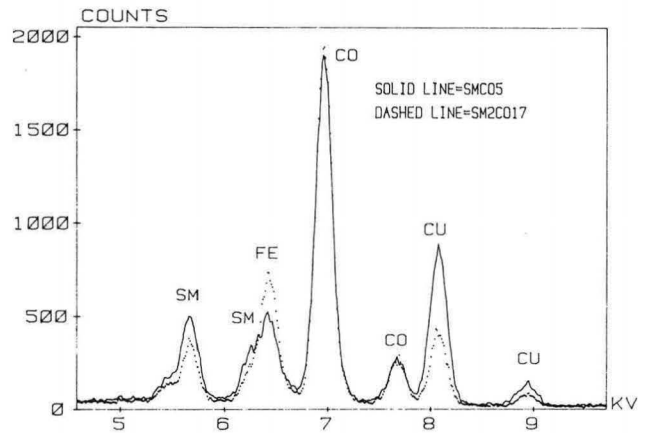


Figure 10-1. Microanalysis of 1:5 and 2:17 phases of overaged alloy. By normalizing both spectra to the Co peak, it is seen that the 2:17 phase is enriched in Fe and the 1:5 phase is enriched in Cu. (XBL 819-2062)

11. Design and Characterization of Mn-Al-C Alloys for Permanent Magnet Applications (Publication 17)

G.S. Gau, R.K. Mishra, and G. Thomas

An experimental study of the processing-structure-property relationships in Mn-Al-C alloys has been undertaken to develop Mn-Al-based permanent magnets.

Extrusion is the most effective means of developing a deformation texture which coincides with the easy axis of magnetization. The resulting microstructure of the extruded magnet contains fine grains, some heavily twinned on {111} planes and some highly dislocated (see Figure 11-1). No antiphase boundaries were found, and no magnetic-domain walls except in the Ni-containing magnet were observed by Lorentz microscopy. The domain walls are believed to be pinned predominantly at grain

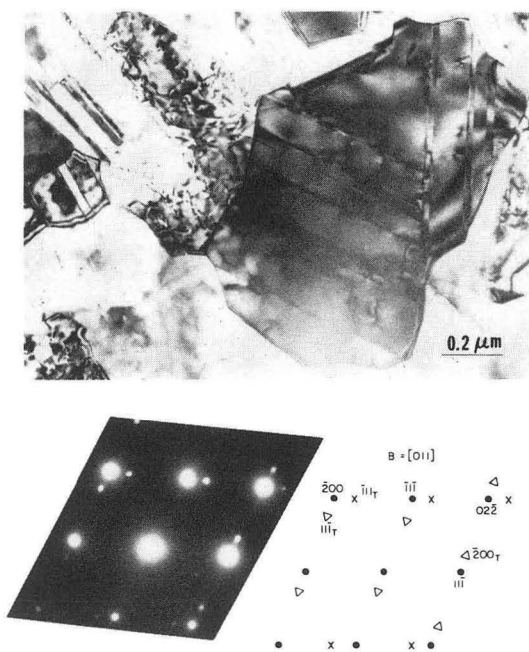


Figure 11-1. Top: A bright-field TEM micrograph taken from a Ni-containing Mn-Al-C alloy illustrates typical microstructural features: dislocation and twins. Bottom: Microdiffraction pattern taken from the grain containing two variants of edge-on twin bands. The corresponding index reveals that the twins lie on $\{111\}$ planes (argon melting sample). (XBB 826-5177)

boundaries. The best properties, those with $(BH)_{\max} = 8.1$ MGOe in the magnet containing 0.8 wt% Ni, are attributed to the strong local Ni-Mn ferromagnetic coupling and improved magnetic anisotropy.

Rapid solidification processing by a melt-spinning technique results in a new nonmagnetic hexagonal ordered phase in the Mn-Al-C system. Magnetic properties of sintered magnets are inferior to those of extruded ones because of the lack of texture, even with a uniaxial hot pressure of 6,000 psi, and the formation of pores during sintering.

12. Determination of Specific-site Occupations in Single Crystals by Channeling-enhanced Microanalysis: Principles and Application (Publications 26, 28, and 35)

K. Krishnan, P. Rez, R.K. Mishra, and G. Thomas

The orientation dependence of electron-induced characteristic x-ray emissions under favorable conditions enhances the potential of energy-dispersive x-ray microanalysis in materials characterization. In

particular, one can determine specific-site occupations in crystalline materials. A detailed technique has been developed and applied to the characterization of garnet materials, where the magnetic anisotropy is attributed to the preferential occupation by certain elemental additions at specific sites in the crystal structure.

Using a theoretical formulation based on the assumption of highly localized inner-shell excitations, a $g = 121$ systematic orientation was predicted to be specific-site sensitive for thin-film magnetic garnets (see Figure 12-1). Experimentally, it has been shown that in these compounds the preference for rare-earth additions is predominantly octahedral, with the probability of octahedral occupation greater than 95%. By monitoring the characteristic x-ray spectrum as a function of incident beam orientation, it was possible to determine that 88.5% of the Mn atoms and 85.1% of the Fe atoms occupy sites in the mixed planes in the $\text{Sm}_2(\text{CoTM})_{17}$ compounds.

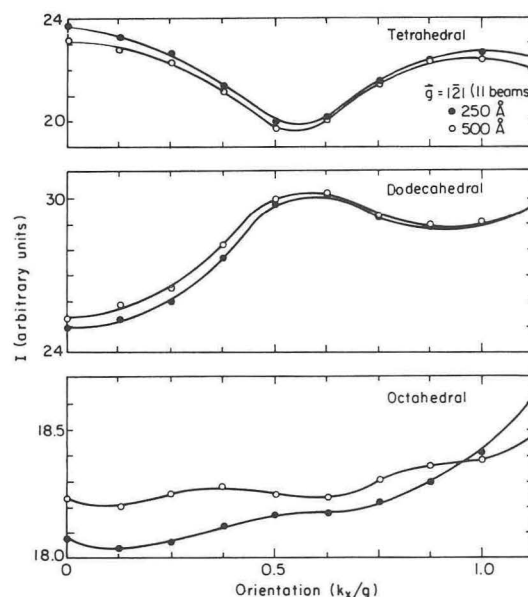


Figure 12-1. Variation of electron-induced characteristic x-ray emission with orientation for a garnet structure. These calculations were carried out for an 11-beam, $g = 121$ systematic row and for a range of incident-beam orientations ($0 < k_x/g < 1.0$). (XBL 831-5156)

13. Work in Progress

The severe embrittlement that accompanies the precipitation of thin films of proeutectoid cementite on austenite grain boundaries has largely precluded the utilization of strongly hypereutectoid (> 1 wt%) carbon steels for mechanical applications. However,

the possibility of developing useful, strongly hypereutectoid steels does exist if the problem of grain-boundary precipitation of proeutectoid cementite can be avoided. As a first step toward achieving this goal, the effect of alloy additions (Fe-C-X, where X = Cu or Mn) on the kinetics and morphology of proeutectoid cementite precipitation is now being examined.

Direct observation of wear as it occurs is difficult because most wear processes are microscopic and instantaneous. Microstructural studies of wear debris may provide important clues to the nature of wear processes and the origin of these wear particles.

In general, TEM studies of the internal structure of debris particles are limited to regions that are thin enough for electron transmission. For a conventional 100-kV microscope, this results in a maximum thickness less than 100 nm. But since most debris particles are thicker than 100 nm, electron penetration is not sufficient. The newly installed 1.5-MV high-voltage TEM is an ideal tool for this study.

The physical metallurgy of low-carbon dual-phase steels is well-understood, but there exists very little experimental data concerning solute partitioning during intercritical (ferrite and austenite) annealing. At the early stages of intercritical annealing, the growth rate of austenite (or ferrite) is controlled primarily by the carbon diffusion rate. However, at later stages the diffusion of substitutional elements governs the development of microstructure. Solute-element concentrations of manganese-bearing steels were measured by a scanning TEM equipped with an energy-dispersive x-ray analyzer. Preliminary experimental results showed similar concentration profiles of Mn through ferrite/martensite to that calculated from the diffusion equations. Further experiments are designed to determine the profiles of Si and P and their effects on the kinetics of microstructure formation.

The stability of austenite in medium-carbon steels with respect to displacive and reconstructive modes of transformation during continuous cooling and subcritical isothermal holding is being studied. In particular, the transition from diffusion-controlled transformation to diffusionless transformation is the focus of this research. The occurrence of the transformation product, bainite, has been noticed in this region. The emphasis is on using electron-microscope techniques to study these transformations.

The volume changes that occur during heating and cooling of low-alloy and plain-carbon steels because of thermal expansion and phase transformations often result in dimensional or shape changes of

heat-treated products. These dimensional changes must be considered in the operation of continuous steel-processing facilities. In addition, very intense internal stresses leading to cracking can result from steep temperature gradients. Finally, differential expansion and contraction can also generate significant differences between phases, because ferrite, cementite, austenite, and martensite all have different specific atomic volumes (densities) and expansion coefficients. Any theoretical interpretation or prediction of the shape and orientation of transformation products requires good data on specific atomic volume as a function of temperature for both the parent and product phases.

For these reasons the volume changes resulting from the transformation of austenite to ferrite plus cementite were computed for a range of carbon contents and temperatures using the best data culled from a rather confusing and conflicting literature. Dilatometry measurements on a series of steels provided a good check on the calculated results.

The results have been used by U.S. Steel with reference to the accurate control of the finished diameter of welded line pipe.

A new project has been undertaken to study the microstructure of audio recording tapes. This is part of a broader study of microstructure and recording characteristics of thin films and dispersed media used for digital and analog recording. Basic questions, such as the valence state of Fe in the γ -Fe₂O₃ tapes, the distribution of alloying elements, and the nature of defects, will be answered in the first phase of this work. Ni-Cr and Co-Co thin films will also be studied.

Piezoelectric materials are being studied to understand the effect of aging phenomena. It is suspected that the domain configuration changes with aging, and transmission microscopy will be used to systematically study these changes in (Pb,La)TiO₃.

Investigation of magnetic properties of a SmCo_{7,4} alloy with Fe and Cu additions will be undertaken to obtain a Sm₂Co₁₇-type magnet containing no cellular morphology, and to design a magnet exhibiting precipitation-hardening characteristics. The characterization of a new class of magnets based on Nd-Fe alloys may also be undertaken this year.

1983 PUBLICATIONS AND REPORTS

Refereed Journals

1. W.J. Salesky and G. Thomas, "Medium Carbon Steel Alloy Design for Wear Applications," *Wear* **75**, 31 (1982); LBL-12447.

2. G. van Tendeloo, K.T. Faber, and G. Thomas, "Characterization of AlN Ceramics Containing Long Period Polytypes," *J. Mat. Sci.* **18**, 525 (1983); LBL-14566.†
3. M. Sarikaya and G. Thomas, "Lath Martensites in Low Carbon Steels," *J. de Physique* **43**, 563 (1982); LBL-14506.
4. M. Sarikaya and G. Thomas, "Lath Martensite in Carbon Steels — Are They Bainitic?" in *Proc. Int. Conf. Solid-Solid Phase Transformations*, Pittsburgh, Pennsylvania, August 1982, p. 999; LBL-13098.
5. M. Sarikaya, A.K. Jhingan, and G. Thomas, "Retained Austenite and Tempered Martensite Embrittlement in Medium Carbon Steel," *Met. Trans. A* **14A**, 1121 (1983); LBL-13876.
6. J.S. Gau and G. Thomas, "Continuous Annealing of a Fe/0.1C/0.45Si/0.05Nb/0.1Mo Dual-phase Steel," *Metallurgy of Continuous-annealed Sheet Steel*, B.L. Bramfitt and P.L. Mangonon, eds., AIME, New York, 1983, p. 333; LBL-13961.
7. N.J. Kim and G. Thomas, "Dual-phase Steel for Pipeline," *Proc. Conf. of Line Pipe and Steel*, London Intl. Conf., The Metals Society, London, **285**, 121 (1983); LBL-14245.
8. L. Rabenberg, R.K. Mishra, and G. Thomas, "Development of the Cellular Microstructure in the SmCo_{7,4}-type Magnets," in *Int. Workshop on Rare-earth Cobalt Magnets and Application in Re-transition Metal Alloys*, Vienna, Austria, 1982, p. 599; LBL-14554.
9. C. Ahn and G. Thomas, "Microstructure and Grain Boundary Composition of Hot Pressed Silicon Nitride with Ytria and Alumina," *J. Am. Ceram. Soc.* **66**, 4 (1983); LBL-14627.†
10. G. Thomas, "Design of Strong, Ductile, Duplex Low Alloy Steels," in *Specialty Steels and Hard Materials*, N.R. Comins and J.B. Clark, eds., Pretoria, South Africa, 1983, p. 55; LBL-15006.
11. W.J. Salesky, R.M. Fisher, R.O. Ritchie, and G. Thomas, "Nature and Origin of Sliding Wear Debris from Steels," in *Proc. Int. Conf. on Wear of Material*, K.C. Ludema, Ed., Book No. H00254, 1983, p. 434; LBL-15059.
12. J.S. Gau, "A New Ordered Phase in Mn-Al-C Alloys," in *Proc. 41st Annual Meeting EMSA*, G.W. Bailey, Ed., 1983, p. 252; LBL-15551A.
13. M. Sarikaya, J.W. Steeds, and G. Thomas, "Lattice Parameter Measurement in Retained Austenite by CBED," in *Proc. 41st Annual Meeting EMSA*, G.W. Bailey, Ed., 1983, p. 206; LBL-15834.
14. G. Thomas and G. Van Tendeloo, "Electron Microscopy Investigations of the ZrO₂-ZrN System — I. Formation of an Incommensurate Superstructure Zr-O-N," *Acta. Met.* **31**, 1611-1618, 1983; LBL-16041.†
15. G. Van Tendeloo, L. Anders, and G. Thomas, "Electron Microscopy Investigation of the ZrO₂-ZrN System — II. Tetragonal and Monoclinic ZrO₂ Precipitation," *Acta. Met.* **31**, 1619-1625, 1983; LBL-17236.
16. T.M. Shaw and G. Thomas, "The Crystallization Behavior of a Mg-Si-O-N Glass," in *Progress in Nitrogen Ceramics*, F.L. Riley, Ed., Martinus Nijhoff, Boston, 1983, pp. 331-336; LBL-17271.‡
17. J.S. Gau, R.K. Mishra, and G. Thomas, "Electron Microscopy of Mn/Al/C Magnets," *IEEE Trans. Mag.* **19** (5) (1983); LBL-15754.
18. I-Nan Lin, R.K. Mishra, and G. Thomas, "EM Study of the Structure and Composition of Grain Boundaries in (Mn,Zn) Fe₂O₄," in *Advances in Materials Characterization*, Plenum Pub., New York, p. 351; LBL-14892.
19. M.H. Harmer, R.K. Mishra, and G. Thomas, "Electron Microscopy of Annealed (Ni,Zn,Co) Fe₂O₄," *Comm. Amer. Cer. Soc.*, **66** (3), (C44), 1983; LBL-11223.
20. T.R. Dinger and G. Thomas, "X-ray Energy Dispersive Spectroscopy of Intergranular Phase in 11 and ' Sialons," in *Advances in Materials Characterization*, Plenum, New York, 1983, p. 339; LBL-14832.
21. C.K. Kwok and G. Thomas, "Microstructural Influence on Abrasive Wear Resistance of High Strength, High Toughness, Medium Carbon Steels," in *Proc. Int. Conf. on Wear of Materials*, K.C. Ludema, Ed., Book No. 00254, 1983, p. 140; LBL-14911.

LBL Reports

22. H. Tokushige (Ph.D. Thesis), "Microstructure-mechanical Property Relationships of Martensite and Lower Bainite in a 0.3%C-3%Cr-2%Mn Steel," LBL-15956.
23. V.B. Dutta, S. Suresh, G. Thomas, and R.O. Ritchie, "Fatigue Resistance and Microstructure of Experimental Dual Phase Fe/2Si/0.1C Steel," International Conference, Rio de Janeiro, Brazil, November 27-December 2, 1983, LBL-16681.
24. J.S. Gau (Ph.D. Thesis), "Design and Characterization of Mn-Al-C Alloys for Permanent Magnet Applications," LBL-16897.

25. A. Nakagawa (Ph.D. Thesis), Microstructure-mechanical Property Relationships in Dual-phase Steel Wire, LBL-17099.
26. K. Krishnan, P. Rez, R.K. Mishra, and G. Thomas, "Determination of the Specific Site Occupation of Rare Earth Additions in $Y_{1.7}Sm_{0.6}Lu_{0.7}Fe_5O_{12}$ Thin Films by the Orientation Dependence of Characteristic X-ray Emissions," Materials Research Society Meeting, Boston, Massachusetts, November 13-17, 1983, LBL-16884.
27. N.J. Kim and G. Thomas, "Structure and Properties of As-hot Rolled Fe/1.5Mn/.06C Steel: Potential for Line Pipe Application," in *Metal Science*, in press, LBL-16881.
28. K. Krishnan, L. Rabenberg, R.K. Mishra, and G. Thomas, "Site Occupation of Ternary Elements in $Sm_2(CoTM)_{17}$ Compounds," J. App. Phys., in press, LBL-16874.
29. L. Rabenberg (Ph.D. Thesis), "Phase Transformations and the Development of Magnetic Coercivity in Samarium-cobalt Based Permanent Magnet Alloys," LBL-16612.
30. G. van Tendeloo and G. Thomas, "High Resolution Microscopy Investigation of the ZrO_2 -ZrN System," J. Am. Ceram. Soc., in press, LBL-16240.[‡]
31. J. Wasynczuk, R. Ritchie, and G. Thomas, "Effects of Microstructure on Fatigue Crack Growth in Duplex Ferrite-martensite Steels," Mat. Sci. and Min. Eng., in press, LBL-16118.
32. R.K. Mishra, G. Thomas, and L. Rabenberg, "Comments on J. Fidler, P. Skalicky and F. Rothwarf, HREM Study of $(Co,Cu,Fe,Zr)_{7.5}$ Magnets," IEEE Trans. Magn., in press, LBL-15995.
33. I.N. Lin, R.K. Mishra, and G. Thomas, "Interaction of Magnetic Domain Walls with Microstructural Features in Spinel Ferrites," IEEE Trans. Magn., in press, LBL-15994.
34. J.J. Rayment, W.J. Salesky, X.M. Meng, and G. Thomas, "Some Observations on the Sliding Wear Behavior and Microstructure of a Laser Heat Treated Experimental Alloy," LBL-15654.
35. K. Krishnan, P. Rez, and G. Thomas, "Effect of Voltage on the Orientation Dependence of Electron Induced Characteristic X-ray Emissions," in *Proc. HVEM Conf. Berkeley, California, 1983*, R.M. Fisher, R. Gronsky, and K. Westmacott, eds., p. 365; LBL-16144.
36. Y. Yoon (M. Eng. Thesis), "Microstructure, Mechanical Properties, and Two-body Abrasive-wear Resistance of an Ultrahigh-strength Shell Based on Fe-3Cr-C," LBL-17277.

Other Publications

37. A. Nakagawa and G. Thomas, "Dual-phase Steels for Rods/wire," U.S. Patent Office File No. PCT US 82-01722, patent pending.

Invited Talks

38. G. Thomas, "Microstructure and Properties of Lower Bainite and Martensite in an 0.3%C/3%Cr/2%Mn Steel," TMS/AIME Conference, Atlanta, Georgia, March 6-10, 1983.
39. G. Thomas, "Structure and Properties of Dual-phase Steel Wire," TMS/AIME Conference, Atlanta, Georgia, March 6-10, 1983.
40. G. Thomas, "Lath Structures in Medium-carbon Steels," Symposium on Phase Transformations in Ferrous Alloys, TMS/AIME, Philadelphia, Pennsylvania, October 2-6, 1983.
41. M. Sarikaya, "Problems Related to Nitrogen Detection in SiALONs by EELS," 11th Western Regional Meeting of Electron Microscopists, Asilomar, California, May 1983.
42. C.K. Kwok, "Microstructural Influence of Abrasive-wear Resistance of High-strength High-toughness Medium-carbon Steel," International Wear Conference, Boston, Massachusetts, April 11-14, 1983.
43. W.J. Salesky, "Microstructural Influence of Abrasive-wear Resistance of High-strength High-toughness Medium-carbon Steel," International Wear Conference, Boston, Massachusetts, April 11-14, 1983.
44. G. Thomas, "Physical Metallurgy of Dual-phase Steels," Melbourne, Australia, February 1983.
45. G. Thomas, "Physical Metallurgy of Dual-phase Steels," Kobe Steel, Japan, February 7, 1983.
46. G. Thomas, "EM and Applications in Materials Science and Engineering," First Thailand Seminar and Workshop on EM, University of Chulalongkorn, Bangkok, Thailand, April 19-23, 1983.
47. G. Thomas, "The National Center for EM in Berkeley," Special Meeting of the Indian Institute of Science and Technology, Delhi, India, April 25, 1983.
48. G. Thomas, "HVEM and its Applications in Materials Science," Bombay Atomic Energy Research Center, Bombay, India, April 27, 1983.

49. G. Thomas, "EM of Ceramics," Stanford Research Institute, Menlo Park, California, January 7, 1983.
50. G. Thomas, "Alloy Design of Microduplex Steels," Stanford University, Stanford, California, January 14, 1983.
51. G. Thomas, "The NCEM, Berkeley, Fulfillment of a Nine-year Project," Keynote Speaker, Biannual Conference of Northern and Southern California EM Societies, Asilomar, California, May 11, 1983.
52. G. Thomas, "Electron Microscopy and Microanalysis of Refractory and Electronic Ceramics," Plenary Lecturer, Japan Society for Ceramics, Toyko, May 17, 1983.
53. G. Thomas, "Characterization of Ceramics," J.S.P.S. Subcommittee, Tokyo, May 19, 1983.
54. G. Thomas, "Characterization of Ceramics," Toshiba R&D Center, Kawasaki, Japan, May 20, 1983.
55. G. Thomas, "Fine Ceramics and Magnetic Materials," NKK R&D Center, Kawasaki, Japan, May 24, 1983.
56. G. Thomas, "New Dual-phase Steels for High-tensile Wire," Michelin R&D Center, Clermont-Ferrand, France, June 30, 1983.
57. G. Thomas, "National Center for Electron Microscopy," Electron Microscopy of Ceramics, Toulouse, France, July 1983.
58. G. Thomas, "The NCEM and the Approach to Atomic Resolution of Solids," Diamond Jubilee Celebrations, Varanasi, India, Plenary Lecture, November 1983.
59. G. Thomas, "Alloy Design of Dual-phase Steels," Keynote Address, Indian Institute of Metals Conference, Varanasi, India, November 14-18, 1983.
60. G. Thomas, "The National Center for Electron Microscopy — Development of Material Research," Plenary Lecture, New England Society for Electron Microscopy, Boston, December 7, 1983.
61. G. Thomas, "ZrO-ZrN Ceramics," ZrO₂ 1983 International Conference, Stuttgart, West Germany, June 21-24, 1983.
62. G. Thomas, "Instrumentation at the NCEM:ARM," EMSA Conference, Phoenix, Arizona, August 6-12, 1983; LBL-16318A.
63. G. Thomas, "The Physical Metallurgy and Alloy Design of Dual-phase Steels," Distinguished Lecture Series, Joint Center for Materials Science of New Mexico, Socorro, New Mexico, December 15, 1983; LBL-16613.

[†]Supported by the National Science Foundation.

[‡]Supported partially by the National Science Foundation.

Solid-State Phase Transformation Mechanisms*

Kenneth H. Westmacott, Investigator

INTRODUCTION

The purpose of this program is to obtain a detailed knowledge of the factors that govern phase changes and phase stability in order to facilitate first-principle alloy design for specific service applications. The powerful observational methods afforded by advanced electron optical techniques, especially high-voltage and high-resolution electron microscopy, are employed to follow directly the mechanisms whereby phase transformations occur. Since accommodation of a new phase of disparate size or structure must involve deformation, the relationship between lattice defects and precipitate phase growth is studied. This approach has been fruitful, and a developing crystallographic theory of precipitation is progressively being tested with a parallel experimental program. Simple model systems are treated initially, followed by studies on complex alloy systems of importance in energy technology applications. The resulting knowledge will contribute to understanding alloy stability in hostile environments and designing superior materials.

1. Plate Precipitate Growth Mechanisms (Publication 17)

K.H. Westmacott and U. Dahmen

The growth mechanisms of plate-shaped precipitates are compared and contrasted for Pt-C, Al-Cu, Mo-HfN, and Al-Ag alloys chosen as models for interstitial, substitutional, and mixed interstitial-substitutional systems. In each case there is a perfect structural match between the precipitate and matrix in the habit plane (i.e., invariant plane strain transformation), and the transformation involves only changes in the stacking or spacing of the planes parallel to the habit. The pattern that emerges is that precipitate growth normal to the habit plane is accomplished by nucleating and propagating lattice

defects that transform the matrix crystal structure into the structure of the precipitate or a structure similar to it. For transformations involving little change in volume, the lattice defects are essentially shear loops and the process is conservative. If these shear loops occur in multiples, they may accommodate each other's strain field. Similarly, the strain field associated with a modified plane spacing (volume change) may be accommodated by the non-conservative formation of prismatic dislocation loops.

Three criteria govern the growth sequence: the minimization of volume change, the avoidance of shape change, and the optimization of the stacking order. Experimental evidence supporting this conclusion is presented.

In spite of the diversity of alloy systems studied, the morphological similarities are striking, as illustrated by Figure 1-1. The precipitates in all the

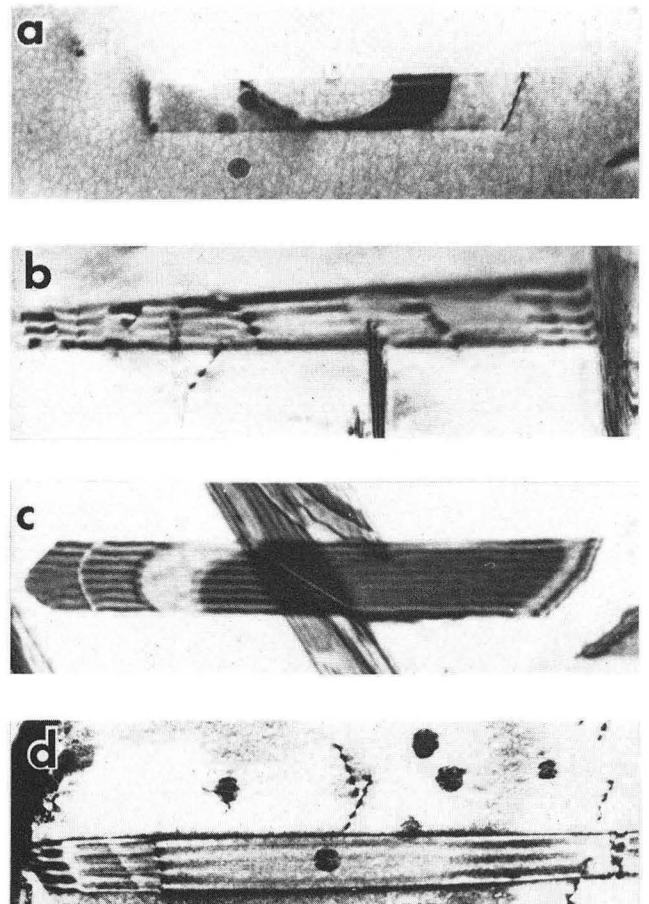


Figure 1-1. Transmission electron micrographs illustrating the morphological similarities between the precipitate plates formed in diverse alloy systems: (a) Pt_2C plate with (001) habit in Pt; (b) θ' (Al_2Cu) plate on (001) in Al-Cu; (c) HfN plate on (001) in Mo; (d) γ' (Al_xAg) plate on (111) in Al-Ag. (XBB 8311-10400)

*This work was supported by the Director, Office of Energy Research, Office of Basic Energy Sciences, Materials Sciences Division of the U.S. Department of Energy under Contract No. DE-AC03-76SF00098.

alloys are plate-shaped due to good match in the habit plane, the habit planes have low crystallographic indices ($\{100\}$ or $\{111\}$), and thickening occurs by propagation of ledges.

2. The Mechanism of θ' Precipitation on Climbing Dislocations in Al-Cu (Publication 12)

U. Dahmen and K.H. Westmacott

A detailed contrast analysis has been performed on the dislocations bounding the spectacular colonies of θ' precipitates that grow in quenched Al-4Cu during high-temperature aging treatments (see Figure 2-1). Large-angle tilting and weak-beam microscopy show that the segments of climbing dislocation that slip into $\{100\}$ planes are dissociated according to the reaction $1/2 [110] \rightarrow 1/2 [100] + 1/2 [010]$. During the

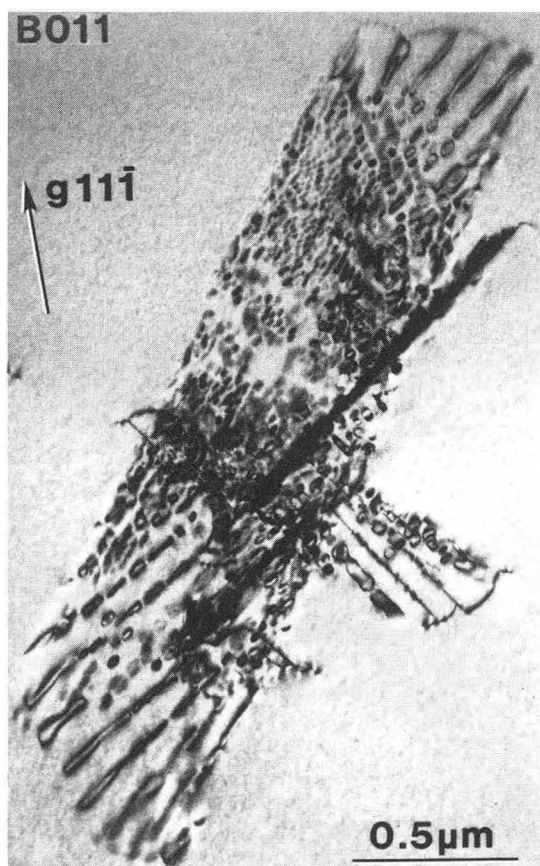


Figure 2-1. Intersecting colonies of θ' precipitates formed on climbing dislocations in Al-4% Cu (note resemblance to golden eagle). The precipitate plates all nucleate on an uncommon fcc partial dislocation $1/2 \langle 100 \rangle$. (XBB 835-3889)

subsequent climb of the dislocation, the $1/2 [010]$ shear loop that forms in its wake provides the ideal structural unit for the heterogeneous nucleation of a unit cell of θ' precipitate. These results are the first direct evidence for the structural role of dislocations in precipitation, as opposed to a purely dilatational role. The results also provide further experimental confirmation of the shear mechanism for θ' growth proposed by the authors earlier.

3. Morphological Aspects of α'' - Fe_{16}N_2 Precipitation in α -Fe (Publication 15)

P. Ferguson, U. Dahmen, and K.H. Westmacott

The curious precipitate morphology observed when α'' - Fe_{16}N_2 plates form in α -Fe has been studied by transmission electron microscopy. Contrast analysis shows that the rosette appearance (Figure 3-1) arises from the precipitate plate being composed of a number of orientation variants.

The different variants are all inclined about 10° to the $\{001\}$ habit plane, and additional segments nucleate as the precipitate diameter increases. The observed inclinations are in good accord with those predicted by linear elastic theory when the appropriate tetragonality ratio is used. A decrease in the total strain energy is postulated as the cause of the puckering of the habit plane.

The results are also compared with other alloy systems in which self-accommodating groupings of several variants have been observed.

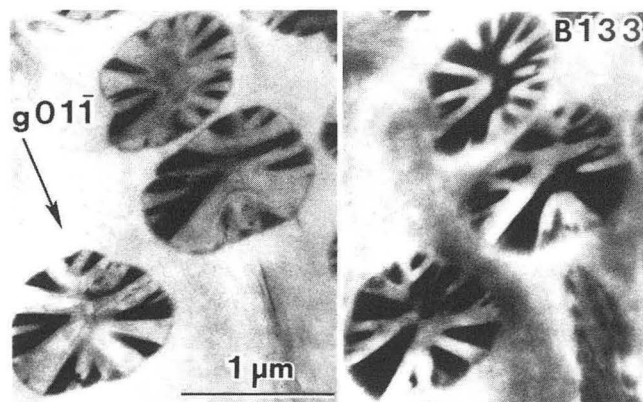


Figure 3-1. Micrographs illustrating the rosette morphology of α'' precipitates in α -Fe resulting from puckering on the $\{001\}$ habit plane. (XBB 838-7678)

4. Work in Progress

A detailed investigation is being made of the mechanism whereby extensive matrix-atom mass transport occurs when certain metal membranes are carburized (or nitrided) on one face and decarburized on the other. An unexpectedly strong coupling between the interstitially dissolved carbon or nitrogen atoms and vacancies is implied. Marked differences in behavior between the grain boundary and matrix regions may provide a direct measure of the GB/matrix-diffusivity ratio.

Development of the crystallographic theory of precipitation is continuing with the extension of the theory to the case of invariant line strain with volume change. We anticipate an analytical solution that will allow prediction of the precipitate habit plane and orientation relationship with the matrix for this general class of transformation.

1983 PUBLICATIONS AND REPORTS

Refereed Journals

1. U. Dahmen, A. Pelton, M.J. Witcomb, and K.H. Westmacott, "The Structural Role of Vacancies in Precipitation Processes," Proc. International Conference on Solid-solid Phase Transformations, Met. Soc. AIME, 637 (1982); LBL-13336.
2. A. Pelton and K.H. Westmacott, "Interstitial Phase Precipitation in Fe-base Alloys: A Comparative Study," Proc. International Conference on Solid-solid Phase Transformations, Met. Soc. AIME, 643 (1982); LBL-13336.
3. U. Dahmen, M.J. Witcomb, and K.H. Westmacott, "Transmission Electron Microscopy Studies of Precipitate Growth Mechanisms in Platinum," Proc. International Conference on Solid-solid Phase Transformations, Met. Soc. AIME, 649 (1982); LBL-13336.
4. U. Dahmen and K.H. Westmacott, "The Role of the Invariant Line in the Nucleation and Growth of Precipitates," Proc. International Conference on Solid-solid Phase Transformations, Met. Soc. AIME, 443 (1982); LBL-13336.
5. J.Y. Laval, K.H. Westmacott, and M.C. Amamra, "Caracterisation et Structure des Phases Vitreuses Intergranulaires dans les Ceramiques," Journal De Physique **43** (12), C9-123 (1982).
6. J.M. Lang, U. Dahmen, and K.H. Westmacott, "The Origin of Mo₂C Precipitate Morphology in Molybdenum," Phys. Stat. Sol. (a) **75**, 409 (1983); LBL-14970.
7. M.J. Witcomb, U. Dahmen, and K.H. Westmacott, "A Study of Precipitation in Interstitial Alloys — II. A New Metastable Carbide Phase in Platinum," Acta Metall. **31** (5), 743 (1983); LBL-14775.
8. U. Dahmen, K.H. Westmacott, and M.J. Witcomb, "A Study of Precipitation in Interstitial Alloys — III. Coherent and Semicoherent Growth Mechanisms," Acta Metall. **31** (5), 749 (1983); LBL-14776.
9. K.H. Westmacott, M.J. Witcomb, and U. Dahmen, "A Study of Precipitation in Interstitial Alloys — IV. The Precipitation Sequence in Pt-C," Acta. Metall. **31** (5), 755 (1983); LBL-14777.
10. R.G. Regnier, N.Q. Lam, and K.H. Westmacott, "Microstructural Transitions in Pt-C Alloys During High-voltage Electron-microscope Irradiation," J. Nucl. Mater. **115**, 286 (1983).
11. A.R. Pelton and K.H. Westmacott, "An AEM Study of Phosphorus Segregation in a Stainless Steel," 41st Ann. Proc. Electron Microscopy Soc. Amer., Phoenix, Arizona (1983).
12. U. Dahmen and K.H. Westmacott, "The Mechanism of θ' Precipitation on Climbing Dislocations in Al-Cu," Scripta Metallurgica **17**, 1241 (1983); LBL-16382.
13. P. Ferguson and K.H. Jack, "The Quench-aging and Strain-aging of Nitrogen Ferrite," Heat Treatment '81, The Metals Society, London, 158 (1983).
14. P. Ferguson, J.H. Driver, and A. Hendry, "Aging of Austenitic Iron Alloys Containing Nitrogen," J. Mat. Sci. **18**, 2951 (1983).

LBL Reports

15. P. Ferguson, U. Dahmen, and K.H. Westmacott, "Morphological Aspects of α'' -Fe₁₆N₂ Precipitation in α -Fe," LBL-16661.
16. U. Dahmen, P. Ferguson, and K.H. Westmacott, "Invariant Line Strain and the Needle-precipitate Growth Directions," LBL-16515.
17. K.H. Westmacott and U. Dahmen, "Plate Precipitate Growth Mechanisms," LBL-16887.

Other Publications

18. P. Ferguson, U. Dahmen, and K.H. Westmacott, "In Situ Study of γ' Precipitation in Fe-N," *Proc. 7th International Conference on HVEM*, Berkeley, California, R.M. Fisher, R. Gronsky, and K.H. Westmacott, eds., 1983, p. 227.
19. U. Dahmen, P. Ferguson, and K.H. Westmacott, "HVEM Studies of Precipitate Morphology Symmetries," *Proc. 7th International Conference on HVEM*, Berkeley, California, R.M. Fisher, R. Gronsky, and K.H. Westmacott, eds., 1983, p. 315.
20. D. Ackland, U. Dahmen, and K.H. Westmacott, "HVEM In Situ Studies of Precipitate Coarsening and Dissolution in a Pt-C Alloy," *Proc. 7th International Conference on HVEM*, Berkeley, California, R.M. Fisher, R. Gronsky, and K.H. Westmacott, eds., 1983, p. 319.
21. R.M. Fisher and K.H. Westmacott, "Structure of Electrodeposited Chromium," *Proc. 7th International Conference on HVEM*, Berkeley, California, R.M. Fisher, R. Gronsky, and K.H. Westmacott, eds., 1983, p. 323.

Invited Talks

22. P. Ferguson, U. Dahmen, and K.H. Westmacott, "A Precipitation Growth Study in Al-Cu," TMS/AIME Fall Meeting, St. Louis, October 24-28, 1982.
23. K.H. Westmacott, "Application of HVEM to Study of Precipitation Reactions," AIME Annual Meeting, Atlanta, February 1983.
24. U. Dahmen, "Invariant Line Strain and the Role of Shear in 2nd Phase Precipitation," invited seminar, Carnegie-Mellon Institute, Pittsburg, Pennsylvania, August 25, 1983.
25. K.H. Westmacott, "Phase Transformation Mechanisms," International Discussion Meeting, Sonnenberg, West Germany, September 18, 1983.
26. K.H. Westmacott, "Precipitation Reaction Studies by TEM," LBL-CAM Metallurgy Workshop, Berkeley, California, October 1983.
27. P. Ferguson, "Nitrogen Steels," invited talk, Northern California Society for Electron Microscopy, University of California at San Francisco, December 1983.

National Center for Electron Microscopy*

Gareth Thomas, Ronald Gronsky, and
Kenneth H. Westmacott, Investigators

INTRODUCTION

The National Center for Electron Microscopy (NCEM) aims to provide state-of-the-art facilities for electron-optical characterization of materials and to develop techniques of imaging, interpretation, and microanalysis.

The very high cost of modern instruments dictates time-sharing of equipment at centers where facilities, support, and staff are available. The Center, available to all qualified researchers, is built around two new microscopes, each housed in its own three-story silo. Installed in 1982, the high-voltage electron microscope (HVEM) accelerates electrons to energies of 1.5 million electron volts (MeV). It is the most powerful microscope of its kind in the United States. The atomic-resolution microscope (ARM), installed in 1983, operates in the 0.4–1.0 MeV range. It offers the highest resolution in the world, with 1.6-Å resolution already proved.

These two microscopes will enable materials scientists and biologists to study samples under the most realistic conditions possible and to distinguish individual atoms even in closely packed metallic and ceramic structures.

Support facilities at the center include 100- and 200-keV transmission electron microscopes, microanalytical instruments, equipment for preparing specimens, image analysis devices, and computer-simulation hardware and software.

The facility will be fully operational in 1984. The Seventh International Conference on High-voltage Electron Microscopy was held at Berkeley on August 16–19, 1983, with approximately 100 participants. See Reference 12 for a list of the participants.

The Center is guided by a Steering Committee, whose present non-LBL members are Drs. J. Hren (University of Florida), Chairman; W.L. Bell (General Electric Company); M. Gibson (Bell Laboratories); D. Howitt (University of California, Davis); M. Simnad (AMES, La Jolla); J.C.H. Spence

(Arizona State University); and A. Taylor (Argonne National Laboratory).

1. 1.5-MeV HIGH-VOLTAGE ELECTRON MICROSCOPE (HVEM)

K.H. Westmacott

Since the modifications to the accelerator-tube bleeder-resistor chain were completed, the HVEM has been performing extremely well. The high-voltage instability problem is completely resolved, and full working-day operation at 1500 kV is now routine.

Of the 67 research proposals received to date, about half are currently active. Research on the instrument covers a wide spectrum of projects, including phase-transformation studies in metals, ceramics, and minerals; semiconductor-device and amorphous-metal investigations; and biological- and medical-science applications.

Usage statistics for 1983 show an average weekly utilization of greater than 80 percent, excluding the three-week down time for the modifications. The ratio of materials-science to biological-science use is now about 6:1.

A list of the new proposals approved during 1983 is given in Table 1-1.

Several improvements in the capabilities for *in situ* studies are in progress. At present hot-stage work in the environmental cell is severely limited by the inability to attain high temperatures in the flowing gas because of heat-dissipation problems. Furnace-type hot stages reach only $\sim 800^\circ\text{C}$, while platinum-strip heaters are notoriously unreliable. An improved direct-heating grid design is being constructed to overcome some of these deficiencies. A second problem, heating the environmental-cell apertures by heat conduction through the gas, is being reduced by a modification that cools the cell walls directly.

In response to a developing demand, a Birmingham-type (after Birmingham University, England) ambient-temperature double-tilting straining stage has been ordered. This well-tested design uses a piezoelectric device or an optional manual drive to impart stress to the specimen. A further advantage is the minimal specimen movement ensured by driving both jaws of the straining stage. When this stage is on line, attempts will be made to add a heating capability to extend its utility to a wider variety of materials. The present video system

*This work was supported by the Director, Office of Energy Research, Office of Basic Energy Sciences, Materials Sciences Division of the U.S. Department of Energy under Contract No. DE-AC03-76SF00098.

Table 1-1
HVEM Research Proposals

Principal Investigator	Affiliation	Proposal Title
A. Evans (Crumley)	Materials Science and Mineral Engineering Department, UC Berkeley	Thin-foil studies of ceramics
R. Ayer	Exxon	Electron-microscopic analysis of formation of surface-oxide films during high-temperature oxidation
T. Cass	Hewlett-Packard	Defect structures in semiconductor devices
G. Brooks	Physical Education Department, UC Berkeley	Adaptations in skeletal-muscle mitochondrial morphology with endurance exercise
C.E. Warble	CSIRO, Australia	Pd/MgO reaction study
R. Gronsky (T. Sands)	LBL, MMRD	<i>In situ</i> study of the degradation of $\text{Cu}_{2-x}\text{S}/\text{Cds}$
R. Stoller	Chemical and Nuclear Engineering Department, UC Santa Barbara	Influence of preinjected helium on void swelling in a model austenitic alloy
E. Dratz	Natural Sciences Department, UC Santa Cruz	High-voltage TEM studies of ocular melanin in retinal-pigment epithelium
		Energy-dispersive spectroscopy of inclusion bodies in the thin sections of retinal-pigment epithelial cells
R. Spohr	GSI Darmstadt	HVEM studies of latent nuclear tracks
G. Reid	Hewlett-Packard	HVEM studies of stress-induced defect generation in CMOS-VLSI devices
J. Dash	Physics Department, Portland State University	Electrodeposition of chromium and copper in magnetic fields
		Phase transformations induced by high pressures and temperatures in a ballistic compressor
J. Clarke (Pelz)	Physics Department, UC Berkeley	Investigation of $1/f$ noise in metal films due to defects
J.W. Morris, Jr. (Katagiri)	Materials Science and Mineral Engineering Department, UC Berkeley	Fatigue-crack-propagation mechanisms of structural alloys at cryogenic temperatures
G. Thomas (Kwok)	Materials Science and Mineral Engineering Department, UC Berkeley	Micromechanisms of wear
M.A. Meyers	New Mexico Institute of Mining and Technology	Metallurgical study of dynamic fracture in metals
A. Evans (Inoue)	Materials Science and Mineral Engineering Department, UC Berkeley	Phase-transformation toughening in 3.2% MgO-ZrO_2
H.J. Ralston, III	UC San Francisco	Three-dimensional structure of thalamic neurons
A.K. Mukherjee	Mechanical Engineering Department, UC Davis	<i>In situ</i> HVEM studies on cavitation in 7475 aluminum alloys
G. Thomas (Wasynczuk)	Materials Science and Mineral Engineering Department, UC Berkeley	Characterization of precipitates within cementite
A. Searcy (Kim)	LBL, MMRD	<i>In situ</i> study of thermal decomposition of $\text{Mg}(\text{OH})_2$
G. Thomas (Krishnan)	Materials Science and Mineral Engineering Department, UC Berkeley	Atom location by channeling-inversion voltage phenomena
R. Wenk (McTigue)	Geology Department, UC Berkeley	Dislocation properties of silicate garnets

has allowed considerable experience to be gained, and the factors limiting the quality of video reproduction have been assessed. A new sophisticated system is now planned; it will be integrated into the entire Center computer network.

A modification to the camera vacuum system is also in progress. The modification will allow a significant reduction in the time needed to resume operation following a change of cassettes. When this improvement is implemented, two-shift operation of the HVEM will commence.

Typical examples of HVEM work in progress are listed below. These examples are taken from work in progress by UCB-LBL investigators. Abstracts of all proposed research projects are approved by the Steering Committee, and copies of the abstracts are on file.

The Transformation Aragonite \rightarrow Calcite and Calcite \rightarrow Lime Observed *In Situ* by HVEM

H.R. Wenk[†] and J.W. McTigue, Jr.[†]

The transformation between calcite and its related phases aragonite and lime is of interest to the geologist as well as the ceramicist. Aragonite is the high-temperature form of CaCO_3 , while calcite is its stable low-temperature form. It is known that the two crystal structures are derivatives of the fcc and hcp structures, respectively, and that the transition involves a 10% change in volume. However, the mechanism of transformation is unknown. This lack of information applies equally to the decomposition of calcite to lime. The loss of CO_2 in this reaction ($\text{CaCO}_3 \rightarrow \text{Ca} + \text{CO}_2$) causes a very large volume change, resulting in a highly porous reaction product.

Because of the sensitivity to radiation damage by 100-keV electrons, HVEM is necessary to study the details of the transformation mechanisms. The available heating stages of the HVEM also provide high stability and good control in the temperature range of transformations (400–500°C). The aragonite-to-calcite transition was found to occur

very rapidly, with a boundary sweeping across the foil, erasing twins and dislocation substructures in aragonite, a feature typical of massive transformations in metal alloys. Videotape recordings will allow a closer examination of this rapid transformation.

The transformation of calcite to lime proceeds more slowly, maintaining a topotaxial relationship of parallel close-packed planes in the two lattices. This relationship suggests a gradual loss of CO_2 from the Ca^{++} framework. The developing porosity begins as thin platelets with a tendency to align parallel to (0001) calcite planes.

[†]Present address: Geology Department, University of California Berkeley

HVEM *In Situ* Study of Precipitate Dissolution in a Pt-C Alloy (Publication 14)

D. Ackland, U. Dahmen, and K.H. Westmacott

Two metastable precipitates, α and α' , are known to form in rapidly quenched and aged dilute platinum-carbon alloys. Both are thin plates on {001} planes, and microdiffraction has revealed that the structure of α is a precursor to the body-centered tetragonal α' carbide. The kinetics of plate shrinkage were measured from sequences of micrographs recorded during *in situ* isothermal annealing, as shown in Figure 1-1. Both types of precipitate were found to exhibit linear-dissolution kinetics but in distinctly different temperature regimes. The α plates shrank at an average rate of 0.02 nm/sec at 450°C, while the measured rate for α' was 0.005 nm/sec at 515°C, indicating a much greater stability of α' . These results are in good agreement with *ex situ* and bulk-coarsening data that suggest the reaction is controlled by vacancy diffusion. Further measurements combined with careful calibration of the microscope's hot stage promise to yield results which may be used quantitatively to determine activation energies.

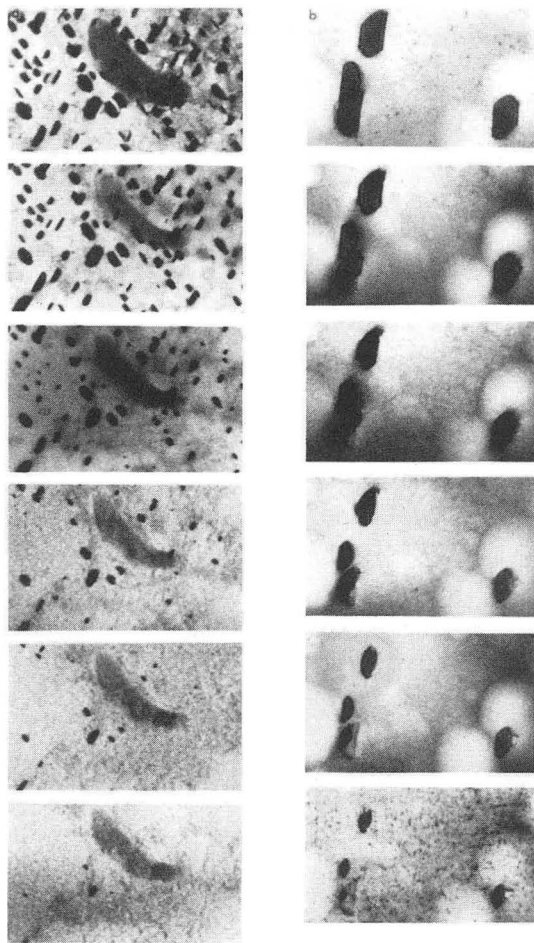


Figure 1-1. Sequences of micrographs showing precipitate shrinkage at linear rate during *in situ* isothermal annealing in the HVEM. Left: field of α precipitates shrinking at 0.02 nm/sec at 725 K; right: field of α' precipitates shrinking at 0.005 nm/sec at 788 K. (XBB 830-11124)

Structure of Electrodeposited Chromium (Publication 15)

R.M. Fisher[†] and K.H. Westmacott

Chromium coatings 5–100 μm thick are widely used to improve corrosion and wear resistance. Their brightness, hardness, and tendency to crack depend on plating conditions. The effect of plating conditions on the columnar-grain structure of electrodeposited chromium, the nature of the residual stresses, and the distribution of entrapped-plating solution (H_2CrO_4) have been studied using high-

voltage and scanning electron microscopy and electron- and ion-beam microanalytical techniques. Electrodeposited chromium is characterized by (1) the occurrence of large tensile stresses in the exposed-surface side that often result in extensive cracking and peeling from the substrate and (2) a substantial amount of entrapped plating solution.

High-voltage electron microscopy has revealed that the microstructure consists of highly elongated columnar grains. A representative 1000-kV transmission electron micrograph of a stripped and ion-thinned sample of hard, bright chromium plating is shown in Figure 1-2. The 0.1- μm -diameter grains (in cross section) exhibit a strong $\langle 111 \rangle$ fiber texture along their columnar axis and contain a dislocation density of about $2 \times 10^{11}/\text{cm}^2$. Heating electrodeposited chromium at 800–900°C results in recrystallization, 1 to 2% shrinkage of the film, relief of tensile stresses through the formation of numerous cracks, evolution of hydrogen, and formation of Cr_2O_3 particles. It appears that the void space in the unequilibrated intercolumnar-grain boundaries contains oxygen and hydrogen (possibly as adsorbed H_2O), resulting in a tendency for the film to shrink as the hydrogen is absorbed by the highly dislocated metal lattice.

[†]Industry Participation Officer, Center for Advanced Materials, Lawrence Berkeley Laboratory.

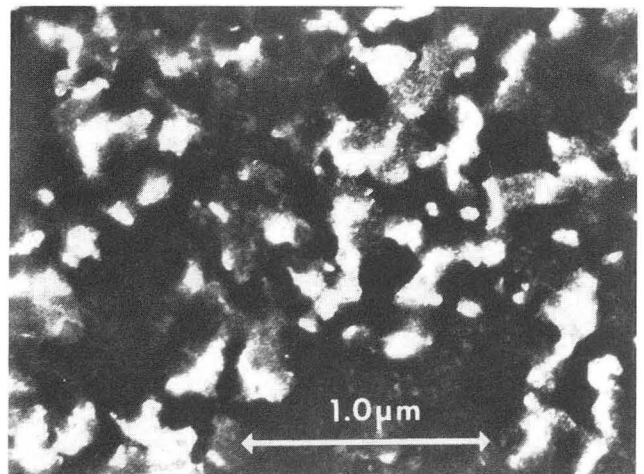


Figure 1-2. Dark-field TEM (1000 kV) showing cross section of columnar grids in hard, bright electrodeposited chromium. (XBB 830-11123)

In Situ Epitaxial Regrowth of Ion-implanted GaAs

T. Sands, D.K. Sadana,[†] J. Washburn, and R. Gronsky

Gallium arsenide is becoming an increasingly attractive semiconducting material for electron and optoelectronic-device applications. However, the science of GaAs processing lags far behind the science (and art) of silicon-device processing. In particular, doping by ion implantation is a much more complex process for GaAs than for Si. In this study high-voltage (HVEM) and high-resolution (HREM) electron microscopy are applied to the study of the annealing behavior of GaAs layers that have been amorphized by the implantation process. HREM images of cross-section specimens show that the as-implanted amorphous-crystalline transition region is finite in width and consists of small pockets of crystalline material in an amorphous matrix (see Figure 1-3). Furnace annealing at 400°C results in epitaxial

regrowth of this transition region. However, once the interface becomes simply connected, stacking-fault bundles are nucleated. Figure 1-4 shows the effect of *in situ* annealing (20 min, 400°C) in the HVEM on the sample imaged in Figure 1-3. Note that the epitaxial regrowth has terminated at the end of the transition region. Further *in situ* HVEM work will be directed toward determining the kinetics of this epitaxial-regrowth process.

[†]Present address: Microelectronics Center of North Carolina, Research Triangle Park, North Carolina 27709.



Figure 1-3. Cross-sectional HREM image ($\langle 110 \rangle$ orientation) of the amorphous-crystalline transition region in as-implanted GaAs (450-keV Se⁺ into (100) GaAs, $1 \times 10^{14}/\text{cm}^2$ dose, room temperature). (XBB 830-9399)

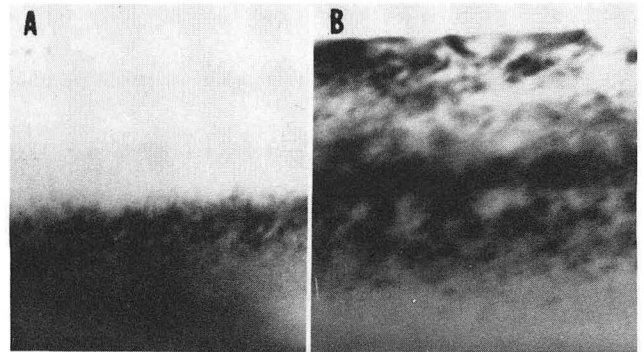


Figure 1-4. Sample of Figure 1-3 before (A) and after (B) *in situ* annealing in HVEM (20 min, 400°C). The buried amorphous layer in the as-implanted material is 190 nm wide. (XBB 830-11122)

A Generalization of Atom Location by Channeling-enhanced Microanalysis

K.M. Krishnan and G. Thomas

The technique of atom location by channeling-enhanced microanalysis (ALCHEMI) has limitations in practical application. A generalization of this technique has been developed with the underlying idea that additional relationships can be generated by performing these experiments at an appropriate number of orientations depending on the stoichiometry of the original compound. The precise number of orientations required to solve the distributions in a whole class of related compounds is expressed in terms of the stoichiometry of the original compound along with the alloying additions.

2. ATOMIC RESOLUTION MICROSCOPE

R. Gronsky

The atomic resolution microscope (ARM) was installed and the instrument formally accepted on July 25, 1983. Figure 2-1 shows the ARM. Nearly all performance specifications were exceeded by the ARM at its LBL site. Most notably, its imaging resolution was demonstrated to be 0.16 nm at 1-MeV accelerating potential (see Figure 2-2). This result clearly establishes the unique capabilities of this instrument for resolving individual atoms in densely packed engineering materials.

Careful attention has since been given to calibrating the microscope and establishing routine user operating conditions. Among these activities has been the simplification of astigmatism correction, enhancement of brightness, determination of proper

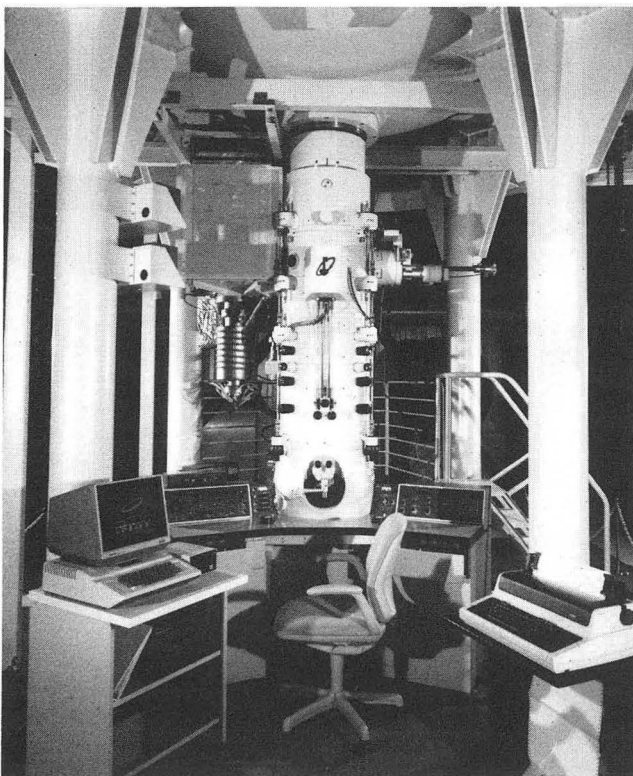


Figure 2-1. Console-level view of the ARM. The large ion-pump mount is visible on the upper left of the column; the diagonal tube attached to the left of the specimen chamber is the mass-spectrometer head. The specimen-exchange rod is attached horizontally to the right, and the manual controls for the goniometer descend in front of the column. The terminal at the lower right addresses all memory locations, digital console display, and text field on micrograph negatives. Console controls are efficiently interfaced to the CPU, thus reducing the total number of controls. (CBB 839-8469)

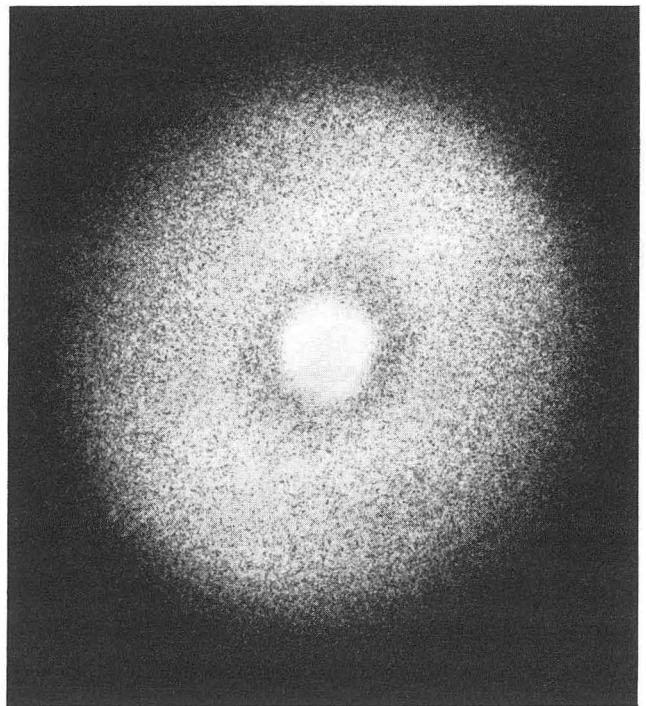


Figure 2-2. Optical diffractogram from a high-resolution image of amorphous Si at the Scherzer defocus, 1000 kV. The diffractogram halo is continuous to a resolution limit of 0.16 nm. (XBB 836-5044)

alignment procedures, and identification of lens settings for convergent-beam electron diffraction (see Figure 2-3).

The ARM opened to the user community in March 1984; the new support laboratory will be

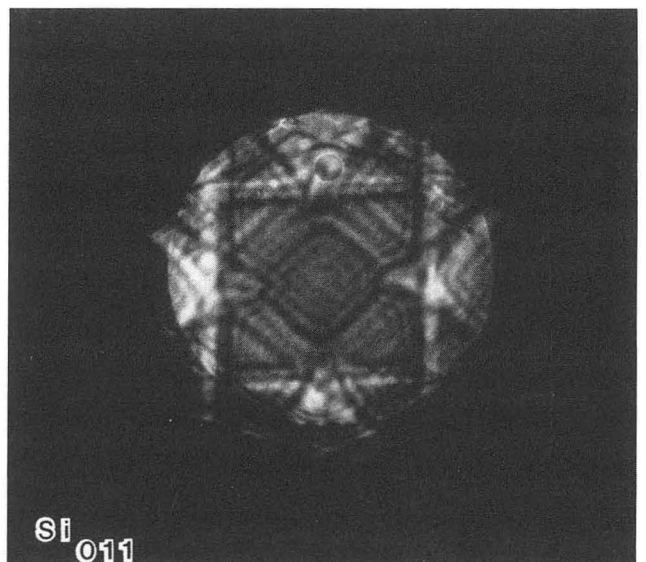


Figure 2-3. Convergent-beam electron-diffraction pattern from a Si specimen in the [011] orientation showing higher-order Laue-zone lines within the central disc. (XBB 836-5048)

available shortly. This addition to NCEM houses three support microscopes, specimen-preparation equipment, and image analysis hardware. Typical research projects on the ARM are listed below.

High-resolution Study of Plate Precipitates in a Mo-Hf-N Alloy

R. Gronsky, K.H. Westmacott, and U. Dahmen

Mo-Hf-N is a mixed-substitutional/interstitial alloy forming plate-shaped precipitates of HfN on {001} planes of the Mo matrix. HfN has the NaCl crystal structure and is related to the bcc-Mo matrix by the Bain correspondence, which for this particular combination of lattice parameters describes an invariant plane strain, a simple extension normal to the precipitate habit plane. Like other precipitates formed by an invariant plane-strain transformation, HfN has been reported to grow by a ledge mechanism. The large-volume change of about 40% that accompanies the transformation must be accommodated by lattice vacancies. If stacking violations of {001} planes are to be avoided, vacancies must condense in double layers. This places discrete limits on the optimal precipitate thicknesses and ledge heights. To test the model, high-resolution structure images of the HfN plates were obtained on the ARM operated at 1 MeV. Figure 2-4 shows an example of an image in the symmetrical Mo $\langle 100 \rangle$ orientation. The thick plate of fcc HfN is viewed precisely edge-on and is readily distinguished from the Mo matrix. Two features are clearly evident: (1) the precipitate-matrix interface is atomically smooth, and (2) the precipitate contains no faults in the stacking sequence. This evidence supports the proposed model, and the resulting plate is predicted to have an 8% interstitial strain field.

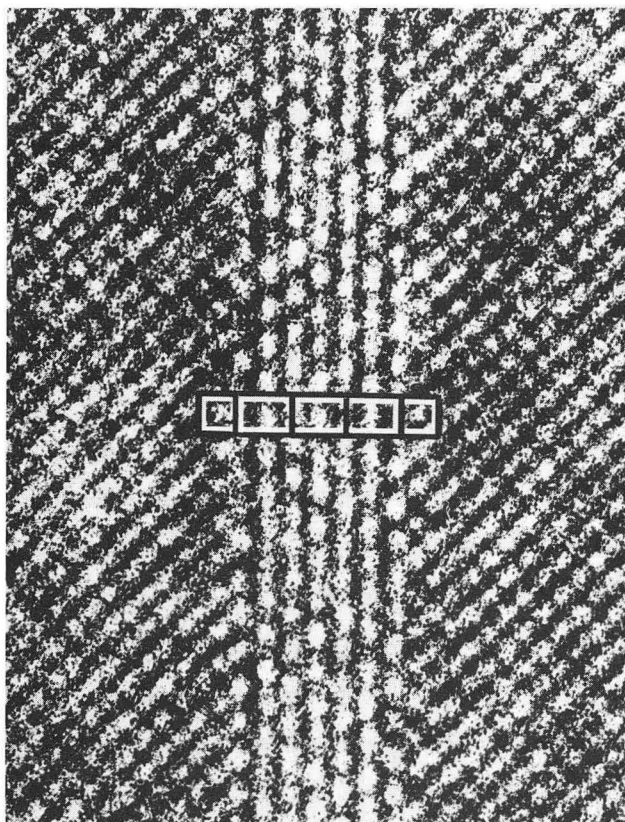


Figure 2-4. High-resolution image of HfN-precipitate plate in a molybdenum matrix. The precipitate is seen to be three unit-cells thick (see outlines), free of stacking faults, and bounded by an atomically smooth interface. (XBB 839-7867)

High-resolution-microscopy Investigation of the ZrO₂-ZrN System (Publications 5 and 6)

G. van Tendeloo[†] and G. Thomas

The ZrO₂-ZrN system has been investigated using different electron-microscopy techniques. From 2.5-mol% to 75-mol% ZrN, an incomen-

urate modulated structure is formed with a rhombohedral $R\bar{3}$ symmetry based on the $Zr_7O_{11}N_2$ structure, which is isostructural to $Zr_5Sc_2O_{13}$. The modulation is most probably due to pseudoperiodic composition fluctuations of nitrogen with respect to oxygen. The final structure can be described as a completely coherent mixture of pure Zr_7O_{14} layers alternating with $Zr_7O_{11}N_2$ layers perpendicular to the rhombohedral threefold axis. The incommensurability arises from local deviations in spacing and/or orientation of these layers. Monoclinic precipitates imbedded in this rhombohedral matrix are characterized with the help of high-resolution electron microscopy combined with optical microdiffraction. Configurations that minimize the strain energy are common (see Figure 2-5).

†Permanent address: RUCA, University of Antwerp, Groenenborgerlaan 171, B-2020 Antwerp, Belgium.

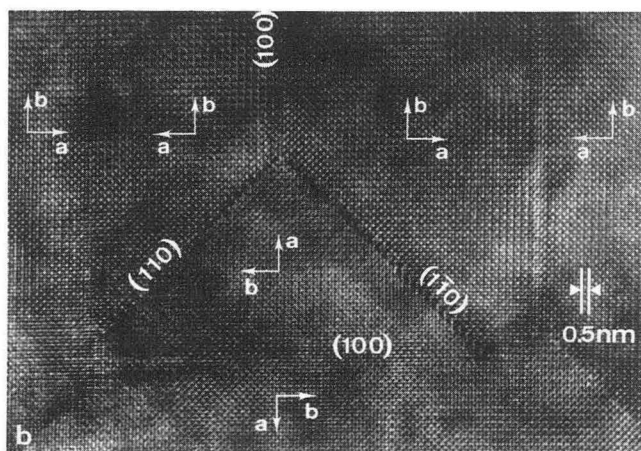
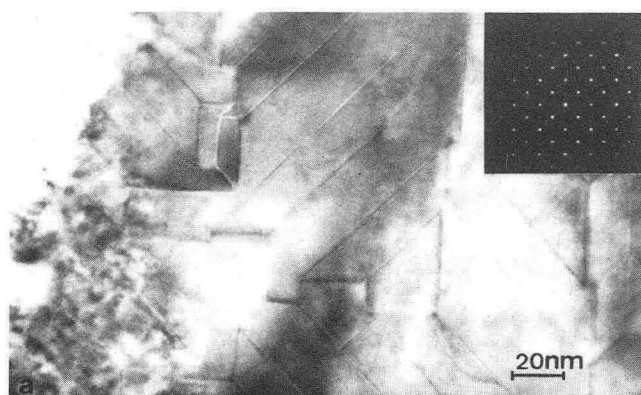


Figure 2-5. High-resolution observation (b) of heavily twinned monoclinic ZrO_2 . All variants have a common c-axis parallel to the electron beam. The orientation of the axes as determined from HREM and optical diffraction is indicated. Part (a) shows a low-resolution view of the same area, with an inset selected-area-diffraction pattern. (XBB 838-7156)

1983 PUBLICATIONS AND REPORTS

Refereed Journals

1. R.G. Regnier, N.Q. Lam, and K.H. Westmacott, "Microstructural Transitions in Pt-C Alloys during High-voltage Electron Microscope Irradiation," *J. Nucl. Mat* **115**, 286 (1983).
2. R. Kilaas and R. Gronsky, "Real Space Image Simulation in High Resolution Electron Microscopy," *Ultramicroscopy* **11**, 289 (1983).
3. G. van Tendeloo, K.T. Faber, and G. Thomas, "Characterization of AlN Ceramics Containing Long Period Polytypes," *J. Mat. Sci.* **18**, 525 (1983); LBL-14566.†
4. M. Sarikaya, J.W. Steeds, and G. Thomas, "Lattice Parameter Measurements in Retained Austenite by CBED," *Proc. EMSA*, G.W. Bailey, Ed., San Francisco Press, Inc, 1983, p. 206; LBL-15834.
5. G. van Tendeloo and G. Thomas, "Electron Microscopy Investigations of the ZrO_2 -ZrN System. I. Formation of an Incommensurate Superstructure Zr-O-N," *Acta Met.* **31**, 1611-1618 (1983); LBL-16041.‡
6. G. van Tendeloo, L. Anders, and G. Thomas, "Electron Microscopy Investigation of the ZrO_2 -ZrN System. II. Tetragonal and Monoclinic ZrO_2 Precipitation," *Acta Met.* **31**, 1619-1625 (1983); LBL-17236.
7. R. Gronsky and G. Thomas, "Instrumentation at the NCEM: The Atomic Resolution Microscope," *Proc. EMSA*, G.W. Bailey, Ed., San Francisco Press, Inc., 1983, p. 310.

LBL Reports

8. K. Krishnan, P. Rez, R.K. Mishra, and G. Thomas, "Determination of the Specific Site Occupation of Rare Earth Additions in $Y_{1.7}Sm_{0.6}Lu_{0.7}Fe_5O_{12}$ Thin Films by the Orientation Dependence of Characteristic X-ray Emissions," Materials Research Society Meeting, Boston Massachusetts, November 13-17, 1983, LBL-16884.
9. K. Krishnan, L. Rabenberg, R.K. Mishra, and G. Thomas, "Site Occupation of Ternary Elements in $Sm_2(CoTM)_{17}$ Compounds," *J. Appl. Phys.*, in press, LBL-16874.
10. G. van Tendeloo and G. Thomas, "High Resolution Microscopy Investigation of the ZrO_2 -ZrN System," *J. Am. Ceram. Soc. Proc. Inst. Conf. ZrO_2 -1983*, Stuttgart, in press, LBL-16240.

11. K. Krishnan, P. Rez, and G. Thomas, "Effect of Voltage on the Orientation Dependence of Electron Induced Characteristic X-ray Emissions," *Proc. 7th Int. Conf. HVEM*, Berkeley, California, 1983, p. 365, LBL-16144.
12. *Proceedings of the 7th International Conference on HVEM, Berkeley, California, August 16-19, 1983*, R.M. Fisher, R. Gronsky, and K.H. Westmacott, eds., LBL-16031.
13. U. Dahmen, P. Ferguson, and K.H. Westmacott, "HVEM Studies of Precipitate Morphology Symmetries," *Proc. 7th Int. Conf. HVEM, Berkeley, California*, R.M. Fisher, R. Gronsky, and K.H. Westmacott, eds., 1983, p. 315, LBL-16031.
14. D. Ackland, U. Dahmen, and K.H. Westmacott, "HVEM *In Situ* Studies of Precipitate Coarsening and Dissolution in a PtC Alloy," *Proc. 7th Int. Conf. HVEM, Berkeley, California*, R.M. Fisher, R. Gronsky, and K.H. Westmacott, eds., 1983, p. 319; LBL-16031.
15. R.M. Fisher and K.H. Westmacott, "Structure of Electrodeposited Chromium," *Proc. 7th Int. Conf. HVEM, Berkeley, California*, R.M. Fisher, R. Gronsky, and K.H. Westmacott, eds., 1983, p. 323; LBL-16031.
16. P. Ferguson, U. Dahmen, and K.H. Westmacott, "*In Situ* Study of γ' Precipitation in Fe-N," *Proc. 7th Int. Conf. HVEM, Berkeley, California*, R.M. Fisher, R. Gronsky, and K.H. Westmacott, eds., 1983, p. 227; LBL-16031.
17. R. Gronsky, "Electron Microscopy at Atomic Resolution," *Proc. Materials Research Soc. Symposium on Electron Microscopy of Materials*, W. Krakow, Ed., North Holland (in press), LBL-16937.

Other Publications

18. R. Gronsky, "High-resolution Transmission Electron Microscopy," *Treatise on Materials Science and Technology*, Vol. 19, part B, H. Herman, Ed., Academic Press, New York, 1983, p. 225; LBL-11243.
19. U. Dahmen and K.H. Westmacott, "A TEM Analysis of Repeated Precipitation on Climbing Dislocations in Al-4Cu," 11th Western Regional Meeting of Electron Microscopists, Pacific Grove, California, 1983, LBL-16382.
20. P. Ferguson, U. Dahmen, and K.H. Westmacott, "Morphological Aspects of α'' -Fe₁₆N₂ Precipitation in α -Iron," 11th Western Regional Meeting of Electron Microscopists, Pacific Grove, California, 1983, LBL-16661.

Invited Talks

21. K.H. Westmacott and R. Gronsky, "National Center for Electron Microscopy," TMS/AIME Meeting, St. Louis, Missouri, October 1982.
22. R. Gronsky, "Developments in Electron Microscopy," Forum of the Solid State Sciences Committee, National Academy of Sciences, Washington, D.C., February 8-9, 1983.
23. K.H. Westmacott, "Applications of HVEM in the Study of Precipitation Reactions," AIME Meeting, Atlanta, Georgia, February 1983.
24. R. Gronsky and G. Thomas, "Atomic Resolution Microscopy of Materials," TMS/AIME and ASM/MD Joint Symposium on Metals Research at User-oriented National Facilities, TMS/AIME Meeting, Atlanta Georgia, March 6-10, 1983.
25. R. Gronsky, "Electron Microscopy: The State of the Art," Industrial Liaison Program, Fifth Annual Conference, University of California Berkeley, March 9-10, 1983.
26. R. Gronsky, "National Center for Electron Microscopy," Invited Poster Session on National Facilities of Importance to Condensed Matter Physics, American Physical Society Annual Meeting, Los Angeles, California, March 22, 1983.
27. G. Thomas, "The National Center for Electron Microscopy, Berkeley," Special Meeting of the Indian Institute of Science and Technology, Delhi, India, April 25, 1983.
28. G. Thomas, "HVEM and its Applications in Materials Science," Bombay Atomic Energy Research Center, Bombay, India, April 27, 1983.
29. R. Gronsky, "Imaging Atomic Structure in the TEM," Department of Chemical and Nuclear Engineering Special Symposium, University of California, Santa Barbara, California, May 2, 1983.
30. G. Thomas, "The NCEM Berkeley—Fulfillment of a Nine-year Project," Keynote Speaker, Biennial Conference of Northern and Southern California E.M. Societies, Asilomar, California, May 11, 1983.
31. G. Thomas, "Characterization of Ceramics," J.S.P.S. Subcommittee, Tokyo, Japan, May 19, 1983.
32. U. Dahmen, "Applications of HV and HR Electron Microscopy," Metals and Welding Conference, San Francisco, California, May 1983.
33. R. Gronsky, "Instrumentation and Interpreta-

- tion in Atomic Resolution Microscopy," EUCHEM Conference on High Resolution Electron Microscopy in Solid State Chemistry, Royal Swedish Academy of Sciences, Stockholm, Sweden, June 12–16, 1983.
34. G. Thomas, "National Center for Electron Microscopy," Electron Microscopy of Ceramics, Toulouse, France, July 1983.
 35. G. Thomas, "Instrumentation at the NCEM: ARM," EMSA Conference, Phoenix, Arizona, August 6–12, 1983.
 36. R. Gronsky, "Atomic Resolution Microscopy," Materials Science Seminar, Department of Materials Science and Mineral Engineering, University of California Berkeley, November 1, 1983.
 37. G. Thomas, "The NCEM and the Approach to Atomic Resolution of Solids," Plenary Lecture, Diamond Jubilee Celebrations, Varanasi, India, November 1983.
 38. G. Thomas, "The National Center for Electron Microscopy—Development of Materials Research," Plenary Lecture, New England Society for Electron Microscopy, December 7, 1983.

[†]Supported by the National Science Foundation.

^{*}Supported partially by the National Science Foundation.

In Situ Investigations of Gas-Solid Reactions by Electron Microscopy*

James W. Evans, Investigator

INTRODUCTION

This investigation is concerned with the relationship between the microstructure of a solid and the kinetics of its reaction with a gas. Examples of such reactions abound in materials and energy technology; three examples are the production of metals by reduction of oxides, the oxidation of metals in gas turbines, and the reduction of oxide refractories in coal conversion reactors.

The research is facilities oriented in that it uses "environmental cells" in the LBL high-voltage transmission electron microscopes to actually observe the reaction between a gas and a solid at elevated temperatures. Such cells are now the principal experimental tool in this investigation, although hitherto much use has been made of an *ex situ* technique whereby the solid is examined after reaction outside the microscope.

1. The Diffusion of Gases in Porous Solids: Monte Carlo Simulations in the Knudsen and Ordinary Diffusion Regimes (Publication 1)[†]

M.H. Abbasi, J.W. Evans, and I.S. Abramson[‡]

Porous solids have been simulated in the computer as assemblages of spheres. When such assemblages contain spheres distributed in size and randomly arranged in space, the structure of the resulting solid resembles that of a real porous solid. Monte Carlo calculations of gas-molecule trajectories through the assemblages were carried out for both the Knudsen and ordinary diffusion regimes. Tortuosities calculated from the simulated diffusion "data" fell within the range obtained experimentally by other investigators. Correlations were obtained that enable the prediction of diffusion rates from

measurement of the porosity, mean pore size, and standard deviation of the pore size.

[†]Supported by DOE-Pittsburgh Energy Technology Center (PETC).

[‡]Present address: Department of Mathematics, University of California San Diego, La Jolla, California.

2. The Hall-Heroult Cell: Some Design Alternatives Examined by a Mathematical Model (Publications 2 and 9)[†]

S.D. Lympany[‡] and *J.W. Evans*

A previously developed mathematical model is used to study the effect of various design or operating changes on the performance of the Hall-Heroult cell. Performance is judged from the flatness of the interface between the aluminum and molten-salt electrolyte and from the current efficiency. The former is found to be particularly sensitive to horizontal currents in the aluminum, and a novel cell design is suggested wherein the minimization of such currents leads to a nearly flat interface. Current efficiency is found to be relatively insensitive to the horizontal currents but to depend on riser design. Computations are carried out for end cells in potlines, for potlines of different spacings, and for cells containing different levels of aluminum.

[†]Supported by DOE-Conservation.

[‡]Present address: Dames & Moore, Golden, Colorado.

3. An Improved Mathematical Model for Melt Flow in Induction Furnaces and Comparison with Experimental Data (Publication 3)

J.W. Evans and S.D. Lympany

A mathematical model (previously developed by Tarapore and Evans¹) for the turbulent, electromagnetically driven flow in an induction furnace was modified. Modifications included a more precise numerical calculation of the electromagnetic-force field and the use of the TEACH computer program for solution of the time-averaged Navier-Stokes equations. The results of the computations were compared with velocity measurements on inductively stirred mercury melts recently published by Moore and Hunt.² The improved model was able to

*This work was supported by the Director, Office of Energy Research, Office of Basic Energy Sciences, Materials Sciences Division of the U.S. Department of Energy under Contract No. DE-AC03-76SF00098.

match the experimental velocity field with a precision better than previously achieved in such modeling.

1. E.D. Tarapore and J.W. Evans, *Met. Trans.* **7B**, 343–351 (1976).

2. D.J. Moore and J.C.R. Hunt, *Proc. 3rd Beer-Sheva Symp. on MHD Flows and Turbulence*, Beer-Sheva, Israel, 1981.

4. An Electron-microscopy Study of the Low-temperature Catalyzed Steam Gasification of Graphite (Publication 4)

*D.J. Coates,[†] J.W. Evans, A.L. Cabrera,[‡]
G.A. Somorjai, and H. Heinemann*

Controlled-atmosphere electron microscopy was used to directly observe the catalyzed low-temperature gasification of graphite. Potassium hydroxide was used as the catalyst in the reaction between steam and graphite. Catalytic channeling of the graphite was observed in the temperature range of 500–600°C, lower temperatures than previously reported for this mechanism using other catalysts. Kinetic studies of the potassium-hydroxide-catalyzed steam-graphite reaction give a constant activation energy of 11 ± 1 kcal/mole at temperatures of 200–600°C, suggesting that one reaction mechanism holds good throughout this range of temperatures.

[†]Present address: METTEK, Santa Ana, California.

[‡]Present address: Air Products & Chemicals, Corporate Science Center, Allentown, Pennsylvania.

5. Magnetohydrodynamic Effects in Aluminum Reduction Cells (Publication 10)[†]

S.D. Lympny, J.W. Evans, and R. Moreau[‡]

Electromagnetic forces have an effect on the electrolytic cells used to produce aluminum. They cause circulation of the molten-salt electrolyte and molten aluminum contained within the cell and impair the current efficiency of the cell. In addition, they deform the interface between the two liquids, thus impeding efforts to reduce electrical energy consumption by the cell. This paper presents two studies aimed at better understanding such magnetohydrodynamic effects. The first has entailed the development of a computer-based mathematical

model which attempts to predict cell performance as a function of design and operating parameters. The second is an analytical approach which, though not incorporating the details of the computer calculations, provides insight into the basic fluid mechanics of the cryolite.

[†]Supported by DOE-Conservation.

[‡]Present address: MADYLAM, Institute National Polytechnique de Grenoble, Saint Martin d'Herès Cedex, France.

6. The Relationship Between Pore Classes in a Solid Computed by a Monte Carlo Technique (Publication 5)[†]

Y. Nakano[‡] and J.W. Evans

Porous solids were simulated in the computer as assemblages of spheres. Simple solids had regular arrays of spheres of uniform size, and more realistic solids were generated wherein both the position and size of the spheres were randomly distributed. Manipulation of the solid (e.g., by removing or by “growing” spheres) enabled an examination of the relationship between pore classes (open pores, closed-end pores, and isolated pores) as a function of total porosity.

[†]Supported by DOE-PETC.

[‡]Present address: Department of Chemical Engineering, Shizuoka University, Hamamatsu 432, Japan.

7. Monte Carlo Simulation of Diffusion of Gases in a Porous Solid: Calculations for a New Class of Solids (Publication 6)[†]

Y. Nakano and J.W. Evans

In a previous paper a Monte Carlo simulation of the Knudsen diffusion of a gas in a porous solid was carried out. The simulated porous solid had pore walls that were convex. In the present paper, the simulation is repeated using simulated solids whose pore walls are concave. It was found that the results of both studies could be correlated by a single equation. This equation enables the prediction of the Knudsen diffusiveness from the porosity and mean pore size without resort to a tortuosity factor.

[†]Supported by DOE-PETC.

8. Fluidized-bed Electrowinning of Metals—A Review (Publication 11)[†]

M. Dubrovsky,[‡] T. Huh, J.W. Evans, and C. Carey[§]

It is now well over a decade since the invention of the fluidized-bed electrode. Despite early enthusiasm and many investigations, published and unpublished, the electrode has yet to be commercially exploited for the electrowinning of metals. It is believed that this is due to the severe operational difficulties and excessive electrical energy consumption encountered by early workers, as well as to the radical nature of the technology and the unusual form of the product. This paper reviews the short history of this device, examines the question of how a fluidized bed can function electrochemically, discusses the factors which govern the performance and scale-up of the electrode, and describes recent improvements in performance that suggest the electrode is at last ripe for commercial development. Emphasis is on research carried out at Berkeley, and the paper includes hitherto unpublished results on the fluidized-bed electrowinning of silver and zinc.

[†]Review of work supported by various government agencies.

[‡]Present address: Chevron Research Laboratory, Richmond, California 94804.

[§]Present address: Homestake Mining Company, Golden, Colorado.

9. The Fluidized-bed Electrowinning of Silver (Publication 7)[†]

T. Huh, J.W. Evans, and C. Carey

Fluidized-bed electrowinning appears to be an alternative to the Zadra cell usually employed to deposit silver electrolytically from cyanide solutions. By using a bench-scale cell it was found that, when using either pure silver or silver-coated copper particles, such electrowinning could be carried out without operating problems and with reasonable current efficiency and cell voltage. Various anodes were examined for use in the cell, and three were found to be satisfactory. By electrolyte analysis and EDAX analysis of the silver deposit, the silver was shown to be free of impurities down to the detection level of the analyses.

[†]Supported by the Homestake Mining Corporation.

10. *In Situ* Observations of the Gasification of Carbon Catalyzed by Calcium Oxide (Publication 8)

D.J. Coates, J.W. Evans, and H. Heinemann

An environmental cell in a transmission electron microscope has been used to examine the gasification of graphite in the presence of calcium oxide formed by hydrolysis and thermal decomposition of calcium nitrate dispersed on the sample. No reaction was observed on exposure to water vapor at 500°C. However, after 90 min of such exposure the environment was changed to a hydrogen-nitrogen mixture, and the catalyzed reaction then proceeded according to a “channeling” mode (see Figure 10-1).

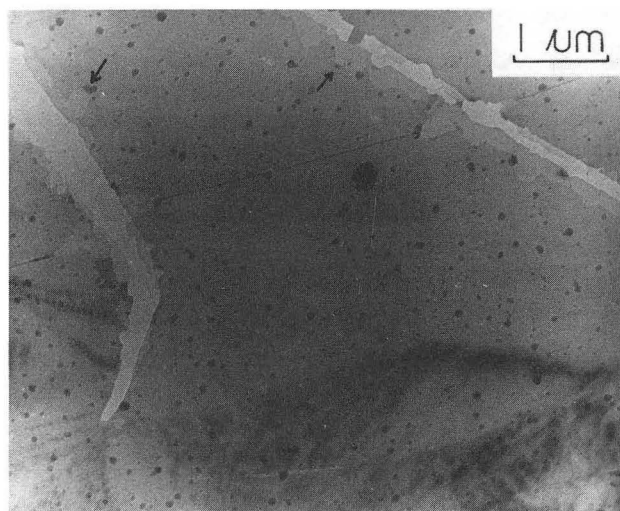


Figure 10-1. Both steps and channels are shown where the gasification rate is increased. (XBB 827-6462)

11. Removal of Nonmetallic Inclusions from Steel Melts (Publication 12)[†]

B.M. Tracy[‡] and J.W. Evans

The difficulties in mathematically predicting the coalescence and removal of inclusions from steel melts are discussed. Results of an experimental investigation in which 6-kg steel melts were deoxidized with silicon are presented. It is shown that such experiments do not yield results that can be scaled up to industrial-scale metals.

[†]Supported by the American Iron and Steel Institute.

[‡]Present address: Materials Engineering Department, Rensselaer Polytechnic Institute, Troy, New York.

12. Work in Progress

The environmental cell presently has a maximum temperature of 600°C in 50 torr of gas. The power supply, cell, and sample holder are being redesigned to operate at temperatures above 1000°C. The higher temperatures will be used to study the effect of the location of iron oxide in a commercial refractory (whether present as large grains or as very small inclusions) on its resistance to hydrogen reduction, along with other aspects of corrosion.

Magnetite single crystals were reduced to Wustite (see Figure 12-1) by 50 torr of the gas mixture 10% H₂/90% Ar at 500°C. The propagation of pores was quicker in one crystallographic direction than in others. The pores also propagated preferentially along dislocations. These pores nucleated at cracks and ran laterally along the surface as channels.

A feasibility study for carrying out *in situ* oxidation of GaAs is in progress.

1983 PUBLICATIONS AND REPORTS

Refereed Journals

1. M.H. Abbasi, J.W. Evans, and I.S. Abramson, "The Diffusion of Gases in Porous Solids: Monte Carlo Simulations in the Knudsen and Ordinary Diffusion Regimes," *AIChE Journal* **29**, 617-624 (1983).[†]
2. S.D. Lympny and J.W. Evans, "The Hall-Heroult Cell: Some Design Alternatives Examined by a Mathematical Model," *Met. Trans.* **14B**, 63-70 (1983); LBL-14386.[‡]
3. J.W. Evans and S.D. Lympny, "An Improved Mathematical Model for Melt Flow in Induction Furnaces and Comparison with Experimental Data," *Met. Trans.* **14B**, 306-308 (1983); LBL-15170.
4. D.J. Coates, J.W. Evans, A.L. Cabrera, G.A. Somorjai, and H. Heinemann, "An Electron

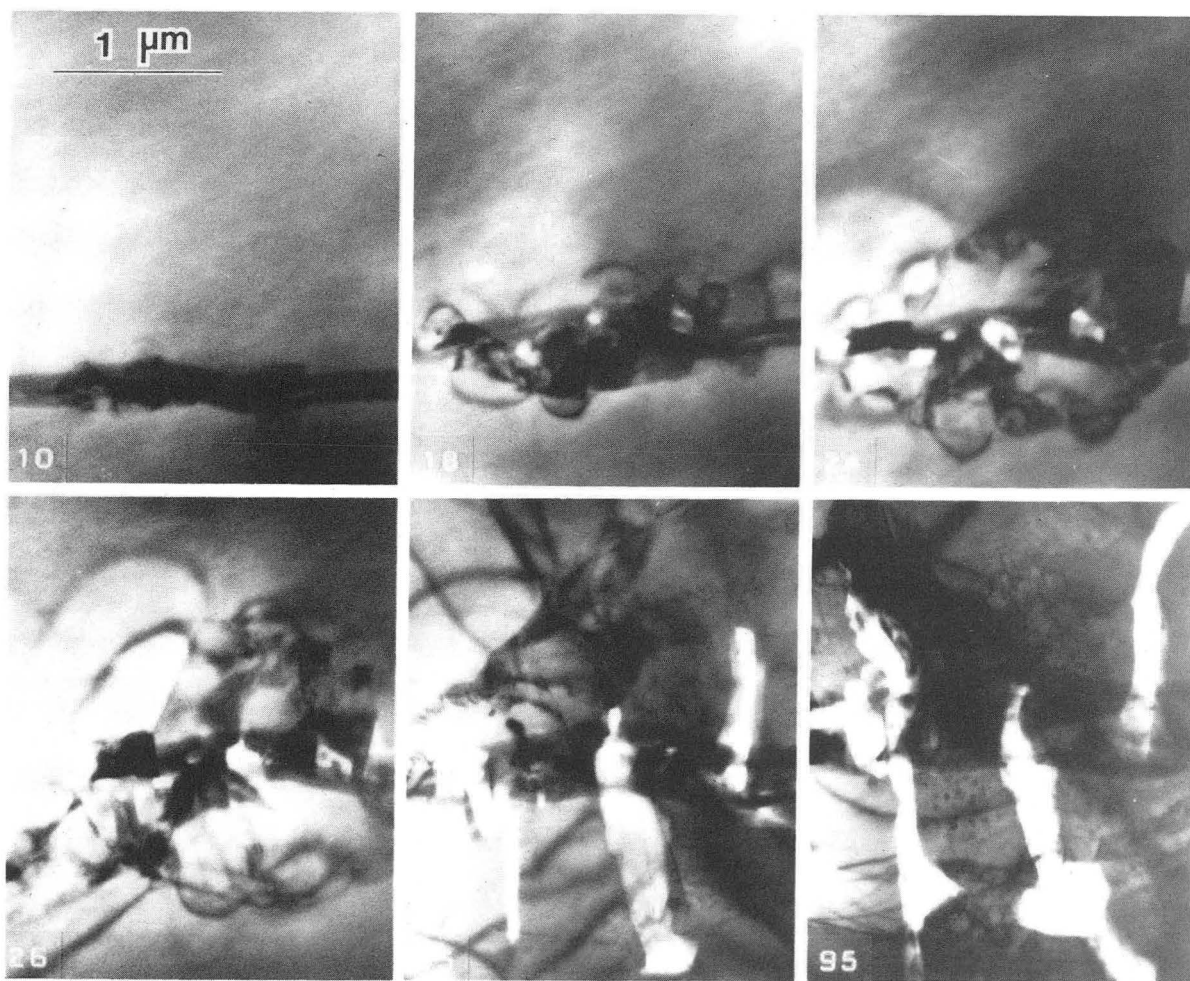


Figure 12-1. Formation of pores as a function of time during reduction of Fe₃O₄ at 514°C. The inset numbers give the time in minutes. (XBB 8311-10290)

Microscopy Study of the Low Temperature Catalysed Steam Gasification of Graphite," *J. Catalysis* **180**, 215-220 (1983); LBL-14463.

5. Y. Nakano and J.W. Evans, "The Relationship Between Pore Classes in a Solid Computed by a Monte Carlo Technique," *Powder Technology* **35**, 115-118 (1983).[†]
6. Y. Nakano and J.W. Evans, "Monte Carlo Simulation of Diffusion of Gases in a Porous Solid: Calculations for a New Class of Solids," *J. Chem. Phys.* **78**, 2568-2572 (1983).[†]
7. T. Huh, J.W. Evans, and C. Carey, "The Fluidized Bed Electrowinning of Silver," *Met. Trans.* **14B**, 353-357, September 1983.[§]
8. D.J. Coates, J.W. Evans, and H. Heinemann, "In Situ Observations of the Gasification of Carbon Catalyzed by Calcium Oxide," *Applied Catalysis* **7**, 233-241, May 1983; LBL-15521.

Other Publications

9. S.D. Lympany and J.W. Evans, "The Hall Cell: Some Design Alternatives Evaluated by a Mathematical Model," in *Light Metals 1983*, The Metals Society AIME, Pittsburgh, 1983; LBL-17344.
10. S.D. Lympany, J.W. Evans, and R. Moreau, "Magnetohydrodynamic Effects in Aluminum Reduction Cells," *Proc. IUTAM Symp. "Metallurgical Applications of Magnetohydrodynamics"*, Cambridge, England, The Metals Society, London, 1983.[‡]

11. M. Dubrovsky, T. Huh, J.W. Evans, and C. Carey, "Fluidized Bed Electrowinning of Metals — A Review," *Proc. 3rd Int. Symp. on Hydrometallurgy*, Atlanta, March 1983.^{||}
12. B.M. Tracy and J.W. Evans, "Removal of Non-metallic Inclusions from Steel Melts," *Proc. SCANINJECT III*, 3rd International Conference on Refining of Iron and Steel by Power Injection, Lulea, Sweden, June 1983.**

Invited Talks

13. J.W. Evans, "Simulation of Diffusion in Porous Solids," U.S.-Japanese seminar on Advances in the Science of Iron- and Steelmaking, Kyoto, Japan, May 1983.
14. J.W. Evans, "Research in Process Metallurgy at Berkeley," Nippon Steel Corporation, Fundamental Research Laboratories, Kawasaki, Japan, May 1983.
15. J.W. Evans, "Research on Iron- and Steelmaking at Berkeley," Kawasaki Steel Corporation, Research Laboratories, Chiba, Japan, May 1983.

[†]Supported by DOE-PETC.

[‡]Supported by DOE-Conservation.

[§]Supported by Homestake Mining Company.

^{||}Review of work supported by various government agencies.

**Supported by the American Iron and Steel Institute.

Local Atomic Configurations in Solid Solutions*

Didier de Fontaine, Investigator

INTRODUCTION

This research is aimed at understanding basic atomic mechanisms that lead to observed microstructures of certain metallic alloys. In particular, work since October 1981 has been focused on two topics: (1) a theoretical study of very regular long-period superstructures observed in some ordered alloys, and (2) a theoretical study of the kinetics of phase transformations responsible for the change of shape from a C-curve to an S-curve in transformation-temperature-time (TTT) diagrams of eutectoid carbon steels upon alloying with ternary substitutional elements. Both of these theoretical studies are being followed by experimental investigations aimed at confirming the models and at suggesting new directions for further basic research and possible applications. Thin foils of Ag_3Mg are being prepared for very high-resolution electron microscopy in order to identify the polytypes (long-period superstructures) observed. Cr and Ni eutectoid alloy steels of various compositions have been prepared, their experimental TTT curves have been determined and compared to theoretical ones, and the degree of partitioning of the substitutional alloy element, measured by analytical transmission electron microscopy, was shown to compare favorably with theoretical predictions. A new study has been initiated, short-range ordering in Au-Fe conducted by electron diffraction and microscopy. The objective is to determine the influence of atomic ordering on the anomalous magnetic behavior in these alloys, a study conducted jointly with Dr. W.M. Stobbs of Cambridge University, Dr. G. Van Tendeloo of the University of Antwerp, and Drs. C. Violet and R. J. Borg of the Lawrence Livermore National Laboratory.

1. Models of Long-period Superstructures (Publication 5)

J. Kulik and D. de Fontaine

The cause of the stability of long-period superstructures is still something of a mystery. Typically, two very different models have been proposed. According to model I, the period of the superstructure (or modulation) is determined by lowering the electronic energy resulting from the formation of a new Brillouin zone. According to model II, competing short-range interactions tend to produce long-period structures, the wavelength of which is determined by configurational entropy considerations. Model I is exemplified by the Sato and Toth theory, apparently applicable to long-period superstructures in Cu-Au, for example. Model II is exemplified by the axial next-nearest neighbor Ising model, for which a low-temperature free-energy expansion has recently been given by Fisher and Selke. The latter model appears to apply to long-period superstructures in Ag_3Mg .

2. Relevance of the ANNNI Model to Binary Alloys (Publication 1)

J. Kulik and D. de Fontaine

The results of a recent low-temperature analysis by Fisher and Selke (FS) of the axial next-nearest neighbor Ising (ANNNI) model appear to have some relevance to long-period superstructures in certain binary alloys, in particular Ag_3Mg and Au_3Zn . The analysis indicates that configurational entropy may be more important in such structures than had been previously thought. We have recalculated the FS results for the anti-ferromagnetic case, which is analogous to the ordered alloy case. It was found that the long-period phases predicted by the low-temperature expansion of the exact free energy had structural formulae $\langle 2^{j+1} \rangle$, replacing the formulae $\langle 2^j \rangle$ of the FS calculations.

*This work was supported by the Director, Office of Energy Research, Office of Basic Energy Sciences, Materials Sciences Division of the U.S. Department of Energy under Contract No. DE-AC03-76SF00098.

3. Synthesis of S-shaped Temperature-time Transformation Diagrams (Publication 2)

O. Dairiki and D. de Fontaine

A mathematical model has been derived for calculating TTT curves of ternary alloy steels FeCM (where M is a substitutional metallic element) based on the knowledge of the corresponding curves for the binary FeC eutectoid steel. The model uses classical nucleation-and-growth theory but allows for variable partitioning of element M between ferrite and carbide phases. The degree of partitioning, determined by maximizing nucleation and growth rates, is found to depend on the temperature and on the nature of the third element. Good agreement was found for calculated and experimentally determined TTT curves of Cr and Ni eutectoid steels.

4. Isothermal Transformation of Ternary Eutectoid Steels with Cr, Ni, and Mn Additions (Publication 3)

E. Colas and D. de Fontaine

TTT diagrams were determined experimentally for eutectoid steels with various amounts of Cr, Ni, and Mn additions. TTT curves of 1.4% Cr, 0.67% C steels compared very well with those determined previously by Chance and Ridley and with those determined theoretically by Dairiki and de Fontaine (see Figure 4-1). Agreement was not as good for the 1.6%

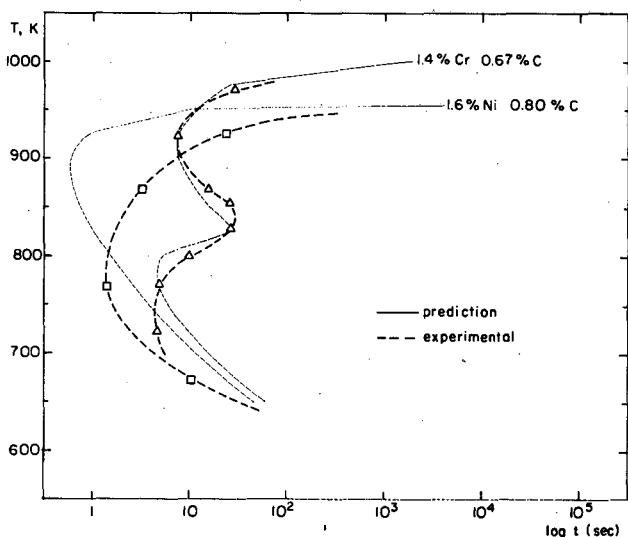


Figure 4-1. Comparison of start times as a function of temperature between theoretical curves and experimental data for indicated compositions. (XBL 839-6331)

Ni, 0.80% C steels, but both experimental and theoretical TTT start curves correctly showed the absence of a "bay," a feature characteristic of the Cr steels. Preliminary analytic transmission electron microscopic determination of local Cr concentration indicated the expected partitioning of Cr among decomposition products.

5. A Comparison of the Short-range Order Exhibited by Different $\langle 1\frac{1}{2} 0 \rangle$ Alloys (Publication 4)

G. Van Tendeloo, S. Amelinckx, W.M. Stobbs, and D. de Fontaine

High-resolution electron microscopic images of the $\langle 1\frac{1}{2} 0 \rangle$ special-point short-range ordering alloys Ni_4Mo , Au_4V , Au_4Cr , and Au_4Fe are compared, and the extent to which optical diffractograms from local regions of such micrographs can be interpreted is discussed. For Au_4Cr and Ni_4Mo the observed state of order can be interpreted as due to the presence of rod-like microclusters extending several unit cells along the c-directions but quite often less than a unit cell wide. For Au_4V and Au_4Fe the observed diffuse intensity is probably too weak to allow decisive conclusions.

6. Work in Progress

Existing models of long-period superstructures are being reexamined in light of the recently developed ANNNI model. In this model, long-period phases are contained in a triangular phase-diagram region located between a Lifshitz point on the uppermost transition temperature line (T_c), a multiphase point at zero absolute temperature, and a point at infinity on the T_c line. Observed periodic antiphase structures result from the modulation of the ordered ground state by either a very regular square wave or by a less regular wave with smoother profile. One-dimensional square-wave modulation results in an infinite series of ordered polytypes whose structures can be determined by expanding the half-period length in continued fractions, following an algorithm developed independently, in different contexts, by Hubbard and by Pokhrovski and Uimin.

Although portions of ANNNI model phase diagrams for long-period superstructures have been calculated by low-temperature expansions and

mean-field theories, no self-consistent calculation of a complete diagram exists at present. Work has now been initiated to compute such diagrams, for both two-dimensional and three-dimensional ordered structures, by the cluster variation method (CVM). Existing computer codes are being modified to accommodate the polytype ground states predicted by the continued-fraction algorithm referred to above.

1983 PUBLICATIONS AND REPORTS

LBL Reports

1. J. Kulik and D. de Fontaine, "Relevance of the ANNNI Model to Binary Alloys," LBL-15519.
2. O. Dairiki (M.S. Thesis), "Synthesis of S-shaped Temperature-time-transformation Diagrams," LBL-17028.
3. E. Colas (M.S. Thesis), "Isothermal Transformation of Ternary Eutectoid Steels with Cr, Ni, Mu Additions," LBL-17029.
4. G. Van Tendeloo, S. Amelinckx, W.M. Stobbs, and D. de Fontaine, "A Comparison of the Short-range Order Exhibited by Different $\langle 1\frac{1}{2} 0 \rangle$ Alloys," LBL-17031.

Other Publications

5. J. Kulik and D. de Fontaine, "Models of Long-period Superstructures," in *International Conference on Phase Transformations in Solids*, Maleme-Chania, Crete, Greece, June 27 - July 1, 1983, T. Tsakalakos, Ed., MRS Publication, Elsevier Science Publishing Co.
6. J. Kulik and D. de Fontaine, "Low Temperature Expansion Ising Model of Long-period Ordered Superstructures," TMS-AIME Annual Meeting, Atlanta, March 9, 1983.
7. S. Kulik and D. de Fontaine, "Long-period Structures in a Simple Ising Model," American Physical Society Meeting, Los Angeles, March 22, 1983; *Bull. Am. Phys. Soc.* **28**, 343 (1983).

Invited Talks

8. D. de Fontaine, "Ordering at Special and Not-so-special Points," Department of Metallurgical Engineering and Materials Science, Carnegie-Mellon University, Pittsburgh, March 10, 1983.
9. D. de Fontaine, "Long-period Superstructures," Solid-state Physics Colloquium, Department of Physics, University of California Berkeley, September 28, 1983; Materials Science Department, Northwestern University, Evanston, Illinois, November 18, 1983.

MECHANICAL PROPERTIES

Theoretical Problems in Alloy Design*

J.W. Morris, Jr., Investigator

INTRODUCTION

This project is a multifaceted program of metallurgical research that is concerned with the science of alloy design. It has three objectives: to build the scientific foundation needed to approach the problem of alloy design in a systematic way, to develop systematic approaches, and to create new alloys that satisfy advanced energy needs. Specific research tasks include: (1) theoretical research on phase transformations in solids and on the influence of microstructure on engineering properties; (2) experimental research on fundamental problems in metallurgy, including the control of microstructure through thermomechanical processing, the influence of microstructure on engineering properties, and the development of techniques for materials testing and characterization; (3) the development of new structural alloys for advanced energy systems, a task that is now mainly concerned with the design of improved structural alloys for low-temperature use; (4) welding metallurgy, including the development of appropriate weld filler metals and weld microstructures to maintain toughness in high-strength welded alloys; and (5) the development of improved superconducting wires for use in high-field superconducting magnets.

*This work was supported by the Director, Office of Energy Research, Office of Basic Energy Sciences, Materials Sciences Division of The U.S. Department of Energy under Contract No. DE-AC03-76SF00098.

1. The Elastic Theory of the Defect Solid Solution (Publication 15)

J.W. Morris, Jr., A.G. Khatchaturyan,[†] and Sheree H. Wen[‡]

This paper reviews the linear elastic theory of the defect solid solution. It outlines the theory in a mathematical form that is suitable for the solution of practical problems. The theory treats solid solutions containing distributions of solute defects that distort the solvent lattice and interact elastically with one another. It determines the total strain of the solvent lattice and the elastic contribution to the free energy of the solution in the strong harmonic approximation. The theory is specifically developed for a binary solution of point defects in the absence of external stress. It can be extended to treat multicomponent solutions, stressed solutions, and solutions of finite defects or macroscopic inclusions. The equations governing these complex systems are also presented. The model is finally used to consider ordering and decomposition reactions in solutions whose components interact elastically.

[†]Present address: Institute of Crystallography, USSR Academy of Sciences, Moscow, USSR.

[‡]Present address: IBM Thomas J. Watson Research Center, Yorktown Heights, New York.

2. The Use of Phase Transformations in the Design of Alloy Steel (Publication 14)

J.W. Morris, Jr.

This paper describes and illustrates the use of phase transformations in the design of new alloy steels. It begins by outlining a systematic recipe for the design of new materials to achieve specific engineering properties and describes the ways in which phase transformations are employed. The general method is illustrated through a discussion of two specific examples: the development of new ferritic structural steels for use at cryogenic temperatures and the development of "dual-phase" steels for automotive use.

3. ^{57}Fe Backscatter Mössbauer Spectrometry (Publication 3)

B. Fultz and J.W. Morris, Jr.

Mössbauer spectra taken from backscattered 14.4-keV γ -rays can be used for nondestructive phase and chemical analysis of iron alloys. U.S. Patent No. 4,393,306 was issued this year for a detector for backscattered 14.4-keV γ -rays. The detector is a gas-filled proportional counter of toroidal geometry. It offers good geometrical collection efficiency of backscattered radiations while providing shielding of the incident beam. A uniform electric-field gradient around the anode, which results in good energy resolution, is provided by an eccentric positioning of the anode wire.

The absorption of resonant radiations as they pass through a specimen distorts the shapes of peaks in Mössbauer spectra. This "thickness distortion" can reduce the apparent intensity of the Mössbauer effect by amounts that can cause errors of 30% in phase analyses of natural iron alloys. The magnitude of this thickness distortion was calculated in exact analytic form for backscatter Mössbauer spectra. The required corrections for backscatter 14.4-keV Mössbauer spectra were shown to be simpler to implement than the corrections required by conventional transmission-geometry experiments.

4. The Influence of Austenite Stability on Fatigue-crack Growth in 18-8 Stainless Steel at Cryogenic Temperature (Publication 7)

G.M. Chang

Mechanically induced martensitic transformations strongly influence the low-temperature mechanical behavior of metastable austenitic steels. The effects were specifically investigated for low-carbon 18Cr/8Ni steels with and without nitrogen additions (304L, 304LN). The fatigue-crack growth rate in 304L decreases as the temperature is lowered, while that in 304LN is relatively insensitive to temperature. This result is apparently a consequence of the strain-induced martensite transformation. 304L is unstable at low temperature, while 304LN is stabilized in the austenite phase by the nitrogen addition. The lower crack growth in 304L is attributed to cyclic closure at the fatigue-crack tip, caused by the volume change associated with the martensitic transformation. This interpretation suggests that the

fatigue-crack growth in metastable austenitic steels should depend on the maximum stress intensity during the fatigue cycle rather than on the variation in the applied stress intensity. It is demonstrated that the fatigue-crack growth curves for 304L coalesce if they are replotted in this way.

5. The Role of the Constituent Phases in Determining the Low-temperature Toughness of 5.5Ni Cryogenic Steel (Publication 9)

J.I. Kim, H. Jae Kim, and J.W. Morris, Jr.

Ferritic Fe-Ni steels that are intended for service at low temperature are usually given an intercritical temper as the final step in their heat treatment. The temper dramatically decreases the ductile-brittle transition temperature T_B . Its metallurgical effect is to temper the lath martensite matrix and precipitate a distribution of fine austenite particles along the lath boundaries. Prior research suggests that the low value of T_B is a consequence of small effective grain size of the ferrite-austenite composite. The present research was done to test this conclusion against an alternative hypothesis that the low T_B is due to the inherent toughness of constituent phases. Toughness specimens were prepared from materials with the compositions of the tempered martensite and precipitated austenite phases in the composite microstructure of tempered 5.5Ni steel. Both austenite and martensite phases were stable in these materials, but they exhibited poor mechanical properties at cryogenic temperatures. This result is consistent with the grain-size effects suggested by previous data and also supports the conclusion that the stability of precipitated austenite is determined mainly by its chemical composition.

6. Sources of Intergranular Embrittlement during High-temperature Testing of an Iron-based Superalloy (Publication 8)

G.X. Hu and J.W. Morris, Jr.

This work was undertaken to investigate the elevated-temperature tensile properties of a new age-hardened iron-based superalloy, EPRI-T (Fe/34.5Ni/5Cr/3Ti/3Ta/1Mo/0.01B), which was designed for both high strength and good fracture toughness at room temperature. The alloy retained

high strength when tested at 650°C in air. However, samples that were aged from the annealed condition were brittle at 650°C. Fractographic analyses of the embrittled specimens showed that they failed in an intergranular mode that initiated at the sample surface. Samples cut longitudinally from material that was aged directly from the as-forged condition were ductile in tension at 650°C. The intergranular surface cracks could not penetrate the elongated grains parallel to the tensile axis. The weakness of the grain boundaries was found to be due to cellular precipitation of the Fe₂Ta Laves phase. An alternate heat treatment was designed to suppress cellular precipitation. Samples given this heat treatment had improved room-temperature ductility and remained ductile when tested at 650°C in vacuum, but were brittle when tested at 650°C in air. The high-temperature brittleness is caused by subsurface oxidation, which induces precipitation of the Laves phase along the grain boundaries ahead of the growing oxide. Hence the alloy embrittles itself when tested at a low strain rate in high-temperature air. A parallel investigation studied the influence of mechanical twinning on the high-temperature deformation of the alloy. Twinning occurs but appears to be a consequence of the embrittling mechanism rather than a cause of embrittlement.

7. Welding Superalloy Sheet for Superconditioning Cable Jackets (Publication 12)

L.T. Summers, M.J. Strum, and J.W. Morris, Jr.

JBK-75, an iron-based superalloy, has been selected for use as the cable-jacket material for the Westinghouse magnet of the Department of Energy's Large Coil Project. Previous investigations of GTA welds of JBK-75 and its sister alloy A-286 have shown that age-hardened weld metal has significantly lower yield and tensile strengths than comparable heat-treated base metal. In this investigation of A-286 weldments, the undermatching properties are shown to be the result of chemical segregation during weld-pool solidification. This chemical segregation results in significant changes in the precipitation kinetics of the gamma-prime hardening phase. The identification of the source of the property mismatch led to the design of alternate welding processes that re-establish comparable properties through modifications of weld-metal chemistry or post-welding heat treatments. The results are applicable to a wide range of problems in superalloy welding.

8. Pulsed Magnetic-field Testing of Multifilamentary Nb₃Sn Superconducting Wire (Publication 13)

J. Glazer, D.R. Dietderich, and J.W. Morris, Jr.

Because high-intensity pulsed magnetic fields are conveniently available at LBL, the feasibility of using pulsed magnetic-field testing as a partial substitute for steady-field testing of high-field superconductors was investigated. The critical-current characteristics of bronze-processed multifilamentary Nb₃Sn wires were determined both in steady magnetic fields and in pulsed magnetic fields. There is good qualitative agreement between the data obtained under pulsed and steady fields and reasonable quantitative agreement for magnetic fields above 11 T. At lower magnetic fields the pulsed-field data lie significantly below the steady-field data. Although we were unable to account for this discrepancy, an empirical understanding of the relationship between the two data sets permits the use of pulsed-field data in evaluating different approaches to superconducting-wire development.

9. The Microstructure and Critical-current Characteristics of a Bronze-processed Multifilamentary Nb₃Sn Superconducting Wire (Publication 4)

I.W. Wu, D.R. Dietderich, J.T. Holthuis, M. Hong, W.V. Hassenzahl, and J.W. Morris, Jr.

The superconducting A15 phase within a bronze-process, multifilamentary Nb₃Sn superconducting wire is formed by reaction at the interface between the Nb filaments and the bronze matrix. The maximum current that could be carried by the wire in an applied magnetic field is known to depend on the time and temperature of the heat treatment. A commercial Airco wire containing 2869 Nb filaments of 3–5 μm diameter in a matrix with a bronze/Nb ratio of 3 was given a variety of reaction heat treatments. The microstructure of the reacted layer was analyzed as a function of heat treatment and found to be divisible into three concentric shells that are morphologically distinct. The central shell consists of fine equiaxed grains. Its areal fraction, grain size, and composition depend on the heat treatment and appear to determine the critical current. The best combination of grain size and composition, and the highest critical current, is obtained with an

intermediate reaction temperature (700–730°C). A further improvement in both microstructure and critical current is achieved by double-aging the wire, starting the reaction at 700°C and finishing it at 730°C. The relation between the heat treatment and the microstructure was revealed by high-resolution transmission electron microscopy, and this relationship was interpreted in light of the apparent mechanisms of the reaction, which are revealed by high-resolution analyses of the reacted layer. The relation between microstructure and properties is consistent with current understanding of the influence of grain size and stoichiometry on the behavior of type-II superconductors.

10. The Critical-current Density of Bronze-processed Nb₃Sn Multifilamentary Wires with Mg Addition to the Bronze Matrix (Publication 10)

I.W. Wu, D.R. Dietderich, J.T. Holthuis, J. Glazer, W.V. Hassenzahl, and J.W. Morris, Jr.

The influence of magnesium additions to the bronze matrix on the current-carrying capacity of bronze-processed 133-filament Nb₃Sn superconducting wires was studied. Preliminary results show that the critical-current density within the A15 layer was enhanced by Mg addition. Microstructural analysis revealed that Mg segregates to the A15 layer during the reaction and that the coarsening of A15 grains is largely suppressed. Further studies of the growth kinetics found that the growth rate varies significantly with heat treatment and bronze composition. To achieve a more valid comparison of J_c , samples with different bronze concentrations were heat-treated isothermally to nearly complete reaction at temperatures from 650 to 800°C. A simple quantitative model is described that connects the superconducting properties to microstructure and composition of the A15 layer.

11. A Microstructural Study on the Processing and Properties of High-field A15 Superconducting Materials (Publication 16)

I.W. Wu

The superconducting properties of high-field A15 materials are related to the physical and chemical

states of the A15 phases. Higher critical current can therefore be achieved through microstructural control, using the relationships between processing variables, microstructure, and the resultant properties. The theories of high-field superconductivity are critically examined, and the results used to interpret the properties of high-field superconducting wires and design means for improving those properties. The A15 materials investigated include the V₃Ga and Nb₃Al phases formed by a direct-precipitation process, the multifilamentary Nb₃Sn formed by the bronze process, and the bronze-processed Nb₃Sn with a Mg addition.

12. Work in Progress

Work in progress in 1984 includes: (1) a theoretical study of the shapes and habits of precipitate phases, using the linear elastic theory; (2) research on the microstructure and chemical state of thermally processed steels, using a combination of high-resolution microscopy, scanning transmission electron microscopy, and Mössbauer spectrometry; (3) research on the influence of grain refinement on resistance to thermal and hydrogen embrittlement in alloy steels; (4) research on the metallurgy and mechanical properties of Fe-Mn steels; (5) research on the influence of weld thermal cycles on the toughness of weldments in ferritic steels; (6) research on the control of the mechanical properties of weldments in superalloy steels; and (7) research on the microstructure-property relations in high-field superconducting wire.

1983 PUBLICATIONS AND REPORTS

Refereed Journals

1. M.J. Strum, L.T. Summers, and J.W. Morris, Jr., "The Aging Response of a Welded Iron-based Superalloy," *Welding J.* **9** (1983), 235–242s; LBL-14999.
2. I.W. Wu, D.R. Dietderich, J. T. Holthuis, W.V. Hassenzahl, and J.W. Morris, Jr., "The Influence of Magnesium Additions to the Bronze on the Critical Current of Bronze-processed Multifilamentary Nb₃Sn," *IEEE Trans MAG* **19**(3), 1437 (1983); LBL-15336.
3. B. Fultz and J.W. Morris, Jr., "The Thickness Distortion of ⁵⁷Fe Backscatter Mössbauer Spectra: II. Effects of Secondary Resonant Absorp-

tions," Nucl. Instr. and Methods **211**, 569-570 (1983); LBL-15433.

4. I.W. Wu, D. Dietderich, J.T. Holthuis, M. Hong, W. Hassenzahl, and J.W. Morris, Jr., "The Microstructure and Critical Current Characteristic of a Bronze-processed Multifilamentary Nb₃Sb Superconducting Wire," J. Appl. Phys. **12** (1983); LBL-15740.

LBL Reports

5. M. Hong, D.E. Wedge, and J.W. Morris, Jr., "The State and Habit of the Fe₁₆N₂ Precipitate in bcc Iron: Elastic Theory," Acta Met., in press, LBL-12973 revised.
6. J.W. Morris, Jr., "Cryogenic Steels," in *Encyclopedia of Materials Science and Engineering*, Pergamon Press, Oxford, England, in press, LBL-15408.
7. G.M. Chang (M.S. Thesis), "Austenite Stability and Its Influence on Mechanical Properties of 18-8 Stainless Steel at Cryogenic Temperatures," LBL-15864.
8. G.-Xiang Hu and J.W. Morris, Jr., "Sources of Intergranular Embrittlement during High Temperature Testing of an Iron Base Superalloy," Met Trans., in press, LBL-16162.
9. J.I. Kim, H. Jae Kim, and J.W. Morris, Jr., "The Role of the Constituent Phases in Determining the Low Temperature Toughness of 5.5Ni Cryogenic Steel," LBL-16231.
10. I.W. Wu, D.R. Dietderich, J.T. Holthuis, J. Glazer, W.V. Hassenzahl, and J.W. Morris, Jr., "The Critical Current Density of Bronze-processed Multifilamentary Nb₃Sn Wires with Magnesium Addition to the Matrix," in *Advances in Cryogenic Engineering*, in press, LBL-16527.
11. D.R. Dietderich, I.W. Wu, J.T. Holthuis, W.V. Hassenzahl, and J.W. Morris, Jr., "The Fabri-

cation and Superconducting Properties of Multifilamentary Nb₃Sn with Mg-doped Bronze," in *Advances in Cryogenic Engineering*, in press, LBL-16529.

12. L.T. Summers, M.H. Strum, and J.W. Morris, Jr., "Welding Superalloy Sheet for Superconducting Cable Jackets," in *Advances in Cryogenic Engineering*, in press, LBL-16530.
13. J. Glazer and J.W. Morris, Jr., "Pulsed Magnet Field Testing of Multifilamentary Nb₃Sn Superconducting Wire," in *Advances in Cryogenic Engineering*, in press, LBL-16535.
14. J.W. Morris, Jr., "The Use of Phase Transformations in the Design of Alloy Steel," in *Proc. Int. Conf. on Phase Transformations*, in press, LBL-16550.
15. J.W. Morris, Jr., A.G. Khatchaturyan, and S. Wen, "The Elastic Theory of the Defect Solid Solution," in *Proc. NATO Advanced Study Inst. in Modulated Structure Materials*, in press, LBL-16551.
16. I.-Wei Wu (Ph.D. Thesis), "A Microstructural Study on the Process and Properties of High-field A15 Superconducting Materials," LBL-16999.

Other Publications

17. K.M. Chang and J.W. Morris, Jr., "Research Toward New Alloys for Generator Retaining Rings," Proc. Microstructural Control Conf., ASM Special Technical Publication No. 792, 1983, pp. 79-103; LBL-13467.
18. B. Fultz, G.M. Chang, and J.W. Morris, Jr., "Effects of Magnetic Fields on Martensite Transformation and Mechanical Properties of Steels at Low Temperatures," in *Proc. Int. Cryogenic Materials Conf.*, Butterworth and Co., England, 1982, pp. 343-348; LBL-15518.

Mechanical Properties of Ceramics*

Anthony G. Evans, Investigator

INTRODUCTION

This project is concerned with the mechanical reliability of ceramics at high temperatures. The principal research topics entail the development of predictive capabilities for the high-temperature failure of ceramics and for microstructure/defect development during sintering. Elevated-temperature failure studies are concerned with the initiation, growth, and coalescence of cracks during creep. Experimental measurements are being correlated with theoretical models containing the dominant microstructural variables. The processes that dictate the presence of retained porosity and defects during solid-state and liquid-phase sintering are being examined.

1. The High-temperature Failure of Polycrystalline Alumina — I. Comparative Microstructures (Publication 8)

B.J. Dalgleish and A.G. Evans

A combination of techniques has been used to compare the compositional and microstructural characteristics of two commercially hot-pressed aluminas: b-Al₂O₃ (so designated because of its black color) and g-Al₂O₃ (light grey). Second-phase material containing Ni was observed in b-Al₂O₃, mainly as small intergranular particles, although significant numbers of much larger second-phase inclusions were present. Thermal treatment in air at temperatures similar to those used for creep testing caused Mg and Ni to concentrate at b-Al₂O₃ surfaces. Color changes, attributed to Ni precipitation, also accompanied oxygen exposure at elevated temperatures. These characterization studies precede a comparative investigation of the creep and creep-rupture characteristics of the two materials.

2. The High-temperature Failure of Polycrystalline Alumina — II. Crack-nucleation Sites (Publication 9)

S.M. Johnson and A.G. Evans

Heterogeneous crack-nucleation sites have been identified during the high-temperature creep of Al₂O₃. These sites include chemical heterogeneities and large-grained zones as well as initial delaminations. A viscous-stress analysis based on creep differentials has been conducted to assess the influence of stress concentrations at the heterogeneities on the crack-nucleation process. The stress concentrations are <2 in all cases and are insufficient to account for the preferred nucleation. Thus additional effects associated with low-viscosity material within the heterogeneity are involved. For example, SiO₂ is present in the chemical heterogeneities, and some Ti exists in the large-grained material.

3. The High-temperature Failure of Polycrystalline Alumina — III. Characterization of Cracks Subject to Creep (Publication 10)

W. Blumenthal and A.G. Evans

The deformation response of small, semi-elliptical, indentation-induced surface cracks in fine-grain alumina has been monitored using crack-opening and surface-displacement measurements. Results indicate values of the secondary-creep exponent n between 1.5 and 2, and a temperature dependence consistent with creep data. However, at temperatures $\geq 1400^\circ\text{C}$, crack-tip damage in the form of grain-boundary cavities exerts a strong influence on the displacement field, as predicted by recent theories. Use of the stress-intensity factor as a loading parameter, based on Newtonian viscous behavior, does not produce adequate correlation with experimental results and is therefore unsuitable for nonlinear creeping polycrystals.

*This work was supported by the Director, Office of Energy Research, Office of Basic Energy Sciences, Materials Sciences Division of the U.S. Department of Energy under Contract No. DE-AC03-76SF00098.

4. The High-temperature Failure of Polycrystalline Alumina — IV. Creep-crack Growth and Blunting (Publication 11)

W. Blumenthal and A.G. Evans

High-temperature crack growth in fine-grain alumina is measured using artificial surface cracks induced by diamond indentation. Particular emphasis is placed on observations of crack-tip cavitation damage. Using the stress-intensity factor as a loading parameter, a narrow power-law growth regime occurs at 1300°C and 1400°C wherein the power-law exponent and activation energy are comparable to steady-state creep values. Crack-tip damage in the form of grain-boundary cavities precedes crack extension in accordance with recent crack-growth models. Asymptotic crack-velocity behavior is exhibited near both the critical stress-intensity factor K_{IC} and the crack-growth threshold K_{th} . The threshold occurs near $0.4 K_{IC}$ at both 1300°C and 1400°C and is associated with a transition in the size and distribution of damage. As K_{th} is approached, damage concentrates in side lobes between 20° to 60° from the plane of the crack. The transition between frontal and side-lobe damage accelerates near-tip crack opening, and damage coalescence leads to crack-tip branching.

5. The High-temperature Failure of Polycrystalline Alumina — V. Failure Times (Publication 12)

B.J. Dalgleish, S.M. Johnson, and A.G. Evans

High-temperature failure data have been obtained for two polycrystalline aluminas, revealing a strongly stress-dependent failure time. The observed stress dependence has been compared with the dependence predicted by models of the nucleation, growth, and coalescence stages of failure. Only models of the coalescence phase indicate sufficient nonlinearity to account for the observations. Further observations and measurements of coalescence involving continuous-crack nucleation and shear-band formation are identified as requirements for further understanding of the rupture process. The observations of shear bands appear to be particularly significant and provide the most important type of future research on creep rupture.

6. On the Nucleation of Cavities During the Creep of Liquid-phase Sintered Materials (Publication 14)

M.D. Thouless and A.G. Evans

The nucleation of cavities within the second phase of liquid-phase sintered ceramics has been studied. A thermodynamic approach has been used to derive the regions of existence for cavities of various morphologies in two-grain channels and three-grain pockets. The nucleation rates for the cavities have also been derived by a classical nucleation approach. It is demonstrated that hole nucleation occurs most readily in three-grain pockets. However, even then the stresses for homogeneous nucleations are relatively large compared with most experimental tests. Transient grain-boundary sliding events are thus deemed to be a major source of the local stress enhancement needed to initiate holes.

7. Some Effects of Ellipsoidal Voids on Sintering and Creep (Publication 7)

M.D. Drory and A.G. Evans

An analysis of the growth and shrinkage of ellipsoidal voids in three-grain channels is presented. The predicted growth rates are compared with the growth of cylindrical pores on the same interfaces. It is demonstrated that the sintering of ellipsoidal pores occurs more rapidly because of the increased surface curvature. The formation of such pores by the Rayleigh-instability mechanism thus appears to constitute an important step in final-stage sintering. Conversely, the growth rates of the ellipsoidal and cylindrical voids subject to creep loading are shown to be similar, indicating that cylindrical-void-growth solutions provide an adequate description of creep rupture.

8. The Mechanical Behavior of Alumina: A Model Anisotropic Brittle Solid (Publication 15)

A.G. Evans and Y. Fu

This article describes the mechanical behavior of alumina at both low and high temperatures. The

brittle behavior at low temperatures is classified into two regions, one due to microcrack coalescence at large grain sizes and the other due to the growth of pre-existing flaws at smaller grain size. The microcracking is predicted on the existence of residual stress due to thermal-expansion anisotropy. Microcracks result in R-curve behavior and a very complex dependence of strength on microstructure. Failure at small grain sizes is more straightforward and relatively well understood. At high temperatures rupture is time-dependent, and failure involves the nucleation and growth of cracks accompanied by creep cavitation. Eventual failure is determined by crack coalescence. Each of these failure processes is discussed and related to microstructure.

9. Work in Progress

Continued studies of creep rupture in solid-state sintered Al_2O_3 have revealed that shear bands exert a major influence on the rupture lifetime. Occasional crack nucleation has been observed at shear-band intersections, and shear bands between cracks have been identified as an invariant source of crack coalescence prior to eventual failure. These recent observations provide the basis for an important change of emphasis in future studies of creep rupture in solid-state sintered ceramics.

Examination of premature crack-nucleation sites in Al_2O_3 has confirmed the predominance of chemical heterogeneities, based on the presence of local zones of SiO_2 , and of large-grain-size inhomogeneities. The chemical heterogeneities have been largely identified with the condensation of SiO_2 onto the specimen surfaces from the test environment by an evaporation/condensation process. The large-grained heterogeneities have been attributed to the presence of Ti impurities: a Ti-rich core has been identified in all instances. The Ti, coupled with alkali impurities, is presumed to locally enhance grain growth by the formation of a eutectic liquid with Al_2O_3 .

Damage-zone models of crack growth in a creeping solid have been subject to continued development by incorporating the sintering stress as a parameter and by examining the role of a local liquid phase. The model has thereby been sufficiently generalized that creep-crack growth rates can be predicted for a wide range of ceramic microstructures.

Creep-crack growth in a liquid-phase-sintered Al_2O_3 has been studied. The failure behavior is entirely different from that observed in solid-state-

sintered Al_2O_3 of essentially the same grain size. The failure strains in the material containing the liquid phase are small, and the cracks, once nucleated, grow continuously without blunting. Failure thus appears to be limited by the creep-crack growth rate and does not entail the blunting and coalescence stages observed in the solid-state sintered materials. The major difference in behavior has been attributed to the ready nucleation of holes within the viscous-liquid phase, leading to a prolific damage mechanism of crack propagation.

Observations of surfaces during the final-stage sintering of MgO specimens within an MgO-powder vehicle have revealed that surface porosity is removed substantially prior to the removal of internal porosity. This phenomenon has been investigated comprehensively, both experimentally and theoretically, because of the obvious potential for improving the surface properties of ceramic components (e.g., improved contact-damage resistance, superior substrate surfaces). Measurements of pore-elimination rates have been compared with calculations for surface-diffusion and evaporation/condensation mechanisms. The comparison indicates that evaporation/condensation in the presence of the fine MgO-powder vehicle is the primary mechanism of surface-pore shrinkage.

Experimental simulations of the influence of powder heterogeneities on sintering stresses and damage have been initiated on an MgO material. Small cylinders of higher initial-density material have been placed into sintering bodies, and the onset and growth of damage has been monitored. The nucleation and growth of creep cracks has thereby been unambiguously identified during sintering when the shrinkage rate differential of the embedded region exceeds a minimum value. Crack blunting and shrinkage have also been observed below the minimum shrinkage-rate differential.

Observations of thin continuous-liquid films that develop during liquid-phase sintering of an Al_2O_3 /anorthite system have been conducted using TEM techniques. The intent of these studies is to provide a comprehensive understanding of the local viscous-flow and solution/precipitation phenomena that accompany liquid-phase sintering. Thus far the studies have revealed that the thickness of the liquid between the sintering-powder particles is in excess of that predicted using a viscous-flow formalism, based on the continuum properties of the liquid. It appears, therefore, that thin liquid layers (10–100 Å in thickness) formed during sintering exhibit some quasi-solid properties in conjunction with their role as a rapid transport path.

1983 PUBLICATIONS AND REPORTS

Refereed Journals

1. J.E. Marion, A.G. Evans, M.D. Drory, and D.R. Clarke, "High Temperature Failure Initiation in Liquid Phase Sintered Materials," *Acta Met* 31 (10), 1445 (1983); LBL-14266.
2. M. Sakarcin, C.H. Hsueh, and A.G. Evans, "An Experimental Assessment of Pore Breakaway During Sintering," *J. Am. Ceram. Soc.* 66 (6), 456 (1983); LBL-14334.
3. M.D. Thouless, C.H. Hsueh, and A.G. Evans, "A Damage Model of Creep Crack Growth in Polycrystals," *Acta Met.* 31 (10), 1675 (1983); LBL-15348.

LBL Reports

4. W. Blumenthal (Ph.D. Thesis), "Mechanical Response of Ceramics to Creep Loading," LBL-16526.
5. M.D. Drory and A.G. Evans, "Some Effects of Ellipsoidal Voids on Sintering and Creep of Polycrystals," *J. Amer. Ceram. Soc.*, in press, LBL-15880.
6. B.J. Dalgleish and A.G. Evans, "The High Temperature Failure of Polycrystalline Alumina — I. Comparative Microstructures," submitted to *J. Am. Ceram. Soc.*, LBL-16167 1/5.
7. S.M. Johnson and A.G. Evans, "The High Temperature Failure of Polycrystalline Alumina — II. Crack Nucleation Sites," submitted to *J. Am. Ceram. Soc.*, LBL-16167 2/5.
8. W. Blumenthal and A.G. Evans, "The High Temperature Failure of Polycrystalline Alumina — III. Characterization of Cracks Subject to Creep," submitted to *J. Am. Ceram. Soc.*, LBL-16167 3/5.
9. W. Blumenthal and A.G. Evans, "The High Temperature Failure of Polycrystalline Alumina — IV. Creep Crack Growth and Blunting," submitted to *J. Am. Ceram. Soc.*, LBL-16167 4/5.
10. B.J. Dalgleish, S.M. Johnson, and A.G. Evans, "The High Temperature Failure of Polycrystalline Alumina — V. Failure Times," submitted to *J. Am. Ceram. Soc.*, LBL-16167 5/5.
11. M.D. Thouless and A.G. Evans, "On the Nucleation of Cavities During the Creep of Liquid Phase Sintered Materials," submitted to *J. Am. Ceram. Soc.*, LBL-16564.
12. A.G. Evans and Y. Fu, "The Mechanical Behavior of Alumina: A Model Anisotropic

Brittle Solid," submitted to *Advances in Ceramics*, LBL-16239.

Other Publications

13. J.R. Porter, W. Blumenthal, and A.G. Evans, "Creep Fracture in Ceramic Polycrystals — I. Creep Cavitation Effects in Polycrystalline Alumina," in *Perspectives in Creep Fracture*, M.F. Ashby and L.M. Brown, eds., Pergamon Press, Oxford, 1983, pp. 125-132; LBL-11560 1/2.
14. C.H. Hsueh and A.G. Evans, "Creep Fracture in Ceramic Polycrystals — II. Effects in Inhomogeneity on Creep Rupture," in *Perspectives in Creep Fracture*, M.F. Ashby and L.M. Brown, eds., Pergamon Press, Oxford, 1983, pp. 133-143; LBL-11560 2/2.
15. A.G. Evans, "Structural Design with Brittle Materials," in *Ceramics for High Performance Applications III: Reliability*, E.M. Lence, R.N. Katz, and J.J. Burke, eds., Plenum Publishing Corp., New York, 1983, pp. 475-502; LBL-10341.

Invited Talks

16. J. Marion and A.G. Evans, "Some Critical Considerations in Liquid Phase Sintering," American Ceramic Society 1983 Annual Meeting, Chicago, April 29, 1983.
17. W. Blumenthal and A.G. Evans, "Creep Crack Growth in Alumina," American Ceramic Society 1983 Annual Meeting, Chicago, April 29, 1983.
18. M.D. Drory and A.G. Evans, "Microstructure Development During Final Stage Sintering," American Ceramic Society 1983 Annual Meeting, Chicago, April 29, 1983.
19. M.C. Lu and A.G. Evans, "The Influence of Cyclic Tangential Loading on Indentation," American Ceramic Society Pacific Coast Regional Meeting, San Diego, October 3, 1983.
20. A.G. Evans and W. Blumenthal, "High Temperature Failure Mechanisms in Ceramic Polycrystals," International Symposium on Plastic Deformation of Ceramic Materials, Pennsylvania State University, State College, Pennsylvania, July 1983, LBL-16192.
21. W. Blumenthal and A.G. Evans, "The High Temperature Failure of Polycrystalline Alumina — Characterization of Cracks Subject to Creep," International Symposium on Plastic Deformation of Ceramic Materials, Pennsylvania State University, State College, Pennsylvania, July 1983, LBL-16510.

22. A.G. Evans, "Fracture Behavior and Reliability of Brittle Solids," Van Horne Lecturer, Case Western Reserve University, Cleveland, Ohio, March 13, 1983.
23. A.G. Evans, "The Reliability of Ceramics: The Role of Toughness," ASEA Conference, Sweden, September 18, 1983.
24. A.G. Evans, "Aspects of Reliability of Ceramics for Engine Applications," 6th International Symposium on Ceramics, Bologna, Italy, September 16, 1983.

Environmentally Affected Crack Growth in Engineering Materials*

Robert O. Ritchie, Investigator

INTRODUCTION

The objective of this program is to examine, from combined continuum and micromechanistic points of view, the role of mechanical, microstructural, and environmental factors involved in the sub-critical crack growth of flaws. Emphasis has been placed on crack growth by fatigue, where models have been developed for the premature closure of cracks at low propagation rates approaching the threshold stress intensity range ΔK_0 for no growth of both long and short cracks. Such crack closure, where the driving force for crack extension is limited by contact behind the crack tip, has been modeled in previous years in terms of the wedging action of corrosion debris (oxide-induced closure) and irregular fracture morphologies (roughness-induced closure). In the past year the latter concept has been utilized to produce exceptionally high fatigue resistance in dual-phase steels. A quantitative model has also been developed for a new mechanism of closure induced by the presence of fluids inside the crack, and studies have been initiated to examine closure resulting from metallurgical phase transformations (see Figure 1-1).

1. Near-threshold Fatigue Crack Closure (Publication 14)

R.O. Ritchie and S. Suresh

In recent years mechanistic and continuum studies on fatigue crack propagation, particularly at near-threshold levels, have highlighted a dominant role of crack closure in influencing growth rate behavior. In this program the various sources of closure induced by cyclic plasticity, corrosion deposits, irregular fracture morphologies, viscous fluids, and metallurgical phase transformations have been modeled (see Figure 1-1). Many of the commonly

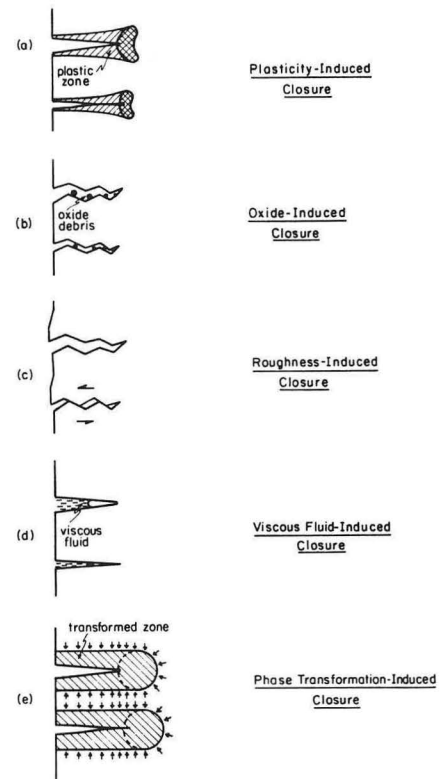


Figure 1-1. Schematic illustration of mechanisms of fatigue crack closure. (XBL 839-6312)

observed effects of mechanical factors (such as load ratio), microstructural factors (such as strength and grain size), and certain environmental conditions can be traced to the extrinsic influence of closure in modifying the effective driving force for crack extension. The implications of such closure mechanisms have been examined in light of constant and variable amplitude fatigue behavior, the existence of a threshold stress intensity for no fatigue crack growth, and the validity of such threshold concepts for the case of short fatigue cracks.

2. Fatigue Crack Propagation in Dual-phase Steels (Publication 15)

R.O. Ritchie, S. Suresh, and V.B. Dutta

Characteristics of fatigue crack propagation in dual-phase steels were investigated in a high-purity Fe-2Si-0.1C steel originally designed by G. Thomas. The objective was to develop duplex ferritic-martensitic microstructures with maximum resistance to fatigue crack extension, while maintaining high strength, by promoting crack closure through

*This work was supported by the Director, Office of Energy Research, Office of Basic Energy Sciences, Materials Sciences Division of the U.S. Department of Energy under Contract No. DE-AC03-76SF00098.

meandering crack paths. Results on fatigue crack propagation in a series of duplex microstructures indicated extraordinarily large effects of the morphology, proportion, and distribution of the ferrite and martensite phases, particularly for tests at low load ratios (see Figure 2-1). Specifically, microstructures containing fine globular or coarse martensite within a coarse-grained ferritic matrix demonstrated exceptionally high fatigue crack growth resistance without loss in strength and yielded, to our knowledge, the highest ambient-temperature fatigue threshold stress intensities ΔK_0 reported to date (see Figure 2-2). Such unusually good fatigue resistance was attributed primarily to the tortuous morphology of the crack path (see Figure 2-3), which results in a reduction in crack-driving force from both crack deflection and roughness-induced crack-closure mechanisms. Analytical models were developed for both deflection and closure processes. These models were used with quantitative metallography and experimental closure measurements to substantiate the interpretations.

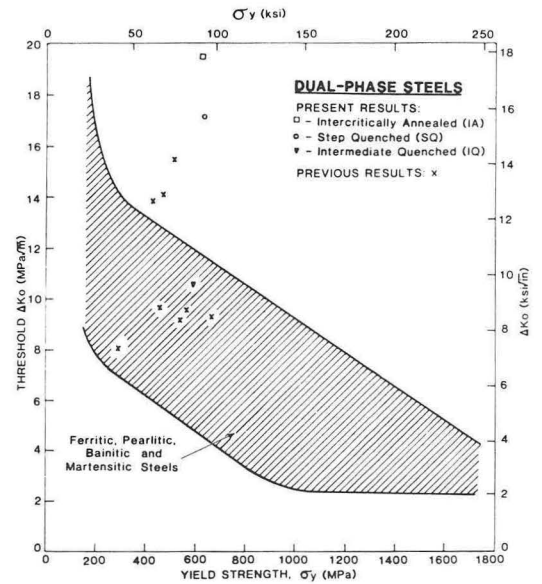


Figure 2-2. Variation of fatigue threshold stress intensity range ΔK_0 at low load ratios as a function of yield strength σ_y for ferrous alloys, showing the exceptional strength and fatigue threshold properties of the present ferritic-martensitic structures in the Fe-2Si-0.1C dual-phase steel. (XBL 838-10895A)

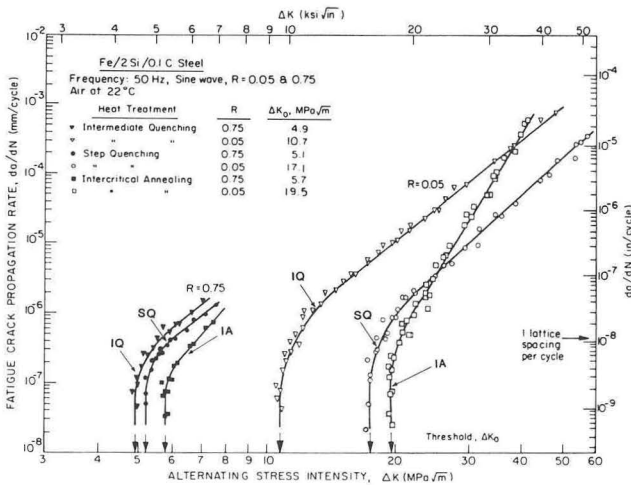


Figure 2-1. Variation in fatigue crack propagation rate da/dN with nominal stress intensity range ΔK for duplex ferrite-martensite microstructures in Fe-2Si-0.1C dual-phase steel. (XBL 838-10897)

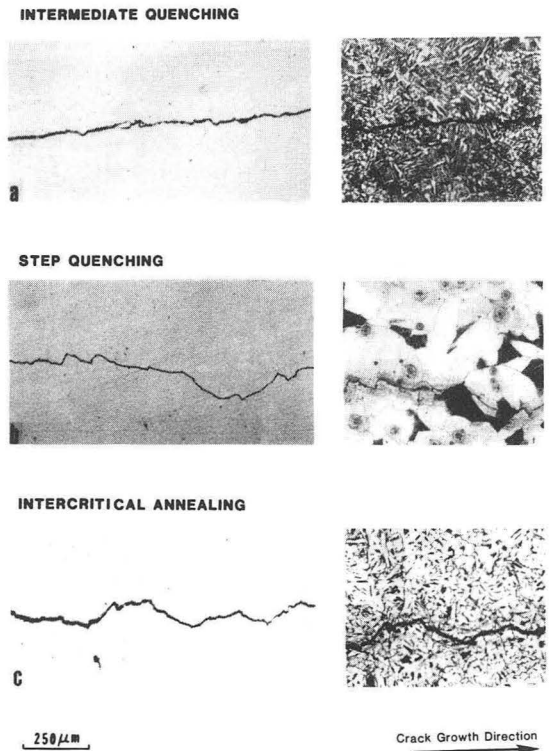


Figure 2-3. Near-threshold crack path morphologies in dual-phase Fe-2Si-0.1C steel, showing linear crack paths in intermediate quenched structures compared to meandering and deflected crack paths in the step-quenched and intercritical annealed structures. (XBB 839-7928)

3. Fatigue Crack Propagation in Oil Environments (Publication 11)

R.O. Ritchie, S. Suresh, and J.-L. Tzou

The influence of dehumidified silicone and paraffin oils with kinematic viscosities varying from 5 to 60,000 cS was examined on fatigue crack propagation in a lower-strength bainitic steel over a range of growth rates from near-threshold levels (10^{-6} to 10^{-8} mm/cycle) to higher growth rates (up to 10^{-3} mm/cycle). Crack growth data for a cyclic frequency of 50 Hz at both low and high load ratios were compared with previous results for environments of moist air, dry gaseous hydrogen, and dry gaseous helium. At low load ratios growth rates in oil exceed those in moist air below 10^{-6} mm/cycle, yet are lower than those in moist air above 10^{-6} mm/cycle (see Figure 3-1). Furthermore, there was a small but definite trend of higher growth rates in the higher-viscosity oils. Such observations are discussed and interpreted in terms of three mutually competitive mechanisms specific to dry viscous environments: suppression of moisture-induced hydrogen embrittlement and/or metal dissolution, minimization of oxide-induced crack closure, and the hydrodynamic wedging action of the oil inside the crack.

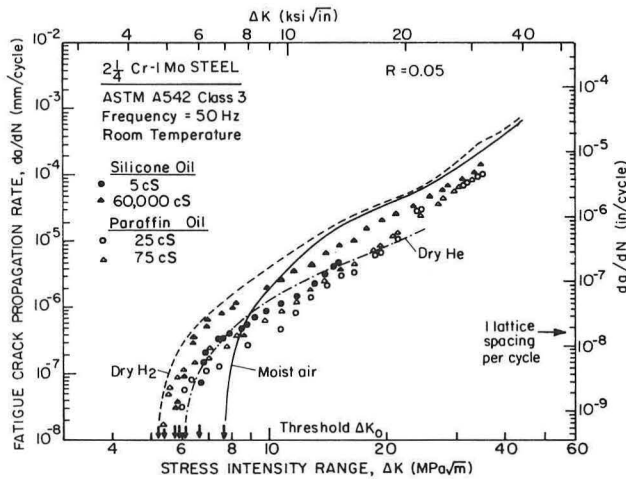


Figure 3-1. Fatigue crack propagation rate da/dN as a function of nominal stress intensity range ΔK for a bainitic $2\frac{1}{4}$ Cr-1Mo steel tested in silicone and paraffin oils, compared to results in moist air, dry helium, and dry hydrogen gases. (XBL 832-5302)

4. Quantitative Modeling of Viscous Fluid-induced Crack Closure (Publication 18)

R.O. Ritchie, J.-L. Tzou, C.H. Hsueh, and A.G. Evans

Several mechanisms, involving cyclic plasticity, corrosion debris, and irregular crack path morphologies, have recently been identified for fatigue crack closure, where contact of the crack faces behind the crack tip can reduce the driving force for crack advance by limiting the effective stress intensity range experienced in the near-tip region (see Figure 1-1). This work examined the concept of crack closure induced by the hydrodynamic wedging action of a viscous fluid within an advancing crack during cyclic loading. Unlike previous analyses, this model treats both the hydrodynamics of the pressure distribution within the crack (see Figure 4-1) and the kinetics of the penetration of the fluid into the crack. The results are presented in fracture mechanics ter-

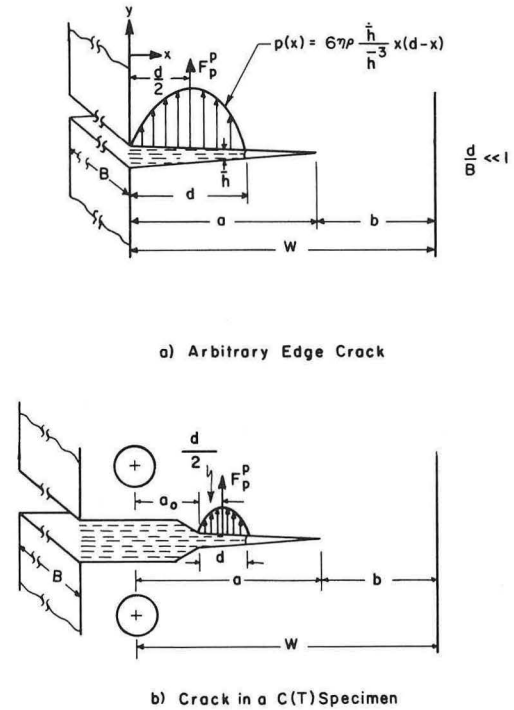


Figure 4-1. Schematic illustration of the internal pressure distribution $p(x)$ and resultant concentrated force f_p due to the partial penetration of a viscous fluid inside a cyclically loaded crack for (a) edge crack and (b) compact tension C(T) geometries. (XBL 834-5540A)

minology in terms of an effective (near-tip) stress intensity range based on the stress intensities due to applied loading and internal pressure distribution. Analyses involving both “full” and “partial penetration” of the viscous fluid inside the crack were used to rationalize the influence of viscosity on fatigue crack propagation in dehumidified oil environments. The roles of stress intensity range, crack size, and frequency on the development of such viscous fluid-induced crack closure were also examined.

5. Macroscopic and Microscopic Analyses for Crack Initiation and Crack Growth Toughness in Ductile Alloys (Publication 16)

R.O. Ritchie and A.W. Thompson

Relationships between crack initiation and crack growth toughness were reviewed by examining the crack tip fields and microscopic (local) and macroscopic (continuum) fracture criteria for the onset and continued quasi-static extension of cracks in ductile materials. By comparing the micromechanisms of crack initiation via transgranular cleavage and crack initiation and subsequent growth via microvoid coalescence (see Figure 5-1), expressions were developed for the fracture toughness of materials in terms of microstructural parameters, including those deduced from fractographic measurements. In particular, the distinction between the deformation fields directly ahead of stationary and nonstationary cracks was explored to explain why microstructure may have a more significant role in influencing the toughness of slowly growing cracks, as opposed to initiating cracks. Utilizing the exact asymptotic crack tip deformation fields recently presented by Rice and his co-workers for the nonstationary Mode I crack, and evoking various microscopic failure criteria for such stable crack growth, a relationship between the tearing modulus T_R and the nondimensionalized crack-initiation fracture toughness J_{IC} was presented. The demonstrated relationship was shown to yield a good fit to experimental toughness data for a wide range of steels.

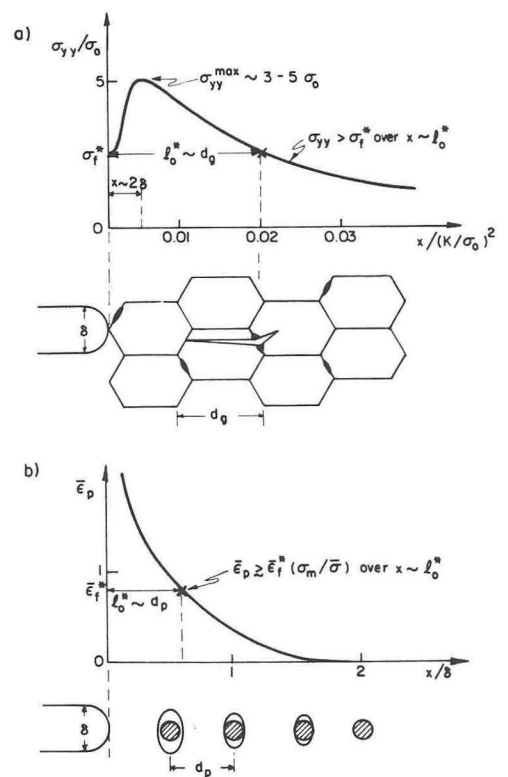


Figure 5-1. Idealization of the micromechanisms of brittle and ductile fracture showing (a) critical stress model for transgranular cleavage and (b) stress-modified critical strain model for microvoid coalescence. (XBL 838-6216)

6. Work in Progress

The role of cyclic frequency on the fatigue threshold stress intensity ΔK_0 is being examined over a change of two orders of magnitude in frequency (5 to 500 Hz) in a bainitic A542 Class-3 pressure vessel steel tested in humid air. Using depth-profiling Auger spectroscopy to characterize crack surface corrosion debris, near-threshold behavior above 50 Hz is found to be insensitive to frequency. This result is consistent with the small amount of measured variation in measured closure loads of oxide debris. However, below 5 Hz, where moisture-induced hydrogen embrittlement becomes significant, ΔK_0 values are decreased, and the corresponding lower crack tip displacements result in

less oxide debris. Such results indicate that, contrary to previous claims, crack-surface oxide debris formation is not necessarily a direct function of frequency but is related to the crack tip opening displacements at ΔK_0 .

1983 PUBLICATIONS AND REPORTS

Refereed Journals

1. R.O. Ritchie, "Why Ductile Fracture Mechanics?" *J. Engineering Materials and Technology, Transactions of ASME Series H* **105** (1), 107 (1983); LBL-13359.
2. S. Suresh and R.O. Ritchie, "On the Influence of Environment on the Load Ratio Dependence of Fatigue Thresholds in Pressure Vessel Steel," *Engineering Fracture Mechanics* **18** (4), 785 (1983); LBL-14280R.
3. H. Nayeb-Hashemi, S. Suresh, and R.O. Ritchie, "On the Contrast between Mode I and Mode III Fatigue Crack Propagation under Variable Amplitude Loading Conditions," *Materials Science and Engineering* **59** (1), L1 (1983); LBL-15690.
4. S. Suresh and R.O. Ritchie, "Some Considerations on the Modelling of Oxide-induced Fatigue Crack Closure Using Solutions for a Rigid Wedge Inside a Linear Elastic Crack," *Scripta Metallurgica* **17** (4), 575 (1983); LBL-15663.
5. J.A. Wasynczuk, R.O. Ritchie, and G. Thomas, "Effects of Microstructure on Fatigue Crack Growth in Duplex Ferrite-martensite Steels," *Materials Science and Engineering* **62** (1983); LBL-14891.
6. S. Suresh, "Micromechanisms of Fatigue Crack Growth Retardation Following Overloads," *Engineering Fracture Mechanics* **18**, 577 (1983); LBL-14482.
7. E.K. Tscheegg, R.O. Ritchie, and F.A. McClintock, "On the Influence of Rubbing Fracture Surfaces on Fatigue Crack Propagation in Mode III," *Int. J. Fatigue* **5** (1), 29 (1983).[†]
8. H. Nayeb-Hashemi, F.A. McClintock, and R.O. Ritchie, "Micro-mechanical Modelling of Mode III Fatigue Crack Growth in Rotor Steels," *Int. J. Fracture* **23** (3), 163 (1983).[†]
9. H. Nayeb-Hashemi, F.A. McClintock, and R.O. Ritchie, "Influences of Overloads and Block Loading Sequences on Mode III Fatigue Crack Propagation in A469 Rotor Steel," *Engineering Fracture Mechanics* **18** (4), 736 (1983).[†]
10. R.O. Ritchie and S. Suresh, "The Fracture Mechanics Similitude Concept: Questions Concerning its Application to the Behavior of Short Fatigue Cracks," *Materials Science and Engineering* **57** (2), L27 (1983).[‡]

LBL Reports

11. J.-L. Tzou, S. Suresh, and R.O. Ritchie, "Fatigue Crack Propagation in Oil Environments: Part I: Crack Growth Behavior in Silicone and Paraffin Oils," submitted to *Acta Met.*, LBL-16028.
12. V.B. Dutta (M.S. Thesis), "Mechanisms of Microstructurally Influenced Fatigue Crack Growth in Dual Phase Steels," LBL-16261.
13. J.-L. Tzou (M.S. Thesis), "Influence of Viscous Environments on Fatigue Crack Propagation in a Lower Strength Steel," LBL-16262.
14. S. Suresh and R.O. Ritchie, "Near-threshold Fatigue Crack Propagation: A Perspective on the Role of Crack Closure," to be published in *Fatigue Crack Growth Threshold Concepts* (TMS-AIME), LBL-16263.
15. V.B. Dutta, S. Suresh, and R.O. Ritchie, "Fatigue Crack Propagation in Dual-phase Steels: Effects of Ferritic-martensitic Microstructures on Crack Path Morphology," submitted to *Met. Trans. A*, LBL-16264.
16. R.O. Ritchie and A.W. Thompson, "On Macroscopic and Microscopic Analyses for Crack Initiation and Growth in Ductile Alloys," submitted to *Met. Trans. A*, LBL-16603.
17. V.B. Dutta, S. Suresh, G. Thomas, and R.O. Ritchie, "Fatigue Resistance and Microstructure of Experimental Dual Phase Fe-2Si-0.1C Steel," to be published in *Fracture Prevention in Energy and Transport Systems* (EMAS), LBL-16681.
18. J.-L. Tzou, C.H. Hseuh, A.G. Evans, and R.O. Ritchie, "Fatigue Crack Propagation in Oil Environments: Part II: A Model for Crack Closure Induced by Viscous Fluids," submitted to *Acta Met.*, LBL-16842.

Other Publications

19. J.-L. Tzou, S. Suresh, and R.O. Ritchie, "Fatigue Crack Propagation in Viscous Environments," in *Mechanical Behavior of Materials, Proceedings of Fourth International Conference (ICM-4)*, Stockholm, Sweden, J. Carlsson and N. G. Olhson, eds., Vol. 2, Pergamon Press, Oxford, 1983, pp. 711-717; LBL-15780.

20. W.J. Salesky, R.M. Fisher, R.O. Ritchie, and G. Thomas, "The Nature and Origin of Sliding Wear Debris from Steels," in *Wear of Materials 1983*, Proc. 3rd Int. Conference, Reston, Virginia, K.C. Ludema, Ed., American Society of Mechanical Engineers, New York, 1983, pp. 434-445; LBL-14482.
21. C.S. White, R.O. Ritchie, and D.M. Parks, "Ductile Growth of Part-through Surface Cracks: Experiments and Analysis," in *Elastic-Plastic Fracture: Vol. 1, Inelastic Crack Analysis*, ASTM STP 803, C.F. Shih and J.P. Gudas, eds., American Society for Testing and Materials, Philadelphia, 1983, pp. I384-I409.[§]
22. S. Suresh, J. Toplosky, and R.O. Ritchie, "Environmentally Affected Near-threshold Fatigue Crack Growth in Steels," in *Fracture Mechanics 14th Symposium: Vol. 1, Theory and Analysis*, ASTM STP 791, J.C. Lewis and G. Sines, eds., American Society for Testing and Materials, Philadelphia, 1983, pp. I329-I347.[§]
23. R.O. Ritchie and S. Suresh, "Mechanics and Physics of the Growth of Small Cracks," in *Behavior of Short Cracks in Airframe Components*, AGARD Conference Proceedings No. 328, North Atlantic Treaty Organization, AGARD, France, 1983, pp. 1.1-1.14.[‡]
30. R.O. Ritchie, "Recent Advances in the Characteristics and Interpretation of Fatigue Crack Propagation," Golden Gate Chapters of ASM and AWS, Berkeley, March 1983.
31. R.O. Ritchie, "Principles of Environmentally Assisted Failure," Department of Aeronautical Structures, Royal Institute of Technology, Stockholm, Sweden, March 1983.
32. R.O. Ritchie, "Near-threshold Fatigue," Royal Institute of Technology, Stockholm, Sweden, March 1983.
33. R.O. Ritchie, "Plane Strain Crack Closure Mechanisms," Aeronautical Research Institute of Sweden (FFA), Stockholm, March 1983.
34. R.O. Ritchie, "Corrosion Fatigue Crack Propagation at Ultralow Growth Rates," Linkoping University, Linkoping, Sweden, March 1983.
35. R.O. Ritchie, "The Development of Fracture Mechanics," Kungliga Tekniska Hogskolam, Stockholm, Sweden, April 1983.
36. R.O. Ritchie, "Design of Low Alloy Steels for Thick Walled Pressure Vessels," AR & TD Fossil Fuel Energy Materials Program, Department of Energy, Germantown, Maryland, May 1983.
37. S. Suresh and R.O. Ritchie, "A Perspective on the Role of Crack Closure," TMS-AIME Fall Meeting, Philadelphia, October 1983.
38. R.O. Ritchie and S. Suresh, "Environmental Effects on Fatigue Crack Propagation," TMS-AIME Fall Meeting, Philadelphia, October 1983.

Invited Talks

24. R.O. Ritchie, "The Problem of Short Cracks in Fatigue," Stanford University, Stanford, California, January 1983.
25. R.O. Ritchie, "The Role of Oxide Wedges Inside Fatigue Cracks," University of California Davis, February 1983.
26. R.O. Ritchie, "Advanced Techniques in Mechanical Testing," ASM Pre-conference Seminar, Golden Gate Welding and Metals Conference, San Francisco, February 1983.
27. J.-L. Tzou, S. Suresh, and R.O. Ritchie, "Influence of Viscous Environments on Fatigue Crack Propagation in Lower Strength Steel," 112th Annual Meeting of AIME, Atlanta, March 1983.
28. J.A. Wasynczuk, R.O. Ritchie, and G. Thomas, "Effects of Microstructure on Fatigue Crack Growth in Duplex Ferrite-martensite Steels," 112th Annual Meeting of AIME, Atlanta, March 1983.
29. R.O. Ritchie, "Advances in Fatigue Research," Industrial Liaison Conference, University of California Berkeley, March 1983.
39. R.O. Ritchie, "Relevance of Crack Closure to Proposed Standard for Fatigue Crack Growth Testing below 10^{-9} m/cycle," ASTM Fall Conference, Pittsburgh, November 1983.
40. R.O. Ritchie, "Advances in Research on Near-threshold Fatigue," Carnegie-Mellon University, Pittsburgh, November 1983.
41. V.B. Dutta, G. Thomas, S. Suresh, and R.O. Ritchie, "The Design of Improved Near-threshold Fatigue-resistant Steels," Conference on Fracture Prevention, Rio de Janeiro, Brazil, November 1983.
42. R.O. Ritchie, "Fracture Mechanics and Fatigue," University of California Los Angeles, December 1983.

[†]Supported in part by the Division of Energy Conservation, U.S. Department of Energy, under Contract No. EX-76-A-01-2295, TO 51.

[‡]Supported by the Air Force Office of Scientific Research under Grant No. AFOSR-82-0181.

[§]Supported in part at M.I.T. by the Office of Basic Energy Sciences of the U.S. Department of Energy under Contract No. DE-AC02-79ER10389.

PHYSICAL PROPERTIES

Interfaces and Ceramic Microstructures*

Joseph A. Pask, Investigator

INTRODUCTION

The purpose of this work is to advance the basic understanding of the nature of interfaces (primarily those between dissimilar materials, such as metals and ceramics), particularly in terms of bonding and the factors that control the development of adherence. This understanding is critical to the development of composites, protective coatings, and glass/ceramic-to-metal seals, and to the reduction of corrosion at interfaces. The work involves studies of thermodynamics and kinetics of reactions at interfaces, and wetting and spreading of liquids.

Another objective in this work is to advance the understanding of the factors that play roles in the development of desired microstructures in ceramic materials, with and without a liquid phase. This understanding depends on a knowledge of the stable and metastable phase equilibrium of interfacial phenomena from a thermodynamics point of view and of mass-transport mechanisms during sintering.

1. Sintering of α -Al₂O₃/Quartz and α -Al₂O₃/Cristobalite Related to Mullite Formation (Publication 1)

Amar P.S. Rana, Osamu Aiko,[†] and Joseph A. Pask

Cristobalite and quartz react differently in mixtures with α -Al₂O₃ at 1415°C. With cristobalite a eutectic liquid forms in accordance with the metastable phase-equilibrium diagram for α -Al₂O₃/SiO₂ (cristobalite) in the absence of mullite. With quartz

a liquid first forms on the surface of quartz because of the occurrence of an intermediate liquid phase on the transformation of quartz to cristobalite. These liquids act as precursors to the formation of mullite by reacting with α -Al₂O₃. Mullite was detected earlier in the cristobalite-containing mixtures under similar firing conditions, because the growth of mullite becomes significant with the formation of the eutectic liquid at the α -Al₂O₃/cristobalite interface since it is already saturated with Al₂O₃. The kinetics of sintering are affected by the rates of the step reactions.

[†]Present address: Asahi Glass Co., Yokohama, Kanagawa, Japan.

2. Influence of Surface-silica Impurities on the Sintering Behavior of Alumina Powders (Publication 10)

Jose Moya and Joseph A. Pask

Impurities generally have a significant effect on the sintering of a ceramic powder. An alumina powder with a surface-silica impurity was studied. When the silica was removed by HF treatment, the compactibility was considerably enhanced because of the modification of the hydration characteristics of the surface. The presence of silica, however, improves the densification process on sintering by decreasing the activation energy of the initial stage of sintering and exerting a moderate inhibitor effect on the grain growth.

3. Effect of Water Vapor on Sintering of Ceramic Oxides (Publication 9)

Joseph A. Pask

Increased rates of densification, i.e. shrinkage, in the initial and intermediate stages of sintering of ceramic powders in the presence of water vapor have been reported by a number of investigators. In this

*This work was supported by the Director, Office of Energy Research, Office of Basic Energy Sciences, Materials Sciences Division of the U.S. Department of Energy under Contract No. DE-AC03-76SF00098.

study the thermodynamic driving forces and mechanisms of mass transport affected by the presence of water vapor were examined.

Densification is the result of mass transport associated with redistribution of material to eliminate the pore volume. The overall process can be considered as having two steps: (1) movement of material from the grain boundaries forming between particles to the neck regions, and (2) movement from the neck regions to the free solid/vapor surfaces. The slower of these two steps determines the kinetics for the overall sintering process. The thermodynamic driving force for mass transport in step (1) is chemical-potential gradients for vacancies generated by initial nonequilibrium solid/vapor/solid dihedral angles that increase and approach equilibrium values with densification. In step (2) the driving force is chemical-potential gradients for vacancies generated by reverse curvatures of solid/vapor surfaces in the neck-pore region.

In the absence of water vapor, step (2) is the slow step, allowing the formation of necks at particle/particle contacts. In the presence of water vapor, step (1) can become the slow step if water vapor increases surface diffusion, thus preventing the formation of necks. If diffusion is not increased, the surface energy is decreased, which causes a decrease in the thermodynamic driving force for sintering.

4. Solid-solution Range and Microstructures of Melt-grown Mullite (Publication 5)

Waltraud M. Kriven[†] and Joseph A. Pask

The solid-solution range of melt-grown mullite was examined by crystal-chemical methods. The maximum Al_2O_3 content as determined by EDAX was ≈ 83.6 wt% (75 mol%), or the nominal composition of $3\text{Al}_2\text{O}_3 \cdot \text{SiO}_2$. For samples with an overall composition of 81 to 83 wt% Al_2O_3 , extra lines indicating crystallographic superstructures appeared in Guinier x-ray patterns. The corresponding transmission electron-microscopy microstructure consisted of a mullite matrix finely twinned on (001), the twins being 0.02 to 0.10 μm wide, with an oriented exsolution of $\alpha\text{-Al}_2\text{O}_3$, often twinned, also being present. An analogy was developed between the mullite superstructure and that of plagioclase feldspars. The relevance of these findings to the $\text{SiO}_2/\text{Al}_2\text{O}_3$ metastable-phase equilibria was shown.

[†]Present address: Department of Ceramic Engineering, University of Illinois, Urbana, Illinois.

5. Wetting of Nickel by Silver (Publication 4)

V.K. Nagesh[†] and Joseph A. Pask

Sessile-drop experiments of molten silver on nickel were performed in air and helium at 970°C. A NiO layer formed at the interface in air; silver formed a 90° contact angle. In helium, silver formed a 9° contact angle on nickel. Solution reactions played a role in forming the angles.

[†]Present address: Hewlett-Packard Co., Palo Alto, California.

6. Work in Progress

Studies are continuing on reactions between metals and glass. The complexity of the reactions increases as the oxidation potential of the substrate metal increases. A result of redox reactions is saturation of the interface with the oxide of the substrate. Such a result leads to thermodynamic equilibrium and chemical bonding at the interface that can be stated as a theory. Particular attention is being addressed to the $\text{Cr}/\text{Na}_2\text{Si}_2\text{O}_5$ system.

1983 PUBLICATIONS AND REPORTS

Refereed Journals

1. A.P.S. Rana, O. Aiko, and J.A. Pask, "Sintering of $\alpha\text{-Al}_2\text{O}_3$ /Quartz and $\alpha\text{-Al}_2\text{O}_3$ /Cristobalite Related to Mullite Formation," *Ceramics International* **8**, 151 (1982); LBL-12458.
2. Y. Oishi, M. Nanba, and J.A. Pask, "Analysis of Liquid-state Interdiffusion in the System $\text{CaO-Al}_2\text{O}_3\text{-SiO}_2$ Using Multiatomic Ion Models," *J. Am. Ceram. Soc.* **65**, 247 (1982).
3. V.K. Nagesh, A.P. Tomsia, and J.A. Pask, "Wetting and Reactions in the Lead Borosilicate Glass - Precious Metal Systems," *J. Mater. Sci.* **18**, 2173 (1983); LBL-15614.
4. V.K. Nagesh and J.A. Pask, "Wetting of Nickel by Silver," *J. Mater. Sci.* **18**, 2665 (1983); LBL-15023.
5. W.M. Kriven and J.A. Pask, "Solid Solution Range and Microstructures of Melt-grown Mullite," *J. Am. Ceram. Soc.* **66**, 649 (1983); LBL-14679.

LBL Reports

6. D.J. Miller and J.A. Pask, "Liquid Phase Sintering of TiC-Ni Composites," *J. Am. Ceram. Soc.*, in press, LBL-16419.

Other Publications

7. H.K. Bowen and J.A. Pask, "Learning from Japan's Developments in High Technology Ceramics," *Bull. Am. Ceram. Soc.* **61**, 916 (1982).
8. J.A. Pask, "Current Understanding of Stable and Metastable Phase Equilibria and Reactions in the $\text{SiO}_2/\alpha\text{-Al}_2\text{O}_3$ System," in *Ceramic Powders*, Vincenzini, Ed., Elsevier Scientific

Publishing Co., Amsterdam, Netherlands, 1983, p. 21; LBL-14678.

9. J.A. Pask, "Effect of Water Vapor on Sintering of Ceramic Oxides," in *Proc. First Int. Symp. on Hydrothermal Reactions*, S. Somiya, Ed., Tokyo Institute of Technology, Tokyo, Japan, 1983, p. 904.
10. J.S. Moya and J.A. Pask, "Influence of Surface Silica Impurities on the Sintering Behavior of Alumina Powders," in *Reactivity of Solids — Materials Science Monograph 10 (Proc. 9th Int. Symp. on Reactivity of Solids, Cracow, 1980)*, K. Dyrek, J. Huber, and J. Nowotny, eds., Elsevier Scientific Publishing Co., Amsterdam, Netherlands, 1982, p. 440; LBL-10392.

High-Temperature Reactions*

Alan W. Searcy, Investigator

INTRODUCTION

The central program objective is to deepen scientific understanding of the kinetics and thermodynamics of high-temperature reactions. Recent emphasis has been on endothermic decomposition reactions (e.g., $\text{CaCO}_3 \rightarrow \text{CaO} + \text{CO}_2$), for which the level of fundamental understanding is exceptionally low despite extensive study. A general theoretical framework for analysis of decomposition-reaction kinetics was developed under this project. With this background a systematic investigation has been conducted on the separate influences of temperature, product-gas pressure, thermal-energy balance, particle size, sample size, and catalysts on decomposition rates and on the structure and properties of solid reaction products. Transmission electron-microscope (TEM) studies of prototype decomposition reactions will complete this phase of the program, and studies of the more complex reactions of the kind illustrated by $\text{BaCO}_3 + \text{TiO}_2 \rightarrow \text{BaTiO}_3 + \text{CO}_2$ are planned. A concurrent investigation of vapor transport through porous solids is being used to obtain quantitative data on high-temperature surface diffusion. Theoretical and experimental studies of surface thermodynamics, chemisorption, and surface-transport processes are receiving increased emphasis. An important objective of the surface studies is to develop a model for the kinetics of molecular exchange between regions of different bond energies in an equilibrium particle.

1. Surface Diffusion of High-temperature Vapors in Porous Alumina (Publication 7)

Elizabeth J. Opila and Alan W. Searcy

The purposes of this study were to determine (a) whether surface diffusion contributed significantly to the transport of zinc vapor through porous aluminas of 0.6- μm and 0.07- μm average pore radii and (b) whether interactions between Zn gas and S_2 gas

perhaps form adsorbed ZnS molecules to modify their rate of transport on alumina surfaces.

Zinc-vapor fluxes through the barriers were determined by a weight-loss technique. The flux of helium through the alumina was also determined from the leak rate at room temperature. After correction for molecular-weight differences, any flux of zinc greater than that of helium was attributed to surface diffusion. In all experiments Knudsen flow was operative in the gaseous phase. The ratio of surface flux to Knudsen flux for $\text{Zn}_{(g)}$ from $\text{Zn}_{(s)}$ in alumina of 0.6- μm average pore size at 647 K was 2.5.

Using alumina of 0.07- μm average pore radius raised the ratio of surface flux to volume flux in proportion to the inverse of the average pore radius, as predicted. The flux of zinc vapor from $\text{Zn}_{(s)}$ at 592 K, and from $\text{Zn}_{(s)}$ at 1092 K where P_{Zn} was nearly equal, was measured using alumina of 0.6- μm average pore radius. The ratio of surface flux to Knudsen flux for zinc was the same in the two experiments. It was concluded that the presence of $\text{S}_{2(g)}$ had no observable effect on the diffusion of zinc vapor in porous alumina.

2. The Thermodynamics and Kinetics of CO_2 Chemisorption on CaO (Publication 9)

Dario Beruto,[†] Rodolfo Botter,[†] and Alan W. Searcy

Equilibrium chemisorption of CO_2 on CaO was measured at 923 to 1013 K, and the kinetics of rapid adsorption and slow dissolution of CO_2 into the CaO, perhaps as CO_3^- at grain boundaries, were measured in 1333 Pa of CO_2 at 983 to 1033 K. Surface areas were measured by the Brunauer-Emmett-Teller (BET) method.

Figure 2-1 shows that equilibrium could be reproduced in desorption and adsorption. From the assumptions that only (100) surfaces of the CaO were exposed and that CO_2 reacted with surface O^- ions to form CO_3^- ions, surface coverage was calculated to approach a complete monolayer. The enthalpy of adsorption was -199 ± 8 kJ/mole, and the thermal entropy of adsorption was -153 ± 8 kJ/mole-deg. Both values were somewhat less negative at $>80\%$ coverage. The apparent activation enthalpy for adsorption was 61 ± 10 kJ/mole. CO_2 was dissolved in the CaO grain boundaries or crystals by a process with an apparent activation enthalpy of 303 ± 15 kJ/mole CaO.

*This work was supported by the Director, Office of Energy Research, Office of Basic Energy Sciences, Materials Sciences Division of the U.S. Department of Energy under Contract No. DE-AC03-76SF00098.

[†]Present address: Instituto Chimica, Faculta di Ingegneria, Universita de Genoa, Italy.

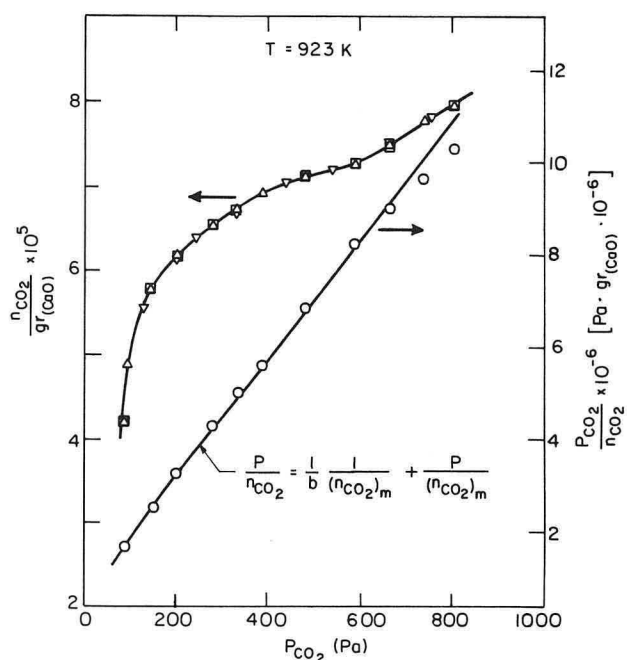


Figure 2-1. Left scale and left curve: number of moles of CO_2 taken up per gram of CaO as a function of P_{CO_2} . The triangles and inverted triangles are desorption measurements, and the boxes are adsorption measurements. Right scales and right curve: fit of the data to a Lungmues isotherm. (XBL 838-6193)

3. Effect of Li_2CO_3 on the Reaction of CO_2 with CaO (Publication 10)

D. Beruto,[†] M.G. Kim, and L. Barco[†]

LiCl , LiBr , NaCl , CaCl_2 , and Li_2CO_3 have been demonstrated in our laboratories to increase the rate of calcite decomposition by 2–5 times, presumably because liquid-phase reaction paths are provided. We report here the effect of Li_2CO_3 on the reverse reaction of CO_2 with low-surface-area CaO at temperatures below, near, and above the Li_2CO_3 - CaCO_3 eutectic temperature (935 K).

Commercial reagent-grade CaO and Li_2CO_3 powders of about 3- μm particle size were used throughout the experiments. Differential thermal analysis and thermogravimetric experiments were done simultaneously using alumina crucibles. The kinetic measurements were supplemented by scanning electron-microscope (SEM) observations of morphologies, BET surface-area measurements, and measurements of the heat effects in a differential thermal analysis (DTA).

Figure 3-1 shows the fraction carbonated as a function of temperature with a constant heating rate.

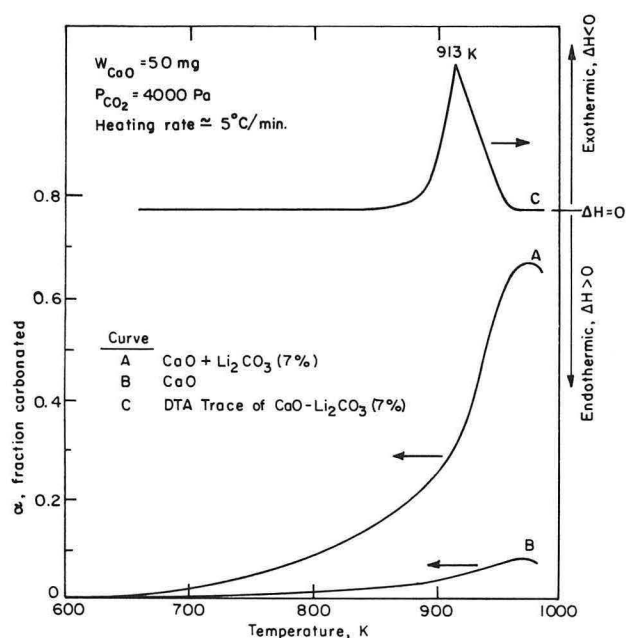


Figure 3-1. Dynamic carbonation of CaO with 7% Li_2CO_3 (A) and without Li_2CO_3 (B). DTA trace for carbonation of CaO with 7% Li_2CO_3 at 913 K (C). (XBL 837-6038A)

At 913 K, if Li_2CO_3 was present an exothermic reaction occurred and the rate of reaction increased rapidly. Probably the highest reaction rate resulted from the formation of the Li_2CO_3 - CaCO_3 eutectic-liquid phase, because DTA analyses on CaO - Li_2CO_3 and CaO - Li_2CO_3 - CaCO_3 showed no heat effect but Li_2CO_3 - CaCO_3 melting, and rapid exothermic carbonation would provide local heating to the eutectic temperature of 945 K. When the Li_2CO_3 content was varied, the maximum degree of carbonation was achieved with about 15% Li_2CO_3 addition. SEM observations of a sample containing 10% Li_2CO_3 and carbonated at 963 K showed calcite-crystal growth, while a sample containing 57% Li_2CO_3 did not. This result implies that, at temperatures where the Li_2CO_3 - CaCO_3 eutectic can form, the CaCO_3 , which forms a protective coating of CaO , is dissolved and reprecipitated as large CaCO_3 crystals, and the reaction proceeds on the CaO surface with a high rate. If enough Li_2CO_3 is present so that the liquid does not become saturated with CaCO_3 , the liquid content of the sample increases as the reaction proceeds, and the liquid phase itself acts as a protective coating.

[†]Present address: Instituto Chimica, Faculta di Ingegneria, Universita de Genoa, Italy.

4. Effects of Particle Size and Shape on Vapor Pressure (Publication 8)

Alan W. Searcy

Thermodynamic theory treats equilibrium in fluid phases separated by an interface as requiring a balance of pressures in each phase with an isotropic tension in the interface. This mechanical model for surface thermodynamics follows from two assumptions in Gibbs' development of surface thermodynamic theory: (1) The influence of interfaces on adjacent phases is limited to regions close to the physical interface. (2) Surfaces are under isotropic tension. The first assumption is shown to be inconsistent with accepted concepts for adsorbed film-vapor equilibrium, and the second assumption is shown to be unnecessary. The predictions of each of two alternate assumptions are used to derive equations for particle-vapor equilibrium. The assumptions are (1) that $(\partial G_p/\partial n)_{T,P} = \mu_v$, where G_p is the particle free energy, n is the number of molecules in the particle, and μ_v is the chemical potential of the vapor; and (2) that $G_p/n = \mu_v$. Either model is shown to yield predictions that agree within reasonable error limits with experimental observations. Reasons are given for preferring the assumption $G_p/n = \mu_v$.

5. On the Nature of the Crystallographic Disorder in Submicrometer Particles of $\text{Ca}(\text{OH})_2$ Produced by Vapor-phase Hydration (Publication 3)[†]

*D. Beruto,[‡] G. Spinolo,[§] L. Barco,[‡]
U. Anselmi Tamburini,[§] and G. Belleri[‡]*

Poorly crystalline forms of $\text{Ca}(\text{OH})_2$ can be produced by the reaction of water vapor at room temperature with CaO powders; these forms are highly reactive toward liquids and gases. Nitrogen-adsorption isotherms, x-ray broadening analysis, and SEM observations were made on different samples either before or after a thermal treatment (essentially an irreversible process) that transforms these hydroxides into more crystalline materials. It is shown that the vapor-phase hydration yields not only small-size particles and high porosities but also crystallographic

defects, and that the irreversible transformation is mainly connected to a recovery of defects.

[†]Supported in Italy by the Italy-USA Exchange Program of the Consiglio Nazionale della Ricerche and the NSF and in the USA by the Division of Materials Sciences, Office of Basic Energy Sciences.

[‡]Present address: Istituto Chimica, Faculta di Ingegneria, Universita de Genoa, Italy.

[§]Present address: Istituto di Chimica Fisica & di Electrochimica della Universita, Pavia, Italy.

6. Interactions of LiBr with Calcite and Calcium Oxide Powders (Publication 4)[†]

D. Beruto,[‡] G. Belleri,[‡] L. Barco,[‡] and V. Longo[§]

The interactions of LiBr with calcite and calcium oxide powders have been studied with and without the calcite decomposition reaction, using DTA and TG analysis plus SEM and RX observations. The LiBr- CaCO_3 system showed two possible phase transformations at 748 and 786 K. The second transformation is due to the formation of a eutectic-liquid phase in the LiBr-rich region. The decomposition rate of calcite powders was measured in dry nitrogen and in a high partial pressure of CO_2 with and without LiBr. The addition of LiBr causes the decomposition reaction to occur at a lower temperature and changes the mechanism of the reaction. The decomposition process occurs through a liquid-phase path given by the eutectic of LiBr- CaCO_3 . The total of reaction rate and the temperature dependence are related to the liquid phase. The CaCO_3 powders obtained have a very dense structure with a high degree of crystallization. Probably the LiBr- CaO eutectic provides a solution path for CaO recrystallization. The effectiveness of salt addition in lowering the decomposition temperature of carbonates seems promising in saving energy, as well as in promoting changes in morphology of important commercial oxide powders.

[†]Supported in Italy by the Italy-USA Exchange Program of the Consiglio Nazionale della Ricerche and the NSF and in the USA by the Division of Materials Sciences, Office of Basic Energy Sciences.

[‡]Present address: Istituto Chimica, Faculta di Ingegneria, Universita de Genoa, Italy.

[§]Present address: Istituto di Chimica Fisica & di Electrochimica della Universita, Pavia, Italy.

7. Work in Progress

The CO_2 decomposition pressures generated by MgCO_3 in Knudsen cells is under investigation for comparison with the anomalous decomposition pressures already measured for CaCO_3 and Mg(OH)_2 . *In situ* TEM measurements are being made of Mg(OH)_2 , MgCO_3 , and their solid products in an effort to determine if transient solid products are responsible for observations of anomalously low decomposition pressures. Measurements are being made of the CO_2 contents of the $\text{MgO}(\text{CO}_2)_{1-\delta}$ and $\text{MgO}-\text{CaO}(\text{CO}_2)_{2-\delta}$ phases as functions of CO_2 pressures and temperatures.

The high-temperature surface diffusion of Cd vapor through porous alumina with and without S_2 vapor present is under study.

At Genoa, Dario Beruto will initiate a joint study on the chemisorption of CO_2 on MgO . Particular emphasis will be placed on determining the effect of very small particles on the shape of CO_2 and N_2 adsorption isotherms when monolayer coverage is approached and the effect of MgO -particle size and shape on the equilibrium decomposition pressure of MgCO_3 . These effects are of use in testing models for the influences of particle size and shape on thermodynamic activity.

Theoretical studies are nearing completion on the influence of particle shapes on stabilities of fcc solids which have 6/12 Leonard Jones potentials (with S.W. Wang and Leo Falicov), and on the thermodynamic stabilities derived for crystalline particles from the assumption that molecular fluxes must be equal between surface regions of different bonding energies (e.g., between edges and adjacent surfaces).

1983 PUBLICATIONS AND REPORTS

Refereed Journals

1. Alan W. Searcy, "The Equilibrium Shapes of Crystals and of Cavities in Crystals," *J. Solid State Chem.* **48**, 93-99 (1983).
2. Alan W. Searcy, Dario Beruto, and Luigi Barco, "Rearrangement of Porous CaO Aggregates During Calcite Decomposition in Vacuum," *J. Am. Ceram. Soc.* **66**, 893 (1983).
3. D. Beruto, G. Spinolo, L. Barco, U. Anselmi Tamburini, and G. Belleri, "On the Nature of the Crystallographic Disorder in Submicrometer Particles of Ca(OH) Produced by Vapor Phase Hydration," *Ceram. Int.* **9**, 22 (1983).[†]

4. D. Beruto, G. Belleri, L. Barco, and V. Longo, "Interactions of LiBr with Calcite and Calcium Oxide Powders," *Ceram. Int.* **9**, 53 (1983).[†]

LBL Reports

5. T.A. Reis, "Thermodynamic Anomaly in Magnesium Hydroxide Decomposition," LBL-15725.
6. J.N. Farnsworth (M.S. Thesis), "Gas Flow through Porous Barriers; the O_2 -Pt, CO -Pt Systems," LBL-15724.
7. E.J. Opila (M.S. Thesis), "Surface Diffusion of High Temperature Vapors in Porous Alumina," LBL-16735.
8. A.W. Searcy, "Effects of Particle Size and Shape on Vapor Pressure," LBL-15533.
9. D. Beruto, R. Botter, and A.W. Searcy, "The Thermodynamics and Kinetics of CO_2 Chemisorption on CaO ," LBL-16589.
10. D. Beruto, M.G. Kim, L. Barco, and A.W. Searcy, "Effect of Li_2CO_3 on CaO and CO_2 Reaction," LBL-16459.
11. D. Beruto, L. Barco, and A.W. Searcy, " CO_2 -catalyzed Surface Area and Porosity Changes in High Surface Area CaO Aggregates," accepted by *J. Am. Ceram. Soc.*, LBL-17191.

Other Publications

12. A.W. Searcy, M.G. Kim, and D. Beruto, "The Kinetics of Decomposition in Powder Beds: Theory and Experiment," *Proc. Symposium on High Temperature Materials Chemistry — II*, Z.A. Munier and D. Cubicciotti, eds., The Electrochemical Society, Pennington, New Jersey, 1983, pp. 133-142; LBL-16069.

Invited Talks

13. A.W. Searcy, M.G. Kim, and D. Beruto, "The Kinetics of Decomposition in Powder Beds: Theory and Experiment," *Symposium on High Temperature Materials Chemistry — II*, Electrochemical Society Meeting, San Francisco, California, May 1983.
14. D. Beruto, M.G. Kim, and L. Barco, "The Effect of Lithium Carbonate on the Reaction of CaO Powder with CO_2 ," 6th International Symposium on Ceramics, Bologna, Italy, September 26-29, 1983.

[†]Supported in Italy by the Italy-USA Exchange Program of the Consiglio Nazionale della Ricerche and the NSF and in the USA by the Division of Materials Sciences, Office of Basic Energy Sciences.

Structure-Property Relationships in Semiconductor Materials*

Jack Washburn, Investigator

INTRODUCTION

The purpose of this research program is to advance the understanding of structural defects including the structure of interfaces in semiconductor materials. Particular emphasis is placed on interfaces and defects that are formed during processing steps used for state-of-the-art solid-state-device manufacture such as ion implantation, oxidation, and contact formation. This approach has also led to several areas of basic research: for example, a continuing series of experiments aimed at a more complete understanding of the mechanism of the crystalline-to-amorphous transformation during ion damage in silicon and gallium arsenide, an investigation of the detailed mechanism of crystal growth into amorphous zones, and a study of the growth of Cu_2S layers on the surface of CdS.

High-resolution lattice-imaging electron microscopy combined with computer simulation of the images has been shown to be a powerful tool for revealing and interpreting fine-scale defects and interface structures, particularly when used in conjunction with complementary observations on the same specimens such as Rutherford backscattering measurements, secondary ion mass spectroscopy, and electrical or optical measurements.

The new atomic-resolution microscope promises to extend the limits of detection to even smaller defects, perhaps making possible more direct correlations between the presence of specific structural defects and their electrical effects.

1. High-resolution Imaging of Oxidized Stepped Silicon Surfaces (Publication 5)

J.H. Mazur and J. Washburn

The Si-SiO₂ system has been the subject of extensive investigation because of its importance for MOS electronic devices. However, an understanding of the correlation between electronic processes, the structure of the Si-SiO₂ interface, and the mechanism of oxidation is still lacking. This study is part of a larger research program that attempts to establish an atomistic model of the Si-SiO₂ interface structure and to clarify the mechanism of oxidation.

In this experiment, the p-type boron-doped 7-17 Ω cm Si wafers used for oxidation had a surface orientation 3° off {111} towards {110}. The wafers were cleaned before oxidation using the RCA procedures. Cleaning was followed by immediate oxidation to various thicknesses ranging from 200 to 1000 Å at 1000°C in dry O₂. Cross sections with a normal parallel to the (101) direction of the Si substrate were prepared for transmission electron microscopy (TEM) using standard procedures. These TEM specimens of thermally grown and native oxides were imaged with point-to-point resolution of 2.6 Å using a JEM200CX electron microscope operating at 200 kV.

Figure 1-1a shows a high-resolution electron-microscope (HREM) image of the Si-SiO₂ interface. The images were taken near a Scherzer focus (-660 Å). Optical diffractograms (Figure 1-1b) and selected-area diffraction (SAD) patterns (Figure 1-1c) demonstrate experimental imaging conditions.

The image in Figure 1-1a indicates the amorphous character of thermally grown oxide. The image shows that {111} planes are inclined 3° off the interface plane. The Si substrate terminates abruptly

*This work was supported by the Director, Office of Energy Research, Office of Basic Energy Sciences, Materials Sciences Division of the U.S. Department of Energy under Contract No. DE-AC03-76SF00098.

at $\{111\}$ terraces with ledges one interplanar distance (3.14 \AA) high. The length of each terrace is close to the calculated value (60 \AA) for a surface orientation 3° from the $\{111\}$ planes. The interpretation of these images in terms of the stepped surface of the Si crystal in contact with the oxide is shown in Figure 1-2. The height of the ledges and the lengths of the terraces were observed to be independent of the temperature and time of the oxidation.

phase is low chalcocite (Cu_2S). A small amount of copper loss due to nonoptimum formation conditions, in-service oxidation, or electromigration under load results in the formation of djurleite ($\text{Cu}_{1.97}\text{S}$) and a corresponding reduction in cell efficiency. The structures of both low chalcocite and djurleite are based on an hcp sulfur network. However, further copper loss encourages the nucleation and growth of low digenite ($\text{Cu}_{1.82}\text{S}$), a metastable phase based on

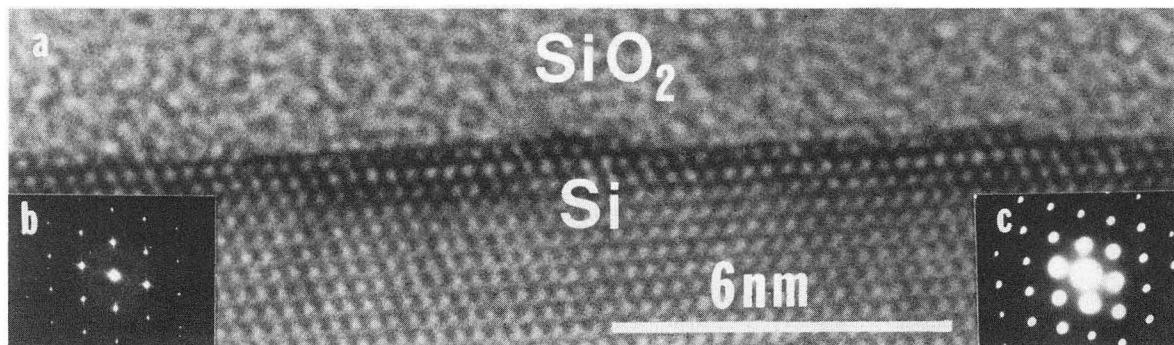


Figure 1-1. (a) HREM image of the Si-SiO₂ interface. The silicon surface orientation is 3° off the (111) plane. The oxide was thermally grown to 1000 \AA thick. (b) Optical diffractogram of the same image. (c) $[10\bar{I}]$ SAD pattern from the specimen imaged in (a). (XBB 832-1793C)

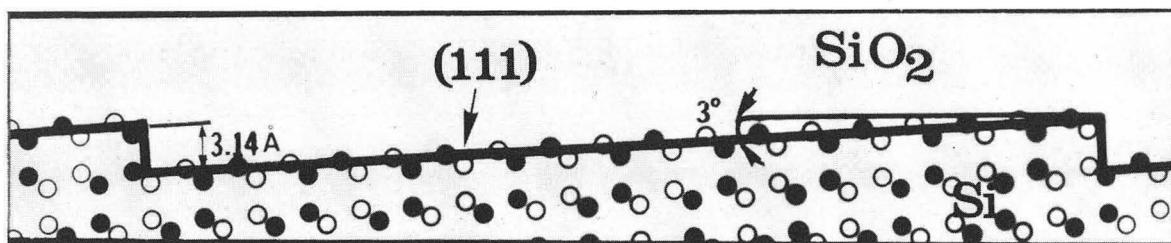


Figure 1-2. Model of the stepped Si-SiO₂ interface. (XBB 832-1793B)

2. Degradation Mechanisms of $\text{Cu}_{2-x}\text{S}/\text{CdS}$ Solar Cells as Revealed by High-resolution Electron Microscopy (Publication 4)

T. Sands and J. Washburn

A major factor preventing the production of inexpensive and efficient p- $\text{Cu}_2\text{S}/\text{n-CdS}$ thin-film solar cells is the inherent sensitivity of the electronic and optical properties of the copper sulfide layer to small changes in composition. This layer can act as an efficient absorber-emitter only if the predominant

an fcc sulfur network.

This study addresses the problem of determining the dominant factors influencing these degradation transformations so that methods to produce more stable layers or device configurations can be systematically developed. High-resolution transmission electron-microscope (HRTEM) images have revealed the structural characteristics of both the low-chalcocite/djurleite and the djurleite/low-digenite transformations.

The degradation sequence starts with the most copper-rich phase, low chalcocite. Exposure to room-temperature air for 4 days leads to the forma-

tion of djurleite domains. Djurleite was found to nucleate coherently at cracks in the low chalcocite films. The relative orientations and shapes of the djurleite domains were observed to be consistent with the minimization of interfacial-lattice misfit. The low-chalcocite-to-djurleite transformation has been shown to proceed by the ordering of copper-vacancy clusters, leaving the sulfur network intact. Further degradation results in the fcc low-digenite phase. The djurleite-to-low-digenite transformation requires the propagation of Shockley partial dislocations on every other close-packed plane, thereby transforming the sulfur network from hcp to fcc.

3. Annealing of Interstitial Loops in Arsenic-implanted Silicon (Publication 6)

N.R. Wu, P. Ling, D.K. Sadana, and J. Washburn

The annealing effects of different gas ambients (N_2 or O_2) on high-dose ($5 \times 10^{15}/cm^2$) arsenic-implanted Si have been investigated by cross-section transmission electron microscopy. The following are the major conclusions:

(1) Two-layer secondary-defect structures are formed during annealing for both O_2 - and N_2 -annealing ambients. (2) The layer of defects closest to the surface was interpreted as As precipitates in the form of hexagonal platelets about 200 Å across, giving rise to electron-diffraction contrast similar to a faulted $1/3 \langle 111 \rangle$ dislocation loop. (3) The deeper-layer defects were shown to be interstitial $1/2 \langle 110 \rangle$ dislocation loops originating from the regrowth of amorphous islands and clustering of excess interstitials below the continuous amorphous-crystalline interface. (4) During annealing in an oxygen atmosphere, growth of interstitial loops was accelerated, suggesting that oxidation occurring at the surface results in interstitial supersaturation. (5) Injection of oxygen during a through-oxide implant resulted in pinning of dislocations and inhibited both growth and shrinkage of the secondary defects during annealing.

4. High-resolution Electron-microscopy Studies of Native Oxide on Silicon (Publication 1)

J.H. Mazur, R. Gronsky, and J. Washburn

This abstract is described in entry 3 under "Structure and Properties of Transformation Interfaces," Ronald Gronsky, Investigator.

5. Work in Progress

Amorphization and recrystallization mechanisms in ion-implanted GaAs are being explored with cross-sectional high-resolution transmission electron microscopy (XHRTEM). Lattice images of as-implanted GaAs cross sections reveal an amorphous-crystalline transition region consisting of well-defined pockets of crystalline material in an amorphous matrix. During low-temperature ($400^\circ C$) annealing, these crystalline pockets act as seeds for epitaxial regrowth. A second regrowth stage begins when the seeds are consumed by the advancing interface to form a simply connected and faceted amorphous-crystalline interface. Stacking-fault bundles propagate from these facets, seriously degrading the structural integrity of the regrown layer. Further work will concentrate on determining the factors which influence stacking-fault nucleation (e.g. impurity clustering and local nonstoichiometry).

Copper sulfide/cadmium sulfide photovoltaic interfaces have been imaged for the first time by the XHRTEM technique. The surface orientation has been found to have a dramatic effect on the copper sulfide phases present at the interface. In terraced off-basal surfaces, a metastable high-pressure polymorph of the stable copper sulfide phase forms at the interface in order to reduce the gradient in the lattice parameter between Cu_2S and CdS . These observations are being used to develop an understanding of the relationship between photovoltaic-cell efficiency and processing variables (e.g. CdS surface preparation and post-barrier heat treatments).

1983 PUBLICATIONS AND REPORTS

Refereed Journals

1. J.H. Mazur, R. Gronsky, and J. Washburn, "High-resolution Electron Microscopy Studies of Native Oxide on Silicon," *Inst. Phys. Conf. Ser. No. 67: Section 2*, p. 77 (1983); LBL-16272.
2. J. Washburn and D.K. Sadana, "Megavolt Electron Induced Regrowth of Amorphous Zones in Silicon," *J. Appl. Phys.* **54**, 2380 (1983); LBL-15487.
3. D.K. Sadana, S. Shatas, and A. Gat, "HEAT-PULSE Annealing of Ion-implanted Silicon; Structural Characterization by Transmission Electron Microscope," *Inst. Phys. Conf. Ser. No. 67: Section 3*, p. 143 (1983); LBL-17320.

Other Publications

4. T. Sands, "Degradation Mechanisms of $\text{Cu}_{2-x}\text{S}/\text{CdS}$ Solar Cells as Revealed by High Resolution Electron Microscopy," *Proc. 41st Annual Meeting of the Electron Microscopy Society of America*, San Francisco Press, Inc., 1983, p. 104, LBL-15536A.
5. J.H. Mazur, "High-resolution Imaging of Oxidized Stepped Silicon Surfaces," *Proc. 41st Annual Meeting of the Electron Microscopy Society of America*, San Francisco Press, Inc., 1983, p. 100, LBL-15592A.
6. N.R. Wu, P. Ling, D.K. Sadana, J. Washburn, and M.I. Current, "Annealing of Interstitial Loops in Arsenic Implanted Silicon," *Proc. Electrochemical Society: Defects in Silicon*, Vol. 83-9, Electrochemical Society, Inc., 1983, p. 366; LBL-17334.

Chemical Properties and Processing of Refractory Ceramics*

Lutgard C. De Jonghe, Investigator

INTRODUCTION

The chemical properties of ceramics are important when their high-temperature stability in gaseous environments is considered. Such properties are particularly significant in industrial processes such as ore reduction. In gaseous reduction of iron-bearing ores by CO/CO₂ mixtures, pronounced product swelling caused by the formation of metallic whiskers is frequently a problem. These investigations are aimed at clarifying the near-interface processes that lead to various product morphologies that can cause swelling during gaseous reduction of oxides.

In the fabrication of multicomponent ceramics, chemical properties are important as well, because solid-state or solid-liquid reactions occur during the densification process and their effects on the development and properties of ceramics for high-temperature applications are very poorly understood. Current efforts are focused on the Al₂O₃-CaO system, which constitutes an important class of high-temperature refractories.

1. Whisker Growth and Swelling in Reduction of Oxides (Publication 3)

Mei Chang and Lutgard C. De Jonghe

Cobalt ferrites were reduced in CO/CO₂ gas mixtures at 1173 K, at total pressures between 6.6×10^3 Pa and 3.3×10^4 Pa. At CO/CO₂ ratios between 11.8 and 2.9, metallic-whisker formation was found to be promoted by the presence of impurities such as CaO and K₂O. The steady-state whisker diameter was found to be inversely proportional to the reaction-gas pressure and was relatively insensitive to the CO/CO₂ ratio. To study these effects, the reducing conditions were changed rapidly during reduction, so that the effects of the gas composition and gas pressure could be evaluated on the same whisker. Figure 1-1 shows a whisker for which the

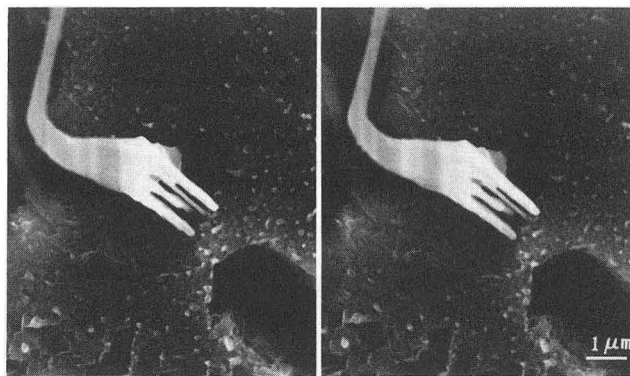


Figure 1-1. Stereo-pair whisker-diameter change for a specimen reduced at 1173 K for 360 sec at 0.66×10^4 Pa, followed by a reduction for 30 sec at 2.6×10^4 Pa. The whisker splits up into several smaller-diameter whiskers. (XBB 832-1115)

pressure was suddenly increased during reduction. The whisker can be seen to split into several smaller-diameter whiskers. Experiments such as these led to a new model that can explain whisker formation in detail. The model considers metal-oxide interface diffusion coupled with a metal-oxide-gas triple-junction reaction at the whisker base. Whisker formation results from a poorly catalyzed triple-junction reaction during which metal-oxide-interface oxygen transport is rapid.

2. Surface-oxygen Chemical Potential in a Gas-solid Reaction (Publication 5)

Lutgard C. De Jonghe and Mei Chang

In certain gas-solid reactions such as oxide reduction by CO/CO₂ mixtures, it may be necessary to define the surface-oxygen chemical potential. This potential is an important quantity because it provides a boundary value for solid-state transport processes that occur as part of the reaction mechanism. For example, in the case of CO/CO₂ reduction of the cobalt ferrites discussed above, the whisker diameter of the reaction product is determined by the rate at which oxygen is removed from under the whisker, i.e., from the metal-oxide interface, and by a surface gas-solid reaction at the triple junction. The situation is shown schematically in Figures 2-1 and 2-2.

A method has been developed for defining the oxygen chemical potential on the surface of the metal or the oxide for cases such as these. The method couples the gas reaction with a solid-state defect reaction. It can be shown that during this

*This work was supported by the Director, Office of Energy Research, Office of Basic Energy Sciences, Materials Sciences Division of the U.S. Department of Energy under Contract No. DE-AC03-76SF00098.

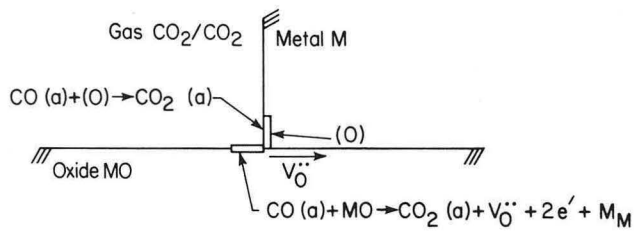


Figure 2-1. Reactions occurring on the metal or oxide phase near the metal-oxide-gas triple junction. Oxygen vacancies or dissolved oxygen may need to be transported along or near the metal-oxide interface when the progress of the reaction requires that oxygen be removed from that interface. (XBL 832-1238)

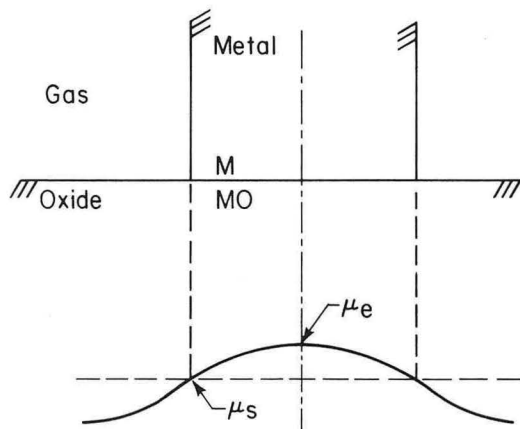


Figure 2-2. Schematic representation of the oxygen chemical potential for a reduction reaction where oxide MO is converted to metal M. (XBL 832-1239)

gas-solid reaction, the surface-oxygen chemical potential μ_s is between that of the gas phase μ_g and that of the metal/metal-oxide equilibrium μ_e . If the absorption-desorption step is slow, μ_s is close to μ_e ; if the absorption-desorption step is fast, μ_s is close to μ_g .

3. Interreaction Between Al_2O_3 and a CaO- Al_2O_3 Melt (Publication 4)

L.C. DeJonghe, H. Schmid, and M. Chang

During reactive sintering of alumina powders containing a small amount of calcia, various chemical changes take place that can affect the densification behavior of the green ceramic body. If matrix- Al_2O_3 powder is sintered above the eutectic temperature, it will react with a minority liquid of approximately eutectic composition. To clarify the reactions that can occur under such conditions, the interreac-

tion between a melt of eutectic composition in the calcia-alumina system and dense alumina at 1800 K was studied. A reaction zone develops consisting of a strongly textured CA_6 layer, (C = calcia, A = alumina), a CA_2 layer, and a layer of unreacted C-A melt (see Figure 3-1). Silica, an impurity in the alumina, is rejected by the advancing $\text{Al}_2\text{O}_3/\text{CA}_6$ reaction interface and accumulates as calcium alumina silicates in channels in the CA_6 layer. These channels assist in the reaction as fast transport paths. The strong texture of the CA_6 layer in the interreaction zone follows from the preferential diffusion of the calcium ions along the CA_6 basal planes and the stresses that arise as a result of the formation of CA_6 from alumina.

When two alpha-alumina blocks are welded by the eutectic mixture, then it is interesting to note that the strength of the weld depends significantly on the amount of melt that was allowed between the contact faces. If a large amount of melt penetration occurs between the blocks to be welded, then an increased amount of porosity develops at the weld interface after complete reaction of the melt to CA_6 . This leads to a weaker weld. The deterioration of the weld is due to reaction-rate heterogeneities that produce a rough interface when the CA_6 bonding phase is formed.

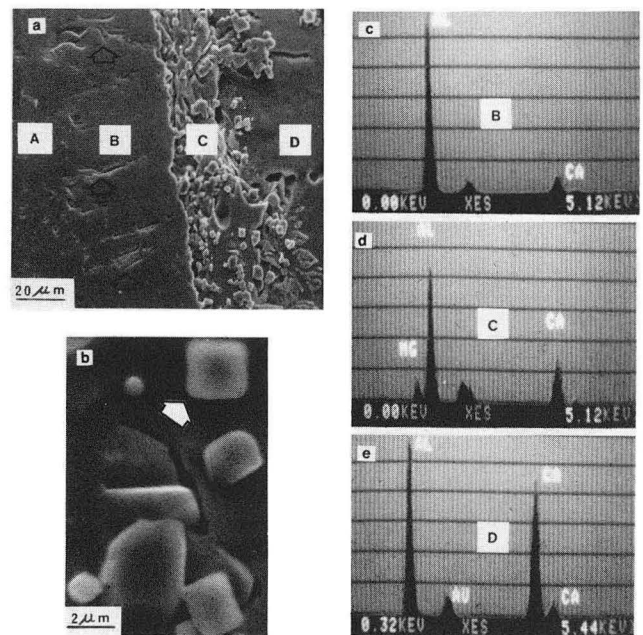


Figure 3-1. a. Cross section of the reaction layer. A = unreacted alumina; B = CA_6 phase; C = CA_2 + spinel; D = CA - C_3A mixture. Some channel-like features in the CA_6 layer are shown by arrows. b. Spinel precipitates (arrows) in the C layer. c,d,e. X-ray dispersive analysis of the B, C, and D layers showing the changing C/A ratios. (XBB 833-2608)

1983 PUBLICATIONS AND REPORTS

Refereed Journals

1. Herbert Schmid and Lutgard C. De Jonghe, "Structure and Nonstoichiometry of Calcium Aluminates," *Phil. Mag. A* **48**, 287-297 (1983).
2. S.C. Hu and Lutgard C. De Jonghe, "Pre-eutectic Densification in $\text{MgF}_2\text{-CaF}_2$," in *Ceramic Powders*, P. Vincenzini, Éd., Elsevier, 1983, pp 719-728.

LBL Reports

3. M. Chang (Ph.D. Thesis), "Origin of Swelling in Gaseous Reduction of Iron Bearing Oxides," LBL-15896.
4. L.C. De Jonghe, H. Schmid, and M. Chang, "Interreaction Between Al_2O_3 and a $\text{CaO-Al}_2\text{O}_3$ Melt," LBL-15885.
5. Lutgard C. De Jonghe and Mei Chang, "Surface Oxygen Chemical Potential in a Gas-solid Reaction," LBL-15732.

Structure and Electrical Properties of Composite Materials*

Robert H. Bragg, Investigator

INTRODUCTION

The purpose of this work is to understand how the properties of hard carbons and soft carbons are related to their structure. The latter undergo a structural transformation, graphitization, and become physically soft when heated above about 2000°C in inert atmosphere, whereas the former do not, even when heated above 3000°C. Soft carbons are fairly well understood, but basic knowledge concerning hard carbons is scant. In this project glassy carbon has been studied as a model hard carbon because it is a chemically pure (i.e., elemental carbon) monolithic solid. The structural differences between the two classes of carbons have been found to be analogous to those between thermosetting resins (hard) and thermoplastic resins (soft). Whereas soft carbons become semimetallic electrical conductors, hard carbons resemble amorphous semiconductors and at low temperatures display one-dimensional conduction. The major unknown in carbon science now is the specific atomic mechanism(s) associated with the structural changes during graphitization. This work has led to the hypothesis that it is the decomposition of a graphite intercalation compound containing hydrogen, and experiments to test this hypothesis via direct synthesis are being performed, as are related studies of the carbon-hydrogen system.

1. The Electrical Conductivity and Hall Effect of Glassy Carbon (Publication 2)

Dennis F. Baker[†] and Robert H. Bragg

The electrical conductivity and Hall effect of glassy carbon heat-treated for 3 hours between 1200 and 2700°C was measured at temperatures from 3 to 300 K in magnetic fields up to 5 tesla. The electrical conductivity, on the order of 200 (ohm-cm)⁻¹ at room temperature, can be empirically written

$$\sigma = A + B \exp(-CT^{-1/4}) - DT^{-1/2}$$

(see Figure 1-1). The first term is a strongly scattering metallic component; the second term is attributed to variable range hopping; and the third term is a negative correction to the metallic conductivity associated with one-dimensionality. The constants A, B, and C were insensitive to heat-treatment temperature (HTT); the constant D decreased and disappeared at about 2200°C.

The Hall coefficient was independent of magnetic field and nearly insensitive to measurement temperature but was a strong function of HTT, crossing over from negative to positive at about 1700°C and ranging from -0.048 to 0.126 cm³/coul (see Figure 1-2).

The idea of one-dimensional filaments in glassy carbon suggested by the correction to the strongly scattering metallic conductivity is compatible with the consensus view of the small scale (10-50 Å) of the microstructure derived from lattice imaging in the transmission electron microscope, wide-range x-ray and neutron scattering, and small-angle x-ray scattering.

[†]Present address: Research Laboratory, Lockheed Missiles and Space Company, Palo Alto, California 94304.

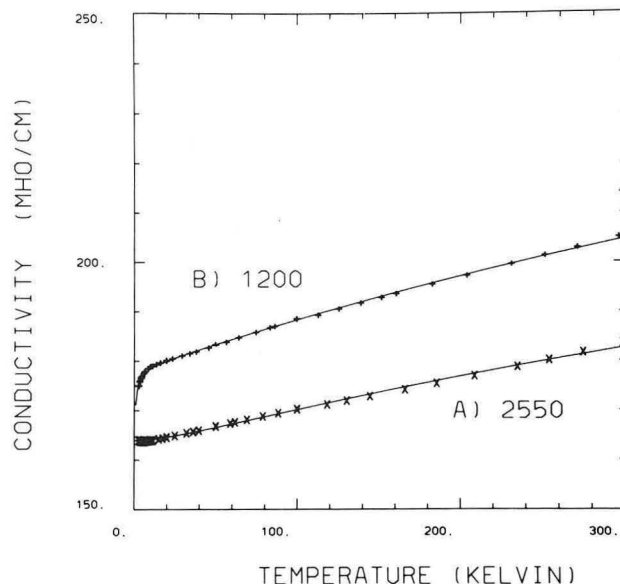


Figure 1-1. Electrical conductivity of glassy carbon as a function of temperature at high-temperature (A — 2550°C) and low-temperature (B — 1200°C) heat treatments. The solid lines are calculated by least squares from the empirical equation $\sigma = A + B \exp(-CT^{-1/4}) - DT^{-1/2}$. (XBL 831-7609)

*This work was supported by the Director, Office of Energy Research, Office of Basic Energy Sciences, Materials Sciences Division of the U.S. Department of Energy under Contract No. DE-AC03-76SF00098.

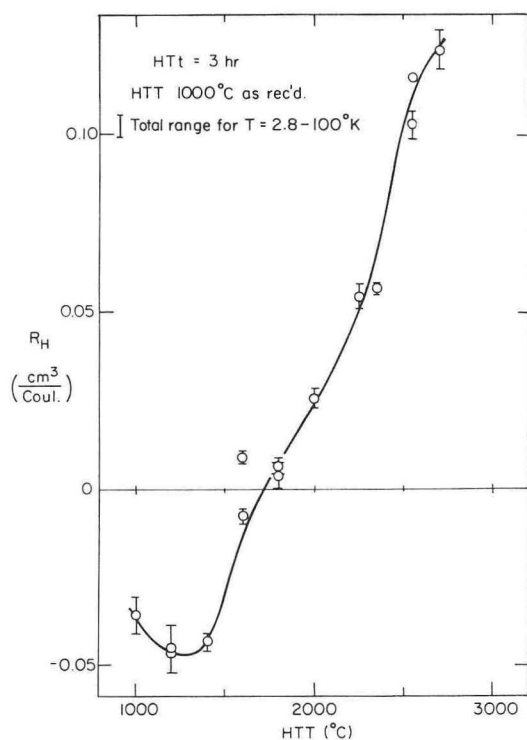


Figure 1-2. Hall coefficient R_H of glassy carbon as a function of heat-treatment temperature. (XBL 816-5907A)

2. Effect of Heat-treatment Temperature on Density, Weight, and Volume of Glass-like Carbon (Publication 2)

Bhola N. Mehrotra, Robert H. Bragg, and A.S. Rao[†]

Room-temperature measurements were made of the density, weight, and linear dimensions of glass-like carbon (GC) that was heat-treated for 3 hours between 1000 and 2700°C in inert gas atmosphere. The density of GC, starting at about 1.5 g/cm³, decreased 12.4%, and the weight loss increased to a maximum of 1.9%. However, the volume increased with a quadratic dependence on HTT, reaching a maximum of 10.2%. Subsequent application of hydrostatic pressure up to 1551 MPa (225,000 psi) produced only a small increase in bulk density. The weight loss is attributed to release of the last vestiges of hydrogen from the carbonaceous precursor, and the volume expansion is shown to be due to two different mechanisms: gas pressure up to about 1600°C and thermal stress due to anisotropy in thermal-expansion coefficients at higher HTT. The irreversibility of the dimensional change is proposed to be

due to creep during heating and reversal of the thermal expansion mismatch during cooling.

[†]Present address: Department of Chemical Engineering, Carnegie-Mellon University, Pittsburgh, Pennsylvania 15213.

3. Negative Magnetoresistance in Glassy Carbon (Publication 3)

Dennis F. Baker[†] and Robert H. Bragg

The magnetoresistance $\Delta\rho/\rho$ of glassy carbon heat-treated for 3 hours between 1200 and 2700°C has been measured at temperatures T from 3 to 100 K in magnetic fields H up to 5 tesla. The magnetoresistance is generally negative and saturates with reciprocal temperature but still increases as a function of magnetic field. The maximum negative $\Delta\rho/\rho$ measured was 2.2% for material heat-treated at 2700°C. The best fit of the data, based on the idea that negative $\Delta\rho/\rho$ is proportional to the square of the magnetic moment, was obtained with the functional form

$$\left[-\frac{\Delta\rho}{\rho} \right]^{1/2} = XH + \Gamma \tanh(\alpha_0 H/T),$$

which is the simplest model combining Curie and Pauli paramagnetism (see Figure 3-1). The parameter α_0 was 6 Bohr magnetons at all temperatures, but

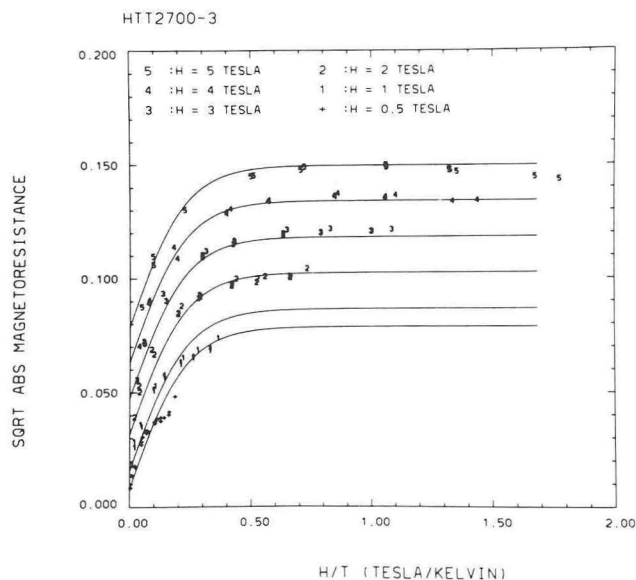


Figure 3-1. Fit of the Curie-Pauli paramagnetism model, with isomagnetic field lines plotted for glassy carbon heat-treated at 2700°C. (XBL 829-11517)

X and Γ increased roughly linearly with HTT. Positive $\Delta\rho/\rho$ was found for HTT less than 1600°C and low measurement temperatures.

†Present address: Research Laboratory, Lockheed Missiles and Space Company, Palo Alto, California 94304.

4. Glass-like Carbon: A C_xH Polymer Intercalation Compound (Publication 4)

Robert H. Bragg

The structure and annealing behavior of glass-like carbon show that it is a polymer carbon but similar to other carbons that have been extensively studied. X-ray and neutron-diffraction studies indicate crystallite sizes of 2.0–5.0 nm and large internal strain. Lattice-fringe images show continuous interwound laths made up of 5–10 layers of carbon atoms arranged as in graphite. During heating above 2000°C the interlayer spacing decreases below the original 0.344 nm, hydrogen diffuses out, and the sign of the Hall coefficient changes. The initial 0.344-nm interlayer spacing is predicted correctly if hydrogen is assumed to be present between the layers as in alkali or halide intercalation compounds (see Figure 4-1). It is proposed that the changes in physical properties are associated with de-intercalation of a compound of stage-1 composition C_3H .

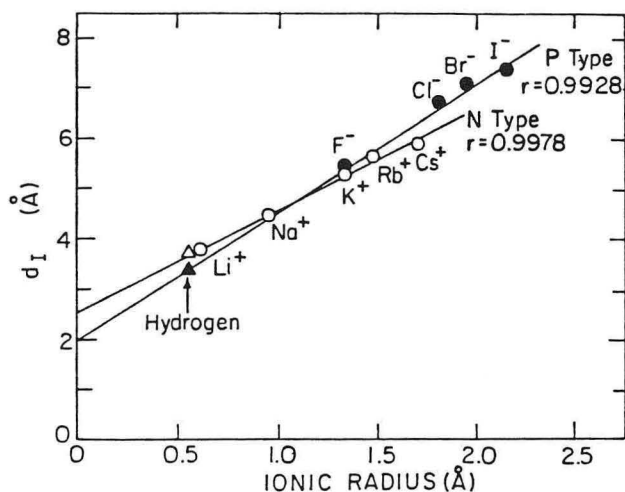


Figure 4-1. Layer spacing d_1 of stage-1 intercalation compounds as a function of ionic radius. (XBL 8210-6712A)

5. One-dimensionality in Glassy Carbon (Publication 5)

Dennis F. Baker† and Robert H. Bragg

A negative $T^{-1/2}$ dependence of a component of the electrical conductivity, indicative of one-dimensional transport, was found in glassy carbon heat-treated below 2200°C (see Figure 5-1). The microstructure as revealed in lattice-fringe images in the electron microscope, the Porod-law dependence obtained from small-angle scattering measurements, and the d_{002} -interlayer spacing as measured by x-ray and neutron diffraction are shown to support this thesis.

†Present address: Research Laboratory, Lockheed Missiles and Space Company, Palo Alto, California 94304.

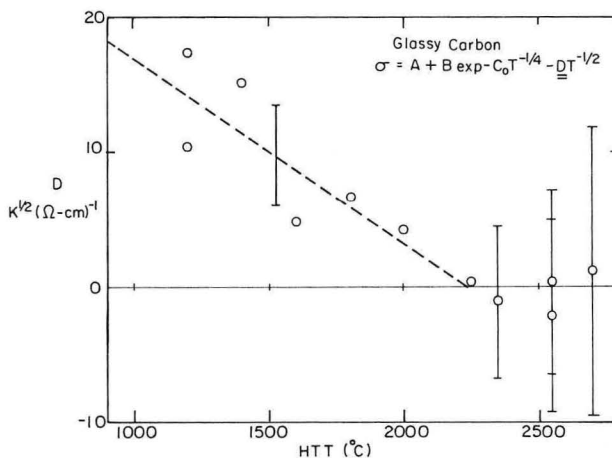


Figure 5-1. One-dimensional electrical-conductivity correction-component parameter D of glassy carbon as a function of heat-treatment temperature. (XBL 828-6436)

6. Work in Progress

The hypothesis is being tested that during carbonization of any hydrocarbon a graphite intercalation compound of hydrogen is formed whose subsequent decomposition (de-intercalation) at temperatures above 2000°C is the long-sought mechanism of “graphitization.” Experiments are being done wherein hydrogen loss or uptake during graphitization or intercalation is measured to permit correla-

tion with lattice parameters and physical properties (e.g., electrical conduction and magnetic susceptibility), a correlation not heretofore attempted or considered.

1983 PUBLICATIONS AND REPORTS

Refereed Journals

1. B.N. Mehrotra, R.H. Bragg, and A.S. Rao, "Effect of Heat Treatment Temperature (HTT) on Density, Weight Loss, and Volume of Glass-like Carbon (GC)," *J. Mat. Sci.* **18**, 2671-2678 (1983); LBL-15072.
2. D.F. Baker and R.H. Bragg, "The Electrical Conductivity and Hall Effect of Glassy Carbon," *J. Non-cryst. Solids* **58**, 57-69 (1983); LBL-15843.
3. D.F. Baker and R.H. Bragg, "Negative Magnetoresistance in Glassy Carbon," *Phil Mag. B* **48** (5), 475-487 (1983); LBL-15747.
4. R.H. Bragg, "Glass-like Carbon: A C_xH Polymer Intercalation Compound," *Synthetic Metals* **7** (1/2), 95-99 (1983); LBL-16615.
5. D.F. Baker and R.H. Bragg, "One Dimensionality in Glassy Carbon," *Phys. Rev. B* **28** (4), 2219-2221 (1983); LBL-15445.

LBL Reports

6. D.F. Baker (Ph.D. Thesis), "The Magnetoresistance, Electrical Conductivity, and Hall Effect of Glassy Carbon," LBL-13562.
7. D.F. Baker, "An Overview of Carbons and Glassy Carbon," LBID-670.

Other Publications

8. R.H. Bragg, D.F. Baker, L.G. Henry, and B.N. Mehrotra, "Graphitization: Decomposition of C_xH ?" *Extended Abstracts*, 16th Biennial International Conference on Carbon, San Diego, California, July 17-22, 1983; LBL-15788 abs.
9. L.G. Henry, R.H. Bragg, J. Rush, and J. Rhyne, "Comparative Line Profile Analyses of Glass-like Carbon Using X-ray and Neutron Diffraction," *Extended Abstracts*, 16th Biennial International Conference on Carbon, San Diego, California, July 17-22, 1983; LBL-15882 abs.
10. B.N. Mehrotra and R.H. Bragg, "Kinetic Studies of Weight Loss and Volume Expansion in Heat Treated Glass-like Carbon," *Extended Abstracts*, 16th Biennial International Conference on Carbon, San Diego, California, July 17-22, 1983; LBL-15790 abs.
11. D.F. Baker and R.H. Bragg, "One Dimensional Conduction in Glassy Carbon," *Extended Abstracts*, 16th Biennial International Conference on Carbon, San Diego, California, July 17-22, 1983; LBL-15784 abs.

High-Temperature Oxidation and Corrosion of Materials*

John Stringer, Acting Investigator[†]

MULTICOMPONENT DIFFUSION

In the development of protective coatings on materials to be exposed to aggressive environments at elevated temperatures, some degree of interdiffusion between the coating and the substrate will take place. In diffusional coatings the coating is prepared by interdiffusing one or more elements with the substrate. Both the coating and the substrate alloy may contain a number of constituents, and the interaction between these can modify the diffusion rates of the major constituents. The diffusion is characterized by a diffusion matrix, the elements of which describe the diffusion of the i th component as a result of a gradient in the j th component. The characterization of a system involves a determination of the diffusion matrix as a function of composition in the system, which in principle can then be used to predict a diffusion path that describes the evolution of the structure during the diffusion.

1. Diffusion in Fe-Cr-Al Systems at 900°C (Publication 3)

H.C. Akuezue

Interdiffusion coefficient matrices (D_{ij}) have been experimentally determined at 31 points in the $\alpha\delta$ -Fe phase field of the Fe-Cr-Al ternary system at 900°C and tested for consistency using the Onsager and Kirkaldy criteria. The diffusion coefficients are strong functions of composition. The variation of the direct coefficient for aluminum, D_{AlAl} , varies with Al content in a manner similar to the interdiffusion coefficient D_{Al} in the Fe-Al system, and $D_{AlAl} \leq D_{Al}$. Interestingly, along the boundary between the single-phase $\alpha\delta$ -Fe region and the two-phase $\alpha\delta + \beta_2$ region, the direct coefficient for aluminum is much

*This work was supported by the Director, Office of Energy Research, Office of Basic Energy Sciences, Materials Sciences Division of the U.S. Department of Energy under Contract No. DE-AC03-76SF00098.

[†]Dr. Stringer is affiliated with the Electric Power Research Institute, Palo Alto, California. He is continuing the research program started by the late Dr. D.P. Whittle.

less than that for chromium, implying that in effect chromium is the only mobile species in this region. The practical applications of these results to the formation of (Cr+Al)-rich coatings on iron-based materials by diffusion are discussed.

CORROSION IN MIXED-OXIDANT ENVIRONMENTS

The presence of a second oxidant such as sulfur, carbon, or chlorine in combination with oxygen can have a profound (and usually deleterious) effect on the development of a protective oxide scale on an alloy. The reasons for this effect are not fully understood, but it appears that the second oxidant can migrate through the oxide and react with the element in the alloy responsible for forming the protective oxide. This migration eventually leads to the development of a morphology that precludes the reestablishment of a protective scale if the initially formed oxide is lost. A variety of other effects is also possible. One important issue is how the second oxidant is transported through the protective oxide: often the apparent transport rate seems too high to be explained by bulk diffusion. It is possible that short-circuit transport is taking place along preferred paths, but the nature of these paths is not understood yet, nor is their manner of formation.

2. High-temperature Corrosion of Iron and Iron-based Alloys in Sulfur-containing Atmospheres (Publication 5)

F.C. Yang

The corrosion morphology and kinetics for some iron-based alloys exposed to atmospheres containing oxygen and sulfur at 871°C have been studied, and a model for the mechanism of the attack has been constructed. In the case of pure iron, oxide protrusions with sulfur-rich cores form on the outer scale surface. It is suggested that the sulfur-rich core acts as a rapid diffusion path for the outward transport of iron.

The addition of sufficient aluminum or chromium results in the formation of a more protective Al_2O_3 or Cr_2O_3 oxide scale. However, sulfur penetration can result in spalling of the scale, and this can lead to catastrophic oxidation of the alloy.

Although it appears that transport of sulfur through the oxide and the eventual breakdown is inevitable, it appears that an alloy designed to form an Al_2O_3 scale, but having sufficient chromium to

form a healing oxide when the alumina spalls, offers the best chance of having an adequate resistance to attack.

3. High-temperature Oxidation of Nickel-cobalt Alloys (Publication 4)

P.Y. Hou

The oxidation of Ni-Co alloys under two widely differing oxygen potentials — 1 atm and 6×10^{-9} atm — at 1000°C has been studied. In both cases an external oxide scale that is a solid solution of NiO and CoO is formed. In the case of the low oxygen potential, there is also considerable internal oxidation in the alloy. The growth of the external oxide scale is described using Wagner's ternary-diffusion model. A more refined model, including all types of vacancy species in the oxide, is used to obtain the diffusivities of cations in the oxide scale as a function of oxygen potential and oxide composition. In addition, correlation effects between elementary jumps of the cations are included to account for an additional composition dependence of the diffusivities. Theoretical calculations of the oxidation-rate constants and of the cation-concentration profiles are compared with experimentally measured data.

4. Work in Progress

Corrosion of alloys by a sulfidation/oxidation process is known to occur at metal temperatures of 600°C and above in fluidized-bed combustors burning coal in the presence of a sulfur acceptor such as CaO. The corrosion is associated with the presence of CaSO₄, often forming a deposit on the metal sur-

face, and with the existence of local transient low-oxygen activities (on the order of 10^{-13} atm) in the dense-emulsion fraction of the fluidized bed. In this work the corrosion of alloys in gaseous environments with oxygen and sulfur activities similar to those expected in these local regions is being studied. To date it has been shown that sulfidation/oxidation corrosion can be induced under these conditions. The variation in the attack with the activities of the two oxidants is being studied, and it is hoped to correlate this variation with the predictions of a thermochemical analysis.

1983 PUBLICATIONS AND REPORTS

Refereed Journals

1. D.P. Whittle and H.C. Akeuzue, "Interdiffusion in the Fe-Al System: Aluminizing," *Metal Sci.* **17**, 27 (1983); LBL-13548.

LBL Reports

2. F.C. Yang (Ph.D. Thesis), "High-temperature Corrosion of Iron and Iron-based Alloys in Sulfur Containing Atmospheres," LBL-16089.
3. H.C. Akuezue (Ph.D. Thesis), "Diffusion in Fe-Cr-Al Systems at 900°C," LBL-16684.
4. P.Y. Hou (M.S. Thesis), "High Temperature Oxidation of Nickel-cobalt Alloys," LBL-16616.

Invited Talks

5. F.C. Yang and J. Stringer, "High Temperature Corrosion of Iron-based Alloys in Sulfur-containing Atmospheres," presented to the Fall Meeting of the Electrochemical Society, Washington, D.C., October 1983.

Ceramic Interfaces*

Andreas M. Glaeser, Investigator

INTRODUCTION

Numerous properties of ceramics depend strongly on the nature of the microstructure, necessitating control of both the microstructural characteristics (grain size, density, pore size, etc.) developed during processing and the stability of the microstructure during subsequent use. The grain size and other microstructural characteristics are generally affected by a number of factors including the chemical and physical nature of the starting powder, the details of the forming and firing operations, and the conditions of subsequent use. The present research program focuses on improving our understanding of several processes which contribute to or control the morphological — and hence microstructural — changes that occur during both materials fabrication and utilization. Specific problems addressed are (1) the development of thermodynamic and kinetic descriptions of the processes by which the closed pore structure characteristic of final-stage sintering develops, and (2) an assessment of the factors that control or influence the nature of the grain boundary migration process and thus directly or indirectly affect the grain size, as well as a number of other microstructural features.

1. Grain Boundary Mobility in MgO-doped Al_2O_3

Andreas M. Glaeser

The mobility of grain boundaries in theoretically dense MgO-doped Al_2O_3 has been measured in the temperature range from 1600 to 1900°C. The time- and spatially-averaged migration behavior of matrix grains has been determined and compared to the behavior characteristic of isolated abnormally growing grains that have developed naturally as a consequence of grain growth or have been artificially introduced by laser melting. The behavior of the abnormally growing grains indicates that a descrip-

tion of grain growth based on the assumption of a single-valued mobility may be seriously in error. Similarly, the interpretation of grain growth data in terms of an average mobility may provide inadequate information to properly model microstructural evolution. Results indicate that the inhomogeneity in mobility may contribute to the initiation of abnormal grain growth; the time dependence of grain size distributions in this material appears consistent with this interpretation.

2. The Stability of Pore Channels: Dihedral Angle Effects (Publication 3)

Andreas M. Glaeser and W. Craig Carter

During the densification of a powder compact, significant changes occur in the pore morphology. During sintering a transition from an initially continuous-pore phase to a closed-pore phase takes place. Frequently the continuous-pore phase located along three grain junctions is modeled as a cylindrical network. Several previous treatments have evaluated the stability of a cylinder to morphological perturbations. The present work has focused on accurately describing the shape of a pore as a function of dihedral angle and reassessing the pore stability condition. The results indicate a strong dependence of the minimum stable wavelength for perturbation growth on dihedral angle. As a consequence, the volumes and mobilities of pores that develop during the transition will also depend on dihedral angle. The theoretical analysis is being extended to describe the stability of continuous second phases at grain boundaries.

3. Boundary-structure Transformation in Lead

Andreas M. Glaeser

Measurements of several boundary-structure-sensitive properties in lead have indicated a change in boundary behavior at a temperature in the vicinity of 0.7–0.8 of T_m , the homologous melting temperature. The changes in dihedral angle, grain boundary mobility, etc., have been interpreted as indicating a change in the atomic structure of the boundary, in particular a disordering of the boundary at elevated temperatures. In contrast, a review of lead grain boundary diffusion data shows no evidence for

*This work was supported by the Director, Office of Energy Research, Office of Basic Energy Sciences, Materials Sciences Division of the U.S. Department of Energy under Contract No. DE-AC03-76SF00098.

a structural transformation, and some dihedral angle measurements at a temperature near T_m indicate an effect of boundary misorientation, contrary to expectations for a disordered boundary. In addition, evidence exists suggesting that the presence of dissolved oxygen may be responsible for the observed changes in migration behavior. High-purity oxygen-free striated-lead single crystals have been grown and grain boundary migration experiments initiated to assess the possibility that the transformation is primarily chemical rather than structural in nature.

4. Work In Progress

Fabrication of alumina powder of controlled morphology and composition is in progress. Attempts to fabricate theoretically dense compacts from sulfate-derived powders were unsuccessful; spherical monodispersed hydroxide precursors have now been produced, but not in sufficient quantity to permit sample fabrication.

A kinetic analysis of pore breakdown due to morphological instabilities is being developed that incorporates the effect of dihedral angle. Considerable changes in the magnitude of the most rapidly growing wavelength are anticipated.

Efforts are being made to fabricate either single-crystal or coarse-grained NaCl by recrystallization of powder compacts. The objective is the fabrication of

samples containing a uniform distribution of fine pores. Subsequent deformation and reintroduction of grain boundaries into the material would permit pore/grain-boundary interactions to be investigated. Approval of funding for the acquisition of an optical hot stage has led to the possibility of *in situ* observations.

1983 PUBLICATIONS AND REPORTS

LBL Reports

1. A.M. Glaeser, "Discussion of Grain Growth Mechanisms in Polysilicon," accepted for publication in J. Electrochem. Soc., LBL-15537.
2. A.M. Glaeser, "Microstructure Development in Ceramics: The Role of Grain Growth," submitted to The Ceramic Society of Japan (Yogyo Kyokai), LBL-17078.
3. W.C. Carter and A.M. Glaeser, "The Stability of Pore Channels: Dihedral Angle Effects," accepted by J. Am. Ceram. Soc., LBL-17079.

Invited Talks

4. A.M. Glaeser, "Microstructure Control During Sintering," Gordon Research Conference on Solid State Studies in Ceramics, Plymouth, New Hampshire, July 24-29, 1983.

ENGINEERING MATERIALS

Abrasive, Erosive, and Sliding Wear of Materials*

Iain Finnie, Investigator

INTRODUCTION

The purpose of this work is to explore the basic mechanisms of abrasive, erosive, and sliding wear in different types of materials. The ultimate objective of this research is to predict wear resistance from simple materials tests. A more modest first step is to identify similarities and differences in the various types of wear so that simple screening tests can be used to evaluate wear resistance. The material properties and microstructural features needed for optimum wear resistance are being studied. With this information and a knowledge of wear mechanisms, quantitative treatments of wear resistance should become feasible.

1. An Experimental Study of Three-body Abrasive Wear (Publication 1)

Abrish Misra[†] and Iain Finnie

Three-body abrasive wear has been studied using a column of abrasive material contained in a tube and pressed against a rotating metal disc. The weight loss of the disc due to abrasion was examined as a function of the length of the wear path, load, speed, abrasive size, abrasive hardness, metal hardness, and temperature. Scanning electron microscopy was used to investigate the mechanism of material removal. Similarities and differences

*This work was supported by the Director, Office of Energy Research, Office of Basic Energy Sciences, Materials Sciences Division of the U.S. Department of Energy under Contract No. DE-AC03-76SF00098.

between three-body abrasion tests and two-body abrasion results are pointed out.

[†]Present address: IBM Research Laboratory, San Jose, California.

2. Flaws, Fracture Mechanisms, and Hertzian Cracks in Brittle Solids (Publication 2)

I. Finnie and D. Dolev[†]

The problem of predicting fracture in a brittle solid loaded by a spherical indenter is considered. Two quite different approaches have been taken in the literature. One is based on the Weibull probabilistic treatment of brittle strength, while the other makes use of concepts from linear elastic-fracture mechanics. It is shown that both approaches provide useful information for this fracture problem, and their advantages and limitations are discussed. Finally, it is shown that the classical Auerbach's law, which relates mean fracture load \bar{P} to the indenter radius R in the form $\bar{P} \sim R$, is a simple consequence of linear elastic-fracture mechanics if the brittle solid is assumed to contain a large range of flaw sizes at all locations.

[†]Present address: Israel Ministry of Defense Research Laboratory, Haifa, Israel.

3. A Comparative Investigation of the Sliding Wear of Some fcc Metals (Publication 4)

R. Glardon[†] and I. Finnie

Experimental investigations of the friction and wear of four copper alloys and pure nickel are presented. Measurements of the shape and dimensions of the wear tracks and of the extent of subsurface layers are also reported. The results are discussed in terms of mechanical behavior, and possible correlations with conventional mechanical properties are considered. The role of cyclic plastic deforma-

tion is emphasized, and areas of interest for future research are suggested.

†Present address: Mettler Instruments, Griefensee, Switzerland.

4. A Study of Friction and Wear of Cartridge- and Free-cutting Brass (Publication 3)

R. Glardon† and I. Finnie

Friction and wear experiments on brasses with and without lead particles are presented and compared. Quantitative results are given for the dimensions of the wear tracks and of the subsurface layers. Differences in the behavior of the two alloys are treated in terms of deformation characteristics and microstructure, and the role of a dispersion of lead particles on friction and wear is discussed.

†Present address: Mettler Instruments, Griefensee, Switzerland.

5. Work in Progress

Additional sliding-wear work describing a large-scale simulation of sliding-wear behavior in a

mechanical test has been submitted for publication. Work on the abrasive and erosive wear of composites and on the effect of temperature on abrasive wear has also been completed.

1983 PUBLICATIONS AND REPORTS

Refereed Journals

1. A. Misra and I. Finnie, "An Experimental Study of Three-body Abrasive Wear," *Wear* **85**, 57 (1983).
2. I. Finnie and D. Dolev, "Flaws, Fracture Mechanisms, and Hertzian Cracks in Brittle Solids," *Proc. 4th Int. Conf. on Mech. Behavior of Materials* **2**, 771 (1983).
3. R. Glardon and I. Finnie, "A Study of the Friction and Wear of Cartridge and Free Cutting Brass," *ASME J. Eng. Mat. & Technology* **105**, 31 (1983).
4. R. Glardon and I. Finnie, "A Comparative Investigation of the Sliding Wear of Some F.C.C. Materials," *ASME J. Eng. Mat. & Technology* **105**, 36 (1983).

Erosion of Brittle Solids*

Anthony G. Evans, Investigator

INTRODUCTION

This project is concerned with the development of a fundamental understanding of erosion and strength degradation of brittle coatings and layers subject to impact by solid particles. The principal research directions involve studies of the damage created by individual particles and the erosion characteristics under multiple-impact conditions. The residual stress in the coating and adherence to the substrate are important variables in the investigation. Hence techniques for ascertaining the magnitude of the residual stress and for characterizing adhesion are essential study topics. Predictions of material removal by spalling after projectile impact constitute the primary product of this investigation.

1. Mechanics of Delamination and Spalling in Compressed Films (Publication 4)

A.G. Evans and J.W. Hutchinson

The mechanics of the delamination and spalling of compressed films or coatings has been analyzed using a combination of fracture mechanics and post-buckling theory. It is demonstrated that the delamination of precompressed films occurs only if the film buckles, whereupon a stress intensification develops at the buckle perimeter. The associated stress intensity depends on the magnitude of the prestress and the film thickness. Conversely, the delamination of indented coatings occurs without buckling; the stress intensity in this instance depends on the indentation volume, the film thickness, and the radius of delamination. Preliminary attempts have also been made to predict critical spall conditions following the incidence of buckling.

2. Measurement of Adherence of Residually Stressed Thin Films by Indentation: I. Mechanics of Interface Delamination (Publication 5)

D.B. Marshall and A.G. Evans.

A fracture analysis of indentation-induced delamination of thin films is presented. The analysis is based on a model system in which the section of film above the delaminating crack is treated as a rigidly clamped disc and the crack extension force is derived from changes in strain energy of the system as the crack extends. Residual-deposition stresses influence the cracking response by inducing buckling of the film above the crack and by providing an additional crack-driving force once buckling occurs. A relation for the equilibrium crack length is derived in terms of the indenter load and geometry, the film thickness and mechanical properties, the residual stress level, and the fracture toughness of the interface. The analysis provides a basis for using controlled-indentation cracking as a quantitative measure of interface toughness and for evaluating contact-induced damage in thin films.

3. Measurement of Adherence of Residually Stressed Thin Films by Indentation: II. Experiments with ZnO/SiO (Publication 6)

C. Rossington, D.B. Marshall, A.G. Evans, and B.T. Khuri-Yakub

Indentation-induced delamination between thin films of ZnO and Si substrates is examined. Delamination occurs by the growth of lateral cracks, either along the interface or within the film adjacent to the interface. The crack path is determined by the indenter load and the film thickness, as well as by residual stresses formed during deposition. A change in crack path from the interface to the film, accompanied by an increase in crack length, is observed

*This work was supported by the Director, Office of Energy Research, Office of Basic Energy Sciences, Materials Sciences Division of the U.S. Department of Energy under Contract No. DE-AC03-76SF00098.

and is interpreted as a buckling-induced stress intensification. The interface-fracture toughness is estimated from the relative crack lengths in the buckled and unbuckled films. A reasonable value is obtained.

4. An Indentation Technique to Measure the Fracture Toughness of Thin Film/Substrate Interfaces (Publication 7)

Carolyn S. Rossington

An indentation technique employing a conventional microhardness tester is developed and used to study the adherence of zinc oxide thin films to silicon substrates. Upon unloading of a Vickers diamond indenter, lateral cracks propagate parallel to the film surface, either along the interface or within the film. A fracture-mechanics model is proposed which relates the adherence in the presence of interface cracking to the interface-crack length, the indentation load, the geometry of the indenter, the material parameters of the film, and the residual stress in the film. The model also predicts the spalling behavior of the film as a function of the interface toughness. Based on the proposed model, the fracture toughness of a ZnO/Si interface is measured.

5. Oxidation-induced Stresses and Some Effects on the Behavior of Oxide Films (Publication 2)

C.H. Hsueh and A.G. Evans

The elastic and viscoelastic stresses created during the oxidation of curved surfaces are calculated. The stress state and amplitude are shown to depend sensitively on the oxidation site (interface or surface) and the oxidation strain (uniaxial or dilatational). The viscoelastic stresses depend, in addition, on the rate of oxidation compared to the viscosity of the oxide. In most cases the stresses increase rapidly as the radius of curvature of the surface decreases. The influence of the stresses on several important oxidation phenomena are discussed. Specifically, corner effects on the oxidation rate, cracking and spalling of the oxide, and plastic deformation of the substrates are briefly addressed.

6. Work in Progress

Coating-spallation studies have been conducted on a model system consisting of ZnO coatings on Si substrates. Indentations emplaced into the ZnO surface have been shown to induce interface cracking above a load threshold and thereafter, at higher loads, to induce spallation of the coating. Similar behavior is expected to obtain subject to projectile impact under erosive conditions. It has been demonstrated that residual compression in the coatings is detrimental because it induces enhanced cracking and spalling. Residual stress thus emerges as an important erosion variable for further investigation. Analysis of the cracking and spalling process reveals that buckling is a prerequisite, and that a buckling-induced stress intensity is the major source of crack extension along the interface. Predictions of cracking and spalling based on buckling theory have been used to correlate data obtained for the ZnO/Si system and to provide a specific rationale for the importance of residual stress and interface adherence (or toughness).

The problem of the impaired adhesion of Al_2O_3 films on superalloys, a problem induced by interface-void formation, has been examined. Cross-sectional transmission electron microscope (TEM) studies coupled with Auger microscopy have shown that Al_2O_3 formation is accompanied by Ni and Cr diffusion through the oxide. Consequently, Al-, Cr-, and Ni-concentration gradients are established in the alloy, consistent with the formation of Kirkendall voids. These voids are then collected by the migrating oxide/alloy interface to cause the initial separation that permits buckling and subsequent spallation. Further studies of this effect are in progress as a basis for interpreting erosion/corrosion behavior in superalloys.

1983 PUBLICATIONS AND REPORTS

Refereed Journals

1. D.B. Marshall, A.G. Evans, and Z. Nisenholz, "Measurement of Dynamic Hardness by Controlled Sharp-projectile Impact," *J. Am. Ceram. Soc.* **66** (8), 580 (1983); LBL-15339.
2. C.H. Hsueh and A.G. Evans, "Oxidation Induced Stresses and Some Effects on the Behavior of Oxide Films," *J. Appl. Phys.* **54**, 6672 (1983); LBL-15818.

LBL Reports

3. A.G. Evans, G. Crumley, and E. Demeray, "The Mechanical Behavior of Brittle Coatings and Layers," *Oxidation of Metals*, in press, LBL-15474.
4. A.G. Evans and J.W. Hutchinson, "On the Mechanics of Delamination and Spalling in Compressed Films," *Intl. J. Solids & Structures*, in press, LBL-15781.
5. D.B. Marshall and A.G. Evans, "Measurement of Adherence of Residually Stressed Thin Films by Indentation: I. Mechanics of Interface Delamination," LBL-16841 1/2.
6. C. Rossington, D.B. Marshall, A.G. Evans, and B.T. Khuri-Yakub, "Measurement of Adher-

ence of Residually Stressed Thin Films by Indentation: II. Experiments with ZnO/SiO," LBL-16841 2/2.

7. C. Rossington (M.S. Thesis), "An Indentation Technique to Measure the Fracture Toughness of Thin Film/Substrate Interfaces," LBL-15892.

Invited Talks

8. G.B. Crumley, A.G. Evans, and E. Demeray, "The High-temperature Failure of Zirconia Thermal-barrier Coatings," *American Ceramic Society 1983 Annual Meeting*, Chicago, April 26, 1983.

SOLID-STATE PHYSICS

EXPERIMENTAL RESEARCH

Far-Infrared Spectroscopy*

Paul L. Richards, Investigator

INTRODUCTION

Improvements in infrared technology are making increases in the sensitivity of many types of infrared measurements possible. In this project improved types of infrared detectors, mixers, and spectrometers are being developed. Improved infrared techniques are being used for experiments in areas of fundamental and applied infrared physics where their impact is expected to be large.

Developments of infrared technology include completion of a liquid-helium-cooled diffraction-grating spectrometer for use with photoconductive detectors for emission spectroscopy, fabrication and testing of ultrasensitive photoconductive detectors for the 50–500 μm wavelength range, improved fabrication techniques for bolometric detectors to increase their ultimate sensitivity, development of a new class of far-infrared dichroic-beam dividers, and development of far-infrared harmonic generation as a spectroscopic source.

Experiments in progress include measurements of the near-infrared absorption spectra of molecules chemically adsorbed on metal surfaces, measurements of the infrared spectra of one-dimensional conductors including charge-density wave systems and organic superconductors, and measurements of the infrared photoconductivity of impurities in semiconductors.

1. Vibrational Spectroscopy of Chemisorbed Molecules by Infrared Emission (Publication 5)

S. Chiang,[†] R.G. Tobin, and P.L. Richards

The technique of infrared emission spectroscopy has been developed in order to observe vibrational modes of molecules adsorbed on clean, single-crystal metal surfaces. A novel apparatus has been constructed which measures the emission from a single-crystal sample in thermal equilibrium at room temperature (see Figure 1-1). The apparatus consists of a liquid-helium-cooled infrared-grating spectrometer coupled to an ultrahigh-vacuum system equipped with surface-preparation and characterization facilities. The system is capable of measuring over the frequency range from 330 to 3000 cm^{-1} with a resolution of 1 to 15 cm^{-1} . Using this technique we have measured the linewidths of both the carbon-metal and carbon-oxygen stretching vibrations of submonolayer coverage of CO on Ni(100).

[†]Present address: IBM Research Laboratory, San Jose, California 95193.

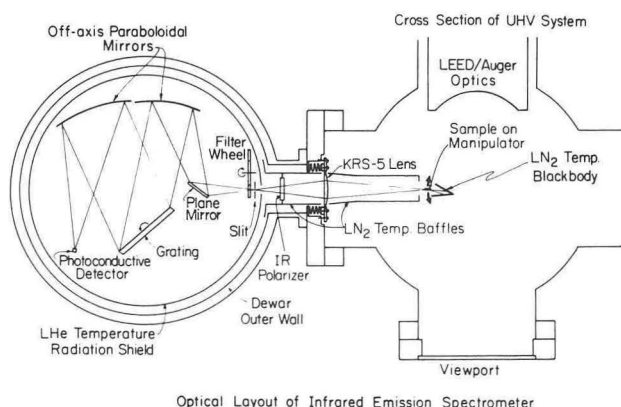


Figure 1-1. Optical layout of infrared-emission apparatus, with LHe-cooled spectrometer on the left and ultrahigh-vacuum system on the right. (XBL 8012-13382 A)

*This work was supported by the Director, Office of Energy Research, Office of Basic Energy Sciences, Materials Sciences Division of the U.S. Department of Energy under Contract No. DE-AC03-76SF00098.

2. The Molecule-substrate Vibration of CO on Ni(100) Studied by Infrared Emission Spectroscopy (Publication 6)

S. Chiang,[†] R.G. Tobin, P.L. Richards, and P.A. Thiel[‡]

We have used a novel infrared-emission technique to make the first measurement of the linewidth of a molecule-substrate vibrational mode on a well-characterized single-crystal surface (see Figure 2-1). At saturation coverage the observed linewidth of the C-Ni mode of CO on Ni(100) is 15 cm^{-1} . This result is in agreement with predictions for broadening caused by de-excitation by two-phonon emission.

[†]Present address: IBM Research Laboratory, San Jose, California 95193.

[‡]Present address: Department of Chemistry, Iowa State University, Ames, Iowa 50011.

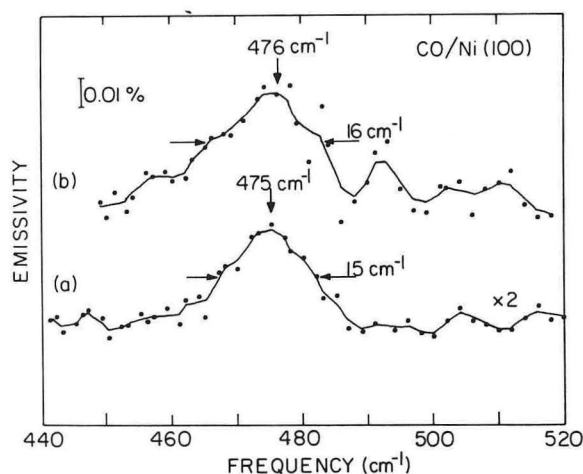


Figure 2-1. Infrared-emission spectra from a saturation coverage of CO on Ni(100) at 310 K. The instrumental resolution was 2.5 cm^{-1} , and a linear baseline has been subtracted from the curves. The solid lines are obtained by computer smoothing of the data. (a) Spectrum of a disordered CO layer on a partially contaminated surface. (b) Spectrum of an ordered $c(2 \times 2)$ CO overlayer on a clean surface. (XBL 8311-6595)

3. The C=O Stretching Vibration of CO on Ni(100) by Infrared Emission Spectroscopy (Publication 7)

R.G. Tobin, S. Chiang,[†] P.A. Thiel,[‡] and P.L. Richards

Infrared emission spectroscopy has been used to study the C=O stretching vibration of CO on Ni(100) at 310 K (see Figure 3-1). In contrast to previous electron-energy-loss and infrared measurements, no bridge-bonded CO is observed at any coverage below $\theta = 0.5$. Variations in the line shape with exposure suggest the presence of $c(2 \times 2)$ islands even at low coverage, though low-energy electron diffraction shows no sign of such ordering.

[†]Present address: IBM Research Laboratory, San Jose, California 95193.

[‡]Present address: Department of Chemistry, Iowa State University, Ames, Iowa 50011.

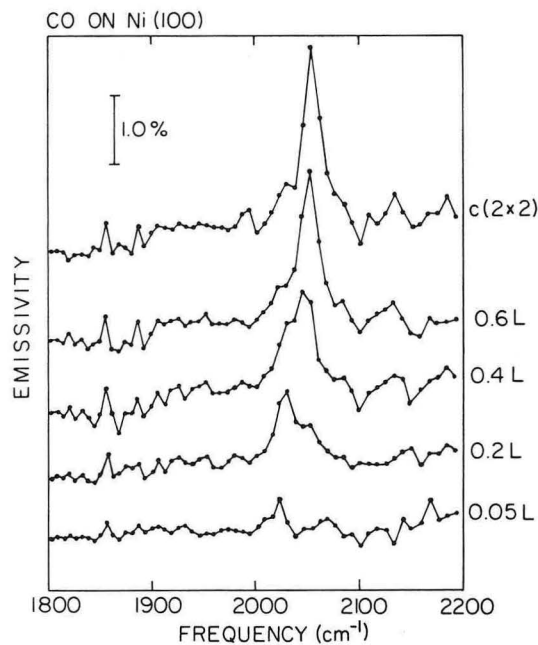


Figure 3-1. Infrared-emission spectra of CO on a clean Ni(100) surface at 310 K. The instrumental resolution was $\sim 18/\text{cm}^{-1}$. (XBL 839-6426)

4. Improved Fabrication Techniques for Infrared Bolometers (Publication 3)[†]

A.E. Lange, E. Kreysa,[‡] S.E. McBride, P.L. Richards, and E.E. Haller

Techniques are described for producing improved infrared bolometers from doped germanium. Ion implantation and sputter metalization have been used to make ohmic electrical contacts to Ge:Ga chips. This method results in a high yield of small monolithic bolometers with very little low-frequency noise. When one of these chips is used as the thermometric element of a composite bolometer, it must be bonded to a dielectric substrate. Figure 4-1 shows a schematic diagram of a composite bolometer. The thermal resistance of the conventional epoxy bond has been measured and found to be undesirably large. A procedure for soldering the chip to a metalized portion of the substrate is described that reduced this resistance.

The contribution of the metal-film absorber to the heat capacity of a composite bolometer has been measured. The heat capacity of a NiCr absorber at 1.3 K can dominate the bolometer performance. A Bi absorber has significantly lower heat capacity.

A low-temperature black-body calibrator has been built to measure the optical responsivity of bolometers. A composite bolometer system with a throughput of ~ 0.1 sr cm² has been constructed using our new techniques. In negligible background it has an optical noise-equivalent power of 3.6×10^{-15} W/ $\sqrt{\text{Hz}}$ at 1.0 K with a time constant of 20 msec. The noise in this bolometer is white above 2.5 Hz and is somewhat below the value predicted

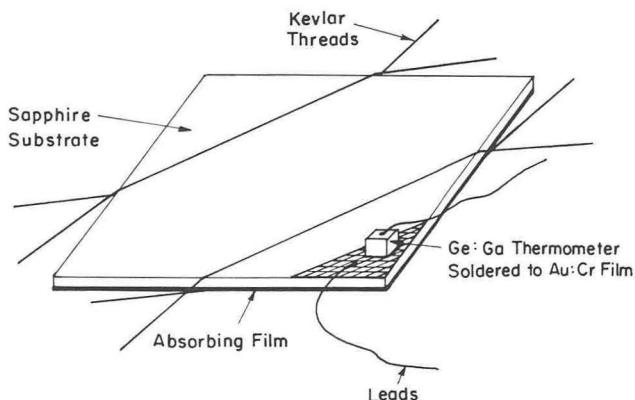


Figure 4-1. Schematic diagram of a composite bolometer. The doped-Ge thermometer is soldered to a metalized portion of the sapphire substrate. (XBL 825-5630)

by thermodynamic-equilibrium theory. It is in agreement with calculations based on a recent non-equilibrium theory.

[†]Support for E.E. Haller was provided by the National Aeronautics and Space Administration under Grant W-14606. During various phases of this work, E. Kreysa was supported by the Deutsche Forschungsgemeinschaft, Sonderforschungsbereich 131, Radioastronomie; and P.L. Richards by the Alexander von Humboldt Foundation Senior U.S. Scientist Program.

[‡]Permanent address: Max-Planck-Institut für Radioastronomie, D-5300 Bonn 1, West Germany.

5. Far-infrared Optical Properties of NbSe₃ (Publication 8)

W.A. Challener[†] and P.L. Richards

We have measured the far-infrared reflectance of NbSe₃ and used models of the frequency-dependent conductivity to fit the data. General arguments show that at 2 K a charge-density-wave (CDW) energy gap exists between 120 and 190 cm⁻¹, the relaxation time(s) of the free carriers and the CDW-pinned mode is $>3 \times 10^{-12}$ sec, and the ratio of the free-carrier concentration to band mass is $>2 \times 10^{20}$ cm⁻³/m₀. Figure 5-1 shows the Kramers-

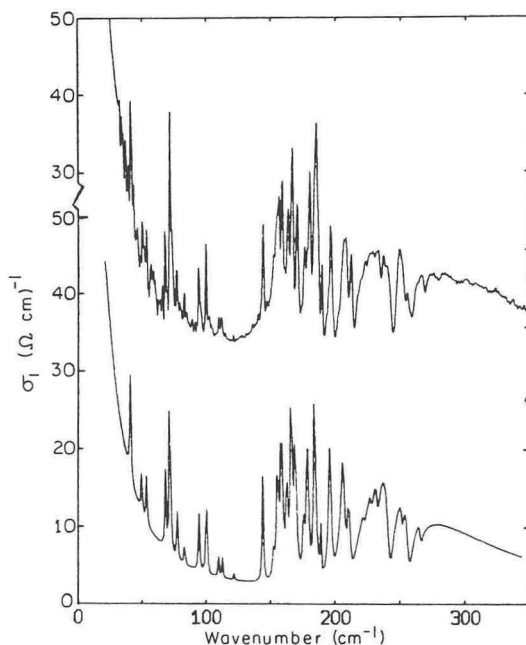


Figure 5-1. Kramers-Kronig calculation of σ_1 using a model that includes a low-frequency pinned mode, coupled-CDW carrier-optical-phonon modes, and a single-particle continuum above a CDW energy gap. (XBL 839-6269)

Kronig calculation of the conductivity σ and the model calculation of σ .

[†]Present address: Los Alamos National Laboratory, Physics Department, Section P-10, Los Alamos, New Mexico 87545.

6. Work in Progress

The success of our new techniques for measuring the infrared spectra of molecules chemisorbed on metal surfaces has led to a second generation of experiments involving CO on Pt to test linewidth mechanisms.

Development of dichroic far-infrared beam dividers is in progress. These dividers are made from Fabry-Perot etalons with resonant inductive-mesh reflectors.

A Schottky-diode microwave harmonic generator in an open-structure antenna will be acquired to test the usefulness of this technology as a source of tunable far-infrared radiation for laboratory spectroscopy.

The infrared optical properties of charge-density-wave compounds TaS_3 , $(\text{TaSe}_4)_2\text{I}$, and $\text{K}_{0.3}\text{MoO}_3$ are being measured.

1983 PUBLICATIONS AND REPORTS

Refereed Journals

1. S. Chiang, R.G. Tobin, and P.L. Richards, "Infrared Emission Spectroscopy of CO on Ni," *J. Electron. Spectr. & Rel. Phenom.* **29**, 113 (1983); LBL-14552.
2. H.J. Levinson, R.G. Tobin, and P.L. Richards, "Infrared Spectra of CO Adsorbed at Low Temperatures on Ni," *J. Electron. Spectr. & Rel. Phenom.* **30**, 65 (1983); LBL-14556.
3. A.E. Lange, E. Kreysa, S.E. McBride, P.L. Richards, and E.E. Haller, "Improved Fabrication Techniques for Infrared Bolometers," *Int. J. I-R and mm Waves* **4** (5), 689 (1983); LBL-13832.[†]
4. A.D. Smith, W.R. McGrath, P.L. Richards, R.E. Harris, F.L. Lloyd, D.E. Prober, and P. Santhanam, "Microwave Mixing and Direct Detection Using SIS and SIS' Quasiparticle Tunnel Junctions," *IEEE Mag.* **19**, 490 (1983).[‡]

LBL Reports

5. S. Chiang, R.G. Tobin, and P.L. Richards, "Vibrational Spectroscopy of Chemisorbed Molecules by Infrared Emission," accepted by *J. Vac. Sci. Technol. A*, LBL-15868.
6. S. Chiang, R.G. Tobin, P.L. Richards, and P.A. Thiel, "The Molecule-substrate Vibration of CO on Ni(100) Studied by Infrared Emission Spectroscopy," accepted by *Phys. Rev. Lett.*, LBL-16779.
7. R.G. Tobin, S. Chiang, P.A. Thiel, and P.L. Richards, "The C=O Stretching Vibration of CO on Ni(100) by Infrared Emission Spectroscopy," accepted by *Surf. Sci.*, LBL-16780.
8. W.A. Challener and P.L. Richards, "Far Infrared Optical Properties of NbSe_3 ," submitted to *Phys. Rev. Lett.*, LBL-16855.
9. S. Chiang (Ph.D. Thesis), "Infrared Emission Spectroscopy of Carbon Monoxide on Nickel," LBL-16151.
10. J.L. Bonomo (Ph.D. Thesis), "Two Instruments for Far Infrared Astrophysics," LBL-14738.
11. W.A. Challener (Ph.D. Thesis), "Far Infrared Optical Properties of the Quasi-one-dimensional Conductors NbSe_3 and $(\text{TMTSF})_2\text{ClO}_4$," LBL-16186.

Other Publications

12. M.R. Hueschen, E.E. Haller, and P.L. Richards, "Ge:Ga Photoconductors: Development and Ideal Performance," abstract for the Seventh International Conference on I-R and mm Waves, Marseille, France, February 14-18, 1983, LBL-14998.
13. S. Chiang, R.G. Tobin, and P.L. Richards, "Infrared Emission Spectroscopy of CO on Ni(100)," *Bull. Am. Phys. Soc.* **28** (3), 503 (1983); LBL-15379.
14. W.A. Challener, P.L. Richards, and R.L. Greene, "Far Infrared Optical Properties of $\text{TMTSF}_2\text{ClO}_4$," *Bull. Am. Phys. Soc.* **28** (3), 445 (1983); LBL-15380.
15. M.R. Hueschen, E.E. Haller, and P.L. Richards, "Ideal Performance of Gallium-doped Germanium Far Infrared Photoconductors," *Bull. Am. Phys. Soc.* **28** (3), 359 (1983); LBL-15395.
16. S. Chiang, R.G. Tobin, and P.L. Richards, "The Adsorption of CO on Ni(100) Studied by Infrared Emission Spectroscopy," abstract for the Third Surface/Interface Research Meeting, Berkeley, California, May 1983; LBL-15868.

17. S. Chiang, R.G. Tobin, and P.L. Richards, "Infrared Emission Spectroscopy of CO Adsorbed on Ni(100)," abstract for the Physical Electronics Conference, Santa Fe, New Mexico, June 20–22, 1983; LBL-16013.
18. W.R. McGrath, A.D. Smith, and P.L. Richards, "Precise Noise Measurements in SIS Mixers," *Bull. Am. Phys. Soc.* **28** (3), 569 (1983).[‡]
25. P.L. Richards, "The Shuttle Infrared Telescope Facility," Colloquium at the Max-Planck Institute for Radio Astronomy, Bonn, West Germany, July 28, 1983.
26. P.L. Richards, "Far Infrared Detectors," seminar at the Battelle Institute, Frankfurt, West Germany, July 29, 1983.
27. R.G. Tobin, "Infrared Emission Spectroscopy of CO Chemisorbed on Ni(100)," American Chemical Society National Meeting, Washington, D.C., August 29–September 2, 1983, LBL-16032.

Invited Talks

19. W.R. McGrath, "SIS Quasiparticle Mixing: Development of a Quantum Limited Receiver," URSI Conference, Boulder, Colorado, January 5–7, 1983.
20. P.L. Richards, "Infrared Measurements of Molecules Chemisorbed on Metal Surface," Symposium on Photoprocesses on Solid Surfaces, American Chemical Society National Meeting, Seattle, Washington, March 21–25, 1983, LBL-15337.
21. P.L. Richards, "Spectrum of the Cosmic Microwave Background," German Astronomical Society, Konstanz, West Germany, March 25, 1983.
22. P.L. Richards, "Infrared Physics," Symposium on Novel Sources of Electromagnetic Radiation, U.S. DOE, Germantown, Maryland, April 21–22, 1983, LBL-15997.
23. P.L. Richards, "Dramatic Improvements in the Sensitivity of Infrared Detectors" and "Applications to Surface Science and Cosmology," colloquium at Xerox Research Laboratories, Palo Alto, California, May 6, 1983.
24. M. R. Hueschen, "Performance of Ge:Ga Far Infrared Detectors," SIRTf preproposal meeting, NASA Ames Laboratory, Moffet Field, California, July 12–13, 1983.
28. P.L. Richards, "In Search of the Big Bang," Alexander von Humboldt Foundation, II Binational Colloquium, Stanford, California, August 30, 1983.
29. P.L. Richards, "The Spectrum of the Cosmic Microwave Background — How Much is Known?" Colloquium at the Institute for Theoretical Physics, University of California Santa Barbara, September 22, 1983.
30. P.L. Richards, "Measurements of the Cosmic Background Radiation," 1983 Annual Meeting of the Optical Society of America, New Orleans, Louisiana, October 17–20, 1983.
31. P.L. Richards, "Vibrational Spectroscopy of Chemisorbed Molecules by Infrared Emission," 30th National Symposium of the American Vacuum Society, Boston, Massachusetts, November 1–4, 1983, LBL-15868.
32. P.L. Richards, "Panel Discussion on Applications of Free Electron Lasers," Lasers 1983, San Francisco, California, December 13, 1983.

[†]Supported partly by NASA, the Deutsche Forschungsgemeinschaft, and the Alexander von Humboldt Foundation.

[‡]Supported partly by the Office of Naval Research.

Experimental Solid-State Physics and Quantum Electronics*

Y.R. Shen, Investigator

INTRODUCTION

The main objective of this program is to further the basic understanding of lasers and laser-related physics. The emphasis is on development of linear and nonlinear optical techniques for material studies and applications of these techniques to probe linear and nonlinear optical properties of gases, liquids, liquid crystals, and solids. For this purpose, both theoretical and experimental research programs on various aspects of the interaction of light with matter are being carried out. Newly developed techniques are being used to study current problems of interest: isotope separation, photochemistry, surface physics, and phase transitions. Nonlinear optical effects in matter that are not yet clearly understood are also being investigated.

1. Determination of Molecular Orientation of Monolayer Adsorbates by Optical Second-harmonic Generation (Publication 4)

T.F. Heinz, H.W.K. Tom, and Y.R. Shen

Optical second-harmonic generation has been used to deduce the average arrangement and orientation of *p*-nitrobenzoic acid molecules adsorbed at air-silica and ethanol-silica interfaces. An adsorption isotherm for the liquid-solid interface has been obtained.

2. Second-harmonic Reflection from Silicon Surfaces and its Relation to Structural Symmetry (Publication 5)

H.W.K. Tom, T.F. Heinz, and Y.R. Shen

Second-harmonic reflection from Si(100) and Si(111) surfaces exhibits a strong dependence on the

angle of rotation of the sample about its surface normal. This behavior can be related directly to the structural symmetry of the crystal and of the surface. Analysis of the results shows that the surface and bulk contributions to the observed second-harmonic signals from Si are generally of the same order of magnitude.

3. Surface-enhanced Second-harmonic Generation and Raman Scattering (Publication 2)

C.K. Chen, T.F. Heinz, D. Ricard, and Y.R. Shen

Emission from a variety of surface optical processes is significantly increased at interfaces with roughened noble metals. A general formalism, applicable to any optical process, is used to predict the enhancement in the radiated power for second-harmonic generation and Raman scattering from an electrochemically reformed silver surface. Experimental results for these enhancements at different wavelengths are reported. The intensity of the second-harmonic radiation can be understood strictly in terms of the strong macroscopic electric fields produced at the roughened surface by resonant structures. For Raman scattering, part of the enhancement also arises from microscopic local-field effects and the direct chemical interaction of the adsorbate and substrate. The surface-enhanced second-harmonic and Raman signals are studied as the silver sample undergoes oxidation and reduction in an electrolyte containing cyanide ions. The behavior of these two easily measurable probes is described and correlated with the system's surface chemistry.

4. Local-field Effect on Linear and Nonlinear Optical Properties of Adsorbed Molecules (Publication 6)

Peixian Ye and Y.R. Shen

A classical point-dipole model is used to calculate the local-field effect on the optical properties of adsorbed molecules on a substrate. The spatially nonvarying component of the local field at the molecules can be described by using a local-field correction factor. Equally important is the spatially varying component of the local field which arises mainly from the molecule-substrate interaction. The

*This work was supported by the Director, Office of Energy Research, Office of Basic Energy Sciences, Materials Sciences Division of the U.S. Department of Energy under Contract No. DE-AC03-76SF00098.

rapid variation over the molecular dimension can appreciably modify the transition-matrix elements and break down the electric-dipole selection rules. The effect becomes insignificant if the molecules are more than 2.5 Å away from the substrate, even in the metal case. Both components of the local field contribute to the effective linear and nonlinear polarizabilities of the adsorbed molecules. Nonlinearity due to molecular response to the harmonic frequency components of the local field discussed by Antoniewicz appears to be less important.

5. Competing Dissociation Channels of the Infrared Multiphoton Decomposition of Ethyl Vinyl Ether (Publication 3)

F. Huisken, D. Krajnovich, Z. Zhang, Y.R. Shen, and Y.T. Lee

Infrared multiphoton decomposition of ethyl vinyl ether (EVE) has been investigated by the crossed-laser/molecular-beam technique. Competition is observed between the two lowest-energy dissociation channels: (1) $\text{EVE} \rightarrow \text{CH}_3\text{CHO} + \text{C}_2\text{H}_4$, and (2) $\text{EVE} \rightarrow \text{CH}_2\text{CHO} + \text{C}_2\text{H}_5$. Center-of-mass product-translational-energy distributions were obtained for both dissociation channels. The products of reactions (1) and (2) are formed with mean translational energies of 31 and 5 kcal/mol, respectively. The branching ratio shifts dramatically in favor of the higher-energy radical-producing channel as the laser intensity and energy fluence are increased, in agreement with the qualitative predictions of statistical unimolecular-rate theory.

6. Competition Between Atomic and Molecular Chlorine Elimination in the Infrared Multiphoton Dissociation of CF_2Cl_2 (Publication 2)

D. Krajnovich, F. Huisken, Z. Zhang, Y.R. Shen, and Y.T. Lee

Infrared multiphoton dissociation of CF_2Cl_2 has been reinvestigated by the crossed-laser/molecular-beam technique using a high-repetition-rate CO_2 TEA laser. Both the atomic and molecular chlorine-elimination channels were observed: (1) $\text{CF}_2\text{Cl}_2 \rightarrow \text{CF}_2\text{Cl} + \text{Cl}$, and (2) $\text{CF}_2\text{Cl}_2 \rightarrow \text{CF}_2 + \text{Cl}_2$. No evidence was found for secondary dissociation of

CF_2Cl at laser-energy fluences up to 8 J/cm². Center-of-mass product-translational-energy distributions were obtained for both dissociation channels. In agreement with previous work, the products of reaction (1) are found to have a statistical translation-energy distribution. The products of reaction (2) are formed with a mean translational energy of 8 kcal/mol, and the distribution peaks rather sharply about this value, indicating a sizeable exit barrier to molecular elimination. The product-branching ratio was directly determined. Reaction (2) accounts for roughly 10% of the total dissociation yield in the fluence range 0.3-8 J/cm². These results provide an additional test of the statistical theory of unimolecular reactions.

1983 PUBLICATIONS AND REPORTS

Refereed Journals

1. C.K. Chen, T.F. Heinz, D. Ricard, and Y.R. Shen, "Surface-enhanced Second-harmonic Generation and Raman Scattering," *Phys. Rev. B* **27**, 1965 (1983); LBL-14840.
2. D. Krajnovich, F. Huisken, Z. Zhang, Y.R. Shen, and Y.T. Lee, "Competition Between Atomic and Molecular Chlorine Elimination in the Infrared Multiphoton Dissociation of CF_2Cl_2 ," *J. Chem. Phys.* **77**, 5977 (1982); LBL-14478.
3. T.F. Heinz, H.W.K. Tom, and Y.R. Shen, "Determination of Molecular Orientation of Monolayer Adsorbates by Optical Second-harmonic Generation," *Phys. Rev. A* **28**, 1883 (1983); LBL-15794.
4. H.W.K. Tom, T.F. Heinz, and Y.R. Shen, "Second-harmonic Generation and its Relation to Structural Symmetry," *Phys. Rev. Lett.* **51**, 1983 (1983); LBL-16442.
5. Peixian Ye and Y.R. Shen, "Local-field Effect on Linear and Nonlinear Optical Properties of Adsorbed Molecules," *Phys. Rev. B* **28**, 4288 (1983); LBL-16006.

LBL Reports

6. H.W.K. Tom, C.M. Mate, X.D. Zhu, J.E. Crowell, T.F. Heinz, G.A. Somorjai, and Y.R. Shen, "Surface Studies by Optical Second-harmonic Generation: The Adsorption of O_2 , CO , and Sodium on the Rh(111) Surface," LBL-16798.

Other Publications

7. T.F. Heinz, H.W.K. Tom, and Y.R. Shen, "Nonlinear Optical Probes of Interfaces," *Laser Focus* **19**, 101 (1983); LBL-15588.
8. S.D. Durbin, S.M. Arakelian, M.M. Cheung, and Y.R. Shen, "Highly Nonlinear Optical Effects in Liquid Crystals," *J. de Phys.* **44**, C2-161 (1983).[†]
9. T.F. Heinz, H.W.K. Tom, and Y.R. Shen, "Nonlinear Optical Detection of Adsorbed Monolayers," in *Surface Studies with Lasers*, F.R. Aussenegg, A. Leitner, and M.E. Lippitsch, eds., Springer-Verlag, Berlin, 1983, p. 79; LBL-15778.
10. H.W.K. Tom, T.F. Heinz, and Y.R. Shen, "Studies of Molecular Adsorbates at Interfaces by Optical Second-harmonic Generation," in *Laser Spectroscopy VI*, B. Weber and W. Luthy, eds., Springer-Verlag, Berlin, 1983, p. 289; LBL-15485.
11. Peixian Ye and Y.R. Shen, "Second-order Nonlinearity of Adsorbed Molecules Arising from the Local Field Effect," *Bull. Am. Phys. Soc.* **28**, 483 (1983); LBL-15403ABS.
12. T.F. Heinz, C.K. Chen, D. Ricard, and Y.R. Shen, "Surface Enhancement of Second-harmonic Generation and Raman Scattering," *Bull. Am. Phys. Soc.* **28**, 493 (1983); LBL-15404ABS.
13. T.F. Heinz, H.W.K. Tom, and Y.R. Shen, "Application of Optical Second-harmonic Generation to the Study of Adsorbed P-nitrobenzoic Acid," *Bull. Am. Phys. Soc.* **28**, 493 (1983); LBL-15402ABS.
14. H.W.K. Tom, T.F. Heinz, and Y.R. Shen, "Studies of Molecular Adsorbates at Interfaces by Optical Second-harmonic Generation," in *Photochemistry and Photobiology: Proceedings of the International Conference*, A.H. Zewail, Ed., Harwood Academic Pub., Chur, Switzerland, 1983; LBL-15485.
15. H.W.K. Tom, T.F. Heinz, and Y.R. Shen, "Nonlinear Optical Techniques as Surface Probes," Abstracts of Papers, 185th American Chemical Society National Meeting, COLL 53, Seattle, Washington, March 20-25, 1983; LBL-15315ABS.
17. T.F. Heinz, H.W.K. Tom, and Y.R. Shen, "Nonlinear Optical Studies of Adsorbed Molecules," Conference on Surface Studies with Lasers, European Physical Society, Mauterndorf, Austria, March 8-11, 1983.
18. T.F. Heinz, H.W.K. Tom, and Y.R. Shen, "Nonlinear Optical Spectroscopy of Surfaces," Conference on Lasers and Electro-optics, Baltimore, Maryland, May 17-20, 1983.
19. H.W.K. Tom, T.F. Heinz, and Y.R. Shen, "Recent Studies on Second-harmonic Generation as a Surface Probe," Vth International Conference on Laser Spectroscopy, Interlaken, Switzerland, June 27-July 1, 1983.
20. Y.R. Shen, "Surface Nonlinear Optics," ETH Honggerberg, Solid State Physics Laboratory, Zurich, Switzerland, July 7, 1983.
21. Y.R. Shen, "Recent Progress in Surface Studies by Optical Second-harmonic Generation," IBM, Yorktown Heights, New York, August 8, 1983.
22. H.W.K. Tom, T.F. Heinz, and Y.R. Shen, "Nonlinear Optics of Surfaces and Adsorbates," Gordon Conference, Wolfboro, New Hampshire, August 1-5, 1983.
23. Y.R. Shen, "Nonlinear Optics and Surface Physics," Electrical Engineering and Computer Science Department, University of California Berkeley, September 28, 1983.
24. Y.R. Shen, "Surface Studies by Optical Second-harmonic Generation," Chemistry Department, University of California Berkeley, October 11, 1983.
25. Y.R. Shen, "Nonlinear Optics and Surface Physics," University of Georgia, Atlanta, Georgia, October 19, 1983.
26. Y.R. Shen, "Surface Nonlinear Optics," Physics Department, San Jose State University, San Jose, California, October 27, 1983.
27. Y.R. Shen, "Surface Studies by Optical Second-harmonic Generation," Exxon Research and Engineering Co., Linden, New Jersey, November 21, 1983.
28. H.W.K. Tom, T.F. Heinz, and Y.R. Shen, "Studies of Surfaces Using Optical Second-harmonic Generation," Lasers '83 Conference, San Francisco, California, December 12-15, 1983.
29. Y.R. Shen, "Fundamentals of Nonlinear Optics, I," "Fundamentals of Nonlinear Optics, II," "Stimulated Light Scattering," "High-resolution Laser Spectroscopy," "Four-wave Mixing," "Detection of Rare Atoms and Molecules," "Coherent Optical Transient

Invited Talks

16. Y.R. Shen, "Applications of Nonlinear Optics to Material Studies," Conference on Condensed Matter Physics and Applications, Beijing, China, December 28, 1982-January 1, 1983.

Effects,” “Nonlinear Optics on Surfaces,” and “Highly Nonlinear Optical Effects,” all at Fudan University, Shanghai, China, December 13–22, 1983.

30. Y.R. Shen, “Surface Studies by Nonlinear Opti-

cal Methods,” Zhungshan University, Canton, China, December 23, 1983.

[†]Supported by the National Science Foundation under Grant DMR81-17366.

Excitations in Solids*

Carson D. Jeffries, Investigator

INTRODUCTION

The central objectives of this program are experimental studies of the onset of instabilities and pseudorandom behavior in solids, together with a detailed analysis and interpretation within the recently developed renormalization group theory of chaotic dynamics. This theory displays universality and predicts that similar and recognizable modes of behavior will be observed in a very broad class of nonlinear phenomena, e.g., turbulence in fluids; plasma instabilities; erratic behavior in nonlinear mechanical, electrical, and chemical systems; and various instabilities in semiconducting, magnetic, ferroelectric, and piezoelectric materials. The turbulence in solids usually has nonlinear microscopic origins; the chaotic dynamics can be viewed as a consequence of strongly driven elementary excited states. To facilitate direct comparison between observed behavior and theoretical models, specific experimental methods have been developed: bifurcation diagrams, phase space portraits, Poincaré sections, return maps, power spectral analysis, real time and transient analysis, and probability density distributions. This program has concentrated to date on spin waves in ferrites and on semiconductors. A detailed and systematic study of the chaotic dynamics of driven p-n junctions in Si and Ge has revealed many universal patterns: periodic doubling bifurcations, onset of chaos, periodic windows, and intermittency. Spin-wave instabilities in ferrite spheres display period doubling, chaos, and intermittency, and can be understood by a two-dimensional quadratic map. Electron-hole plasma density waves in crystals of Ge exhibit a period doubling route to chaos, periodic windows, and quasi-periodicity. These results have a bearing on devices of high technological interest and on a very general class of nonlinear problems of practical importance.

*This work was supported by the Director, Office of Energy Research, Office of Basic Energy Sciences, Materials Sciences Division of the U.S. Department of Energy under Contract No. DE-AC03-76SF00098.

1. Direct Observation of Crises of the Chaotic Attractor in a Nonlinear Oscillator (Publication 1)

Carson Jeffries and Jose Perez

For a driven nonlinear oscillator we report direct evidence for three cases of an interior crisis of the attractor, as conjectured by Grebogi, Ott, and Yorke. These crises are sudden and discontinuous changes in the attractor, observed directly from bifurcation diagrams and attractor diagrams (Poincaré sections) in real time. The crises arise from intersection of an unstable orbit with the chaotic attractor.

2. Study of a One-dimensional Map with Multiple Basins (Publication 2)

James Testa and G.A. Held

The cubic iterative equation $x_{n+1} = ax_n^3 + (1 - a)x_n$ has two critical points, and in the periodic regime it displays a dependence on the initial condition. This dependence results from the presence of two critical points and leads to two attractors and a "split bifurcation" not found in maps with one critical point. We determined the sequence and pattern of the periodic orbits; these differ from those observed for maps with a single critical point. We noted that a conjugacy principle divides the periodic windows into two distinct categories. Also, we observed a correlation between crises of the attractors and the locations of unstable orbits.

3. Electrically Detected Electron Paramagnetic Resonance (EPR) in Germanium Single Crystals (Publication 3)

E.J. Pakulis

The results of ultrahigh-sensitivity EPR studies of Ge single crystals are discussed. Maximum sensitivity was achieved by using high-Q microwave resonant samples together with an electric detection technique. Under subband-gap optical excitation, two sets of lines were detected: four lines with axial symmetry about the four $\langle 111 \rangle$ axes with $g_{\parallel} = 0.34$ and $g_{\perp} = 1.94$, and 24 lines with $g_{\parallel} = 0.73$ and $g_{\perp} = 1.89$, axially symmetric about $\langle 111 \rangle$ axes with a six-fold 1.2° distortion. Detection involved monitoring

the absorption of energy from the microwave electric field by photoexcited electrons. Due to spin-dependent scattering of the electrons by dangling bonds located in the core of dislocations within the crystal, a resonant change in this absorption was observed on each passage through spin resonance. Both increases and decreases in the absorption were observed, depending on sample characteristics. The spin-dependent scattering was observed to persist for hours after the removal of optical excitation, indicating the existence of a conducting dislocation band with a very long lifetime.

4. Observation of Luminescence from Bound Multiexciton Complexes in Gallium-doped Germanium (Publication 4)

G.A. Held, E.E. Haller, and C.D. Jeffries

Spectrally resolved luminescence associated with the decay of bound multiexciton complexes in optically excited Ge:Ga is observed. This is the first reported observation of multiexciton complexes in p-type germanium. The observed spectra are consistent with the shell model for bound multiexciton complexes. No-phonon, TA, LA, and TO-phonon-assisted luminescences are observed. From these spectra, the energies of the LA, TA, and TO phonons in Ge:Ga are determined.

5. Observation of Period Doubling and Chaos in Spin Wave Instabilities in Yttrium Iron Garnet (Publication 6)

George Gibson and Carson Jeffries

Ferromagnetic resonance in a polished 0.047-cm sphere of gallium-doped yttrium iron garnet is studied at 1.3 GHz in a magnetic field of 460 gauss. A second-order Suhl instability is observed, owing to the nonlinear coupling of the precessing uniform magnetization with spin waves. This is detected by the onset of auto-oscillations of the magnetization. One of these modes with frequency ≈ 16 kHz corresponds to the lowest spherical dimensional resonance of a packet of spin waves of small wave vector and long lifetime ($\approx 10^3$ cycles). From real time signals, spectral analysis, and return maps this mode is found to display chaotic dynamics as the driving rf field is increased: thresholds for the onset of

period-doubling bifurcations, chaos, and periodic windows. Some observed return maps bear resemblance to the two-dimensional area-preserving quadratic map of Henon. The system has several attractors and displays "solid-state turbulence," analogous to that in fluids.

6. Experimental Study of a Driven Oscillator with a Nonlinear Inductive Element (Publication 8)

Paul Bryant and Carson Jeffries

Observations are made of the behavior of a driven negative-resistance oscillator incorporating a saturable inductor with a magnetic core displaying hysteretic dissipation. This system exhibits a Hopf bifurcation to quasi-periodic and phase-locked states. The behavior in the low-frequency regime is shown to be governed by a mapping that for much of the region of interest can be approximated as a map of the plane. Much of the behavior relating to the resonance horns is explored: period-doubling and symmetry-breaking bifurcations; heteroclinic tangencies, crises, and other bifurcations taking place at the horn boundaries; and some of the bifurcations that take place in connection with strong resonances. The effects of magnetic core symmetry on frequency spectra and bifurcations is discussed, along with the effects of asymmetric perturbations. The system is shown to exhibit a Hopf bifurcation from a phase-locked state to periodic islands, similar to those found in Hamiltonian systems. Similarity is shown between the loss of smoothness of the invariant circle in the quasi-periodic regime and the development of chaos in nearby weak resonances via period doubling. This very simple physical system shows dynamical behavior that is representative of behavior found in more complex systems, e.g., turbulence in fluids. It provides a detailed test of current theoretical methods and concepts in nonlinear dynamics.

7. Observation of Chaotic Behavior in an Electron-hole Plasma in Ge (Publication 9)

G.A. Held, Carson Jeffries, and E.E. Haller

Spontaneous current oscillations which develop chaotic behavior are reported for an electron-hole

plasma in a crystal of Ge at 77 K in parallel electric and magnetic fields. The observed behavior includes a period doubling route to chaos (see Figure 7-1) with increasing applied electric field, regions of broadband noise which contain noise-free periodic windows, and bifurcations from quasi-periodic states to turbulence (see Figure 7-2). A rate equation model which includes nonlinear coupling between unstable and damped plasma density waves is presented.

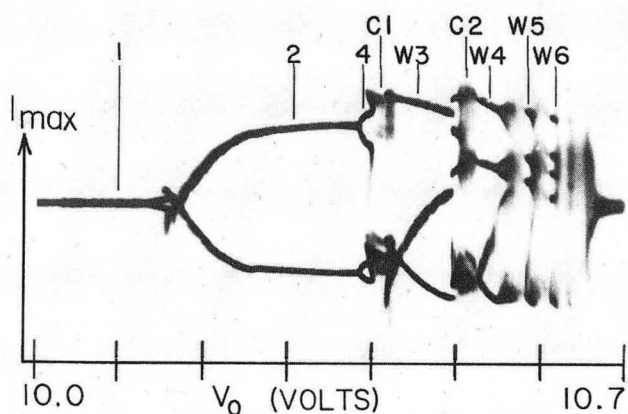


Figure 7-1. Bifurcation diagram (I_{\max} vs driving voltage V_0) for electron-hole plasma current through a Ge crystal at 77 K in an external B field. Current oscillations at $f_0 \approx 118$ kHz show successive period-doubling bifurcations to a chaotic state C1, to period 3 window W3, to chaotic state C2, etc. (XBB 830-10360)

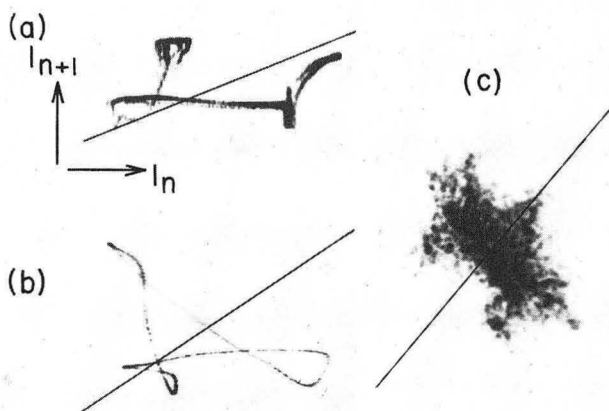


Figure 7-2. Return maps of I_{n+1} vs I_n , where I_n is the set of local current maxima. (a) For sample of Figure 7-1, region C2. (b) For a different sample which showed oscillations at two incommensurate frequencies prior to turbulence. (c) Same as (b), just after turbulence, showing higher dimension attractor.

(XBB 830-10361)

8. Work in Progress

Experiments are in progress to compute various measures of the "dimension" of the chaotic attractor in driven p-n junctions and in electron-hole plasma waves in Ge. The measures include the fractal or Hausdorff dimension, the information dimension, the metric entropy, and the correlation exponent. Chaotic dynamics of electron-hole plasma waves will be studied in different geometries of Ge crystals, some including a large number of probe contacts to establish the spatial variation. Preliminary experiments indicate possible chaotic dynamics in acoustic nonlinearities in ferroelectrics.

1983 PUBLICATIONS AND REPORTS

Refereed Journals

1. Carson Jeffries and Jose Perez, "Direct Observation of Crises of the Chaotic Attractor in a Nonlinear Oscillator," *Phys. Rev. A* **27**, 601 (1983); LBL-14653.
2. James Testa and G.A. Held, "Study of a One-dimensional Map with Multiple Basins," *Phys. Rev. A* **28**, 3085 (1983); LBL-14559 Rev.
3. E.J. Pakulis, "Electrically Detected Electron Paramagnetic Resonance in Germanium Single Crystals," *J. Mag. Res.* **51**, 490 (1983); LBL-14802.
4. G.A. Held, E.E. Haller, and C.D. Jeffries, "Observation of Luminescence from Bound Multiexciton Complexes in Gallium Doped Germanium," *Solid State Comm.* **47**, 459 (1983); LBL-15557.

LBL Reports

5. Jose Maria Perez (Ph.D. Thesis), "Chaotic Behavior of a Driven p-n Junction," LBL-16898.
6. George Gibson and Carson Jeffries, "Observation of Period Doubling and Chaos in Spin Wave Instabilities in Yttrium Iron Garnet," *Phys. Rev. A*, February 1984, LBL-15202.
7. James Clifford Culbertson (Ph.D. Thesis), "Photo-excited States in Germanium at Liquid Helium Temperatures," LBL-15472.
8. Paul Bryant and Carson Jeffries, "Experimental Study of a Driven Oscillator with a Nonlinear Inductive Element," LBL-16949.
9. G.A. Held, Carson Jeffries, and E.E. Haller, "Observation of Chaotic Behavior in an Electron-hole Plasma in Ge," submitted to *Phys. Rev. Lett.*, LBL-16948.

Other Publications

10. Carson Jeffries and George Gibson, "Observation of Period Doubling, Chaos, and Periodic Windows in Spin Wave Instabilities in Yttrium Iron Garnet," *Bull. Am. Phys. Soc.* **28**, 383 (1983), abstract; LBL-15643.
11. G.A. Held, E.E. Haller, and C.D. Jeffries, "Observation of Luminescence from Bound Multiexciton Complexes in Ge:Ga," *Bull. Am. Phys. Soc.* **28**, 542 (1983), abstract; LBL-15644.
12. James Testa and G.A. Held, "Period Doubling, Bifurcations, Chaos, and Periodic Windows of the Cubic Map," *Bull. Am. Phys. Soc.* **28**, 383 (1983), abstract; LBL-15645.
13. Jose Perez and Carson Jeffries, "New Chaotic Sequence in a p-n Junction," *Bull. Am. Phys. Soc.* **28**, 383 (1983), abstract.

Invited Talks

14. C.D. Jeffries, "Observation of Instability and Chaos in a p-n Junction," Solid State Devices Seminar, Department of Electrical Engineering, University of California Berkeley, January 28, 1983.
15. C.D. Jeffries, "Solid State Turbulence: Experiment and Analysis," Colloquium, Los Alamos National Laboratory, Center for Nonlinear Studies, Los Alamos, New Mexico, March 1, 1983; NATO Advanced Research Workshop, Haverford, Pennsylvania, June 5-9, 1983.
16. C.D. Jeffries, "Deterministic Chaotic Dynamics: Experiment and Interpretation," Colloquium, Physics Department, University of California Berkeley, April 14, 1983.

Time-Resolved Spectroscopies in Solids*

Peter Y. Yu, Investigator

INTRODUCTION

Interactions between elementary excitations (such as electrons and phonons) in condensed matter occur in picoseconds (10^{-12} sec). The purpose of this project is to use picosecond, tunable pulses from mode-locked dye lasers to study these fast processes in real time and to deduce from these measurements the strengths and dynamics of the interaction. Spectroscopic techniques used to probe the response of the sample to the excitation laser pulses include light-scattering spectroscopy and photoluminescence. Areas which have been investigated include the behavior of hot electron-hole plasmas in GaAs and excitons in Cu_2O .

1. Study of Nonequilibrium Electron-hole Plasma in GaAs by Light Scattering with Picosecond Laser Pulses (Publication 5)

C.L. Collins and P.Y. Yu

Whenever intense laser beams are used to heat up materials, such as in laser annealing and welding, the energy in the radiation is usually first transferred to the electrons in the material. This process typically occurs at subpicosecond time scales. The heated electrons subsequently transfer their energy to high-energy vibrational modes in picoseconds. It takes nanoseconds for the sample temperature to rise since temperature is determined by distribution of low-energy acoustic phonons. The properties of the hot electron-hole plasma created in solids by these intense laser pulses are not well known. As a result, proposals suggesting that laser annealing is produced by the plasma without melting the sample can be neither verified nor disproved.

We have used picosecond laser pulses to create a high-density electron-hole plasma (density $\lesssim 10^{19} \text{ cm}^{-3}$) in GaAs, and we have studied its properties

by light scattering. We show that the plasma density can be determined directly from the light-scattering spectra of the coupled phonon-plasmon modes (see Figure 1-1). We can determine the electron distribution function from the scattering spectra of single-particle excitations. We find that the electron distribution within the first ~ 40 psec of excitation is highly nonequilibrium, and the plasma expands into the sample with a velocity of 10^7 cm/sec . Work is still in progress to follow the plasma properties as a function of time.

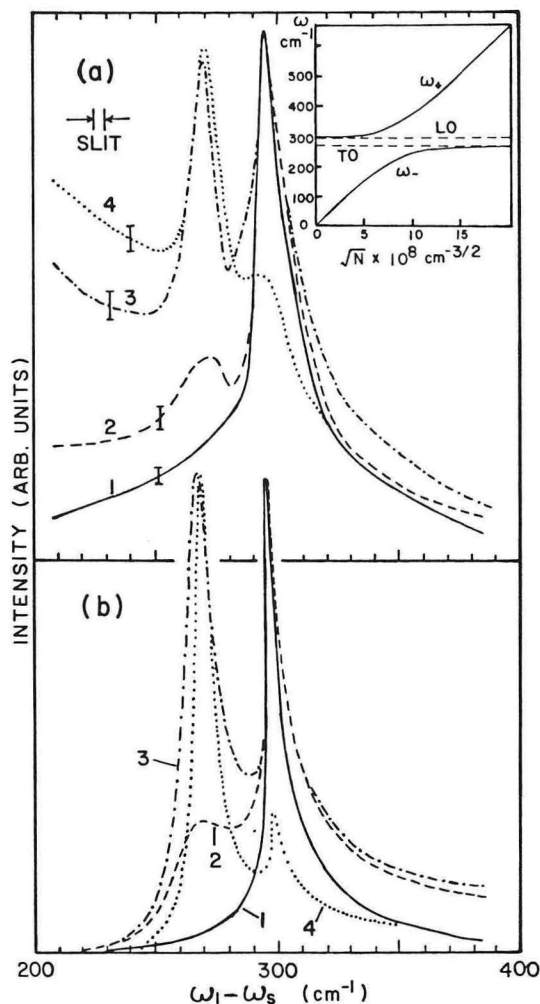


Figure 1-1. Experimental (a) and theoretical (b) Raman spectra of the coupled modes of electron-hole plasma in GaAs. The nominal plasma densities calculated from the laser intensities for the four experimental curves are: (1) -3.4 , (2) -7.0 , (3) -13.6 , and (4) -28 (in units of 10^{18} cm^{-3}). The plasma density used in computing the theoretical curves are: (1) -1.0 , (2) -2.5 , (3) -4.6 , and (4) -9 (10^{18} cm^{-3}). The insert in (a) shows the frequencies of the coupled modes vs electron density predicted by theory. (XBL 8312-4326)

*This work was supported by the Director, Office of Energy Research, Office of Basic Energy Sciences, Materials Sciences Division of the U.S. Department of Energy under Contract No. DE-AC03-76SF00098.

2. Distinction of Resonant Raman Scattering and Hot Luminescence in Cu_2O by Time-resolved Measurements (Publication 4)

J.S. Weiner and P.Y. Yu

Resonant Raman scattering (RRS) with a continuous-wave (cw) laser is a very powerful technique for obtaining information on electronic and vibrational properties of crystals, chemicals, and biological materials. Resonant Raman results can often be understood by assuming that the scattering process at resonance becomes a two-step absorption-followed-by-emission process. Such processes have been known as hot luminescence (HL) in the literature. A controversy over whether RRS and HL are identical or distinct has been going on for ten years now. It has been suggested, first by Y.R. Shen and later by other theorists, that RRS and HL can be distinguished by time-resolved measurements. We have now performed such a measurement in Cu_2O . We show that in Cu_2O the scattering is dominated by HL, and we further show that the time-resolved measurements produce new information on relaxation mechanisms in Cu_2O not obtainable by cw measurements.

1983 PUBLICATIONS AND REPORTS

Refereed Journals

1. C.L. Collins and P.Y. Yu, "Nonequilibrium Phonon Spectroscopy: A New Technique for Studying Intervalley Scattering in Semiconductors," *Phys. Rev. B* **27**, 2602 (1983); LBL-14992.
2. J.S. Weiner, N. Caswell, P.Y. Yu, and A. Mysyrowicz, "Ortho- to Para-exciton Conversion in Cu_2O : A Subnanosecond Time-resolved Photoluminescence Study," *Solid State Commun.* **46**, 105 (1983).
3. C.L. Collins and P.Y. Yu, "Optical Pumping of Hot Phonons in GaAs," *Physica* **117B** and **118B**, 386 (1983); LBL-15350.

LBL Reports

4. J.S. Weiner and P.Y. Yu, "Time-resolved Hot Luminescence and Resonant Raman Scattering: Cu_2O Revisited," LBL-16156.
5. C.L. Collins and P.Y. Yu, "Light Scattering from Non-equilibrium Electron-hole Plasma Excited by Picosecond Laser Pulses in GaAs," LBL-16635.
6. J.S. Weiner and P.Y. Yu, "Free Carrier Lifetime in Semi-insulating GaAs from Time-resolved Band-to-band Photoluminescence," LBL-16966.

Other Publications

7. C.L. Collins and P.Y. Yu, "Light Scattering from High Density e-h Plasmas in GaAs with a Picosecond Dye Laser," *Bull. Am. Phys. Soc.* **28**, 534 (1983).
8. J.S. Weiner, P.Y. Yu, and A. Mysyrowicz, "A Study of Ortho-para-exciton Conversion in Cu_2O by Subnanosecond Time-resolved Photoluminescence," *Bull. Am. Phys. Soc.* **28**, 283 (1983).
9. J.S. Weiner and P.Y. Yu, "Time-resolved Study of Resonant Raman Scattering and Hot Luminescence in Cu_2O ," *Bull. Am. Phys. Soc.* **28**, 283 (1983).

Invited Talks

10. P.Y. Yu, "Study of GaAs with Picosecond Lasers," Electronic Materials Seminar, Department of Materials Science and Mineral Engineering, University of California Berkeley, October 6, 1983.
11. J.S. Weiner, "A Subnanosecond Time-resolved Emission Study of Cu_2O ," Bell Laboratories, Holmdel, New York, November 9, 1983; Philips Research Laboratories, Briarcliff Manor, New York, November 11, 1983; University of Rochester, Laboratory for Laser Energetics, Rochester, New York, November 14, 1983; Eastman Kodak, Rochester, New York, November 15, 1983.

Superconductivity, Superconducting Devices, and 1/f Noise*

John Clarke, Investigator

INTRODUCTION

Dc superconducting quantum interference devices (SQUIDs) are being developed and used in a wide variety of applications, including geophysical measurements, noise thermometry in the millikelvin temperature range, nonequilibrium superconductivity, and the measurement of electrical noise. An ultralow-noise SQUID amplifier has been operated at frequencies up to 100 MHz and is being used to improve the sensitivity of nuclear-magnetic-resonance and quadrupole-resonance measurements. SQUIDs are also being operated at temperatures down to 20 mK to study their ultimate noise limitations for such applications as transducers for gravity-wave antennas. Novel experiments are being used to investigate macroscopic quantum tunneling in Josephson tunnel junctions at millikelvin temperatures. The nonlinear dynamics of circuits containing a Josephson junction are being studied, with particular regard to the noise in such systems. A detailed study is being made of the excess noise induced in metal films by electron bombardment in an electron microscope. This type of measurement may produce a new technique for characterizing the defect concentration of metals.

1. Charge Imbalance Induced by a Temperature Gradient in Superconducting Aluminum (Publications 7 and 14)

H. Jonathon Mamin, Dale J. Van Harlingen, and John Clarke

Although the familiar thermoelectric effects observed in normal metals vanish in superconductors, thermoelectric effects do exist in superconductors but manifest themselves in different ways. For

example, a temperature gradient ∇T is predicted to produce a quasiparticle current $j_N = L_T(-\nabla T)$ that is cancelled everywhere by a counterflowing supercurrent j_S ; here, $L_T(T)$ is the thermoelectric coefficient. We have observed this effect by measuring directly the charge imbalance Q^* associated with the normal current in the region near the end of a superconducting film where j_N diverges. Each sample consisted of an aluminum film about 300 nm thick evaporated onto a glass substrate. A closely spaced array of probes about 3 μm wide were deposited over this film near one end and at right angles to it. The charge imbalance produced by a temperature gradient was determined by measuring the voltage developed at each probe with a SQUID voltmeter. Figure 1-1 shows the voltage $V(x)$ as a function of the distance from the end of the aluminum film for four different temperatures. The solid lines fit to a theory that takes into account the nonuniformity of the temperature gradient near the end of the aluminum film. The fit to the theory is excellent and yields values of L_T that agree well with values measured on the film in the normal state.

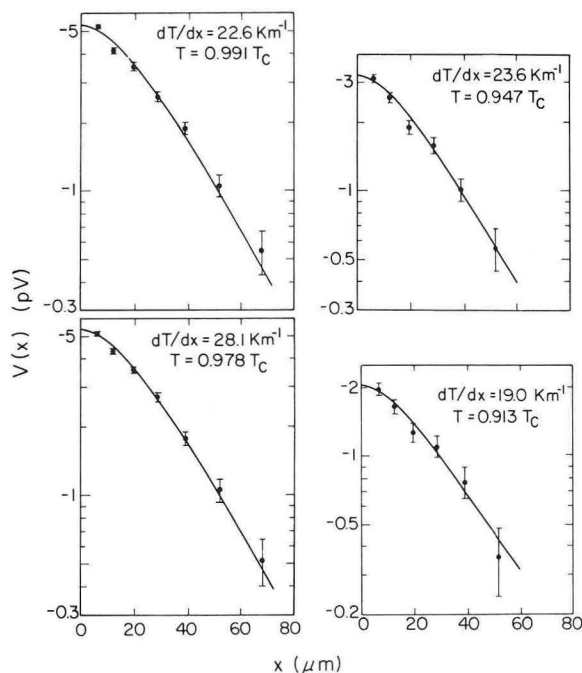


Figure 1-1. Voltage $V(x)$ vs distance from the end of the film x for aluminum film in the presence of a temperature gradient at four different temperatures. Solid lines are fits to theory.
(XBL 839-6440)

*This work was supported by the Director, Office of Energy Research, Office of Basic Energy Sciences, Materials Sciences Division of the U.S. Department of Energy under Contract No. DE-AC03-76SF00098.

2. Phonon-induced Enhancement of the Energy Gap and Critical Current of Superconducting Aluminum Films (Publication 6)

Daniel Seligson and John Clarke

Enhancements of the energy gap Δ and the critical current I_c have been induced in thin superconducting aluminum films near the transition temperature T_c by pulses of phonons at frequencies ν of approximately 9 GHz. In terms of the change in temperature $|\delta T/T_c|$ necessary to produce the same enhancement in equilibrium, the gap enhancement increased smoothly with phonon power at fixed temperature and decreased with decreasing temperature at fixed phonon power. However, at temperatures very close to T_c the enhancement rolled off. At relatively low phonon powers, the data were in good agreement with the theory of Eckern, Schmid, Schmutz, and Sohön (ESSS), as illustrated in Figure 2-1, where we have plotted $\delta T/T_c$ vs T/T_c for 6 levels of phonon power. The solid lines represent a fit to the ESSS theory. At higher power levels the data fell markedly below the predictions of the theory. The critical-current enhancements in terms of $|\delta T/T_c|$ were always larger than the gap enhancements at the same temperature and phonon power. At fixed-phonon power the critical-current enhancements were nearly independent of temperature except at temperatures very close to T_c , where the

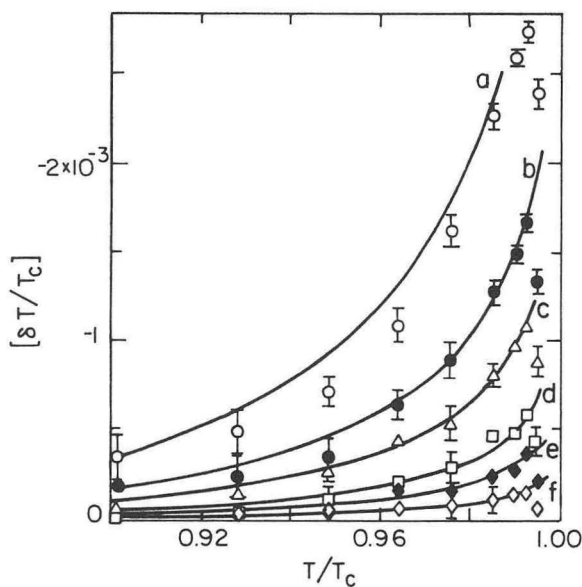


Figure 2-1. Gap enhancement $\delta T/T_c$ vs T/T_c ($h\nu/k_B T_c = 0.333$). Solid lines represent predictions of the ESSS theory, fitted at -10 dB power level. Power levels: a: -7 dB; b: -10 dB; c: -12 dB; d: -17 dB; e: -20 dB. (XBL 835-5602)

enhancement became small. The inclusion of the nonequilibrium quasiparticle distribution and the kinetic energy of the supercurrent in the theory relating the critical-current enhancement to the gap enhancement did not resolve the discrepancies between the two enhancements. It appears likely that there is an additional mechanism for critical-current enhancement that has not yet been identified.

3. Radio-frequency Amplifier Based on a dc SQUID (Publication 5)

Claude Hilbert and John Clarke

We have developed a reliable and sensitive dc SQUID that we are using in a wide variety of applications. The SQUIDs are fabricated in batches of 9 on silicon wafers using state-of-the-art photolithographic techniques. Signals are coupled-in via thin-film planar coils deposited directly on top of the SQUID. An example with a 50-turn coil is shown in Figures 3-1 and 3-2. In one application the SQUID

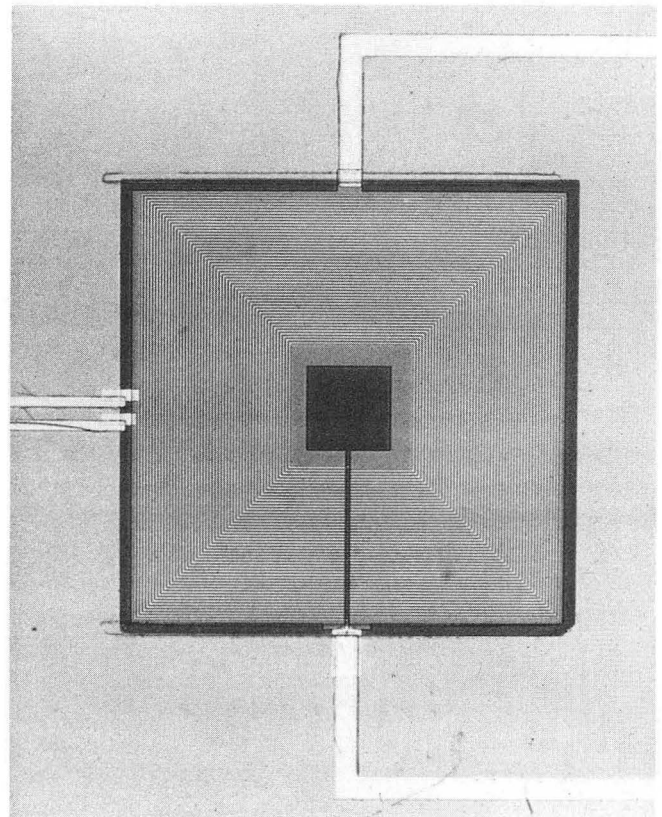


Figure 3-1. Photograph of planar dc SQUID with 50-turn spiral input coil; the SQUID is about 1 mm square.

(CBB 837-5927)

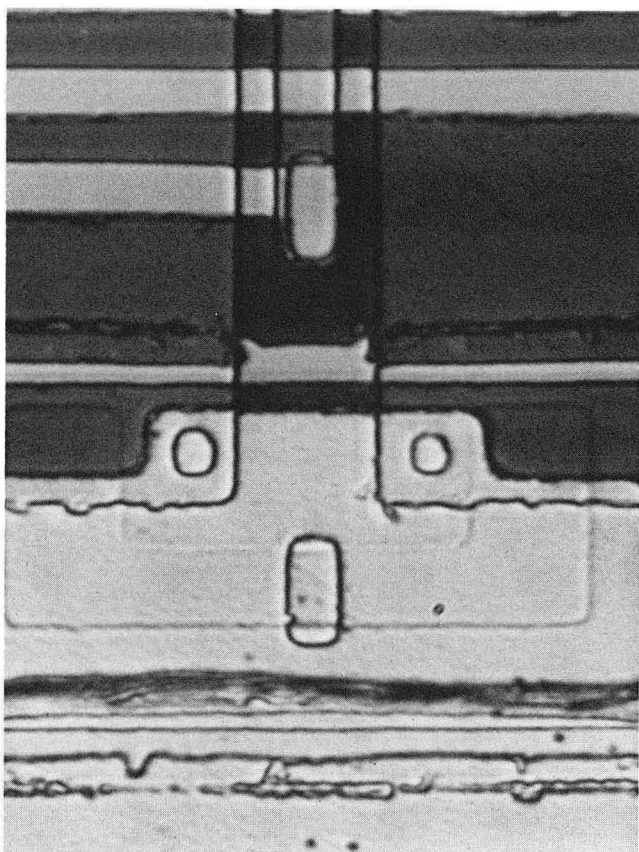


Figure 3-2. Enlargement of Figure 3-1 showing two Josephson tunnel junctions which are about $2 \mu\text{m}$ across. (CBB 837-5925)

is used as an rf amplifier at frequencies up to 100 MHz. The voltage source is coupled to the input coil in series with a 50Ω resistor, and the amplified signal produced across the SQUID is amplified further by a conventional room-temperature amplifier. Typical values of the gain G and noise temperature T_N are shown in Table 3-1 for two different

operating temperatures. These noise temperatures are the lowest ever achieved at these frequencies. The SQUID can be used for nuclear-magnetic and nuclear-quadrupole resonance, and it should lead to a major advance in the sensitivity of these methods.

4. Integrated dc SQUID Magnetometer with a High Slew Rate (Publication 16)

Frederick Wellstood, C. Heiden, and John Clarke

For a number of years we have used cylindrical dc SQUIDS as magnetometers for magnetotelluric measurements. Although the sensitivity ($10 \text{ fT}\cdot\text{Hz}^{-1/2}$) has been more than adequate, the slew rate has been limited by the associated electronics to about $30 \mu\text{T}/\text{sec}$. This slew rate has proved to be inadequate during periods of high electrical activity, where "sferics" may cause the magnetometer to become unlocked. We have converted the SQUID shown in Figure 3-1 to a magnetometer by depositing a thin-film pickup loop on the same silicon wafer; the pickup loop is connected to the spiral coil. The magnetic-flux sensitivity of this SQUID is an order of magnitude greater than that of the cylindrical SQUID. The electronics package has also been redesigned to produce a higher slew rate. The combination of the higher flux sensitivity and improved electronics has enabled us to retain the same sensitivity as the cylindrical SQUID but increase the slew rate by more than two orders of magnitude to $4 \text{ mT}/\text{sec}$ at 6 KHz . The frequency response has been extended to 70 KHz . This device, which is eminently suitable for 3-axis magnetometers for geophysical applications, can be operated under almost any conditions encountered in the field without losing lock.

Table 3-1
Gain G and noise temperature T_N for a typical dc SQUID at two different temperatures

Frequency (MHz)	Gain (dB)		Noise Temperature T_N (K)	
	T=4.2 K	T=1.5 K	T=4.2 K	T=1.5 K
60	20.0 ± 0.5	24.0 ± 0.5	4.5 ± 0.6	1.2 ± 0.3
80	18.0 ± 0.5	21.5 ± 0.5	4.1 ± 0.7	0.9 ± 0.3
100	16.5 ± 0.5	19.5 ± 0.5	3.8 ± 0.9	1.0 ± 0.4

5. Excess Noise in Josephson Parametric Amplifiers (Publication 4)

Robert F. Miracky and John Clarke

Three- and four-photon Josephson parametric amplifiers have been plagued by the problem of "noise rise," a noise temperature that increases roughly as the power gain increases. The origin of this effect, which has prevented the amplifier from becoming a useful device, has been the subject of considerable discussion. However, our recent studies of chaos in a Josephson tunnel junction shunted by a resistor with self-inductance have brought to light the phenomenon of noise-induced hopping between nearby subharmonic modes, resulting in large levels of excess noise. To test whether such hopping effects can occur in a Josephson parametric amplifier, we have simulated the three-photon device with an analog simulator that includes both a calibrated thermal-noise source and a model for the microwave circulator that couples the signal to and from the junction. To establish the correct operating conditions, we applied a signal at approximately one-half the pump frequency ω_p and adjusted the dc-bias and ac-pump levels until maximum gain was achieved. Just above the optimum bias and pump levels, the system bifurcated to an oscillation at $\omega_p/2$, and the gain dropped abruptly. In the absence of thermal noise, the amplifier showed large amounts of gain with no associated noise rise. However, in the presence of thermal noise, the gain was lower and, more importantly, accompanied by very large levels of noise. This noise arises from random hopping, induced by thermal noise, between the ω_p and $\omega_p/2$ modes. Thus, the noise rise inevitably accompanies the gain process and can be eliminated only by operating the amplifier at extremely low temperatures.

1983 PUBLICATIONS AND REPORTS

Refereed Journals

1. Roger H. Koch, John Clarke, W.M. Goubau, J.M. Martinis, C.M. Pegrum, and D.J. Van Harlingen, "Flicker (1/f) Noise in Tunnel Junction dc SQUIDS," *J. Low Temp. Phys.* **51**, 207 (1983); LBL-14973.
2. H.F. Miracky, Roger H. Koch, and John Clarke, "Chaotic Noise Observed in a Resistively Shunted Self-resonant Josephson Tunnel Junction," *Phys. Rev. Lett.* **50**, 856 (1983); LBL-15221.
3. John Clarke, T.D. Gamble, W.M. Goubau, R.H. Koch, and R.F. Miracky, "Remote-reference Magnetotellurics: Equipment and Procedures," *Geophys. Pros.* **31**, 149 (1983); LBL-13559.
4. R.F. Miracky and John Clarke, "Simulation of the Noise Rise in Three-photon Josephson Parametric Amplifiers," *Appl. Phys. Lett.* **43**, 508 (1983); LBL-16091.
5. Claude Hilbert and John Clarke, "Radio-frequency Amplifier Based on a dc Superconducting Quantum Interference Device," *Appl. Phys. Lett.* **43**, 694 (1983); LBL-16293.
6. D. Seligson and J. Clarke, "Phonon-induced Enhancement of the Energy Gap and Critical Current of Superconducting Aluminum Films," *Phys. Rev. B* **28**, 6297 (1983); LBL-16323.
7. H.J. Mamin, J. Clarke, and D.J. Van Harlingen, "Observation of Thermoelectrically Induced Charge Imbalance in Superconducting Aluminum," *Phys. Rev. Lett.* **51**, 1480 (1983); LBL-16456.
8. J. Clarke, R.F. Miracky, J. Martinis, and R.H. Koch, "Chaos and Noise in Josephson Tunnel Junctions," in *Noise in Physical Systems and 1/f Noise*, M. Savelli, G. Lecoy, and J-P. Nougier, eds., Elsevier, 1983, p.117; LBL-16127.
9. John Clarke, "Geophysical Applications of SQUIDS," *IEEE Trans. Magn.* **MAG-19**, 288 (1983); LBL-15312.
10. J.M. Martinis and John Clarke, "Measurements of Current Noise in dc SQUIDS," *IEEE Trans. Magn.* **MAG-19**, 446 (1983); LBL-15313.
11. R. H. Koch, J. Clarke, J.M. Martinis, W. M. Goubau, C. M. Pegrum, and D.J. Van Harlingen, "Investigation of 1/f Noise in Tunnel Junction dc SQUIDS," *IEEE Trans. Magn.* **MAG-19**, 449 (1983); LBL-15314.
12. W.M. Goubau, P. Maxton, and J. Clarke, "Correlation Lengths in Magnetotellurics," LBL-15484.
13. Daniel Seligson (Ph.D. Thesis), "Phonon-induced Enhancements of the Energy Gap and Critical Current in Superconducting Aluminum," LBL-16290.
14. H.J. Mamin, J. Clarke, and D.J. Van Harlingen, "Charge Imbalance Induced by a Temperature Gradient in Superconducting Aluminum," LBL-16693.

LBL Reports

15. K. Wiesenfeld, E. Knobloch, R.F. Miracky, and J. Clarke, "Calculation of Period-doubling in a Josephson Circuit," LBL-16873.
16. F. Wellstood, C. Heiden, and J. Clarke, "Integrated dc SQUID Magnetometer with a High Slew Rate," LBL-17127.

Other Publications

17. John Clarke, "Fundamental Limits on SQUID Technology," in *Advances in Superconductivity*, B. Deaver and John Ruvalds, eds., Plenum, New York, 1983, p.13; LBL-14972.
18. R. Miracky, J. Clarke, and R. Koch, "Chaos in Resistively Shunted Self-resonant Josephson Tunnel Junctions: Experiments and Simulation," *Bull. Am. Phys. Soc.* **28**, 568 (1983); LBL-15316ABS.
19. C. Hilbert and J. Clarke, "Dc SQUID as a Radiofrequency Amplifier," *Bull. Am. Phys. Soc.* **28**, 570 (1983); LBL-15317ABS.
20. K.A. Wiesenfeld, E. Knobloch, R. Miracky, and J. Clarke, "Period-doubling in a Josephson Circuit: Analytic Approach," *Bull. Am. Phys. Soc.* **28**, 1313 (1983); LBL-16619ABS.

Invited Talks

21. J. Clarke, "SQUIDs and Geophysics: New Applications for Sensitive Magnetometers," Colloquium at Francis Bitter National Magnet

Laboratory, Cambridge, Massachusetts, April 19, 1983.

22. J. Clarke, "SQUIDs, Brains, and Gravity Waves," Annual Meeting of the Association of North Bay Scientists, College of the Redwoods, Eureka, California, April 30, 1983.
23. J. Clarke, "Chaotic Noise in Josephson Tunnel Junctions," 7th International Conference on Noise in Physical Systems, Montpellier, France, May 17-20, 1983; LBL-16127.
24. J. Clarke, "SQUIDs in the Real World," Colloquium at IBM, Zurich, Switzerland, May 24, 1983.
25. J. Clarke, "Chaos and Noise in Josephson Tunnel Junctions," Colloquium at University of California at Santa Cruz, Santa Cruz, California, June 2, 1983.
26. J. Clarke, "Nonequilibrium Superconductivity and Quantum Noise," Workshop on Problems in Superconductivity, Copper Mountain, Colorado, August 21-22, 1983.
27. J. Clarke, W.M. Goubau, P.M. Maxton, and R.H. Koch, "Noise Correlations in Remote Reference Magnetotellurics," Fall Meeting of the American Geophysical Society, San Francisco, California, December 5-9, 1983.
28. F.C. Wellstood, C. Heiden, and J. Clarke, "Integrated SQUID Magnetometer with High Slew Rate," Fall Meeting of the American Geophysical Society, San Francisco, California, December 5-9, 1983.

THEORETICAL RESEARCH

Theoretical Studies of the Electronic Properties of Solid Surfaces*

L.M. Falicov, Investigator

INTRODUCTION

The purpose of this program is to study properties of solid surfaces. In particular the interest is in determining (a) structural properties of surfaces, namely the organization and arrangement of atomic constituents at equilibrium; (b) constitutional properties of the surface, in particular the segregation properties of alloys at the surface as a function of crystal structure, surface orientation, nominal chemical composition, and temperature; (c) electronic structure of surfaces, in particular electron states and electron densities in the neighborhood of the surface; (d) vibronic properties of surfaces; (e) magnetic properties of surfaces, both in magnetic solids (ferromagnetic and antiferromagnetic) and in nonmagnetic solids that may develop a magnetic surface layer; and (f) chemical properties of solids — in particular their catalytic properties — as they are related to all the basic physical properties listed above.

A variety of theoretical techniques and models have been developed to focus on the various properties (band-structure models, many-body electron physics, numerical relaxation techniques), but the emphasis is on physical aspects and their implication to experiments rather than on techniques *per se*.

Since 1978 we have worked with Dr. Eugene Haller and his group to study a set of unusual impurities in very pure semiconductors. These impurities had never been seen before and include hydrogen complexes, lithium-based complexes, carbon-nitrogen complexes, and ordinary substitutional impurities in an unusual charge state.

1. Calculation of the Magnetic States of Cobalt Overlayers on Cu(111) (Publication 4)

R.H. Victora and L.M. Falicov

One- and two-atom layers of cobalt on a Cu(111) surface were found to be magnetic with a spin polarization close to the bulk value. The calculation was performed in a tight-binding scheme, with single-site full-orbital interactions treated self-consistently. Antiferromagnetic and ferromagnetic states with a two-atom periodicity were examined. A new type of "spatially modulated" state was found. The density of states and the spatial distribution of magnetization were obtained for each configuration. The ferromagnetic state was found to have the lowest total energy; the energy of the spatially modulated state was, however, calculated to be only 0.03 Ry per surface atom higher. Agreement with photoemission experiments is satisfactory: it is excellent for a one-atom layer of Co on Cu(111), but a theoretically predicted shift in peak location with Co-layer thickness was not found experimentally. Calculations for both pure Cu(111) and Co on Cu(111) show that the spectral features observed at the corner of the surface-Brillouin zone arise from the totally symmetric electronic states.

2. Three Holes Bound to a Double Acceptor: Be⁺ in Germanium (Publication 3)

E.E. Haller, Robert E. McMurray, Jr., L.M. Falicov, N.M. Haegel, and W.L. Hansen

A double acceptor that binds three holes has been observed for the first time with photoconductive far-infrared spectroscopy in beryllium-doped germanium single crystals. The new center, Be⁺, has a hole-binding energy of ~5 meV and is only present when free holes are generated by ionization of either neutral shallow acceptors or neutral-Be double acceptors. The Be⁺ center thermally ionizes above 4 K. It disappears at a uniaxial stress $\geq 10^9$ dyn/cm² parallel to [111] as a result of the lifting of the valence-band degeneracy.

*This work was supported by the Director, Office of Energy Research, Office of Basic Energy Sciences, Materials Sciences Division of the U.S. Department of Energy under Contract No. DE-AC03-76SF00098.

3. Work in Progress

Magnetic and electronic properties of the Fe-Co alloys are being studied. In particular, the enhancement of the magnetization of each atomic component in the alloy compared to the elemental solid and the enhancement of the magnetization of the surface of the alloy with respect to its bulk are now understood.

1983 PUBLICATIONS AND REPORTS

Refereed Journals

1. B. Koiller and L.M. Falicov, "Theory of Inelastic Electron Scattering from Antiferromagnetic NiO: Surface and Bulk Effects," *Phys. Rev. B* **27**, 346 (1983).[†]
2. B. Koiller and L.M. Falicov, "Theory of Electron Scattering from a Heisenberg Antiferromagnet: Surface and Bulk Effects," *J. Magn. Mater.* **31-34**, 907 (1983).[†]
3. E.E. Haller, Robert E. McMurray, Jr., L.M. Falicov, N.M. Haegel, and W.L. Hansen, "Three Holes Bound to a Double Acceptor: Be⁺ in Germanium," *Phys. Rev. Lett.* **51**, 1089 (1983); LBL-15988.
4. R.H. Victora and L.M. Falicov, "Calculation of the Magnetic States of Cobalt Overlayers on Copper (111)," *Phys. Rev. B* **28**, 5232 (1983); LBL-16072.
5. B. Koiller, M.O. Robbins, M.A. Davidovich, and C.E.T. Goncalves da Silva, "Renormalization Group Treatment for the Electronic Spectrum of Partially Ordered One-dimensional Alloys," *Solid State Commun.* **45**, 955 (1983).[†]
6. M.O. Robbins and B. Koiller, "Renormalization-group Methods for the Spectra of Disordered Chains," *Phys. Rev. B* **27**, 7703 (1983).[†]
7. J. Oliva, "Self-consistent Hellmann-Feynman Theorem for Tight-binding Models," *Phys. Rev. B* **28**, 1798 (1983).[†]
8. J.L. Morán-López and L.M. Falicov, "Theory of Hydrogen Chemisorption on Ferromagnetic Transition Metals," in *Electronic Structure and Properties of Hydrogen in Metals*, P. Jena and C.B. Satterthwaite, eds., Plenum Press, New York, 1983, p. 635.[‡]
9. J.L. Morán-López and L.M. Falicov, "Theory of Surface Effects in Binary Alloys," in *Alloy Phase Diagrams*, L.H. Bennett, T.B. Massalski, and B.C. Geissen, eds., North-Holland, New York, 1983, p. 29.[‡]
10. M.O. Robbins and L.M. Falicov, "Electronic Energy and Short-range Order in Binary Alloys," in *Alloy Phase Diagrams*, L.H. Bennett, T.B. Massalski, and B.C. Geissen, eds., North-Holland, New York, 1983, p. 53.[†]
11. R.H. Victora and L.M. Falicov, "Magnetization of Thin Cobalt Films," *Bull. Am. Phys. Soc.* **28**, 250 (1983).
12. B. Koiller and L.M. Falicov, "Theory of Inelastic Electron Scattering from Antiferromagnetic NiO: Surface and Bulk Effects," *Bull. Am. Phys. Soc.* **28**, 297 (1983).[†]
13. J. Oliva and L.M. Falicov, "Self-consistent Hellmann-Feynman Theorem for Tight-binding Models," *Bull. Am. Phys. Soc.* **28**, 329 (1983).[†]
14. L.M. Falicov and J. Oliva, "Theory of Hydrogen-based Dynamic Acceptor Complexes in Ge," *Bull. Am. Phys. Soc.* **28**, 329 (1983).[†]
15. E.E. Haller, N.M. Haegel, R.E. McMurray, Jr., and L.M. Falicov, "A⁺ Centers in Beryllium-doped Germanium Single Crystals," *Bull. Am. Phys. Soc.* **28**, 411 (1983).

Invited Talks

16. L.M. Falicov, "Dynamic Effects in Semiconductor Shallow Impurities," Brazilian Summer School on the Physics of Semiconductors, Campinas, Brazil, January 31, 1983.
17. L.M. Falicov, "Ordering and Segregation in Intermetallic Alloys," March Meeting of the American Physical Society, Los Angeles, California, March 22, 1982 (presented by M.O. Robbins).
18. L.M. Falicov, "Ferromagnetism of Thin Ni Films," March Meeting of the American Physical Society, Los Angeles, California, March 23, 1983 (presented by J. Tersoff).
19. L.M. Falicov, "Magnetic Properties of Thin Films and Surfaces of Transition Metals," IBM Lecture Series: Current Problems in Magnetism, IBM Research Laboratory, San Jose, California, June 13, 1983.
20. L.M. Falicov, "Chemical, Electronic, and Magnetic Properties of Transition-metal Films, Overlayers, Surfaces, and Interfaces," Gordon Conference on Catalysis, Colby-Sawyer College, New London, New Hampshire, June 27, 1983.
21. L.M. Falicov, "Dynamic Impurities Involving Hydrogen in Very Pure Germanium," Exxon Laboratories, Linden, New Jersey, July 5, 1983; VII Latin American Symposium on Solid State Physics, Oaxtepec, Mexico, July 18, 1983;

- University of Brasilia, Brazil, August 4, 1983; Solid State Division Seminar, Oak Ridge National Laboratory, Oak Ridge, Tennessee, December 14, 1983.
22. L.M. Falicov, "Dynamic Impurities in Ultrapure Germanium: Tunneling Hydrogen," IBM Research Laboratory, Yorktown Heights, New Jersey, July 8, 1983.
 23. L.M. Falicov, "Hydrogen in Metals," Universidad Autonoma, San Luis Potosi, Mexico, July 26, 1983.
 24. L.M. Falicov, "Chemical, Electronic, and Magnetic Properties on Transition Films, Overlayers, Surfaces, and Interfaces," Petroleum Institute, Mexico City, July 22, 1983.
 25. L.M. Falicov, "Spin-off of Science and Technology," topic of a round-table discussion, Rio de Janeiro, Brazil, July 29, 1983.
 26. L.M. Falicov, "Current Status of Condensed Matter Physics," Second Symposium on Pan-American Collaboration, Rio de Janeiro, Brazil, August 1, 1983.
 27. L.M. Falicov, "Surface Magnetism," Pennsylvania State University, University Park, Pennsylvania, November 2, 1983.
 28. L.M. Falicov, "Condensed Matter Physics: Past, Present, and Future," Society of Physics Students, University of California Berkeley, December 2, 1983.
 29. L.M. Falicov, "Magnetic Properties of Surfaces, Interfaces, and Overlayers," Symposium on Electron, X-ray, and Ion Spectroscopies and their Application to Surfaces, 38th Northwest Regional Meeting, American Chemical Society, University of Hawaii, Honolulu, Hawaii, December 28, 1983.

[†]Supported in part by the National Science Foundation through Grant DMR81-06494.

[‡]Supported in part by the National Science Foundation through Grant DMR81-06494 and INT80-18688.

Theoretical Solid-State Physics*

Marvin L. Cohen, Investigator

INTRODUCTION

The purpose of this research is to provide a microscopic theory of solids capable of explaining and predicting the physical properties of real materials. During the past few years a successful theory has been developed here. The theory is based on a quantum-mechanical pseudopotential/local-density/total-energy approach, and the inputs are essentially only the atomic number and atomic mass of the constituent atoms making up a solid. Applications of the method have been made to surfaces, interfaces, optical properties, superconductivity, electronic structure, vibrational properties, static structural properties, high-pressure solid-phase transitions, transport phenomena, photoemission characteristics, chemisorption properties, and properties of molecules.

Direct collaborations with experimental projects have been frequent, and the predictive power of the theoretical approach has been tested successfully.

SURFACES

1. Pseudopotential Total-energy Calculations for Si(111)-(2 × 1) (Publication 2)

John E. Northrup and Marvin L. Cohen

The total energies of several models of the Si(111) surface have been calculated with the pseudopotential method and the local-spin-density functional formalism. The 2 × 1 chain model has the lowest calculated total energy of those structures considered.

2. Atomic Geometry and Surface-state Spectrum for Ge(111)-(2 × 1) (Publication 5)

John E. Northrup and Marvin L. Cohen

The π -bonded chain model is studied for Ge(111)-(2 × 1). The minimum-energy chain geometry is found with the use of the Hellmann-Feynman forces. A buckling of the surface atoms in the chain is energetically favorable. This buckling is associated with rehybridization (sp^3 to sp^2) effects.

STRUCTURAL AND ELECTRONIC PROPERTIES OF SEMICONDUCTORS AND INSULATORS

3. Structural Properties of III-V Zincblende Semiconductors under Pressure (Publication 1)

Sverre Froyen and Marvin L. Cohen

The pseudopotential method within the local-density approximation is used to investigate the static and structural properties of some III-V compound semiconductors. Comparisons of calculated total energies as a function of volume and structure yield information about solid-solid phase transformations. At high pressure the results indicate that several metallic structures are lower in energy than the zincblende structure. From our results the compounds AlP, AlAs, GaP, and GaAs can be divided into two classes. In the Ga compounds we find a pressure-induced phase transformation to either rock salt, β -Sn, or NiAs, whereas in the Al compounds rock salt and NiAs are stabilized with respect to β -Sn. All structures except zincblende are metallic. We discuss the electronic structure of each phase and show how it relates to structural stability.

4. Will Diamond Transform under Pressure? (Publication 6)

M.T. Yin and Marvin L. Cohen

It is predicted that among the fcc, bcc, hcp, simple-cubic, and β -tin phases, diamond will first transform to the simple-cubic phase under a hydrostatic pressure of 23 Mbar. The absence of p electrons in the core causes remarkably strong sp^3 bond-

*This work was supported jointly by the Director, Office of Energy Research, Office of Basic Energy Sciences, Materials Science Division of the U.S. Department of Energy under Contract No. DE-AC03-76SF00098, and by the National Science Foundation under Grant No. DMR7822465.

ing in diamond. This stabilizes diamond against the other five phases under high pressures. The study is carried out using *ab initio* pseudopotential theory within the local-density-functional formalism.

5. The Electronic Band Structures for Zincblende and Wurtzite BeO (Publication 7)

K.J. Chang, Sverre Froyen, and Marvin L. Cohen

The self-consistent electronic band structures for zincblende and wurtzite BeO are calculated using first-principles pseudopotentials. The calculated direct band gap for wurtzite BeO is consistent with experimental measurement, and the valence-band width is also in good agreement with experiment; however, the value for the forbidden band gap is underestimated. For the hypothetical zincblende structure, an indirect band gap is found. We present the band structure, density of states, and the valence charge density in a (110) plane for both crystal structures.

6. Electronic Band Structures for Zincblende and Wurtzite CdS (Publication 14)

K.J. Chang, Sverre Froyen, and Marvin L. Cohen

The electronic band structures for zincblende and wurtzite CdS are calculated within the local-density approximation with the use of first-principles pseudopotentials. Incorporating the d state into the valence band substantially improves the main valence-band width and yields valence-band features in good agreement with experiment. The maximum effect of the d band occurs at Γ_{15} for zincblende CdS and at $\Gamma_1 \Gamma_6$ for wurtzite CdS. We find that the local-density approximation does not accurately predict the position of localized Cd 4d state.

STRUCTURAL AND ELECTRONIC PROPERTIES OF METALS

7. Calculation of High-pressure Phases of Al (Publication 4)

Pui K. Lam and Marvin L. Cohen

Possible high-pressure phases of Al are examined by comparing the total energies for three structures: fcc, bcc, and hcp. The energies are calculated using the density-functional formalism and the *ab initio* self-consistent pseudopotential approach. At zero pressure the most stable structure is the fcc structure, in agreement with experiment. At about 2 Mbar the hcp structure is predicted to be the most stable, whereas at about 4 Mbar the bcc structure is the most stable. The stability of the bcc phase at compressed volumes is found to be caused by the lowering of the d states. This conclusion is based on an analysis of the occupancy of s, p, and d states at normal and compressed volumes.

8. Calculation of the Compton Profile of Beryllium (Publication 9)

M.Y. Chou, Pui K. Lam, and Marvin L. Cohen

A calculation of the Compton profiles of beryllium is presented. The wave functions are obtained from an *ab initio* calculation with the use of the pseudopotential approach within the local-density-functional approximation. The calculated anisotropic profiles are in excellent agreement with experiments. The directional profiles are also in good agreement except for a small discrepancy with experiment that can be improved by the inclusion of the effects of correlation in an approximate way.

9. *Ab initio* Study of Structural and Electronic Properties of Beryllium (Publication 13)

M.Y. Chou, Pui K. Lam, and Marvin L. Cohen

An *ab initio* calculation of the structural and electronic properties of beryllium is presented. The calculation method used is the self-consistent pseudopotential approach within the local-density-functional scheme. The calculated lattice constants, cohesive energy, bulk modulus, Poisson's ratio, electronic band structure, density of states, and charge density are all in good agreement with the experimental measurements.

STRUCTURAL AND ELECTRONIC PROPERTIES OF MOLECULES

10. Pseudopotential Local-spin-density Calculations for Si (Publication 12)

John E. Northrup, M.T. Yin, and Marvin L. Cohen

Pseudopotential local-spin-density calculations of the bond lengths, vibrational energies, and dissociation energies for the $^3\Sigma_g^-$, $^3\Sigma_u^+$, and two $^1\Sigma_g^+$ states of the silicon dimer have been performed. The bond lengths are within 1% of experimental values, and the vibrational frequencies are within 5% of experimental values. The dissociation energy of the ground state is larger than experiment by ~ 1.25 eV. These results are near the limits of accuracy of the local-spin-density approximation.

11. Work in Progress

The structural and electronic properties of the (2×1) -antiferromagnetic and (1×1) -paramagnetic states of Si(111) are being studied. Adatom geometries are also being investigated to examine their possible role in the (2×1) and (7×7) structures.

A structural theory of graphitic carbon and silicon is being developed. A detailed calculation of the momentum distribution for graphite and lithium-intercalated graphite is being done to unravel Compton-scattering experiments. A theory of the pressure dependence of semiconductor and insulator band gaps has been applied to a variety of materials. A complete *ab initio* theory of the structural and

vibrational properties of NaCl is being done. This work will serve as a prototype calculation for alkali halides.

The temperature- and pressure-induced crystallographic transitions in Be are being computed. Possible pressure-induced transitions are being examined. A calculation illustrating the dependence of lattice constants and bulk moduli on pseudopotential properties of metals is in progress.

A pseudopotential local-spin-density calculation of the bond length, vibrational frequency, and binding energy of the germanium dimer is being done.

1983 PUBLICATIONS AND REPORTS

Refereed Journals

1. Sverre Froyen and Marvin L. Cohen, "Static and Structural Properties of III-V Zincblende Semiconductors," *Proc. 16th Int. Conf. Physics of Semiconductors, Montpellier, 1982, Part I*, North Holland, Amsterdam, 1983, p. 561 (Physica **117B** and **118B**).
2. John E. Northrup and Marvin L. Cohen, "Pseudopotential Total Energy Calculations for Si(111)-(1 \times 1) and Si(111)-(2 \times 1)," *Proc. 16th Int. Conf. Physics of Semiconductors, Montpellier, 1982, Part II*, North Holland, Amsterdam, 1983, p. 774 (Physica **117B** and **118B**).
3. M.T. Yin and Marvin L. Cohen, "Valence-electron Density in Silicon under High Pressure," *Phys. Rev. Lett.* **50**, 1172 (1983).
4. Pui K. Lam and Marvin L. Cohen, "Calculation of High-pressure Phases of Al," *Phys. Rev. B* **27**, 5986 (1983).
5. John E. Northrup and Marvin L. Cohen, "Atomic Geometry and Surface-state Spectrum for Ge(111)-(2 \times 1)," *Phys. Rev. B* **27**, 6553 (1983).
6. M.T. Yin and Marvin L. Cohen, "Will Diamond Transform under Megabar Pressures?" *Phys. Rev. Lett.* **50**, 2006 (1983).
7. K.J. Chang, Sverre Froyen, and Marvin L. Cohen, "The Electronic Band Structures for Zincblende and Wurtzite BeO," *J. Phys. C* **16**, 3475 (1983).
8. Marvin L. Cohen, "Pseudopotentials for Calculating the Bulk and Surface Properties of Solids," *Revista Brasileira de Fisica, Volume Especial*, **10** (1983).
9. M.Y. Chou, Pui K. Lam, and Marvin L. Cohen, "Calculation of the Compton Profile of

- Beryllium," Phys. Rev. B **28**, 1696 (1983).
10. Pui K. Lam and Marvin L. Cohen, "Correlation of Superconductivity with Material Properties," Phys. Lett. A **97**, 114 (1983).
 11. Sverre Froyen and Marvin L. Cohen, "Structural Properties of III-V Zincblende Semiconductors under Pressure," Phys. Rev. B **28**, 3258 (1983).
 12. John E. Northrup, M.T. Yin, and Marvin L. Cohen, "Pseudopotential Local-spin-density Calculations for Si₂," Phys. Rev. A **28**, 1945 (1983).
 13. M.Y. Chou, Pui K. Lam, and Marvin L. Cohen, "*Ab initio* Study of Structural and Electronic Properties of Beryllium," Phys. Rev. B **28**, 4179 (1983).
 14. K.J. Chang, Sverre Froyen, and Marvin L. Cohen, "Electronic Band Structures for Zincblende and Wurtzite CdS," Phys. Rev. B **28**, 4736 (1983).

Other Publications

15. M.T. Yin and M.L. Cohen, "Theoretical Study of Phase Stability for Diamond," Bull. Am. Phys. Soc. **28**, 429 (1983).
16. M.Y. Chou, P.K. Lam, and M.L. Cohen, "Theoretical Study of Beryllium: Structural Properties, Electronic Properties, and Phase Transitions," Bull. Am. Phys. Soc. **28**, 1327 (1983).

Invited Talks

17. Marvin L. Cohen, "Atomic Structure of Solids: Surface and Bulk," Center for Advanced Materials (CAM) Scientific Review, Lawrence Berkeley Laboratory, Berkeley, California, January 10, 1983.
18. Marvin L. Cohen, "Pseudopotentials for the Electronic Structure of Solids and Surfaces: Electronic Energy Band Theory," "Surfaces and Interfaces," "Total Energy and Structure I," and "Total Energy and Structure II," Summer School on Semiconductor Physics, Campinas, Brazil, January 31–February 3, 1983.
19. Marvin L. Cohen, "Fifty Years of Pseudopotentials," International Sanibel Symposia, Palm Coast, Florida, March 10, 1983; Naval Research Laboratory, Washington, D.C., April 27, 1983; Department of Physics, Harvard University, Cambridge, Massachusetts, September 30, 1983; 22nd Eastern Theoretical Physics Conference, Brookhaven National Laboratory, Upton, New York, October 22, 1983.
20. Marvin L. Cohen, "Predicting the Properties of Solids," Department of Physics, Sonoma State University, Rohnert Park, California, April 11, 1983.
21. Marvin L. Cohen, "Electronic Structure of Solids," Symposium to Mark the 70th Birthday of Gregory Wannier, University of Oregon, Eugene, Oregon, May 20, 1983.
22. Marvin L. Cohen, "Overview: Science and Technology," Symposium to Establish the Pacific International Center for High Technology Research, Honolulu, Hawaii, May 31, 1983.
23. Marvin L. Cohen, "The Fermi Atomic Pseudopotential: Applications to Non-metals; Mostly Bulk Properties," International School of Physics "Enrico Fermi," Varenna, Italy, June 30, 1983.
24. Marvin L. Cohen, "The Fermi Atomic Pseudopotential: Applications to Non-metals; Mostly Surface and Interface Properties," International School of Physics "Enrico Fermi," Varenna, Italy, July 1, 1983.
25. Marvin L. Cohen, "Theory of GaAs: Bulk and Interfaces," CAM Workshop, Lawrence Berkeley Laboratory, Berkeley, California, October 11, 1983.
26. Marvin L. Cohen, "Pseudopotential Calculations for Surfaces," American Chemical Society, Pacific Conference on Chemistry and Spectroscopy, Pasadena, California, October 27, 1983.

MATERIALS CHEMISTRY

CHEMICAL STRUCTURE

Low-Temperature Properties of Materials*

Norman E. Phillips, Investigator

INTRODUCTION

Measurements of low-temperature properties of condensed-matter systems, particularly heat capacities, are used to obtain information that contributes to an understanding of the behavior of materials. There are numerous special cases in which specific heat data provide either a test of theoretical models or values of important parameters that could not otherwise be obtained. Much of the work is in the region below 1 K, where the temperature scale is not well defined and temperature-measuring techniques are not well established. Because accurate temperature determinations are important in obtaining useful heat-capacity data, research is also conducted on methods of temperature measurement.

An accurate temperature scale has been developed to below 10 mK. Specific-heat measurements on ^3He in the Fermi-liquid region have established the correct values of parameters that are important to understanding the superfluid states. The specific heats of potassium, rubidium, and cesium have been measured to 0.1 K to search for predicted charge-density wave effects. Although analysis of the data is not complete, the preliminary conclusion is that charge-density wave effects are not present. Measurements on CuMn in high magnetic fields have mapped out the theoretically predicted phase boundary.

*This work was supported by the Director, Office of Energy Research, Office of Basic Energy Sciences, Materials Sciences Division of the U.S. Department of Energy under Contract No. DE-AC03-76SF00098.

1. Specific-heat Anomaly and Phase Boundary for the Spin-glass/Paramagnet Transition in CuMn (Publication 1)

William E. Fogle, James D. Boyer, R.A. Fisher, and Norman E. Phillips

Examination of the second derivatives of specific-heat data on 2790-at. ppm CuMn between 0.3 and 30 K and in fields to 75 kOe show a small field-dependent specific-heat anomaly that is, apart from magnitude, in qualitative agreement with recent theoretical predictions for the spin-glass transition (see Figure 1-1). The results support the approximate validity of mean-field theory for real spin glasses and, indirectly, the reality of the predicted phase transition. The specific-heat measurements give the entropy as a function of both temperature and field, which has been compared with the Parisi-Toulouse hypothesis. Although the total entropy does not show the predicted behavior, the small part of the entropy associated with the anomaly does.

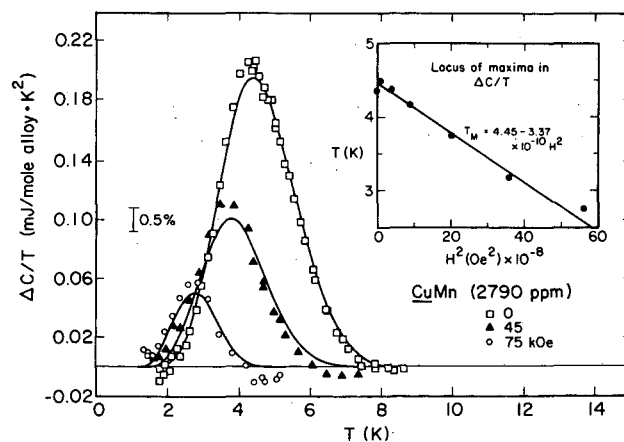


Figure 1-1. Representative heat capacity anomalies for CuMn at three magnetic fields, extracted from the data by analysis of the second derivatives. The inset shows a comparison of the temperatures of the maxima with the predicted H^2 dependence. (XBL 832-8411)

2. Specific Heat of ^3He in the Fermi-liquid Region (Publication 2)

M.C. Mayberry, William E. Fogle, and Norman E. Phillips

In recent years a controversy has developed over the correct magnitude and temperature dependence of the specific heat of ^3He in the Fermi-liquid region — the discrepancies between measurements from different laboratories have been as great as 40%. Since the parameters derived from the Fermi-liquid data are important to an understanding of the superfluid states, new measurements have been made on a temperature scale that is expected to represent the thermodynamic temperature (see Figure 2-1). Specific-heat data on ^3He between 6.5 and 200 mK are in good agreement with recent data from Bell Laboratories and in substantial disagreement with all other data. It is shown that many of the discrepancies would arise from demonstrable discrepancies in the different laboratory temperature scales.

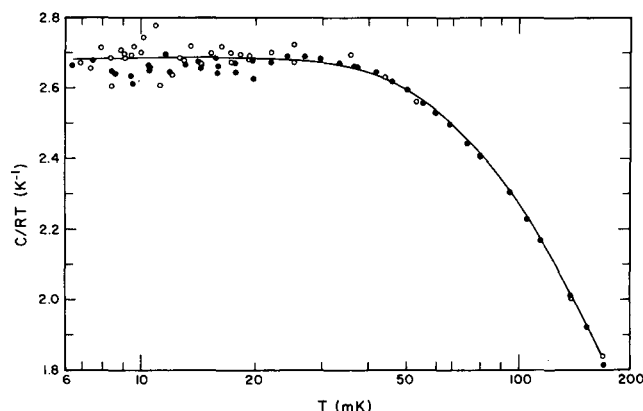


Figure 2-1. The specific heat of ^3He . The solid symbols represent points taken with 10 cm^3 of liquid. The open symbols represent points with 5 cm^3 of liquid and are consequently of lower precision, but they demonstrate the absence of surface effects. (XBL 8311-4671)

3. Work in Progress

Recent measurements¹ have been interpreted as showing a charge-density wave contribution to the specific heat of potassium, but it has been suggested² that the reported anomaly may reflect temperature-scale errors. Since the question is of fundamental importance in the theory of metals, new measurements to 0.1 K have been made on potassium,

rubidium, and cesium. A preliminary report³ on the potassium data shows that there is no anomaly of the magnitude and temperature reported earlier. More detailed analysis is in progress.

Significant improvements have been made in the capability for making high-pressure specific-heat measurements. A new cell withstands pressures of 25 kbar at room temperature and is expected to retain approximately 20-kbar pressure at low temperatures. It will be used to extend the measurements on $\alpha\text{-Ce}$ into the more interesting part of the phase diagram and for measurements on other "mixed-valence" materials.

¹C.D. Amarasekara and P.H. Keesom, *Phys. Rev. Lett.* **47**, 1311 (1981).

²N.E. Phillips, *Phys. Rev. Lett.* **48**, 1504 (1982).

³J. Van Curen, E.W. Hornung, J.C. Lasjaunias, and N.E. Phillips, *Phys. Rev. Lett.* **49**, 1653 (1982).

1983 PUBLICATIONS AND REPORTS

Refereed Journals

1. William E. Fogle, James D. Boyer, R.A. Fisher, and Norman E. Phillips, "Specific-heat Anomaly and Phase Boundary for the Spin-glass-paramagnet Transition in CuMn ," *Phys. Rev. Lett.* **50**, 1815 (1983); LBL-16309.
2. M.C. Mayberry, William E. Fogle, and Norman E. Phillips, "Specific Heat of ^3He in the Fermi-liquid Region," *Quantum Fluids and Solids, Am. Institute of Phys.*, AIP Conference Proceedings No. 103, 1983, p. 161; LBL-15646 Rev.
3. G.E. Brodale, R.A. Fisher, W.E. Fogle, N.E. Phillips, and J. Van Curen, "The Effect of Spin-glass Ordering on the Specific Heat of CuMn ," *J. Magnetism and Magnetic Materials* **31** (34), 1331 (1983); LBL-17109.
4. James D. Boyer, J.C. Lasjaunias, R.A. Fisher, and Norman E. Phillips, "The Low-temperature Specific Heat of PTFE (Teflon) at Pressures to 5.2 kbar," *J. Non-Cryst. Solids* **55**, 413 (1983); LBL-17110.

Invited Talks

5. N.E. Phillips, "Specific Heat of CuMn : Evidence for a Phase Transition," Centre de Recherches sur les tres Basses Temperatures, Grenoble, France, March 15, 1983.

6. N.E. Phillips, "Resolution of the Controversy over the Fermi-liquid Specific Heat of ^3He ?" Centre de Recherches sur les tres Basses Temperatures, Grenoble, France, March 17, 1983.
7. N.E. Phillips, "Calorimetric Evidence for the Reality of the Gabay-Toulouse Line in CuMn ," C.N.R.S., Universite de Paris Sud, Orsay, France, March 22, 1983.
8. M.C. Mayberry, "Specific Heat of ^3He in the Fermi-liquid Region," Conference on Quantum Fluids and Solids, Sanibel Island, Florida, April 13, 1983.
9. N.E. Phillips, "Specific Heat of the Spin-glass CuMn ," Department of Physics, University of California Berkeley, December 7, 1983.

Electrochemical Processes*

Charles W. Tobias, Investigator

INTRODUCTION

This program is designed to advance the scientific foundations of electrochemical engineering and to broaden the range of useful applications of electrochemical transformations. Electrolysis processes have inherent advantages over thermochemical methods with respect to material yield and energy efficiency. However, in spite of their long history of economically significant applications, cell processes have not achieved their potential with respect to performance and range of applications in chemical synthesis, nor in energy conversion or storage. A major reason for this condition is the complex nature of transport phenomena in ionic media, as these phenomena relate to charge-transfer processes at the electrode surface. The present emphasis in this program is on exploring novel methods for reducing mass-transfer resistance in high-rate applications, including electroforming of metals and electro-organic synthesis. The effects of fixed-flow obstacles, and suspended inert solid particles in flowing electrolytes, on transport rates and current distribution are measured over broad ranges of process variables. Theoretical models are advanced for the interpretation of mechanisms. A major part of this effort is directed jointly with Dr. Rolf H. Muller.

Nonaqueous ionizing solvents are evaluated for potential use at ambient temperatures in electrosynthesis processes. Emphasis is placed on the thermodynamic and kinetic properties of various electrode reactions not feasible in aqueous media.

Applied research on Surface Morphology of Metals in Electrodeposition, Engineering Analysis of Electrolytic Gas Evolution, and Metal Couples in Nonaqueous Electrolytes is supported by the Office of Advanced Conservation Technologies, DOE, and is reported under Electrochemical Energy Storage.

1. Effects of Small Flow Obstacles on the Limiting Current and Pressure Drop in a Square Duct (Publication 2)

Daniel S. Fischl, Rolf H. Muller, and Charles W. Tobias

This work investigated the effectiveness of mass-transfer enhancement by small obstacles attached to the cathode in an electrochemical flow cell 0.5 by 0.5 cm in cross section and 50.8 cm long. Pressure drops and limiting currents for the reduction of ferricyanide were measured in the range of $80 \leq Re \leq 3200$. Rectangular obstacles extending 0.0254 to 0.160 cm from the surface were used, and the spacing-to-height ratio ranged from 9 to 170. Suspensions of inert materials were used to make the flow patterns around obstacles visible. The patterns were recorded by means of dark-field photography.

Depending on the flow rate, addition of the obstacles can increase mass-transfer rates by as much as five times over those in the unobstructed system (see Figure 1-1). The maximum enhancement occurs when the spacing is approximately 15 times the obstacle size, corresponding to the largest elongation of the recirculation zone observed downstream from an obstacle.

At $Re \approx 100$, the mass-transfer rate is approximately doubled on addition of the optimal number of obstacles without appreciably affecting the pressure drop. The largest enhancement (5-fold) occurs at the upper laminar flow regime with a 2.7-fold increase in the pressure drop. These comparisons are made at the same flow rate.

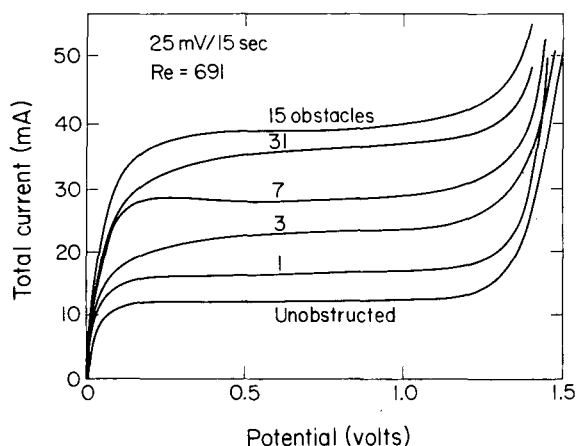


Figure 1-1. Limiting current densities for the cathodic reduction of ferricyanide on a 50.8-cm-long electrode in a channel. Equally spaced $0.16 \times 0.16 \times 5$ mm plastic slabs are glued to the electrode surface, normal to the flow direction.

(XBL 835-2635)

*This work was supported by the Director, Office of Energy Research, Office of Basic Energy Sciences, Materials Sciences Division of the U.S. Department of Energy under Contract No. DE-AC03-76SF00098.

In the unobstructed system, improved mass-transfer rates (limiting currents) are achieved by increasing the flow rate to produce turbulent flow. This approach involves large pressure drops and consequently large pumping-power requirements. An increase in the limiting current by the addition of obstacles, on the other hand, requires only 2-5 percent of the pumping power required to obtain the same limiting current achieved by increasing the flow rate in the unobstructed system (see Figure 1-2). Obstacles therefore produce efficient mixing near the electrode surface and correspondingly high mass-transfer rates without causing large energy dissipation in the bulk fluid.

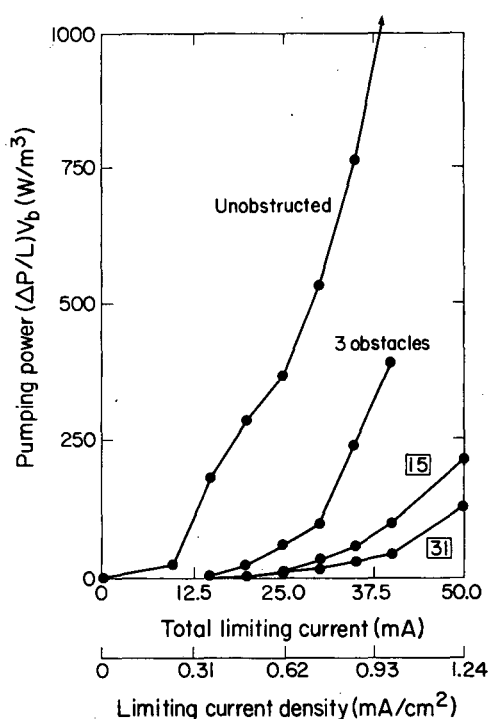


Figure 1-2. Pumping power required to achieve a specified limiting current density on a planar electrode imbedded in the wall of a channel as a function of number of equally spaced $0.76 \times 0.76 \times 5$ mm plastic obstacles attached to the 50.8-cm-long by 5-mm-wide nickel electrode. (XBL 838-3062)

2. Work in Progress

Experimental and theoretical work is in progress on the control of rate and composition in the codeposition of metals with dissimilar standard potentials. Two model systems are under investigation: cadmium-telluride and lead-tin alloys. Of particular interest is the role of solution-side ionic trans-

port on alloy composition. A theoretical model has been established for the description of the effects of periodic (pulsed) current on solution-side surface composition, alloy composition, and electrode potential.

Copper deposits approximately 1 mm thick are being electroformed at current densities from 1–10 amp/cm². A cell containing a cylindrical cathode rotating coaxially with the stagnant outer cylinder (anode) has been constructed to allow the formation of metallic shapes at these high deposition rates. Control of deposit morphology is investigated without the usual additives by using electrical variables (e.g., pulsed current).

The effects of suspended solids on transport rates at rotating-disk electrodes facing upward are being measured. Macroscopic and microscopic models are under development for the interpretation of transport-rate enhancement relative to the particle-free case.

Firm evidence has been obtained that a moisture content on the order of 10 ppm renders propylene carbonate and its analogues unstable with respect to both strong oxidizing and reducing agents. Solvent preparation by fractional freezing is under evaluation as a promising method for removal of water to below 1 ppm.

A review of the electrochemistry in ethylene carbonate is in preparation. This solvent has a dielectric constant higher than water, and in certain applications it may have advantages over propylene carbonate.

1983 PUBLICATIONS AND REPORTS

LBL Reports

1. C.W. Tobias, D. Rajhenbah, and J. Faltemier, "Mass Transfer Limiting Currents of Zinc Deposition in Acidic ZnCl₂ and ZnSO₄ Solutions," LBL-15338.†
2. D.S. Fischl (M.S. Thesis), with R.H. Muller and C.W. Tobias, "Effects of Small Flow Obstacles on the Limiting Current and Pressure Drop in a Square Duct," LBL-16422.
3. J.L. Faltemier (Ph.D. Thesis), with C.W. Tobias, "The Effect of Hydrodynamic Flow on the Morphology of Electrodeposited Zinc," LBL-16485.†
4. J. Faltemier, M. Jaksic, C.W. Tobias, and T. Tsuda, "An Inventory of Photographs of Zinc Electrodeposited from Acid Electrolytes," LBL-16601.†

5. D.W. Dees (Ph.D. Thesis), with C.W. Tobias, "Mass Transfer at Gas Evolving Surfaces in Electrolysis," LBL-16176.[†]

Other Publications

6. A. Kindler and C.W. Tobias, "The Morphology of Copper Electrodeposition; Powder Deposition," Electrochemical Society Meeting, San Francisco, May 8-13, 1983, Ext. Abstr. 83-1, no. 583, pp. 879-880; based on LBL-12838.[†]
7. P.C. Foller, M.L. Goodwin, and C.W. Tobias, "Glassy Carbon Anodes and Air-depolarized Cathodes for the Generation of Ozone," Electrochemical Society Meeting, San Francisco, May 8-13, 1983, Ext. Abstr. 83-1, no. 578.[‡]
8. D.W. Dees and C.W. Tobias, "Development of a Data Acquisition and Control System for the Study of Mass Transfer Phenomena on a Micromosaic Electrode," Electrochemical Society Meeting, San Francisco, May 8-13, 1983, Ext. Abstr. 83-1, no. 469.[†]
9. Process for Producing Ozone (1983): U. S. Patent No. 4,375,395 (with P.C. Foller and M.L. Goodwin); based on LBL-16176.[‡]

Invited Talks

10. C.W. Tobias (with Douglas Bennion, E.J. Cairns, Karl Kordesch, John Newman, and William Tiedemann, instructors), short course on electrochemical engineering of batteries, Marriott Hotel, Berkeley, California, June 20-24, 1983.
11. C.W. Tobias, "Electrochemical Techniques for the Studies of Mass Transport Phenomena," invited colloquia lectures, The University of Pennsylvania, Philadelphia, October 3, 1983; Carnegie-Mellon University, Pittsburgh, Pennsylvania, October 5, 1983.
12. C.W. Tobias, "Effect of Hydrodynamic Flow on the Morphology of Zinc Deposited from Acid Electrolytes," workshop on zinc/halogen batteries under the auspices of LBL and EPRI, Palo Alto, California, November 30-December 2, 1983.[†]

[†]Supported by the Office of Advanced Conservation Technologies, U. S. Department of Energy.

[‡]Supported entirely from University funds.

HIGH-TEMPERATURE AND SURFACE CHEMISTRY

High-Temperature Thermodynamics*

Leo Brewer, Investigator

INTRODUCTION

High-temperature chemistry is characterized by the occurrence of unusual species and phases that are often unstable at conventional temperatures. Because of the difficulty of carrying out measurements under high-temperature conditions, it is important to design experiments to yield information that can be used with predictive models. In this manner one can often calculate chemical behavior under conditions where measurements have not been made or would not be practical.

Since 1943 the research of this program has led to the development of successful models of predictive capability for the behavior of gases at high temperatures, of refractory containment materials, and of many metallic systems. For many alloys, understanding the interactions is adequate to provide quantitative predictive models. As an example, in 1980 a tabulation of the thermodynamic properties and phase diagrams of 100 binary systems of molybdenum was published. The main thrust of the present research is aimed at providing quantitative predictive models for the strongly interacting alloys exhibiting generalized Lewis acid-base behavior. A variety of experimental methods are being used to characterize the thermodynamics of these systems.

*This work was supported by the Director, Office of Energy Research, Office of Basic Energy Sciences, Materials Sciences Division of the U.S. Department of Energy under Contract No. DE-AC03-76SF00098.

1. Solute Stabilization for hcp-fcc Transitions: Co-Mo (Publication 1)

Leo Brewer and Drucilla G. Davis†

The structural change from the low-temperature form of cobalt to the high-temperature form is very sluggish. Experimentally reported phase studies contradicting the predictions of the Brewer-Engel theory were believed to be due to lack of equilibration. Samples were equilibrated in a temperature-gradient furnace, and a crystal-growth catalyst was used to find the optimum conditions for equilibration. An unambiguous confirmation of the theory was obtained by demonstration that molybdenum stabilizes the hexagonal phase of cobalt. The temperature range of stability is increased from $427 \pm 40^\circ\text{C}$ for pure cobalt to $849 \pm 6^\circ\text{C}$ for an alloy with five atomic percent molybdenum.

†Present address: Shell Development Co., Houston, Texas 77001.

2. Systematics of the Properties of the Lanthanides (Publication 8)

Leo Brewer

The trends in the properties of the lanthanide metals and their compounds were analyzed in terms of the electronic configurations involved. For the various distributions of valence electrons among the 4f, 5d, 6s, and 6p orbitals, the energies of the lowest states of each configuration were fixed either from experimental data or by the use of predictive models. These values were used to analyze the abnormal trends of the boiling points of the metals. The thermodynamic properties of lanthanide solid oxides and the gaseous LnO, Ln₂O₂, Ln₂O, and LnO₂ species were characterized. Data were given for the gaseous diatomic molecules, and the thermodynamic stability of lanthanide and actinide intermetallic binary systems was characterized in terms of electronic configurations, internal pressures, and size factors.

3. Mathematical Representation of Size and Electronic Factors (Publication 9)

Leo Brewer

The modifications of the regular-solution model to incorporate the contributions of different electronic configurations is discussed, and mathematical equations are presented that use electronic configuration, internal pressure, and size to characterize the thermodynamics of metallic solutions.

4. Calculations of Boundaries of Saturated Phases (Publication 3)

Leo Brewer and Susie Hahn

Mathematical equations and calculator programs are presented for the calculation of the phase boundaries of binary systems. The programs can be applied to pairs of saturating solids, liquids, or a combination of a solid and liquid.

5. The Responsibility of High-temperature Scientists (Publication 4)

Leo Brewer

The complexity of high-temperature systems and the difficulty of making reliable measurements sets severe limits on the amount of information that can be obtained by direct experiment. Theoretical models are needed to provide the information needed by technology, but a sound base of critically evaluated data is needed for the development and testing of these models. Specialists in each field collect and critically evaluate data in their field for their own use. It is most important that they take the additional effort to make these compilations available to those who do not have the background to adequately evaluate the possible sources of error. Sometimes such an effort requires collaboration by a number of individuals.

As an example, it was necessary to know the thermodynamic data for the gaseous actinides. A number of specialists in the field of actinide atomic spectroscopy collaborated in providing the most

complete set of spectroscopic data available. Various models were used to predict the positions of yet unobserved levels. It was thus possible to calculate the thermodynamic properties of the elements francium to lawrencium with high accuracy. For many of the elements, values of $-(G^\circ - H^\circ_{298})/RT$ could be provided up to 3000 K with an uncertainty of ± 0.0001 . Analytical equations were developed that allow calculation of values between 298 and 3000 K.

6. The Generalized Lewis Acid-base Theory: Surprising Recent Developments (Publication 2)

Leo Brewer

An unexpected application of the G.N. Lewis acid-base theory has been to mixtures of the transition metals, including the lanthanides and actinides with the platinum-group metals. The Engel theory of metals assigns empty d orbitals to transition metals on the left side of the Periodic Table and nonbonding electron pairs to the platinum-group metals. Very strong acid-base interactions have been demonstrated in confirmation of the theory. When 10M HCl is added to an excess of 10M NaOH, the activity of the hydrogen ion only drops by a factor of 10^{16} . The same mixing of Hf or U with an excess of Pd or Pt at room temperature would reduce the activity of Hf or U by a factor of more than 10^{90} . This type of interaction is important in many metal systems.

7. Work in Progress

The thermodynamics of strongly interacting metallic systems is being investigated by a variety of methods, including phase-equilibrium measurements, electrochemical-cell measurements using solid-electrolyte cells, and vapor-pressure measurements using atomic fluorescence. Thermodynamic data are being critically evaluated and compiled in analytical form for all of the elements and their oxides. Calculator programs have been developed for calculation of thermodynamic properties of a variety of gaseous molecules. The results are being tabulated. The theoretical models for prediction of the properties of metallic systems are being tested against available data, and improved models are being developed.

1983 PUBLICATIONS AND REPORTS

Refereed Journals

1. L. Brewer and D.C. Davis, "Solute Stabilization for hcp-fcc Transitions: Co-Mo," *Met. Trans.* **15A**, 67-72 (1984); LBL-16649.
2. L. Brewer, "The Generalized Lewis Acid-base Theory: Surprising Recent Developments," *J. Chem. Educ.* **61** (2), 101-104 (1984); LBL-14867.

LBL Reports

3. L. Brewer and S. Hahn, "Calculations of Boundaries of Saturated Phases," LBL-16726.
4. L. Brewer, "The Responsibility of High Temperature Scientists," accepted by *High Temperature Science* **17**, LBL-17310.
5. J.K.M. Gibson (Ph.D. Thesis), "Thermochemistry of Acid-base Stabilized Transition Metal Alloys by Carbide and Nitride Equilibria and Knudsen Effusion Vapor Pressures," LBL-16233.
6. J.K. Gibson, L. Brewer, and K.A. Gingerich, "Thermodynamics of Several Lewis Acid-base Stabilized Transition Metal Alloys," submitted to *Met. Trans.*, LBL-16815.
7. R.H. Lamoreaux, D.L. Hildenbrand, and L. Brewer, "High Temperature Vaporization Behavior of Oxides, II. Oxides of Be, Mg, Ca, Sr, Ba, B, Al, Ga, In, Tl, Si, Ge, Sn, Pb, Zn, Cd, and Hg," submitted to *J. Phys. Chem. Ref. Data*, LBL-17309.[†]
8. L. Brewer, "Systematics of the Properties of the Lanthanides," in *NATO ASI Series C: Mathematical and Physical Sciences No. 109*, S.P. Sinha, Ed., D. Reidel, Boston, 1983, pp. 17-69; LBL-14811.

9. L. Brewer, "Mathematical Representation of Size and Electronic Factors," *Materials Research Society Symposium Proceedings*, Vol. 19, L.H. Bennett, T.B. Massalski, and B.C. Giessen, eds., North-Holland, New York, 1983, pp. 129-134; LBL-15220.
10. L. Brewer, "Gases: (A) Spectroscopy of Interest to High-temperature Chemistry, and (B) Reactions Between Gases and Condensed Phases," in *Bibliography on the High-temperature Chemistry and Physics of Materials*, Vol. 27, Part 2, M.B. Hocking and V. Vasantasree, eds., IUPAC Commission on High Temperatures and Refractory Materials, London, 1983.

Invited Talks

11. L. Brewer, "The Role of Electronic Configurations in Determining Structure," The Metallurgical Society of AIME, Atlanta, Georgia, March 7, 1983.
12. L. Brewer, "Chemical Bonding in Metallic Systems," Arizona State University, Tempe, Arizona, March 23, 1983.
13. L. Brewer, "Surprises in Chemistry — Unexpected Strong Lewis Acid-base Interactions in Metallic Systems," Drew University, Madison, New Jersey, April 11, 1983.
14. L. Brewer, "A Review of High-temperature Chemistry," Midwest High Temperature Conference, Lawrence, Kansas, June 10, 1983.
15. L. Brewer, "Chemical Bonding Concepts Applied to Metals and Their Alloys," Materials Research Society Symposium, Boston, Massachusetts, November 14, 1983.

[†]Supported partially by the U.S. Bureau of Standards through the Stanford Research Institute.

Chemistry and Materials Problems in Energy Production Technologies*

Donald R. Olander, Investigator

INTRODUCTION

The goal of this program is to characterize the chemical and physical behavior of materials in the high-temperature radiation environment of fission and fusion reactors. The materials of the uranium-based fuels and the zirconium-based cladding materials of light-water nuclear reactors are of principal interest. The processes and properties studied include rapid transient vaporization of fuel materials by laser pulsing, high-temperature corrosion of zirconium by steam, and the release of volatile fission products from irradiated UO_2 . Another aspect of the program involves molecular-beam studies of the chemical kinetics of gas-solid reactions, including hydrogen-atom reactions with silicon and its compounds and the etching of metals by halogens.

1. Kinetic Study of Zirconium-iodine Reaction by Modulated Molecular-beam Mass Spectrometry (Publication 1)

Mehdi Balooch and Donald R. Olander

The reaction of molecular iodine with polycrystalline zirconium was studied by modulated molecular-beam/mass-spectrometric methods. The reaction was investigated in the 400 to 1400 K temperature range and equivalent iodine pressures of 10^{-5} to 10^{-4} torr. ZrI_4 was identified as the sole detectable reaction product at low temperatures (<850 K), achieving a maximum reaction probability at about 600 K. At high temperatures, molecular dissociation and atomic desorption of iodine play a predominant role in the gas-surface reaction. The molecular-beam data, in conjunction with Auger and ESCA analysis of the surface after the experiment, support a reaction model involving a thin scale of a lower iodide present on the surface at low temperatures during the reaction. The kinetics of the reac-

tion are governed by the diffusional properties and the reactivity of this scale with respect to adsorbed iodine atoms. At high temperatures the reaction mechanism consists of adsorption and dissociation of I_2 on the metal, which is partially covered with the iodide scale, followed by desorption of atomic iodine.

2. Stress-corrosion Cracking of Zircaloy by Cadmium, Iodine, and Metal Iodides (Publication 2)

S.H. Shann and D.R. Olander

In order to examine the cause of the reactor-fuel-pin pellet-cladding-interaction phenomenon (PCI), stress corrosion cracking (SCC) experiments of Zircaloy under iodine, iron iodide, aluminum iodide, cesium iodide, and cadmium were undertaken. The rupture lifetime was measured as a function of stress, temperature, and the equivalent pressure of the corrosive agents. Tests with CsI and simultaneous irradiation were also performed to check whether radiation decomposition can induce Zircaloy SCC. Iodine, iron iodide, and aluminum iodide substantially reduced the failure times in comparison to the failure times of control specimens at the same stress and temperature. A critical stress of ~ 370 MPa for iodine and iron iodide separates burst-type failure from low-stress short-slit failures. Both types showed brittle-cleavage fracture surfaces. The presence of cesium iodide did not have any influence on the failure time of Zircaloy. The failure was the burst type, and the fractography was ductile. Simultaneous radiation tests with cesium iodide did not cause reduction in failure time either. All specimens failed under cadmium vapor by the burst mode, but the fractography showed brittle-cleavage characteristics, and the failure times were much smaller than those of control specimens.

3. Work in Progress

Tracer spreading experiments have provided measurements of surface self-diffusion coefficients on UO_2 . Laser-pulse evaporation of this refractory oxide has been related to high-temperature vapor pressure; this work will continue with uranium carbide and the ternary oxide $(\text{U,Nd})\text{O}_2$.

Reaction of chlorine with various liquid and solid metals is being investigated by modulated

*This work was supported by the Director, Office of Energy Research, Office of Basic Energy Sciences, Materials Sciences Division of the U.S. Department of Energy under Contract No. DE-AC03-76SF00098.

molecular-beam mass spectrometry. Various aspects of the oxidation of zirconium by steam at high temperatures are being studied experimentally and theoretically.

1983 PUBLICATIONS AND REPORTS

Refereed Journals

1. D.R. Olander and M. Balooch, "Kinetic Study of the Zirconium-iodine Reaction by Modulated Molecular Beam Mass Spectrometry," *J. Electrochem. Soc.* **130**, 151 (1983); LBL-14518.
2. D.R. Olander and S.H. Shann, "Stress Corrosion Cracking of Zircaloy by Cadmium, Iodine, and Metal Iodides," *J. Nucl. Mater.* **113**, 234 (1983); LBL-13855.
3. D.R. Olander, "The UO_2 -Zircaloy Chemical Interaction," *J. Nucl. Mater.* **115**, 271 (1983); LBL-14353.
4. D.R. Olander, "Multiphoton Laser Ionization Mass Spectrometry of Cesium Iodide and Atomic Iodine," *J. Mass Spectrometry & Ion Phys.* **51**, 155 (1983); LBL-14989.

LBL Reports

5. F. Tehranian (Ph.D. Thesis), "The Kinetics of Laser Pulse Vaporization of Uranium Carbide by Mass Spectrometry," LBL-15982.
6. S.G. Prussin, D.R. Olander, P. Goubeault, and D. Bayen, "Release of Volatile Fission Products from UO_2 ," LBL-16893.
7. M.K. Farnaam (Ph.D. Thesis), "The Surface Chemistry of Epitaxial Silicon Deposition by Thermal Cracking of Silane," LBL-15448.
8. M. Balooch, W.J. Siekhaus, and D.R. Olander, "Reaction of Modulated Molecular Beam Chlorine with Polycrystalline Iron," submitted to *J. Chem. Soc. (London)*, UCRL-88163.
9. S.Y. Zhou and D.R. Olander, "Tracer Surface Diffusion on Uranium Dioxide," submitted to *Surf. Sci.*, LBL-16070.
10. D.R. Olander, "Dissolution of ZrO_2 by Liquid Zircaloy," submitted to *J. Nucl. Mater.*, LBL-15695.
11. M. Balooch, W.J. Siekhaus, and D.R. Olander, "Reaction of Chlorine with Liquid Metals — I. Indium," submitted to *J. Phys. Chem.*, LBL-16357.
12. M. Balooch, W.J. Siekhaus, and D.R. Olander, "Reaction of Chlorine with Liquid Metals—II.

Lead," submitted to *J. Phys. Chem.*, LBL-16356.

13. D.R. Olander, "The Distribution in Space and Time of the Heat of Reaction During Oxidation of Zircaloy and its Effects on Corrosion Kinetics," submitted to *J. Electrochem. Soc.*, LBL-15465.
14. Chuen-Hong Tsai and D.R. Olander, "Rapid Heating and Vaporization of Binary Solids by Absorbing Radiation — II. Laser Pulse Vaporization of Uranium Dioxide," submitted to *J. Nucl. Mater.*, LBL-15124.
15. M.K. Farnaam and D.R. Olander, "The Surface Chemistry of the Thermal Cracking of Silane on (111) Silicon," submitted to *Surf. Sci.*, LBL-16921.

Other Publications

16. D.R. Olander, "The Kinetics of Laser Pulse Vaporization of Uranium Dioxide by Mass Spectrometry," *Trans. Amer. Nucl. Soc.* **44**, 252 (1983).
17. D.R. Olander, "Tracer Surface Diffusion on UO_2 ," *Trans. Amer. Nucl. Soc.* **45**, 281 (1983); LBL-16282.

Invited Talks

18. M. Balooch, "The Kinetics of Gas/Solid/Liquid Reactions," 163rd Meeting of the Electrochemical Society, San Francisco, May 9, 1983.
19. F. Tehranian, "Laser Pulse Vaporization of Uranium Dioxide," 163rd Meeting of the Electrochemical Society, San Francisco, May 11, 1983.
20. D.R. Olander, "Zircaloy Corrosion by Steam," Osaka University, Department of Nuclear Engineering, Osaka, Japan, May 14, 1983.
21. D.R. Olander, "Fission Product Release from UO_2 ," Kyushu University, Department of Nuclear Engineering, Kyushu, Japan, May 16, 1983.
22. D.R. Olander, "Chemistry and Materials Problems in Nuclear Energy Technology," Tokyo University, Department of Nuclear Engineering, Tokyo, May 23, 1983.
23. D.R. Olander, "Fundamental Research on Nuclear Fuel Behavior," Meeting of the Atomic Energy Society of Japan, Tokyo, May 24, 1983.
24. D.R. Olander, "Laser Pulse Vaporization of Refractory Nuclear Fuels," Japan Atomic Energy Research Establishment, Tokai, Japan, May 25, 1983.

25. D.R. Olander, "Stress Corrosion Cracking of Zircaloy," Power Reactor and Nuclear Fuel Development Corporation, Tokai, Japan, May 26, 1983.
26. D.R. Olander, "The Gas Centrifuge for Uranium Isotope Separation," Atomic Vapor Laser Isotope Separation Group, Lawrence Livermore National Laboratory, Livermore, California, July 18, 1983.
27. D.R. Olander, "Severe Fuel Damage," Materials Science and Technology Division of the American Nuclear Society Annual Awards Luncheon, San Francisco, California, November 2, 1983.
28. D.R. Olander, "Tracer Surface Diffusion on UO_2 ," Bay Area Conference on High-temperature Science and Technology, Sandia Laboratory, Livermore, California, November 10, 1983.

Plasma-Enhanced Deposition of Thin Films*

Dennis W. Hess, Investigator

INTRODUCTION

This program is designed to establish scientific foundations for the rf plasma-enhanced deposition of thin films and thereby create a unique synthetic capability for a wide spectrum of film materials whose chemical, physical, and electrical properties can be controlled by variation of deposition parameters. Film structures (amorphous, polycrystalline, and crystalline), chemical composition, optical properties, and conductivity are correlated with plasma deposition variables such as rf power, rf frequency, substrate temperature, gas pressure, gas dynamics, source materials, and electrode spacing. Kinetic models are being developed so that increased understanding of the relationships between the deposition parameters and the resulting film properties can be obtained. Furthermore, these endeavors will assist in the elucidation of the chemistry occurring within the plasma. Results from these studies will be applied to such technologically important areas as solar-cell fabrication and structure-property relationships in catalyst support materials.

1. Structural Properties of Titanium Dioxide Films Deposited in an rf Glow Discharge (Publication 1)

Larry M. Williams and Dennis W. Hess

An rf glow discharge has been used to promote the reaction between titanium tetrachloride and oxygen in order to deposit thin films of titanium dioxide at low temperatures. Structural properties of the films have been studied as functions of deposition temperature (25 to 700°C) and of substrate material (Si, sapphire, glass, NaCl, and Ti). Films deposited onto glass substrates were amorphous at temperatures below 300°C, anatase at 300°C and 400°C, a mixture of anatase and rutile at 500°C, and only

rutile at 600°C and above. Films deposited on the other substrates showed similar behavior, but the temperatures for specific crystalline forms differed for each substrate material. Deposition at low power densities and 400°C resulted in large (~5- μ m) anatase crystallites in 1-2 μ m films.

2. Capacitance-voltage Technique for the Determination of Carrier Concentrations in Thin-film Photoanodes (Publication 2)

Christopher S. Blair and Dennis W. Hess

Carrier concentrations in thin-film iron oxide and titanium oxide photoanodes are determined using a metal/insulator/semiconductor structure. Capacitance-voltage measurements on this structure are distinct from the usual liquid-junction impedance measurements because results of the present study do not depend on electrolyte/semiconductor interface properties. Furthermore, determination of the conductivity of the photoanode films permits the calculation of carrier mobilities.

1983 PUBLICATIONS AND REPORTS

Refereed Journals

1. L.M. Williams and D.W. Hess, "Structural Properties of Titanium Dioxide Films Deposited in an rf Glow Discharge," *J. Vac. Sci. Technol. A1*, 1810 (1983); LBL-14994.

LBL Reports

2. C.S. Blair and D.W. Hess, "Capacitance-voltage Technique for the Determination of Carrier Concentrations in Thin Film Photoanodes," LBL-16285.

Invited Talks

3. D.W. Hess, "Plasma-enhanced CVD: Oxides, Nitrides, Transition Metals, and Transition Metal Silicides," AVS Meeting, Boston, Massachusetts, November 1-4, 1983.

*This work was supported by the Director, Office of Energy Research, Office of Basic Energy Sciences, Materials Sciences Division of the U.S. Department of Energy under Contract No. DE-AC03-76SF00098.

Electrochemical Phase Boundaries*

Rolf H. Muller, Investigator

INTRODUCTION

The purpose of this work is to advance the understanding of boundary layers and thin films at electrochemical interfaces. Boundary layers control the chemical environment in which electrode processes take place and are often responsible for limiting the specific rate at which reactions can be conducted. Thin films and adsorbed layers on electrodes greatly affect the kinetics of electrode reactions, such as the electrodeposition and dissolution of metals, and control the chemical properties of most metals in liquid environments.

New optical techniques for the observation of electrode surfaces in liquid media are developed and used. They include spectroscopic ellipsometry combined with light-scattering measurement and Auger spectroscopy, interferometry, thin-film interference, and Doppler velocimetry. Research on electrochemical mass transfer and high-rate electrodeposition and dissolution, conducted jointly with C.W. Tobias, is described under "Electrochemical Processes," C.W. Tobias, Investigator. Applied research, "Surface Layers on Battery Materials," supported by DOE's Office of Advanced Conservation Technologies, is reported under "Electrochemical Energy Storage."

1. Macroscopic Optical Model for the Ellipsometry of an Underpotential Deposit: Lead on Copper and Silver (Publication 1)

Rolf H. Muller and Joseph C. Farmer[†]

Submonolayers of underpotential deposits of Pb on Ag and Cu substrates have been investigated *in situ* by ellipsometry during cyclic voltammetry. Predictions based on two extrapolated macroscopic optical-film models, an effective-medium model and an island-film model, were compared to measurements. The island model, in which film growth is assumed to occur by the spreading of monolayer film

*This work was supported by the Director, Office of Energy Research, Office of Basic Energy Sciences, Materials Sciences Division of the U.S. Department of Energy under Contract No. DE-AC03-76SF00098.

patches, provided good agreement with measurements. In this model the state of polarization of reflected light is determined by the coherent superposition of polarization states resulting from reflection on adjacent film-covered and bare surface elements. Fractional surface coverage and optical constants of the deposit, the independent variables in the model, were determined by multidimensional optimization over the entire range of coverage (see Figure 1-1), and confidence intervals for the parameters were determined by statistical analysis of the measurements.

[†]Present address: Sandia Laboratory, Livermore, California.

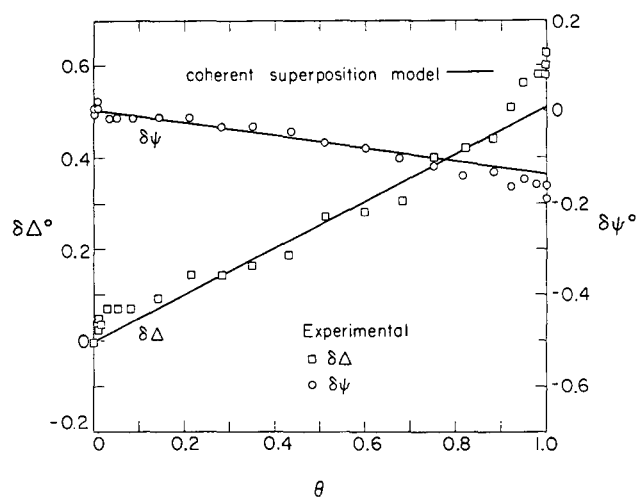


Figure 1-1. Optimized island model (lines) and measured points for the relative-phase (Δ) and relative-amplitude (ψ) ellipsometer parameters of Pb-underpotential deposits of coverage θ on Cu(111). (XBL 8212-12370)

2. Anodic Films (Publication 12)

Rolf H. Muller

Surface layers formed on many metals by anodic reaction are reviewed. Such layers include the products of charge and discharge in many storage batteries, dielectric films used in electronic and optical circuits and display devices, layers responsible for passivity and corrosion protection, and films generated in metal shaping and finishing operations such as anodization, coloring, electropolishing, electrochemical machining, and deburring. Anodic films may be formed by solid-solid transformations or by

dissolution-precipitation processes, but the choice between the two reaction paths is often not clear. Film properties and mechanisms of formation can be determined *in situ* by a number of optical techniques which have recently become available.

3. Automatic Self-nulling Spectral-scanning Ellipsometer: Software for the LSI-11 Data-acquisition System (Publication 2)

Rolf H. Muller and Joseph C. Farmer

The automatic magneto-optic ellipsometer with spectral-scanning capabilities in the visible UV has been interfaced to an LSI-11/2 for data acquisition. FORTRAN software is documented for the acquisition of both fixed-wavelength and spectroscopic data from an automatic self-nulling ellipsometer. Additional programs are presented to aid in the interpretation of the acquired ellipsometry data. Software is categorized as being for (a) fixed-wavelength data collection; (b) spectroscopic data collection, reduction, and simulation; (c) graphics; or (d) modeling and optimization. The most basic ellipsometry equations have also been programmed for a Texas Instruments 59 calculator and are presented because of their proven usefulness, convenience, and popularity.

4. Work in Progress

The combination of depth-profiling Auger spectroscopy with spectroscopic ellipsometry has shown that Pb layers of 500 and 1000 Å thickness, prepared by electrodeposition or evaporation, are transformed into island films by the ion-etching process. Film models derived from the optical interpretations agree with electron-microscope images. The uniformity of the original deposit and the effect of oxide layers formed during specimen transfer on the ion-etching process are being investigated.

Electrolyte films on metal surfaces are being investigated to determine surface forces responsible for film formation. The effect of temperature changes on film thickness has been linked to solvent evaporation and condensation. A theoretical model in which the interaction of two double layers is considered predicts film thicknesses smaller than those observed.

1983 PUBLICATIONS AND REPORTS

Refereed Journals

1. R.H. Muller and J.C. Farmer, "Macroscopic Optical Model for the Ellipsometry of an Underpotential Deposit: Lead on Copper and Silver," *Surf. Sci.* **135**, 521 (1983); LBL-15833 Rev.

LBL Reports

2. R.H. Muller and J.C. Farmer, "Automatic, Self-nulling, Spectral-scanning Ellipsometer: Software for the LSI-11 Data Acquisition System," LBL-15525.
3. J.C. Farmer (Ph.D. Thesis), with R.H. Muller, "Effect of Organic Adsorbates on the Initial Stage of Electrolytic Metal Deposition: Development and Use of a Spectroscopic Ellipsometer," LBL-15607.
4. J.C. Farmer and R.H. Muller, "Nucleation of Pb Electrodeposits on Ag and Cu," submitted to *J. Electrochem. Soc.*, LBL-15458.
5. J.C. Farmer and R.H. Muller, "Effect of Rhodamine-B on the Electrodeposition of Lead on Copper," submitted to *J. Electrochem. Soc.*, LBL-15459.
6. R.H. Muller and J.C. Farmer, "Fast, Self-compensating Spectral-scanning Ellipsometer," accepted by *Rev. Sci. Instr.*, LBL-16703.
7. R.E. Acosta, R.H. Muller, and C.W. Tobias, "Transport Processes in Narrow Gap Channels," accepted by *J. AIChE.*, LBL-16067.
8. D.S. Fischl (M.S. Thesis), with R.H. Muller and C.W. Tobias, "Effects of Small Flow Obstacles on the Limiting Current and Pressure Drop in a Square Duct," LBL-16422.

Other Publications

9. F.R. McLarnon, R.H. Muller, and C.W. Tobias, "Interferometric Study of Combined Forced and Natural Convection" (Discussion), *J. Electrochem. Soc.* **120**, 1444 (1983).
10. J.C. Farmer and R.H. Muller, "Effect of Rhodamine-B on Pb Electrodeposition on Ag and Cu," *Electrochemical Society Meeting, San Francisco, May 8-13, 1983, Ext. Abstr.* 822.
11. J.C. Farmer and R.H. Muller, "Nucleation of Pb Electrodeposits on Ag and Cu," *Electrochemical Society Meeting, San Francisco, May 8-13, 1983, Ext. Abstr.* 823.

Invited Talks

12. R.H. Muller, "Anodic Films," American Institute of Chemical Engineers Meeting, Denver, Colorado, August 28-31, 1983, submitted to AIChE Symp. Volume; LBL-16511.
13. R.H. Muller and J.C. Farmer, "Fast Self-nulling Spectroscopic Ellipsometer: Instrumentation and Application," International Conference on Ellipsometry and Other Optical Methods for Surface and Thin Film Analysis, Paris, France, June 7-10, 1983, submitted to Editions de Physique; LBL-15918 and 15918 Rev.
14. R.H. Muller, "Effect of Adsorbed Organic Material on the Micromorphology of the Initial Stages of Electrolytic Metal Deposition," University of Bern, Switzerland, May 25, 1983; Brown Boveri Ltd., Baden, Switzerland, May 26, 1983; Watch Research Laboratory, Neuchatel, Switzerland, May 27, 1983; Institute of Technology, Lausanne, Switzerland, May 30, 1983; University of Karlsruhe, West Germany, June 3, 1983.

Solid-State and Surface Reactions*

Gabor A. Somorjai, Investigator

INTRODUCTION

This research program is centered on studies of catalyzed surface reactions and investigations of the atomic structure and chemical composition of solid surfaces and adsorbed monolayers. The kinetics and mechanisms of catalytic surface reactions are studied for well-characterized crystal surfaces at low and high pressures by using a combination of surface-science techniques.

The materials that are the focus of our studies are platinum, molybdenum, rhenium, rhodium, iron and its compounds, alkali metals, and bimetallic alloys. The adsorbates and reactants are mostly hydrocarbons, oxygen, hydrogen, and water.

Part of the investigation is directed toward atomic-scale understanding of the structure and catalytic behavior of metal surfaces. The other part is aimed at developing new catalyst materials which substitute for precious metals and exhibit high reaction rates and selectivity.

SURFACE STRUCTURE AND CHEMISORPTION BY LOW-ENERGY ELECTRON DIFFRACTION (LEED) AND ELECTRON SPECTROSCOPY

1. The Structure of Rh(111)(2 × 3)-3CO from LEED Intensities: Simultaneous Bridge and Near-top Adsorption in a Distorted Compact-hexagonal CO Overlayer (Publication 15)

M.A. Van Hove, R.J. Koestner, J.C. Frost,[†] and G.A. Somorjai

The first LEED intensity analysis of molecular adsorption on multiple sites is presented. A 3/4-monolayer CO overlayer on Rh(111) is found to involve one bridge site and two near-top sites in each unit cell. This finding supports the bridge and

top assignment based on earlier high-resolution electron energy loss spectroscopy (HREELS) data. The near-top site is asymmetrical, with the CO axis close to the surface normal (but possibly tilted about 5°), yielding a bent Rh-C-O species. The near-top CO molecules are forced sideways about 0.53 Å from the ideal top site by bridge-bonded CO molecules located 2.85 Å away. This short CO-CO separation is somewhat smaller than corresponding intermolecular separations found in metal carbonyl clusters and crystalline CO and CO₂. The resulting CO overlayer has a hexagonal geometry that is distorted both parallel and perpendicular to the surface because of the strong metal-CO bonding. The Zanazzi-Jona and Pendry R-factors for the best structure are 0.25 and 0.47, respectively. The LEED analysis exhibits the use of different levels of approximation in the multiple-scattering theory in order to show the value of approximate but fast calculations in preliminary structural searches. A new algorithm to obtain experimental I-V curves from digitized images of LEED patterns is described.

[†]Permanent address: Department of Chemistry, Heriot-Watt University, Edinburgh, Scotland.

2. Efficient Scheme for the Calculation of LEED Intensities in the Presence of Large Superlattices, with Application to the Structural Analysis of Benzene Adsorbed on Rh(111) (Publication 20)

M.A. Van Hove, Rongfu Lin, and G.A. Somorjai

A powerful calculational LEED scheme is introduced for surface superlattices with unit cells of any size. The scheme is called beam-set neglect. It removes the traditional limitation on the two-dimensional unit-cell size for a large and important class of surface structures. It can furthermore be easily extended to disordered overlayer structures, whether atomic or molecular.

The method is applied to the first structural analysis from LEED intensities of a large molecule — benzene — adsorbed on a single-crystal metal surface, Rh(111). In a $\begin{pmatrix} 3 & 1 \\ 1 & 3 \end{pmatrix}$ lattice, benzene is found to lie flat on the surface, in agreement with results for HREELS obtained in this research group. The molecule is centered over hcp-type hollow sites. A planar, possibly distorted C₆ ring is found, with Rh-C bond lengths of 2.35 ± 0.05 Å, corresponding to a Rh-C layer spacing of 2.15 ± 0.05 Å.

*This work was supported by the Director, Office of Energy Research, Office of Basic Energy Sciences, Materials Sciences Division of the U. S. Department of Energy under Contract No. DE-AC03-76SF00098.

3. An HREELS Study of the Surface Structure of Benzene Adsorbed on the Rh(111) Crystal Face (Publication 29)

B.E. Koel,[†] J.E. Crowell, C.M. Mate, and G.A. Somorjai

Benzene adsorption on the Rh(111) crystal surface has been studied using HREELS, LEED, and temperature-programmed thermal desorption (TPD). The vibrational spectra indicate that benzene adsorbs molecularly at 300 K and is π -bonded to the surface with the ring plane parallel to the surface plane. Recent dynamic-LEED calculations, together with the angle-dependent HREELS studies reported here, establish a $C_{3v}(\sigma d)$ -bonding symmetry for the $c(2\sqrt{3} \times 4)\text{rect-C}_6\text{H}_6$ structure. Several other ordered benzene overlayers can be formed between 300-400 K depending on the benzene coverage. No large changes occur in the chemisorption-bonding mode or geometry coincident with the two-dimensional-ordering phase transitions in this temperature range. The vibrational spectra show that two molecular adsorption sites can be populated. Benzene adsorption is only partially reversible; less than 20% of the adsorbed benzene desorbs molecularly upon heating. The remaining benzene decomposes irreversibly, evolving hydrogen and leaving a carbon-covered surface. The TPD and HREELS data on Rh(111) and other single-crystal surfaces show correlations between the metal-benzene bond strength, the work function of the clean surface, and the frequency shifts of some of the molecular-benzene vibrational modes.

[†]Miller Institute Postdoctoral Fellow.

4. Video LEED Technique Development

D.F. Ogletree, J.E. Katz, and G.A. Somorjai

A new system of collecting LEED I-V data using a sensitive vidicon camera has been developed. The camera can be used with any traditional LEED optics without modification to the vacuum system. LEED images are recorded on videotape while the electron gun is controlled by computer. All the LEED spots at a given energy are recorded in 1-2 sec. The recorded images are then digitized using commercial video digitizer equipment with an LSI 11/23 computer. Images can be digitized with 512-

line by 480-line spatial resolution and 256 grey levels at the standard video rate of 30 images/sec.

Computer programs have been developed to analyze the digitized LEED images. Spots in a LEED pattern are located by the program, and the integrated intensity, position, and dimensions of the spot are determined. The programs follow spots as the electron energy changes, producing integrated intensity profiles as a function of incident electron energy. The analysis programs take about 0.5 sec per spot per energy level. The video digitizer can work from videotape or directly from a live video image. The use of a videotape recorder reduces the total electron-beam exposure during an experiment.

This method has been used to record I-V curves for the Pt(111) surface. The I-V curves agreed very well with published I-V data obtained by other techniques.

5. The Surface Structure of Copper-aluminum Single Crystals (Publication 77)

D.F. Ogletree, M.A. Van Hove, G.A. Somorjai, and R. Baird[†]

Copper-aluminum alloys containing up to 25 atomic percent (at%) aluminum form crystals similar to pure copper. X-ray-diffraction data indicate that aluminum is randomly substituted for copper, except that aluminum nearest-neighbor pairs occur much less often than would be predicted by a pure random distribution. The lattice constant changes by less than 1% from that of pure copper.

When Cu-Al single crystals are annealed and cooled below about 600 K, a $\sqrt{3}$ -rotated 30° LEED pattern is observed on the (111) crystal face. There is a reversible surface-phase transition between the (1×1) structure and the $\sqrt{3}$ -rotated 30° structure. This transition seems to be due to aluminum surface segregation, and it has been observed over a range of alloy compositions from approximately 3- to 20-at% aluminum.

LEED-IV profiles for the $\sqrt{3}$ -rotated 30° structure have been recorded for a Cu/17-at% Al alloy crystal at normal and off-normal incidence. The LEED data were recorded and analyzed using the vidicon-video digitizer-computer system described above. Dynamic-LEED structure calculations are being performed for this system. Preliminary results indicate that Al atoms are substituted for Cu atoms in the top layer in a $\sqrt{3}$ pattern, with slight contrac-

tion and buckling of the top layer (~ 0.05 Å). This is the first alloy structure determined by dynamic-LEED calculation.

[†]Present address: Ford Motor Co., Dearborn, Michigan.

6. The Growth and Alloy Formation of Copper on the Pt(111) and Stepped-Pt(553) Crystal Surfaces. Characterization by LEED, Auger Electron Spectroscopy (AES), and CO Thermal Desorption (Publication 32)

R.C. Yeates and G.A. Somorjai

Epitaxial layers of copper were formed on Pt(111) and Pt(553) single-crystal surfaces by condensation of copper atoms from the vapor. Surface alloys were formed by diffusing the copper atoms into the platinum substrate at temperatures above 550 K. The activation energy for this process was found to be ~ 120 kJ/mole. These Pt/Cu surfaces were characterized by LEED, AES, and thermal desorption mass spectroscopy (TDS) of CO. The copper grows in islands on the Pt(111) surface, and one monolayer is completed before another begins. There is an apparent repulsive interaction between the copper atoms and the step sites of the Pt(553) surface that causes a second layer of copper to begin forming before the first layer is complete. Epitaxial copper atoms block CO-adsorption sites on the platinum surface without affecting the CO-desorption energy. However, when the copper is alloyed with the platinum, the desorption energy of CO from the platinum was reduced by as much as 20 kJ/mole. This reduction in the desorption energy suggests an electronic modification that weakens the Pt-CO bond.

7. HREELS of Propylene Chemisorbed on the Pt(111) and Rh(111) Single-crystal Faces (Publication 50)

B.E. Koel, J.E. Crowell, B.E. Bent, C.M. Mate, and G.A. Somorjai

We have extended our comparison using HREELS of the structures of hydrocarbon monolayers on Pt(111) and Rh(111). We find that propylene chemisorbs at 310 K on these surfaces to different structures. The HREELS spectrum for a

monolayer of propylene on Pt(111) supports the propylidyne ($\equiv\text{CCH}_2\text{CH}_3$) model proposed on the basis of LEED experiments in this laboratory. A $p(2 \times 2)$ -LEED pattern was found in both experiments. The HREELS spectrum was assigned by comparison with the vibrational frequencies from a normal-coordinate calculation on 1,1,1-trichloropropane.

Under the same chemisorption conditions on Rh(111), propylene produces an entirely different HREELS spectrum. The most likely assumption is that the spectrum is caused by decomposition of propylene by carbon-carbon-bond scission to an ethylidyne ($\equiv\text{CCH}_3$) moiety plus a CH fragment. No structure with both carbon-carbon bonds intact adequately fits the spectrum. Methyl acetylene (C_3H_4) chemisorbed at 310 K on Rh(111) gives an identical spectrum.

Attempts to thermally decompose the Pt(111) propylidyne to the Rh(111) structure(s) were unsuccessful. HREELS studies of propylene chemisorption at low temperatures on Rh(111) are in progress to see if propylidyne is an intermediate in the decomposition.

8. A Thermal Desorption Study of Thiophene Adsorbed on the Clean and Sulfided Mo(100) Crystal Face (Publication 31)

A.J. Gellman, M.H. Farias, M. Salmeron, and G.A. Somorjai

The adsorption of thiophene ($\text{C}_4\text{H}_4\text{S}$) on the clean and sulfided Mo(100) crystal surface has been studied. A fraction of the adsorbed thiophene desorbs molecularly while the remainder decomposes upon heating, evolving H_2 and leaving carbon and sulfur deposits on the surface. The reversibly adsorbed thiophene exhibits three distinct desorption peaks at 370 K, 240–300 K, and 150–180 K, corresponding to binding energies of 22, 13–16, and 7–9 kcal/mole, respectively. Sulfur on the Mo(100) surface preferentially blocks the highest-energy binding site and causes an increase in the amount of thiophene bound in the low-binding-energy multilayer state. The thiophene-decomposition reactions yield H_2 desorption peaks in the 300–700 K temperature range. We estimate that 50–66% of the thiophene adsorbed to the clean Mo(100) surface decomposes. The decomposition reaction is blocked by the presence of $c(2 \times 2)$ islands of sulfur and is blocked completely at $\theta_{\text{S}} = 0.5$, at which thiophene adsorption is entirely reversible.

9. The Coadsorption and Reactions of Sulfur, Hydrogen, and Oxygen on Clean and Sulfided Mo(100) and MoS₂(0001) Crystal Faces (Publication 35)

M.H. Farias,[†] A.J. Gellman and G.A. Somorjai

The chemisorption and reactivity of O₂ and H₂ with the sulfided Mo(100) surface and the basal-(0001) plane of MoS₂ have been studied by TDS, AES, and LEED. These studies have been carried out at both low (10⁻⁸-10⁻⁵ torr) and high (1 atm) pressures of O₂ and H₂. Sulfur desorbs from Mo(100) both as an atom and as a diatomic molecule. Sulfur adsorbed on Mo(100) blocks sites of hydrogen adsorption without noticeably changing the hydrogen-desorption energies.

TDS of ¹⁸O coadsorbed with sulfur on the Mo(100) surfaces produced the desorption of SO at 1150 K, and of S, S₂, and O, but not of SO₂. A pressure of 10⁻⁷ torr of O₂ was sufficient to remove sulfur from Mo(100) above 1100 K. The basal plane of MoS₂ was unreactive in the presence of 1 atm of O₂ at 520 K. Sputtering of the MoS₂ produced a marked uptake of oxygen and the removal of sulfur under the same conditions.

[†]CONACYT-CINVESTAV (Mexico) Fellow.

10. The Coadsorption of CO and K on Rh(111): An HREELS, TPD, AES, and LEED Study (Publication 40)

J. E. Crowell and G.A. Somorjai

Alkali-metal additives are commonly used to alter the reactivity and selectivity of transition metals that catalyze important chemical reactions. It is thought that by transferring substantial electronic charge to the transition-metal substrate, alkali additives increase the electron density at the surface. As a consequence, the chemisorptive properties of these surfaces are modified, resulting in changes in catalyst activity and product distribution.

One such reaction catalyzed by several transition metals that are often altered in activity by alkali additives (e.g., Fe, Ni, Rh, and Ru) is the hydrogenation of carbon monoxide. In order to understand the role of the alkali adatoms in promoting this reaction, it is important to elucidate the nature of the interaction between the alkali and the coadsorbed species.

Hence we have combined AES, LEED, TPD, and HREELS to determine the effect of potassium on the adsorption of carbon monoxide on the Rh(111) surface.

11. Energetics and Reversibility of Hydrocarbon Sequential Dehydrogenation on Platinum Single-crystal Surfaces: Thermal Desorption and Carbon-14 Radiotracer Studies (Publication 24)

S.M. Davis, F. Zaera, M. Salmeron, B.E. Gordon, and G.A. Somorjai

The energetics and reversibility of hydrocarbon sequential dehydrogenation on the Pt(100), Pt(111), and Pt(10,8,7) single-crystal surfaces has been investigated at 200-700 K using carbon-14 radiotracer studies and hydrogen TDS. Propylene, cis-2-butene, n-hexane, ¹⁴C-ethylene, and ¹⁴C-benzene all displayed similar sequential-dehydrogenation energetics with activation energies from 18-45 kcal/mole. Radiotracer studies revealed "active" and "inactive" forms of partially dehydrogenated carbon on the platinum surfaces that differ greatly in their reactivity for hydrogenation and hydrogen-transfer reactions with H₂ or unlabeled hydrocarbons. The inactive fraction increased with increasing adsorption temperature as the surface species became more hydrogen deficient. Removal of the active ¹⁴C-containing species by hydrogen transfer occurred more slowly than direct hydrogenation. The C-H bond-breaking processes are discussed in connection with recent LEED, photoemission, and vibrational-spectroscopy studies that revealed atomic structures for the surface species.

12. Core- and Valence-band Energy-level Shifts in Small Two-dimensional Islands of Gold Deposited on Pt(100): The Effect of Step-edge, Surface, and Bulk Atoms (Publication 18)

M. Salmeron, S. Ferrer, M. Jazzar, and G.A. Somorjai

Photoemission techniques were used to study the electronic properties of two-dimensional islands of Au deposited on Pt(100) in the submonolayer range. Shifts of approximately 0.6 eV were observed in both

valence-band and core-level binding energies from $\Theta=1$ to 0.1. These shifts are interpreted in terms of the increasing proportion of island edges as the gold coverage approaches zero. Above $\Theta=1$ the surface/bulk-energy shift was found to agree with previously published data.

13. A New Model for CO Ordering at High Coverages on Low-index Metal Surfaces: A Correlation Between LEED, HREELS, and Infrared Spectroscopy (IRS). II. CO Adsorbed on fcc(111) and hcp(0001) Surfaces (Publication 54)

J.P. Biberian and M.A. Van Hove

The approach used in earlier work to understand the high-coverage structures of carbon monoxide overlayers on fcc(100) metal surfaces has been extended to metal surfaces that have a threefold rotational symmetry: fcc(111) and hcp(0001). The proposed structures consist of ordered domains composed of simple superlattices such as $(\sqrt{3} \times \sqrt{3})R30^\circ$ and $c(4 \times 2)$, in which only well-defined sites (mostly top and/or bridge sites) are occupied by the CO molecules. Laser simulation is used to test the validity of the proposed models. These models for the first time satisfy both the LEED-pattern observations and the vibrational-loss data obtained by HREELS and IRS.

STUDIES OF CATALYZED SURFACE REACTIONS

14. HREELS of the Rh(111) Single Crystal after Reactions at Atmospheric Pressures: An HD-exchange Study of the Role of Ethylidyne in Ethylene Hydrogenation (Publication 51)

B.E. Koel, B.E. Bent, and G.A. Somorjai

Little direct evidence exists for the mechanisms of surface reactions in heterogeneous catalysis. To study the reactivity of the adsorbed monolayer at metal/gas interfaces, we are using HREELS to determine the structure of monolayers remaining after atmospheric-pressure gas exposures. Isotopic labeling is used to distinguish between composition and structure changes.

We have used this new HREELS/high-pressure-low-pressure system combination to study hydrogen-deuterium (HD) exchange in ethylidyne ($\equiv\text{CCH}_3$) on Rh(111). Monolayers of ethylidyne formed by chemisorbing ethylene at 310 K do not irreversibly hydrogenate upon exposure to 1 atm of hydrogen. The HREELS spectrum after exposure to 1 atm of deuterium has new peaks corresponding to partial exchange in the methyl group. Comparison with UHV HD-exchange data shows the amount of exchange depends weakly on the D_2 pressure but strongly on the available bare-metal surface area. We suggest that ethylidene ($\equiv\text{CDCH}_3$) is the exchange intermediate.

We find in studying ethylene hydrogenation on Rh(111) that an ethylidyne monolayer forms during the reaction. Hydrogenation over a $\equiv\text{CCD}_3$ monolayer shows no formation of $\equiv\text{CCH}_3$. We conclude that the turnover rate for ethylene hydrogenation is greater than that for ethylidyne hydrogenation or HD exchange. Ethylidyne is not, therefore, an intermediate in ethylene hydrogenation on the Rh(111) single-crystal face. The ordered $c(4 \times 2)$ ethylidyne monolayer formed in this reaction makes the metal sites unavailable for ethylene adsorption, although hydrogen can still chemisorb. We propose that hydrogenation occurs on top of this stable ethylidyne monolayer. Ethylidene is a likely intermediate for transfer of surface deuterium to gas-phase ethylene.

15. The Hydrogenation of Ethylene Over Pt(111) Single-crystal Surfaces (Publication 36)

F. Zaera and G.A. Somorjai

The hydrogenation of ethylene with both hydrogen and deuterium was studied over Pt(111) single-crystal surfaces under a total pressure of 110 torr and temperatures from 300–370 K. An activation energy of 10.8 ± 0.1 kcal/mole and kinetic orders with respect to hydrogen and ethylene partial pressure of 1.31 ± 0.05 and -0.60 ± 0.05 , respectively, were observed. The deuterium-atom distribution in the product from the reaction with D_2 was found to peak at 1–2 deuterium atoms per ethane molecule produced, a result similar to that reported for supported catalysts. The reaction takes place on a partially ordered carbon-covered surface where the carbonaceous deposits have a morphology similar to that of ethylidyne. However, this ethylidyne does not directly participate in the hydrogenation of ethylene because both its hydrogenation and its deuterium

exchange are much slower than the ethane production. A mechanism is proposed to explain the experimental results.

16. Surface Structure and Temperature Dependence of Light-alkane Skeletal-rearrangement Reactions Catalyzed Over Platinum Single-crystal Surfaces (Publication 22)

S.M. Davis, F. Zaera, and G.A. Somorjai

The structure sensitivity of isobutane, n-butane, and neopentane hydrogenolysis and isomerization catalyzed over a series of flat, stepped, and kinked platinum single-crystal surfaces was investigated near atmospheric pressure and at 540–640 K. The atomic structure and surface composition of the active catalyst were determined before and after reaction studies using LEED and AES. Catalytic activities for butane isomerization and consecutive-rearrangement reactions were maximized on platinum surfaces with high concentrations of (100) microfacets. Maximum rates for the competing hydrogenolysis reactions were obtained on platinum surfaces that contain high concentrations of steps and kinks. Hydrogenolysis-product distributions varied markedly with terrace structure. The symmetries of d-orbitals which emerge from the surfaces with different atomic structure have been used to rationalize the structure sensitivity of light-alkane isomerization.

17. Surface Structure and Temperature Dependence of n-hexane Skeletal-rearrangement Reactions Catalyzed Over Platinum Single-crystal Surfaces: Marked Structure Sensitivity of Aromatization (Publication 27)

S.M. Davis, F. Zaera, and G.A. Somorjai

The surface structure and temperature dependence of n-hexane skeletal rearrangement were investigated near atmospheric pressure and at 520–700 K over a series of five platinum single-crystal surfaces with variable terrace, step, and kink structures. The atomic structure and surface composition of the active catalyst were determined before and after the reactions using LEED and AES. Aromatization of n-hexane to benzene displayed unique structure sensitivity in which the rates and specificity for this

important reforming reaction were maximized on platinum surfaces with a hexagonal (111) terrace structure. The rates of competing isomerization, C5-cyclization, and hydrogenolysis reactions displayed little dependence on surface structure, although hydrogenolysis-product distributions were influenced markedly by terrace structure. Platinum surfaces with (100) terraces favored internal C-C bond scission, whereas surfaces with (111) terraces displayed high selectivity for terminal hydrogenolysis.

Skeletal rearrangement was dominated by cyclic mechanisms involving both 1,5- and 1,6-ring closure. Marked variations in reaction selectivity with reaction conditions were related to a change in the most abundant surface intermediate that resulted from changes in the surface concentration of chemisorbed hydrogen. Catalyst deactivation resulted from the formation of disordered carbonaceous deposits on the platinum surfaces that acted as a nonselective poison.

18. Ammonia Synthesis Over Re Catalysts (Publication 49)

M. Asscher and G. A. Somorjai

Our continuous interest in studying the mechanism of catalyzed ammonia synthesis was directed toward the detailed understanding of Re as a new catalyst. Our group recently found that a polycrystalline foil of Re is as efficient a catalyst for NH_3 synthesis as the most active face of the traditional catalyst, the Fe(111) single-crystal surface. In order to explore the details of the NH_3 -synthesis mechanism with this new catalyst, we used pressure-dependence and isotopic studies. We conclude that the rate-determining step in both cases involves the adsorption and dissociation of the nitrogen molecules.

Next we studied the efficiency of this synthesis on different Re single-crystal surfaces. As with the iron single crystals but even more dramatically, this synthesis was found to be surface-structure sensitive. The (0001) face was found to be practically inactive, while the (1120) single-crystal surface, an open face that exposes C_7 coordination atoms, is extremely active. The difference in activity between the (0001) and (1120) crystal surfaces exceeds 3 orders of magnitude. An intermediate activity was found with the (1010) crystal that does not expose C_7 coordination atoms and is slightly more tightly packed as compared with the (1120) face.

19. Partial Oxidation of Methane with Nitrous Oxide Over Molybdena-silica Catalyst (Publication 52)

M.M. Khan and G.A. Somorjai

Supported molybdenum oxide (1.7%) on silica was found to catalyze the partial oxidation of methane to methanol and formaldehyde from 520–610°C in the presence of nitrous oxide and steam under 1 atm pressure. It was possible to carry out the process at a turnover rate of 5.2×10^{-4} molecules/site-sec over a week without any drastic reduction in activity. Methanol formation below 550°C had an activation energy of 27 ± 2 kcal/mole. Formaldehyde formation occurred through two distinct mechanisms, one with an activation energy (E_{act}) of 58 ± 4 below 550°C and the other with an E_{act} of 34 ± 2 at higher temperatures. This result indicates parallel reactions leading to both methanol and formaldehyde below 550°C and consecutive oxidation processes at higher temperatures.

20. The Hydrodesulfurization of Thiophene on the Mo(100) Crystal Face (Publication 41)

A.J. Gellman, M.H. Farias, and G.A. Somorjai

We have carried out studies of the hydrodesulfurization of thiophene over single-crystal Mo(100) surfaces. We have primarily looked at the hydrodesulfurization reaction at thiophene pressures of 1.0–5.0 torr in the presence of H_2 at 100–800 torr. The products, in increasing abundance, are butane, butadiene, cis-2-butene, trans-2-butene, and 1-butene. The temperature dependence of the production rates is Arrhenius-like for the butadiene only. The reaction is zero-order in thiophene pressure. The H_2 -pressure dependence is zero-order for butadiene, half-order for the butenes, and first-order for the butane. In addition we have identified a previously unobserved hexagonal structure of sulfur on the Mo(100) surface that is stable under reaction conditions. The reaction has been shown to be catalytic, having run to as many as 10,000 turnovers at frequencies as high as 0.1/sec.

21. Cyclohexane Dehydrogenation Catalyzed by Bimetallic Au-Pt(111) Single-crystal Surfaces (Publication 43)

J.W.A. Sachtler[†] and G.A. Somorjai

Cyclohexane dehydrogenation was investigated using two-phase epitaxial Au on Pt(111) single-crystal surfaces and single-phase Au-Pt(111) surface alloys as catalysts, with 20-mbar cyclohexane and 133-mbar H_2 at 573 K. Benzene production was found to be strongly enhanced by Au, reaching a maximum at a surface composition of 50-at% Au and declining thereafter. The clean Pt(111) crystal face did not produce detectable amounts of cyclohexene; its formation by the single crystal was completely attributable to the crystal edges. The addition of gold to the Pt(111) surface also induced production of cyclohexene. Surfaces containing about 90-at% Au were the most active. In both cases, the effects were similar for epitaxial and alloy surfaces, but the latter usually gave larger enhancements. The enhancement by Au of the cyclohexane dehydrogenation to benzene is interpreted as a reduction of the product poisoning of Pt sites by benzene. This, and the observation that only Au-containing Pt(111) surfaces produced cyclohexene, are both explained by ensemble-size effects.

[†]Permanent address: UOP Research Center, The Signal Companies, Des Plaines, Illinois 60016.

22. The Dynamics of Atomic Hydrogen and Deuterium (HD) Recombination on the Stepped-Pt(557) Crystal Surface (Publication 39)

T.H. Lin and G.A. Somorjai

The velocity distribution of HD produced on the Pt(557) crystal surface from atomic hydrogen and deuterium incident beams was measured from 150–700 K. The striking results are: (1) The average kinetic energy of the desorbing HD increases as the crystal temperature decreases from 300 to 200 K. (2) At 200 K the velocity distribution is considerably wider than the Maxwellian distribution, and there is

a significant amount of HD leaving the surface with translational energy corresponding to 1900 K. (3) For a fraction of the incident atoms, the residence time decreases as the crystal temperature decreases from 300 to 200 K. It appears that some of the incident atoms can react with chemisorbed atoms at high coverage before they achieve thermal equilibrium with the surface.

23. Vibrational Excitation and Deexcitation Rates of Molecules Adsorbed on Metal Surfaces (Publication 42)

M. Asscher,[†] Yehuda Zeiri,[†] and G.A. Somorjai

The rates for vibrational excitation and deexcitation of adsorbed molecules on metal surfaces were studied. The desorption of the adsorbed molecules was shown to compete with the excitation process, resulting in "vibrationally cold" desorbing molecules. Simple rate equations were used with the available experimental data to estimate the rates for vibrational excitation and deexcitation of NO molecules on Pt(111) surfaces as a function of the crystal temperature. The application of this approach to other systems is discussed.

[†]Chaim Weizmann Postdoctoral Fellow.

24. Angular and Velocity Distributions of HD Molecules Produced by the H₂-D₂ Exchange Reaction on the Stepped Pt(557) Crystal Surface (Publication 38)

T.H. Lin and G.A. Somorjai

The H₂-D₂ exchange reaction on the Pt(557) crystal surface was investigated using a molecular-beam/surface-scattering technique. The angular and velocity distributions of the HD product were measured at various crystal temperatures (500-1170 K). It was found that the exchange reaction occurred via interactions of adsorbed H and D atoms (the Langmuir-Hinshelwood mechanism). Although the HD produced desorbs with a $\cos^2\theta$ angular distribution, its translational energy corresponds to a temperature slightly colder than that of the substrate, with the mean energy of the desorbing molecules depending on the desorption angle. As the desorbing angle increases away from the surface normal, the

mean translational energy decreases. The exchange reactivity was found to depend on the incident azimuthal angle, while the translational energy of the product HD is independent of the azimuthal angle of detection. Models explaining the results are discussed.

25. A Molecular-beam Surface-scattering Study of Ammonia Oxidation on The Pt(111) Crystal Face (Publication 34)

M. Asscher, T.H. Lin, W.L. Guthrie, and G.A. Somorjai

The catalyzed reaction of ammonia and molecular oxygen on a Pt(111) single-crystal surface was studied over the crystal temperature range of 550-1100 K. A molecular-beam/surface-scattering technique was used, and two-photon ionization was used to probe the NO product. Two different NO production paths were observed. These could be characterized by activation energies of 29 ± 4 and 14 ± 3 kcal/mole for the faster and slower processes, respectively. The internal-energy distributions of the scattered-NO product, e.g., rotational and vibrational energies, were found to have a lower temperature than the crystal temperature. Possible reaction mechanisms are discussed.

26. Work in Progress

The oxidation of molybdenum and the catalytic behavior of molybdenum oxides and sulfides are under investigation.

The surface structures of large aromatic organic molecules are under investigation by LEED and HREELS on Fe and Pt crystal surfaces.

The structure and chemistry of surfaces produced by plasma deposition or modified by laser heating are being investigated.

The modification of metal catalytic behavior by deposition on TiO₂ single crystals is being studied.

1983 PUBLICATIONS AND REPORTS

Refereed Journals

1. N.D. Spencer and G.A. Somorjai, "Catalysis, in British Institute of Physics," Rep. Prog. Phys.

- 46, 1-49 (1983); LBL-13536.
2. G.A. Somorjai, "The Surface Science of Heterogeneous Catalysis," Robert A. Welch Conference Proceedings, Heterogeneous Catalysis XXV, 83-138 (1983); LBL-14135.
 3. W. McLean, C.A. Colmenares, R.L. Smith, and G.A. Somorjai, "The Chemisorption of CO and CO₂ on Gold Supported ThO₂ Films," *J. Phys. Chem.* **87**, 788 (1983); UCRL-86251.
 4. S.M. Davis and G.A. Somorjai, "The Surface Science of Heterogeneous Catalysis," *Chemtech* **13**, 502-511 (1983); LBL-14285.
 5. R.J. Koestner, M.A. Van Hove, and G.A. Somorjai, "Origins of the Behavior of Hydrocarbons on Metal Surfaces," *Chemtech* **13** (6), 376-384 (1983); LBL-13982.
 6. N.D. Spencer and G.A. Somorjai, "Ammonia Synthesis Catalyzed by Rhenium," *J. Catal.* **78**, 142-146 (1982); LBL-14298.
 7. E. Lang, K. Muller, K. Heinz, M.A. Van Hove, R.J. Koestner, and G.A. Somorjai, "LEED Intensity Analysis of the (1 × 5) Reconstruction of Ir(100)," *Surf. Sci.* **127** (2), 347 (1983); LBL-14338.
 8. J.W.A. Sachtler and G.A. Somorjai, "Influence of Ensemble Size on CO Chemisorption and Catalytic n-hexane Conversion with Au-Pt(111) Bimetallic Single Crystal Surfaces," *J. Catal.* **81**, 77-94 (1983); LBL-14406.
 9. R.J. Koestner, M.A. Van Hove, and G.A. Somorjai, "The Molecular Structure of Hydrocarbon Monolayers on Metal Surfaces," *J. Phys. Chem.* **87**, 203 (1983); LBL-13962.
 10. M. Salmeron, R. Chianelli, and G.A. Somorjai, "A LEED-AES Study of the Structure of Sulfur Monolayers on the Mo(100) Crystal Face," *Surf. Sci.* **127** (3), 526 (1983); LBL-14551.
 11. G.A. Somorjai, "Molecular Ingredients of Heterogeneous Catalysis," *New Horizons of Quantum Chem.*, 305 (1983); LBL-14406.
 12. M. Asscher, W.L. Guthrie, T.H. Lin, and G.A. Somorjai, "Energy Redistribution Among Internal States of Nitric Oxide Molecules Upon Scattering from Pt(111) Crystal Surface," *J. Chem. Phys.* **78** (11), 6992 (1983); LBL-15034.
 13. S.T. Ceyer, W.L. Guthrie, T.H. Lin, and G.A. Somorjai, "D₂O Product Angular and Translational Energy Distributions from the Oxidation of Deuterium on Pt(111)," *J. Chem. Phys.* **78** (11), 6982 (1983); LBL-15035.
 14. E.L. Garfunkel, J.J. Maj, J.C. Frost, M.H. Farias, and G.A. Somorjai, "The Interaction of Potassium with II-electron Orbital Containing Molecules on Pt(111)," *J. Phys. Chem.* **87** (19), 3629 (1983); LBL-15504.
 15. M.A. Van Hove, R.J. Koestner, J.C. Frost, and G.A. Somorjai, "The Structure of Rh(111)(2 × 2)-3CO from LEED Intensities: Simultaneous Bridge and Near-top Adsorption in a Distorted Compact Hexagonal CO Overlayer," *Surf. Sci.* **129**, 482-506 (1983); LBL-15271.
 16. B.E. Koel and G.A. Somorjai, "Vibrational Spectroscopy Using HREELS of Benzene Adsorbed on the Rh(111) Crystal Surface," *J. Elect. Spectroscopy and Related Phenomena* **29**, 287-292 (1983).
 17. S. Mark Davis and G.A. Somorjai, "Surface Science Studies of Catalyzed Reactions on Platinum Surfaces. The Role of the Atomic Structure of Platinum Single Crystals in Determining Selectivity," *Platinum Metals Review* **27** (2), 54-64 (1983).
 18. M. Salmeron, S. Ferrer, M. Jazzar, and G.A. Somorjai, "Core and Valence Band Energy Shifts in Small Two-dimensional Islands of Gold Deposited on Pt(100): The Effect of Step-edge, Surface, and Bulk Atoms," *Phys. Rev. Lett. B, Rapid Communications* **28** (2), 1158-1160 (1983); LBL-16109.
 19. M. Salmeron and G.A. Somorjai, "LEED, Auger, and TDS Study of the Structure and Chemistry of Sulfur Overlayers on Mo(100)," *Surf. Sci.* **126**, 410 (1983).
 20. M.A. Van Hove, Rongfu Lin, and G.A. Somorjai, "Efficient Scheme for LEED Calculations in the Presence of Large Superlattices, with Application to the Structural Analysis of Benzene Adsorbed on Rh(111)," *Phys. Rev. Lett.* **51** (9), (1983); LBL-16255.
 21. R.F. Lin, R.J. Koestner, M.A. Van Hove, and G.A. Somorjai, "The Adsorption of Benzene and Naphthalene on the Rh(111) Surface: A LEED, AES, and TDS Study," *Surf. Sci.* **134** (1), 161-183 (1983); LBL-15820.
 22. S.M. Davis, F. Zaera, and G.A. Somorjai, "Surface Structure and Temperature Dependence of Light-alkane Skeletal Rearrangement Reactions Catalyzed over Platinum Single-crystal Surfaces," *J. Am. Chem. Soc.* **104**, 7453-7461 (1982).
- LBL Reports**
23. F. Zaera and G.A. Somorjai, "The Effect of Potassium on the Catalyzed Reactions of n-hexane over Pt(111) Single Crystal Surfaces,"

- submitted to J. Crystals, LBL-15734.
24. S. M. Davis, F. Zaera, M. Salmeron, B.E. Gordon, and G.A. Somorjai, "Energetics and Reversibility of Hydrocarbon Sequential Dehydrogenation on Platinum Single Crystal Surfaces: Thermal Desorption and Carbon-14 Radiotracer Studies," submitted to J. Am. Chem. Soc., LBL-14611.
 25. U. Bardi, P.N. Ross, and G.A. Somorjai, "LEED and AES Study of Structural and Chemisorptive Properties of Zr Overlayers on the Pt(100) Crystal Face," submitted to J. Vac. Sci. Technol., LBL-15294.
 26. M.A. Van Hove, Rongfu Lin, R.S. Koestner, B.E. Koel, M. Mate, J.E. Crowell, and G.A. Somorjai, "LEED and HREELS Studies of Benzene Adsorbed on Rh(111)," submitted to ISSC-6, LBL-15822.
 27. S. Mark Davis, Francisco Zaera, and G.A. Somorjai, "Surface Structure and Temperature Dependence of n-hexane Skeletal Rearrangement Reactions Catalyzed Over Platinum Single Crystal Surfaces: Marked Structure Sensitivity of Aromatization," submitted to J. Catal., LBL-15826.
 28. J.R. Anderson, M. Boudart, and G. A. Somorjai, "Surface Structural Chemistry," submitted to *Catalysis: Science and Technology*, LBL-16002.
 29. B.E. Koel, J.E. Crowell, C.M. Mate, and G.A. Somorjai, "An HREELS Study of the Surface Structure of Benzene Adsorbed on the Rh(111) Crystal Face," submitted to J. Phys. Chem., LBL-16012.
 30. R. Yates and G.A. Somorjai, "The Surface Science of Heterogeneous Catalysis," submitted to J. Electrochem. Soc., LBL-16062.
 31. A.J. Gellman, M.H. Farias, M. Salmeron, and G.A. Somorjai, "A Thermal Desorption Study of Thiophene Adsorbed on the Clean and Sulfided Mo(100) Crystal Face," submitted to Surf. Sci., LBL-15934.
 32. R.C. Yeates and G.A. Somorjai, "The Growth and Alloy Formation of Copper on the Platinum(111) and Stepped (553) Crystal Surfaces. Characterization by LEED, AES, and CO Thermal Desorption," submitted to Surf. Sci., LBL-16229.
 33. U. Bardi, P.N. Ross, and G.A. Somorjai, "Ligand Effects for CO and H₂ Chemisorption on a Polycrystalline Pt₃Ti Surface," submitted to J. Catal., LBL-15603.
 34. M. Asscher, W.L. Guthrie, T.H. Lin, and G.A. Somorjai, "Molecular Beam Surface Scattering Study of Ammonia Oxidation on a Pt(111) Single Crystal Surface," submitted to J. Phys. Chem., LBL-16353.
 35. M.H. Farias, A.J. Gellman, R. Chianelli, and G.A. Somorjai, "The Chemisorption and Reaction of Hydrogen and Oxygen on Clean and Sulfided Mo(100) and on MoS₂," submitted to Surf. Sci., LBL-16412.
 36. F. Zaera and G.A. Somorjai, "The Hydrogenation of Ethylene Over Platinum(111) Single Crystal Surfaces," submitted to J. Am. Chem. Soc., LBL-16423.
 37. G.A. Somorjai, "The Molecular Surface Science of Heterogeneous Catalysis, History and Perspective," submitted to ISSS Book, LBL-16573.
 38. T.H. Lin and G.A. Somorjai, "HD Product Angular and Velocity Distribution from the H₂-D₂ Exchange Reaction on the Pt(557) Surface," submitted to J. Chem. Phys., LBL-16598.
 39. T.H. Lin and G.A. Somorjai, "The Dynamics of Atomic Hydrogen and Deuterium Recombination on Pt(557) Surface," submitted to J. Chem. Phys., LBL-16599.
 40. J.E. Crowell and G.A. Somorjai, "The Coadsorption of CO and K on Rh(111): An HREELS, TPD, AES, and LEED Study," submitted to J. Vac. Sci. Technol., LBL-16691.
 41. A. Gellman, M. Farias, and G.A. Somorjai, "The Catalytic Hydrodesulfurization of Thiophene on the Mo(100) Surface," submitted to J. Catal., LBL-17144.
 42. M. Asscher and G.A. Somorjai, "Vibrational Excitation and Deexcitation Rates of Molecules Adsorbed on Metal Surfaces," submitted to J. Chem. Phys., LBL-16830.
 43. J.W.A. Sachtler and G.A. Somorjai, "Cyclohexane Dehydrogenation Catalyzed by Bimetallic Au-Pt(111) Single Crystal Surfaces," submitted to J. Catal., LBL-16845.
 44. M. Salmeron, S. Ferrer, M. Jazsar, and G.A. Somorjai, "Photoelectron-spectroscopy Study of the Electronic Structure of Au and Ag Overlayers on Pt(100), Pt(111), and Pt(997)," submitted to Phys. Rev., LBL-16942.
 45. G.A. Somorjai, "Molecular Ingredients of Heterogeneous Catalysis," submitted to Trans. Faraday Soc., LBL-16983.
 46. J.E. Crowell and G.A. Somorjai, "The Effect of Potassium on the Chemisorption of Carbon Monoxide on the Rh(111) Crystal Face," submitted to Applications of Surf. Sci., LBL-16984.
 47. W.T. Tysoe, F. Zaera, and G.A. Somorjai, "On

- the Absolute Coverage of Ethylene on Pt(111) Single Crystal Surfaces," submitted to Surf. Sci., LBL-17122.
48. W.T. Tysoe, J. Carrazza, and G.A. Somorjai, "The Adsorption and Catalyzed Reactions of CO and CO₂ on Graphite Surfaces," submitted to preprint volume of the ACS Division of Fuel Chemistry on the Symposium on the Gasification of Chars and Carbonaceous Materials, LBL-17004.
 49. M. Asscher and G.A. Somorjai, "The Remarkable Surface Structure Sensitivity of the Ammonia Synthesis Over Rhenium Single Crystal," submitted to Surf. Sci. Lett., LBL-17176.
 50. B.E. Koel, J.E. Crowell, B.E. Bent, C.M. Mate, and G.A. Somorjai, "High-resolution Electron Energy Loss Spectroscopy of Propylene Chemisorbed on the Pt(111) and Rh(111) Single-crystal Faces," LBL-17410.
 51. B.E. Koel, B.E. Bent, and G.A. Somorjai, "High-resolution Electron Energy Loss Spectroscopy of the Rh(111) Single Crystal after Reactions at Atmospheric Pressures: An HD-exchange Study of the Role of Ethylidene in Ethylene Hydrogenation," LBL-17493.
 52. M.M. Khan and G.A. Somorjai, "Partial Oxidation of Methane with Nitrous Oxide over Molybdena-silica Catalyst," submitted to J. Catal., LBL-17408.
 57. G.A. Somorjai, "Chemical Energy Conversion Strategies," American Public Works Association, Northern California Chapter, Berkeley Meeting, Berkeley, California, February 18, 1983.
 58. M. Asscher, W.L. Guthrie, T.H. Lin, and G.A. Somorjai, "Vibrational and Rotational Excitation of NO on a Pt(111) Crystal Surface is Monitored by Molecular Beam Surface Scattering," American Chemical Society, Seattle, Washington, March 22, 1983.
 59. A.J. Gellman, M. Farias, and G.A. Somorjai, "A Study of Sulfur on Mo(100) and its Effects on Hydrodesulfurization Catalysis," American Chemical Society, Seattle, Washington, March 22, 1983.
 60. B.E. Koel and G.A. Somorjai, "Vibrational Studies of Alkene Decomposition on the Rh(111) Surface," American Chemical Society, Seattle, Washington, March 23, 1983.
 61. E.L. Garfunkel and G.A. Somorjai, "Effects of Alkali Promoters on Model Transition Metal Catalysts," American Chemical Society, Seattle, Washington, March 23, 1983.
 62. G.A. Somorjai, "The Surface Science of Heterogeneous Catalysis, the Building of New Catalysts," The Lemieux Lectures, 1983, University of Ottawa, Ottawa, Ontario, May 2-4, 1983.
 63. G.A. Somorjai, "Molecular Ingredients of Heterogeneous Catalysis," 163rd Meeting, The Electrochemical Society, San Francisco, California, May 6, 1983; NASA Langley Research Center, Hampton, Virginia, June 20, 1983.

Other Publications

53. U. Bardi, P.N. Ross, and G.A. Somorjai, "Summary Abstract: Adsorptive and Catalytic Properties of Zirconium Overlayers on Pt(100)," J. Vac. Sci. Technol. A 1, (2), April-June 1983; LBL-17401.
54. J.P. Biberian and M.A. Van Hove, "A New Model for CO Ordering at High Coverage on Low-index Metal Surfaces: A Correlation Between LEED, HREELS, and IRS. II. CO Adsorbed on fcc(111) and hcp(0001) Surfaces," accepted by Surf. Sci.
64. G. A. Somorjai, "The Structure of Surface Monolayers. Techniques and Results," American Crystallographic Association, San Diego, California, August 17, 1983.
65. G.A. Somorjai, "The Surface Science of Heterogeneous Catalysis," Sixth International Summer Institute in Surface Science (ISSS 1983), University of Wisconsin, Milwaukee, August 22, 1983.
66. G.A. Somorjai, "The Determination of the Structure and Composition of Surfaces," University of Lausanne, Switzerland, September 12, 1983.
67. G.A. Somorjai, "The Structure and Composition of Surface Monolayers," University of Lausanne, Switzerland, September 13, 1983.
68. G.A. Somorjai, "Elementary Surface Reactions and Heterogeneous Catalysis," University of Lausanne, Switzerland, September 14, 1983.

Invited Talks

55. G.A. Somorjai, "The Surface Science of Heterogeneous Metal Catalysis," University of Florida, January 4, 1983.
56. G.A. Somorjai, "The Search for Catalysts for New Chemical Processes," The Michigan Catalysis Society, Romulus, Michigan, February 8, 1983.

69. G.A. Somorjai, "The Surface Science of Energy Conversion. New Reactions, New Catalysts," The 43rd Frontiers in Chemistry Conference, Case Western Reserve University, Cleveland, Ohio, October 20, 1983.
70. M.A. Van Hove and G.A. Somorjai, "LEED and HREELS Used in the Structure Determination of Organic Monolayers on Surfaces of Metal Single Crystals," Symposium on Surface Analysis Techniques and Reactions, Pasadena, California, October 26, 1983.
71. G.A. Somorjai, "The Surface Chemical Bond," Royal Society Centenary Lectures, Cardiff, Wales, November 4, 1983.
72. G.A. Somorjai, "The Molecular Ingredients of Heterogeneous Catalysis," Royal Society Centenary Lectures; London and Bradford, England, and Heriot-Watt University, Edinburgh, Scotland, November 7, 10, and 11, 1983.
73. M.A. Van Hove, "Structure Determination by Low-energy Electron Diffraction of Molecular Surface Structures: CO and Hydrocarbons Adsorbed on Rh(111) and Pt(111)," York University, York, England, April 12, 1983; Heriot-Watt University, Edinburgh, Scotland, April 22, 1983.
74. M.A. Van Hove, "Determination by LEED of Complex Surface Structures: New Methods Applied to Molecular Overlayers," Daresbury SERC Laboratory, Daresbury, England, April 14, 1983; Imperial College, London, April 27, 1983.
75. M.A. Van Hove, "Hydrocarbon Adsorption Structures on Rh(111) and Pt(111) Determined by LEED," Cambridge University, Cambridge, England, April 25, 1983.
76. M.A. Van Hove, "The Structure of Organic Molecules Adsorbed on Single-crystal Metal Surfaces Studied by LEED and HREELS," Surface Canada 1983 Meeting, Vancouver, B.C., June 23, 1983.
77. D.F. Ogletree, M.A. Van Hove, and G.A. Somorjai, "The Surface Structure of an Alloy by Dynamical LEED Analysis: The (111) Face of Cu/16at% Al," American Physical Society 1984 Meeting, March 26-30, 1984.

Nuclear Magnetic Resonance*

Alexander Pines, Investigator

INTRODUCTION

The primary objective of the nuclear magnetic resonance (NMR) program is to develop methods in magnetic-resonance spectroscopy and to use them to study molecular behavior in condensed phases. This objective demands an understanding of the interaction of nuclear spins with each other; with other degrees of freedom such as molecular translations, vibrations, and rotations; and with external radiation such as light or radiofrequency sources. Novel methods developed under the program include multiple quantum spectroscopy, high-resolution solid-state NMR and magic-angle spinning, zero-field NMR, pulsed-laser nuclear double resonance, and nuclear magnetic-isotope separation. These methods are being applied to help understand structure and dynamics at the molecular level in a number of materials including ferroelectrics, liquid crystals, polymers, organic crystals, and zeolites. Some molecular properties change with light excitation, and laser magnetic double resonance is being used to examine how these changes dictate the course of photochemical reactions. New methods of detection are being developed to increase the sensitivity of detection, in particular the use of rapidly switched superconducting fields and Josephson-junction devices such as superconducting quantum interference devices (SQUIDS).

1. Multiple-quantum NMR (MQNMR) in Solids (Publication 1)

Yu-Sze Yen[†] and A. Pines

MQNMR has typically been observed in small groups of spins in isolated molecules. Because of the profusion of spin transitions in a solid, individual lines are unresolved. Excitation of high-quantum transitions by normal schemes is thus difficult. To ensure that overlapping lines add constructively and

*This work was supported by the Director, Office of Energy Research, Office of Basic Energy Sciences, Materials Sciences Division of the U.S. Department of Energy under Contract No. DE-AC03-76SF00098.

to enhance sensitivity, time-reversal pulse sequences were used to generate all lines in phase. Up to 38-quantum absorption in solid adamantane was observed. This technique is now being used to develop NMR imaging in solids.

[†]Present address: IBM Thomas J. Watson Research Center, P.O. Box 218, Yorktown Heights, New York 10598.

2. Zero-field NMR (Publication 3)

D.P. Weitekamp, A. Bielecki, D. Zax, K. Zilm,[†] and A. Pines

NMR "powder spectra" in polycrystalline samples are broad, and much structural information is lost as a result of the orientational disorder of these samples. A new technique, Fourier-transform NMR in zero magnetic field, has been developed. With no preferred direction in space, all crystallites contribute equivalently, and resolved splittings can be interpreted directly in terms of internuclear distances. This method opens the possibility of molecular-structure determination without the need for single crystals or oriented samples. Initial experiments have been done on hydrogen groups in metal-hydrogen complexes.

[†]Present address: Department of Chemistry, Yale University, New Haven, Connecticut 06520.

3. Spin Diffusion and Orientation Dependence of Deuterium T_1 in Solids (Publication 5)

C. Ye,[†] R. Eckman,[‡] and A. Pines

A theory has been developed to describe the process of spin diffusion (transport of magnetization energy) between quadrupolar nuclei. Experiments confirmed the dependence of T_1 (spin-lattice relaxation time) on the inverse square $\frac{1}{\Delta\omega^2}$ of the frequency difference. Thus sample rotation can be an effective means of enhancing the diffusion.

[†]Present address: Wuhan Institute of Physics, Academia Sinica, Wuhan, People's Republic of China.

[‡]Present address: Chemical Technology Department, Exxon Chemical Company, Baytown, Texas 77522.

4. Total-spin Coherence-transfer Echo Spectroscopy (Publication 6)

J.R. Garbow,[†] D.P. Weitekamp, and A. Pines

The sensitivity of multiple-quantum NMR transitions to both magnetic-field inhomogeneity and the relative phases and amplitudes of multiple-quantum lines is discussed. Total-spin coherence-transfer echo spectroscopy (TSCTES) is described and experimentally demonstrated. The TSCTES method allows multiple-quantum spectra to be obtained that are free of inhomogeneous-magnet broadening yet remain sensitive to spin-spin couplings and chemical-shift differences. The method takes advantage of the properties of the total-spin coherence, the unique transition between the extreme eigenstates of a coupled-spin system. Experimental results are reported for partially oriented acetaldehyde and are analyzed in terms of irreducible-tensor operators. Limitations on the method and extensions to heteronuclear-spin systems are also discussed.

[†]Present address: Monsanto Company, St. Louis, Missouri 63167.

5. Broadband Population Inversion (Publication 9)

R. Tycko, J. Baum, E. Schneider, and A. Pines

A theory is presented for construction of sequences of phase-shifted radiation pulses for coherently inverting populations over a broad band of transition frequencies. Such sequences have applications in NMR and coherent optics. Examples of sequences are derived together with computer simulations of their inversion properties. These sequences allow excitation of molecules over a broad bandwidth with considerably less power than previously possible.

6. MQNMR Study of Molecular Structure and Ordering in a Liquid Crystal (Publication 10)

S.W. Sinton,[†] D. Zax, J.B. Murdoch,[‡] and A. Pines

Proton MQNMR spectroscopy was used to investigate the anisotropic ordering in a magnetic field and molecular structure for the nematic phase

of 4-cyano-4'-n-pentyl-d₁₁-biphenyl(5CB-d₁₁). The multiple-quantum spectra exhibited a greater resolution of line splittings than the conventional single-quantum Fourier-transform NMR spectrum of 5CB-d₁₁. This finding greatly simplifies a spectral analysis for the proton dipole-dipole-coupling constants. Splittings among the five-, six-, and seven-quantum spectra were used to obtain the biphenyl-proton couplings for 5CB-d₁₁. Two models for the biphenyl symmetry were considered in the analysis. In one model (D₄ symmetry), the two phenyl rings were assumed to be equivalent. In the other model (D₂ symmetry), the rings were inequivalent by virtue of structural or motion differences between them. Both models produced acceptable fits to the splittings assigned from the experimental spectra, but only the D₂-symmetry case predicted all the structure of the seven-quantum spectrum. The proton-dipolar couplings obtained in both cases were used to derive values for internuclear distances and the biphenyl-order parameters. The D₄-symmetry dipolar couplings produced the most reasonable structural description of the biphenyl unit, in which the phenyl-ring geometry is close to that of benzene. The twist angle between the ring planes was determined to be 30 ± 2°. The order parameters from the D₄-symmetry analysis are in good agreement with results reported by others for the same liquid crystal but with a higher degree of deuterium substitution.

[†]Present address: Exxon Production Research Company, Houston, Texas 77001.

[‡]Present address: Earth Sciences Division, Lawrence Berkeley Laboratory, Berkeley, California 94720.

7. Fourier-transform Pure Nuclear-quadrupole Resonance (NQR) by Pulsed-field Cycling (Publication 11)

A. Bielecki, J.B. Murdoch,[†] D.P. Weitekamp, D.B. Zax, K.W. Zilm,[‡] H. Zimmermann,[§] and A. Pines

We report the observation of Fourier-transform pure NQR by pulsed-field cycling. For deuterium, well-resolved spectra were obtained with high sensitivity showing the low-frequency ν_0 lines and allowing assignments of quadrupole couplings and asymmetry parameters to inequivalent deuterons. The technique is ideally applicable to nuclei with low-quadrupolar frequencies (e.g., ²D, ⁷Li, ¹¹B, ²⁷Al,

^{23}Na , ^{14}N) and makes possible high-resolution structure determination in polycrystalline or disordered materials such as polymers and zeolites.

[†]Present address: Earth Sciences Division, Lawrence Berkeley Laboratory, Berkeley, California 94720.

[‡]Present address: Department of Chemistry, Yale University, New Haven, Connecticut 06511.

[§]Present address: Max-Planck-Institut, Abteilung Molekulare Physik, D-6900 Heidelberg 1, West Germany.

8. Computer Simulations of MQNMR Experiments. I. Nonselective Excitation (Publication 12)

J.B. Murdoch,[†] W.S. Warren,[‡] D.P. Weitekamp, and A. Pines

The multiple-quantum (MQ) evolution of anisotropic-spin systems with four to eight coupled protons was analyzed using a computer for the basic three-pulse sequence. MQ intensities were first investigated as a function of preparation time. The concept of time-independent intensities was then introduced, and an algorithm for efficient computation of these quantities was described. A correlation between the distribution of dipolar coupling values and the intensity of high-quantum lines was discussed. In many cases these intensities were predicted to be considerably larger than a simple statistical argument would suggest. The effect of varying the preparation and detection times independently was analyzed as a random-walk problem.

[†]Present address: Earth Sciences Division, Lawrence Berkeley Laboratory, Berkeley, California 94720.

[‡]Present address: Department of Chemistry, Princeton University, Princeton, New Jersey 08540.

9. MQ Spectrum of Oriented Hexane (Publication 14)

G. Drobny,[†] D.P. Weitekamp, and A. Pines

The proton MQNMR spectrum of methyldeuterated hexane- d_6 was obtained in a nematic solvent. Simulation was achieved with a simple model of conformer probabilities and ordering. The advantages and prospects of MQNMR for the conforma-

tional analysis of ordered nonrigid molecules are discussed. The nematic ordering has a strong influence on the proportion of molecules in the all-trans configuration.

[†]Present address: Department of Chemistry, University of Washington, Seattle, Washington 98125.

10. Work in Progress

We are presenting theory, simulations, and experimental demonstrations of composite π pulses for population inversion in coupled-spin systems such as occur in solid-state NMR. The composite π pulses are phase-shifted rf-pulse sequences designed to invert spins over a larger range of dipole or quadrupole couplings than a conventional π pulse for a given rf power. We discuss a previously proposed theory for constructing composite pulses in the specific context of solids. Two particular sequences, $45_0 180_{90} 90_{180} 180_{90} 45_0$ and $180_0 180_{120} 180_0$, are examined in detail. Their performance in coupled-spin systems of various sizes is evaluated in simulations. Experiments are performed on two solid compounds, $\text{Ba}(\text{ClO}_3)_2 \cdot \text{H}_2\text{O}$ and $\text{C}_4\text{O}_4\text{H}_2$. The results reveal markedly less spectral distortion after composite-pulse inversion than after conventional π -pulse inversion at low-rf powers.

An apparatus has been constructed for zero-field NMR at low temperatures. The apparatus involves a mechanical shuttling of the sample together with rapid magnetic-field switching. Using this apparatus will allow us to obtain structural information as well as molecular dynamics in polycrystalline or disordered materials where x-ray crystallography is of little avail.

The spectra of a mixture of compounds can be separated into their individual spectra by two-dimensional techniques. These techniques, used with MQNMR, allow the determination of molecular ordering in liquid crystals and its relationship to the macroscopic properties of these important materials.

NMR imaging has been used as a medical tool and is beginning to surpass x-ray scanning in its capabilities. Our current work involves extending the NMR-imaging methods so that they can also be used in solid materials. By a combination of multiple-pulse excitation and magnetic-field gradients, high-resolution frequency dependences can be observed in solids. These dependences are being developed to obtain one-dimensional projections of solid samples.

1983 PUBLICATIONS AND REPORTS

Refereed Journals

1. Yu-Sze Yen and A. Pines, "Multiple-quantum NMR in Solids," *J. Chem. Phys.* **78**, 3579 (1983); LBL-14821.
2. D. Zax and A. Pines, "Study of Anisotropic Diffusion of Oriented Molecules by Multiple Quantum Spin Echoes," *J. Chem. Phys.* **78**, 6333 (1983); LBL-14997.
3. D.P. Weitekamp, A. Bielecki, D. Zax, K. Zilm, and A. Pines, "Zero-field Nuclear Magnetic Resonance," *Phys. Rev. Lett.* **50**, 1807 (1983); LBL-15809.
4. R. Eckman, A. Pines, R. Tycko, and D.P. Weitekamp, "Spin Diffusion between Inequivalent Quadrupolar Nuclei by Double-quantum Flip-flops," *Chem. Phys. Lett.* **99**, 35 (1983); LBL-15853.
5. C. Ye, R. Eckman, and A. Pines, "Spin Diffusion and Orientation Dependence of Deuterium T_1 in Solids," *J. Mag. Reson.* **55**, 334 (1983); LBL-15698.
6. J.R. Garbow, D.P. Weitekamp, and A. Pines, "Total Spin Coherence Transfer Echo Spectroscopy," *J. Chem. Phys.* **79**, 5301 (1983); LBL-15810.
7. R. Eckman, "Enhanced Nuclear Spin Relaxation of Deuterium in Solids by Sample Rotation," *J. Chem. Phys.* **79**, 524 (1983); LBL-17183.
8. J. Baum, R. Tycko, and A. Pines, "Broadband Population Inversion by Phase-modulated Pulses," *J. Chem. Phys. Comm.* **79**, 4643 (1983); LBL-16098.
9. R. Tycko, "Broadband Population Inversion," *Phys. Rev. Lett.* **51**, 775 (1983); LBL-16052.
10. S.W. Sinton, D. Zax, J.B. Murdoch, and A. Pines, "Multiple-quantum NMR Study of Molecular Structure and Ordering in a Liquid Crystal," *Mol. Phys.*, in press, LBL-16685.
11. A. Bielecki, J.B. Murdoch, D.P. Weitekamp, D.B. Zax, K. Zilm, and A. Pines, "Fourier Transform Nuclear Quadrupole Resonance by Pulsed Field Cycling," *J. Chem. Phys.*, in press, LBL-17167.
12. J.B. Murdoch, W.S. Warren, D.P. Weitekamp, and A. Pines, "Computer Simulations of Multiple-quantum NMR Experiments. I. Non-selective Excitation," submitted to *J. Mag. Reson.*, LBL-17184.
13. W.S. Warren, J.B. Murdoch, and A. Pines, "Computer Simulations of Multiple-quantum NMR Experiments. II. Selective Excitation," submitted to *J. Mag. Reson.*, LBL-17185.
14. G. Drobny, D.P. Weitekamp, and A. Pines, "Multiple-quantum Spectrum of Oriented Hexane," submitted to *J. Chem. Phys.*, LBL-17168.
15. J.R. Garbow (Ph.D. Thesis), "Heteronuclear Dipolar Couplings, Total Spin Coherence, and Bilinear Rotations in NMR Spectroscopy," LBL-16119.
16. S. Sinton, J.R. Garbow, J.L. Ackerman, G. Drobny, D.J. Ruben, and A. Pines, "Spec-Doc: A User's Guide to Spectrometer Software," PUB-3033.

Invited Talks

17. A. Pines, "Irreversibility?" Trumbull Lecture, Yale University, New Haven, Connecticut, January 1983.
18. A. Pines, "Multiple Quantum NMR of Oriented Molecules," British Radiofrequency Group, Spring Meeting, Leeds, England, April 1983.
19. A. Pines, "New Angles in Solid State NMR," 24th Experimental NMR Conference, Asilomar, California, April 1983.
20. A. Pines, "New Angles in NMR Spectroscopy," Louis A. Strait Award Lecture, Northern California Society for Spectroscopy, San Francisco, May 1983.
21. A. Pines, "A Review of Multiple-quantum NMR," Eighth Waterloo Summer Institute on Nuclear Magnetic Resonance, University of Waterloo, Waterloo, Ontario, June 13-18, 1983.
22. A. Pines, "Multiple-quantum Methods (Theory and Practice of Multiple-quantum Methods, Spectral Simplification, and Application to Structural and Dynamical Problems)," NATA ASI on Magnetic Resonance Techniques in Fossil Energy Problems, Maleme, Crete, July 1983.
23. A. Pines, "Recent Developments in Multiple-quantum Spectroscopy," Sixth International Meeting on NMR Spectroscopy, Edinburgh, Scotland, July 1983.
24. A. Pines and K. Zilm, "Zero Field NMR," 25th Rocky Mountain Conference, Denver, August 1983.
25. A. Pines and K. Zilm, "NMR with no Magnetic Field," Eighth Meeting of the International Society of Magnetic Resonance, Chicago, August 22-26, 1983.

LBL Reports

26. A. Pines, "Multiple Quantum Resonance in Quadrupole Spectroscopy," 6th Specialized International *Colloque Ampere* Congress, Kreta, Crete, September 1983.
27. A. Pines, "Coherent Transfer and Two-dimensional Spectroscopy," Physical Chemistry Seminar, Department of Chemistry, University of California Berkeley, October 1983.
28. A. Pines, "Zero Field Nuclear Magnetic Resonance," Department of Chemistry, University of Edmonton, Edmonton, Alberta, November 1983.
29. A. Pines, "Zero Field Nuclear Magnetic Resonance," Department of Chemistry, University of British Columbia, Vancouver, British Columbia, November 1983.
30. A. Pines, "Zero Field Nuclear Magnetic Resonance," Department of Chemistry, Princeton University, Princeton, New Jersey, December 1983.
31. A. Pines, "Will the Magnet Lab. Stay in Business? — Zero-field NMR," Massachusetts Institute of Technology, Cambridge, Massachusetts, December 1983.

Chemical
Sciences

FUNDAMENTAL INTERACTIONS

PHOTOCHEMICAL AND RADIATION SCIENCES

Photon-Assisted Surface Reactions, Materials, and Mechanisms*

Gabor A. Somorjai, Investigator

INTRODUCTION

This project explores the photocatalyzed dissociation of water (H_2O) at both the solid-liquid and solid-vapor interfaces to produce hydrogen and oxygen gases. The purposes of these studies are to explore the mechanism of the photon-assisted surface reaction, to characterize the semiconductor catalyst, and to establish the optimum conditions of surface structure, composition, temperature, and electrolyte solution that maximize both the rate of hydrogen and oxygen production and the power-conversion efficiency of the process. Materials used include silicon- and magnesium-doped iron oxides as small particles, thin films, and single crystals.

1. Photoelectrochemical Studies of Doped Iron Oxide Diodes (Publication 2)

J. Turner, M. Hendewerk, and G.A. Somorjai

Previous work in this laboratory has shown that photodissociation of water can be accomplished without external bias using electrodes of Mg-doped (p-type) and Si-doped (n-type) iron oxide and illumination by visible light. This unbiased p/n-diode assembly has recently been characterized through stability studies, oxygen detection, and the determination of an energy-level diagram for the short-circuited assembly.

Stability studies on an illuminated assembly showed photocurrents which persisted undiminished

throughout 320 hours of continuous testing, indicating that hydrogen and oxygen production from the cell is, in fact, catalytic. Auger analysis before and after extended operation showed that electrode deterioration did not occur. Oxygen production was detected from an assembly using isotopically labeled water ($H_2^{18}O$) and a mass spectrometer to monitor $^{34}O_2$ production. These results showed that near-stoichiometric amounts of O_2 were produced from the cell. An energy-level diagram for the short-circuited p/n assembly was established using a capacitance method to locate conduction- and valence-band edges for the semiconductor electrodes. An energetics analysis of the assembly proved that simultaneous evolution of H_2 and O_2 was thermodynamically feasible from this iron-oxide-based assembly.

Laser and monochromator studies of the p/n assembly have provided further information on carrier production and transport in iron oxide. Measurement of open-circuit voltage and short-circuit photocurrent as a function of illumination intensity have shown that both n-type and p-type iron oxides are low-mobility, high-carrier-density semiconductors.

2. Work in Progress

Several modifications are being investigated to improve the solar-energy-conversion efficiency of the p/n assembly. Thin films of Mg- and Si-doped Fe_2O_3 have been prepared by a plasma-sputtering technique in an attempt to reduce bulk recombination of carriers beyond the depletion layer. In separate studies, iron oxide electrodes have been coated with thin metal overlayers (20–100 Å) of Pt, Rh, and RuO_2 . Such coatings may enhance photoelectrolysis by a reduction of surface-carrier recombination or by catalyzing hydrogen or oxygen production at the electrode surface. Preliminary results show a substantial improvement in hydrogen and oxygen production rates.

In addition, alternative p-type and n-type semiconductors are being investigated for use in photoelectrochemical cells. Requirements for these elec-

*This work was supported by the Director, Office of Energy Research, Office of Basic Energy Sciences, Chemical Sciences Division of the U.S. Department of Energy under Contract No. DE-AC03-76SF00098.

trodes are a demonstrated stability in aqueous solutions, appropriately located conduction- and valence-band edges, and a bandgap that can utilize a large proportion of incident solar radiation.

An electrochemical cell is under construction that may be interfaced directly to an ultrahigh-vacuum chamber. Photoelectrochemical studies on semiconductor electrodes will then be performed in conjunction with analysis by surface spectroscopies (AES, XPS, UPS). These techniques will be useful in identifying surface states and intermediates in photoelectrochemical reactions.

1983 PUBLICATIONS AND REPORTS

Refereed Journals

1. C. Leygraf, M. Hendewerk, and G.A. Somorjai, "The Preparation and Selected Properties of Mg-doped p-type Iron Oxide as Photocathode for the Photoelectrolysis of Water Using Visible Light," *J. Solid State Chem.* **48**, 357-367 (1983); LBL-15269.

LBL Reports

2. J.E. Turner, M. Hendewerk, and G.A. Somorjai, "The Photodissociation of Water by Doped Iron Oxides: The Unbiased p/n Assembly," submitted to *Chem. Phys. Lett.*, LBL-16134.
3. J.E. Turner, M. Hendewerk, D. Neiman, and G.A. Somorjai, "The Characterization of p-type and n-type Doped Iron Oxide Electrodes for the Photodissociation of Water-locations of Band Edges, Oxygen Detection, and Long-term Stability," submitted to *J. Electrochem. Soc.*, LBL-16412.

Invited Talks

4. G.A. Somorjai, "New Strategies for Energy Conversion Through Basic Research. The Photochemical Dissociation of Water," Commonwealth Club of California, Environmental and Energy Section, San Francisco, California, January 31, 1983.

5. G.A. Somorjai, "Dissociation of Water Catalyzed by Light and Iron Oxide," American Chemical Society, Midland, Michigan, February 7, 1983.
6. G.A. Somorjai, "Mg- and Si-doped Iron Oxide for the Photocatalyzed Production of Hydrogen from Water by Visible Light," U.S.-Japan Seminar on Photoelectrochemical Energy Conversion, San Diego, California, March 18, 1983.
7. G.A. Somorjai, C. Leygraf, and M. Hendewerk, "Mg- and Si-doped Iron Oxides for the Photocatalyzed Production of Hydrogen from Water by Visible Light ($2.2 \text{ eV} \leq h\nu \leq 2.7 \text{ eV}$)," American Chemical Society, Seattle, Washington, March 22, 1983.
8. C. Leygraf, M. Hendewerk, and G.A. Somorjai, "Photodissociation of Water with Thin Film p-type and n-type Doped $\alpha\text{-Fe}_2\text{O}_3$ in a Photoelectrochemical Diode Assembly," American Chemical Society, Seattle, Washington, March 22, 1983.
9. G.A. Somorjai, "Mg- and Si-doped Iron Oxide for the Photocatalyzed Production of Hydrogen from Water by Visible Light," Tenth Annual Symposium on Surfaces and Interfaces of the North Central Chapter, American Vacuum Society, Detroit, Michigan, May 17, 1983.
10. G.A. Somorjai, "Solar Energy Conversion by the Photochemical Dissociation of Water," Third Surface/Interface Research Meeting of the Northern California Chapter American Vacuum Society, Lawrence Berkeley Laboratory, Berkeley, California, May 26, 1983.
11. J. Turner, M. Hendewerk, and G.A. Somorjai, "Photodissociation of Water by Mg-doped p-type and Si-doped n-type Oxide Diodes," Seventh DOE Solar Photochemistry Research Conference, Mills College, Oakland, California, June 13, 1983.
12. J. Turner and G.A. Somorjai, "Photodissociation of Water Over Doped Iron Oxides," 43rd Annual Conference on Physical Electronics, Santa Fe, New Mexico, June 20, 1983.
13. G.A. Somorjai, "Catalysts for New Chemical Processes: The Photodissociation of Water and the Reactions of Carbon with Water," Royal Society Centenary Lectures, Liverpool, Great Britain, November 8, 1983.

Photochemistry of Materials in the Stratosphere*

Harold S. Johnston, Investigator

INTRODUCTION

This research is concerned with fundamental gas phase photochemistry, emphasizing chemical species that occur in the stratosphere. Laboratory studies are carried out to obtain optical cross sections, quantum yields, information about microscopic states, and macroscopic rate coefficients for molecules and reactions important in interpreting atmospheric observations. The experimental methods include visible and ultraviolet laser flash photolysis, laser resonance absorption, resonance fluorescence, and infrared diode lasers. Theoretical methods include some molecular quantum mechanics and some numerical atmospheric modeling. This research has applications to problems of atmospheric ozone, and recently it has become apparent that this field of research is applicable to the role of gases other than carbon dioxide in the "greenhouse effect."

1. Measurement of Vibration-rotation Line Strengths of HO Using a Tunable Diode Laser (Publication 1)

James R. Podolske and Harold S. Johnston

Line strengths were measured for four transitions of the HO radical near $2.93 \mu\text{m}$ in the fundamental vibration-rotation band using a tunable infrared diode laser coupled to a molecular modulation spectrometer (see Figure 1-1). The hydroxyl radical was produced by modulated photolysis of O_3 at 253.7 nm in the presence of H_2O , and its number density was obtained from numerical simulation of the complete photochemical system. The strongest line observed was at 3407.607 cm^{-1} , with a measured line strength of $(3.3 \pm 1.5) \times 10^{-20} \text{ cm}^2/\text{molecule}\cdot\text{cm}$.

*This work was supported by the Director, Office of Energy Research, Office of Basic Energy Sciences, Chemical Sciences Division of the U.S. Department of Energy under Contract No. DE-AC03-76SF00098.

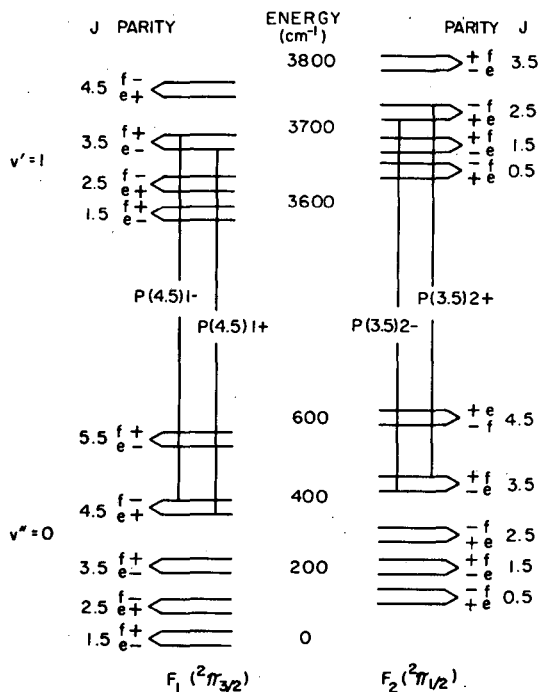


Figure 1-1. Energy level diagram for the HO radical. The transitions observed in this study are indicated, with the notations following Maillard *et al.*¹ (XBL 818-6377)

1. Maillard, *et al.*, J. Mol. Spectrosc. **63**, 120 (1976).

2. Rate of the Resonant Energy-transfer Reaction Between $\text{O}_2(^1\Delta_g)$ and HOO (Publication 2)

James R. Podolske and Harold S. Johnston

Photolysis of ozone at 253.7 nm in a flow system with helium carrier gas was performed, both without and with added water vapor, and steady-state ozone concentrations were measured by ultraviolet absorption at 315.0 nm . The $\text{O}_2(^1\Delta_g)$ is a primary product of UV ozone photolysis, and in a pure ozone system each $\text{O}_2(^1\Delta_g)$ is responsible for the destruction of two additional ozone molecules. With water present, the $\text{O}(^1\text{D})$ formed by O_3 photolysis reacts with H_2O to form hydroxyl radicals, and these radicals initiate an ozone-destroying chain reaction carried by HO and HOO radicals. The experimental results upon addition of water differed qualitatively from predictions based on the 1981 reaction set (see Figure 2-1), but these differences could be explained in terms of inhi-

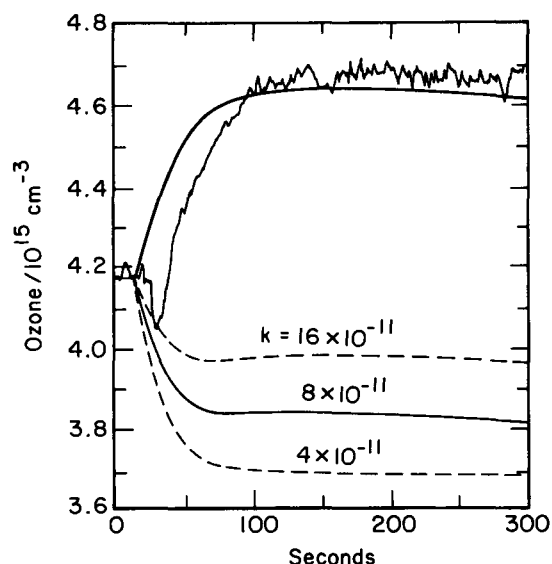
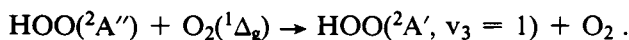


Figure 2-1. Calculated and observed changes in the steady-state concentration of photolyzed ozone as water is added to a dry system. The three lower curves are the calculated ozone concentrations omitting the $O_2(^1\Delta_g) + HOO$ reaction and using three different values for the rate constant $HO + HOO$. The upper curve is that calculated using the two respective rate constants: $3 \times 10^{-11} \text{ cm}^3/\text{molecule}\cdot\text{sec}$, and $8 \times 10^{-11} \text{ cm}^3/\text{molecule}\cdot\text{sec}$. (XBL 824-9236)

hibition of $O_2(^1\Delta_g)$ destruction of ozone by way of HOO quenching of $O_2(^1\Delta_g)$:



An experimental study under a variety of conditions and the interpretation of the data indicate this rate constant to be $(3.3 \pm 1.6) \times 10^{-11} \text{ cm}^3/\text{molecule}\cdot\text{sec}$. The sensitivity of this result to the uncertainty in the rate constant for radical termination ($HO + HOO$) was also investigated.

3. NO_3 Quantum Yields from N_2O_5 Photolysis (Publication 3)

Diane Swanson, Brian Kan, and Harold S. Johnston

The technique of laser flash photolysis/laser resonance absorption was used directly to measure the quantum yield for NO_3 production upon ultraviolet photolysis of N_2O_5 . The average NO_3 quantum yield was found to be 0.89 ± 0.15 . There appeared to be a slight decrease in quantum yield as the concentration of N_2O_5 increased and as the pressure of the carrier gas (N_2 or O_2) increased. The indicated

NO_3 quantum yield at low N_2O_5 concentration and low gas pressure is 1.0, but there is uncertainty from experimental error. After flash photolysis, a fast rise in the concentration of $NO_3(v=0)$ was observed, and the rise time depended on N_2O_5 concentration and on N_2 pressure (see Figure 3-1). These data are interpreted to give rate constants for the deactivation process:



where $k(N_2O_5) = (4.0 \pm 1.0) \times 10^{-12} \text{ cm}^3/\text{molecule}\cdot\text{sec}$, and $k(N_2) = (1.6 \pm 0.3) \times 10^{-13} \text{ cm}^3/\text{molecule}\cdot\text{sec}$.

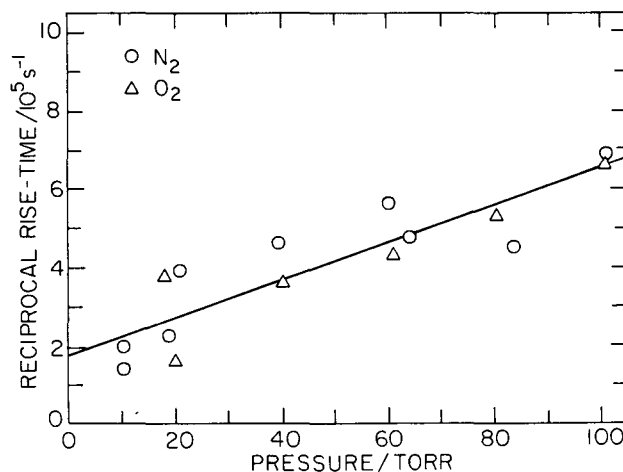


Figure 3-1. Reciprocal rise time of $NO_3(v=0)$ as a function of carrier-gas pressure (\circ, N_2 ; Δ, O_2) at constant concentration of N_2O_5 , $1.5 \times 10^{16} \text{ molecules}/\text{cm}^3$. (XBL 8312-4310)

4. Oxygen Absorption Cross Sections in the Herzberg Continuum and Between 206 and 327 K (Publication 4)

Harold S. Johnston, Mark Paige, and Francis Yao

The ultraviolet absorption cross sections for molecular oxygen have been determined for wavelengths between 205 and 225 nm, for temperatures between 206 and 327 K, and at pressures from 100 to 750 torr. No temperature effect on the O_2 cross sections was observed in the Herzberg continuum. It was necessary to separate the extremely weak O_2 absorption from the stronger absorption by the collision complex O_4 . These experimental data and similar data by others were interpreted in terms

of a theoretical expression for the shape of the Herzberg continuum absorption spectrum. The O_2 absorption cross sections are in good agreement with the values measured in the stratosphere by Herman and Mentall¹ (see Figure 4-1), even though these results are substantially lower than those previously reported in the literature.

1. J.R. Herman and J.E. Mentall, *J. Geophys. Res.* **87**, 8967 (1982).

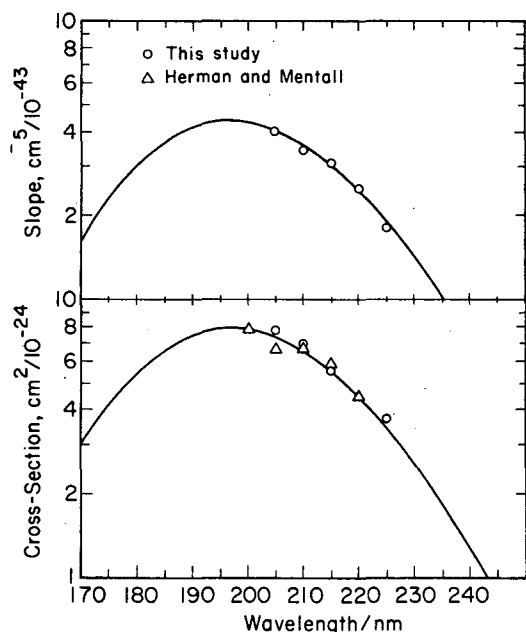


Figure 4-1. Lower panel: These laboratory observations, Herman and Mentall's atmospheric measurements, and the vertically adjusted theoretical curve for O_2 absorption in the Herzberg continuum. Upper panel: similar plot for O_4 absorption; the plotted quantity is the product of the equilibrium constant ($2O_2 = O_4$) and the O_4 cross section. (XBL 8312-4309)

5. Work in Progress

The diode laser is being used to measure the high-resolution absorption spectrum of the ν_2 band of the unstable but atmospherically important molecule HOCl. The line positions, absolute absorption strengths, and pressure-broadening coefficients are being measured.

The quantum yield for NO_3 fluorescence is being measured. A program is being started to measure the "nascent" vibrational distribution of NO_3 after N_2O_5 is photolyzed.

1983 PUBLICATIONS AND REPORTS

Refereed Journals

1. James R. Podolske and Harold S. Johnston, "Measurement of Vibration-rotation Line Strengths of HO Using a Tunable Diode Laser," *J. Chem. Phys.* **79**, 3633 (1983); LBL-16370.
2. James R. Podolske and Harold S. Johnston, "Rate of the Resonant Energy-transfer Reaction Between $O_2(^1\Delta_g)$ and HOO," *J. Phys. Chem.* **87**, 628 (1983); LBL-14961.

LBL Reports

3. Diane Swanson, Brian Kan, and Harold S. Johnston, "NO₃ Quantum Yields from N₂O₅ Photolysis," submitted to *J. Phys. Chem.*, LBL-16951.
4. Harold S. Johnston, Mark Paige, and Francis Yao, "Oxygen Absorption Cross Sections in the Herzberg Continuum and Between 206 and 327 K," submitted to *J. Geophys. Res.*, LBL-17062.

Invited Talk

5. Harold S. Johnston, "Resonant Energy Transfer Between $O_2(^1\Delta_g)$ and HOO," CMA Fluorocarbon Program, Jet Propulsion Laboratory, Pasadena, California, January 18, 1983.

CHEMICAL PHYSICS

Energy Transfer and Structural Studies of Molecules on Surfaces*

Charles B. Harris, Investigator

INTRODUCTION

A proper description of the ways in which internal energy is transferred between molecules and surfaces through electromagnetic-field interactions, particularly in the short-distance regime, is crucial to the understanding of a wide variety of molecule-surface interactions. The purpose of this research is to develop new optical techniques for investigating molecule-surface interactions and for determining how energy in excited states of atoms and molecules is redistributed in the surface states of metals and semiconductors. The long-range goals of this research are to understand, in a general way, how energy redistribution occurs in these systems and how the electromagnetic interactions with metal surfaces give rise to other phenomena such as photofragmentation and Raman scattering.

1. Photochemistry on Metal Surfaces (Publication 7)

*Gary M. Goncher, Craig A. Parsons, and
Charles B. Harris*

The enhanced electric fields present at microstructured silver surfaces in the presence of laser radiation in the visible and near-UV region of the spectrum lead to pronounced increases in the Raman signal observed from molecules adsorbed at the surface and provide a mechanism for enhancing photochemical reactions occurring with molecules at the

surface. If field enhancement is sufficiently high near certain structured metal surfaces, increased absorption by molecules near the surface more than compensates for energy damping by energy transfer to the surface.

Resonant photodecomposition of a variety of aromatic molecules has been observed on roughened silver surfaces with excitation between 350 and 410 nm. These surfaces have been shown to enhance the Raman signal in the green region of the spectrum by a factor of 10^3 . A continuous laser source was used to produce graphitic carbon on the surface, which was monitored by Raman spectroscopy at the 1580 cm^{-1} band of surface carbon. For most molecules the initial excitation appears to be a two-photon process, followed by subsequent absorption steps and fragmentation. Benzaldehyde absorbed on silver, however, shows a one-photon resonant absorption at 350.7 nm followed by rapid decomposition to carbon atoms. Distance-dependence studies of photofragmentation rates by use of an inert spacer layer to separate the molecules undergoing photochemistry from the surface show a maximum decomposition rate 15–20 Å from the surface, corresponding to a balance between enhanced excitation of the molecule and quenching by the surface. The results have been compared to a variety of photochemical mechanisms involving ion and/or neutral intermediates.

2. Distance Dependence of Electronic-energy Transfer to Semiconductor Surfaces: $^3n\pi^*$ Pyrazine/GaAs(110) (Publication 1)

*Paul M. Whitmore, Paul Alivisatos, and
Charles B. Harris*

Energy transfer from $^3n\pi^*$ pyrazine to GaAs(110) has been studied. Within experimental error, a classical dielectric model quantitatively reproduces measurements of the distance-dependent lifetime for emitter-surface separations from 430 to 20 Å. Analysis of the energy transfer shows that the molecular electronic excitation is dissipated through the

*This work was supported by the Director, Office of Energy Research, Office of Basic Energy Sciences, Chemical Sciences Division of the U.S. Department of Energy under Contract No. DE-AC03-76SF00098.

creation of electron-hole pairs in the solid by the high-wave-vector components of the dipole near field.

3. Transient-stimulated Raman Scattering in High-laser Depletion and its Effects on Vibrational Dynamics Experiments (Publication 3)[†]

Dor Ben-Amotz, Steve M. George, and Charles B. Harris

The progress of laser depletion and Stokes growth in transient-stimulated Raman scattering (TSRS) is investigated using a Rayleigh-scattering technique. High-laser depletion is found to dominate the behavior of TSRS under conditions relevant to excite-and-probe vibrational-dynamics experiments. The results are used to explain differences between recent vibrational-dephasing experiments. Implications of the results on both energy-relaxation (T_1) and phase-relaxation (T_2) experiments utilizing TSRS excitation are discussed.

[†]National Science Foundation program using DOE equipment.

4. Picosecond Studies of the Temperature Dependence of Homogeneous and Inhomogeneous Vibrational-linewidth Broadening in Liquid Acetonitrile (Publication 4)[†]

Steve M. George, Alexander L. Harris, Mark Berg, and Charles B. Harris

The temperature dependence of homogeneous and inhomogeneous vibrational-linewidth broadening is reported for the symmetric CH_3 -stretching vibration in acetonitrile over its entire liquid range at $P=1$ atm. A selective excite-and-probe vibrational-dephasing experiment based on TSRS in high-laser depletion is used to measure the homogeneous-dephasing times T_2 . Homogeneous- and inhomogeneous-broadening processes are separated using the combined results of isotropic spontaneous Raman studies and selective picosecond vibrational-dephasing experiments. As a function of temperature, the relative contributions of homogeneous and inhomogeneous broadening are shown to

change significantly in opposing directions. Agreement between experiment and theory supports previous suggestions that homogeneous broadening is caused by rapidly varying processes which affect the vibration via short-range repulsive forces. The results also suggest that inhomogeneous broadening is caused by slowly varying local-density sites which interact with the vibration through long-range attractive forces.

[†]National Science Foundation program using DOE equipment.

5. Generation of Widely Tunable Nanosecond Pulses in the Vibrational Infrared by Stimulated Raman Scattering from the Cesium 6s-5d Transition (Publication 6)[†]

Alexander L. Harris, Keenan Brown, Mark Berg, and Charles B. Harris

The first use of a pulsed rhodamine-dye laser to generate widely tunable nanosecond light pulses in the vibrational infrared by stimulated electronic Raman scattering is reported. Narrowband pulses of up to $120 \mu\text{J}$ were generated from 3450 cm^{-1} to 900 cm^{-1} ($2.9 \mu\text{m}$ to $11.1 \mu\text{m}$), and broadband pulses up to $75 \mu\text{J}$ were generated from 3390 cm^{-1} to 1800 cm^{-1} ($2.9 \mu\text{m}$ to $5.5 \mu\text{m}$) by scattering from the 6s-5d transition in cesium vapor. Cesium-dimer effects on tuning-curve structure and efficiency are discussed.

[†]National Science Foundation program using DOE equipment.

6. Generation of Tunable Picosecond Pulses in the Vibrational Infrared by Stimulated Electronic Raman Scattering of Rhodamine-dye Laser Pulses from the 6s-5d Cesium Transition (Publication 5)[†]

Mark Berg, Alexander L. Harris, Keenan Brown, and Charles B. Harris

The first use of a rhodamine-dye laser to generate tunable high-power picosecond pulses in the vibrational infrared is reported. By using stimulated electronic Raman scattering from the 6s-5d transition in a superheated cesium vapor, one-picosecond pulses from an amplified rhodamine-dye laser

(568–590 nm) have been shifted to 3040–2320 cm^{-1} (3.3–4.3 μm). Somewhat longer pulses have been shifted to 1950 cm^{-1} (5.1 μm). Peak infrared energies of 11 μJ , representing a quantum efficiency of 4.6%, were obtained at a 10-Hz repetition rate. Tuning to longer wavelengths with short pulses is limited by nonlinear processes but should be possible by further reductions of cesium dimer effects.

†National Science Foundation program using DOE equipment.

1983 PUBLICATIONS AND REPORTS

Refereed Journals

1. P.M. Whitmore, A.P. Alivisatos, and C.B. Harris, "Distance Dependence of Electronic Energy Transfer to Semiconductor Surfaces: $^3n\pi^*$ Pyrazine/GaAs(110)," *Phys. Rev. Lett.* **50** (14), 1092 (1983); LBL-15638.
2. S.M. George and C.B. Harris, "Theory for Selective Vibrational Dephasing Experiments Using Transient Stimulated Raman Scattering in High Laser Depletion," *Phys. Rev. A.* **28** (2), 863 (1983); LBL-15640.†
3. D. Ben-Amotz, S.M. George, and C.B. Harris, "Transient Stimulated Raman Scattering in High-laser Depletion and Its Effects on Vibrational Dynamics Experiments," *Phys. Rev. Lett.* **50** (14), 1092 (1983); LBL-15639.†
5. M. Berg, A.L. Harris, J.K. Brown, and C.B. Harris, "Generation of Tunable Picosecond Pulses in the Vibrational Infrared by Stimulated Electronic Raman Scattering of Rhodamine Dye Laser Pulses from the 6s-5d Cesium Transition," *Optics Letters* (in press), LBL-17021.†
6. A.L. Harris, J.K. Brown, M. Berg, and C.B. Harris, "Generation of Widely Tunable Nanosecond Pulses in the Vibrational Infrared by Stimulated Raman Scattering from the Cesium 6s-5d Transition," *Optics Letters* (in press), LBL-17022.†
7. G.M. Goncher, C.A. Parsons, and C.B. Harris, "Photochemistry on Metal Surfaces," LBL-17000.
8. S.M. George (Ph.D. Thesis), "Picosecond Studies of Vibrational Linewidth Broadening in Liquids," LBL-15842.†

LBL Reports

4. S.M. George, A.L. Harris, M. Berg, and C.B. Harris, "Picosecond Studies of the Temperature Dependence of Homogeneous and Inhomogeneous Vibrational Linewidth Broadening in Liquid Acetonitrile," *J. Chem. Phys.* (in press), LBL-15641.†
9. C.B. Harris, "Enhanced Photochemistry on Metal Surfaces," American Chemical Society Meeting, Seattle, Washington, March 1983.
10. C.B. Harris, "Energy Transfer and Photochemistry on Metal Surfaces," American Chemical Society Meeting, Toronto, Ontario, June 1983.
11. C.B. Harris, "The Temperature Dependence of Homogeneous and Inhomogeneous Vibrational Linewidth Broadening Studies Using Coherent Picosecond Stokes Scattering," NATO Workshop on Applications of Picosecond Spectroscopy to Chemistry, Italy, June 1983.†
12. C.B. Harris, "A New Picosecond Infrared Source, and Its Use for Studying Chemical Dynamics," Sixth International Conference on Lasers '83, San Francisco, December 1983.†

†National Science Foundation program using DOE equipment.

Selective Photochemistry*

C. Bradley Moore, Investigator

INTRODUCTION

The fundamental goal of this program is to understand the photophysics of selective excitation of molecules, the dynamics of energy transfer and specificity loss, and the chemical reactions of specifically excited states. For low levels of vibrational excitation in small molecules, chemical reaction rate constants are defined for each quantum state. For larger, more highly excited molecules, energy is transferred among vibrational modes more rapidly than chemical reactions occur. Mode-selective chemical reactions usually do not occur.

Is there a critical molecular size and excitation energy for mode selectivity to disappear? How is this energy flow affected by the environment: gas phase, liquids, inert matrices, and surfaces? Can direct laser excitation of the reaction coordinate defeat this energy transfer and give mode-selective reactions? Answers to these questions may lead to new types of chemical reactions. They may find applications in chemical purification and synthesis, in photobiology, and in surface chemistry.

The rates and mechanisms of free-radical reactions are often best studied by flash kinetic spectroscopy, using lasers for thermal heating, photolyzing, and spectroscopic probing. A fundamental understanding of these reactions is sought to serve as a basis for modeling combustion processes.

1. Reaction and Relaxation of Vibrationally Excited Formyl Radicals (Publication 6)

Andrew O. Langford and C. Bradley Moore

Ground-state and vibrationally excited formyl radicals were produced by excimer-laser (308-nm) photolysis of formaldehyde and glyoxal at 295 K. The subsequent evolution of the (0,1,0) and (0,0,0)

*This work was supported by the Director, Office of Energy Research, Office of Basic Energy Sciences, Chemical Sciences Division of the U.S. Department of Energy under Contract No. DE-AC03-76SF00098.

vibrational levels was monitored through time-resolved laser resonance absorption. Rate constants of $(6.4 \pm 1.0) \times 10^{-12}$, $(3.0 \pm 0.5) \times 10^{-12}$, $(2.5 \pm 0.3) \times 10^{-13}$, $(2.5 \pm 0.8) \times 10^{-13}$, $(3.4 \pm 0.4) \times 10^{-11}$, and $(9.4 \pm 1.1) \times 10^{-12}$ cm³/molecule-sec were determined for removal of HCO(0,1,0) by (HCO)₂, H₂CO, He, N₂, NO, and O₂, respectively. Upper limits of 8.0×10^{-12} and 4.4×10^{-12} cm³/molecule-sec were established for reactive removal of HCO(0,1,0) by NO and O₂. The rate constant for relaxation of an unidentified higher vibrational level of HCO to (0,1,0) by (HCO)₂ was measured to be $(2.4 \pm 0.4) \times 10^{-11}$ cm³/molecule-sec, and rate constants of $(7 \pm 2) \times 10^{-13}$ and $(2.6 \pm 0.6) \times 10^{-11}$ cm³/molecule-sec, respectively, were determined for removal of DCO(0,1,0) by D₂CO and NO. The relaxation and reaction rates with NO and O₂ are understood in terms of the formation and decomposition of an HCONO and HCOO₂ collision complex.

2. Collision Complex Formation in the Reactions of Formyl Radicals with Nitric Oxide and Oxygen (Publication 7)

Andrew O. Langford and C. Bradley Moore

The laser-photolysis/resonance-absorption technique has been used to measure absolute rate constants for the reactions of HCO and DCO with NO and O₂ at 295 K. The values of $(1.26 \pm 0.2) \times 10^{-11}$ and $(4.65 \pm 0.6) \times 10^{-12}$ cm³/molecule-sec for the reactions of HCO with NO and O₂, respectively, are in good agreement with previously reported values. Deuterium substitution was found to increase the rate constants by 25% and 10% in reactions with NO and O₂, respectively. These results are not explained within the framework of a direct hydrogen transfer mechanism and suggest that collision complexes are formed in reactions. Simple RRKM calculations for a complex with a long lifetime, when compared to vibrational energy redistribution times, reproduce the experimental isotope effects semiquantitatively, as well as reproduce the experimentally observed decreases in rate constant which result from vibrational excitation of the HCO or from an increase in temperature. Figure 2-1 shows the potential-energy diagram for the collision-complex mechanism of the reaction HCO + NO → HNO + CO.

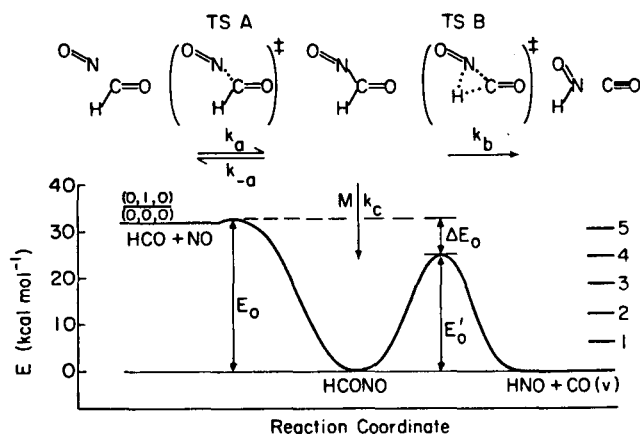


Figure 2-1. Schematic potential-energy diagram for the collision-complex mechanism of the reaction $\text{HCO} + \text{NO} \rightarrow \text{HNO} + \text{CO}$. The collision-complex formation rate is determined experimentally as the rate of vibrational relaxation plus decay reaction for $\text{HCO}(0,1,0) + \text{NO}$. The complex is assumed to decay statistically to reactants [$\text{HCO}(0,0,0) + \text{NO}$] and products [$\text{HCO} + \text{NO}$] or to be stabilized by collisions. The experimental data fix a value for ΔE_0 of about 8 kcal/mole. The "inverse" isotope effect and the decrease in reactivity with vibrational excitation follow necessarily from the RRKM calculated rates for complex decay to reactants and products. (XBL 8312-4308)

3. Activation and Cleaning of Oxide Surfaces by a Continuous Wave (cw) CO_2 Laser (Publication 5)

Alison D. Abbate, Tomoji Kawai, C. Bradley Moore, and Chi-Tsung Chin

Silica, alumina, and zinc oxide surfaces have been dehydroxylated by a cw CO_2 laser. Power densities of $3\text{--}7 \text{ W/cm}^2$ produce the same surfaces spectroscopically as does heating at $400\text{--}1000^\circ\text{C}$. Varying the laser power while keeping the total number of photons constant shows that this is not a linear photochemical process and may be purely thermal desorption. Laser heating has a number of practical advantages over traditional heating methods which have been used for surface cleaning and activation.

1983 PUBLICATIONS AND REPORTS

Refereed Journals

1. J.M. Jasinski, J.K. Frisoli, and C.B. Moore, "High Vibrational Overtone Photochemistry of Cyclobutene," *J. Chem. Phys.* **79**, 1312 (1983); LBL-15502.

2. J.M. Jasinski, J.K. Frisoli, and C.B. Moore, High Vibrational Overtone Photochemistry of 1-Cyclopropylcyclobutene, *J. Phys. Chem.* **87**, 3826 (1983); LBL-15503.
3. C.B. Moore and J.C. Weisshaar, "Formaldehyde Photochemistry," *Ann. Rev. Phys. Chem.* **34**, 525 (1983); LBL-15785.[†]

LBL Reports

4. C.-K. Cheng, P. Ho, and C.B. Moore, "Infrared Studies of CO Produced by the Photodissociation of Formaldehyde and Other Small Carbonyls," accepted by *J. Phys. Chem.*, LBL-17111.[†]
5. A.D. Abbate, T. Kawai, C.B. Moore, and C.-T. Chin, "Activation and Cleaning of Oxide Surf. by Heating With a CO_2 Laser," accepted by *Surf. Sci. Lett.*, LBL-16678.
6. A.O. Langford and C.B. Moore, "Reaction and Relaxation of Vibrationally Excited Formyl Radicals," accepted by *J. Chem. Phys.*, LBL-17026.
7. A.O. Langford and C.B. Moore, "Collision Complex Formation in the Reactions of Formyl Radicals With Nitric Oxide and Oxygen," accepted by *J. Chem. Phys.*, LBL-17027.

Invited Talks

8. C.B. Moore, "Applications of Lasers in Chemistry at Berkeley," Third Meeting of the Bay Area Chapter of the Quantum Electronics and Applications Society (Institute of Electrical and Electronics Engineering), University of California Berkeley, February 17, 1983.
9. C.B. Moore, "Vibrational Photochemistry," Nobel Laureate Signature Award Symposium, American Chemical Society National Meeting, Seattle, Washington, March 22, 1983.
10. C.B. Moore, "The Chemical Dynamics of Highly Vibrationally Excited Molecules," Department of Chemistry Seminar, University of Southern California, Los Angeles, California, April 6, 1983.
11. C.B. Moore, "Vibrational Photochemistry," Department of Chemistry Colloquium, Arizona State University, Tempe, Arizona, April 13, 1983.
12. C.B. Moore, "Photochemistry with Lasers," Department of Chemistry Colloquium, University of Arizona, Tucson, Arizona, April 14, 1983.
13. J.M. Jasinski, J.K. Frisoli, and C.B. Moore, "Unimolecular Reactions Induced by Overtone

- Excitation of C-H Bonds" (delivered by J.M. Jasinski), The Royal Society of Chemistry Faraday Division, General Discussion No. 75 on Intramolecular Kinetics, Warwick University, Warwick, England, April 18-20, 1983.
14. C.B. Moore, "Photochemistry Using High Overtone Excitation," Seminar, Avco Everett Research Laboratories, Everett, Massachusetts, April 25, 1983.
 15. C.B. Moore, "Dynamics and Chemistry of Highly Vibrationally Excited Molecules," Physics Colloquium, Physikalisches Institut für Theoretische Physik III, Bayreuth, Germany, June 21, 1983.
 16. C.B. Moore, "Flash Kinetic Spectroscopy of Methylene and Formyl Radicals," Department of Physical Chemistry Seminar, University of Wuppertal, Wuppertal, West Germany, June 24, 1983.
 17. C.B. Moore, "Reaction and Relaxation of Excited Free Radicals," Eighth International Conference on Molecular Energy Transfer (COMET VIII), Cirencester, England, July 3-8, 1983.
 18. C.B. Moore, "Physique des Milieux Ionisés, les spectres et la Relaxation Vibrationnelle en Plasma," Ecole Polytechnique, Palaiseau, France, October 21, 1983.
 19. C.B. Moore, "Spéctres Infrarouge à Haute Résolution des Espèces de Courte Durée de Vie," Ecole Normale Supérieure, Paris et Université de Paris V, Paris, October 26, 1983.
 20. C.B. Moore, "Spéctre Infrarouge et Processus de Transfert d'Energie des Radicaux et des Ions," Université de Paris VI, Institut de Photophysique Moléculaire, Orsay, France, October 29, 1983.

[†]Supported in part by the Assistant Secretary for Nuclear Energy, Office of Advanced Systems and Nuclear Projects, Advanced Isotope Separation Division of the U.S. Department of Energy under Contract No. DE-AC03-76SF00098.

Physical Chemistry With Emphasis on Thermodynamic Properties*

Kenneth S. Pitzer, Investigator

INTRODUCTION

The purpose of this program is the discovery and development of methods of calculation of thermodynamic and related properties of important chemical systems by the use of quantum and statistical mechanics, together with experimental measurements for key systems. Current efforts include relativistic quantum mechanical methods for the calculation of energies, bond distances, and other properties of the ground and excited states of molecules containing very heavy atoms where conventional nonrelativistic methods are inadequate. Such results are important in evaluating possible laser systems and for models of catalytic entities including heavy atoms such as platinum.

Another general area is that of ionized systems, electrolyte solutions, and plasmas. Systems comprising fused salts mixed in any proportion with water are being studied experimentally and with semi-empirical theory. Recent theoretical advances include treatments of the dielectric constant of H_2O , the thermodynamics of ionic solutions in H_2O above its critical temperature, and the critical properties of pure ionic fluids such as NaCl. Earlier advances yielded improved equations for electrolyte solutions which are now being applied to a wide variety of systems of industrial or geological interest, including geothermal brines.

1. Thermodynamics of Unsymmetrical Electrolyte Mixtures. Enthalpy and Heat Capacity (Publication 7)

Kenneth S. Pitzer

There is a purely electrostatic contribution to the thermodynamic properties of electrolytes for the mixing of ions of different charge but the same sign. The previous treatment, which was limited to

*This work was supported by the Director, Office of Energy Research, Office of Basic Energy Sciences, Chemical Sciences Division of the U.S. Department of Energy under Contract No. DE-AC03-76SF00098.

activity or osmotic coefficients, is extended to enthalpies and heat capacities and applied to the measurements of Cassel and Wood on the heat of mixing in the systems NaCl-BaCl₂ and NaCl-Na₂SO₄. The results for the latter system are shown in Figure 1-1.

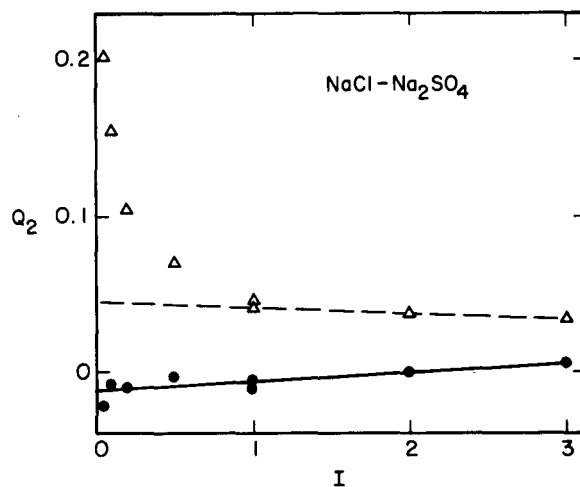


Figure 1-1. The interaction Q_2 from short-range forces for the heat of mixing ions of the same sign, calculated two ways: including (circles) and excluding (triangles) the higher-order unsymmetrical mixing term for electrostatic forces. This interaction should be linear in the ionic strength I .

(XBL 8312-2555)

2. The Ground and Excited States of PtH and PtH⁺ by Relativistic *Ab Initio* Electronic Structure Calculations: A Model Study for Hydrogen Chemisorption on Platinum Surfaces and Related Photoemission Properties (Publication 12)

S. W. Wang and Kenneth S. Pitzer

Relativistic electronic-structure calculations for the ground and excited states of PtH and PtH⁺ are performed, first using a spin-averaged relativistic effective core potential (AREP) at the self-consistent field (SCF) level, and later incorporating the spin dependence at the configuration-interaction (CI) level. These calculations lead to the following conclusions. (1) Both the 6s and 5d orbitals of Pt interact strongly with the H orbitals, clearly indicating that the bonding involves both 6s and 5d electrons. (2) Correlation energies contribute significantly to the PtH binding energy but have little effect

on the force constant. (3) The polarization functions centered on H are much more important than those centered on Pt in affecting the binding energy. (4) The two lowest states, ${}^2\Delta_{5/2}$ and ${}^2\Sigma_{1/2}$, are calculated to have almost exactly the same energy; either may be the lower one. The lowest 3/2 state is mixed ${}^2(\pi+\Delta)_{3/2}$ and lies a little higher in energy. (5) Both the first ionization potential and the ionization energy of the H-like level agree reasonably well with the experimental data. (6) Finally, the absolute binding energy of PtH is 2.45 eV, to be compared with the experimental value of 3.44 eV. The discrepancy is due to our computational limitations.

3. Relativistic Molecular Structure Calculations Including CI for Several Low-lying States of SnO (Publication 13)

K. Balasubramanian and Kenneth S. Pitzer

Relativistic quantum calculations, including configuration interaction and spin-orbit interaction, are described for seven low-lying Λ -S states of SnO and the corresponding ω - ω states with spin-orbit interaction. Spectroscopic properties of these states are computed and compared with experimental results. Properties are predicted for several low-lying electronic states that have not yet been observed experimentally.

4. Dielectric Constant of Water at Very High Temperature and Pressure (Publication 14)

Kenneth S. Pitzer

Pertinent statistical mechanical theory is combined with the available measurements of the dielectric constant of water at high temperature and pressure to predict the dielectric constant at still higher temperature. The dielectric constant is needed in connection with studies of electrolytes such as NaCl/H₂O at very high temperature. Figure 4-1 indicates the accuracy of agreement of the equation with experimental data, which extend in temperature to 823 K, in terms of the Kirkwood g factor.

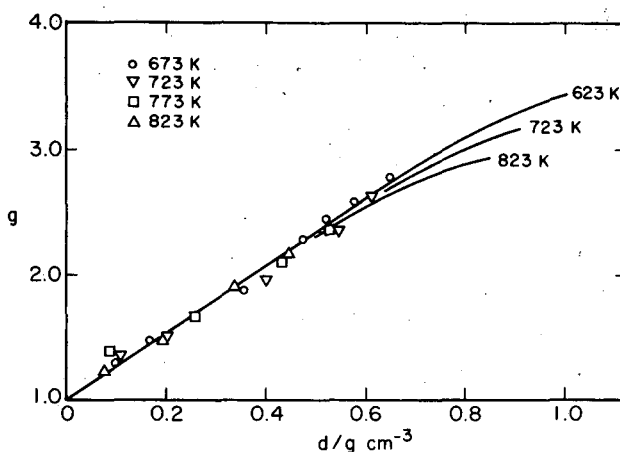


Figure 4-1. The Kirkwood g factor for H₂O at high temperature. The points are based on experimental measurements at the indicated temperatures. The curves are calculated. (XBL 834-167)

5. Relativistic Configuration-interaction Calculations for Several Low-lying States of PbO: Comparison with Chemiluminescent Spectra (Publication 17)

K. Balasubramanian and Kenneth S. Pitzer

Relativistic quantum calculations, including configuration interaction and spin-orbit interaction, are described for eleven low-lying states of PbO. Comparison calculations are presented for 8 Λ -S states obtained in the absence of spin-orbit interaction. These calculations were carried out using relativistic effective core potentials. Spectroscopic properties of these low-lying states of PbO are computed and compared with the spectra resulting from chemiluminescent reactions of Pb with O₃, N₂O, etc. Possible assignments of the experimentally observed bands are suggested. Spectroscopic properties are predicted for several low-lying electronic states that have not yet been observed experimentally. The effect of spin-orbit interaction and the nature of CI wave functions are discussed and comparisons made with SnO.

6. Relativistic Quantum Calculations of Low-lying States of PbH: Comparison with Experimental Spectra (Publication 18)

K. Balasubramanian and Kenneth S. Pitzer

Relativistic quantum calculations, including configuration interaction and spin-orbit interaction, are described for five low-lying states of PbH. Two of these states have not been observed experimentally. Spectroscopic properties are calculated and discussed in comparison with experimental spectra. The calculated dissociation energy of 1.64 eV agrees well with experiment (1.59 eV). From the nature of the CI wave function, it is shown that the low-lying electronic states are heavily mixed by spin-orbit interaction and cannot be assigned to any Λ -S state uniquely.

7. Relativistic Quantum Calculations of Low-lying States of SnH: Comparisons with the Electronic Spectra of SnH and with the Properties of PbH (Publication 21)

K. Balasubramanian and Kenneth S. Pitzer

Relativistic quantum calculations, including spin-orbit interaction and configuration interaction, are described for several low-lying states of SnH. The spectroscopic properties of these states are compared with the experimental electronic spectra. The properties of the $^2\Pi$, $^4\Sigma^-$, and $^2\Delta$ states are discussed in both Λ -S and ω - ω coupling schemes and compared with appropriate states of PbH. The dissociation energy is calculated to be 2.30 eV.

8. Critical Point and Vapor Pressure of Ionic Fluids Including NaCl and KCl (Publication 24)

Kenneth S. Pitzer

Theoretical results for the liquid density and vapor pressure of a hard-core ionic fluid are compared with experimental data for NaCl. From extrapolations to higher temperature, estimates are presented for the critical properties for the primitive model and for pure NaCl and KCl. For NaCl, $T_c = 3900$ K, $V_c = 490$ cm³ · mol⁻¹, and $p_c = 258$ bar. The degree of conformity of these ionic fluids to the principle of corresponding states is examined.

9. Work in Progress

Electronic-structure calculations are nearly complete for small clusters of copper atoms by methods which should be extendible to larger clusters. This will allow calculations for models of surfaces and edges in small crystals. Effective-potential methods are used in a local-spin-density formalism including terms for core polarizability. Good agreement is obtained with experimental data for Cu₂ and Cu₃.

1983 PUBLICATIONS AND REPORTS

Refereed Journals

1. Rabindra N. Roy, James J. Gibbons, Mark D. Wood, Rick W. Williams, J. Christopher Peiper, and Kenneth S. Pitzer, "The First Ionization of Carbonic Acid in Aqueous Solutions of Potassium Chloride Including the Activity Coefficients of Potassium Bicarbonate," *J. Chem. Thermodynamics* **15**, 37 (1983); LBL-13482.†
2. K. Balasubramanian, "Operator and Algebraic Methods in NMR Spectroscopy. I. Generation of Spin Species," *J. Chem. Phys.* **78**, 6358 (1983); LBL-14548/1.
3. K. Balasubramanian, "Operator and Algebraic Methods in NMR Spectroscopy. II. Projection Operators and Spin Functions," *J. Chem. Phys.* **78**, 6369 (1983); LBL-14548/2.
4. K. Balasubramanian and K.S. Pitzer, "Electron Structure Calculations Including CI for Ten Low Lying States of Pb₂ and Sn₂. Partition Function and Dissociation Energy for Sn₂," *J. Chem. Phys.* **78**, 321 (1983); LBL-14723.
5. K.S. Pitzer, "Thermodynamics of Sodium Chloride Solutions in Steam," *J. Phys. Chem.* **87**, 1110 (1983); LBL-14886.†
6. M. Conceição P. de Lima and Kenneth S. Pitzer, "Thermodynamics of Saturated Aqueous Solutions Including Mixtures of NaCl, KCl, and CsCl," *J. Solution Chem.* **12**, 171 (1983); LBL-15301.†
7. K.S. Pitzer, "Thermodynamics of Unsymmetrical Electrolyte Mixtures. Enthalpy and Heat Capacity," *J. Phys. Chem.* **87**, 2360 (1983); LBL-15318.
8. Rabindra N. Roy, James J. Gibbons, J. Christopher Peiper, and Kenneth S. Pitzer, "Thermodynamics of the Unsymmetrical Mixed Electrolyte HCl-LaCl₃," *J. Phys. Chem.* **87**, 2365 (1983); LBL-15319.†

9. Ramesh C. Phutela and Kenneth S. Pitzer, "Thermodynamics of Aqueous Calcium Chloride," *J. Solution Chem.* **12**, 201 (1983); LBL-15322.†
10. M. Conceição P. de Lima and Kenneth S. Pitzer, "Thermodynamics of Saturated Electrolyte Mixtures of NaCl with Na₂SO₄ and with MgCl₂," *J. Solution Chem.* **12**, 187 (1983); LBL-15323.†
11. K. Balasubramanian, "Computer Generation of the Symmetry Elements of Non-rigid Molecules," *J. Comput. Chem.* **4**, 302 (1983); LBL-15455.
12. S.W. Wang and Kenneth S. Pitzer, "The Ground and Excited States of PtH and PtH⁺ by Relativistic *Ab Initio* Electronic Structure Calculations: A Model Study for Hydrogen Chemisorption on Platinum Surfaces and Related Photoemission Properties," *J. Chem. Phys.* **79**, 3851 (1983); LBL-15648.
13. K. Balasubramanian and Kenneth S. Pitzer, "Relativistic Molecular Structure Calculations Including CI for Several Low Lying States of SnO," *Chem. Phys. Lett.* **100**, 273 (1983); LBL-15852.
14. K.S. Pitzer, "Dielectric Constant of Water at Very High Temperature and Pressure," *Proc. Nat. Acad. Sci. USA* **80**, 4574 (1983); LBL-15941.
15. Robert H. Wood, David Smith-Magowan, Kenneth S. Pitzer, and P.S.Z. Rogers, "Comparison of Experimental Values of \bar{V}_2^0 , C_{p2}^0 , and C_{v2}^0 for Aqueous NaCl with Predictions Using the Born Equation at Temperatures from 300 to 573.15 K at 17.7 MPa," *J. Phys. Chem.* **87**, 3297 (1983).†
19. Rabindra N. Roy, James J. Gibbons, Rick Williams, Lehman Godwin, Gigi Baker, John M. Simonson, and Kenneth S. Pitzer, "The Thermodynamics of Aqueous Carbonate Solutions Including Mixtures of Potassium Carbonate, Bicarbonate, and Chloride," submitted to *J. Chem. Thermodynamics*, LBL-16317.†
20. Kenneth S. Pitzer and Yi-gui Li, "Thermodynamics of Aqueous Sodium Chloride to 823 K and 1 kbar," submitted to *Proc. Nat. Acad. Sci. USA*, LBL-16561.†
21. K. Balasubramanian and Kenneth S. Pitzer, "Relativistic Quantum Calculations of Low-lying States of SnH: Comparisons with the Electronic Spectra of SnH and with the Properties of PbH," submitted to *J. Molec. Spectroscopy*, LBL-16474.
22. Kenneth S. Pitzer and John M. Simonson, "Ion Pairing in a System Continuously Miscible from the Fused Salt to Dilute Solution," submitted to *J. Am. Chem. Soc.*, LBL-16562.†
23. Kenneth S. Pitzer and Yi-gui Li, "Critical Phenomena and Thermodynamics of Dilute Aqueous Sodium Chloride to 823 K," submitted to *Proc. Nat. Acad. Sci. USA*, LBL-16831.†
24. Kenneth S. Pitzer, "Critical Point and Vapor Pressure of Ionic Fluids Including NaCl and KCl," submitted to *Chem. Phys. Lett.*, LBL-16888.
25. Kenneth S. Pitzer, "Ionic Fluids," submitted to *J. Phys. Chem.*, LBL-16991.
26. John Michael Simonson (Ph.D. Thesis), "Thermodynamic Properties of Very Concentrated Electrolyte Solutions," LBL-16625.

LBL Reports

16. K.S. Pitzer, J.C. Peiper, and R.H. Busey, "Thermodynamic Properties of Aqueous Sodium Chloride Solutions," submitted to *J. Phys. Chem. Ref. Data*, LBL-15512.†
17. K. Balasubramanian and K.S. Pitzer, "Relativistic Configuration Interaction Calculations for Several Low Lying States of PbO. Comparisons of Chemiluminescent Spectra," submitted to *J. Phys. Chem.*, LBL-16014.
18. K. Balasubramanian and K.S. Pitzer, "Relativistic Calculations of Low-lying States of PbH: Comparison with Experimental Spectra," submitted to *Chem. Phys. Lett.*, LBL-16315.
27. Kenneth S. Pitzer, "Thermodynamics of Condensed Ionic Systems," presented at a NATO Advanced Study Institute, Cambridge, England, September 5-17, 1983, to be published by D. Reidel Publishing Co., LBL-16634.
28. K. Balasubramanian, "Non-rigid Molecular Group Theory and Its Applications," a chapter in *Chemical Applications of Topology and Graph Theory*, to be published by Elsevier Publishing Co., LBL-14598.

Other Publications

†This work was supported by the Director, Office of Energy Research, Office of Basic Energy Sciences, Division of Engineering, Mathematics, and Geosciences of the U.S. Department of Energy under Contract No. DE-AC03-76SF00098.

Molecular Interactions*

William A. Lester, Jr., Investigator

INTRODUCTION

This program is directed at extending fundamental knowledge of the interactions that govern the dynamics of energy-transfer, reactive, and photodissociative molecular processes. The approach is based on the reliable description of the potential-energy surfaces and coupling-matrix elements needed in theoretical approaches for the evaluation of cross sections and rates. Emphasis is placed on the use of state-of-the-art Hartree-Fock (HF), multiconfiguration HF (MCHF), and configuration-interaction (CI) *ab initio* methods for the accurate description of molecular interactions. A variety of methods is used to describe collision dynamics. The electronic-structure studies emphasize the determination of the critical geometries and energetics that govern reaction pathways and include the computation of global potential-energy surfaces where appropriate. The dynamics studies include fully quantum-mechanical approaches to ro-vibrational energy transfer in molecules by collision, and an adiabatic approach to single-photon photodissociation of small polyatomic molecules and to chemical reaction.

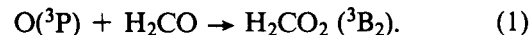
A novel method that solves the Schrödinger equation stochastically is also being studied to ascertain its usefulness for determining the binding energy of molecules and other molecular properties.

1. Hydrogen-atom Migration in the Oxidation of Aldehydes: $O(^3P) + H_2CO$ (Publication 10)

Michel Dupuis and William A. Lester, Jr.

Mechanistic and kinetic studies indicate that the reactions of $O(^3P)$ with aldehydes proceed mostly via abstraction of the weak aldehydic hydrogen atom. In the reaction with H_2CO , the expected products are the formyl and hydroxyl radicals. However, Chang and Barker¹ recently reported the measurement of a

substantial yield (30%) of a primary product of mass 44 (presumably CO_2) in that reaction, and suggested that the addition reaction may be an important channel,



The methylenebis(oxy) H_2CO_2 adduct would then undergo isomerization



followed by fragmentation to form $H + HOCO$, $H + HCO_2$, and $HCO + OH$. Further fragmentation of $HOCO$ and HCO_2 would lead to CO_2 . We report the results of an *ab initio* study of the H-atom migration reaction channel (2). Figure 1-1 shows structures of the stationary points for reaction (2).

From energy barriers calculated by HF, MCHF, and CI, we estimate the activation energy to be no less than 30 kcal/mole. We conclude that the hydrogen-migration channel is not accessible in recent room-temperature experiments on the $O(^3P) + H_2CO$ reaction.

Figure 1-2 shows the energy correlation diagram for the $H_2CO_2 \rightarrow HCOOH$ reaction.

¹J.S. Chang and J.R. Barker, *J. Phys. Chem.* **83**, 3059 (1979).

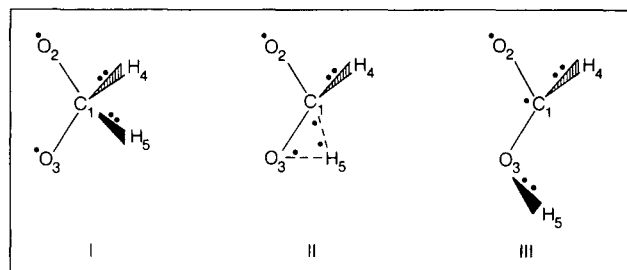


Figure 1-1. Structures of stationary points for the $H_2CO_2 \rightarrow HCOOH$ reaction. (XBL 839-862)

*This work was supported by the Lawrence Berkeley Laboratory Director's Program Development Fund and by the Director, Office of Energy Research, Office of Basic Energy Sciences, Chemical Sciences Division of the U. S. Department of Energy under Contract No. DE-AC03-76SF00098.

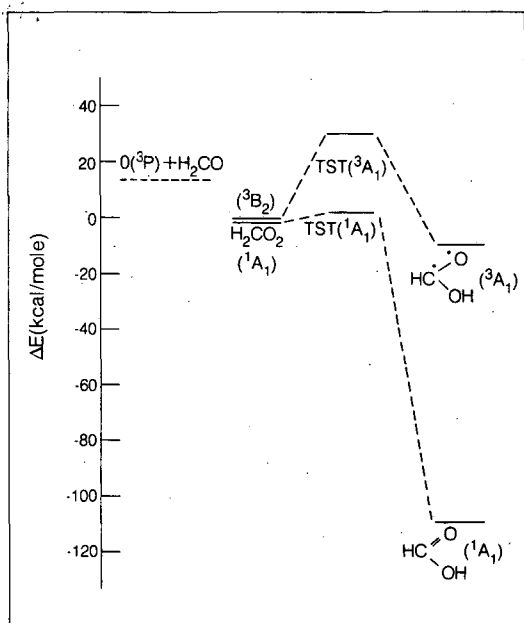


Figure 1-2. Energy correlation diagram for the $\text{H}_2\text{CO}_2 \rightarrow \text{HCOOH}$ reaction. (XBL 839-860)

2. *Ab Initio* Study of Cyanogen (C_2N_2) (Publications 11 and 12)

Christopher E. Dateo, Michel Dupuis, and William A. Lester, Jr.

An *ab initio* MCHF study of the $X^1\Sigma_g^+$, $\tilde{a}^3\Sigma_u^+$, $\tilde{B}^1\Delta_u$, and $\tilde{C}^1\Pi_u$ states of cyanogen (C_2N_2) is presented. Equilibrium structures, harmonic vibrational frequencies, excitation energies, and dissociation energies have been calculated and found to be in semiquantitative agreement with available experimental data.

This study confirms the $\pi \rightarrow \pi^*$ character of the $^3\Sigma_u^+$ and $^1\Delta_u$ states, and the $n \rightarrow \pi^*$ character of the $^1\Pi_u$ state near their equilibrium geometries. Configuration mixing among the n and π electrons is needed to correct the broken-symmetry description given by the HF method and leads to a qualitatively correct description of these excited states. For the $\pi \rightarrow \pi^*$ states, the harmonic force constants show a strong through-bond interaction due to the dominance of the charge-transfer configuration $^+\text{NCCN}^-$. For the $n \rightarrow \pi^*$ state the trans-bending mode and the cis-bending mode lead to different Renner-Teller splittings. The lower $^1A'$ state most likely has a slightly trans-bent minimum-energy structure.

Figure 2-1 shows the energy correlation diagram of C_2N_2 . Figure 2-2 shows the qualitative bending potential of C_2N_2 ($\tilde{C}^1\Pi_u$).

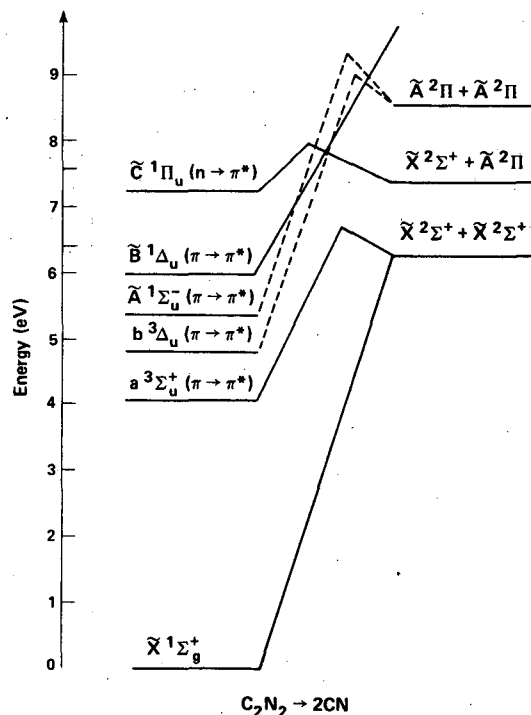


Figure 2-1. Energy correlation diagram of C_2N_2 . (XBL 832-1235)

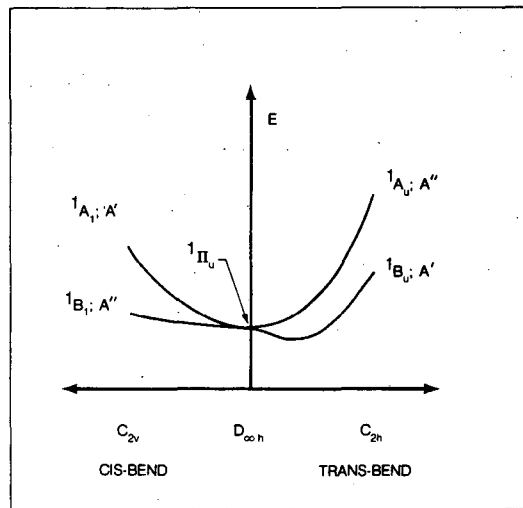


Figure 2-2. Qualitative bending potential of C_2N_2 ($\tilde{C}^1\Pi_u$). (XBL 839-863)

3. Reaction Hamiltonian and the Adiabatic Approach to the Dynamics of Chemical Reaction (Publication 13)

Vladimir Z. Kresin and William A. Lester, Jr.

A new approach for the evaluation of product energy distributions of chemical reactions is presented. The approach is characterized by two main features. The first is the introduction of a specific reaction Hamiltonian (in second quantization) that facilitates the description of a chemical reaction as a quantum transition from reactants to products. The second is the use of a specific adiabatic method to describe the dynamics of nuclear motion of both reactants and products. To illustrate the method, the determination of the product-energy distribution is discussed for $\text{OH} + \text{D} \rightarrow \text{OD} + \text{H}$ and $\text{C} \ell \text{I} + \text{D} \rightarrow \text{C} \ell + \text{ID}$ and carried out for the latter system.

4. The Adiabatic Method in the Theory of Many-body Systems (Publication 17)

Vladimir Z. Kresin and William A. Lester, Jr.

The adiabatic approach is presented as a method in quantum many-body theory. Recent advances in adiabatic theory for solids, molecules, and nuclei are described. The application of adiabatic methods to systems with comparable masses is presented and applied to the problem of nuclear motion of polyatomic systems. Different types of nonadiabatic interactions (e.g., the electron-phonon interaction in metals, the pair correlation in superconducting systems, and the electron-vibrational interaction in molecules) are discussed. The continuity of electron and phonon spectra in solids and the potential energy surface crossings in molecular systems are shown to lead to large nonadiabaticity.

5. Quantum Monte Carlo for Molecules (Publication 19)

Peter J. Reynolds and William A. Lester, Jr.

An alternative approach to conventional quantum-chemistry techniques for molecular studies is the quantum Monte Carlo (QMC) method. In this approach the many-body Schrödinger equation is re-

interpreted as a diffusion equation. Simulating the appropriate random-walk process allows one to calculate expectation values of molecular properties. In principle these expectation values can be calculated exactly, subject only to statistical errors, which may be made arbitrarily small through sufficient computation. In preliminary work on small molecules (H_2 , LiH , Li_2 , and H_2O), we have used a simple but accurate approximation to treat Fermi statistics. In that approximation the calculated total energy remains an upper bound to the true energy. The quality of the bound, as well as the magnitude of the statistical error, depends on the "importance function" which guides the diffusion through phase space. With exceptionally simple importance functions, we have obtained 80–100% of the correlation energy for the above-mentioned molecules.

6. Achieving Chemical Accuracy by Quantum Monte Carlo (Publication 23)

William A. Lester, Jr. and Peter J. Reynolds

In order to better understand the processes resulting in the release of chemical energy, one needs a computational technique of high accuracy. One promising alternative approach to the current quantum-chemistry techniques for molecular studies is the QMC method. Simulating an appropriate random-walk process enables one to calculate expectation values of molecular properties exactly, in principle, subject only to statistical errors. The computational effort with QMC rises roughly as N^2 , where N is the number of electrons. Thus calculations on relatively large systems are feasible. Using a simple but accurate fixed-node approximation, the calculated total energy remains an upper bound to the true energy. The quality of the bound and the magnitude of the statistical error depend on an "importance function" which guides the diffusion through phase space. The location of the nodes of this function determines the accuracy which can be obtained. Even with very simple importance functions, we have obtained 80–100% of the correlation energy of two- to ten-electron molecules.

The QMC procedure applies equally well in situations away from the equilibrium geometry. In calculations of the ground-state energy of Li_2 at a few different nuclear separations, we chose the same importance function (with the same parameters) for all nuclear separations. Although this choice is hardly optimal, point-wise agreement with the exact

results strayed at roughly 90–95% of the correlation energy.

7. Chemical Application of Diffusion Quantum Monte Carlo (Publication 24)

Peter J. Reynolds and William A. Lester, Jr.

The diffusion QMC method is receiving increasing attention for molecular applications because of its high accuracy. However, reducing statistical uncertainty remains a priority because molecular properties are often obtained as small differences of large numbers. An example of such a problem occurs in calculating the energy difference of the lowest singlet and triplet states of methylene (CH_2). One direction for reducing variances is to increase the number of time steps using the power of parallel and vector computers.

We have implemented the QMC algorithm on the Cyber 205, first as a direct transcription of the algorithm running on a DEC VAX 11/780, and second by explicitly writing vector code for all loops longer than a crossover length C^* . Present studies show that $C^* = 15$ is the optimal crossover point for the Cyber. Since CH_2 has only eight electrons, most of the loops in this application are fairly short and thus do not take maximum advantage of the Cyber architecture. The longest inner loops run over the set of atomic-basis functions. The CPU time dependence obtained versus the number of basis functions is linear for both the Cyber and the VAX. However, the slope on the Cyber is near zero, implying little extra cost for enlarging the basis set. Traditional quantum-chemistry codes scale with the fourth to seventh power of the number of basis functions. Finally, we note that restructuring the algorithm to compute the separate Monte Carlo realizations in parallel will potentially allow vectors of unlimited length and could result in an additional order-of-magnitude reduction in variance for comparable computing times.

8. Work in Progress

We have calculated the polarizability components of H_2 ($B^1\Sigma_u^+$) using noncorrelated HF, correlated MCHF, and CI wavefunctions. The results show that electron-correlation contributions to the H_2 ($B^1\Sigma_u^+$) polarizability are significant ($\sim 25\%$), with the largest contribution arising from

angular correlation. The calculated polarizability components are $\alpha_{\perp} = 53 \pm 3$ a.u. and $\alpha_{\parallel} = 265 \pm 15$ a.u.

A systematic study of the effects of electron correlation on the structure, dipole moment, and dipole-moment derivatives of ozone (O_3) has been carried out. The importance of a proper description of charge-transfer effects for qualitative and quantitative accuracy is demonstrated. An electronic configuration corresponding to charge transfer from the center oxygen atom to the end atoms plays a critical role in providing an accurate determination of the dipole moment of ozone and the intensities of the fundamental vibrations. Calculated properties, with the experimental values in parentheses, are: $R_e = 1.295 \text{ \AA}$ (1.271 \AA); $\theta_e = 116.5^\circ$ (116.8°); $\mu = -0.507 \text{ D}$ (-0.536 D); ω_1 (sym. st., cm^{-1}) = 1.096 (1110); ω_2 (bond, cm^{-1}) = 689 (705); ω_3 (asym. st., cm^{-1}) = 1040 (1042). The calculated ratio of infrared intensities, with the experimental values in parentheses, is $I_1:I_2:I_3 \equiv -:1.0:14.3$ (0.6:1.0:19.4).

1983 PUBLICATIONS AND REPORTS

Refereed Journals

1. T. Takada and M. Dupuis, "On the Electronic Structure of Cubene C_8H_6 ," *Chem. Phys. Lett.* **93**, 193 (1982); LBL-14584.
2. J. Pacansky and M. Dupuis, "Assignment of the Infrared Spectrum for the Ethyl Radical," *J. Am. Chem. Soc.* **104**, 415 (1982); LBL-17452.
3. T. Takada, M. Dupuis, and H.F. King, "Molecular Symmetry IV: the Coupled Perturbed Hartree-Fock Method," *J. Comp. Chem.* **4**, 234 (1983); LBL-14470.
4. T. Takada and M. Dupuis, "Theoretical Study of the Allyl Radical: Structure and Vibrational Analysis," *J. Am. Chem. Soc.* **105**, 1713 (1983); LBL-14314.
5. N. Abusalbi, R.A. Eades, T. Nam, D. Thirumalai, D. Dixon, D.G. Truhlar, and M. Dupuis, "Electron Scattering by Methane: Elastic Scattering and Rotational Excitation Cross Sections Calculated with *Ab Initio* Interaction Potentials," *J. Chem. Phys.* **78**, 1213 (1983); LBL-14871.
6. J. Rys, M. Dupuis, and H.F. King, "Computation of Electron Repulsion Integrals Using the Rys Quadrature Method," *J. Comp. Chem.* **4**, 154 (1983); LBL-17299.
7. S. Chapman, M. Dupuis, and S. Green, "Theoretical Three-dimensional Potential

- Energy Surface for the Reaction of Be with HF," Chem. Phys. **78**, 93 (1983); LBL-17302.
8. M.E. Colvin, G.P. Raine, H.F. Schaefer, III, and M. Dupuis, "Infrared Intensities of H_3O^+ , H_2DO^+ , HD_2O^+ , and D_3O^+ ," J. Chem. Phys. **79**, 1551 (1983); LBL-16092.
 9. M. Dupuis, W.A. Lester, Jr., B.H. Lengsfeld, and B. Liu, "Accurate MCHF/CI Calculation of the $\text{H}_2\text{CO} \rightarrow \text{H}_2 + \text{CO}$ Dissociation," J. Chem. Phys. **79**, 6167 (1983); LBL-16714.

LBL Reports

10. M. Dupuis and W.A. Lester, Jr., "Hydrogen Atom Migration in the Oxidation of Aldehydes: $\text{O}(^3\text{P}) + \text{H}_2\text{CO}$," LBL-16274.
11. C.E. Dateo, M. Dupuis, and W.A. Lester, Jr., "Ab Initio Study of Cyanogen (C_2N_2). I: The $\tilde{a}^3\Sigma_u^+$ and $\tilde{B}^1\Delta_u$ States," LBL-16627.
12. C.E. Dateo, M. Dupuis, and W.A. Lester, Jr., "Ab Initio Study of Cyanogen (C_2N_2). II: The $\tilde{C}^1\Pi_u$ State," LBL-16648.
13. V.Z. Kresin and W.A. Lester, Jr., "Reaction Hamiltonian and the Adiabatic Approach to the Dynamics of Chemical Reaction," submitted to Chem. Phys., LBL-16739.

Other Publications

14. W.A. Lester, Jr. and Michel Dupuis, "Theoretical Study of Oxidation Reactions: Mechanism of the $\text{O}(^3\text{P}) + \text{H}_2\text{CO}$ Reaction," DOE/BES Combustion Research Contractor's Meeting, Upton, New York, May 24-26, 1983, LBL-15953.
15. P.J. Reynolds, M. Dupuis, and W.A. Lester, Jr., "Quantum Monte Carlo Calculation of the Singlet-triplet Energy Splitting in Methylene," 1983 Sanibel Symposia, Palm Coast, Florida, March 7-12, 1983, LBL-16751.
16. W.A. Lester, Jr. and V.Z. Kresin, "A New Theoretical Method for Polyatomic Photodissociation," Bull. Am. Phys. Soc. **2**, 556 (1983), LBL-16858A.
17. V.Z. Kresin and W.A. Lester, Jr., "The Adiabatic Method for Many-body Systems," chapter accepted for *Mathematical Analysis of Physical Systems*, R. Mickens, Ed., Van Nostrand Reinhold, New York; LBL-16712.

Invited Talks

18. M. Dupuis, "MCHF Calculations on Midi- and Super-computers," Sanibel Symposium on

Computers in Chemistry, Palm Coast, Florida, March 1983.

19. W.A. Lester, Jr., "Quantum Monte Carlo for Molecules," Tenth Annual Meeting of the National Organization for the Professional Advancement of Black Chemists and Chemical Engineers, Nashville, Tennessee, May 25-28, 1983, LBL-16753.
20. M. Dupuis, "Applications of the MCHF Method: Determination of the Electronic Structure of Excited States and Reaction Pathways," University of California Berkeley, April 1983; National Bureau of Standards, Washington, D.C., June 1983.
21. P.J. Reynolds, "Quantum Monte Carlo," Center for Polymer Studies Seminar, Boston University, Boston, Massachusetts, June 10, 1983.
22. W.A. Lester, Jr., "Computers and Their Role in Energy Research: Current Status and Future Needs," testimony before the Subcommittee on Energy Development and Applications and the Subcommittee on Energy Research and Production of the Committee on Science and Technology, U. S. House of Representatives, Ninety-eighth Congress, First Session, Washington, D. C., June 15, 1983.
23. W.A. Lester, Jr., "Achieving Chemical Accuracy by Quantum Monte Carlo," Office of Naval Research Program Workshop on Energetic Material Decomposition Fundamentals, Chestertown, Maryland, August 15-17, 1983, LBL-16752.
24. P.J. Reynolds, "Chemical Application of Diffusion Quantum Monte Carlo," Joint NASA/Goddard-CDC Symposium on Cyber 205 Applications, Lanham, Maryland, October 11-12, 1983, LBL-16754.
25. W.A. Lester, Jr., "Potential Energy Surfaces and Collision Dynamics," Institute of Chemistry, Academia Sinica, Beijing, China, November 8, 1983.[†]
26. W.A. Lester, Jr., "Quantum Monte Carlo for Molecules," Institute for Molecular Science, Okazaki, Japan, November 16, 1983.

[†]Supported by private U. S. sources and the China Association of Science and Technology.

Spectroscopy and Structures of Reactive Intermediates*

Richard J. Saykally, Investigator

INTRODUCTION

The objective of this research is to advance our knowledge of the reaction intermediates which are the essence of combustion processes. Structures and important molecular properties (e.g., dipole moments, collision cross sections, electron distributions) of reaction intermediates are studied with several complimentary new high-resolution laser-spectroscopy techniques. Photolytically generated paramagnetic-reaction intermediates are studied by far-infrared laser-magnetic-resonance (LMR) rotational spectroscopy. Polar species, generated and cooled to ultralow temperatures in a supersonic beam, are investigated by a completely new technique called molecular-beam laser-electric resonance. A more general new technique for studying rotational spectra of reactive intermediates is under development. In this technique a tunable far-infrared laser is the light source, and laser photolysis is used to generate reactive molecules. The theoretical formalism required to analyze spectra obtained by these approaches is being developed concurrently.

1. LMR Rotational Spectroscopy of $^2\Sigma$ Radicals: Ethynyl (CCH) (Publication 3)

Richard J. Saykally, Leif Veseth, and Kenneth M. Evenson

Many reactive intermediates in combustion processes possess electronic ground states in which electronic spin is very weakly coupled to the rotational angular momentum. These species exhibit complex magnetic-resonance spectra and have not been accessible to the otherwise very powerful LMR technique.

In this work a new approach to predicting, assigning, and analyzing LMR rotational spectra of molecules with such weakly coupled electronic states is developed and applied to CCH, an important reactive intermediate in hydrocarbon combustion.

The first terrestrial measurement of the free ethynyl radical CCH made by far-infrared LMR is described. The $N = 6 \rightarrow 7$ rotational transition was observed for the lowest vibrational level of the $^2\Sigma^+$ ground state. Because of the very weak spin coupling in this state, the LMR spectrum is complex and badly overlapped (see Figure 1-1). A theoretical formalism for the prediction and analysis of such weakly coupled $^2\Sigma$ states is presented in which frequencies, linewidths, and intensities of all transitions are computed as a function of magnetic-flux density, and the total absorption coefficient is computed at each field point in order to simulate the magnetic-resonance spectrum (see Figure 1-2). This formalism is used to analyze the LMR spectra of CCH. A combined least-squares analysis of existing microwave, astronomical, and LMR data was carried out to determine an improved set of molecular parameters for this important interstellar molecule.

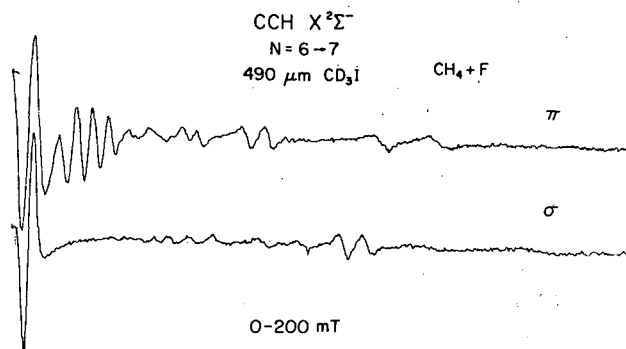


Figure 1-1. The LMR spectrum observed for the $N = 6 \rightarrow 7$ transition of CCH with the $490\text{-}\mu\text{m}$ laser line of CD_3I . Only the strong lines at low fields (4 for π , 1 for σ) are due to this transition; the others are unassigned. (1 mT = 10 Gauss).

(XBL 841-294)

*This work was supported by the Director, Office of Energy Research, Office of Basic Energy Sciences, Chemical Sciences Division of the U.S. Department of Energy under Contract No. DE-AC03-76SF00098.

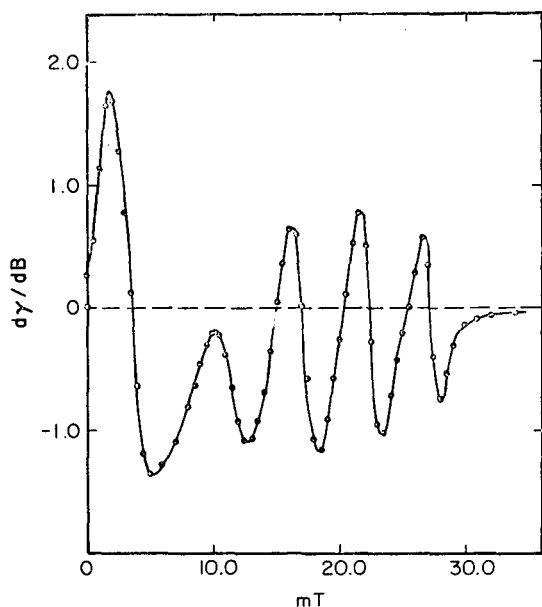


Figure 1-2. Synthetic LMR- π spectrum of CCH: computed values of the derivative of the absorption coefficient (arbitrary units) with respect to the external field for $\Delta M_F = 0$ transitions (half width $\Delta\nu = 2.0$ MHz). Compare with the top trace in Figure 1-1. (XBL 841-295)

2. A Search for the $^2\Pi$, $N = 1$, $J = 3/2$ Lambda-doubling Transition of CH (Publication 1)[†]

L.M. Ziurys, C. Henkel, and R.J. Saykally

We report negative results for an astronomical search for the $^2\Pi$, $N = 1$, $J = 3/2$ Λ -doubling transition of the CH molecule. Upper limits to the column densities calculated from these observations are in agreement with those previously derived from the 3-GHz ground-state transitions, provided that the excitation temperature within the $^2\Pi$, $N = 1$, $J = 3/2$ Λ -doublet is $\lesssim 10$ – 100 K, depending on the source. Toward Cas A, Ori A, and Sgr B2, upper limits to the optical depth for the transition are an order of magnitude lower than those obtained from the ground-state measurements (Ori A: $\tau \lesssim 1.2 \times 10^{-3}$, Sgr B2: $\tau \lesssim 4.8 \times 10^{-4}$, Cas A: $\tau \lesssim 3.9 \times 10^{-4}$). Calculations show that neither collisions nor far-infrared radiation are particularly effective in populating the $^2\Pi$, $N = 1$, $J = 3/2$ levels.

[†]Supported by the California Space Association (CalSpace) (Grant No. 1-539578-19900-3) and the National Science Foundation (Grant No. CHE80 070420).

3. SiN in Space? A Search for Interstellar Silicon Nitride (Publication 4)[†]

L.M. Ziurys, D.P. Clemens, R.J. Saykally, M. Colvin, and H.F. Schaefer

We have searched for the $N = 2-1$ rotational transition of silicon nitride, SiN, at 87 GHz using the 14-m antenna of the Five-College Radio Astronomy Observatory and one of the 6-m antennas of the Radio Astronomy Laboratory at Hat Creek (University of California Berkeley). Upper limits to the SiN column densities are $N_{\text{SiN}} \leq 10^{12-15} \text{ cm}^{-2}$. The ratio of the abundances of SiN to CN toward the four sources observed here gives SiN/CN ≤ 0.002 – 0.05 , significantly less than the silicon-to-carbon ratio of 0.1. These ratios suggest that either silicon is depleted onto grains where CN is present, or that ion-molecule chemistry does not favor the production of SiN. Upper limits to the SiN/SiO ratios are significantly less than the nitrogen-to-oxygen ratio for Orion-KL and IRC+10216, indicating that the chemistry responsible for producing SiO does not correspondingly produce SiN. We also report detection of interstellar ^{30}SiS toward IRC+10216 and obtain terrestrial abundance ratios for the silicon isotopes of this molecule.

[†]Supported by NSF Grant No. CHE8207307 and CalSpace Grant No. 1-539578-19900-3. Schaefer and Colvin were supported by NSF Grant No. CHE8218785.

4. Velocity-modulation Electronic-absorption Spectroscopy of Molecular Ions (Publication 2)

C.S. Gudeman, C.C. Martner, and R.J. Saykally

A new technique for measurement of electronic spectra of molecular ions generated in low-density reactive plasmas is described. This method permits such spectra of ions to be obtained with minimal interference from the vastly more abundant neutral species also present in these media. The technique is demonstrated for the cases of Ar^+ , N_2^+ ($A^2\Pi - X^2\Sigma$), and CO^+ ($A^2\Pi - X^2\Sigma$) generated in helium plasmas containing small amounts of the respective precursor gases. For N_2^+ , this constitutes the first measurement of the (1,5), (2,6), and (3,7) bands in this system, which are usually obscured by strong overlapping spectra from neutral N_2 . The potential application of this method for measurement of quantum-state selected plasma properties (drift, diffusion, charge transfer, etc.) is discussed.

5. Measurement of the Rotational Spectrum of HF⁺ by LMR (Publication 5)

D.C. Hovde, E. Schäfer, S.E. Strahan, C.A. Ferrari, D. Ray, K.G. Lubic, and R.J. Saykally

Rotational transitions in the X²Π state of the HF⁺ molecular ion were measured by LMR spectroscopy. Hyperfine splittings from both the fluorine and hydrogen nuclei were resolved. An analysis of the J = 3/2 → 5/2 transitions yielded the following molecular parameters (MHz): B₀ = 513,070.2(99), D₀ = 66.23(27), A₀ = -8,736,727(400), A_D = -847(14), P₀ = 7741(19), q₀ = -1214.9(2), h = 3353(12), b = 1384(130). Figure 5-1 shows the LMR spectrum of HF⁺.

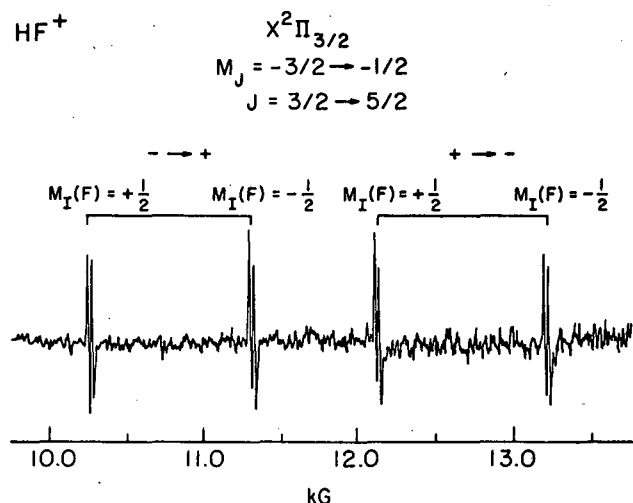


Figure 5-1. The LMR Spectrum of HF⁺, measured in a plasma containing 1 torr of helium with a trace of HF.

(XBL 841-296)

6. Work in Progress

The molecular-beam laser-electric-resonance technique has been used to measure rotational spectra of two stable molecules, CH₃F and PH₃. Sub-Doppler resolution is effected due to the intracavity measurement of the absorption, resulting in inverse Lamb-dip spectra. Currently the data are being examined to ascertain the nature and extent of the cooling achieved in the supersonic expansion. Extension of the technique to the measurement of rotational spectra of ultracold reaction intermediates is planned.

1983 PUBLICATIONS AND REPORTS

Refereed Journals

1. L.M. Ziurys, C. Henkel, and R.J. Saykally, "A Search for ²Π, N = 1, J = 3/2 Lambda Doubling Transitions of CH," *Astrophys. J.*, December 1, 1983.[†]

LBL Reports

2. C.S. Gudeman, C.C. Martner, and R.J. Saykally, "Velocity Modulation Electronic Absorption Spectroscopy of Molecular Ions," LBL-16854.

Other Publications

3. R.J. Saykally, L. Veseth, and K.M. Evenson, "Laser Magnetic Resonance Rotational Spectroscopy of ²Σ Radicals: Ethynyl (CCH)," accepted by *J. Chem. Phys.*
4. L.M. Ziurys, D.P. Clemens, R.J. Saykally, M. Colvin, and H.F. Schaefer, "SiN in Space? A Search for Interstellar Silicon Nitride," *Astrophys. J.*, in press.[†]
5. D.C. Hovde, E. Schäfer, S.E. Strahan, C.A. Ferrari, D. Ray, K.G. Lubic, and R.J. Saykally, "Measurement of the Rotational Spectrum of HF⁺ by Laser Magnetic Resonance."

Invited Talks

6. R. J. Saykally, "Laser Spectroscopy of Molecular Ions," Department of Chemistry and Joint Institute for Laboratory Astrophysics, University of Colorado, Boulder, Colorado, February 4, 1983; Department of Chemistry, California Institute of Technology, Pasadena, California, February 22, 1983; University of California, Davis, California, May 12, 1983; Department of Chemistry, University of Utah, Salt Lake City, Utah, November 1, 1983; Department of Chemistry, University of California, Irvine, California, November 15, 1983.
7. R.J. Saykally, "Laser Spectroscopy of Discharge and Flame Plasmas," Department of Electrical Engineering, University of California Berkeley, February 9, 1983.
8. R.J. Saykally, "Laser Magnetic Resonance of Molecular Ions," Symposium on Organic Free Radicals, ACS National Meeting, Seattle, Washington, March 22-25, 1983.
9. R.J. Saykally, "Rotational Spectroscopy of Molecular Ions," Department of Chemistry,

- University of Pittsburgh, Pittsburgh, Pennsylvania, April 5, 1983.
10. R.J. Saykally, "Optogalvanic Spectroscopy of Atoms and Molecules in Hollow Cathode Plasmas with Tunable Infrared and Visible Lasers," Symposium on New Laser Techniques in Chemistry, ACS Mid-Atlantic Regional Meeting, Hershey Pocono Resort, White Haven, Pennsylvania, April 6-8, 1983.
 11. R.J. Saykally, "Velocity Modulation Laser Absorption Spectroscopy of Molecular Ions," SPIE 27th Annual Symposium, San Diego, California, August 23, 1983.
 12. R.J. Saykally, "Velocity Modulation Laser Absorption Spectroscopy of Molecular Ions," Symposium on Spectra of Molecular Ions, Optical Society of America National Meeting, New Orleans, October 18, 1983.

†Supported by Calspace and the National Science Foundation.

Theory of Atomic and Molecular Collision Processes*

William H. Miller, Investigator

INTRODUCTION

This research is primarily involved with the development of theoretical methods and models for describing atomic and molecular collision processes. Specific topics of interest include the theory of inelastic and reactive scattering, collision processes involving electronically excited atoms or molecules, collisional ionization phenomena, statistical theories of chemical reactions, scattering of atoms and molecules from surfaces, and the interactions of molecular systems with high-power laser radiation.

Much of this research is involved with the development and application of a general semiclassical mechanics that allows one to combine classical mechanics and quantum mechanics in a correct and useful manner. This has been extremely successful in providing an understanding of the various quantum effects that are seen in molecular phenomena, and it also often provides simpler computational methods for carrying out quantitative calculations. Certain research topics are more amenable to a completely quantum mechanical approach, and these sorts of theoretical techniques are also used.

The ability to understand — and thus to model and to predict — chemical kinetic phenomena in the gas phase has widespread practical importance in a number of different areas. Among these are atmospheric chemistry and physics, the interactions of molecules with strong laser fields, and energy transfer and chemical reactions in flames and combustion.

*This work was supported by the Director, Office of Energy Research, Office of Basic Energy Sciences, Chemical Sciences Division of the U.S. Department of Energy under Contract No. DE-AC03-76SF00098.

1. Application of the Semiclassical Perturbation (SCP) Approximation to Diffraction and Rotationally Inelastic Scattering of Atoms and Molecules from Surfaces (Publication 4)[†]

Lynn M. Hubbard[‡] and William H. Miller

The SCP approximation of Miller and Smith¹ is applied to the scattering of atoms and molecules from crystal surfaces. Specifically, diffraction of He from LiF and diffraction and rotationally inelastic scattering of H₂ from LiF are treated, and the SCP model is seen to agree well with earlier coupled-channel and quantum sudden calculations. These tests of the SCP model are all for “soft” interaction potentials, e.g., of the Lennard-Jones Devonshire variety, but it is also shown that the model behaves correctly in the limit of an impulsive hard-wall potential function. The SCP picture thus appears to have a wide range of validity for describing the dynamics of gas-surface collisions.

[†]The calculations were carried out on a Harris H800 minicomputer supported by the National Science Foundation under Grant CHE-79-20181.

[‡]Present address: Department of Chemistry, Princeton University, Princeton, New Jersey 08540.

1. Miller and Smith, *Phys. Rev. A* **17**, 17 (1978).

2. Structure and Tunneling Dynamics of Malonaldehyde, a Theoretical Study (Publication 5)[†]

Jozef Bicerano,[‡] Henry F. Schaefer III, and William H. Miller

The geometry and harmonic vibrational frequencies of equilibrium malonaldehyde and of the transition state for the symmetric intramolecular hydrogen atom transfer have been determined at the SCF level of theory (using a slightly better than double-zeta basis set). All geometrical parameters were fully and simultaneously optimized using SCF gradient techniques. Comparison of the equilibrium structure with the structure determined from microwave spectra shows good agreement in most respects, although there are a few differences. At the C_s equilibrium geometry and the C_{2v} transition state, large-scale configuration-interaction (all single and double excitations) calculations were carried out to determine the barrier height for the symmetric hydrogen atom transfer; including a correction for quadruple excita-

tions, this gives a classical, or "bare," barrier height of 8.0 kcal/mole. A one-dimensional model for the tunneling dynamics of H-atom transfer leads to a tunneling splitting in the ground vibrational state $\sim 18 \text{ cm}^{-1}$, in relatively good agreement with the experimental value. It is noted, though, that the value of the splitting is sensitive to the potential surface parameters (i.e., bare height, frequencies) and that there is also uncertainty about the accuracy of the one-dimensional description of the tunneling.

[†]Jozef Bicerano has been supported by the National Science Foundation under Grant CHE-79-20181.

[‡]Present address: ECD, Inc., 1675 West Maple Rd., Troy, Michigan.

3. Symmetry-adapted Transition-state Theory and a Unified Treatment of Multiple Transition States (Publication 6)

William H. Miller

It is shown how a recently discussed symmetry-adapted transition-state theory leads to a unified treatment of reactions that involve multiple transition states that are symmetry-related. If the two (or more) transition states are well separated, the present description reduces to the standard prescription based on symmetry numbers, but it also applies more generally to the case that the transition states are close enough to interact dynamically, and even to the limit that they merge into a single transition state.

4. Multichannel Distorted Wave Born Approximation for Reactive Scattering (Publication 7)[†]

Lynn M. Hubbard,[‡] Sheng-hua Shi, and William H. Miller

Previous applications of the distorted wave Born approximation (DWBA) to reactive scattering have often given reasonably good *relative* cross sections (i.e., angular distributions, product state distributions, etc.), but *absolute* reactive cross sections have been poor. It is argued in this paper, however, that the DWBA for reactive scattering should be accurate

if (1) the reaction probability is sufficiently small (as it is, for example, in the threshold region of a reaction), and (2) the nonreactive scattering is described "sufficiently accurately." This paper utilizes a nonreactive coupled-channel scattering wave function for distorted waves in the DWBA. Application to a standard test problem (collinear H + H₂) shows this multichannel DWBA indeed to be extremely accurate if the reaction probability is no larger than 0.1 and if about 3 to 4 vibrational states are included in the nonreactive coupled-channel expansion. This approach thus provides an excellent description of the threshold region of a reaction which has an activation barrier.

[†]The calculations were carried out on a Harris H800 minicomputer supported by the National Science Foundation under Grant CHE-79-20181. Lynn M. Hubbard has also been supported by this NSF grant.

[‡]Present address: Department of Chemistry, Princeton University, Princeton, New Jersey 08540.

5. Effect of Electronic-transition Dynamics on Iodine-atom Recombination in Liquids (Publication 8)[†]

Domenic P. Ali[‡] and William H. Miller

The Langevin stochastic-trajectory model used by Hynes, Kapral, and Torre¹ to describe the secondary recombination of iodine atoms in solution has been generalized to allow for electronically inelastic transitions between the ten I-I potential curves that dissociate to ground state iodine atoms. The electronic transitions are treated via the Miller-George version of the Tully-Preston surface-hopping model. The main qualitative result is that electronically inelastic processes substantially slow down the rate (and ultimate probability) of recombination. It is also seen that the electronic inelasticity goes from strong at large *r*, where an essentially Boltzmann distribution is maintained over the various electronic states, to weak at small *r*, where the distribution is far from Boltzmann.

[†]The calculations were carried out on a Harris H800 minicomputer supported by the National Science Foundation under Grant CHE-79-20181.

[‡]Present address: Department of Chemistry, University of Colorado, Boulder, Colorado 80309.

1. Hynes, Kapral, and Torre, *J. Chem. Phys.* **72**, 177 (1980).

6. System-bath Decomposition of the Reaction-path Hamiltonian. II. Rotationally Inelastic Reactive Scattering of $H + H_2$ in Three Dimensions (Publication 9)[†]

Steven D. Schwartz and William H. Miller

Earlier work by the authors¹ has shown how the reaction-path Hamiltonian of Miller, Handy, and Adams² can be divided into a "system" of the reaction coordinate and modes strongly coupled to it, plus a "bath" of more weakly coupled modes. Quantum mechanical perturbation theory was used to show how one can combine an exact description of the "system" dynamics with an approximate (perturbative) treatment of the effect of the "bath." The present paper applies this approach to the 3-d $H + H_2$ reaction, where the two collinear degrees of freedom constitute the "system," and the two bending modes the "bath." Comparison with the accurate scattering calculations of Schatz and Kupperman³ shows the approach to provide a good description of the coupling between bending (i.e., rotational) and collinear modes.

[†]The calculations were carried out on a Harris H800 minicomputer supported by the National Science Foundation under Grant CHE-79-20181.

1. Schwartz and Miller, *J. Chem. Phys.* **77**, 2378 (1982).
2. Miller, Handy, and Adams, *J. Chem. Phys.* **72**, 99 (1980).
3. Schatz and Kupperman, *J. Chem. Phys.* **65**, 4668 (1976).

7. Symmetry-adapted Transition-state Theory: Non-zero Total Angular Momentum (Publication 10)[†]

William H. Miller

It is shown how nonzero total angular momentum is incorporated in a recently proposed symmetry-adapted transition-state theory. The analysis is carried through explicitly for the unimolecular dissociation of formaldehyde, $H_2CO \rightarrow H_2 + CO$, for which the transition state is planar, i.e., C_s symmetry. The main qualitative result for this example is that mode specificity between the A' and

A'' states — i.e., the difference of the rate-constant ratio $k_{A'}/k_{A''}$ from unity — diminishes with increasing J but does not completely disappear even in the limit $J \rightarrow \infty$.

[†]The calculations were carried out on a Harris H800 minicomputer supported by the National Science Foundation under Grant CHE-79-20181.

8. Quantum Mechanical Rate Constants for Bimolecular Reactions (Publication 12)[†]

William H. Miller, Steven D. Schwartz, and John W. Tromp

Several formally exact expressions for quantum mechanical rate constants (i.e., bimolecular reactive cross sections suitably averaged and summed over initial and final states) are derived and their relation to one another analyzed. It is suggested that they may provide a useful means for calculating quantum mechanical rate constants accurately without having to solve the complete state-to-state quantum mechanical reactive-scattering problem. Several ways are discussed for evaluating the quantum mechanical traces involved in these expressions, including a path-integral evaluation of the Boltzmann operator/time propagator and a discrete-basis set approximation. Both these methods are applied to a one-dimensional test problem (the Eckart barrier).

[†]The calculations were carried out on a Harris H800 minicomputer supported by the National Science Foundation under Grant CHE-79-20181.

9. Work in Progress

Further developments and applications in the area of polyatomic reaction dynamics are in progress, including generalizations of the original "reaction-path" model on which all applications to date have been based. Several new ideas for carrying out quantum mechanical reactive-scattering calculations are also under development.

1983 PUBLICATIONS AND REPORTS

Refereed Journals

1. S.K. Gray and W.H. Miller, "Classical Model for Electronic Degrees of Freedom: Charge Transfer in Na + I Collisions," *Chem. Phys. Lett.* **93**, 341 (1982); LBL-14808.
2. W.H. Miller, "Dynamical Effects of Symmetry along a Reaction Path; Mode Specificity in the Unimolecular Dissociation of Formaldehyde," *J. Am. Chem. Soc.* **105**, 216 (1983); LBL-14300.
3. B.A. Waite, S.K. Gray, and W.H. Miller, "Mode Specificity in the Unimolecular Dissociation of Formaldehyde ($\text{H}_2\text{CO} \rightarrow \text{H}_2 + \text{CO}$), a Two-mode model," *J. Chem. Phys.* **78**, 259 (1983); LBL-14855.
4. L.M. Hubbard and W.H. Miller, "Application of the Semiclassical Perturbation (SCP) Approximation to Diffraction and Rotationally Inelastic Scattering of Atoms and Molecules from Surfaces," *J. Chem. Phys.* **78**, 1801 (1983); LBL-15068.[†]
5. J. Bicerano, H.F. Schaefer, and W.H. Miller, "Structure and Tunneling Dynamics of Malonaldehyde, a Theoretical Study," *J. Am. Chem. Soc.* **105**, 2550 (1983); LBL-15155.[†]
6. W.H. Miller, "Symmetry-adapted Transition State Theory and a Unified Treatment of Multiple Transition States," *J. Phys. Chem.* **87**, 21 (1983); LBL-15069.
7. L.M. Hubbard, S. Shi, and W.H. Miller, "Multichannel Distorted Wave Born Approximation for Reactive Scattering," *J. Chem. Phys.* **78**, 2381 (1983); LBL-15226.[†]
8. D.P. Ali and W.H. Miller, "Effect of Electronic Transition Dynamics on Iodine Atom Recombination in Liquids," *J. Chem. Phys.* **78**, 6640 (1983); LBL-15329.[†]
9. S. Schwartz and W.H. Miller, System-bath Decomposition of the Reaction Path Hamiltonian. II. Rotationally Inelastic Reactive Scattering of H + H₂ in Three Dimensions," *J. Chem. Phys.* **79**, 3759 (1983); LBL-15464.[†]
10. W.H. Miller, "Symmetry Adapted Transition State Theory: Non-zero Total Angular Momentum," *J. Phys. Chem.* **87**, 2731 (1983); LBL-15443.[†]
11. W.H. Miller, "Reaction Path Dynamics for Polyatomic Systems," *J. Phys. Chem.* **87**, 3811 (1983); LBL-16093.
12. W.H. Miller, S.D. Schwartz, and J.W. Tromp, "Quantum Mechanical Rate Constants for Biomolecular Reactions," *J. Chem. Phys.* **79**, 4899 (1983); LBL-16339.[†]
13. S.K. Gray, "Classical Aspects of the Laser Excitation of a Morse Oscillator," *Chem. Phys.* **75**, 67 (1983); LBL-14717.
14. Shenghua Shi, "A New Semiclassical Approach to the Molecular Dynamics: Label Variable Classical Mechanics," *J. Chem. Phys.* **79**, 1314 (1983); LBL-15763.

LBL Reports

15. S.K. Gray and P.S. Dardi, "Classical and Quantum Mechanical Studies of Overtone and Multiphoton Absorption of HF in an Intense Laser Field," submitted to *J. Chem. Phys.*, LBL-16719.
16. S.D. Schwartz, "Adiabatic Frequency Variation Along a Reaction Path," submitted to *Chem. Phys. Lett.*, LBL-16720.
17. D.P. Ali and W.H. Miller, "Classical Models for Electronic Degrees of Freedom: Quenching of $\text{Br}^*(^2\text{P}_{1/2})$ by Collision with H₂ in Three Dimensions," submitted to *Chem. Phys. Lett.*, LBL-16721.
18. S. Shi, "T-V and V-V Energy Transfer in Collinear Collision of Two Diatomic Molecules — an Application of Label Variable Classical Mechanics," submitted to *J. Chem. Phys.*, LBL-17094.
19. L.M. Hubbard and W.H. Miller, "Application of the Semiclassical Perturbation Approximation to Scattering from Surfaces: Generalization to Include Phonon Inelasticity," submitted to *J. Chem. Phys.*, LBL-17095.
20. G.C. Schatz, L.M. Hubbard, P.S. Dardi, and W.H. Miller, "Coupled Channel Distorted Wave Calculations for the Three Dimensional H + H₂ Reaction," submitted to *J. Chem. Phys.*, LBL-17190.

Invited Talks

21. W.H. Miller, "On the Question of Mode Specificity in Unimolecular Reaction Dynamics," International Conference on Photochemistry and Photobiology, University of Alexandria Research Center, Alexandria, Egypt, January 5–10, 1983, LBL-15463.
22. W.H. Miller, "Mode Specificity in Unimolecular Reaction Dynamics," Symposium on Molecular Scattering Theory and Quantum Chemistry in honor of Professor David Bates, Palm Coast, Florida, March 3–5, 1983.

[†]Supported in part by the National Science Foundation under Grant CHE-79-20181.

Photoelectron Spectroscopy*

David A. Shirley, Investigator

INTRODUCTION

This program addresses both experimental and theoretical aspects of electron spectroscopy for the investigation of electronic structure of matter in the gaseous and condensed phases. Research is conducted using both laboratory sources at LBL and synchrotron radiation in the energy range 5–5000 eV available at the Stanford Synchrotron Radiation Laboratory, where there is participation in developing the spectroscopy of this newly accessible range of the electromagnetic spectrum. Time-of-flight measurements with synchrotron radiation are used to measure angular distributions of photoelectrons and resonant photoemission phenomena in the gas phase. Ultrahigh-resolution photoelectron spectroscopy based on molecular beams is yielding new information about small molecules and about the transition from single metal atoms to behavior characteristic of a three-dimensional solid. Employing angle-resolved variable-energy photoemission and electron-energy-loss spectroscopy, this program examines the electronic structure of solids as well as geometric and electronic structure of surface-adsorbate systems with photoelectron diffraction, angle-resolved photoemission extended fine structure (ARPEFS), and surface extended x-ray absorption fine structure (EXAFS).

1. Photoelectron Asymmetries and Two-electron Satellites Near the $3p \rightarrow 3d$ Giant-resonance Region in Atomic Mn (Publication 12)

P.H. Kobrin,[†] U. Becker,[‡] C.M. Truesdale,[§] D.W. Lindle, H.G. Kerkhoff,[‡] and D.A. Shirley

The $3p$ absorption spectrum of MnI is dominated by a strong, broad asymmetric resonance at

*This work was supported by the Director, Office of Energy Research, Office of Basic Energy Sciences, Chemical Sciences Division of the U.S. Department of Energy under Contract No. DE-AC03-76SF00098. It was performed at the Stanford Synchrotron Radiation Laboratory, which is supported by the Department of Energy, Office of Basic Energy Sciences and the National Science Foundation, Division of Materials Research.

~50 eV. Discrete features below and above the largest resonance are also seen as well as a broad modulation in the continuum absorption immediately above the $3p$ threshold. The "giant resonance" is attributed to transitions from the ground state $3p^6 3d^5 4s^2 6S$ to the dipole-allowed states $3p^5(3d^6 5D)4s^2 6P_{3/2,5/2,7/2}$. The shape and width of the resonance are explained by the mixing of the $6P$ resonance with the $3p^6 3d^4 4s^2 f 6P$ continuum.

In this paper we report the photon-energy dependence of partial cross sections and angular distributions for the main lines and several satellite peaks in the photoelectron spectrum of Mn. An analysis is made of the intensities of the satellite lines based on Hartree-Fock configuration-interaction (HF-CI) calculations. Of particular interest is the enhancement of the satellite intensities relative to the main $3d$ line at ~55 eV near the $3p$ threshold.

[†]Department of Chemistry, Pennsylvania State University, University Park, Pennsylvania 16802.

[‡]Fachbereich Physik, Technische Universität Berlin, 1000 Berlin 12, West Germany.

[§]Research and Development Division, Corning Glass Works, Corning, New York 14831.

2. Resonance Photoelectron Spectroscopy of $5p$ Hole States in Atomic Barium (Publication 11)

*P.H. Kobrin,[†] R.A. Rosenberg,[‡] U. Becker,[§] S. Southworth,^{||} C.M. Truesdale,^{**} D.W. Lindle, G. Thornton,^{††} M.G. White,^{‡‡} E.D. Poliakoff,^{§§} and D.A. Shirley*

We have recorded photoelectron spectra of atomic barium at several photon energies in the range $20 \text{ eV} \leq h\nu \leq 29 \text{ eV}$. The variations of the $\text{Ba}^+ 5p^6 nl$ ($nl = 6s, 5d, 6p, 7s, \text{ and } 6d$) photoelectron peak intensities were measured in the 20–21 eV autoionization region. The results indicated that each autoionizing state decays to the various states of the ion in a characteristic way. Above 21 eV, $5p$ ionization begins to dominate, and the Auger spectra were used to monitor the production of the various $5p$ hole states. As the photon energy was scanned over the autoionizing resonances, these Auger spectra indicated a propensity to produce very low-energy photoelectrons ($\leq 2 \text{ eV}$) and the corresponding high-energy Auger electrons from two-step autoionization. Calculations suggest that a heretofore unobserved $5p^5 6p^2 2P_{3/2} 5d$ autoionizing level is responsible for the Auger distribution measured at $h\nu = 28.9 \text{ eV}$.

[†]Department of Chemistry, Pennsylvania State University, University Park, Pennsylvania 16802.

[‡]Physics Division, Naval Weapons Center, Michelson Laboratory, China Lake, California 93555.

[§]Fachbereich Physik, Technische Universität Berlin, 1000 Berlin 12, West Germany.

^{||}National Bureau of Standards, Washington, D.C. 20234.

^{**}Research and Development Division, Corning Glass Works, Corning, New York 14831.

^{††}Department of Chemistry, University of Manchester, Manchester, England.

^{‡‡}Department of Chemistry, Brookhaven National Laboratory, Upton, New York 11973.

^{§§}Department of Chemistry, Boston University, Boston, Massachusetts 02215.

3. Photoemission from the 3d Subshell of Atomic Kr (Publication 26)

*D.W. Lindle, P.H. Kobrin,[†] C.M. Truesdale,[‡]
P.A. Heimann, T.A. Ferrett, U. Becker,[§]
H.G. Kerkhoff,[§] and D.A. Shirley*

Angular-distribution asymmetry parameters are presented for Kr 3d photoemission using photon energies from 100 to 600 eV. The asymmetry parameter fell below the Hartree-Fock-theory prediction at high photon energies and showed resonant interchannel-coupling effects near the 3p threshold. The intensities of 4p → np satellites relative to the 3d main line were found to decrease with photon energy in the range 180 to 270 eV, and the average asymmetry parameter for these shakeup states showed a marked increase over the same energy range.

[†]Department of Chemistry, Pennsylvania State University, University Park, Pennsylvania 16802.

[‡]Research and Development Division, Corning Glass Works, Corning, New York 14831.

[§]Fachbereich Physik, Technische Universität Berlin, 1000 Berlin 12, West Germany.

4. Nitrogen K-shell Photoemission and Auger Emission from N₂ and NO (Publication 23)

*D.W. Lindle, C.M. Truesdale,[†] P.H. Kobrin,[‡]
T.A. Ferrett, P.A. Heimann, U. Becker,[§]
H.G. Kerkhoff,[§] and D.A. Shirley*

The first gas-phase photoelectron measurements near the N K edges of N₂ and NO are reported.

Shape-resonance behavior is exhibited in the cross sections for both N 1s photoemission and N KVV Auger emission. The angular-distribution asymmetry parameters for N 1s photoemission show larger contrast ratios than the cross-section data and agree with multiple-scattering calculations except for a small energy shift.

[†]Research and Development Division, Corning Glass Works, Corning, New York 14831.

[‡]Department of Chemistry, Pennsylvania State University, University Park, Pennsylvania 16802.

[§]Fachbereich Physik, Technische Universität Berlin, 1000 Berlin 12, West Germany.

5. Vibrationally Angle-resolved Photoelectron Studies of CO₂ and OCS (Publication 18)

*C.M. Truesdale,[†] S. Southworth,[‡] P.H. Kobrin,[§]
U. Becker,^{||} D.W. Lindle, and D.A. Shirley*

We have measured the vibrationally averaged and vibrationally resolved partial cross sections and asymmetry parameters for the CO₂ A²Π_u(1π_u⁻¹) and OCS C²Σ⁺(8σ⁻¹) ionic channels. As an example of our studies, the vibrationally resolved cross section and asymmetry parameter (β) for the (0,0,0) vibrational channel of the CO₂ A²Π_u ionic channel are shown in Figure 5-1. The present measurements correspond to the filled circles. For the β(ε) curve, the non-Franck-Condon MSM calculation of Swanson et al.¹ and measurements of Grimm et al.² are presented with our measurements. There is good agreement with the previous measurements and the MSM calculation except near threshold (17.31 eV). The feature in the cross section and asymmetry parameter near 20.5 eV is attributed to a π_g shape resonance.¹ These studies yield information about the dependence of nuclear geometry and the effects of resonances on cross sections and asymmetry parameters.

[†]Research and Development Division, Corning Glass Works, Corning, New York 14831.

[‡]National Bureau of Standards, Washington, D.C. 20234.

[§]Department of Chemistry, Pennsylvania State University, University Park, Pennsylvania 16802.

^{||}Fachbereich Physik, Technische Universität Berlin, 1000 Berlin 12, West Germany.

1. J.R. Swanson, D. Dill, and J.L. Dehmer, *J. Phys. B* **14**, L207 (1981).

2. F.A. Grimm, J.D. Allen, Jr., T.A. Carlson, M.O. Krause, D. Mehaffy, P.R. Keller, and J.W. Taylor, *J. Chem. Phys.* **75**, 92 (1981).

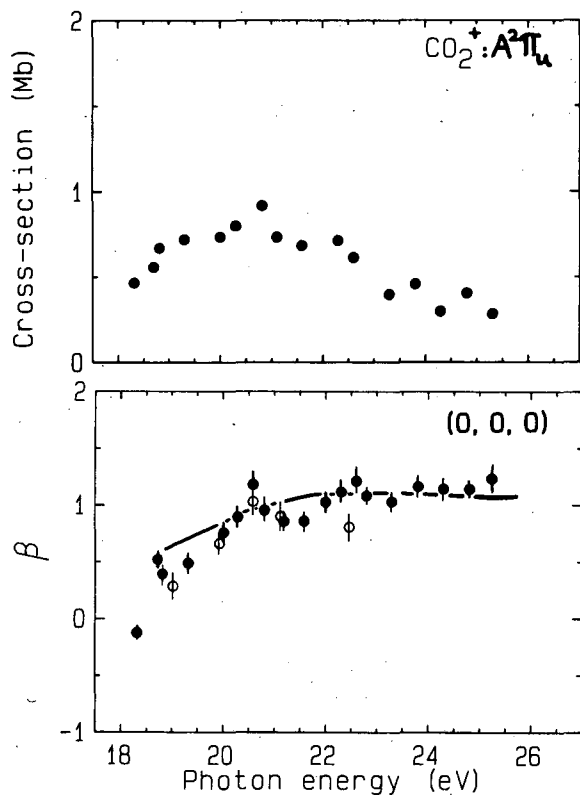


Figure 5-1. Photoionization cross section and asymmetry parameter $\beta(\epsilon)$ for the (0,0,0) vibrational channel for the $A^2\Pi_u$ ionic state of CO_2 . For $\beta(\epsilon)$, the solid curve is the MSM calculation of Swanson et al.¹ and the open circles are the measurements of Grimm et al.² (XBL 833-8545)

6. Core-level Photoelectron and Auger Shape-resonance Phenomena in CF_4 and OCS (Publication 15)

C.M. Truesdale,[†] S. Southworth,[‡] P.H. Kobrin,[§] U. Becker,^{||} D.W. Lindle, H.G. Kerkhoff,^{||} T.A. Ferrett, P.A. Heimann, and D.A. Shirley

We are continuing the investigation of carbon K-shell shape-resonance phenomena for small molecules from our earlier work on CO^1 and CO_2 . Resonances in cross sections and variations in the asymmetry parameter β are associated with the scattering of the outgoing electron by the molecular potential in a quasi-bound state. Our work can be used to test theoretical predictions which describe the effects of the shape resonances on the cross section and asymmetry parameter. The carbon K-shell of OCS has been studied using a multiple-scattering model by Grimm,² but the carbon 1s shell of CF_4 has not been investigated theoretically.

The asymmetry results for molecular core levels are the first of their kind. As an example, the carbon 1s asymmetry parameter of OCS is shown in Figure 6-1, along with the localized-hole MSM calculation of Grimm.² There is excellent agreement with Grimm's work. The two minima in the asymmetry parameter result from the effects of the σf and g-wave shape resonances, respectively.²

[†]Research and Development Division, Corning Glass Works, Corning, New York 14831.

[‡]National Bureau of Standards, Washington, D.C. 20234.

[§]Department of Chemistry, Pennsylvania State University, University Park, Pennsylvania 16802.

^{||}Fachbereich Physik, Technische Universität Berlin, 1000 Berlin 12, West Germany.

1. C.M. Truesdale, S. Southworth, P.H. Kobrin, U. Becker, H.G. Kerkhoff, and D.A. Shirley, Phys. Rev. Lett. **50**, 1265 (1983).

2. F.A. Grimm, Chem. Phys. **53**, 71 (1980).

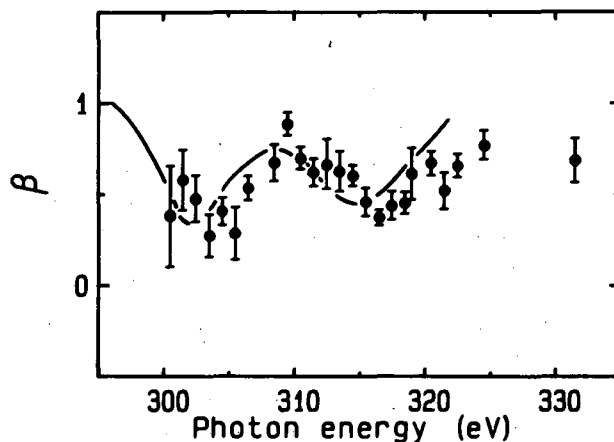


Figure 6-1. The asymmetry parameter for the C 1s peak in OCS. The present results are shown as filled circles. The solid curve represents the localized-hole MSM calculation of Grimm,² lowered by 0.3. (XBL 833-8920A)

7. Inner-shell Photoemission from the Iodine Atom in CH_3I (Publication 22)

D.W. Lindle, P.H. Kobrin,[†] C.M. Truesdale,[‡] T.A. Ferrett, P.A. Heimann, H.G. Kerkhoff,[§] U. Becker,[§] and D.A. Shirley

The first photoemission measurements on the I 4d and I 4p subshells in methyl iodide are presented. Cross sections and angular-distribution asymmetry parameters were measured from threshold to 300-eV photon energy for the I 4d level (to 440 eV for the asymmetry parameter) and from 175

to 300 eV for the I 4p level. The I 4d results exhibit atomic-like behavior throughout this energy range, mimicking the behavior of the Xe 4d subshell. Theoretical calculations for the Xe 4d subshell agree very well with the I 4d asymmetry-parameter results and indicate that the I 4d subshell is localized on the iodine atom in CH_3I . Near threshold, the spin-orbit final states $4d_{5/2}$ and $4d_{3/2}$ were resolved in these measurements, and they exhibited nonstatistical intensity ratios mainly due to a kinetic-energy effect. The I 4p asymmetry-parameter results are essentially identical to the asymmetry-parameter results for the I 4d subshell, suggesting strong interchannel coupling.

[†]Department of Chemistry, Pennsylvania State University, University Park, Pennsylvania 16802.

[‡]Research and Development Division, Corning Glass Works, Corning, New York 14831.

[§]Fachbereich Physik, Technische Universität Berlin, 1000 Berlin 12, West Germany.

8. Torsional Potential and Intramolecular Dynamics in the C_2H_4^+ Photoelectron Spectra (Publication 21)

J.E. Pollard,[†] D.J. Trevor,[‡] J.E. Reutt, Y.T. Lee, and D.A. Shirley

The 584-Å photoelectron spectrum of ethylene was reexamined at higher resolution using a supersonic molecular-beam source for rotational cooling. The vibrational frequencies of the $\text{C}_2\text{H}_4^+ \tilde{X}^2\text{B}_3$ state were measured with improved accuracy, which permitted the torsional potential-energy curve to be characterized. The measured equilibrium torsional angle is $27 \pm 2^\circ$, and the inversion barrier is $270 \pm 150 \text{ cm}^{-1}$. The $\tilde{A}^2\text{B}_3$ state is shown to be in reasonable agreement with a recent theoretical calculation which takes into account strong nonadiabatic effects. The correlation function calculated for this state is consistent with this calculation and recent calculations on the unimolecular dissociation of this state. The $\text{B}^2\tilde{A}$ state correlation function indicates that a rapid decay mechanism is operative. The broadened vibrational structure in the fourth band results from a saddle point in the $\tilde{\text{C}}^2\text{B}_2$ potential-energy surface from which the ion relaxes to the $\tilde{\text{X}}$ state by moving along a repulsive degree of freedom, which in this case is internal rotation. The $\tilde{\text{C}}$ state vibrational

broadening as well as the decay of the correlation function yield a lifetime for this process of 14 fsec.

[†]The Aerospace Corporation, Los Angeles, California 90009.

[‡]EXXON Research and Engineering Company, Linden, New Jersey 07036.

9. Auger Decay Mechanism in Photon-stimulated Desorption from Sodium Fluoride (Publication 8)[†]

*C.C. Parks,[‡] Z. Hussain,[§] D.A. Shirley, M.L. Knotek,^{||} G. Loubriel,^{||} and R.A. Rosenberg***

Results of photon-stimulated desorption (PSD) from NaF at the Na(K) edge are presented (see Figure 9-1). PSD of Na^+ and F^+ occurs from a NaF(100) cleaved surface upon Na(1s) excitation. In agreement with the Auger decay model¹ of desorption, both sodium and fluorine positive-ion yields (versus photon energy) are similar to total electron yield in the vicinity of the Na K-edge, except for a pre-edge peak observed predominantly in Na^+

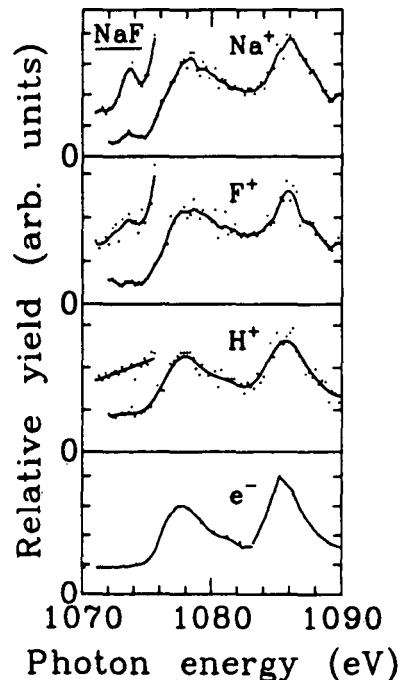


Figure 9-1. A comparison of total electron yield to Na^+ , F^+ , and H^+ desorption. The sums of several scans are shown in the prethreshold region of the ion-desorption spectra. Curves are drawn through the data as a visual aid. (XBL 836-10083)

desorption. Intra-atomic Auger decay of the Na(1s) core hole followed by charge transfer from adjacent halogens is shown to initiate desorption. The resulting neutral or positively charged halogens provide the driving force for desorption of sodium ions from the surface. Expressions are developed for the maximal energy available to the desorbing Na⁺ or F⁺ ions in terms of the Madelung energy and the Mott-Littleton polarization.

[†]Supported in part by Sandia National Laboratories, which is supported by the U.S. Department of Energy under Contract No. DE-AC04-76-DP00789.

[‡]IBM, General Technology Division, Poughkeepsie, New York 12602.

[§]Department of Physics, University of Petroleum and Minerals, Dhahran, Saudi Arabia.

^{||}Sandia National Laboratory, Albuquerque, New Mexico 87108.

^{**}Michelson Laboratory, Physics Division, Naval Weapons Center, China Lake, California 93555.

1. M.L. Knotek and P.J. Feibelman, Phys. Rev. Lett. **40**, 964 (1978).

10. Beam Exposure Dependence and Mechanisms of Photon-stimulated Desorption from Alkali Fluorides (Publication 19)[†]

C.C. Parks,[‡] D.A. Shirley, and G. Loubriel[§]

Photon-stimulated desorption experiments were performed on the (001) face of LiF for photon energies near the F(2s) and Li(1s) edges (from 37 to 72 eV). There are structures in the F⁺ yield above the F(2s) edge that are absent in the Li⁺ and H⁺ spectra, differences in detail in the Li⁺ and F⁺ yields near the Li(1s) edge, and considerable broadening of the desorption yields as compared to the bulk photoabsorption spectrum. These results helped clarify the role of the Auger decay mechanism in ion desorption from LiF. The first observation of a strong x-ray, and visible, beam exposure dependence of ion yields from LiF and NaF is also presented. For instance, in Figure 10-1 a cleaved NaF crystal was exposed to zero-order (intense polychromatic) light and to 1.96-eV (red) laser light; ion yields were monitored with 160-eV light. The zero-order and laser exposures dramatically changed the H⁺ or Na⁺ yields. These results are discussed in terms of electronic and defect properties of alkali halides.

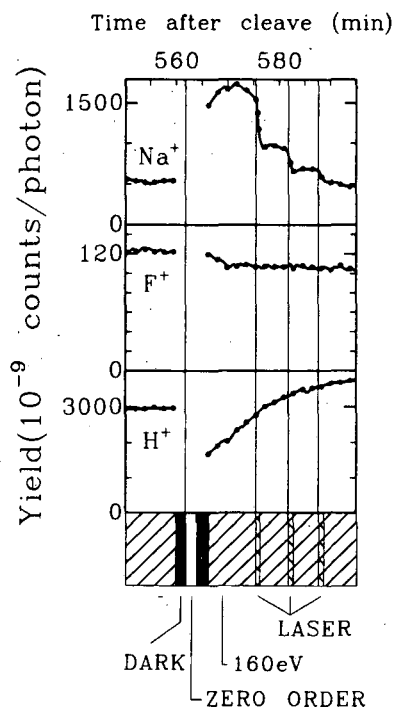


Figure 10-1. Na⁺, F⁺, and H⁺ yields at 160 eV versus time after cleavage. The following exposure sequence was performed: 160 eV, dark, zero order, dark, 160 eV. During the latter period, three laser exposures occurred. For clarity one out of each three data points is enlarged. (XBL 8310-896)

[†]Supported in part by Sandia National Laboratories, which is supported by the U.S. Department of Energy under Contract No. DE-AC04-76-DP00789.

[‡]IBM, General Technology Division, Poughkeepsie, New York 12602.

[§]Sandia National Laboratory, Albuquerque, New Mexico 87108.

11. Work in Progress

Recent development of the angle-resolved photoemission extended fine structure (ARPEFS) technique of photoelectron diffraction continues to provide exciting breakthroughs. The ARPEFS oscillations are observed by measuring the angle-resolved photoemission intensity as the photon energy — and hence the photoelectron kinetic energy — is scanned. These oscillations are caused by interference between direct and scattered photoelectron current. Different emission directions pick up scattering signals from different substrate atoms. Recent experiments at high electron kinetic energies (50–500 eV) show that

ARPEFS is dominated by single scattering that is well-predicted by our single-scattering theory. At high energies we can also use our angle-resolved spectrometer to measure in different emission directions, picking up scattering signals from different substrate atoms.

Recent progress includes:

- (i) We have discovered that the curvature of the photoelectron final state has a significant effect on the scattering amplitude and phase; all previous theoretical work has ignored this effect.
- (ii) The generalized Ramsauer-Townsend effect has also been demonstrated for electron scattering at certain energies and angles. This effect will allow us to precisely determine bond angles for adsorbate atoms and molecules on surfaces.
- (iii) We have completed the design and construction of a new electron spectrometer optimized for ARPEFS and 10–100 times more efficient than our present spectrometer. This new spectrometer should allow us to determine many more adsorption geometries than before and also to explore the nature of ARPEFS more fully.

Gas-phase photoionization experiments have been completed on the S 2p and S 1s shells of SF₆. Angular distributions and cross-section measurements for these levels have been made over a range of energies where shape-resonant and autoionization effects are important. In addition, the photon-energy dependence of the cross section for an S 2p satellite (excited ionic state) has been studied to determine the extent of many-electron interactions in SF₆ photoemission.

1983 PUBLICATIONS AND REPORTS

Refereed Journals

1. S.Y. Tong, W.M. Kang, D.H. Rosenblatt, J.G. Tobin, and D.A. Shirley, "Photoelectron-diffraction Analysis of the Structure of c(2 × 2)O on Ni(001)," *Phys. Rev. B* **27**, 4632 (1983); LBL-15152.
2. J.G. Nelson, W.J. Gignac, R.S. Williams, S.W. Robey, J.G. Tobin, and D.A. Shirley, "Angle-resolved Photoelectron Spectroscopy Investigation of Intrinsic Surface States on the Ge(001)-(2 × 1) Reconstructed Surface," *Phys. Rev. B* **27**, 3924 (1983); LBL-15250.[†]
3. C.M. Truesdale, S.H. Southworth, P.H. Kobrin, U. Becker, D.W. Lindle, H.G. Kerkhoff, and D.A. Shirley, "Shape Resonance Phenomena in CO Following K-shell Photoexcitation," *Phys. Rev. Lett.* **50**, 1265 (1983); LBL-12873.
4. P.H. Kobrin, P.A. Heimann, H.G. Kerkhoff, D.W. Lindle, C.M. Truesdale, T.A. Ferrett, U. Becker, and D.A. Shirley, "Photoelectron Measurements of the Mercury 4f, 5p, and 5d Subshells," *Phys. Rev. A* **27**, 3031 (1983); LBL-14759.
5. C.M. Truesdale, S. Southworth, P.H. Kobrin, D.W. Lindle, and D.A. Shirley, "Photoelectron Angular Distributions of the N₂O Outer Valence Orbitals in the 19–31 eV Photon Energy Range," *J. Chem. Phys.* **78**, 7117 (1983); LBL-15287.
6. S. Southworth, U. Becker, C.M. Truesdale, P.H. Kobrin, D.W. Lindle, S. Owaki, and D.A. Shirley, "Electron-spectroscopy Study of Inner-shell Photoexcitation and Ionization of Xe," *Phys. Rev. A* **28**, 261 (1983); LBL-13697.
7. J.J. Barton, C.C. Bahr, Z. Hussain, S.W. Robey, J.G. Tobin, L.E. Klebanoff, and D.A. Shirley, "Direct Surface Structure Determination with Photoelectron Diffraction," *Phys. Rev. Lett.* **51**, 272 (1983); LBL-14645.
8. C.C. Parks, Z. Hussain, D.A. Shirley, M.L. Knotek, G. Loubriel, and R.A. Rosenberg, "Auger Decay Mechanism in Photon-stimulated Desorption from Sodium Fluoride," *Phys. Rev. B* **28**, 4793 (1983); LBL-14240.[‡]
9. J.G. Tobin, S.W. Robey, L.E. Klebanoff, and D.A. Shirley, "Ag/Cu(001): Observation of the Development of the Electronic Structure in Metal Overlayers from Two to Three Dimensionality," *Phys. Rev. B* **28**, 6169 (1983); LBL-14187.
10. J.G. Nelson, W.J. Gignac, R.S. Williams, S.W. Robey, J.G. Tobin, and D.A. Shirley, "Mapping Bulk Ge Electronic Energy Bands along Delta Using ARPES Spectra of the (001) 2 × 1 Surface," *Surf. Sci.* **131**, 290 (1983); LBL-15691.[§]
11. P.H. Kobrin, R.A. Rosenberg, U. Becker, S. Southworth, C.M. Truesdale, D.W. Lindle, G. Thornton, M.G. White, E.D. Poliakoff, and D.A. Shirley, "Resonance Photoelectron Spectroscopy of 5p Hole States in Atomic Barium," *J. Phys. B* **16**, 4339 (1983); LBL-15442.

LBL Reports

12. P.H. Kobrin, U. Becker, C.M. Truesdale, D.W. Lindle, H.G. Kerkhoff, and D.A. Shirley, "Photoelectron Asymmetries and Two-electron Satellites Near the $3p \rightarrow 3d$ Giant-resonance Region in Atomic Mn," LBL-14545.
13. J.G. Tobin (Ph.D. Thesis), "Dimensionality and Its Effect Upon the Valence Electronic Structure of Ordered Metallic Systems," LBL-14704.
14. D.W. Lindle, T.A. Ferrett, U. Becker, P.H. Kobrin, C.M. Truesdale, H.G. Kerkhoff, and D.A. Shirley, "Photoionization of Helium Above the $He^+(n = 2)$ Threshold: Autoionization and Final-state Symmetry," submitted to Phys. Rev. A, LBL-15094.
15. C.M. Truesdale, D.W. Lindle, P.H. Kobrin, U.E. Becker, H.G. Kerkhoff, P.A. Heimann, T.A. Ferrett, and D.A. Shirley, "Core-level Photoelectron and Auger Shape-resonance Phenomena in CO, CO₂, CF₄, and OCS," accepted by J. Chem. Phys., LBL-15540.
16. P.H. Kobrin (Ph.D. Thesis), "Atomic Photoelectron Spectroscopy Studies Using Synchrotron Radiation," LBL-15591.
17. C.M. Truesdale (Ph.D. Thesis), "Molecular Photoemission Studies Using Synchrotron Radiation," LBL-15902.
18. C.M. Truesdale, S. Southworth, P.H. Kobrin, U. Becker, D.W. Lindle, and D.A. Shirley, "Vibrationally Angle-resolved Photoelectron Studies of CO₂ and OCS," LBL-15990.
19. C.C. Parks, D.A. Shirley, and G. Loubriel, "Beam Exposure Dependence and Mechanisms of Photon-stimulated Desorption from Alkali Fluorides," submitted to Phys. Rev. B., LBL-16065.[†]
20. J.J. Barton, C.C. Bahr, Z. Hussain, S.W. Robey, L.E. Klebanoff, and D.A. Shirley, "Direct Determination of Surface Structures From Photoelectron Diffraction," submitted to J. Vac. Sci. Technol., LBL-16314.
21. J.E. Pollard, D.J. Trevor, J.E. Reutt, Y.T. Lee, and D.A. Shirley, "Torsional Potential and Intramolecular Dynamics in the C₂H₄⁺ Photoelectron Spectra," LBL-16576.
22. D.W. Lindle, P.H. Kobrin, C.M. Truesdale, T.A. Ferrett, P.A. Heimann, H.G. Kerkhoff, U. Becker, and D.A. Shirley, "Inner-shell Photoemission from the Iodine Atom in CH₃I," LBL-16746.
23. D.W. Lindle, C.M. Truesdale, P.H. Kobrin, T.A. Ferrett, P.A. Heimann, U. Becker, H.G. Kerkhoff, and D.A. Shirley, "Nitrogen K-shell Photoemission and Auger Emission From N₂ and NO," LBL-16861.
24. D.W. Lindle (Ph.D. Thesis), "Inner-shell Photoemission From Atoms and Molecules Using Synchrotron Radiation," LBL-16864.
25. C.C. Parks (Ph.D. Thesis), "The Auger Decay Mechanism in Photon-stimulated Desorption of Ions From Surfaces," LBL-16892.
26. D.W. Lindle, P.H. Kobrin, C.M. Truesdale, P.A. Heimann, T.A. Ferrett, U. Becker, H.G. Kerkhoff, and D.A. Shirley, "Photoemission From the 3d Subshell of Atomic Kr," LBL-16941.

Other Publications

27. D.A. Shirley, P.H. Kobrin, C.M. Truesdale, D.W. Lindle, T.A. Ferrett, P.A. Heimann, U. Becker, H.G. Kerkhoff, and S. Southworth, "Gas-phase Photoemission with Soft X-rays: Cross Sections and Angular Distributions," in *Proceedings for Brookhaven Conference on Advances in Soft X-ray Science and Technology*, Brookhaven National Laboratory, Upton, New York, October 17-19, 1983; LBL-16296.
28. J.J. Barton, C.C. Bahr, Z. Hussain, S.W. Robey, L.E. Klebanoff, and D.A. Shirley, "Angle-resolved Photoemission Extended Fine Structure," in *Proceedings for Brookhaven Conference on Advances in Soft X-ray Science and Technology*, Brookhaven National Laboratory, Upton, New York, October 17-19, 1983; LBL-16298.
29. D.A. Shirley, "Synchrotron Radiation and Surface Chemistry," a report for the National Academy of Sciences Report, *Chemistry—Opportunities and Needs*, February 1983; LBL-15564.

Invited Talks

30. D.A. Shirley, "Angle-resolved Photoemission Extended Fine Structure," Chemistry Department, University of California, Los Angeles, California, April 18, 1983; Chemistry and Physics departments, Oregon State University, Corvallis, Oregon, May 25, 1983; Physics Department, Free University, Berlin, West Germany, July 27, 1983; and Northwest Regional ACS Meeting, University of Hawaii, Honolulu, Hawaii, December 28-30, 1983.
31. D.A. Shirley, "High Energy Photoemission from Atoms and Molecules," Gordon Research Conference on Atomic Physics, Colby-Sawyer College, New London, New Hampshire, July 8,

- 1983; and International Workshop on Atomic and Molecular Photoionization, Fritz-Haber-Institut, Berlin, West Germany, July 26, 1983.
32. D.A. Shirley, "Center for Advanced Materials," Scientific and Engineering Colloquium, University of Colorado, Colorado Springs, Colorado, November 18, 1983.
 33. D.W. Lindle, "Photoelectron Spectroscopy of Gases Using Synchrotron Radiation," Department of Chemistry, Indiana University, Bloomington, Indiana, March 10, 1983.
 34. D.W. Lindle, "Resonant Photoemission: Autoionization in He and Shape Resonances in Molecules," National Bureau of Standards, Washington, D.C., July 11, 1983.
 35. P.H. Kobrin, "Photoelectron Spectroscopy of Gases Using Synchrotron Radiation," The Aerospace Corporation, Los Angeles, California, February 11, 1983.
 36. J.J. Barton, "Surface Structure Determination with Angle-resolved Photoemission Extended Fine Structure," 185th National ACS Meeting, Seattle, Washington, March 20-25, 1983.
 37. J.G. Tobin, "Ag/Cu(001): The Interface, Dimensionality, and the Convergence of the Overlayer to Bulk Behavior," Department of Chemistry, Iowa State University, Ames, Iowa, March 10, 1983; Microelectronics Seminar, University of Minnesota, Minneapolis, Minnesota, March 15, 1983; and Analytical Chemistry Seminar, University of Wisconsin, Madison, Wisconsin, February 3, 1983.

[†]Partially supported (a student salary) by the Research Corporation, Occidental Research Corporation, and the NSF under Grant No. CHE79-10965.

[‡]Partially supported by the Naval Weapons Center Independent Research Fund, the U.S. Navy Office of Naval Research, and Sandia National Laboratories, which is supported by the U.S. Department of Energy under Contract No. DE-AC04-76-DP00789.

[§]Partially supported (a student salary) by the Research Corporation, Occidental Research Corporation, and the NSF under Grant CHE79-10965.

[¶]Partially supported by Sandia National Laboratories, which is supported by the U.S. Department of Energy under Contract No. DE-AC04-76-DP00789.

Crossed Molecular Beams*

Yuan T. Lee, Investigator

INTRODUCTION

The major goals of this research are to elucidate detailed dynamics of simple elementary reactions that are theoretically important and to use the molecular-beams method to unravel the mechanism of complex chemical reactions or photochemical processes that play an important role in many macroscopic processes. Molecular beams of reactants are used to study individual encounters between molecules or to monitor photodissociation events in a collision-free environment. Most of the information is derived from measurement of the product-fragment energy and angular distributions using a unique molecular-beam apparatus designed for these purposes. Recent activities have been centered on the following areas: (1) direct probing of transition states of the $F + H_2$ reaction through the experimental observation of quantum-mechanical-resonance phenomena; (2) the mechanisms of elementary chemical reactions involving oxygen atoms with unsaturated hydrocarbons; (3) the dynamics of chemical reactions of electronically excited atoms; (4) the primary photochemical processes of polyatomic molecules, radicals, and ions; (5) the intramolecular energy transfer of chemically activated and locally excited molecules using overtone-excitation processes; and (6) the interaction potential of open-shell atoms with rare-gas atoms.

1. Infrared-laser Multiple-photon Dissociation of $CDCl_3$ in a Molecular Beam (Publication 3)[†]

Irving P. Herman,[‡] Frank Magnotta,[‡]
Richard J. Buss,[§] and Yuan T. Lee

Pulsed CO_2 -laser multiple-photon dissociation of $CDCl_3$ was examined in a molecular beam using 11- μm radiation. The main purpose of this work was to understand the competition between simple bond rupture and 3-center elimination of DCl in the

*This work was supported by the Director, Office of Energy Research, Office of Basic Energy Sciences, Chemical Sciences Division of the U.S. Department of Energy under Contract No. DE-AC03-76SF00098.

primary-dissociation process. At fluences as high as several J/cm^2 , the only observed dissociation channel was hydrogen chloride elimination ($>99.1\%$), with no evidence of simple chloride-atom cleavage ($<0.9\%$). Implications for isotope separation are discussed.

[†]This work was carried out in collaboration with Lawrence Livermore National Laboratory and was supported in part by the U.S. Department of Energy by the Lawrence Livermore National Laboratory under Contract W-7405-ENG-48.

[‡]Permanent address: Lawrence Livermore National Laboratory, Livermore, California 94550.

[§]Present address: Sandia National Laboratory, Albuquerque, New Mexico 87185.

2. Reactive Scattering of $O(^3P) + CF_3$ (Publication 5)

R.J. Buss,[†] S.J. Sibener,[‡] and Y.T. Lee

The reaction of $O(^3P) + CF_3I$ has been studied using an RF-discharge supersonic-oxygen atom-beam source in a crossed-beams arrangement. At a collision energy of 2.2 kcal/mole, the reaction yields exclusively $IO + CF_3$ radical products. The angular and velocity distributions of the products show that the reaction involves complex formation, with the intermediate living a time greater than or equal to one rotational period. Only a small fraction of the available energy is partitioned into product translation, in good agreement with a statistical model. The reaction is believed to remain confined to the triplet surface forming a CF_3-I-O complex.

[†]Present address: Sandia National Laboratory, Albuquerque, New Mexico 87185.

[‡]Permanent address: The James Franck Institute, University of Chicago, Chicago, Illinois 60637.

3. Reactive Scattering of $O(^3P)$ with Toluene (Publication 13)[†]

R.J. Baseman,[‡] R.J. Buss,[§] P. Casavecchia,^{||} and Y.T. Lee

In a crossed molecular-beam study, the reaction of $O(^3P) +$ toluene at 9.7 kcal/mole collision energy is shown to give primarily radical products ($CH_3 +$ phenoxy and $H +$ cresoxy) under single-collision con-

ditions. There is no evidence of intersystem crossing to a stable-singlet species, cresol, as was previously observed in the O + benzene reaction. The isotropic angular distributions of the product suggest that the mechanism involves formation of a long-lived triplet biradical intermediate.

[†]R.J. Baseman was supported by the Fannie and John Hertz Foundation as a Graduate Fellow.

[‡]Present address: Sperry Univac, Semiconductor Division, St. Paul, Minnesota 55164-0525.

[§]Present address: Sandia National Laboratory, Albuquerque, New Mexico 87185.

[¶]Present address: Department of Chemistry, University of Perugia, Perugia, Italy.

4. Photodissociation of 1,2-chloroiodoethane at 248 and 266 nm (Publication 10)

D. Krajnovich, Z. Zhang, L. Butler, and Y.T. Lee

The photochemistry of CF_2Br_2 at 248 nm has been studied using the crossed-laser/molecular-beam technique. The only primary reaction channel observed is atomic-bromine elimination: $\text{CF}_2\text{Br}_2 \rightarrow \text{CF}_2\text{Br} + \text{Br}$. Laboratory angular and time-of-flight distributions of the CF_2Br and Br primary products were measured and used to derive the center-of-mass (c.m.) product recoil energy and angular distributions for this reaction. The average c.m. recoil energy of the products is 21.3 kcal/mole. The shape of the c.m. angular distribution indicates that the transition dipole moment is polarized parallel to the Br-Br direction in CF_2Br_2 . The molecular-bromine elimination reaction, $\text{CF}_2\text{Br}_2 \rightarrow \text{CF}_2 + \text{Br}_2$, does not occur to a measurable extent at 248 nm. However, CF_2 radicals are produced in abundance under collision-free conditions, due to the efficient secondary photodissociation of some of the CF_2Br primary product.

5. Work in Progress

The photodissociation of 1,2-chloroiodoethane has been investigated at 248 and 266 nm. The experimental set-up consisted of a supersonic molecular beam of $\text{CH}_2\text{ClCH}_2\text{I}$ crossed at right angles by a UV laser. The photodissociation products were detected in the plane of the laser and molecular beams by a rotatable mass spectrometer.

By fitting the experimental time-of-flight and angular distributions, we obtained the center-of-mass

recoil-translational-energy distribution $P(E_T)$, as well as the center-of-mass angular distribution of the products. At 248 nm the ratio of I^* to I formation is 1.5, while at 266 nm $\text{I}^*/\text{I} = 3$. Analysis of the angular distributions suggests that both iodine channels at both wavelengths proceed by a transition which is nearly parallel to the C-I bond.

A comparison of the translational-energy distributions for the I fragment and for the $\text{C}_2\text{H}_4\text{Cl}$ fragment shows that if the internal energy of the chloroethyl-radical product is above 24.5 ± 2 kcal/mole, then the radical will dissociate. Thus, $D_0^\circ(\text{C-Cl})$ for $\text{C}_2\text{H}_4\text{Cl}$ is determined.

We have studied the unimolecular decay of vibrationally hot isopropyl toluene (ITOL) by crossing a supersonic molecular beam of isopropylcycloheptatriene (ICHT) with the output of a frequency-quadrupled Nd:YAG laser. After absorption of a UV photon, ICHT is known to undergo very rapid internal conversion to its electronic ground state. The vibrationally hot molecules then isomerize to form ITOL. In the absence of collisional deactivation, unimolecular decomposition of ITOL prepared with an average internal energy of 140 kcal/mole can then be observed.

We have measured angular and velocity distributions of the dissociation products and found evidence for two dissociation channels: loss of a methyl group and loss of the isopropyl group.

In order to gather some lifetime information, we modified our experimental set-up so that the intersection of laser and molecular beam could be moved upstream of the region viewed by the mass spectrometer. This corresponds to the introduction of a variable time delay between laser excitation and probing of the dissociation products. The isomerization of ICHT to ITOL and the subsequent dissociation were found to have an overall lifetime of 5 μsec . Since this value corresponds to the known isomerization rate, we conclude that the dissociation of ITOL must be significantly faster. Statistical-model calculations (RRKM) of the latter are in progress.

The absorption of an infrared (IR) photon from a tunable-IR laser causes the negative ion CH_2^- to photodetach to the neutral CH_2 . Very efficient ion detection allows small changes in the number of ions to be detected. Our experimental goal is to determine the threshold for photodetachment of $\text{CH}_2^- 2\text{B}$ to the 3B ground-electronic state of CH_2 . Because the difference in energy between the $\text{CH}_2^- 2\text{B}$ and $\text{CH}_2 1\text{A}$ states is well-known, the $\text{CH}_2 3\text{B}$ -to- $\text{CH}_2 1\text{A}$ energy splitting can be found. Determination of the singlet-triplet splitting has been the goal of much work, both experimental and theoretical. The

methylene radical is small enough to study using *ab initio* calculations, and thus a direct comparison can be made between experimental and theoretical studies. While most studies yield a splitting of 8–10 kcal/mole, the photoelectron spectrum of CH_2^- by Lineberger et al.¹ gave a value of 19.5 kcal/mole. The discrepancy between the photoelectron spectrum and other measurements can be explained if, in the photoelectron-spectroscopy work, the CH_2^- ions were formed with vibrational excitation energy. Recent theoretical calculations support this hypothesis.

A key requirement of this experiment is to obtain the CH_2^- ions with no vibrational-excitation energy, so that the true photodetachment threshold will be measured. To ensure that our ions are not vibrationally hot, they are trapped in an octapole ion guide for up to 0.5 sec to cool radiatively before they are photodetached to the neutral. We tuned our IR source, an optical parametric oscillator, and compared photodetachment cross sections as a function of trap time. At the higher energies, which are above threshold (0.65 eV), the photodetachment drops ~50% from a 10-msec trap time to a 501-msec trap time. In contrast, at photon energies below the expected threshold, we see the photodetachment drop by about 90%. This decrease in photodetachment cross section is attributed to the radiative relaxation of the initially hot CH_2^- ions. Our experimental results support our hypothesis that the ions in the photoelectron study were vibrationally hot.

In addition to the threshold for photodetachment of the cooled CH_2^- , the radiative lifetimes of the vibrational levels of CH_2^- are being determined.

An experimental study of proton and deuteron transfer in $\text{H}_2^+ + \text{He}$ and $\text{HD}^+ + \text{He}$ has been carried out as a function of kinetic and vibrational energy. The data give evidence that at lower kinetic energies the spectator-stripping mechanism indeed plays an important role when H_2^+ or HD^+ is vibrationally excited. The $\text{H}_2^+(v=0)$ reaction has a much smaller cross section and seems to go through intimate, small-impact-parameter collisions involving all the atoms.

The competition between both the proton and deuteron transfer channels for the HD^+ case shows that the vibrational enhancement toward forming the HeD^+ product, falls off sooner with increasing kinetic energy than does the HeH^+ product, again in accordance with the spectator-stripping model. The higher yield for HeH^+ production at both higher vibrational levels of HD^+ and lower kinetic energy, and the behavior of translational-energy dependence of HeH^+ , seem to indicate the importance of the induced orientation of HD^+ during the collision with

He. Because of the displacement of the center of mass from the center of charge in HD^+ , the charge-induced dipole interaction between He and HD^+ tends to swing the H atom more toward He during the approach of He and HD^+ .

The infrared spectrum of the hydrogen-bonded water dimer in the gas phase was obtained at 2 cm^{-1} resolution. The water dimer was formed by expanding a mixture of 0.5% water vapor in 4 atm of helium carrier gas through a 3-mil nozzle into a vacuum chamber via two stages of differential pumping. The dimer is detected by electron-bombardment ionization and a quadrupole mass spectrometer set for mass 19. H_3O^+ is the dominant fragment formed from the dimer.

The tunable infrared radiation from a Nd:YAG-pumped optical parametric oscillator overlaps the molecular beam in an antiparallel arrangement. The spectrum is obtained by observing the depletion in the dimer signal that occurs when the predissociating state formed by the absorption of an infrared photon predissociates, resulting in the excited dimers scattering out of the path to the detector.

Significantly narrower dimer spectral features were found than were previously observed. While this result is partially due to the improved resolution of the infrared source, the production of rotationally cold dimers with little trimer contamination is thought to be the main reason for the narrower lines.

In addition to recording the dimer spectrum in the region corresponding to the symmetric and asymmetric stretches of the water monomer, we have seen spectra corresponding to the first overtone of the bend (at 3180 cm^{-1}) and a combination band of the stretch and bend (at 5332 cm^{-1}). These results are consistent with the stretches being "red" shifted on hydrogen bonding, but the bend is shifted to the "blue."

The $3^2\text{P}_{3/2}$ state of sodium has a lifetime of only 16.6 nsec. We have been able to study the reaction dynamics of this short-lived excited electronic state by preparing it directly in the interaction region of our universal crossed molecular-beam machine. The ground-state $\text{Na} + \text{HCl} \rightarrow \text{NaCl} + \text{H}$ reaction is endothermic by 4.6 kcal/mole.

An atomic beam of sodium was optically pumped to produce a steady-state fraction of 30% of the sodium atoms in the $3\text{P } F=3$ state. This excitation was accomplished using a single-mode single-frequency continuous-wave (cw) dye laser whose frequency was locked to the maximum of the subsequent sodium fluorescence. The sodium beam was crossed with a supersonic HCl beam. Product angular distributions were measured at relative collision

energies of 5.38 and 19.4 kcal/mole. Product velocity measurements were made at 5.38 kcal/mole. Also, at the lower collision energy the alignment and orientation of the excited p-orbital was varied by changing the laser polarization. (Both linear and circular polarization were used.)

At 19.4 kcal/mole of collision energy, there was no difference between the product angular distributions given by the ground and excited electronic states. At 5.38 kcal/mole, however, there was an enormous enhancement of the reaction with the laser excitation. This is clearly because the ground-state reaction is very nearly thermoneutral at the lower collision energy.

The excited-state measurements at a collision energy of 5.38 kcal/mole were deconvoluted to give product center-of-mass energy and angular distributions. The NaCl product was found to be largely backscattered with some forward-sideways peaking. This is indicative of a direct reaction in which low-impact-parameter collisions lead to reaction. No dependence of the reactivity on the laser polarization was observed. We attribute this to the predominance of depolarizing events (e.g., fine-structure changing collisions), because these events have large cross sections as compared to those of reactive scattering.

The concept of a transition state (TS) was introduced by Henry Eyring in the 1930s when he developed a reaction-rate theory based on the structure of the intermediate unbound molecule that must be formed *en route* from reactants to products. Until now our knowledge of the TS has been limited by the theoretical calculations. Direct experimental probing of TS has not been successful. We have recently completed crossed molecular-beam experiments which reveal evidence for a very short-lived quasi-bound FH_2 molecule. The reactive scattering that is a result of this complex-formation mechanism provides a very direct experimental probe of the potential-energy surface (PES) in the neighborhood of the TS. Two torr of pure F_2 is thermally dissociated in a resistively heated oven. An effusive beam of F atoms is then velocity selected to a peak velocity of 870 m/sec with full-width half maximum of 11% by a set of six slotted disks. The H_2 beam is a very intense supersonic jet, collimated by an electroformed skimmer without differential pumping. The reaction products are detected using a triply differentially pumped, ultrahigh-vacuum, rotatable-quadrupole mass spectrometer. Two measurements are made, both as a function of lab angle: total intensity and time-of-flight velocity measurement of product. From these data the product-flux contour

map in the center-of-mass reference frame is derived by forward convolution.

The two major channels are the formation of $v=2$ and $v=3$. The $v=3$ channel is the reaction of F with H_2 ($J=2$). The $v=2$ product is scattered primarily in the backward direction. This means that for $v=2$ formation low-impact-parameter collisions are the most productive, corresponding to a nearly collinear TS. It also means that the reaction is direct: there is no time for rotation of the complex through the course of the reaction. This is consistent with classical trajectory results on the Muckerman-5 PES. This surface favors a collinear TS and has no wells in it. The flux map for $v=3$ formation is much different. At all energies a strong forward peak is found.

This forward scattering is the result of a quasi-bound FH_2 molecule which lives a fraction of a rotational period. In order for a quasi-bound molecule to form on a PES with no wells, there must be a well in some effective PES with barriers in both the entrance channel and the exit channel. In the past this has been explained in terms of vibrationally adiabatic surfaces. Specifically, the product $v=3$ exit-channel and reactant $v=0$ entrance-channel barriers were postulated to cause formation of a quasi-bound molecule that then decays to $v=2$ of the product. The fact that the resonance is found in $v=3$ indicates that the $v=3$ adiabatic exit-channel barrier in the Muckerman-5 PES (used in theoretical calculations) needs to be improved. We must at least lower this barrier so that the product can decay to the correct vibrational state. It is hoped that these data will serve as a very rigorous test of future theoretically derived PESs and scattering calculations.

1. P.C. Engelking, R.R. Corderman, J.J. Wendoloski, G.B. Ellison, S.V. O'Neil, and W.C. Lineberger, *J. Chem. Phys.* **74** (1981), 5460.

1983 PUBLICATIONS AND REPORTS

Refereed Journals

1. F. Huisken, D. Krajnovich, Z. Zhang, Y.R. Shen, and Y.T. Lee, "Competing Dissociation Channels in the Infrared Multiphoton Decomposition of Ethyl Vinyl Ether," *J. Chem. Phys.* **78**, 3806 (1983).[†]
2. L.J. Butler, D. Krajnovich, G. Ondrey, R. Bersohn, and Y.T. Lee, "The Photodissociation of

- Nitromethane at 193 nm," *J. Chem. Phys.* **79**, 1708 (1983).[†]
3. Irving P. Herman, Frank Magnotta, Richard J. Buss, and Y.T. Lee, "Infrared Laser Multiple-photon Dissociation of CDCl_3 in a Molecular Beam," *J. Chem. Phys.* **79**, 1789 (1983); LBL-15901.[‡]
 4. J.W. Hepburn, R.J. Buss, L.J. Butler, and Y.T. Lee, "A Molecular Beam Study of the Photochemistry of S_1 Glyoxal," *J. Phys. Chem.* **87**, 3638 (1983); LBL-15467.
 5. R.J. Buss, S.J. Sibener, and Y.T. Lee, "Reactive Scattering of $\text{O}(^3\text{P}) + \text{CF}_3\text{I}$," *J. Phys. Chem.* **87**, 4840 (1983); LBL-16114.
 6. Yuan T. Lee, "Molecular Beam Studies of Primary Photochemical Processes," *Laser Chemistry* **2**, 219 (1983), LBL-15480.
 7. L.J. Butler, R.J. Buss, R.J. Brudzynski, and Y.T. Lee, "Energy Partitioning to Product Translation in the Infrared Multiphoton Dissociation of Diethyl Ether," *J. Phys. Chem.* **87**, 5106 (1983).[†]
 15. Y.T. Lee, "Crossed Molecular Beams Studies Using the Seeded Supersonic Beams Method," John Fenn Symposium, Yale University, New Haven, Connecticut, March 14-15, 1983.
 16. Y.T. Lee, "Dynamic Resonances in Reactive Scattering," Department of Chemistry, Rice University, Houston, Texas, March 16, 1983.
 17. Y.T. Lee, "Elucidation of Reaction Mechanism by the Crossed Molecular Beams Method," Kolthoff Lecture, Department of Chemistry, University of Minnesota, Minneapolis, Minnesota, April 25, 1983.
 18. Y.T. Lee, "Molecular Beam Studies of Primary Photochemical Processes," Kolthoff Lecture, Department of Chemistry, University of Minnesota, Minneapolis, Minnesota, April 27, 1983.
 19. Y.T. Lee, "Dynamic Resonances in $\text{F} + \text{H}_2$ Reaction," Kolthoff Lecture, Department of Chemistry, University of Minnesota, Minneapolis, Minnesota, April 29, 1983.
 20. Y.T. Lee, "High Brilliance VUV Photochemistry," Workshop on Synchrotron Radiation Source, Lawrence Berkeley Laboratory, Berkeley, California, May 10, 1983.

LBL Reports

8. Douglas John Krajnovich (Ph.D. Thesis), "Molecular Beam Studies of Photodissociation Reactions," LBL-15354.
9. Matthew Fowler Vernon (Ph.D. Thesis), "Molecular Beam Scattering," LBL-15855.
10. D. Krajnovich, Z. Zhang, L. Butler, and Y.T. Lee, "Photodissociation of CF_2Br_2 at 248 nm by the Molecular Beam Method," submitted to *J. Phys. Chem.*, LBL-16431.
11. Sanford Will Bustamente (Ph.D. Thesis), "Molecular Ion Photofragment Spectroscopy," LBL-16633.
12. Jeremy G. Frey, "Excited Vibrational States Near Dissociation in Weakly Bound Triatomic Systems," submitted to *Chem. Phys. Lett.*, LBL-16709.
13. R.J. Baseman, R.J. Buss, P. Casavecchia, and Y.T. Lee, "Reactive Scattering of $\text{O}(^3\text{P})$ with Toluene," submitted to *J. Am. Chem. Soc.*, LBL-17103.[§]
21. R.J. Buss, "Further Investigation on the Reaction of $\text{O}(^3\text{P})$ with Acetylene by the Crossed Molecular Beams Method," DOE/BES Combustion Research Contractors' Meeting, Brookhaven National Laboratory, Upton, New York, May 24-26, 1983, LBL-15916ABS.
22. Y.T. Lee, "The Effect of Internal Excitation in Promoting a Chemical Reaction," Workshop on Elementary Chemical Reactions, University of Paris, Orsay, France, June 10, 1983.
23. Y.T. Lee, "Recent Advances in Molecular Beam Chemistry," Workshop on Elementary Chemical Reactions, University of Paris, Orsay, France, June 10, 1983.
24. Y.T. Lee, "Reactive Scattering, Advances and Perspectives," International Symposium on Molecular Beams, Freiburg, West Germany, June 13-17, 1983.
25. O. Dutuit, "Effect of Vibrational and Translational Energy on the Reactions Between H_2^+ and HD^+ with He," International Symposium on Molecular Beams, Freiburg, West Germany, June 13-17, 1983.

Invited Talks

14. Y.T. Lee, "Primary Photochemical Processes by Molecular Beam Photofragmentation Translational Spectroscopy," International Conference on Photochemistry and Photobiology, January 3-8, 1983, Alexandria, Egypt, LBL-15480.
26. Y.T. Lee, "Introductory Remark on Reactive Scattering," Conference on Dynamics of Molecular Collisions, Gull Lake, Brainard, Minnesota, June 27-July 1, 1983.
27. Daniel M. Neumark, "Molecular Beam Studies of the $\text{F} + \text{H}_2$, D_2 , and HD Reactions," Confer-

- ence on Dynamics of Molecular Collisions, Gull Lake, Brainard, Minnesota, June 27–July 1, 1983, LBL-15996ABS.
27. Alec M. Wodtke, "The Investigation of Dynamic Resonances in $F + HD$," Conference on Dynamics of Molecular Collisions, Gull Lake, Brainard, Minnesota, June 27–July 1, 1983, LBL-16113ABS.
 28. Y.T. Lee, "Molecular Beam Studies of Primary Photodissociation Processes," XIth International Conference on Photochemistry, University of Maryland, College Park, Maryland, August 21–26, 1983.
 29. D.J. Krajnovich, L.J. Butler, and Y.T. Lee, "UV Photodissociation of $1,2-C_2F_4BrI$: Bond Selective Photodissociation through Electronic Transition," Herrsching Workshop on Primary Photophysical Processes, Herrsching, West Germany, October 16–21, 1983, LBL-16710ABS.
 30. Y.T. Lee, "Molecular Beam Studies of Primary Photochemical Processes of Polyatomic Molecules," Department of Chemistry, California Institute of Technology, Pasadena, California, October 28, 1983.
 31. Y.T. Lee, "Elucidation of Reaction Mechanism Involving Oxygen Atom with Unsaturated Hydrocarbons," FMC Lecture, Department of Chemistry, Princeton University, Princeton, New Jersey, November 2, 1983.
 32. Y.T. Lee, "Experimental Investigations of Resonance Phenomena in Elementary Chemical Reactions," FMC Lecture, Department of Chemistry, Princeton University, Princeton, New Jersey, November 2, 1983.
 33. Y.T. Lee, "Photodissociation of Alkyl Polyhalides Using an Excimer Laser," FMC Lecture, Department of Chemistry, Princeton University, Princeton, New Jersey, November 2, 1983.
 34. Y.T. Lee, "Reaction of Oxygen Atoms With Unsaturated Hydrocarbons," Frontier Lecture, Texas A&M University, College Station, Texas, November 27, 1983.
 35. Y.T. Lee, "Promotion of Chemical Reaction by Reagent Translational and Internal Excitation," Frontier Lecture, Texas A&M University, College Station, Texas, November 28, 1983.
 36. Y.T. Lee, "Experimental Probing of the Transition State in the $F + H_2$ Reaction," Frontier Lecture, Texas A&M University, College Station, Texas, November 29, 1983.
 37. Y.T. Lee, "Infrared Multiphoton Dissociation of Polyatomic Molecules," Frontier Lecture, Texas A&M University, College Station, Texas, November 30, 1983.
 38. Y.T. Lee, "Molecular Beam Photofragmentation Translational Spectroscopy," Frontier Lecture, Texas A&M University, College Station, Texas, December 1, 1983.
 39. Y.T. Lee, "Dynamics in Mechanisms of Primary Photochemical Processes of Polyatomic Molecules," Department of Chemistry, University of Rochester, Rochester, New York, December 4, 1983.
 40. Y.T. Lee, "Molecular Beam Studies of Elementary Chemical Reactions," Harrison Howe Award Lecture, Rochester Section of the ACS, Rochester, New York, December 4, 1983.
 41. Y.T. Lee, "Direct Probing of the Transition State: Dynamic Resonances in the $F + H_2$ Reaction," Department of Chemistry, California Institute of Technology, Pasadena, California, December 8, 1983.

[†]Supported by the Office of Naval Research under Contract N00014-75-C-0671.

[‡]This work was carried out in collaboration with Lawrence Livermore National Laboratory and was supported in part by the U.S. Department of Energy by the Lawrence Livermore National Laboratory under Contract W-7405-ENG-48.

[§]Supported partly by the Fannie and John Hertz Foundation.

Potential-Energy Surfaces for Chemical Reactions*

Henry F. Schaefer III, Investigator

INTRODUCTION

This research program has two goals, related yet distinct. The first goal is the development of new theoretical and/or computational methods for the description of "what electrons are doing in molecules," to use the words of Robert S. Mulliken. Specifically, the single outstanding problem in the field is the correlation problem, that of formulating models for going beyond the single-particle or Hartree-Fock approximation. The second goal of our research is to apply these theoretical methods to significant problems of broad chemical interest. Currently two areas are of special concern: (1) model theoretical studies of chemisorption, metal clusters, and organometallic species, and (2) potential-energy surfaces that govern gas-phase chemical reactions. Research in the former area is ultimately aimed at a truly molecular understanding of catalysis, a subject pertinent to future energy requirements; but the research sometimes tends toward molecules that are potentially important in interstellar space, atmospheric chemistry, and the development of high-power laser systems. It is to be emphasized that in recent years theoretical chemistry has become a significant source not only of broad generalities, but also of specific predictions concerning molecular systems that may be very important but inaccessible to experiment.

1. Singlet Cyclobutylene: A Relative Minimum on the C_4H_4 Potential-energy Hypersurface? (Publication 2)[†]

George Fitzgerald, Paul Saxe,[‡] and Henry F. Schaefer III

The lowest singlet and triplet electronic states of cyclobutylene have been investigated by using the

nonempirical molecular electronic-structure theory. Initially, singlet cyclobutylene was studied with two-configuration self-consistent-field (TCSCF) methods, and triplet cyclobutylene was studied with single-configuration SCF theory. Three standard-basis sets of double-zeta (DZ) through double-zeta plus polarization (DZ+P) caliber were employed, the largest being designated C(9s 5p 1d/4s 2p 1d), H(4s 1p/2s 1p). Geometrical structures and harmonic-vibrational frequencies were determined by analytic-gradient techniques. Subsequently, the different stationary points were subjected to electron-correlation studies, including in a fully variational manner as many as 74,625 configurations. From purely geometrical considerations, the short carbon-carbon bond in singlet cyclobutylene may be labeled a weak (or long) triple bond, with $r_e(C\equiv C) = 1.258 \text{ \AA}$. For triplet cyclobutylene a much longer carbon-carbon distance (1.323 \AA) is predicted, consistent with the sort of C=C double bond expected for this diradical species. The triple-bond CC harmonic-stretching frequency for singlet cyclobutylene is predicted to be 1911 cm^{-1} , while the analogous stretching frequency for the triplet diradical species is 1779 cm^{-1} . Vibrational analyses demonstrate that (at the levels of theory considered) both singlet and triplet cyclobutylene are relative minima on the C_4H_4 potential-energy hypersurface. For the former, the lowest frequency predicted at the DZ plus carbon-d function (DZ+d) TCSCF level of theory is 276 cm^{-1} , corresponding to the ring-puckering mode. These remarks notwithstanding, it is to be emphasized that singlet cyclobutylene is a highly energetic species, predicted to lie $\sim 78 \text{ kcal}$ above vinyl acetylene, $HC\equiv C-CH=CH_2$, the absolute minimum among C_4H_4 molecules. Finally, singlet cyclobutylene is predicted to lie 13 kcal below its triplet diradical.

Figure 1-1 shows the predicted molecular structures for singlet and triplet cyclobutylene at several levels of theory.

[†]The Berkeley minicomputer for theoretical chemistry is supported by the National Science Foundation, Grant CHE80-09320.

[‡]Present address: Ballistic Research Labs, DRDAR-BLI, Aberdeen Proving Ground, Aberdeen, Maryland 21005.

*This work was supported by the Director, Office of Energy Research, Office of Basic Energy Sciences, Chemical Sciences Division of the U.S. Department of Energy under Contract No. DE-AC03-76SF00098.

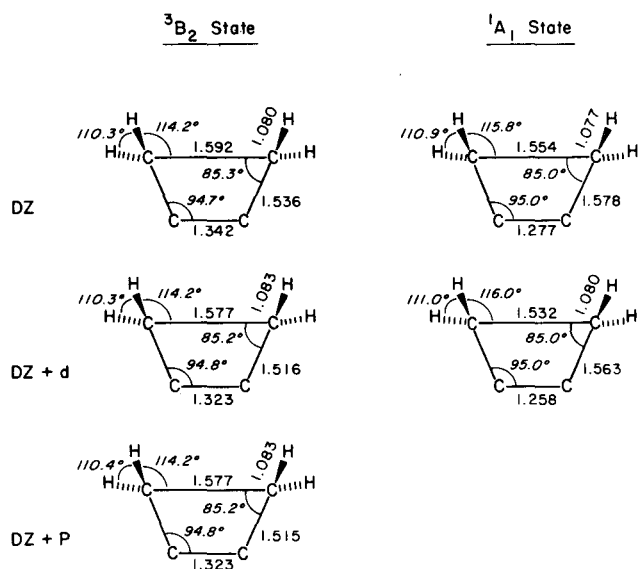


Figure 1-1. Predicted molecular structures at several levels of theory for singlet (1A_1) and triplet (3B_2) cyclobutene. Singlet structures were determined with two basis sets, DZ and DZ+d, from two-configuration SCF wave functions. Triplet structures were obtained from three different basis sets (DZ, DZ+d, and DZ+P) in conjunction with single-configuration SCF theory. All bond distances are in Å. (XBL 841-380)

2. Molecular Clustering About a Positive Ion: Structures, Energetics, and Vibrational Frequencies of the Protonated Hydrogen Clusters H_3^+ , H_5^+ , H_7^+ , and H_9^+ (Publication 4)

Yukio Yamaguchi, Jeffrey F. Gaw, and Henry F. Schaefer III

The positive hydrogen clusters $H^+(H_2)_n$ for $n=1,2,3$, and 4 have been studied via nonempirical molecular electronic-structure theory. Using DZ and DZ+P basis sets, wave functions are reported at both the SCF and configuration-interaction (CI) levels, including all single- and double-excitations (CISD) levels of theory. In each case analytic-gradient techniques have been used to locate stationary-point geometries and to predict harmonic-vibrational frequencies. The effects of electron correlation are shown to be greater for these loose molecular complexes than for ordinary molecules. Although H_5^+ in its lowest energy conformation is not qualitatively described as $H_3^+ \cdot H_2^+$, the larger molecular ions do fit the qualitative picture $H_3^+(H_2)_n$, with H_3^+ as a nucleating center. Of special interest here are the "new" normal modes of these clusters; i.e., those modes having no counterpart in the isolated H_3^+ or H_2 species. There are 15 such vibrational degrees of

freedom for H_9^+ , and the resulting harmonic-vibrational frequencies range from 775 cm^{-1} all the way down to 63 cm^{-1} . Dissociation energies as a function of cluster size follow the pattern established experimentally by Hiraoka and Kebarle.

Figure 2-1 shows the normal vibration corresponding to the highest-frequency mode of H_9^+ .

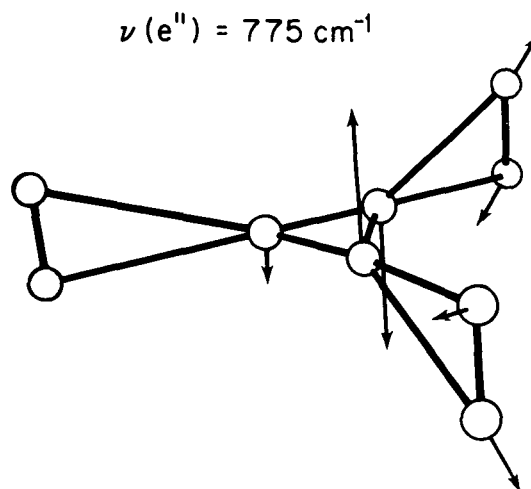


Figure 2-1. The normal vibration corresponding to the highest-frequency new mode of H_9^+ . The term "new mode" is meant to imply that there is no comparable vibrational frequency for either the nucleating center H_3^+ or the three isolated H_2 ligands. This is the e'' vibrational frequency at 775 cm^{-1} (DZ+P-SCF level of theory). (XBL 827-3963)

3. Vibrational Frequencies for Silacetylene and Its Silylidene and Vinylidene Isomers (Publication 6)[†]

Mark R. Hoffmann, Yasunori Yoshioka,[‡] and Henry F. Schaefer III

The molecular structures, vibrational frequencies, and relative energies of silacetylene and its vinylidene and silylidene isomers have been investigated via nonempirical molecular-electronic theoretical methods. Basis sets of DZ and DZ+d quality have been used for this purpose, in conjunction with SCF and CI wave functions. The largest CI included in a completely variational manner 8001 configurations, and analytic CI-gradient methods were used to determine the structure and harmonic-vibrational frequencies of silacetylene itself. The absolute minimum on the potential-energy hypersurface is the silylidene, $:\text{Si}=\text{CH}_2$, which lies $\sim 50\text{ kcal}$ below the linear silacetylene. The vinylidene isomer $\text{H}_2\text{Si}=\text{C}:$

is either an extremely shallow minimum, or, more likely, not a genuine relative minimum at all. Silaacetylene is predicted to have a *trans*-bent equilibrium geometry, with HSiC angle 128.8° , HCSi angle 150.1° , and a silicon-carbon bond distance of 1.635 \AA , about 0.08 \AA shorter than a "standard" Si=C double-bond distance. The silicon-carbon stretching-vibrational frequency is predicted to be $\sim 1100 \text{ cm}^{-1}$, or 10% higher than found experimentally for dimethylsilaethylene. It is concluded that the silicon-carbon linkage in *trans*-bent silaacetylene is intermediate between a double and triple bond. There appears to be no *cis* isomer of silaacetylene.

Figure 3-1 shows the transition state for the rearrangement of *trans*-bent silaacetylene to its silylidene isomer.

†The Berkeley theoretical chemistry minicomputer is supported by the U.S. National Science Foundation, Grant CHE80-09320.

‡Present address: Department of Chemistry, Faculty of Engineering Science, Osaka University, Toyonaka, Osaka 560, Japan.

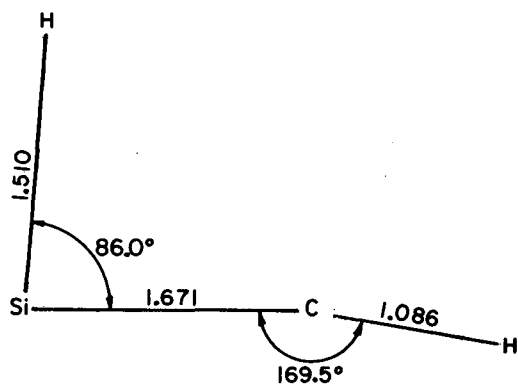


Figure 3-1. Transition state for the rearrangement of *trans*-bent silaacetylene to its silylidene isomer (DZ+d-CI level of theory). (XBL 829-4135)

4. Structure and Tunneling Dynamics of Malonaldehyde. A Theoretical Study (Publication 7)

Jozef Bicerano,[†] Henry F. Schaefer III, and William H. Miller

The geometry and harmonic-vibrational frequencies of equilibrium malonaldehyde and of the transition state for the symmetric intramolecular hydrogen-atom transfer have been determined at the SCF level of theory (using a slightly better than DZ basis set). All geometrical parameters were fully and simultaneously optimized by using SCF-gradient techniques. Comparison of the equilibrium structure with the structure determined from microwave spectra shows good agreement in most respects, although there are a few differences. At the C_s equilibrium geometry and the C_{2v} transition state, large-scale CI (all single and double excitations) calculations were carried out to determine the barrier height for the symmetric hydrogen-atom transfer. Including a correction for quadruple excitations, this gives a classical or "bare" barrier height of 8.0 kcal/mole . A one-dimensional model for the tunneling dynamics of H-atom transfer leads to a tunneling splitting in the ground-vibrational state of $\sim 18 \text{ cm}^{-1}$, in relatively good agreement with the experimental value. It is noted, though, that the value of the splitting is sensitive to the potential-surface parameters (i.e., bare height, frequencies), and that there is also uncertainty about the accuracy of the one-dimensional description of the tunneling.

Figure 4-1 shows the experimental and theoretical structures for malonaldehyde, and a theoretical structure for the degenerate rearrangement of malonaldehyde.

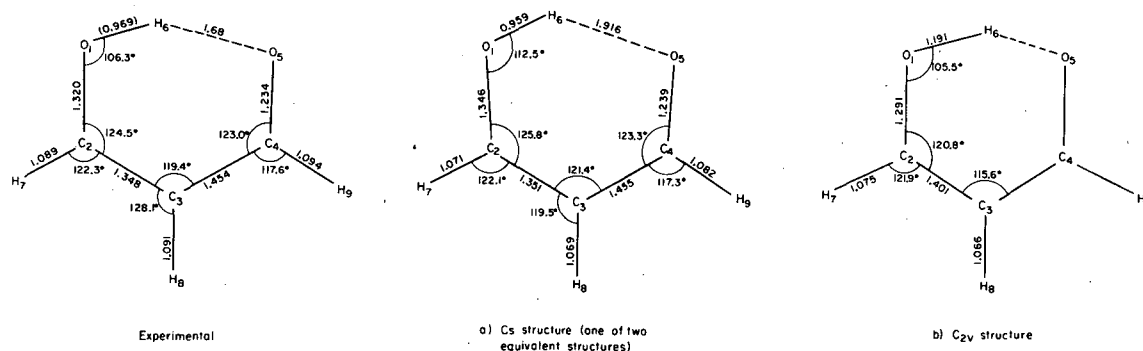


Figure 4-1. Experimental (left) and theoretical (center) structures for malonaldehyde, and a theoretical structure (right) for the transition state for the degenerate rearrangement of malonaldehyde. All bond distances are in Å .

(XBL 827-3965)

[†]Present address: Energy Conversion Devices, Inc., Troy, Michigan 48084.

5. The Convergence of the Cluster Model for the Study of Chemisorption: Be_{36}H (Publication 8)

Paul S. Bagus,[†] Henry F. Schaefer III, and Charles W. Bauschlicher, Jr.[‡]

A three-layer cluster (with 14, 8, and 14 atoms comprising the three layers) has been used to model the chemisorption of atomic hydrogen on the (0001) surface of beryllium. *Ab initio* molecular electronic-structure theory was employed at the SCF level with a minimum basis set (Be 1s, 2s, 2p, and H 1s functions). The properties of the Be_{36} cluster are discussed in some detail, as is the adsorption of H on each of four different high-symmetry surface sites. Significant differences are reported for chemisorption on this model surface relative to the results obtained previously with a two-layer Be_{22} cluster. Changes in chemisorptive bond energies range from 0.2 to 9.7 kcal, while Be_nH distances change by 0.01 to 0.04 Å in going from Be_{22} to Be_{36} . It is concluded that some properties related to chemisorption (e.g., bond distances) converge reasonably rapidly with respect to cluster size, while others (e.g., dissociation energies) converge more slowly.

[†]Present address: IBM Research Laboratory, San Jose, California 95193.

[‡]Present address: NASA Ames Research Center, Moffett Field, California 94035.

6. Vibrational Frequencies of the HCCN Molecule. A Near Degeneracy Between Bent Cyanocarbene and Linear Allene-related Geometries (Publication 9)[†]

Kwang S. Kim,[‡] Henry F. Schaefer III, Leo Radom,[§] John A. Pople,^{||} and J. Stephen Binkley^{††}

The geometrical structure and vibrational frequencies of the ground-triplet electronic state of HCCN have been examined at a wide range of levels of *ab initio* electronic-structure theory. The potential-energy surface of HCC bending is very flat for HCCN, owing to a competition between linear-allene $\text{HC}=\text{C}=\text{N}$ and bent-carbene $\text{HCC}\equiv\text{N}$ valence

structures. Evidence is presented that both the restricted Hartree-Fock (RHF) and unrestricted Hartree-Fock (UHF) methods treat this potential surface in a somewhat uneven manner. When the effects of electron correlation are included, however, RHF- and UHF-based methods converge to a similar set of structural and energetic predictions. The most reliable levels of theory suggest that HCCN is a quasi-linear molecule, with $\theta_e(\text{HCC}) \approx 138^\circ$ and a barrier to linearity of only about 2 kcal/mole.

Figure 6-1 shows stationary-point geometries predicted for linear and bent HCCN.

[†]The Berkeley theoretical chemistry minicomputer is supported by the U.S. National Science Foundation, Grant CHE80-09320.

[‡]Present address: IBM (D55/966-2), Poughkeepsie, New York 12606.

[§]Present address: Research School of Chemistry, Australian National University, Canberra ACT 2600, Australia.

^{||}Present address: Department of Chemistry, Carnegie-Mellon University, Pittsburgh, Pennsylvania 15213.

^{††}Present address: Sandia Laboratory, Livermore, California 94550.

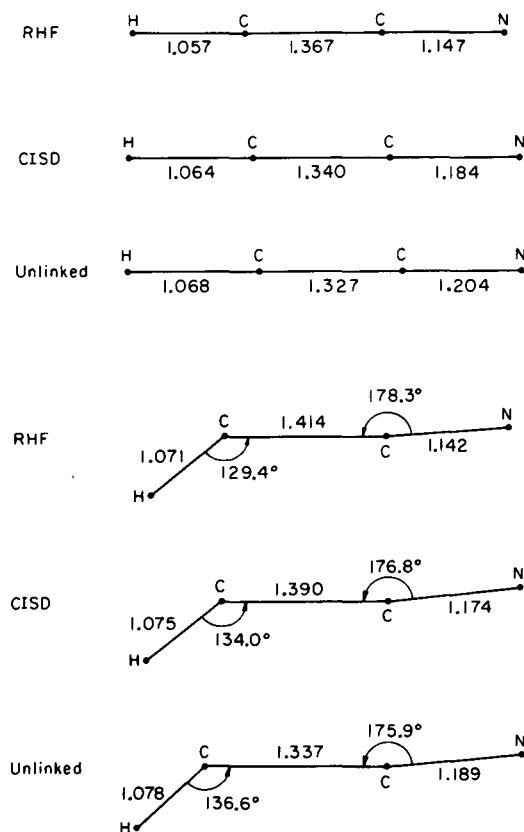


Figure 6-1. Stationary-point geometries predicted for linear (upper) and bent (lower) HCCN. Bond distances are given in Å. RHF refers to the spin-restricted SCF method; CISD refers to CI including single and double excitations; unlinked refers to the results obtained by appending the Davidson correction for quadruple excitations to the CISD variational energies. All results were obtained using a DZ+P basis set. (XBL 825-3837)

7. Molecular and Electronic Structure of Phosphonium Cyclopropylide $\text{H}_3\text{P}=\text{C}(\text{CH}_2)_2$: A Theoretical Study (Publication 10)[†]

Mark A. Vincent,[‡] Henry F. Schaefer III,
Annette Schier,[§] and Hubert Schmidbaur[§]

Theoretical studies have been carried out for a phosphonium cyclopropylide model, $\text{H}_3\text{P}=\text{C}(\text{CH}_2)_2$. The molecule was shown to have a ground-state equilibrium geometry (structure I) with a pyramidal carbanion center, the details being in satisfactory agreement with experimental findings for the tri-phenylphosphine cyclopropylide homologue. One of the PH_3 hydrogen atoms is affected by the carbanion (partial) negative charge, and its position shows substantial distortion away from the idealized tetrahedral phosphorus geometry. In the energy profile for the carbanion inversion, the stationary point of maximum energy (two imaginary vibrational frequencies) occurs not for the planar carbanion configuration but well beyond in a situation with a dihedral angle HOPC1C2 of 123° instead of 90° . The rotated configuration (a genuine transition state) is virtually the eclipsed analogue of structure I. The barriers to inversion and rotation are predicted to be 6.3 to 5.8 kcal, respectively. Calculated bond distances, bond angles, dihedral angles, total-energy values, and total-electron populations on atoms are given for all three conformations. Atomic-orbital components and energies of frontier orbitals of the ground state are also discussed.

Figure 7-1 shows a perspective drawing of the phosphonium cyclopropylide model.

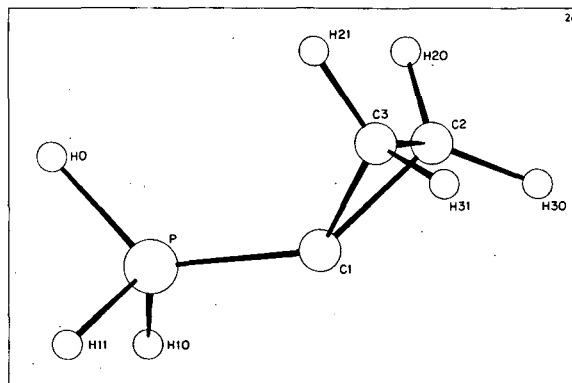


Figure 7-1. Perspective drawing of the phosphonium cyclopropylide model, with molecular dimensions predicted from theory. (XBL 841-381)

8. Infrared Intensities of H_3O^+ , H_2DO^+ , HD_2O^+ , and D_3O^+ (Publication 11)

Michael E. Colvin, Gwendolyn P. Raine,
Henry F. Schaefer III, and Michel Dupuis

Saykally and co-workers have recently observed the infrared spectra of HCO^+ and HN_2^+ , and their spectroscopic technique shows promise for the detection of a large number of other polyatomic molecular ions. An immediate target is H_3O^+ , for which the subtleties of the rotation-inversion problem may make assignments difficult. In this respect the availability of theoretical predictions for the infrared intensities may be of some help in unraveling the observed vibrational spectra. Moreover, because the deuterated molecules H_2DO^+ and HD_2O^+ remove the problems associated with C_{3v} symmetry, the identification of these species may in fact be simpler. Therefore, in this note we report infrared intensities for all four isotopic molecules H_3O^+ , H_2DO^+ , HD_2O^+ , and D_3O^+ . Table 8-1 gives these intensities, along with theoretical harmonic-vibrational frequencies in all cases.

[†]The Berkeley theoretical chemistry minicomputer is supported by the U.S. National Science Foundation, Grant CHE80-09320.

[‡]Present address: School of Molecular Science, University of Sussex, Brighton BN1 9QT, England.

[§]Present address: Anorganisch-chemisches Institut, Technische Universität, Munich, 8046 Garching, West Germany.

Table 8-1

Theoretical harmonic vibrational frequencies ν and infrared intensities a_1 (in parentheses) for H_3O^+ and three isotopically substituted forms. The ν values are in cm^{-1} , and the intensity values are in $\text{D}^2/(\text{\AA}^2 \text{amu})$. As noted in the text, the predicted harmonic OH stretching frequencies are expected to be $\sim 12.3\%$ above the yet-to-be-observed fundamentals. Results obtained with the DZ+P basis set are given beside those from the larger extended (Ext) basis set.

	Normal-mode Species							
	H_3O^+		D_3O^+		H_2DO^+		HD_2O^+	
	Ext	DZ+P	Ext	DZ+P	Ext	DZ+P	Ext	DZ+P
$\nu_1(a_1)$	3831(1.0)	3868(1.2)	2722(0.6)	2749(0.7)	2843(4.4) [†]	2879(4.8) [†]	2781(2.1) [†]	2811(2.3) [†]
$\nu_2(a_1)$	814(13.9)	803(14.5)	617(6.6)	609(6.9)	753(11.5) [†]	743(12.0) [†]	686(9.0) [†]	677(9.4) [†]
$\nu_3(e)$	3948(13.5)	4004(14.8)	2907(7.0)	2950(7.7)	3948(13.5) [‡]	4004(14.8) [‡]	3913(9.9) [†]	3964(10.9) [†]
					3874(5.8) [†]	3919(6.5) [†]	2908(7.2) [‡]	2950(7.9) [‡]
$\nu_4(e)$	1794(3.2)	1788(3.2)	1304(1.3)	1299(1.3)	1774(3.4) [‡]	1768(3.4) [‡]	1625(2.7) [†]	1620(2.7) [†]
					1509(1.7) [†]	1503(1.7) [†]	1332(1.2) [‡]	1326(1.2) [‡]

[†] a_1'

[‡] a_1''

9. Structures, Energetics, and Vibrational Frequencies of Cyclopropyne (Publication 12)[†]

George Fitzgerald[‡] and Henry F. Schaefer III

The electronic structure of the lowest singlet and triplet states of cyclopropyne have been investigated using *ab initio* molecular quantum mechanics. Both DZ and DZ+d basis sets have been used in conjunction with SCF, multiconfiguration SCF (MCSCF), and CI methods. Singlet cyclopropyne is predicted to be a transition state for the degenerate rearrangement of propadienylidene ($\text{H}_2\text{C}=\text{C}=\text{C}:$). However, triplet cyclopropyne is a minimum on the C_3H_2 potential-energy hypersurface, and vibrational frequencies are predicted at two levels of theory. Structures and vibrational frequencies are compared with those of the relatively stable cyclopropene molecule.

Figure 9-1 shows the predicted stationary-point geometries for singlet and triplet cyclopropyne.

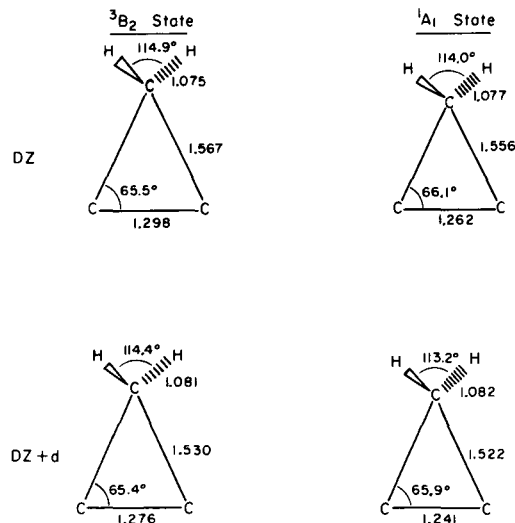


Figure 9-1. Predicted stationary-point geometrical structures for singlet (1A_1) and triplet (3B_2) cyclopropyne at two levels of theory, DZ and DZ+d. Bond distances are given in Å.

(XBL 8211-4244)

[†]The Berkeley theoretical chemistry minicomputer is supported by the U.S. National Science Foundation, Grant CHE80-09320.

[‡]National Science Foundation Predoctoral Fellow, 1980-83.

10. Electronic Symmetry Breaking in Polyatomic Molecules. MCSCF Study of the Cyclopropenyl Radical, C_3H_3 (Publication 13)[†]

Mark R. Hoffmann, William D. Laidig,[‡]
Kwang S. Kim,[§] Douglas J. Fox,^{||} and
Henry F. Schaefer III

For equilateral-triangle geometries (point group D_{3h}), the C_3H_3 radical has a degenerate ${}^2E''$ electronic ground state. Although the 2A_2 and 2B_1 components separate in energy for C_{2v} geometries, these two components should have identical energies for equilateral-triangle structures. In fact, when approximate wave functions are used and the orbitals are not required to transform according to the D_{3h} irreducible representations, an energy separation between the 2A_2 and 2B_1 components is observed. At the single-configuration SCF level of theory, this separation is 2.8 kcal with a DZ basis set and 2.4 kcal with a DZ+P basis set.

It has been demonstrated that this spurious separation may be greatly reduced using MCSCF (up to 7474 variationally optimum configurations) and CI interaction (up to 60,685 space- and spin-adapted configurations) techniques. Configurations differing by three and four electrons from the Hartree-Fock reference function are found necessary to reduce the ${}^2A_2 - {}^2B_1$ separation to below 0.5 kcal.

[†]The Berkeley minicomputer for theoretical chemistry is supported by the U.S. National Science Foundation, Grant CHE-8218785.

[‡]Present address: Quantum Theory Project, University of Florida, Gainesville, Florida 32611.

[§]Present address: IBM (D55/966-2), Poughkeepsie, New York 12606.

^{||}Present address: Department of Chemistry, Carnegie-Mellon University, Pittsburgh, Pennsylvania 15213.

11. The HO_2^+ Molecular Ion. Geometrical Structure and Vibrational Frequencies (Publication 14)[†]

Gwendolyn P. Raine, Henry F. Schaefer III, and
Nicholas C. Handy[‡]

The equilibrium geometry and harmonic-vibrational frequencies of HO_2^+ have been predicted at seven distinct levels of *ab initio* theory. In this regard, SCF and CI methods were used in conjunction with DZ, DZ+P, and extended-basis sets of con-

tracted gaussian functions. The molecular structure of HO_2^+ predicted at the DZ+P-CI level of theory is $r_e(H-O) = 1.005$ Å, $r_e(O-O) = 1.239$ Å, and $\theta_e(HOO) = 111.5^\circ$, compared to the experimental structure of neutral HO_2 , $r_o(H-O) = 0.977$ Å, $r_o(O-O) = 1.334$ Å, and $\theta_o(HOO) = 104.2^\circ$. Anharmonic vibrational frequencies were also predicted at four different levels of theory, with the DZ+P-CI results being $\nu_1 = 3204$ cm^{-1} , $\nu_2 = 1572$ cm^{-1} , and $\nu_3 = 1144$ cm^{-1} . For comparison, the observed fundamentals for the neutral HO_2 molecule are $\nu_1 = 3436$ cm^{-1} , $\nu_2 = 1392$ cm^{-1} , and $\nu_3 = 1098$ cm^{-1} .

Figure 11-1 shows theoretical structures for the HO_2^+ molecular ion predicted by different basis sets.

[†]The Berkeley theoretical chemistry minicomputer is supported by the U.S. National Science Foundation, Grant CHE-8218785.

[‡]Present address: Department of Theoretical Chemistry, University Chemical Laboratories, Cambridge CB2 1EW, England.

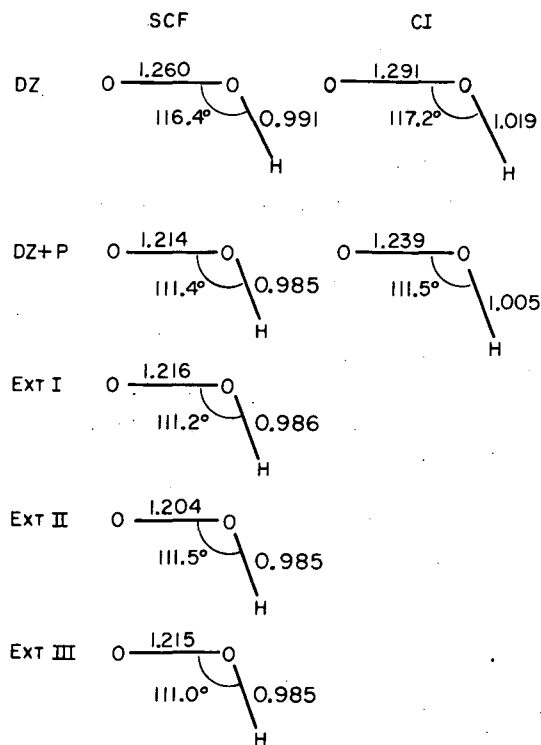


Figure 11-1. Theoretical structures for the HO_2^+ molecular ion, predicted by different basis sets. Bond distances are given in Å. The abbreviation EXT refers to several basis sets of size greater than DZ+P. (XBL 835-3764)

12. Applications of Molecular Quantum Mechanics to Problems in Chemistry (Publication 15)[†]

Henry F. Schaefer III

The past decade has witnessed remarkable progress in the development of rigorous quantum mechanical methods for the study of molecular electronic structure. Key developments include the emergence of large-scale CI methods (including more than one million variational parameters) and of analytic first and second energy-derivative techniques. These advances have greatly increased the scope of current applications of quantum mechanics to chemistry. Present and anticipated future developments with respect to the fields of physical, organic, and inorganic chemistry are surveyed.

[†]Supported in part by the U.S. National Science Foundation, Grant CHE-8218785.

13. Vibrational Frequencies and Infrared Intensities for H₂CN⁺, Protonated HCN (Publication 16)[†]

Timothy J. Lee and Henry F. Schaefer III

During the past year the infrared spectra of a number of polyatomic molecular ions, including HCO⁺, HN₂⁺, H₃O⁺, and NH₄⁺, have been observed at high resolution using the velocity-modulated absorption technique developed by Saykally and co-workers. Several of these experiments have been assisted by theoretical predictions. Here we predict the infrared spectrum of H₂CN⁺, a prime candidate for immediate observation. A summary of the results is given in Table 13-1.

[†]The Berkeley minicomputer for theoretical chemistry is supported and maintained by the National Science Foundation, Grant CHE-8218785.

Table 13-1
Vibrational frequency and intensity predictions for H₂CN⁺
made at the DZ+P-SCF and DZ+P-CI levels of theory

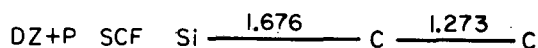
Normal Mode Description	DZ+P—SCF level			DZ+P—CI level		
	Vibrational frequency (cm ⁻¹)		Intensity, (debye/Å) ² /amu	Vibrational frequency (cm ⁻¹)		Intensity, (debye/Å) ² /amu
	Predicted	Estimated		Predicted	Estimated	
ν ₁ (σ) N-H stretch	3869	3455	12.81	3754	3474	11.23
ν ₂ (σ) C-H stretch	3501	3188	8.36	3423	3201	8.44
ν ₃ (σ) C≡N stretch	2434	2132	1.46	2283	2161	0.93
ν ₄ (π) HCN bend	937	779	1.21	836	790	2.52
ν ₅ (π) HNC bend	799	--	3.52	700	--	2.20

14. An Energetically Low-lying Silacyclopropyne Isomer of SiC_2 (Publication 17)[†]

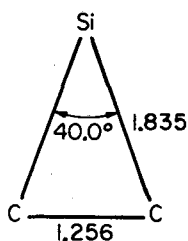
Roger S. Grev and Henry F. Schaefer III

We have discovered a low-lying cyclic isomer of Si-C-C which is best described as a three-membered ring with a weak carbon-carbon triple bond. In these theoretical studies a DZ+P basis set was used initially. At the SCF and TCSCF levels of theory, the ring structure is a transition state leading to linear Si-C-C. A CI treatment at the SCF optimized cyclic geometry, however, shows it to lie 1.1 kcal/mole below the linear structure. Extension of the basis set to include a second set of d functions on each atom gives a final prediction that the ring structure lies ~5 kcal below linear Si-C-C.

Figure 14-1 shows predicted stationary-point geometric structures for the SiC_2 molecule at different levels of theory.



DZ+P SCF



DZ+P TCSCF

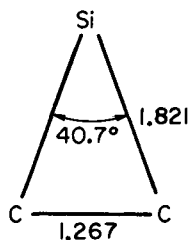


Figure 14-1. Predicted stationary-point geometric structures for the SiC_2 molecule at different levels of theory. All bond distances are given in Å. (XBL 842-606)

15. Analytic Second Derivatives for Renner-Teller Potential-energy Surfaces. Examples of the Five Distinct Cases (Publication 18)[†]

Timothy J. Lee, Douglas J. Fox,[‡]
Henry F. Schaefer III, and Russell M. Pitzer

Force constants at Renner-Teller stationary points fall into five distinct categories, which are readily explored using recently developed analytic-energy second-derivative methods. The nature of the Renner-Teller effect has been derived using symmetry principles and many-electron perturbation theory. By considering the BH_2 , CH_2 , NH_2 , and CuH_2 molecules, examples of all five cases are illustrated via *ab initio* molecular electronic-structure theory (see Figure 15-1).

[†]The Berkeley theoretical chemistry minicomputer is supported by the U.S. National Science Foundation, Grant CHE-8218785.

[‡]Present address: Department of Chemistry, Carnegie-Mellon University, Pittsburgh, Pennsylvania 15213.

FIVE RENNER-TELLER CASES

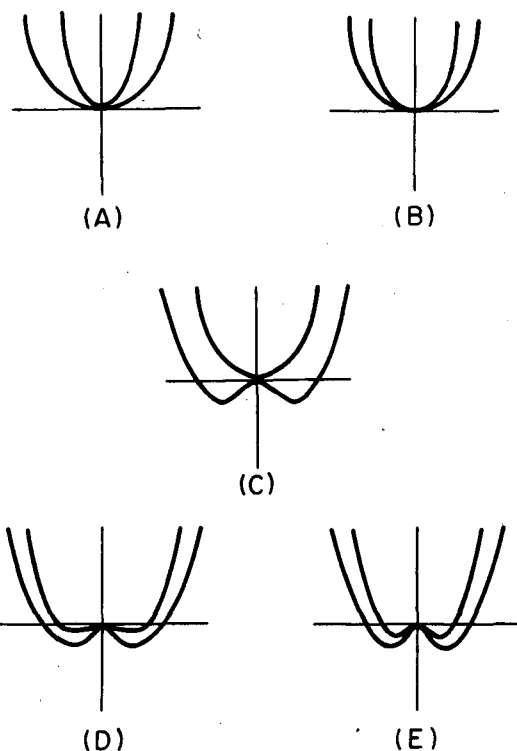


Figure 15-1. Illustrations of the five qualitatively different types of Renner-Teller potential-energy surfaces. (XBL 835-3763)

16. Where to Look for the Electronic Spectrum of Hydrogen Isocyanide, HNC (Publication 19)[†]

William D. Laidig,[‡] Yukio Yamaguchi, and Henry F. Schaefer III

The geometrical structures and vibrational frequencies of the ground and first-excited electronic states of HNC have been predicted by *a priori* theoretical methods. Using a standard DZ+P basis set, both the SCF and CISD levels of theory have been employed. To allow a reasonable assessment of the reliability of the HNC theoretical predictions, analogous studies of the experimentally characterized HCN molecule are also reported. It is hoped that the HNC theoretical predictions will assist in identifying its electronic spectrum. The HNC electronic

spectrum should be readily distinguishable from that observed for HCN by Herzberg and Innes for two reasons: (1) The $\tilde{X}^1\Sigma^+ - \tilde{A}^1A''$ energy difference is predicted to be $\sim 5,000 \text{ cm}^{-1}$ less for HNC than for HCN. (2) For HNC the upper-state vibrational frequencies ν_2 and ν_3 are nearly equal (to within 100 cm^{-1}), while for HCN the $\text{C}\equiv\text{N}$ stretch occurs more than 50% higher in frequency than the bending mode.

Figure 16-1 shows predicted equilibrium structures for the ground and first-excited singlet states of HCN and HNC at different levels of theory and experiment.

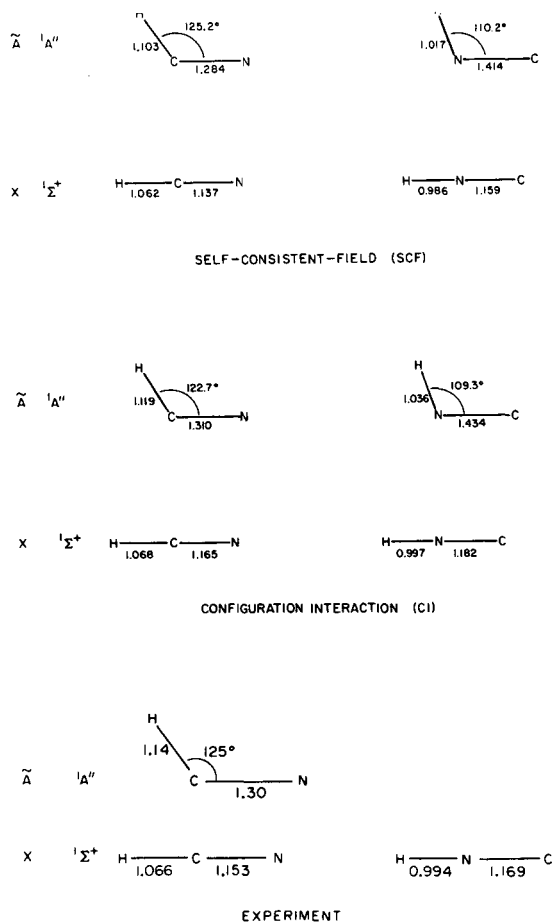


Figure 16-1. Predicted equilibrium structures for the ground and first-excited singlet states of HCN and HNC for SCF and CI levels of theory, along with experimental data. Bond distances are given in Å. (XBL 817-3992)

[†]The Berkeley minicomputer for theoretical chemistry is supported and maintained by the National Science Foundation, Grant CHE-8218785.

[‡]Present address: Quantum Theory Project, University of Florida, Gainesville, Florida 32611.

17. Vibrational-frequency Shifts in Hydrogen-bonded Systems: The Hydrogen Fluoride Dimer and Trimer (Publication 20)[†]

Jeffrey F. Gaw, Yukio Yamaguchi, Mark A. Vincent,[‡] and Henry F. Schaefer III

Ab initio molecular electronic-structure theory has been used to predict the structures and harmonic-vibrational frequencies of $(\text{HF})_2$ and $(\text{HF})_3$. Standard Huzinaga-Dunning DZ and DZ+P basis sets have been used in conjunction with SCF and CI methods. As many as 29,161 configurations were included variationally, with analytic CI-gradient methods used to precisely locate stationary-point geometries. The DZ-SCF, DZ+P-SCF, and DZ+P-CI methods all give qualitative agreement with recent high-resolution spectroscopic measurements of the H-F dimer vibrational frequency shifts. Trimer-equilibrium and transition-state structures and vibrational frequencies have similarly been predicted at the DZ-SCF and DZ+P-SCF levels of theory.

Figure 17-1 shows the transition state for 6-atom exchange and the equilibrium geometry for the HF trimer.

[†]The Berkeley minicomputer for theoretical chemistry is supported and maintained by the National Science Foundation, Grant CHE-8218785.

[‡]Present address: School of Molecular Science, University of Sussex, Brighton BN1 9QT, England.

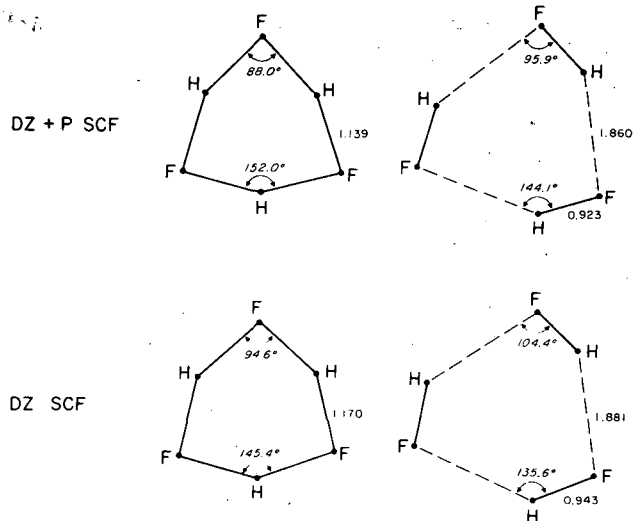
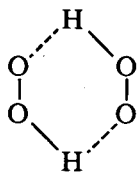


Figure 17-1. Left — transition state for six-atom exchange. Right — equilibrium geometry for the HF trimer. Both figures are shown at the DZ+P-SCF and DZ-SCF levels of theory. All bond distances are in Å. (XBL 841-382)

18. Work in Progress

The HO_2 molecule has in recent years come to be appreciated as one of the most important of atmospheric molecules. E.K.C. Lee and his co-workers at the University of California Irvine have recently reported the infrared spectrum of the HO_2 dimer, discussing several possible isomeric structures. A theoretical study of this molecule is approaching conclusion, with special emphasis on the hydrogen-based cyclic structure



Michael Bowers and his co-workers at the University of California Santa Barbara have recently reported some fascinating electronic spectra for the $(\text{NO})_2^+$ molecular-ion dimer. These spectra have no counterpart for the neutral species NO or $(\text{NO})_2$. Theoretical studies are in progress to determine the structure of the $(\text{NO})_2^+$ system in its *cis*, *trans*, and cyclic forms. Examination of the upper-state potential-energy hypersurface should allow an explanation of the Bowers' experiments.

Refereed Journals

1. D.J. Fox and H.F. Schaefer, "Terminal vs. Bridge Bonding of Methylene to Metal Systems. Al_2CH_2 as a Model System," *J. Chem. Phys.* **78**, 328 (1983); LBL-14339.
2. G. Fitzgerald, P. Saxe, and H.F. Schaefer, "Singlet Cyclobutyne: A Relative Minimum on the C_4H_4 Potential Energy Hypersurface?" *J. Am. Chem. Soc.* **105**, 690 (1983); LBL-14622.[†]
3. P. Saxe and H.F. Schaefer, "Cyclic D_{6h} Hexazabenzene — A Relative Minimum on the N_6 Potential Energy Hypersurface?" *J. Am. Chem. Soc.* **105**, 1760 (1983); LBL-15156.
4. Y. Yamaguchi, J.F. Gaw, and H.F. Schaefer, "Molecular Clustering About a Positive Ion. Structures, Energetics, and Vibrational Frequencies of the Protonated Hydrogen Clusters H_3^+ , H_5^+ , H_7^+ , and H_9^+ ," *J. Chem. Phys.* **78**, 4074 (1983); LBL-15154.
5. S. Saebo, L. Radom, and H.F. Schaefer, "The Weakly Exothermic Rearrangement of Methoxy Radical (CH_3O) to the Hydroxymethyl Radical (CH_2OH)," *J. Chem. Phys.* **78**, 845 (1983); LBL-15495.
6. M.R. Hoffmann, Y. Yoshioka, and H.F. Schaefer, "Vibrational Frequencies for Silacetylene and its Silylidene and Vinylidene Isomers," *J. Am. Chem. Soc.* **105**, 1084 (1983); LBL-14312.[†]
7. J. Bicerano, H. F. Schaefer, and W.H. Miller, "Structure and Tunneling Dynamics of Malonaldehyde, a Theoretical Study," *J. Am. Chem. Soc.* **105**, 2550 (1983); LBL-15155.
8. P.S. Bagus, H.F. Schaefer, and C.W. Bauschlicher, Jr., "The Convergence of the Cluster Model for the Study of Chemisorption: Be_{36}H ," *J. Chem. Phys.* **78**, 1390 (1983); LBL-15496.
9. K.S. Kim, H.F. Schaefer, L. Radom, J.A. Pople, and J.S. Binkley, "Vibrational Frequencies of the HCCN Molecule. A Near Degeneracy Between Bent Cyanocarbene and Linear Allene-related Geometries," *J. Am. Chem. Soc.* **105**, 4148 (1983); LBL-15166.[†]
10. M.A. Vincent, H.F. Schaefer, A. Schier, and H. Schmidbaur, "The Molecular and Electronic Structure of Phosphonium Cyclopropylide $\text{H}_3\text{P}=\text{C}(\text{CH}_2)_2$: A Theoretical Study," *J. Am. Chem. Soc.* **105**, 3806 (1983); LBL-15399.[†]

11. M.E. Colvin, G.P. Raine, H.F. Schaefer, and M. Dupuis, "Infrared Intensities of H_3O^+ , H_2DO^+ , HD_2O^+ , and D_3O^+ ," *J. Chem. Phys.* **79**, 1551 (1983); LBL-16092.
12. G. Fitzgerald and H.F. Schaefer, "Structures, Energetics, and Vibrational Frequencies of Cyclopropyne," *Israel J. Chem.* **23**, 93 (1983); LBL-15288.[†]

LBL Reports

13. M.R. Hoffmann, W.D. Laidig, K.S. Kim, D.J. Fox, and H.F. Schaefer, "Electronic Symmetry Breaking in Polyatomic Molecules. Multiconfiguration Self-consistent-field Study of the Cyclopropenyl Radical, C_3H_3 ," LBL-14092.[‡]
14. G.P. Raine, H.F. Schaefer, and N.C. Handy, "The HO_2^+ Molecular Ion. Geometrical Structure and Vibrational Frequencies," LBL-16717.[‡]
15. H.F. Schaefer, "Applications of Molecular Quantum Mechanics to Problems of Chemistry," in *Chemistry for the Future*, H. Grunewald, Ed., Pergamon Press, Oxford, England, in press, LBL-15762.[§]
16. T.J. Lee and H.F. Schaefer, "Vibrational Frequencies and Infrared Intensities for H_2CN^+ , Protonated HCN," LBL-17098.[‡]
17. R.S. Grev and H.F. Schaefer, "An Energetically Low-lying Silacyclopropyne Isomer of SiC_2 ," LBL-16718.^{||}
18. T.J. Lee, D.J. Fox, H.F. Schaefer, and R.M. Pitzer, "Analytic Second Derivatives for Renner-Teller Potential Energy Surfaces. Examples of the Five Distinct Cases," LBL-17097.[‡]
19. W.D. Laidig, Y. Yamaguchi, and H.F. Schaefer, "Where to Look for the Electronic Spectrum of Hydrogen Isocyanide, HNC," LBL-14203.[‡]
20. J.F. Gaw, Y. Yamaguchi, M.A. Vincent, and H.F. Schaefer, "Vibrational Frequency Shifts in Hydrogen Bonded Systems: The Hydrogen Fluoride Dimer and Trimer," LBL-17096.[‡]
23. H.F. Schaefer, XVII Organosilicon Symposium, North Dakota State University, Fargo, North Dakota, June 2-4, 1983.
24. H.F. Schaefer, 29th International Congress of Pure and Applied Chemistry, Cologne, West Germany, June 4-12, 1983.
25. H.F. Schaefer, "Vectorization of Advanced Methods for Molecular Electronic Structure," NATO, Colorado Springs, Colorado, September 25-29, 1983.
26. H.F. Schaefer, Baekeland Award Symposium, American Chemical Society, Kean College, Union, New Jersey, October 24, 1983.
27. H.F. Schaefer, Department of Theoretical Chemistry, Cambridge University, Cambridge, England, March 22, 1983.
28. H.F. Schaefer, Chemistry Department, Michigan State University, East Lansing, Michigan, July 8, 1983.
29. H.F. Schaefer, Chemistry Department, University of British Columbia, Vancouver, British Columbia, September, 1983.
30. H.F. Schaefer, Chemistry Department, University of Victoria, Victoria, British Columbia, September, 1983.
31. H.F. Schaefer, Chemistry Department, University of Miami, Coral Gables, Florida, November 10, 21, and 29, 1983 (three invited talks).
32. H.F. Schaefer, Chemistry Department, University of Florida, Gainesville, Florida, November 18, 1983.
33. H.F. Schaefer, Chemistry Department, Florida Atlantic University, Boca Raton, Florida, December 9, 1983.

Invited Talks

21. H.F. Schaefer, International Symposium on the Quantum Theory of Matter, Palm Coast, Florida, March 7-12, 1983.
22. H.F. Schaefer, Science and Engineering Research Council, St. Catharine's College,

Cambridge University, Cambridge, England, March 25-27, 1983.

[†]Use of the Berkeley minicomputer for theoretical chemistry was supported by the National Science Foundation, Grant CHE80-09320.

[‡]Use of the Berkeley minicomputer for theoretical chemistry was supported by the National Science Foundation, Grant CHE-8218785.

[§]Supported in part by the National Science Foundation, Grant CHE-8218785.

^{||}Supported partly by an unrestricted grant from Energy Conversion Devices, Inc.

PROCESSES AND TECHNIQUES

CHEMICAL ENERGY

Formation of Oxyacids of Sulfur from SO_2^*

Robert E. Connick, Investigator

INTRODUCTION

The primary purpose of this research is to investigate the fundamental chemistry of sulfur dioxide in aqueous solution, as well as to investigate species formed from it. There is strong interest currently in this chemistry because of the pernicious effects of acid rain, formed when sulfur-containing fuels such as coal are burned and the gaseous products allowed to escape into the atmosphere. The initial combustion yields sulfur dioxide, ultimately forming sulfuric acid. Presently the best way to control acid rain is to remove the sulfur dioxide from the stack gases of coal-burning power plants with aqueous scrubbers. Thus understanding the chemistry of sulfur dioxide and the species formed from it at low acidity is vital to the understanding and design of these massive installations. In addition, the aqueous chemistry of sulfur dioxide is important because it is believed that the oxidation to sulfuric acid in the atmosphere occurs in water films on suspended dust particles.

A secondary and not closely related goal is to determine the factors controlling the rate of substitution reactions in the first coordination sphere of metal ions. These reactions are important in almost all processes involving metal ions in solution. This includes metal-ion-complex formation, some oxidation-reduction reactions, and many biological processes involving metal ions.

*This work was supported by the Director, Office of Energy Research, Office of Basic Energy Sciences, Chemical Sciences Division of the U.S. Department of Energy under Contract No. DE-AC03-76SF00098.

1. Computer Modeling of Rare-solvent Exchange (Publication 1)[†]

R.E. Connick and B.J. Alder[‡]

A simplified two-dimensional model was used to simulate solvent exchange from the first coordination sphere of a metal ion. With realistic activation energies the computer-calculation time per exchange becomes excessive for a freely evolving system. Computer calculations in which the system is equilibrated in constrained states along the reaction trajectory agree with unconstrained simulations at relatively low activation energy, but the constrained-state calculations are orders of magnitude more efficient. For a more realistic activation energy, the two-dimensional computer model shows that at the top of the barrier the two exchanging particles are at an intermediate distance between the first and second coordination shell, separated in angle by the solvent molecules in the first coordination shell. This configuration allows more efficient local packing. Exchange occurs by a highly collective motion involving very many small displacements of all the particles in the first two coordination shells. The crossing of the barrier is more akin to diffusion rather than to unidirectional motion of a particle with an effective mass in a constant-potential field, as envisioned in the transition-state model.

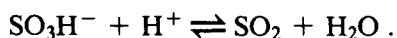
[†]Supported in part by the Lawrence Livermore National Laboratory.

[‡]Present address: Lawrence Livermore National Laboratory, Livermore, California.

2. Work in Progress

A nuclear magnetic resonance study of the exchange of oxygens between bisulfite ion and water has been completed and the results are being written up. The following interpretation has been made. Bisulfite ion appears to exist in two different forms in aqueous solution, one with the proton attached to an oxygen (SO_3H^-), and the other with the proton attached to the sulfur (HSO_3^-). Only the SO_3H^-

form exchanges oxygen with water at a detectable rate, presumably through the reaction:



At pH around 3 the equilibration of the two forms of bisulfite is sufficiently slow that the HSO_3^- form shows a distinct ^{17}O resonance, while at the same time the resonance of the SO_3H^- form is merged with that of water by rapid oxygen exchange with water. At pH 5 the two bisulfite resonances are averaged to a single peak by exchange and, because of the slow exchange with water, appear as a resonance separate from that of water. Rate laws have been determined and mechanisms proposed for these processes.

Rates at which ligands coordinated to metal ions are substituted by other ligands have received a great deal of attention, particularly in recent years. Yet the factors controlling the liability of these ligands are incompletely understood. The present work is aimed at trying to resolve the relative importance of ionic, electronic, and steric effects by using a single metal ion, Ni^{2+} , partially complexed by a variety of ligands, and measuring the exchange rate of the attached water molecules. Four nickel complexes with iminodiacetate, methyl iminodiacetate, ethyl iminodiacetate, and nitrilotriacetate have now been studied. The nitrilotriacetate shows two separate water-exchange rates differing by about a factor of 60 and corresponding to the two different waters present. The iminodiacetate also shows two different water-exchange rates, but differing by only a factor of about 3. The methyl and ethyl iminodiacetates each show only a single water-exchange rate. These wholly unexpected results for the last two species seem best explained by two concurrent events: (1) a rapid Bailar-twist process in which the two different

kinds of water are made "equivalent," along with (2) a slower rate of exchange from one of the positions into the solvent. The possibility then arises that with iminodiacetate the two apparent water-exchange rates are in reality the Bailar-twist rate and exchange from just one of the water positions.

1983 PUBLICATIONS AND REPORTS

Refereed Journals

1. R.E. Connick and B.J. Alder, "Computer Modeling of Rare Solvent Exchange," *J. Phys. Chem.* **87**, 2764 (1983).[†]

Invited Talks

2. R.E. Connick, "The Use of Nuclear Magnetic Resonance to Follow Exchange Reactions," University of Geneva, Switzerland, August 25, 1983; University of Neuchatel, Switzerland, August 22, 1983.
3. R.E. Connick, "The Mechanism of the Chain Reaction Between Bisulfite Ion and Oxygen," University of Neuchatel, Switzerland, August 24, 1983.
4. R.E. Connick, "NMR Studies of Water and Other Ligand Exchange on Partially Complexed Nickelous Ion," University of Neuchatel, Switzerland, August 23, 1983.
5. R.E. Connick, "Computer Simulation of Ligand Exchange from Metal Ions in Solution," University of Geneva, Switzerland, August 26, 1983.

[†]Supported in part by Lawrence Livermore National Laboratory.

Catalytic Hydrogenation of CO*

Gabor S. Somorjai and Alexis T. Bell, Investigators

INTRODUCTION

The purpose of this program is to develop an understanding of the fundamental processes involved in catalytic conversion of carbon monoxide and hydrogen to gaseous and liquid fuels. Attention is focused on defining the factors which limit catalyst activity, selectivity, and resistance to poisoning, and the relationship between catalyst composition/structure and performance. To meet these objectives, a variety of surface diagnostic techniques are used to characterize supported and unsupported catalysts before, during, and after reactions. These techniques include low-energy electron diffraction (LEED), Auger electron spectroscopy (AES), x-ray photoelectron spectroscopy (XPS), electron-energy-loss spectroscopy (EELS), infrared spectroscopy (IRS), and temperature-programmed desorption (TPD). The information thus obtained is combined with detailed studies of reaction kinetics to elucidate reaction mechanisms and the influence of modifications in catalyst composition and/or structure on the elementary reactions involved in carbon monoxide hydrogenation.

1. The Effect of Potassium on the Chemisorption of Carbon Monoxide on the Rh(111) Crystal Face (Publication 1)

J.E. Crowell and G.A. Somorjai

The adsorption of CO on the clean and potassium-predosed Rh(111) crystal surface has been studied using TPD and high-resolution EELS (HREELS). When 10% of a potassium monolayer is preadsorbed, the thermal desorption spectrum of CO broadens in temperatures by 100 K. In the presence of 10–36% of a coadsorbed potassium monolayer, two new high-temperature desorption maxima develop because of dissociation of CO. The CO-stretching vibrations decrease continuously with either increasing potassium coverage or decreasing

CO coverage. Substantial population shifts in site occupancy from the atop to the bridge sites occur as a function of increasing potassium coverage. The results indicate both strengthening of the M-C bond and weakening and breaking of the C-O bond in the presence of potassium, presumably because of increased electron occupancy of the $2\pi^*$ orbital of CO. Broadening and asymmetry of the vibrational peaks suggest that the proximity of the CO molecules to the potassium adatoms influences the chemisorption behavior, although nonlocal interactions are also indicated.

2. Studies of the Coverage of Ruthenium by Carbon and Hydrogen Adspecies During CO Hydrogenation (Publication 11)

P. Winslow and A.T. Bell

Isotopic-tracer techniques have been used to identify the coverages of adsorbed CO, carbon, and hydrogen on the surface of a Ru-black catalyst during CO hydrogenation. The coverage by adsorbed CO is close to a monolayer. Two forms of carbon are identified, C_α and C_β , which differ in the dynamics of their formation and conversion to hydrocarbons. C_α is more reactive than C_β and is the principal intermediate in the synthesis of methane and C_2^+ hydrocarbons. C_β accumulates continuously during the reaction but does not strongly inhibit the adsorption of CO or hydrogen. A remarkable finding is that under reaction conditions a monolayer of hydrogen is adsorbed on the Ru surface. Additional hydrogen is found to be associated with the C_β form of carbon.

3. ^{13}C Nuclear-magnetic-resonance (NMR) Spectra of Carbonaceous Deposits on Silica-supported Ruthenium Catalysts (Publication 3)

T.M. Duncan, P. Winslow, and A.T. Bell

^{13}C -NMR spectroscopy has been used to characterize the carbonaceous species deposited on a silica-supported ruthenium catalyst during methanation. The NMR spectra reveal the presence of at least three forms of nonoxygenated carbon. These forms are interpreted to be multiple-coordinated carbides on ruthenium, reactive carbon bonded to silicon, and unreactive aggregates of carbon. Although the indi-

*This work was supported by the Director, Office of Energy Research, Office of Basic Energy Sciences, Chemical Sciences Division of the U.S. Department of Energy under Contract No. DE-AC03-76SF00098.

vidual spectra of the species overlap, the features may be separated by NMR techniques that differentiate on the basis of spin-lattice and spin-spin relaxation times. Thus, with the results of this preliminary study, it is demonstrated that ^{13}C -NMR spectroscopy allows one to characterize and quantify carbon intermediates on heterogeneous catalysts.

4. An XPS Study of Metal-support Interactions on Pd/SiO₂ and Pd/La₂O₃ (Publication 8)

T.H. Fleisch, R.F. Hicks, and A.T. Bell

The activity of Pd/La₂O₃ is unusually high compared to Pd supported on other metal oxides. This is believed to be due to interactions between the metal and the support. In this investigation the electronic properties of palladium supported on SiO₂ and La₂O₃ were examined by XPS. Spectra were collected after each stage of catalyst preparation: deposition of the palladium chloride precursor, oxidation in air at 623 K, and reduction in H₂ at 573 K. The Pd-3d_{5/2} binding energies recorded following precursor deposition and oxidation were the same on both catalysts. However, after reduction the Pd-3d_{5/2} binding energies of the Pd/La₂O₃ samples shifted below the corresponding values for metallic Pd, while the Pd-3d_{5/2} binding energies of the Pd/SiO₂ samples did not. Furthermore, the binding energies for the Pd/La₂O₃ samples decreased with increasing metal loading, with the largest Pd particles apparently exhibiting the greatest interaction. A maximum shift of -0.7 eV relative to bulk-Pd foil was observed for 8.8% Pd/La₂O₃. This binding-energy shift is interpreted as arising from a change in the chemical state of Pd, i.e., that Pd supported on La₂O₃ is more electronegative than zero-valent Pd alone. A model is proposed which suggests that a thin covering of the La₂O₃ support lies on a portion of the Pd surface. This covering is partially reduced during H₂ treatment at 573 K, and because of the electropositive nature of La, the additional charge is distributed among the surface Pd atoms. It should be noted that the La₂O₃-support surface after H₂ reduction was a complex mixture of La(OH)₃, LaO(OH), La₂O₃, and La₂(CO₃)₃. The exact composition of the support depended strongly on the reduction temperature and the amount of Pd deposited.

5. Influence of Adsorption and Mass-transfer Effects on Temperature-programmed Desorption (TPD) from Porous Catalysts (Publication 6)

J.S. Rieck and A.T. Bell

TPD spectroscopy is an effective technique for probing the influence of metal-support interactions on the strength of adsorption of H₂ and CO on supported-metal catalysts. The aim of this study is to identify the influence of adsorption and mass-transfer effects on the determination of activation energies and preexponential factors for desorption from a bed of catalyst perfused by a flow of carrier gas. The bed is modeled either as a single stirred-tank reactor or as multiple stirred-tank reactors connected in series. The number of stirred-tank reactors required is governed by the product of Schmidt and Reynold's numbers, ScRe. The model developed in this paper is used to calculate TPD spectra for the desorption of CO and H₂ from the surface of a Group VIII metal. It is established that the position and shape of the spectra are sensitive functions of catalyst-particle size, catalyst-bed depth, carrier-flow rate, and carrier-gas composition. The effects of nonuniformities in the initial distribution of adsorbate are also examined. For small particle diameters such nonuniformities are rapidly annealed by intraparticle diffusion and as a consequence have little effect on the shape or position of the TPD spectrum. For larger particle diameters distortions of the spectrum due to nonuniform-adsorbate distribution are expected. The theoretically generated TPD spectra are used to evaluate the applicability of a relationship developed for describing equilibrium desorption in the absence of mass-transfer effects. Reasonably accurate estimates of the enthalpy of adsorption can be obtained from this relationship, but its use to determine the preexponential factor for desorption produces large errors when significant mass-transfer effects are present.

6. Work in Progress

Studies of the combined reactions of CO, H₂, and N₂ to produce amines using rhenium and iron catalysts are in progress. Molybdenum and

molybdenum compounds are being tested as catalysts for the hydrogenation of CO in a combined catalytic and XPS study. The CO/H₂ reaction on palladium foils is being explored. (Directed by G.A. Somorjai.)

The synthesis of methanol and ethanol over rare-earth oxide-supported rhodium is being studied. The interactions of CO with rhodium and palladium supported on SiO₂, Al₂O₃, MgO, TiO₂, and La₂O₃ are being investigated using TPD and Fourier-transform infrared spectroscopy (FTIR). The structure and concentration of carbonaceous species presented on ruthenium catalysts is being investigated using isotopic-tracer techniques and ¹³C and ²D solid-state NMR. (Directed by A.T. Bell.)

1983 PUBLICATIONS AND REPORTS

Refereed Journals

1. L.H. Dubois and G.A. Somorjai, comments on "Why CO₂ Does not Dissociate on Rh at Low Temperature," by W.H. Weinberg, *Surf. Sci.* **128** (2/3), L231-L235 (1983); LBL-17178.
2. A.A. Chin and A.T. Bell, "Kinetics of H₂ Desorption from Silica-supported Rhodium," *J. Phys. Chem.* **87**, 3482 (1983).[†]
3. T.M. Duncan, P. Winslow, and A.T. Bell, "¹³C NMR Spectra of Carbonaceous Deposits on Silica-supported Ruthenium Catalysts," *Chem. Phys. Lett.* **102**, 163 (1983).[‡]

LBL Reports

4. J.E. Crowell and G.A. Somorjai, "The Coadsorption of CO and K on Rh(111): An HREELS, TPD, AES, and LEED Study," Summary Abstract for the American Vacuum Society 30th National Vacuum Symposium, Boston, Massachusetts, November 1-4, 1983; accepted by *J. Vac. Sci. and Tech.*, LBL-16691.
5. J.E. Crowell and G.A. Somorjai, "The Effect of Potassium on the Chemisorption of Carbon Monoxide on the Rh(111) Crystal Face," accepted by *Appl. Surf. Sci.*, LBL-16984.
6. J.S. Rieck and A.T. Bell, "Influence of Adsorption and Mass Transfer Effects on Temperature Programmed Desorption from Porous Catalysts," submitted to *J. Catal.*, LBL-16071.
7. P. Winslow and A.T. Bell, "Application of Transient Response Techniques for Quantitative Determination of Adsorbed Carbon Monoxide and Carbon Present on the Surface

of a Ruthenium Catalyst During Fischer-Tropsch Synthesis," submitted to *J. Catal.* LBL-16265.

8. T.H. Fleisch, R.F. Hicks, and A.T. Bell, "Characterization of Pd/SiO₂ and Pd/La₂O₃ Methanol Synthesis Catalysts by X-ray Photoelectron Spectroscopy," submitted to *J. Catal.*, LBL-16570.
9. A.T. Bell, "Fourier-transform Infrared Spectroscopy in Heterogeneous Catalysis," submitted to *Adv. in Chem.*, LBL-16621.
10. R.F. Hicks, Q.J. Yen, T.H. Fleisch, and A.T. Bell, "The Chemical State and Structure of Palladium Supported on Lanthanum Oxide," submitted to *Appl. Surface Sci.*, LBL-16757.
11. P. Winslow and A.T. Bell, "Studies of the Surface Coverage of Ruthenium by Carbon and Hydrogen Adspecies During CO Hydrogenation," submitted to *Proc. 8th Int. Congress on Catalysis*, LBL-17199.

Invited Talks

12. M.A. Logan, P.R. Watson, and G.A. Somorjai, "Hydrogenation of CO Catalyzed by Rhodium and Rhodium-containing Compounds," California Catalysis Society Spring Meeting 1983, Claremont Hotel, Berkeley, California, March 17, 1983.
13. M.A. Logan and G.A. Somorjai, "Catalytic Hydrogenation of Carbon Monoxide by Rhodium and Rhodium-containing Compounds," American Chemical Society, Seattle, Washington, March 22, 1983.
14. G.A. Somorjai, "Surface Science Approach to New Catalytic Processes for Energy Conversion," The Lemieux Lectures 1983, University of Ottawa, Ottawa, Ontario, May 4, 1983.
15. G.A. Somorjai, "Catalysis for Energy Conversion," University of Lausanne, Switzerland, September 16, 1983.
16. G.A. Somorjai, "Selective Catalysis of the Hydrogenation of Carbon Monoxide. The Building of New Catalysts," Royal Society Centenary Lectures, Egham, England, October 31, 1983; Royal Society Centenary Lectures, Southampton, England, November 2, 1983.
17. A.T. Bell, "Applications of *In Situ* Infrared Spectroscopy to Studies of Catalyzed Reactions," Department of Chemistry, University of California, Riverside, California, January 1983.
18. A.T. Bell, "Theoretical and Experimental Studies of Temperature Programmed Desorption from Supported Metal Catalysts," W.R. Grace & Co., Columbia, Maryland, January 1983;

- Exxon Research & Engineering, Linden, New Jersey, February 1983; Department of Chemical Engineering, University of Delaware, Newark, Delaware, February 1983; California Catalysis Society, Berkeley, California, March 1983.
19. A.T. Bell, "Methanol Synthesis Over Group VIII Metals," Chemistry and Geochemistry Department, Colorado School of Mines, Boulder, Colorado, February 1983.
 20. A.T. Bell, "Effects of Metal-support Interactions on Methanol Synthesis Over Palladium," Frontiers in Catalysis, California Institute of Technology, Pasadena, California, March 1983; Department of Chemical Engineering, Brigham Young University, Provo, Utah, April 1983; 1983 International Conference on Coal Science, Pittsburgh, Pennsylvania, August 1983.
 21. A.T. Bell, "The Role of CH_x ($x = 1-3$) Species in Fischer-Tropsch Synthesis," 185th American Chemical Society National Meeting, Seattle, Washington, March 1983.
 22. A.T. Bell, "Detection of Reactive Intermediates Formed During Fischer-Tropsch Synthesis," 185th American Chemical Society National Meeting, Seattle, Washington, March 1983.
 23. A.T. Bell, "Identification and Quantification of Intermediates Formed During Fischer-Tropsch Synthesis Over Ruthenium Catalysts," Department of Chemical Engineering, University of Washington, Seattle, May 1983.
 24. A.T. Bell, "*In Situ* Studies of Catalyzed Reactions by Transmission FTIR," ACS Summer Symposium on Analytical Chemistry, Lincoln, Nebraska, June 1983.
 25. A.T. Bell, "Modification of the Physical, Chemical, and Catalytic Properties of Palladium as a Consequence of Metal-support Interactions," Gordon Conference on Catalysis, New London, New Hampshire, June 1983.
 26. A.T. Bell, "Reaction Mechanisms in Fischer-Tropsch Synthesis," Canadian Workshop on Fischer-Tropsch Synthesis, Queens University, Kingston, Ontario, July 1983.
 27. A.T. Bell, "Methanol Synthesis Over Supported Palladium Catalysts," Eastman Kodak Company, Rochester, New York, July 1983.
 28. A.T. Bell, "Fourier Transform Infrared Spectroscopy in Heterogeneous Catalysis," 6th International Institute in Surface Science, University of Wisconsin, Milwaukee, August 1983.
 29. A.T. Bell, "Mechanistic Studies of Fischer-Tropsch Synthesis Over Ru Catalysts," Department of Chemical Engineering, University of Houston, Houston, Texas, September 1983; Exxon Research Laboratories, Baton Rouge, Louisiana, September 1983.
 30. A.T. Bell, "The Chemical State and Structure of Lanthana-supported Palladium," 1983 Materials Research Society Meeting, Boston, Massachusetts, November 1983.
 31. A.T. Bell, "Applications of FTIR Spectroscopy to Studies of Catalyzed Reactions," IBM Research Laboratories, San Jose, California, November 1983.
 32. A.T. Bell, "Applications of Various Spectroscopic Techniques to Characterization of Supported-metal Catalysts," Department of Physics, University of California Berkeley, December 1983.

[†]Supported in part by the National Science Foundation.

^{*}Supported in part by Bell Laboratories.

Organometallic Chemistry of Coal Conversion*

K. Peter C. Vollhardt, Investigator

INTRODUCTION

The basic program objective is to apply organometallic processes and techniques to the solution of problems concerned with the conversion of coal and coal-related molecules to liquid and gaseous fuels. The potential of novel organometallic systems as catalysts is being explored.

A new method of constructing fulvalene complexes has allowed the exploitation of unprecedented binuclear chemistry of homo- and heteronuclear transition-metal derivatives. Several of these compounds have shown novel and distinct chemistry of relevance to catalysis and photochemical storage cycles. These systems are being investigated as potential models in heterogeneous Fischer-Tropsch polymerization, particularly as mimics of carbon-carbon and carbon-hydrogen bond-breaking and bond-making processes on surfaces. The preparation and isolation of soluble, defined molecular systems has allowed structural and mechanistic information to be assembled in unprecedented detail.

1. Synthesis, Structure, and Photochemistry of Fulvalene Diruthenium Tetracarbonyl. Thermally Reversible Photoisomerization Involving Carbon-carbon Bond Activation at a Dimetal Center (Publication 2)

K. Peter C. Vollhardt and Timothy W. Weidman

The synthesis of several new fulvalene dimetal complexes has been accomplished by direct reaction of dihydrofulvalene with metal carbonyls. The x-ray structure of $\eta^5:\eta^5$ -fulvalene diruthenium tetracarbonyl exhibits a bent π -ligand with a Ru-Ru bond length of 2.821(1) Å and four terminally bound carbonyl ligands. The complex undergoes a variety of substitution reactions. Upon irradiation at 350 nm, it rearranges via cleavage of the Ru-Ru and carbon-carbon single bond to form an isomeric $\eta^1:\eta^5$ - C_5H_4 bridged complex (see Figure 1-1). Upon heating, this species reverts to the starting material. Crossover experiments verify the intramolecularity of both the photochemical and thermal isomerizations (see Figure 1-1).

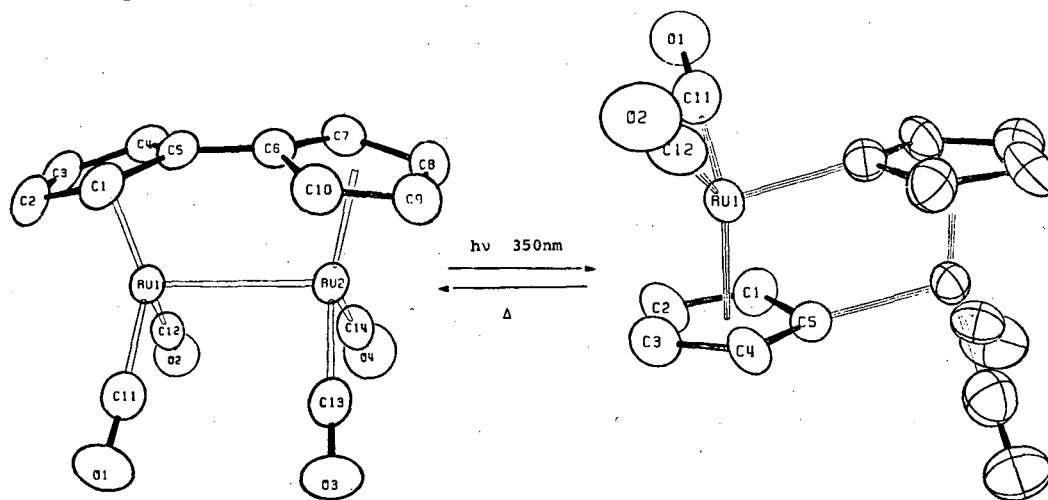


Figure 1-1. The thermally reversible photochemical rearrangement of fulvalene diruthenium tetracarbonyl. (XBL 8312-2556)

*This work was supported by the Director, Office of Energy Research, Office of Basic Energy Sciences, Chemical Sciences Division of the U.S. Department of Energy under Contract No. DE-AC03-76SF00098.

2. Efficient Syntheses of New Fulvalene Bridged Carbonyl Complexes of Cobalt, Ruthenium, Chromium, Molybdenum, and Tungsten (Publication 5)

K. Peter C. Vollhardt and Timothy W. Weidman

A variety of new dimetallafulvalene carbonyl complexes have been prepared by slow addition of cold purified dihydrofulvalene in heptane to boiling solutions of metal carbonyls. Reaction of $\text{Co}_2(\text{CO})_8$ with dihydrofulvalene allows efficient preparation of $(\eta^5:\eta^5\text{-C}_{10}\text{H}_8)(\text{CO})_4\text{Co}_2$. $\text{Ru}_3(\text{CO})_{12}$, $\text{Mo}(\text{CO})_6$, $\text{Cr}(\text{NCEt})_3(\text{CO})_3$, and $\text{W}(\text{NCEt})_3(\text{CO})_3$ react to form the intramolecularly metal-metal-bonded complexes $(\eta^5:\eta^5\text{-C}_{10}\text{H}_8)(\text{CO})_4\text{Ru}_2$ and $(\eta^5:\eta^5\text{-C}_{10}\text{H}_8)(\text{CO})_6\text{M}_2$ ($\text{M} = \text{Cr}, \text{Mo}, \text{ and } \text{W}$). Attempts to generate the analogous iron complex were unsuccessful. Reaction of a mixture of $\text{Ru}_3(\text{CO})_{12}$ and $\text{Mo}(\text{CO})_6$ with dihydrofulvalene affords a better than statistical yield of the mixed metal-metal-bonded complex $(\eta^5:\eta^5\text{-C}_{10}\text{H}_8)(\text{CO})_5\text{MoRu}$.

3. Elemental Sulfur and Selenium Induced Intramolecular Carbyne-carbyne Coupling in Trinuclear Bis(carbyne) Cobalt Clusters. A Novel Entry Into Metalladithiolenes and Metalladiselenolenes (Publication 4)[†]

K. Peter C. Vollhardt and Eric C. Walborsky

$[\mu_3\eta^1\text{-CR}^1][\mu_3\eta^1\text{-CR}^2][\text{CpCo}]_3$ clusters 1 ($\text{Cp} = \eta^5\text{-C}_5\text{H}_5$) react with sulfur and selenium to furnish metalladithio- and selenolenes derived by intramolecular carbyne-carbyne coupling, as shown by crossover experiments (see Figure 3-1). A plausible model for the initial step of this cluster degradation is obtained by edge-thiomethylation of 1 ($\text{R}^1 = \text{R}^2 = n\text{-Bu}$), resulting in a salt characterized by x-ray analysis. CpM-dichalcogenolenes undergo CpM exchange, but not Cp or alkyne transfer, as proven by crossover studies involving, respectively, MeC_5H_4 , Cp, Co, Rh, S, Se, and $\text{R}^1 = \text{R}^2 = n\text{-Bu}$ or C_6H_5 , in various permutations.

[†]Supported in part by equipment funds of the National Science Foundation.

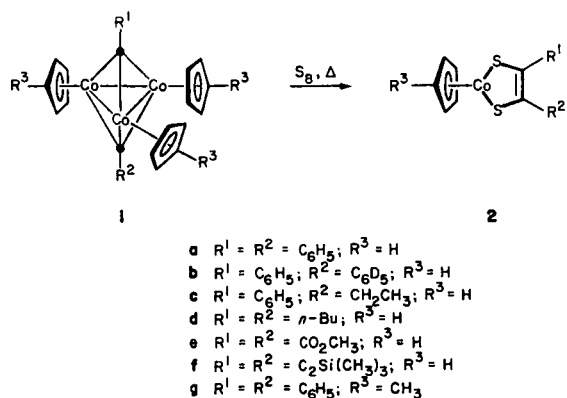


Figure 3-1. The degradation of trinuclear cobalt biscarbyne complexes to metalladithiolenes. (XBL 8312-2557)

4. Work in Progress

The photoisomer of fulvalene diruthenium tetracarbonyl has been shown to undergo novel solid- and solution-phase photochemical transformations. Several fulvalene metal-carbonyl complexes have been investigated with respect to photochemical and thermal activation. Unprecedented photosubstitution chemistry has been observed. Fulvalene dimolybdenum hexacarbonyl has been converted to a Fischer-carbene carbonyl complex, the first Fischer carbene to exhibit fluxional character. The thermal degradation of this complex has revealed novel pathways by which hydrocarbons can be extruded from dinuclear metal systems. It has also led to the recognition of new surface chemical mechanisms involving hydrocarbon formation and rearrangements.

1983 PUBLICATIONS AND REPORTS

Refereed Journals

1. N.T. Allison, J.R. Fritch, K.P.C. Vollhardt, and E.C. Walborsky, "An Unprecedented Biscarbyne Cluster Rearrangement Involving Simultaneous Coupling and Decoupling of Carbyne Fragments: A New Homogeneous Model for C-C Bond-forming and Bond-breaking on Surfaces," *J. Am. Chem. Soc.* **105**, 1384 (1983); LBL-15414.

2. K.P.C. Vollhardt and T.W. Weidman, "Synthesis, Structure, and Photochemistry of Fulvalene Diruthenium Tetracarbonyl. Thermally Reversible Photoisomerization Involving Carbon-carbon Bond Activation at a Dimetal Center," *J. Am. Chem. Soc.* **105**, 1676 (1983); LBL-15541.
3. J.A. King, Jr. and K.P.C. Vollhardt, "Vinyl Hydrogen Activation in Mono- and Dinuclear η^5 -C₅H₅-Hexatriene Cobalt Complexes, Thermal and Photochemical Hydrogen Shifts of Complementary Stereochemistry," *J. Am. Chem. Soc.* **105**, 4846 (1983); LBL-16374.[†]
4. K.P.C. Vollhardt and E.C. Walborsky, "Elemental Sulfur Induced Intramolecular Carbyne-carbyne Coupling in Trinuclear Bis(carbyne) Cobalt Clusters. A Novel Entry into Metalladithiolenes and Metalladiselenolenes," *J. Am. Chem. Soc.* **105**, 5507 (1983); LBL-16375.[‡]

LBL Reports

5. K.P.C. Vollhardt and T.W. Weidman, "Efficient Syntheses of New Fulvalene Bridged Carbonyl Complexes of Cobalt, Ruthenium, Chromium, Molybdenum, and Tungsten," *Organometallics*, in press, LBL-17005.
6. G.A. Ville, K.P.C. Vollhardt, and M.J. Winter, "Thermally Induced Diastereoisomerization of Cyclobutadiene Cobalt Complexes as a Probe for the Reversibility of Their Formation From Complexed Alkynes," submitted to *Organometallics*, LBL-17006.[§]
7. J.S. Drage, M. Tilset, K.P.C. Vollhardt, and T.W. Weidman, "First Photosubstitution of Fulvalene-bridged Metal-metal Bonded Carbonyls. Synthesis and Structural Determination of Novel Homo- and Heterobimetallic Alkyne Complexes," submitted to *Organometallics*, LBL-17007.

Invited Talks

8. K.P.C. Vollhardt, "Remarkable Rearrangements in the Coordination Sphere of Transition Metals," Plenary Lecturer, 185th ACS National

Meeting, Seattle, Washington, March 20-25, 1983.

9. K.P.C. Vollhardt, "Nonbiomimetic Transition Metal Mediated Approaches to the Total Synthesis of Steroids," Adolf Windaus Medal Lecturer, University of Göttingen, West Germany, June 3, 1983.
10. K.P.C. Vollhardt, "Transition Metal Mediated [2+2+2]Cycloadditions: A Better Version of the Diels-Alder Reaction," Plenary Lecturer, 19th IUPAC Congress, Cologne, West Germany, June 5-10, 1983.
11. K.P.C. Vollhardt, "The Remarkable Chemistry of Biscarbyne Cobalt and Fulvalene Diruthenium Complexes," University of Hamburg, West Germany, June 10, 1983.
12. K.P.C. Vollhardt, "Transition Metal Mediated Approaches to the Total Synthesis of Natural Products," University of Paderborn, West Germany, June 13, 1983.
13. K.P.C. Vollhardt, "Excessively Unhappy Hydrocarbons," University of Erlangen-Nuremberg, West Germany, June 14, 1983.
14. K.P.C. Vollhardt, "Cobalt Mediated Total Synthesis of Steroids," University of Hawaii, Honolulu, August 3, 1983; Plenary Lecturer, 2nd Annual Esther Humphrey Symposium, University of Vermont, September 30-October 1, 1983; Plenary Lecturer, 1983 Fall Symposium, Northwestern University, Evanston, Illinois, November 4, 1983; ACS-Corpus Christi Section, Texas, November 9, 1983; and John E. Mahler Lectureship, University of Texas at Austin, November 11, 1983.
15. K.P.C. Vollhardt, "Remarkable Organometallic Rearrangements," Texas A & M University, College Station, Texas, November 10, 1983; University of California, Davis, December 1, 1983.

[†]Supported in part by a postdoctoral student stipend of the National Science Foundation.

[‡]Supported in part by equipment funds of the National Science Foundation.

[§]Supported in part by a partial summer salary provided by the National Science Foundation.

Synthetic and Physical Chemistry*

William L. Jolly, Investigator

INTRODUCTION

The purpose of this project is to use photoelectron spectroscopy to determine the nature of the bonding in significant inorganic and organometallic compounds. By measuring core-electron binding energies of appropriate transition-metal compounds, it is possible to study the interaction of metal d electrons with various ligands and to identify various modes of ligand-metal bonding that have analogues in the intermediates of catalyzed organic reactions. Core binding energies can also be used in conjunction with valence shell ionization potentials to quantify the bonding or antibonding character of molecular orbitals.

1. The Partnership of Gas-phase Core and Valence Photoelectron Spectroscopy (Publication 8)

William L. Jolly

This review article summarizes the theoretical background of the method of using core-electron binding energies to correct shifts in valence-electron ionization potential for the effects of potential and relaxation energy. The article describes applications of this method to a wide variety of compounds in which the bonding or antibonding character of molecular orbitals is quantified. The review effectively summarizes the current research effort of this group.

2. The Use of Core Binding Energies in the Assignment of the Ultraviolet Photoelectron Spectra of the Manganese Pentacarbonyl Halides (Publication 1)

William L. Jolly

The ultraviolet photoelectron spectra of the manganese pentacarbonyl halides, $\text{Mn}(\text{CO})_5\text{X}$, have received considerable attention. However, at least three assignments have been proposed for the first four bands of each spectrum, and until recently there was no consensus regarding the assignment. By using core binding energy data to correct for the effects of potential (atomic charges) and relaxation energy, one can largely resolve the ambiguities in the assignment of the first four bands in the spectra.

3. A Gas-phase X-ray Photoelectron Spectroscopy (XPS) Study of Iron Cluster Compounds (Publication 2)

David B. Beach, James L. Hoskins, William L. Jolly, Steven P. Smit, and Si Fen Xiang

Because of current interest in the function of iron clusters in catalytic systems and biological electron carriers, we have investigated the nature of the bonding in the following iron-cluster complexes using gas-phase XPS: $\text{Fe}_2\text{C}_4\text{H}_4(\text{CO})_6$, $\text{Fe}_2\text{S}_2(\text{CO})_6$, $\text{Fe}_2(\text{SCH}_3)_2(\text{CO})_6$, $\text{FeCo}_3(\text{CO})_{12}\text{H}$, $\text{Fe}_3(\text{CO})_{12}$, $\text{C}_4\text{H}_6\text{Fe}(\text{CO})_3$, and $(\text{CH}_2)_3\text{CFe}(\text{CO})_3$. The iron atoms in $\text{Fe}_2\text{C}_4\text{H}_4(\text{CO})_6$ have structurally different environments and might be expected to have quite different charges. However, the iron core binding energies were found to be essentially identical, a result which suggests that the compound is best

*This work was supported by the Director, Office of Energy Research, Office of Basic Energy Sciences, Chemical Sciences Division of the U.S. Department of Energy under Contract No. DE-AC03-76SF00098.

looked upon as a cluster complex in which the $\text{Fe}(\text{CO})_3$ groups provide two cluster electrons each. The binding-energy data of the other compounds can be rationalized in terms of their structures and the electronegativities and polarizabilities of the groups.

4. Lone-pair and Core Ionization Potentials of Planar Ammonia and Phosphine. The Use of Core and Valence Ionization Potentials to Quantify the Bonding and Antibonding Character of Molecular Orbitals of Compounds of Nitrogen and Phosphorus (Publication 3)

Charles J. Eyermann and William L. Jolly

For both ammonia and phosphine, the differences between the ionization potentials of the pyramidal and planar forms were calculated by an *ab initio* SCF method. The lone-pair ionization-potential differences, $\text{IP}(\text{planar})-\text{IP}(\text{pyramidal})$, are -1.0 and -2.3 eV for NH_3 and PH_3 , respectively. The core binding-energy shifts, $E_B(\text{planar})-E_B(\text{pyramidal})$, are -0.3 and -0.4 eV for NH_3 and PH_3 , respectively. By combining these data with appropriate experimental valence and core ionization potentials, it is possible to quantify the bonding or antibonding character of molecular orbitals of nitrogen and phosphorus compounds. The method is illustrated by using data for several nitrogen- and phosphorus-containing species.

5. Lone-pair/Lone-pair Repulsion in the Halogen Molecules (Publication 4)

William L. Jolly and Charles J. Eyermann

A simple molecular-orbital treatment of the diatomic homonuclear halogens, in which the overlap integral is ignored when estimating the resonance integral, leads to the conclusion that the antibonding π^* level is raised above the atomic p level as much as the bonding π level is lowered below that level. This result is equivalent to having the eight π electrons of an X_2 molecule occupy four strictly nonbonding lone-pair orbitals. However, if the overlap integral is included in the treatment, it is found that the antibonding level is raised more than the bonding level is lowered, resulting in a net π -antibonding interaction, or "lone-pair/lone-pair repulsion."

By using both core and valence ionization potentials, it is possible to evaluate the ionization potentials that atomic orbitals (in molecules) would have if they were nonbonding. We report the results of applying this method to the data for both the homonuclear and the heteronuclear diatomic halogens. The localized-orbital ionization potentials (LOIPs), the π and π^* ionization potentials, and the differences Δ between the average of the π and π^* ionization potentials and the LOIP values are presented in Table 5-1. A Δ value of zero corresponds to no lone-pair/lone-pair repulsion; a negative value indicates lone-pair/lone-pair repulsion. In the case of the homonuclear molecules, the only Δ value that is definitely negative (with the ± 0.1 -eV uncertainty of the method taken into account) is that of F_2 . We believe that these data constitute the first unequivocal evidence for lone-pair repulsion in F_2 . Other effects may contribute to the weakness of the F-F bond, but clearly lone-pair repulsion is very significant.

Table 5-1
LOIPs, ionization potentials (IP), and Δ values (all in eV) for halogens and interhalogens

Molecule	LOIP	IP(π)	IP(π^*)	Δ
F_2	17.94	18.80	15.84	-0.62
Cl_2	13.12	14.42	11.61	-0.10
Br_2	11.85	12.85	10.68	-0.08
I_2	10.35	11.21	9.51	0.01
ClF	15.09	17.06	12.79	-0.16
ICl	11.56	12.88	10.24	0.0
IBr	10.59	12.09	9.99	0.45

6. Photoelectron Spectroscopic Study of the Bonding in Tetracarbonyl(ethylene)iron (Publication 5)

David B. Beach and William L. Jolly

The iron $2p_{3/2}$, carbon 1s, and oxygen 1s binding energies of gaseous $\text{Fe}(\text{CO})_4\text{C}_2\text{H}_4$ have been measured. Atomic-charge calculations based on binding-

energy shifts indicate that the ethylene group of $\text{Fe}(\text{CO})_4\text{C}_2\text{H}_4$ is negatively charged. Interpretation of the published ultraviolet photoelectron spectroscopy spectrum of $\text{Fe}(\text{CO})_4\text{C}_2\text{H}_4$ with the aid of core binding-energy shifts leads to the following conclusions: (1) There is significant σ interaction between the ethylene ligand and the $\text{Fe}(\text{CO})_4$ group of $\text{Fe}(\text{CO})_4\text{C}_2\text{H}_4$. (2) The energy of the (d_{xy} , $d_{x^2-y^2}$) orbitals of $\text{Fe}(\text{CO})_4\text{C}_2\text{H}_4$ is affected by the two equatorial CO ligands and the ethylene ligand to the same extent that the energy of the (d_{xy} , $d_{x^2-y^2}$) orbitals of $\text{Fe}(\text{CO})_5$ is affected by three equatorial CO ligands. (3) The total back-bonding of the (d_{xz} , d_{yz}) orbitals of $\text{Fe}(\text{CO})_4\text{C}_2\text{H}_4$ is less than that of $\text{Fe}(\text{CO})_5$, as expected from the orthogonality of these orbitals and the π^* orbital of coordinated C_2H_4 in $\text{Fe}(\text{CO})_4\text{C}_2\text{H}_4$.

7. Study of Hyperconjugation in Trifluoramine Oxide and Related Molecules Using Core and Valence Ionization Potentials (Publication 6)

C.J. Eyermann, W.L. Jolly, S.F. Xiang, J.M. Shreeve, and S.A. Kinkad

The oxygen, nitrogen, and fluorine core binding energies of ONF_3 have been redetermined. The data indicate strong hyperconjugation, with N-O π bonding and weak N-F σ bonding. The core and valence ionization potentials together indicate that the highest occupied molecular orbital of ONF_3 (derived mainly from the O $p\pi$ orbitals) is weakly antibonding. This result is consistent with other data if it is assumed that the latter orbital has considerable fluorine lone-pair character and that the orbital derived mainly from the N-F σ orbitals (at lower energy) has considerable N-O π character. The core and valence ionization potentials of OPF_3 and OPCl_3 indicate that the oxygen "lone-pair" orbitals of these molecules are at lower energies than the corresponding hypothetical nonbonding oxygen p orbitals. These results imply significant participation of phosphorus $3d\pi$ orbitals in the P-O bonds.

8. Analysis of $p\pi \rightarrow d\pi$ Bonding in Halogen Compounds of Silicon, Germanium, and Tin (Publication 7)

William L. Jolly

Halogen lone-pair ionization potentials for the main-group IV compounds MX_4 and MH_3Cl are corrected for the effects of potential and relaxation energy using the corresponding halogen core binding energies. The corrected data indicate significant $p\pi \rightarrow d\pi$ bonding in MX_4 (for M = Si, Ge, and Sn), significant repulsion between the lone pairs and CH_3 group in CH_3Cl , and little or no $p\pi \rightarrow d\pi$ bonding in SiH_3Cl and GeH_3Cl .

9. Work in Progress

We have just completed an XPS study of σ and π bonding in iron tetracarbonyl complexes involving the ligands pyridine, trimethyl phosphine, and a variety of substituted olefins. We have also just completed a determination of proton affinities and isocyanide-to-nitrile isomerization energies from core binding energies by use of the equivalent-cores approximation. We are studying N-S π bonding in a variety of sulfur-nitrogen-fluorine compounds derived from NSF and NSF_3 .

1983 PUBLICATIONS AND REPORTS

Refereed Journals

1. W.L. Jolly, "The Use of Core Binding Energies in the Assignment of the Ultraviolet Photoelectron Spectra of the Manganese Pentacarbonyl Halides," *J. Phys. Chem.* **87**, 26 (1983); LBL-15161.
2. D.B. Beach, J.L. Hoskins, W.L. Jolly, S.P. Smit, and S.F. Xiang, "A Gas Phase XPS Study

- of Iron Cluster Compounds," *J. Electron Spectrosc. Relat. Phenom.* **28**, 299 (1983); LBL-14798.
3. C.J. Eyermann and W.L. Jolly, "Lone-pair and Core Ionization Potentials of Planar Ammonia and Phosphine. The Use of Core and Valence Ionization Potentials to Quantify the Bonding and Antibonding Character of Molecular Orbitals of Compounds of Nitrogen and Phosphorus," *J. Phys. Chem.* **87**, 3080 (1983); LBL-14951.
 4. W.L. Jolly and C.J. Eyermann, "Lone-pair-lone-pair Repulsion in the Halogen Molecules," *Inorg. Chem.* **22**, 1566 (1983); LBL-15609.
 5. D.B. Beach and W.L. Jolly, "Photoelectron Spectroscopic Study of the Bonding in Tetracarbonyl(ethylene)iron," *Inorg. Chem.* **22**, 2137 (1983); LBL-15355.
 6. C.J. Eyermann, W.L. Jolly, S.F. Xiang, J.M. Shreeve, and S.A. Kinkead, "Study of Hyperconjugation in Trifluoramine Oxide and Related Molecules using Core and Valence Ionization Potentials," *J. Fluorine Chem.* **23**, 389 (1983); LBL-13972.
 7. W.L. Jolly, "Analysis of $p\pi \rightarrow d\pi$ Bonding in Halogen Compounds of Silicon, Germanium, and Tin," *Chem. Phys. Lett.* **100**, 546 (1983); LBL-16159.

8. W.L. Jolly, "The Partnership of Gas-phase Core and Valence Photoelectron Spectroscopy," *Acc. Chem. Res.* **16**, 370 (1983); LBL-15610.

Invited Talks

9. W.L. Jolly, "The Partnership of Core and Valence Photoelectron Spectroscopy," Chemistry Department, University of Arizona, Tucson, March 8, 1983; Chemistry Department, University of New Mexico, Albuquerque, March 10, 1983; Institut für Anorganische Chemie der Universität Frankfurt, West Germany, April 14, 1983; Instituto di Chimica Generale ed Inorganica, Università di Padova, Italy, April 22, 1983; Physikalisch-Chemisches Institut der Universität Basel, Switzerland, April 28, 1983; Institut für Anorganische and Angewandte Chemie der Universität Hamburg, West Germany, May 2, 1983; Vakgroep Anorganische en Theoretische Chemie, Vrije Universiteit, Amsterdam, Holland, May 4, 1983; Gmelin Institut für Anorganische Chemie, Frankfurt, West Germany, May 9, 1983; Institut de Chimie, Université de Strasbourg, France, May 10, 1983; Chemistry Department, California State University, Los Angeles, October 4, 1983.

Chemistry and Morphology of Coal Liquefaction

Heinz Heinemann, Investigator, with Alexis T. Bell, R.H. Fish, and Gabor A. Somorjai, Investigators

For the complete entry under this title, see "Chemistry and Morphology of Coal Liquefaction" in the Fossil Energy Section of this Annual Report.

Electrochemical Systems*

John Newman, Investigator

INTRODUCTION

This program includes the investigation of fluid-flow and electrochemical transport, the analysis of mass-transfer rates and current distribution, the design of practical electrochemical systems, and the investigation of corrosion processes. Coupled kinetic, mass-transfer, and fluid-flow phenomena are investigated in semiconductor-electrode systems, with emphasis on the optimization of configurational and operating parameters of liquid-junction photovoltaic cells.

1. Mathematical Modeling of Liquid-junction Photovoltaic Cells: I. Governing Equations (Publication 1)

Mark E. Orazem[†] and John Newman

The equations that govern the liquid-junction photovoltaic cell are presented in the context of a one-dimensional mathematical model. This model treats explicitly the semiconductor, the electrolyte, and the semiconductor-electrolyte interface in terms of potentials and concentrations of charged species. The model incorporates macroscopic transport equations in the bulk of the semiconductor and electrolyte coupled with a microscopic model of the semiconductor-electrolyte interface. Homogeneous and heterogeneous recombination of electron-hole pairs is included within the model. Recombination takes place at the semiconductor-electrolyte interface through interfacial sites that can enhance the recombination rate. The coupled nonlinear ordinary differential equations of the model were posed in finite-difference form and solved numerically. The results are presented in the following two abstracts.

[†]Present address: University of Virginia, Charlottesville, Virginia.

*This work was supported by the Director, Office of Energy Research, Office of Basic Energy Sciences, Chemical Sciences Division of the U.S. Department of Energy under Contract No. DE-AC03-76SF00098.

2. Mathematical Modeling of Liquid-junction Photovoltaic Cells: II. Effect of System Parameters on Current-potential Curves (Publication 2)

Mark E. Orazem[†] and John Newman

The one-dimensional mathematical model described above was used to calculate the effect of system variables on the performance of an n-type GaAs semiconducting anode in contact with an 0.8M K₂Se/0.1M K₂Se₂/1.0M KOH electrolytic solution. The performance of the semiconductor electrode is influenced by kinetic limitations to interfacial reactions, dopant concentration, semiconductor thickness, the direction of illumination, and the amount of light absorbed in the semiconductor. An optimal dopant concentration and semiconductor thickness can be calculated for a given system.

[†]Present address: University of Virginia, Charlottesville, Virginia.

3. Mathematical Modeling of Liquid-junction Photovoltaic Cells: III. Optimization of Cell Configurations (Publication 3)

Mark E. Orazem[†] and John Newman

The liquid-junction photovoltaic cell is an electrochemical system with one or two semiconducting electrodes. This system provides a means of converting solar energy to chemical or electrical energy. A one-dimensional mathematical model of the liquid-junction photovoltaic cell has been developed. The one-dimensional model of the liquid-junction cell was coupled with primary-resistance calculations to predict the optimal performance of three cell configurations. Two cells are considered in which the semiconductor is illuminated from the electrolyte side, and one is considered in which the semiconductor is illuminated from the current-collector side. An economic analysis is presented based on these results. The performance of the liquid-junction photovoltaic cell depends on the design, surface area, and placement of the counterelectrode and current collectors.

[†]Present address: University of Virginia, Charlottesville, Virginia.

4. Primary Current Distribution and Resistance of a Slotted-electrode Cell (Publication 4)

Mark E. Orazem[†] and John Newman

The primary-current distribution and resistance of a cell containing a slotted electrode were calculated using numerical methods coupled with the Schwarz-Christoffel transformation. Results are presented and compared to asymptotic solutions. An approximate analytic expression for the cell resistance is presented.

[†]Present address: University of Virginia, Charlottesville, Virginia.

5. Mathematical Modeling and Optimization of Liquid-junction Photovoltaic Cells (Publication 5)

Mark E. Orazem[†]

The liquid-junction photovoltaic cell is an electrochemical system with one or two semiconducting electrodes. This system has been studied since the early 1970s as a means of converting solar energy to chemical or electrical energy. Most of these studies have been oriented toward developing an understanding of the semiconductor electrode.

The design of a liquid-junction photovoltaic cell requires selection of an appropriate semiconductor-electrolyte combination as well as an efficient cell configuration. The selection of a semiconductor is based on the band gap, which provides an upper limit to the conversion efficiency of the device, and the choice of electrolyte is governed by the need to limit corrosion. The objective of this work was to develop a mathematical model of the liquid-junction cell which could predict the effect of design parameters on cell performance. The one-dimensional model of the liquid-junction cell was coupled with primary-resistance calculations to predict the effect of cell design on performance.

[†]Present address: University of Virginia, Charlottesville, Virginia.

6. Activity Coefficients of Electrons and Holes in Semiconductors (Publication 6)

Mark E. Orazem[†] and John Newman

Dilute-solution transport equations with constant activity coefficients are commonly used to model semiconductors. These equations are consistent with a Boltzmann distribution and are invalid in regions where the species concentration is close to the respective site concentration. A more rigorous treatment of transport in a semiconductor requires activity coefficients of electrons and holes in semiconductors. These activity coefficients are functions of concentration and are thermodynamically consistent. The use of activity coefficients in macroscopic-transport relationships allows a description of electron transport in a manner consistent with the Fermi-Dirac distribution.

[†]Present address: University of Virginia, Charlottesville, Virginia.

7. Fundamental Mathematical Principles for Electrochemical Engineering (Publication 8)

John Newman

Principles of current distribution are related to fundamental transport equations. These equations include both mass transfer and applications of potential theory, where the potential distribution satisfies Laplace's equation. It is important to include the potential as a variable, because it is the difference in potential between the electrode and the solution that governs the electrochemical reactions that will occur. Emphasis is also placed on the mathematical techniques used to treat the effects of convective mass transfer and ohmic potential simultaneously.

8. Current Distribution and Cell Design (Publication 9)

John Newman

The motivation and direction for electrochemical engineering are reviewed briefly. The use of comput-

ers in the practical development of mathematical models is outlined and illustrated by examples in the design of molten-salt batteries. The use of the Schwarz-Christoffel transformation is detailed for obtaining the primary resistance of a cell for photoelectrochemical-energy production.

9. Work in Progress

A bench-scale flow-through porous electrode has been designed for the removal of dilute concentrations of mercury from contaminated brine solutions. The porous-electrode reactor, made of reticulated vitreous carbon, has been used not only to demonstrate the efficiency of this method for waste treatment but also to provide accurate data on the mass-transfer behavior of the packed bed. These data will be used to evaluate the scale-up of the process.

Computer models of the behavior of electrochemical systems during cyclic voltammetry have been developed. A comparison of these models with available data for the iodine-iodide-triiodide redox system in propylene carbonate has been made, and the models have been found to predict the behavior accurately in many cases. Future work will focus on improvements of the agreement between theory and experiment.

1983 PUBLICATIONS AND REPORTS

LBL Reports

1. Mark E. Orazem and John Newman, "Mathematical Modeling of Liquid-junction Photovoltaic Cells: I. Governing Equations," submitted to *J. Electrochem. Soc.*, LBL-16210.
2. Mark E. Orazem and John Newman, "Mathematical Modeling of Liquid-junction Photovoltaic Cells: II. Effect of System Parameters on Current-potential Curves," submitted to *J. Electrochem. Soc.*, LBL-16211.
3. Mark E. Orazem and John Newman, "Mathematical Modeling of Liquid-junction Photovoltaic Cells: III. Optimization of Cell Configurations," submitted to *J. Electrochem. Soc.*, LBL-16212.
4. Mark E. Orazem and John Newman, "Primary Current Distribution and Resistance of a Slotted Electrode Cell," submitted to *J. Electrochem. Soc.*, LBL-15494.
5. Mark E. Orazem (Ph.D. Thesis), with John Newman, "Mathematical Modeling and Optimization of Liquid-junction Photovoltaic Cells," LBL-16131.
6. Mark E. Orazem and John Newman, "Activity Coefficients of Electrons and Holes in Semiconductors," submitted to *J. Electrochem. Soc.*, LBL-16786.
7. John Newman, "Design of Photoelectrochemical Energy Conversion Cells," Department of Chemical Engineering Seminar, University of California Davis, Davis, California, May 2, 1983.
8. John Newman, "Fundamental Mathematical Principles for Electrochemical Engineering," invited review for the Symposium on Inorganic Electrosynthesis and Electrochemical Engineering Principles, Denver meeting of the American Institute of Chemical Engineers, August 29, 1983; submitted to the AIChE Symp. Volume, LBL-16785.
9. John Newman, "Current Distribution and Cell Design," invited plenary lecture at the Erlangen, Germany, meeting of the International Society of Electrochemistry, September 22, 1983, Ext. Abstr. (P)IV.4; lecture for Faculty of Technology, Split, Yugoslavia, September 28, 1983.
10. John Newman, "Photoelectrochemical Cells," invited plenary lecture before the Serbian Chemical Society, Belgrade, Yugoslavia, September 27, 1983.

Invited Talks

Surface Chemistry — Application of Coordination Principles*

Earl L. Muetterties, Investigator[†]

INTRODUCTION

The goal of this research program is to compare the coordination chemistry of transition-metal surfaces with that of molecular metal complexes and molecular metal clusters. Displacement reactions supplemented with diffraction and spectroscopic data are used in the elucidation of structural, bonding, and chemical features of the nickel and platinum metal surfaces with chemisorbed molecules. Initial studies are focused on the chemisorption states of aromatic hydrocarbons, olefins, and acetylenes on nickel and platinum surfaces. Catalytic reactions of these molecules will be examined in an ultrahigh-vacuum chamber equipped with an isolation cell. These catalytic reactions will be closely correlated with metal-cluster research to obtain a precise comparison between homogeneous and heterogeneous catalysis. Theoretical analysis, based on symmetry matching of energetically available metal-surface orbitals with those of molecules and molecular fragments of hydrocarbon, have been developed for a further comparison with structural data.

1. Mechanisms of $\text{Re}_2(\text{CO})_{10}$ Substitution Reactions: Crossover Experiments with $^{185}\text{Re}_2(\text{CO})_{10}$ and $^{187}\text{Re}_2(\text{CO})_{10}$ (Publication 2)

A.M. Stolzenberg and E.L. Muetterties

$^{185}\text{Re}_2(\text{CO})_{10}$ and $^{187}\text{Re}_2(\text{CO})_{10}$ were prepared separately and then used in combination in crossover experiments to probe for fragmentation to mononuclear rhenium species in thermal and photochemically initiated substitution reactions. For the $\text{CO-Re}_2(\text{CO})_{10}$ exchange reaction, a reaction separately analyzed for ^{13}CO - ^{12}CO interchange, no crossover was observed at 150°C after 14 half-lives of

reaction (14 hr). Similarly, the thermal-reaction sequences of $\text{Re}_2(\text{CO})_{10} + \text{P}(\text{C}_6\text{H}_5)_3 \rightleftharpoons \text{Re}_2(\text{CO})_9\text{P}(\text{C}_6\text{H}_5)_3 + \text{CO}$ and $\text{Re}_2(\text{CO})_9\text{P}(\text{C}_6\text{H}_5)_3 + \text{P}(\text{C}_6\text{H}_5)_3 \rightleftharpoons \text{Re}_2(\text{CO})_8[\text{P}(\text{C}_6\text{H}_5)_3]_2 + \text{CO}$ were examined at 150°C (maintaining a CO pressure of ~ 560 – 640 mm). No crossover was detectable in either $\text{Re}_2(\text{CO})_{10}$ or $\text{Re}_2(\text{CO})_9\text{P}(\text{C}_6\text{H}_5)_3$ (relative to blank experiments). Hence phosphine substitution reactions proceed without a detectable formation of mononuclear rhenium species. These observations support a CO-dissociative mechanism. A model based on this mechanism can accurately reproduce the mass spectra observed during ^{13}CO - ^{12}CO interchange. In the absence of a CO atmosphere, $^{185}\text{Re}_2(\text{CO})_{10}$ and $^{187}\text{Re}_2(\text{CO})_{10}$ formed ^{185}Re - $^{187}\text{Re}(\text{CO})_{10}$, and this interchange was nearly complete at 150°C within 14–16 half-lives. All photochemically initiated reactions with the two labeled decacarbonyls led to complete crossover within short reaction times. It appears that the primary mode of reaction for $\text{Re}_2(\text{CO})_{10}$ under photolysis conditions involves Re-Re bond scission as an early elementary step. Also, the reversible steps leading to the precursor(s) to $\text{Re}_2(\text{CO})_{10}$ decomposition include scission of the rhenium-rhenium bond.

2. Orientation of Complex Molecules Chemisorbed on Metal — Near-edge X-ray Absorption Studies (Publication 5)

Allen L. Johnson, E.L. Muetterties, and J. Stöhr[†]

Near-edge x-ray-absorption fine-structure (NEX-AFS) spectra for aromatic organic molecules chemisorbed on Pt(111) show a dramatic polarization dependence that arises from dipole-allowed transitions to π^* - and σ^* -symmetry final states. The spectra unambiguously establish the orientation of the ring plane with respect to the surface plane. As expected, at room temperature benzene, toluene, and hexafluorobenzene chemisorb in a plane parallel to the Pt(111) surface plane. Benzonitrile is similarly bound, and the CN-bond vector of the nitrile functional group is either in the C_6 -ring plane or displaced from that plane to a slight degree. Chemisorbed pyridine, in contrast, is in a plane perpendicular to the surface plane. Pt(111) toluene, when heated to the first region of thermal decomposition, generates tolyl surface species, either $\text{C}_6\text{H}_5\text{CH}$ or $\text{C}_6\text{H}_5\text{C}$, in which the C_6 -ring plane is perpendicular to, or tipped substantially from, the Pt(111)-surface plane. These studies demonstrate the utility of

*This work was supported by the Director, Office of Energy Research, Office of Basic Energy Sciences, Chemical Sciences Division of the U.S. Department of Energy under Contract No. DE-AC03-76SF00098.

[†]Dr. Muetterties died in January 1984. This report has been prepared by T.M. Gentle.

NEXAFS as a general structural probe for chemisorbed molecules and for surface "intermediates" generated from such molecules, in particular in the presence of π orbitals.

[†]Present address: Corporate Research Science Laboratories, Exxon Research and Engineering Corp., Linden, New Jersey 07036.

3. Catalytic Chemistry of Palladium Surfaces under Ultrahigh-vacuum Conditions (Publication 4)

T.M. Gentle, V.H. Grassian, D.G. Klarup, and E.L. Muetterties

Catalytic reactions of hydrocarbons on clean transition-metal surface planes are not typically observed under ultrahigh-vacuum conditions. However, catalytic-hydrocarbon reactions have now been observed for the clean low-Miller-index planes of palladium. Catalytic reactions described are the hydrogenation of alkynes, alkenes, and arenes, as well as the hydrogenation of nitriles to amines. Also observed was catalytic hydrosilylation of acetylene with $(\text{CH}_3)_3\text{SiH}$ and $(\text{CH}_3)_2\text{SiClH}$. The major catalytic reaction common to the three palladium surfaces was trimerization of acetylene to benzene with Pd(111), the most effective surface. Benzene also formed from propyne and from trimethylsilylacetylene. Reaction of acetylene with hydrogen cyanide produced small amounts of pyridine.

4. Silane Surface Chemistry of Palladium: Synthesis of Silaethylene Silacyclobutadiene and Silabenzene (Publication 1)

Thomas M. Gentle and E.L. Muetterties

The clean surface of Pd(110) proved effective in the dehydrogenation of organosilanes. After chemisorption of $(\text{CH}_3)_3\text{SiH}$ on Pd(110) at -135°C , rapid heating of the crystal led to desorption of $(\text{CH}_3)_3\text{SiH}$, $(\text{CH}_3)_2\text{Si}=\text{CH}_2$, H_2 , and a minor amount of $\{(\text{CH}_3)_2\text{SiCH}_2\}_2$. Silacyclohexane on Pd(110) partially desorbed reversibly and partially dehydrogenated to give silabenzene, SiC_5H_6 . Silacyclobutane on Pd(110) yielded silacyclobutadiene, $\text{H}_2\text{Si}=\text{CH}_2$, and $\{\text{H}_2\text{SiCH}_2\}_2$. $(\text{CH}_3)_2\text{Si}=\text{CH}_2$ was also partially formed in the thermal desorption of

$(\text{CH}_3)_3\text{SiOSi}(\text{CH}_3)_3$, $(\text{CH}_3)_3\text{SiNHSi}(\text{CH}_3)_3$, and $(\text{CH}_3)_3\text{SiN}_3$. The azide also formed $\{(\text{CH}_3)_2\text{SiNCH}_3\}_2$.

5. A Theoretical Model of Metal-surface Reactions (Publication 3)

Evgeny Shustorovich,[†] Roger C. Baetzold,[†] and E.L. Muetterties

Metal-surface reactions are modeled with a novel theoretical construct in which periodic trends can be scrutinized. The theoretical model is succinctly presented, and a wide range of periodic trends, based on the model, is explored. Periodic trends are discussed in the contexts of chemisorption bond energies, electron transfer between metal surface and adsorbate, stereochemical features of chemisorption states for closed-shell diatomic and linear X-CN or X-NC molecules, and hydrocarbon reactions. Hydrocarbon C-H bond-breaking processes are analyzed in terms of d-level occupancy, electron transfer, and stereochemistry of intermediates. Conceptually and computationally the metal surface is characterized as a good electron donor: antibonding molecular orbitals of the adsorbate species appear to be significant contributors to the chemisorption bond and also play a decisive role in bond-breaking processes. No aspect of the model projections is inconsistent with the experimental data, although the electronic characterization of some chemisorption states is counter to commonly held perceptions.

[†]Present address: Research Laboratories, Eastman Kodak Company, Rochester, New York 14650.

6. Work in Progress

A series of surface-science experiments was designed to factor the electronic and steric features that affect the structure and bond strength of hydrocarbons chemisorbed on metal surfaces. Specifically, the benzene chemisorption state on Pt(111) has been probed using benzene molecules progressively substituted by fluorine. The van der Waals radii of hydrogen and fluorine are similar, but their electronegativities are disparate. Hence this system of benzene and fluorobenzenes should be a sensitive probe of electronic structure of the chemisorption state. Also considered is the thermal reactivity of these benzene

and fluorobenzene chemisorption states. The mechanism of C-H and C-F bond scission will be discussed in the context of isotopic labeling studies.

Solutions of $^{101}\text{Ru}_3(\text{CO})_{12}$ and $^{104}\text{Ru}_3(\text{CO})_{12}$ were used to monitor intermolecular metal-atom scrambling under thermal and photochemical conditions. Both scrambling and ligand exchange were monitored by mass spectrometry. Carbon monoxide interchange occurred at rates about two orders of magnitude greater than scrambling rates. The scrambling-reaction rate was not affected by the presence of CO at low activities but was slightly decreased by the presence of CO at high pressures (~ 1.5 atm). Intermolecular metal-atom scrambling was also effected by light.

A detailed kinetic analysis has been prepared for the thermal desorption of alkyl and perfluoroalkyl cyanides (nitriles) from Ni(111). The activation energy for the desorption of the perfluoroalkyl derivatives was about 8 kcal/mole greater than for the alkyl analogs.

The coordination chemistry of methyl-substituted pyridine molecules on Ni(100) has been studied. The position of methyl substitution has a profound effect on pyridine surface chemistry.

PUBLICATIONS AND REPORTS

Refereed Journals

1. Thomas M. Gentle and E.L. Muetterties, "Silane Surface Chemistry of Silaethylene, Sila-cyclobutadiene, and Silabenzene," *J. Am. Chem. Soc.* **105**, 304-305 (1983); LBL-15129.
2. A.M. Stolzenberg and E.L. Muetterties, "Mechanisms of $\text{Re}_2(\text{CO})_{10}$ Substitution Reactions: Crossover Experiments with $^{185}\text{Re}_2(\text{CO})_{10}$ and $^{187}\text{Re}_2(\text{CO})_{10}$," *J. Am. Chem. Soc.* **105**, 822-827 (1983).
3. Evgeny Shustorovich, Roger C. Baetzold, and E.L. Muetterties, "A Theoretical Model of Metal Surface Reactions," *J. Phys. Chem.* **87**, 1100-1113 (1983); LBL-16267.
4. T.M. Gentle, V.H. Grassian, D.G. Klarup, and E.L. Muetterties, "Catalytic Chemistry of Palladium Surfaces Under Ultrahigh Vacuum Conditions," *J. Am. Chem. Soc.* (communication); LBL-16555.
5. Allen L. Johnson, E.L. Muetterties, and J. Stöhr, "Orientation of Complex Molecules Chemisorbed on Metal Surfaces — Near Edge X-ray Absorption Studies," *J. Am. Chem. Soc.* (communication); LBL-16614.

Other Publications

6. R.M. Wexler and E.L. Muetterties, "Metal Clusters and Metal Surfaces," in *Survey of Progress in Chemistry*, Vol. 10, pp. 62-128 (1983).
7. E.L. Muetterties, "Pentaco-ordination," Citation Classic No. 31, August 1, 1983.

Invited Talks

8. E.L. Muetterties, "Clusters and Surfaces in Catalysis and Electrochemistry," Proceedings of the Electrochemical Society Symposium, San Francisco, May 1983.
9. E.L. Muetterties, Camille and Henry Dreyfus Lecturer, University of Florida, Gainesville, Florida, 1983.
10. E.L. Muetterties, Priestley Lecturer, Pennsylvania State University, University Park, Pennsylvania, 1983.

High-Energy Oxidizers and Delocalized-Electron Solids*

Neil Bartlett, Investigator

INTRODUCTION

The main aim of this program is the synthesis and characterization of new materials. The synthetic work tests models and theories which correlate physical properties (such as electrical conductivity) with chemical composition and structure. The present emphasis is on the study of two-dimensional extended-atomic networks such as those derived from graphite, layer-form boron nitride, and their relatives. Electron oxidation of such materials (with accompanying intercalation to form salts) generates durable and conductive materials (some conducting better than aluminum). Chemical, stoichiometric, and structural requirements for the best conductivity are being defined. The layered materials can often be oxidized (and intercalated) electrochemically in a reversible process. Thus graphite may be reversibly converted by electrochemical means to a graphite fluoride of approximate composition $C_{2.5}F$. This novel material, which could be important as a high-energy electrode, possesses a π -electron system which appears to be similar to that in pristine graphite. Physical and chemical studies are being applied to this and related materials to determine the structure and bonding changes which accompany oxidation and reduction. Salts that are either proton conductors or fluoride-ion conductors, and that are resistant to oxidation but are not metallic, are being sought as solid electrolytes for use with the metallic layer-material salts.

1. Chemical and Structural Relationships of the Products of the Interaction of Graphite with AsF_5 , AsF_5 and F_2 , and O_2AsF_6 (Publication 2)

Fujio Okino and Neil Bartlett

The F/As molar ratio in the vacuum-stable solid products obtained by treating graphite at 20° with (1)

AsF_5 , (2) AsF_5 plus F_2 , and (3) O_2AsF_6 has in all cases been established to be 6. Route (1) gives mixtures of first- and second-stage salts, whereas routes (2) and (3) readily yield first-stage material. This effect is attributed to the greater oxidizing potential of the reagents in (2) and (3). The volatiles from the route (1) synthesis are AsF_5 and AsF_3 , and AsF_5 is the volatile from the route (2) synthesis. The interlayer spacing I_c of the occupied graphite galleries in the vacuum-stable hexafluoroarsenates is $\sim 7.6 \text{ \AA}$, and $c_0 \approx 7.6 + 3.34(n-1) \text{ \AA}$, where n is the stage. For such salts the composition approximates the formula $C_{14n}AsF_6$; in the first-stage salt the approximate charge on carbon is C_{14}^+ . Where neutral molecules occur in the galleries, as in the products of routes (1) and (2), $I_c \approx 8.0 \text{ \AA}$ and $c_0 \approx 8.0 + 3.35(n-1) \text{ \AA}$ prior to removal of volatiles.

2. The Crystal Structure of the First-stage Graphite Salt $C_{14}^+AsF_6^-$ and the First-stage Precursor Prepared from Graphite and Arsenic Pentafluoride (Publication 3)

Fujio Okino and Neil Bartlett

X-ray powder-diffraction data for the first-stage graphite salt $C_{14}^+AsF_6^-$ have shown that the AsF_6^- species are nestled in contiguous threefold sets of carbon-atom hexagons of the graphite. This pattern requires a staggering of the enclosing carbon-atom layers as in hexagonal graphite. Each gallery of the graphite contains an ordered, closest-packed, nestled assembly, appropriate for the stoichiometry $C_{14}AsF_6$. Apart from the restrictions imposed by AsF_6^- nesting, the layers of composition $C_{14}AsF_6$ are otherwise randomly stacked. Materials prepared by direct interaction of graphite and AsF_5 (from which AsF_5 and AsF_3 are removable in a vacuum) have a larger interlayer spacing ($I_c = 8.0 \text{ \AA}$) than $C_{14}AsF_6$ ($I_c = 7.6 \text{ \AA}$). X-ray powder data for such samples are accounted for by a random distribution of un-nestled AsF_x species. The carbon-atom sheets in these c -axis-expanded materials are, however, eclipsed. Introduction at $\sim 20^\circ C$ of AsF_5 or AsF_3 to $C_{14}AsF_6$ ($I_c = 7.6 \text{ \AA}$ and staggered layer arrangement) slowly yields the $I_c = 8.0 \text{ \AA}$ material, with eclipsed carbon layers.

*This work was supported by the Director, Office of Energy Research, Office of Basic Energy Sciences, Chemical Sciences Division of the U.S. Department of Energy under Contract No. DE-AC03-76SF00098.

3. The Fluorobasicities of ReF_7 and IF_7 as Measured by the Enthalpy Change $\Delta H^\circ(\text{EF}_{7(\text{g})} \rightarrow \text{EF}_{6(\text{g})}^+ + \text{F}_{(\text{g})}^-)$ (Publication 6)

Neil Bartlett, Sam Yeh, Kostantinos Kourtakis, and Tom Mallouk

Iridium hexafluoride oxidizes ReF_6 (via an ReF_6^+ salt), and at room temperatures IrF_6 , ReF_6 , ReF_7 , and $(\text{IrF}_5)_4$ are each present in the equilibrium mixture. From these and related findings, $\Delta H^\circ(\text{ReF}_6^+ \rightarrow \text{ReF}_6^+ + e^-) = 1092 \pm 27$ kJ/mole (261 ± 6 kcal/mole), which is in harmony with an accepted ionization potential derived from photoelectron spectroscopic work. From this and other selected thermodynamic data, consistent with the observed chemistry, $\Delta H^\circ(\text{ReF}_{7(\text{g})} \rightarrow \text{ReF}_{6(\text{g})}^+ + \text{F}_{(\text{g})}^-) = 911 \pm 33$ kJ/mole (218 ± 8 kcal/mole). From observations on the stability of $\text{IF}_6^+\text{BF}_4^-$ and the lattice-enthalpy evaluation for the salt, $\Delta H^\circ(\text{IF}_{7(\text{g})} \rightarrow \text{IF}_6^+ + \text{F}_{(\text{g})}^-) = 870 \pm 24$ kJ/mole (208 ± 6 kcal/mole). These values fit the quantitative displacement of ReF_7 from $\text{ReF}_6^+\text{MF}_6^-$ salts by IF_7 , which thereby forms $\text{IF}_6^+\text{MF}_6^-$ salts. Nevertheless, the basicities for ReF_7 and IF_7 are close, and similar to the basicities of the hypervalent molecules (enthalpy changes, in kJ/mole, in parentheses): XeF_6 (874), XeF_4 (925), XeF_2 (906), and SF_4 (883). By way of contrast, the nonhypervalent fluoride ONF (786 kJ/mole) is a much stronger base. This suggests that the bonding in ReF_7 may be very similar to that in the hypervalent molecules.

4. Work in Progress

Electrical-conductivity studies have shown that first-stage salts $\text{C}_x^+\text{MF}_6^-$ are poorer conductors (in layer plane) than higher-stage relatives. When M is As, it has been shown that the introduction of neutral fluorides AsF_3 or AsF_5 can increase the conductivity twofold, perhaps more. These conductivity changes and their reversibility are being correlated with structure as well as composition.

^{13}C nmr spectra of graphite fluoride powders $[\text{C}_x\text{F}_{1-\delta}(\text{HF})_\delta]_n$, for which C/F = 3.70 and 2.05, have been obtained. The technique used, $^{19}\text{F} \rightarrow ^{13}\text{C}$ cross-polarization, enhances the ^{13}C signal and simultaneously removes the ^{19}F scalar and dipolar couplings. For both C/F ratios, two peaks separated by 47 ppm were observed, and the similarity of the spectra indicate that the same bonding environments are found in both materials. The low-field peak ($\delta = +135$ ppm relative to TMS) indicates that such

carbon is graphite-like. The high-field peak has been attributed to the carbon attached directly to the fluorine. Work now in progress aims to count the number of carbon atoms in each environment.

1983 PUBLICATIONS AND REPORTS

Refereed Journals

1. Thomas Mallouk and Neil Bartlett, "Reversible Intercalation of Graphite by Fluorine: A New Bifluoride, C_{12}HF_2 , and Graphite Fluorides, C_xF ($5 > x > 2$)," *J. Chem. Soc., Chem. Commun.* **103**, 102-105 (1983); LBL-13815.

LBL Reports

2. Fujio Okino and Neil Bartlett, "Chemical and Structural Relationships of the Products of the Interaction of Graphite with (a) AsF_5 , (b) AsF_5 and F_2 , and (c) O_2AsF_6 ," submitted to Carbon, LBL-17161.
3. Fujio Okino and Neil Bartlett, "The Crystal Structure of the First-stage Graphite Salt $\text{C}_{14}^+\text{F}_6^-$, and of the First-stage Precursor Prepared from Graphite and Arsenic Pentafluoride," submitted to Carbon, LBL-17162.
4. T.E. Mallouk, G.L. Rosenthal, G. Müller, R. Brusasco, and N. Bartlett, "The Fluoride Ion Affinities of GeF_4 and BF_3 from Thermodynamic and Structural Data for $(\text{SF}_3)_2\text{GeF}_6$, ClO_2GeF_5 , and ClO_2BF_4 ," submitted to *Inorg. Chem.*, LBL-13817.
5. T.E. Mallouk, B. Desbat, and N. Bartlett, "Structural Studies of Salts of *cis* and *trans* μ -fluoro-bridged Polymers of GeF_5^- and GeF_5^- Monomer," submitted to *Inorg. Chem.*, LBL-13816.
6. N. Bartlett, Sam Yeh, Kostantinos Kourtakis, and Tom Mallouk, "The Fluorobasicities of ReF_7 and IF_7 as Measured by the Enthalpy Change $\Delta H^\circ(\text{EF}_{7(\text{g})} \rightarrow \text{EF}_{6(\text{g})}^+ + \text{F}_{(\text{g})}^-)$," submitted to *J. Fluorine Chem.*, LBL-17081.
7. T.E. Mallouk (Ph.D. Thesis), with N. Bartlett, "Reversible Intercalation of Graphite by Fluorine, and Related Synthetic and Thermodynamic Studies," LBL-16778.

Invited Talks

8. N. Bartlett, "Thermodynamic and Kinetic Aspects of the Intercalation of Graphite by Fluorine and Fluorides," 6th Winter Fluorine

- Conference, Daytona Beach, Florida, February 6-11, 1983; based on LBL-13815 and LBL-15457.
9. N. Bartlett, "From the Oxidation of Oxygen to Synthetic Metals — An Oxidative Odyssey," symposium organized for the Nichols Medal Award (to Neil Bartlett), New York Section, American Chemical Society, Marymount College, Tarrytown, New York, March 4, 1983; based on LBL-12475 and LBL-13815.
 10. N. Bartlett, "New Aspects of the Intercalation of Graphite by Fluorine and Fluorides," 8th European Symposium on Fluorine Chemistry, Jerusalem, Israel, August 21-26, 1983; based on LBL-13815, LBL-17161, and LBL-17162.
 11. N. Bartlett, "Noble-gas Chemistry," New Zealand Institute of Chemistry, Christchurch, New Zealand, September 19, 1983; Chemistry Department, Otago University, New Zealand, October 10, 1983; Waikato University, New Zealand, October 27, 1983; University of Auckland, New Zealand, October 28, 1983; Massey University, New Zealand, November 1, 1983; Chemistry Department, Australian National University, November 21, 1983; Australian Chemical Institute, Melbourne University Chemical Society, November 23, 1983.
 12. N. Bartlett, "From Metals to Insulators: Some Studies in the Oxidative Intercalation of Graphite," Chemistry Department, University of Canterbury, Christchurch, New Zealand, September 27, 1983; based on LBL-17161, LBL-17162, and LBL-13815.
 13. N. Bartlett, "Quantitative Evaluation of Fluoro-acid and Fluoro-base Strengths (Including Novel Evaluation for Lattice Energies and Entropies)," Chemistry Department, University of Canterbury, Christchurch, New Zealand, October 4, 1983; based on LBL-13817 and LBL-17081.
 14. N. Bartlett, "The Oxidative Intercalation of Graphite by Fluorine and Fluorides: New Metals and Novel Bonding for Carbon," Chemistry Department, University of Otago, New Zealand, October 10, 1983; Chemistry Department, Australian National University, November 22, 1983; Chemistry Department, Monash University, November 29, 1983; based on LBL-17161, LBL-17162, and LBL-13815.
 15. N. Bartlett, "From $C_6F_6^+$ Salts to Synthetic Metals," Chemistry Department, La Trobe University, Melbourne, Australia, December 5, 1983; based on LBL-12475 and LBL-13815.

Transition-Metal-Catalyzed Conversion of CO, NO, H₂, and Organic Molecules to Fuels and Petrochemicals*

Robert G. Bergman, Investigator

INTRODUCTION

The goal of this project is the discovery of new chemical reactions in which transition metals interact with organic materials, and the understanding of how these reactions work. The approach begins with the synthesis and structural characterization of new types of stable organotransition metal complexes. Then the self-reactions of these materials (induced, for example, by heat or light) are investigated, as well as their reactions with small molecules and organic compounds. A recent discovery on this project was the finding that a certain class of iridium complexes undergo oxidative addition into the carbon-hydrogen bonds of completely saturated hydrocarbons. This is the first example of this long-sought reaction, and work on this project is now directed at examining the scope, selectivity, and mechanism of this reaction. Efforts are also being directed at converting the alkyl(hydrido)iridium products of the oxidative addition into functionalized organic molecules.

1. Reversible C-H Insertion/Reductive Elimination in (η^5 -pentamethylcyclopentadienyl)(trimethylphosphine)iridium Complexes. Use in Effecting Selective Primary Functionalization, Determining Relative Metal-carbon Bond Energies, and Thermally Activating Methane (Publication 16)

Michael J. Wax, Jeffrey M. Stryker,
J. Michael Buchanan, Caroline A. Kovac, and
Robert G. Bergman

Heating causes reductive elimination of alkane from Cp'(L)Ir(R)(H) complexes (Cp' = η^5 -penta-

methylcyclopentadienyl, L = trimethylphosphine), leading to an intermediate capable of undergoing oxidative addition to the C-H bonds in other alkanes. As shown in Figure 1-1, this property has been used to convert the mixture of primary and secondary hydridoalkyliridium complexes obtained on irradiation of Cp'(L)IrH₂ in n-pentane into the single, thermodynamically most stable isomer, Cp'(L)Ir(1-pentyl)H (complex 2). The reversibility of this process has also provided a means of equilibrating hydridoalkyliridium complexes formed by attack on the C-H bonds of different hydrocarbons. Thus, the equilibrium constant for interconversion of 1-n-pentyl complex 2 and cyclohexane with cyclohexyliridium complex 6 and n-pentane has been measured as 10.8 at 140°C. Using this K_{eq} and some reasonable assumptions, it can be estimated that the primary metal-carbon bond in complex 2 is 5.5 kcal/mole stronger than the secondary metal-carbon bond in complex 6.

Finally, the thermodynamic stability of the corresponding hydridomethyl complex has allowed use of these equilibrating conditions to develop the first thermal oxidative addition of methane to a soluble transition-metal complex. Thus, as illustrated in Figure 1-2, heating hydrido(cyclohexyl)iridium complex 6 in cyclooctane solvent under 20 atm of CH₄ for 14 hr at 140–150°C led to a 58% yield of Cp'(L)Ir(CH₃)(H) (complex 7). Complex 7 can be converted to the corresponding chloromethyliridium complex 9 by treatment with CHCl₃. Chloride (complex 9) can be prepared independently by methylation of Cp'(L)IrCl₂, and converted to hydride (complex 7) by treatment with LiBH₄.

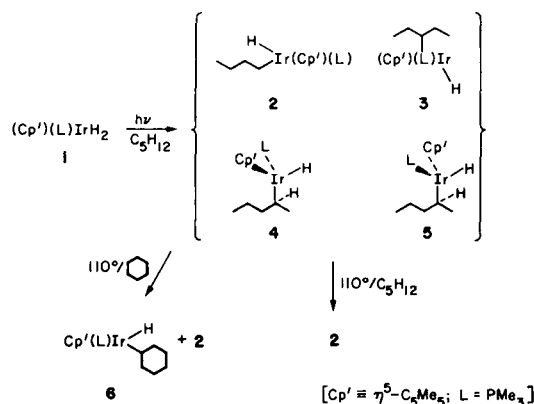


Figure 1-1. Irradiation of Cp'(L)IrH₂ (complex 1) in n-pentane and thermolysis of the resulting product mixture in cyclohexane and n-pentane. (XBL 841-29)

*This work was supported by the Director, Office of Energy Research, Office of Basic Energy Sciences, Chemical Sciences Division of the U.S. Department of Energy under Contract No. DE-AC03-76SF00098.

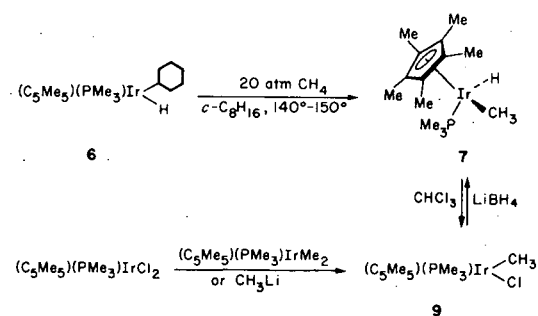


Figure 1-2. Use of complex 6 in the activation of methane and reactions used in identifying the product complex 7.

(XBL 841-30)

2. Oxidative Addition of Rhodium to Alkane C-H Bonds: Enhancement in Selectivity and Alkyl-group Functionalization, and the First Structurally Characterized Derivative of a C-H Insertion Product (Publication 14)

Roy A. Periana and Robert G. Bergman

As shown by the data in Table 2-1, UV irradiation of $(\eta^5\text{-C}_5\text{Me}_5)\text{RhPMe}_3\text{H}_2$ (complex 2 in Figure 2-1) in alkanes below -30°C results in the formation of $(\eta^5\text{-C}_5\text{Me}_5)\text{RhPMe}_3(\text{R})(\text{H})$ (complex 4), with significantly greater selectivity toward different C-H bonds than the iridium analogue. The mechanism is proposed to be a concerted oxidative process proceeding via the unsaturated intermediate $[(\eta^5\text{-C}_5\text{Me}_5)\text{RhPMe}_3]$ (complex 3). Conversion of the thermally labile complexes 4 to $(\eta^5\text{-C}_5\text{Me}_5)\text{RhPMe}_3(\text{R})(\text{Br})$ (complex 5) by treatment with CHBr_3 allowed characterization of these derivatized C-H activation products by both spectrometric and analytical methods. In the case where R is cyclopropyl (complex 5c), the molecular structure (illustrated in Figure 2-2) was determined by x-ray crystallography. Treatment of complex 5 with Br_2 at 25°C results in the formation of $(\eta^5\text{-C}_5\text{Me}_5)\text{RhPMe}_3\text{Br}_2$ (complex 7) and bromoalkane.

Table 2-1

Relative rate constants (k_{rel})^a for attack at a single C-H bond in different molecules by $(\eta^5\text{-C}_5\text{Me}_5)(\text{PMe}_3)\text{M}$, where M = Rh and Ir at -60°C .

C-H Bond	$k_{\text{rel}}(\text{Rh})$	$k_{\text{rel}}(\text{Ir})$
Benzene	19.5	3.9
Cyclopropane	10.4	2.1
n-Hexane (1°)	5.9	2.7
n-Hexane (2°) ^b	0 ^c	0.2
Propane (1°)	2.6	1.5
Propane (2°)	0 ^c	0.3
Cyclopentane	1.8	1.1
Cyclohexane	1.0	1.0

a. Relative rate constants are determined from competition experiments (see text) carried out with each individual metal complex in mixtures of two solvents, and are normalized by arbitrarily setting the rate constant for cyclohexane equal to 1.0 in each case.

b. Average k_{rel} for attack on both types of secondary hydrogens.

c. A k_{rel} larger than 0.1 could have been detected.

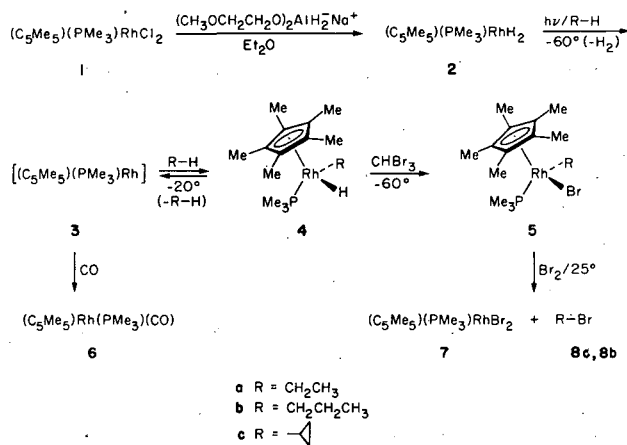


Figure 2-1. Synthesis and reaction chemistry developed using $\text{Cp}^*(\text{L})\text{RhH}_2$ (complex 2). (XBL 841-31)

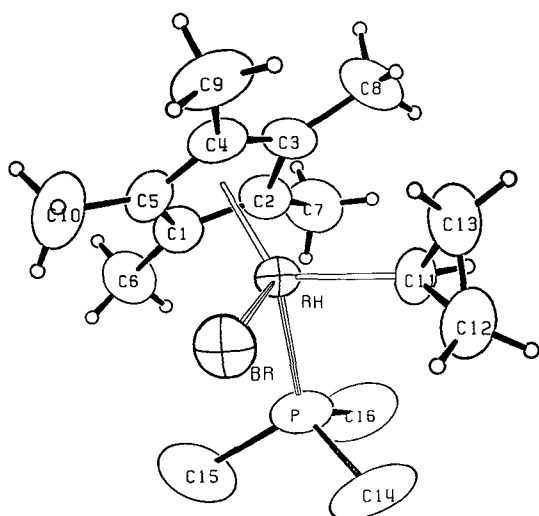


Figure 2-2. ORTEP diagram illustrating the structure of (η^5 - C_5Me_5)(PMe_3) $Rh(C_3H_5)Br$ (complex 5c). (XBL 841-32)

3. Preparation and Reactions of Tetrahydrido(pentamethylcyclopentadienyl)-iridium: A Novel Iridium(V) Polyhydride (Publication 9)

Thomas M. Gilbert and Robert G. Bergman

The new complex $[C_5(CH_3)_5]IrH_4$ (complex 1 in Figure 3-1), a rare example of a formal iridium(V) species, has been synthesized and its chemistry investigated. As summarized in Figure 3-1, synthesis of the complex was achieved by preparing the

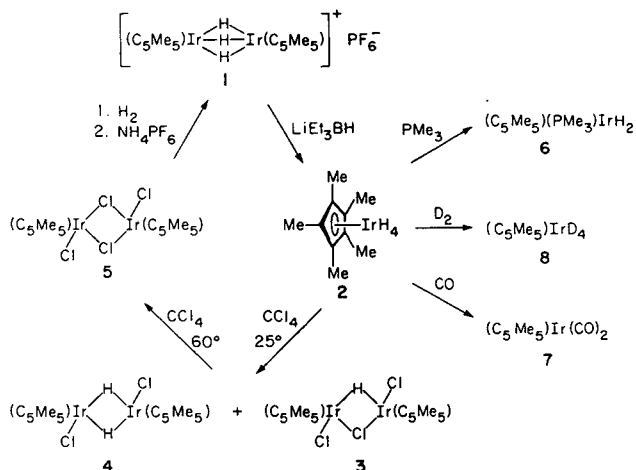


Figure 3-1. Synthesis and chemical reactions of Cp^*IrH_4 (complex 2). (XBL 841-33)

cationic dinuclear trihydride (complex 1) and reducing it with a strong hydride donor. Complex 1 was characterized by standard analytical and spectroscopic methods, as well as by a single-crystal x-ray diffraction study.

Ultraviolet irradiation of the dihydride (complex 2) in the presence of PMe_3 leads to the known dihydride (complex 6), while irradiation under an atmosphere of CO leads to the dicarbonyl (complex 7). Similar photolysis under an atmosphere of D_2 yields complex 8, the tetradeutero analogue of complex 2, which may also be prepared by thermal hydrogen exchange. Reaction with carbon tetrachloride initially leads to dinuclear hydridochlorides (complexes 3 and 4), followed by conversion of these materials back to the tetrachloride (complex 5).

4. Mechanism of the Reaction of Molybdenum Carbonyl Alkyls with Molybdenum Hydrides: A Model for the Aldehyde-producing Step of the Oxo Process (Publication 13)

Michael J. Wax and Robert G. Bergman

The reaction of $CpMo(CO)_3R$ (1; $Cp = \eta^5-C_5H_5$; $R = CH_3, C_2H_5$) with $CpMo(CO)_3H$ (2), which produces $RCHO$, $[CpMo(CO)_2]_2$, and $[CpMo(CO)_3]_2$, occurs by way of two competing pathways. One involves reversible solvent-assisted migratory insertion (k_1) to form $CpMo(CO)_2(solvent)COR$, followed by attack of metal hydride on this intermediate (k_4). The other route involves the direct reaction of 1 with 2 (k_5). No hydrogen-deuterium kinetic-isotope effect is observed on either k_4 or k_5 when $CpMo(CO)_3D$ is substituted for 2. Enhancing the Lewis basicity of the hydride by replacement of a carbonyl ligand with a phosphine to produce $CpMo(CO)_2(PMe_3)H$ increases k_5 , while the larger metal-hydrogen bond strength of $CpW(CO)_3H$ is reflected in a decrease in k_4 . Qualitative experiments further indicate that ionic intermediates or free radicals are present in neither pathway, and that a metal-metal bond is created prior to or concomitant with aldehyde release. These results suggest the presence of at least some metal-hydrogen bond breaking in the rate-limiting transition state of the reaction of $CpMo(CO)_3H$ with $CpMo(CO)_2(solvent)COR$, (k_4). In contrast with this, the rate-determining formation of some dinuclear complex containing an intact Mo-H bond characterizes the direct reaction of 2 with $CpMo(CO)_3R$ (k_5). The structure of this intermediate cannot be determined unambiguously, but it may

be the datively bound species $\text{Cp}(\text{CO})_3\text{HMo}-\text{Mo}(\text{COR})(\text{CO})_2\text{Cp}$.

5. Work in Progress

Research in this program is now focused entirely on the use of metals to activate C-H bonds in organic molecules. In the iridium and rhodium systems, the thermal hydridoalkylmetal reductive-elimination/oxidative-addition reaction is being used to measure equilibrium constants for interchange of various alkyl groups on iridium; these data will provide important information on relative metal-carbon bond energies. Experiments are being carried out in both the iridium and rhodium systems designed to develop methods for converting the products of C-H activation into functionalized organic molecules, especially oxygenated compounds. Efforts are also under way aimed at expanding the range of substrates which will be subjected to reaction with the intermediate $(\text{C}_5\text{Me}_5)(\text{PMe}_3)\text{Ir}$. Initial experiments will be directed toward examining the reactivity of alcohols, amines, halides, and ethers. Finally, preliminary results have been obtained demonstrating that a pentamethylcyclopentadienyl complex of rhenium successfully activates C-H bonds. Studies have been initiated aimed at examining this reaction further and comparing its characteristics with those of the iridium and rhodium systems.

1983 PUBLICATIONS AND REPORTS

Refereed Journals

1. K.H. Theopold and R.G. Bergman, "Synthesis and Reaction Chemistry of a New Class of μ -alkylidene Dicobalt Complexes. Crystal and Molecular Structure of μ -methylene-bis(η^5 -methylcyclopentadienyl)carbonylcobalt," J. Am. Chem. Soc. **105**, 464 (1983).[†]
2. W.P. Weiner and R.G. Bergman, "Kinetics and Mechanism of the Formation of Nitrosoalkane Complexes by Migratory Insertion of Coordinated Nitric Oxide into Cobalt-carbon Bonds," J. Am. Chem. Soc. **105**, 3922 (1983).[‡]
3. P.N. Becker and R.G. Bergman, "Transition-metal-based Method for 1,2-diamination of Alkenes. Synthesis of Cobalt Dinitrosoalkanes from Alkenes, Nitric Oxide, and (η^5 -cyclopentadienyl)nitrosylcobalt Dimer and

Their Reduction to Primary Vicinal Diamines," Organometallics **2**, 787 (1983).[‡]

4. P.N. Becker and R.G. Bergman, "Reversible Exchange of (η^5 -cyclopentadienyl)(dinitrosoalkane)cobalt Complexes with Alkenes. Kinetic and Spectroscopic Evidence for $\text{C}_5\text{H}_5\text{Co}(\text{NO})_2$ as a Reactive Intermediate," J. Am. Chem. Soc. **105**, 2985 (1983).[‡]
5. A.H. Janowicz and R.G. Bergman, "Activation of C-H Bonds in Saturated Hydrocarbons on Photolysis of (η^5 - C_5Me_5)(PMe_3) IrH_2 . Relative Rates of Reaction of the Intermediate with Different Types of C-H Bonds, and Functionalization of the Metal-bound Alkyl Groups," J. Am. Chem. Soc. **105**, 3929(1983); LBL-15145.
6. W.H. Hersh, F.J. Hollander, and R.G. Bergman, "Synthesis, Crystal and Molecular Structures, and Reactions of a Benzodicobaltacyclohexene, a Thermally Derived Mononuclear o-xylylene Complex, and an Unsymmetrical Phosphine-derived Dinuclear Complex," J. Am. Chem. Soc. **105**, 5834 (1983).[†]
7. W.H. Hersh and R.G. Bergman, "Kinetics and Mechanism of Decomposition of a Benzodicobaltacyclohexene: Reversible Dinuclear Elimination of o-xylylene via a Dimetalla-Diels-Alder Reaction," J. Am. Chem. Soc. **105**, 5846 (1983).[†]
8. G.K. Yang and R.G. Bergman, "Stereochemistry of Metallacycle Formation in the Double Alkylation of Bis(triphenylphosphine)-nitrogen-(1+) Bis(η^5 -cyclopentadienyl)bis(μ -carbonyl)dicobaltate with α - γ -diiodoalkanes," J. Am. Chem. Soc. **105**, 6045 (1983).[†]
9. T.M. Gilbert and R.G. Bergman, "Preparation and Reactions of Tetrahydrido(pentamethylcyclopentadienyl)iridium: A Novel Iridium(V) Polyhydride," Organometallics **2**, 1458 (1983); LBL-16325.
10. G.K. Yang and R.G. Bergman, "Characterization and Evidence for Alkylation of $\text{CpRe}(\text{CO})_2\text{H}^-$ in the Conversion of $\text{CpRe}(\text{CO})_2\text{H}_2$ to $\text{CpRe}(\text{CO})_2\text{R}_2$. Synthesis of a Rhenacyclopentane and its Thermolysis to Methylcyclopropane," J. Am. Chem. Soc. **105**, 6500 (1983).[†]
11. P.F. Seidler, H.E. Bryndza, J.E. Frommer, L.S. Stuhl, and R.G. Bergman, "Synthesis of Trinuclear Alkylidyne Complexes from Dinuclear Alkyne Complexes and Metal Hydrides. CIDNP Evidence for Vinyl Radical Intermediates in the Hydrogenolysis of These Clusters," Organometallics **2**, 1071 (1983).[†]

LBL Reports

12. R.G. Bergman, "Activation of Alkanes in Homogeneous Solution Using Organotransition Metal Complexes," *Science*, in press, LBL-16320.
13. M.J. Wax and R.G. Bergman, "Mechanism of the Reaction of Molybdenum Carbonyl Alkyls with Molybdenum Hydrides: A Model for the Aldehyde-producing Step of the Oxo Process," submitted to *Organometallics*, LBL-16364.
14. R.A. Periana and R.G. Bergman, "Oxidative Addition of Rhodium to Alkane C-H Bonds: Enhancement in Selectivity and Alkyl Group Functionalization, and the First Structurally Characterized Derivative of a C-H Insertion Product," submitted to *Organometallics*, LBL-16548.
15. M.J. Wax (Ph.D. Thesis), with R.G. Bergman, "Phosphine- and Metal Hydride-induced Migratory Insertion in Molybdenum Carbonyl Alkyls," LBL-16586.
16. M.J. Wax, J.M. Stryker, J.M. Buchanan, C.A. Kovac, and R.G. Bergman, "Reversible C-H Insertion/Reductive Elimination in (η^5 -pentamethylcyclopentadienyl)(trimethylphosphine)iridium Complexes. Use in Effecting Selective Primary Functionalization, Determining Relative Metal-carbon Bond Energies, and Thermally Activating Methane," submitted to *J. Am. Chem. Soc.*, LBL-16617.

Other Publications

17. A.H. Janowicz, C.A. Kovac, R.A. Periana-Pillai, J.M. Buchanan, T.M. Gilbert, and R.G. Bergman, "Oxidative Addition of Soluble Iridium and Rhodium Complexes to Carbon-hydrogen Bonds in Alkanes," in *Organometallic Compounds: Proceedings of the First IUCCP Symposium*, Texas A&M University Press, 1983, LBL-17186.

Invited Talks

18. R.G. Bergman, "Activation of C-H Bonds in Completely Saturated Hydrocarbons Using Soluble Iridium and Rhodium Complexes," Department of Chemistry, Georgia Institute of Technology, Atlanta, Georgia, February 7, 1983.
19. R.G. Bergman, "Activation of C-H Bonds in Completely Saturated Hydrocarbons Using Soluble Iridium Complexes," 7th Conference on Structure-energy Relationships, Asilomar Conference Center, Monterey, California,

March 14, 1983.

20. R.G. Bergman, "Intermolecular Oxidative Addition of Iridium to C-H Bonds in Saturated Hydrocarbons," 12th Sheffield-Leeds International Symposium on Organometallic, Inorganic, and Catalytic Chemistry, Department of Chemistry, The University of Sheffield, Sheffield, England, March 30, 1983.
21. R.G. Bergman, lectures on (a) Formation of Carbon-hydrogen Bonds in the Hydrogenolysis of Metal Alkyl Complexes and in Metal Hydride/Metal Alkyl Reactions, (b) Synthesis and Chemistry of Dinuclear Metallacycles, (c) Migratory Insertion and Cycloaddition Reactions Involving Metal Nitrosyl Complexes, and (d) Homogeneous, Intermolecular Oxidative Addition of Rhodium and Iridium to Carbon-hydrogen Bonds in Completely Saturated Hydrocarbons; all at Department of Chemistry, The University of Texas at Austin, Austin, Texas, April 11-15, 1983.
22. R.G. Bergman, "Activation of C-H Bonds in Completely Saturated Hydrocarbons Using Soluble Iridium and Rhodium Complexes," IUCCP Symposium in Organometallic Chemistry, Department of Chemistry, Texas A&M University, College Station, Texas, April 20, 1983.
23. R.G. Bergman, "The Use of Soluble Iridium and Rhodium Complexes for Activation of Carbon-hydrogen Bonds in Completely Saturated Hydrocarbons," MIT Chemical Sciences/Industry Forum, Department of Chemistry, Massachusetts Institute of Technology, Cambridge, Massachusetts, May 31, 1983.
24. R.G. Bergman, lectures on (a) Synthesis and Chemistry of Dinuclear Metallacycles, (b) Reactions of Mono- and Polynuclear Organotransition Metal Alkyl Complexes with Metal Hydrides and with H₂, (c) The Use of Coordinated Nitric Oxide in the Formation of New C-N Bonds in Organic Molecules, and (d) Activation of Alkane C-H Bonds Using Soluble Organotransition Metal Complexes; all at Department of Chemistry, University of Colorado at Boulder, Boulder, Colorado, August 15, 1983.
25. R.G. Bergman, "Homogeneous Intermolecular Oxidative Addition of Rhodium and Iridium to Carbon-hydrogen Bonds in Completely Saturated Hydrocarbons," Inorganic C-H Activation Symposium, 186th National American Chemical Society Meeting, Washington, D.C., August 30, 1983,

26. R.G. Bergman, "Activation of Alkanes in Homogeneous Solution Using Organotransition Metal Complexes," Dains Memorial Lecture, Department of Chemistry, University of Kansas, Lawrence, Kansas, September 30, 1983.
27. R.G. Bergman, "Oxidative Addition of Soluble Transition Metal Complexes to Carbon-hydrogen Bonds in Alkanes," Plenary Lecture at the XI International Conference on Organometallic Chemistry, Callaway Gardens, Pine Mountain, Georgia, October 12, 1983.
28. R.G. Bergman, "Oxidative Addition of Transition Metals to Alkane C-H Bonds in Homogeneous Solution," Department of Chemistry, Columbia University, New York, November 10, 1983.

[†]Supported by the National Science Foundation (Grant No. CHE79-26291).

^{*}Supported by the National Institutes of Health (Grant No. GM-25459).

CHEMICAL ENGINEERING SCIENCES

High-Pressure Phase Equilibria in Hydrocarbon-Water (Brine) Systems*

John M. Prausnitz, Investigator

INTRODUCTION

Phase equilibria are required for the efficient design of large-scale separation processes (e.g. distillation and extraction) in the chemical and related industries. In this context "efficient" refers to optimum use of raw materials and conservation of energy.

Since the variety of technologically important fluid mixtures is extremely large, it is not possible to obtain all desired equilibria from experiment. Therefore the objective of this research is development of molecular thermodynamics for interpretation and correlation of selected phase-equilibrium data toward reliable general prediction of phase equilibria for engineering. The correlations are expressed through semitheoretical physicochemical models in a form suitable for computer-aided design. Particular attention is given to those systems that are of primary interest in energy-related industries, especially those concerned with fossil fuels and fossil-fuel/water mixtures.

Development of molecular thermodynamics calls for a combination of theoretical, computational, and experimental work. It further demands simultaneous awareness of progress in molecular science and of realistic requirements for engineering design.

1. Mutual Solubilities and Vapor Pressures of Hydrocarbon-water Systems (Publication 13)

Frank E. Anderson and John M. Prausnitz

An apparatus has been constructed for measuring mutual solubilities and vapor pressures for liquid-liquid systems in the region ambient to 200°C. Both phases are sampled and analyzed using gas-liquid chromatography. The apparatus has been used to obtain data for binary water-hydrocarbon systems in the 100–200°C range. Special care must be taken to assure reliable sampling because mutual solubilities are very small. It is especially important to avoid entrainment, phase change (due to temperature gradients or pressure drops), and adsorption when removing samples for chemical analysis. Experimental results are reported for binary aqueous mixtures containing benzene, toluene, and m-xylene. These results are in good agreement with diverse data reported in the literature.

2. High-pressure Phase Equilibria for the Water/Methane System (Publication 6)

Eldon R. Larsen[†] and John M. Prausnitz

A semitheoretical method has been established for superimposing the residual thermodynamic properties of pure water over wide ranges of pressure (0.01 to 1000 MPa) and temperature (triple point to

*This work was supported by the Director, Office of Energy Research, Office of Basic Energy Sciences, Chemical Sciences Division of the U.S. Department of Energy under Contract No. DE-AC03-76SF00098.

twice the critical temperature). Using reasonable mixing rules with two binary parameters, this superposition also gives mixture properties, including high-pressure vapor-liquid equilibria.

†Present address: Union Carbide Corporation, Charleston, West Virginia 25303.

3. Supercritical Fluid Extraction with Mixed Solvents (Publication 12)

D.K. Joshi and J.M. Prausnitz

The solubility of high-boiling solid or liquid in a compressed gas can be raised substantially when a suitable entrainer is added to the compressed gas. Illustrative calculations for several cases indicate that solubilities can be raised by one or two orders of magnitude.

4. Thermodynamics of Associated Solutions. Henry's Constants for Nonpolar Solutes in Water (Publication 7)

Ying Hu,[†] Edmundo Azevedo,[‡] Dorothea Lüdecke, and John M. Prausnitz

A systematic derivation is presented for the Helmholtz energy of a van der Waals fluid mixture whose nonideality is ascribed to both chemical and physical interactions. This derivation, applicable to all fluid densities, leads to an equation of state which contains chemical-equilibrium constants in addition to the customary physical van der Waals constants *a* and *b*. Attention is given to the need for simplifying assumptions and to the variety of simplifying assumptions that can lead to useful results. A particular equation of state is used to correlate Henry's constants of nonpolar solutes in water over a wide temperature range. The correlation is only partially successful because we do not yet have a truly satisfactory theory for thermodynamic properties of mixtures containing molecules that differ appreciably in size.

†Present address: East China Institute of Chemical Technology, Shanghai, China.

‡Present address: Instituto Superior Tecnico, Lisbon, Portugal.

5. Molecular Thermodynamics of Fluid Mixtures Containing Molecules that Differ in Size and Potential Energy (Publication 8)

Ying Hu,[†] Dorothea Lüdecke, and John M. Prausnitz

Recent computer-simulation work by Shing and Gubbins¹ for binary mixtures has shown that common semiempirical models (van der Waals *n*-fluid models) are in error when the molecules of the two components differ appreciably in size; the error is most severe in the dilute region. While perturbation theories are much better, they, like computer simulations, are not yet useful for engineering work because of prohibitive computer requirements.

This work proposes an algebraic expression for the Helmholtz energy of a mixture; the expression gives results in very good agreement with those reported by Shing and Gubbins.¹ This expression, using the local-composition concept, is based on a simplified but realistic picture of a fluid mixture: short-range order and long-range disorder. The proposed expression uses the Mansoori-Carnahan-Starling-Leland equation for the contribution of repulsive forces. For the contribution of attractive forces, it uses a new expression based on several radii for the first-neighbor shell, with one radius for each component.

With reasonable simplifications, the resulting equation for the Helmholtz energy indicates that van der Waals "constant" *a* is a strict quadratic function of mole fraction only at very low densities. At advanced densities there are small deviations from the quadratic-mixing rule. For practical calculations computer requirements are nearly the same as those for conventional engineering models.

†Present address: East China Institute of Chemical Technology, Shanghai, China.

1. K.S. Shing and K.D. Gubbins, *Molecular Physics* (in press).

6. A Thermodynamic Method for Simultaneous Representation of Ternary Vapor-liquid and Liquid-liquid Equilibria (Publication 9)

T.H. Cha and J.M. Prausnitz

When common expressions for the excess Gibbs energy g^E are used to predict ternary phase equilibria on the basis of binary data alone, calculated vapor-liquid equilibria (VLE) are generally satisfactory, but

calculated liquid-liquid equilibria (LLE) are often poor. This work proposes that a usual ternary expression for g^E be multiplied by a composition-dependent correction factor C such that $C=1$ whenever the ternary degenerates to a binary. This correction factor C is always near unity and therefore has little effect on the ternary VLE; however, its effect on LLE is large. Illustrative results are given for 19 ternary systems. When reliable binary-VLE data and reliable ternary-LLE data are available, the method proposed here gives a good thermodynamic representation of ternary VLLE suitable for computer-aided design of separation processes.

7. An Experimental Technique for Determining Solubilities of Complex Liquid Mixtures in Dense Gases (Publication 1)

Augustine Monge[†] and John Prausnitz

A flow method has been developed for measuring solubilities of heavy complex mixtures in compressed gases to 100 bar and 600 K. A quantitative analysis of the effluent gas is not required; therefore, this method is suitable for liquid mixtures containing many unidentified components. The method is also suitable for gaseous mixtures containing a subcritical component such as water.

[†]Present address: E.I. du Pont de Nemours and Co., Inc., LaPlace, Louisiana 70068.

8. Phase Equilibria for Mixtures Containing Very Many Components. Development and Application of Continuous Thermodynamics (Publication 10)

R.L. Cotterman, R. Bender, and J.M. Prausnitz

For some multicomponent mixtures where detailed chemical analysis is not feasible, the composition of the mixture may be described by a continuous-distribution function of some convenient macroscopic property such as normal boiling point or molecular weight. To attain a quantitative

description of phase equilibria for such mixtures, this work has developed thermodynamic procedures for continuous systems: the procedure is called continuous thermodynamics. To illustrate the procedure, continuous thermodynamics is used here to calculate dew points for natural-gas mixtures, solvent loss in a high-pressure absorber, and liquid-liquid phase equilibria in a polymer-fractionation process.

Continuous thermodynamics provides a rational method for calculating phase equilibria for those mixtures where complete chemical analysis is not available but where composition can be given by some statistical description. While continuous thermodynamics is only the logical limit of the well-known pseudocomponent method, it is more efficient than that method because it is less arbitrary and the required computer time is much lower.

9. Phase Equilibria for Complex Fluid Mixtures (Publication 2)

John M. Prausnitz

After complex mixtures are defined, attention is given to the canonical procedure used for the thermodynamics of fluid mixtures. First a suitable, idealized reference system is established, and then a perturbation (or excess function) that corrects the idealized system for real behavior is established. For complex mixtures containing identified components (e.g. alcohols, ketones, water), discussion is directed at possible techniques for extending to complex mixtures our conventional experience with reference systems and perturbations for simple mixtures. Possible extensions include generalization of the quasi-chemical approximation (local compositions) and superposition of chemical equilibria (association and solvation) on a "physical" equation of state.

For complex mixtures containing unidentified components (e.g. coal-derived fluids), a possible experimental method is suggested for characterization. Conventional procedures can then be used to calculate phase equilibria using the concept of pseudocomponents whose properties are given by the characterization data. Finally, as an alternative to the pseudocomponent method, a brief introduction is given to phase-equilibrium calculations using continuous thermodynamics.

10. Thermodynamics of Gas Solubility. Relation Between Equation-of-state and Activity-coefficient Models (Publication 11)

E. Bender,[†] U. Klein,[‡] W. Schmitt,[‡] and J.M. Prausnitz

The Krichevsky-Ilinskaya equation for gas solubility is derived from an equation of state. First the ratio of fugacity to mole fraction for the solute is obtained by calculating the fugacity coefficient of the solute at infinite dilution. Then the logarithm of this ratio is expanded in a double Taylor series with respect to pressure and composition. Only first-order terms are retained. Using a simple equation of state with conventional mixing rules, an experimental value of Henry's constant is used to obtain the equation of state's characteristic binary parameter. The remaining parameters in the Krichevsky-Ilinskaya equation (partial molar volume and Margules constant) are then obtained from the equation of state.

To illustrate, results are given for the solubility of hydrogen in ethylene diamine and the solubilities of methane in n-hexane and water.

[†]Deceased December 22, 1982.

[‡]Present address: Departments of Mechanical and Chemical Engineering, University of Kaiserslautern, West Germany.

1983 PUBLICATIONS AND REPORTS

Refereed Journals

1. Augustine Monge and John M. Prausnitz, "An Experimental Technique for Determining Solubilities of Complex Liquid Mixtures in Dense Gases," *I&EC Fund.* **22**, 505 (1983).
2. John M. Prausnitz, "Phase Equilibria for Complex Fluid Mixtures," *Fluid Phase Equilibria* **14**, 1 (1983).
3. Y. Hu, E.G. Azevedo, and J.M. Prausnitz, "The Molecular Basis for Local Compositions in Liquid-mixture Models," *Fluid Phase Equilibria* **14**, 351 (1983).
4. E.M. Pawlikowski and J.M. Prausnitz, "Estimation of Setchenow Constant for Nonpolar Gases in Common Salts at Moderate Temperatures," *I&EC Fund.* **22**, 896 (1983).[†]
5. E.M. Pawlikowski, J.S. Newman, and J.M. Prausnitz, "Vapor-liquid Equilibria for NH₃ and H₂ in the 100 to 150°C Region: Effect of

Low Levels of Phenol on Partial Pressure of Ammonia," *AIChE J.* **29**, 869 (1983).[†]

LBL Reports

6. Eldon R. Larsen and John M. Prausnitz, "High Pressure Phase Equilibria for the Water/Methane System," presented at the American Institute of Chemical Engineers 1983 Spring National Meeting and Petro Expo '83, Houston, Texas, March 27-31, 1983, LBL-15501.
7. Ying Hu, Edmundo Azevedo, Dorothea Lüdecke, and John Prausnitz, "Thermodynamics of Associated Solutions. Henry's Constants for Nonpolar Solutes in Water," submitted to *Fluid Phase Equilibria*, LBL-16804.
8. Ying Hu, Dorothea Lüdecke, and John Prausnitz, "Molecular Thermodynamics of Fluid Mixtures Containing Molecules that Differ in Size and Potential Energy," submitted to *Fluid Phase Equilibria*, LBL-16803.
9. T.H. Cha and J.M. Prausnitz, "A Thermodynamic Method for Simultaneous Representation of Ternary Vapor-liquid and Liquid-liquid Equilibria," LBL-17153.
10. R.L. Cotterman, R. Bender, and J.M. Prausnitz, "Phase Equilibria for Mixtures Containing Very Many Components. Development and Application of Continuous Thermodynamics," submitted to *I&EC Proc. Des. Dev.*, LBL-16940.
11. E. Bender, U. Klein, W. Schmitt, and J.M. Prausnitz, "Thermodynamics of Gas Solubility. Relation Between Equation-of-state and Activity-coefficient Models," LBL-17152.
12. D.K. Joshi and J.M. Prausnitz, "Supercritical Fluid Extraction with Mixed Solvents," LBL-17154.
13. Frank E. Anderson and John M. Prausnitz, "Mutual Solubilities and Vapor Pressures of Hydrocarbon-water Systems," LBL-17333.

Other Publications

14. Y. Hu, E.G. Azevedo, and J.M. Prausnitz, "The Molecular Basis for Local Compositions in Liquid Mixture Models," presented at the Third International Conference on Fluid Properties and Phase Equilibria for Chemical Process Design, Callaway Gardens, Georgia, April 10-15, 1983.
15. A. Monge and J.M. Prausnitz, "An Experimental Method for Measuring Solubilities of Heavy Fossil-fuel Fractions in Compressed Gases to

100 Bar and 300°C," in *Chemical Engineering of Supercritical-fluid Conditions*, M.Paulaitis, Ed., Ann Arbor Science Publishers, 1983, Chapter 7.

Invited Talks

16. J.M. Prausnitz, "Thermodynamics of Complex Mixtures," Keynote Lecture, Third International Conference on Fluid Properties and Phase Equilibria for Chemical Process Design, Callaway Gardens, Georgia, April 10–15, 1983.
17. J.M. Prausnitz, "Reality and Abstraction. The Two Sources of Chemical Thermodynamics," acceptance address (receipt of honorary Doctor of Engineering degree), The University of L'Aquila, L'Aquila, Italy, October 1983.
18. J.M. Prausnitz, "Continuous Thermodynamics for Phase Equilibria in Complex Mixtures," Annual Meeting of European Thermodynamicists in Chemical Engineering, Dortmund, Germany, October 1983; Chemical Engineering Department, Stanford University, Stanford, California, December 1983; Annual Meeting, AIChE, Washington, D.C., November 1983.

†Supported partly by a Fanny and John Hertz fellowship.

Nuclear
Sciences

LOW-ENERGY NUCLEAR SCIENCES

HEAVY-ELEMENT CHEMISTRY

Actinide Chemistry*

Norman M. Edelstein, Richard A. Andersen,
Neil Bartlett, John G. Conway,
Kenneth N. Raymond, Glenn T. Seaborg,
Andrew Streitwieser, Jr., David H. Templeton, and
Alan Zalkin, Investigators

INTRODUCTION

The purpose of this project is to study actinide materials in order to provide the basic knowledge necessary for their safe and economic use in present and future technology. The program includes the preparation of new gaseous, liquid, and solid phases and studies of their physical and chemical properties. Techniques for characterization include x-ray diffraction, optical and vibrational spectroscopy, magnetic resonance, and magnetic susceptibility. Equilibrium and kinetic data for complex formation are measured. From these complementary studies, new insights into the structural and chemical principles of actinide compounds are obtained with which to design new synthetic schemes to produce new materials.

A major aspect of the program is the design and synthesis of sequestering agents for actinide ions. These compounds are intended for use in the treatment of actinide poisoning and for possible application in the treatment of spent reactor fuels. Preparative, structural, and physical studies of new types of organoactinide, related organolanthanide, and new actinide inorganic complexes are continuing. Studies on optical spectra of free ions and actinide ions in crystals are being pursued in order to understand their electronic structure. Applications of new spectroscopic techniques for characterization of actinide species in solution are being undertaken.

*This work was supported by the Director, Office of Energy Research, Office of Basic Energy Sciences, Chemical Sciences Division of the U.S. Department of Energy under Contract No. DE-AC03-76SF00098.

SPECIFIC SEQUESTERING AGENTS FOR THE ACTINIDES

1. The Preparation of Praseodymium(III) Chloranilate and the Crystal Structures of $\text{Pr}_2(\text{C}_6\text{Cl}_2\text{O}_4)_3 \cdot 8\text{C}_2\text{H}_5\text{OH}$ and $\text{Na}_3[\text{C}_6\text{H}_2\text{O}(\text{OH})(\text{SO}_3)_2] \cdot \text{H}_2\text{O}$ (Publication 2)

P.E. Riley,[†] S.F. Haddad,[‡] and K.N. Raymond

The crystal structure of $\text{Pr}_2(\text{C}_6\text{Cl}_2\text{O}_4)_3 \cdot 8\text{C}_2\text{H}_5\text{OH}$ (1), a complex obtained by slow hydrolysis of *o*-chloranil ($\text{C}_6\text{Cl}_4\text{O}_2$) in acidic ethanol solution, has been determined by single-crystal x-ray-diffraction techniques with data collected by counter methods (see Figure 1-1). The structure of $\text{Na}_3[\text{C}_6\text{H}_2\text{O}(\text{OH})(\text{SO}_3)_2] \cdot \text{H}_2\text{O}$ (2), the trianion of tiron, has also been determined by x-ray crystallography. Crystals of 1 form in triclinic space group *P1* with $a = 8.990(1) \text{ \AA}$, $b = 10.503(2) \text{ \AA}$, $c = 13.589(1) \text{ \AA}$, $\alpha = 99.02(1)^\circ$, $\beta = 91.50(1)^\circ$, and $\gamma = 94.44(1)^\circ$. The observed density of 1.643 g/cm^3 is in agreement with the calculated value of 1.671 g/cm^3 for one unit of $\text{Pr}_2(\text{C}_6\text{Cl}_2\text{O}_4)_3 \cdot 8\text{C}_2\text{H}_5\text{OH}$ per unit cell. The crystal structure is a three-dimensional network of alternating $(\text{C}_6\text{Cl}_2\text{O}_4)^{2-}$ and Pr^{3+} ions in which the chloranilate rings lie about crystallographic inversion centers. The resulting coordination sphere about Pr^{3+} consists of six chloranilate oxygen atoms from three symmetry-independent chloranilate ions and three ethanol oxygen atoms (six of the eight ethanol molecules in the full formula—the remaining two are simply in the crystal lattice), arranged in an approximately tricapped trigonal prismatic fashion. Full-matrix least-squares refinement of the structure has converged with *R* and *R_w* indices (on $|F|$) of 0.025 and 0.040 using 3057 symmetry-independent reflections with $F_o^2 > 3\sigma(F_o^2)$. Crystals of 2 form from aqueous solution in orthorhombic space group *Pnma* with $a = 16.108(2) \text{ \AA}$, $b = 6.972(2) \text{ \AA}$, and $c = 9.700(1) \text{ \AA}$. The $[\text{C}_6\text{H}_2\text{O}(\text{OH})(\text{SO}_3)_2]^{3-}$ species exhibits rigorous *C_s* symmetry with only the two symmetry-related oxygen atoms of each SO_3 moiety lying out of the plane of the anion. There are no unusual aspects of the molecular geometry of 2.

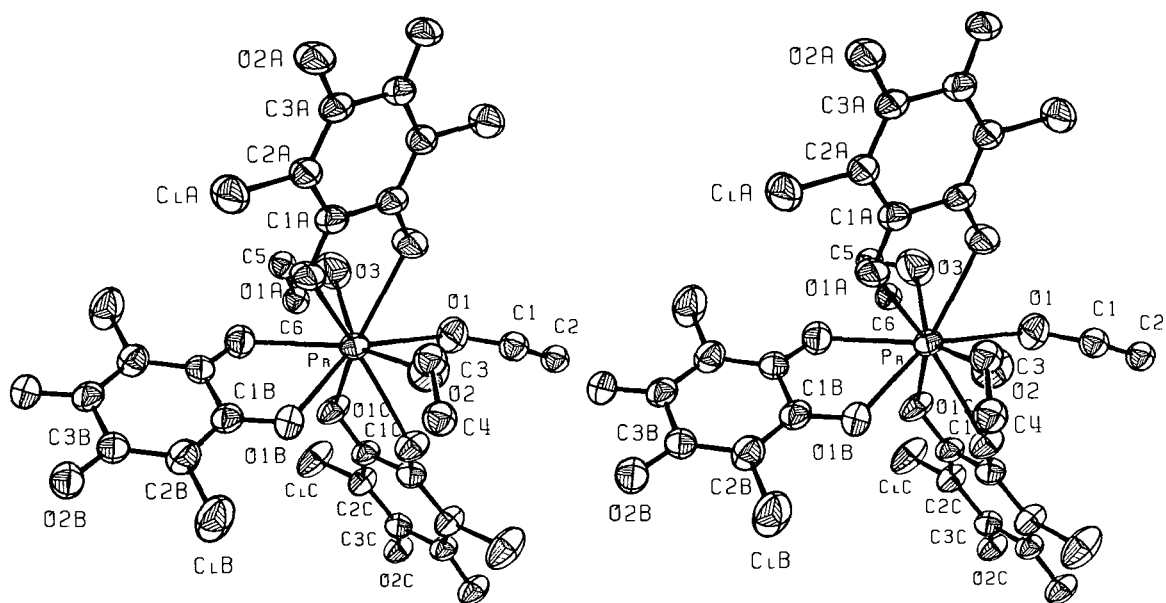


Figure 1-1. Stereoscopic view of the Pr^{3+} complex illustrating the atom-numbering scheme. Atoms are drawn as spheres of 50 percent probability. The thermal motion of the ethanol carbon atoms has been artificially reduced and hydrogen atoms omitted for clarity. (XBL 829-9628)

Full-matrix least-squares refinement of the structure has converged with R and R_w indices (on $|F|$) of 0.034 and 0.045, using the 805 observations with $F_o^2 > 3\sigma(F_o^2)$.

†Present address: Department of Chemistry, University of California, Berkeley, California 94720.

‡On leave from the Department of Chemistry, University of Jordan, Amman, Jordan.

2. Specific Sequestering Agents for the Actinides. 9. Synthesis of Metal Complexes of 1-hydroxy-2(1H)-pyridinone and the Crystal Structure of Tetrakis(1-hydroxy-2(1H)-pyridinone)aquothorium(IV) Dihydrate (Publication 14)†

P.E. Riley,‡ K. Abu-Dari, and K.N. Raymond

The Zr(IV), Ce(IV), Th(IV), and U(IV) complexes of 1-hydroxy-2(1H)-pyridinone anion ($\text{C}_5\text{H}_4\text{NO}_2^-$) have been prepared, and the crystal structure of the dihydrate of the nine-coordinate complex $(\text{C}_5\text{H}_4\text{NO}_2)_4(\text{H}_2\text{O})\text{Th}$ has been determined

by single-crystal x-ray-diffraction techniques with data obtained by counter methods (see Figure 2-1). The compound crystallizes as colorless parallelepipeds in orthorhombic space group $Pbcn$ with $a = 12.880(1) \text{ \AA}$, $b = 8.812(2) \text{ \AA}$, and $c = 20.826(2) \text{ \AA}$. The calculated density of 2.041 g/cm^3 agrees well with the measured value of 2.04 g/cm^3 and is consistent with four formula units of the dihydrate per unit cell. Full-matrix least-squares refinement of the structure with use of the 2100 reflections with $F_o^2 > 3\sigma(F_o^2)$ has converged with r and R_w indices of 0.026. The Th(IV) complex consists of neutral molecules of rigorous C_2 symmetry in which Th(IV) and the coordinated water molecule lie along the C_2 axis parallel to b . The immediate coordination sphere about Th is completed by the eight oxygen atoms of the four bidentate $\text{C}_5\text{H}_4\text{NO}_2^-$ ligands, such that the resulting nine-coordinate complex resembles a D_{3h} tricapped trigonal prism.

†Supported in part by the National Institute of Health through Grant HL24775.

‡Present address: Department of Chemistry, University of California, Berkeley, California 94720.

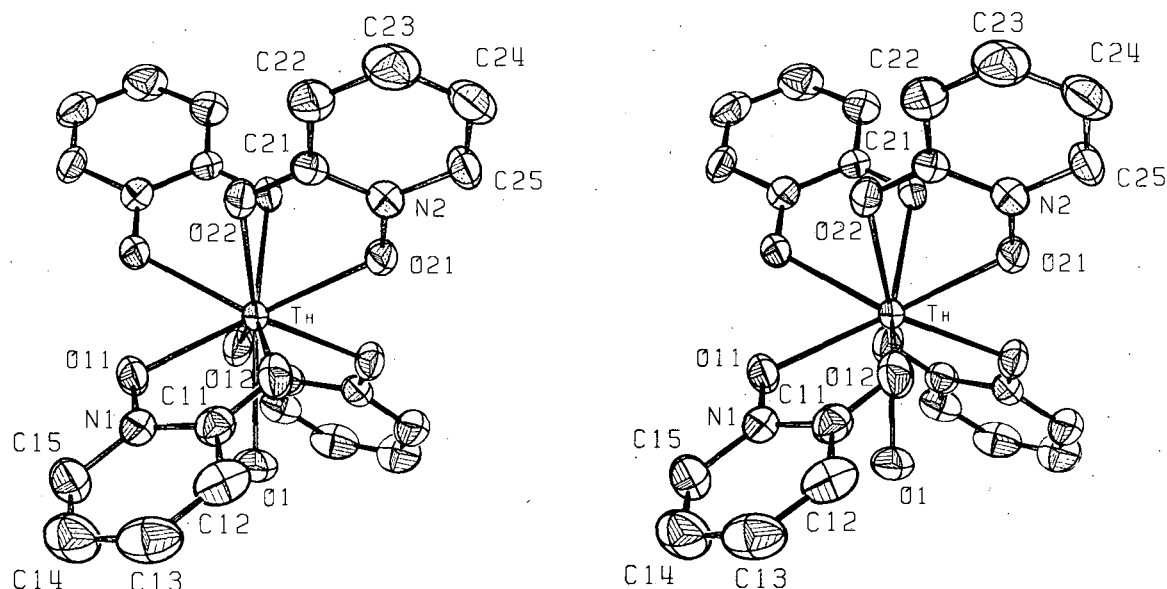


Figure 2-1. Stereoscopic view of $(C_5H_4NO_2)_2Th$, illustrating the atom-numbering scheme. Atoms are drawn as ellipsoids of 50 percent probability; hydrogen atoms have been omitted for clarity. A crystallographic C_2 axis is coincident with the Th-O(1) bond and thus carries the left and right halves of the molecule into each other.

(XBL 821-7742)

SYNTHETIC AND STRUCTURE STUDIES OF ACTINIDES AND OTHER COMPOUNDS

3. Tetraalkyl-phosphine Complexes of the f-block Metals; Preparation and Crystal Structure of $Th(CH_2Ph)_4(Me_2PCH_2CH_2PMe_2)$ and $U(CH_2Ph)_3Me(Me_2PCH_2CH_2PMe_2)$ (Publication 16)

P.G. Edwards, R.A. Andersen, and A. Zalkin

Reaction of four molar equivalents of $PhCH_2Li$ with $MCl_4(Me_2PCH_2CH_2PMe_2)_2$ gives $M(CH_2Ph)_4(Me_2PCH_2CH_2PMe_2)_2$, where M is Th or U. Reaction of a mixture of three molar equivalents of $PhCH_2Li$ and one molar equivalent of $MeLi$ with $MCl_4(Me_2PCH_2CH_2PMe_2)_2$ gives the unsymmetrical alkyls, $M(CH_2Ph)_3Me(Me_2PCH_2CH_2PMe_2)_2$, where M is Th or U. The molecular structures of $Th(CH_2C_6H_5)_4(Me_2PCH_2CH_2PMe_2)_2$ and $U(CH_2C_6H_5)_3Me(Me_2PCH_2CH_2PMe_2)_2$ were determined by

single-crystal x-ray-diffraction methods. Crystals of $Th(CH_2Ph)_4(Me_2PCH_2CH_2PMe_2)_2$ are triclinic, $P1$, with cell dimensions $a = 11.463(2)$ Å, $b = 16.151(3)$ Å, $c = 21.527(3)$ Å, $\alpha = 106.28(2)^\circ$, $\beta = 95.85(2)^\circ$, and $\gamma = 107.78(2)^\circ$; there are 4 molecules in the unit cell. Crystals of $U(CH_2Ph)_3Me(Me_2PCH_2CH_2PMe_2)_2$ are monoclinic, $P2_1/c$, with cell dimensions $a = 13.035(2)$ Å, $b = 15.381(2)$ Å, $c = 14.540(2)$ Å, and $\beta = 98.06(2)^\circ$; there are 4 molecules in the unit cell. In the Th complex there are two independent molecules in the unit cell. The Th atoms are each bonded to four benzyl groups and to two phosphorus atoms from the dimethylphosphinoethane ligands; the average Th-C distance is $1.55(2)$ Å, and the average Th-P distance is $3.17(3)$ Å. In the U complex the uranium atom is bonded to a methyl group, three benzyl groups, and the two phosphorus atoms of the dimethylphosphinoethane ligand. The U-C(methyl) distance is $2.41(1)$ Å; the average U-C(benzyl) distance is $2.50(4)$ Å.

ORTEP drawings of the structures of the two compounds are shown in Figures 3-1 and 3-2.

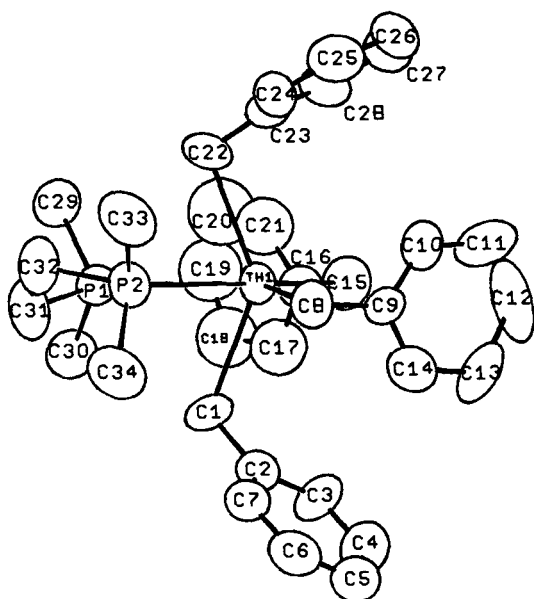


Figure 3-1. ORTEP drawing of $\text{Th}(\text{CH}_2\text{Ph})_4(\text{Me}_2\text{PCH}_2\text{CH}_2\text{PMe}_2)$. (XBL 838-11150)

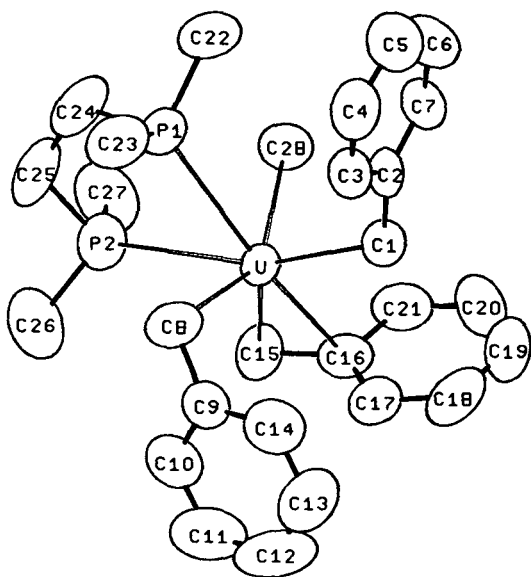


Figure 3-2. ORTEP drawing of $\text{U}(\text{CH}_2\text{Ph})_3\text{Me}(\text{Me}_2\text{PCH}_2\text{CH}_2\text{PMe}_2)$. (XBL 824-9117)

4. Dialkyl Bis[bis(trimethylsilyl)amido] Group 4A Metal Complexes. Preparation of Bridging Carbene Complexes by γ Elimination of Alkane. Crystal Structure of $\text{ZrCHSi}(\text{Me})_2\text{NSiMe}_3[\text{N}(\text{SiMe}_3)_2]_2$ (Publication 4)

R.P. Planalp, R.A. Andersen, and A. Zalkin

The dialkyls of zirconium of the type $\text{R}_2\text{Zr}[\text{N}(\text{SiMe}_3)_2]_2$, where R is Me, Et, or CH_2SiMe_3 , thermally decompose (at 60°C and 10^{-2} mm) by elimination of alkane (MeH, EtH, or Me_4Si , respectively) to give the bridging carbene compound $\text{ZrCHSi}(\text{Me})_2\text{NSiMe}_3[\text{N}(\text{SiMe}_3)_2]_2$. The 1:1 complex with pyridine is described. The related hafnium dialkyls decompose in a related manner, though in this case the decomposition product could only be characterized as its pyridine complex, $\{\text{HfCHSi}(\text{Me})_2\text{NSiMe}_3[\text{N}(\text{SiMe}_3)_2][\text{NC}_5\text{H}_5]_2\}$. The NMR spectra of the pyridine complexes of zirconium and hafnium are similar. In contrast, $\text{Me}_2\text{Ti}[\text{N}(\text{SiMe}_3)_2]_2$ is thermally stable to 190°C . The titanium-carbene $\text{TiCHSi}(\text{Me})_2\text{NSiMe}_3[\text{N}(\text{SiMe}_3)_2]_2$ may be prepared by sodium-amalgam reduction of $\text{Cl}_2\text{Ti}[\text{N}(\text{SiMe}_3)_2]_2$. The crystal structure of $\text{ZrCHSi}(\text{Me})_2\text{NSiMe}_3[\text{N}(\text{SiMe}_3)_2]_2$ was determined by single-crystal x-ray crystallography. The crystals are orthorhombic of space group $Pbca$ with cell dimensions $a = 18.307(7)$ Å, $b = 26.036(6)$ Å, and $c = 19.425(6)$ Å; for $Z = 8$, $d_{\text{calcd}} = 1.18$ g/cm³. The structure was refined to a conventional R factor of 0.061 by using 3149 data where $F^2 > 3\sigma(F^2)$. The structure consists of three fused, planar, four-membered rings giving the molecule a "tub" conformation. The Zr-C distances are 2.16 and 2.21 Å, and the Zr-N distances range from 2.04 to 2.09 Å.

A view that emphasizes the central structure of the molecule is shown in Figure 4-1.

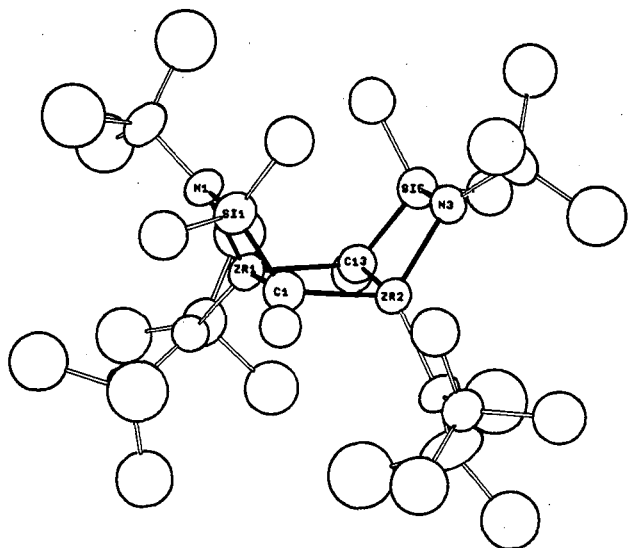


Figure 4-1 ORTEP drawing of $\{ZrCHSi(Me)_2NSiMe_3-[NSiMe_3]_2\}_2$ (XBL 816-10257)

5. Divalent Lanthanide Chemistry; Preparation and Crystal Structures of Sodium

Tris[bis(trimethylsilyl)amido]-europate(II) and -ytterbate(II), $NaM[N(SiMe_3)_2]_3$ (Publication 27)

T.D. Tilley, R.A. Andersen, and A. Zalkin

A new synthetic method for high-yield preparations of the divalent silylamides $M[N(SiMe_3)_2]_2[MeOCH_2CH_2OMe]_2$, where M is Eu or Yb, has been developed that involves reaction of Ml_2 and $NaN(SiMe_3)_2$ in $MeOCH_2CH_2OMe$. Reaction of EuI_2 and $NaN(SiMe_3)_2$ in Et_2O yields $NaEu[N(SiMe_3)_2]_3$. Reaction of YbI_2 with $NaN(SiMe_3)_2$ in Et_2O yields two products, depending on the crystallization conditions. If Et_2O is used, $Yb[N(SiMe_3)_2]_2(OEt)_2$ is isolated. In contrast, if toluene is used, $NaYb[N(SiMe_3)_2]_3$ is isolated. The crystal structures of $NaEu[N(SiMe_3)_2]_3$ and $NaYb[N(SiMe_3)_2]_3$ were determined by x-ray-diffraction methods. Crystals of $NaEu[N(SiMe_3)_2]_3$ are monoclinic, $P2_1/n$, with cell dimensions $a = 17.586(6)$ Å, $b = 19.170(6)$ Å, $c = 21.808(6)$ Å, and $\beta = 107.90(4)^\circ$; for $Z = 8$, the calculated density is 1.246 g/cm³. Crystals of $NaYb[N(SiMe_3)_2]_3$ are orthorhombic, $Pbca$, with cell dimensions $a = 19.334(6)$ Å, $b = 18.534(6)$ Å, and $c = 20.020(6)$ Å; for $Z = 8$, the calculated density is 1.254 g/cm³. The structures were refined to conventional R factors of 0.043 [6757 data, $F^2 > 3\sigma(F^2)$] for the Eu complex, and 0.056 [2546 data, $F^2 > 3\sigma(F^2)$] for the Yb com-

plex. In the europium complex there are two crystallographically distinct but chemically equivalent molecules. The molecular structures of the Eu and Yb complexes are similar. The lanthanide atom bonds to one of the silylamido ligands exclusively and shares the two others with the sodium atom. The Eu-N and Yb-N (unshared) distances are $2.46(1)$ Å and $2.38(2)$ Å, respectively; the average Eu-N and Yb-N (shared) distances are $2.55(2)$ Å and $2.46(2)$ Å, respectively; the average Na-N distance is $2.46(1)$ Å. Several noteworthy close contacts between the metal ions and methyl carbon atoms have been noted; i.e., Na-C, 2.70 Å; Eu-C, 2.97 Å; and Yb-C, 2.86 Å.

ORTEP drawings of the two complexes are shown in Figures 5-1 and 5-2.

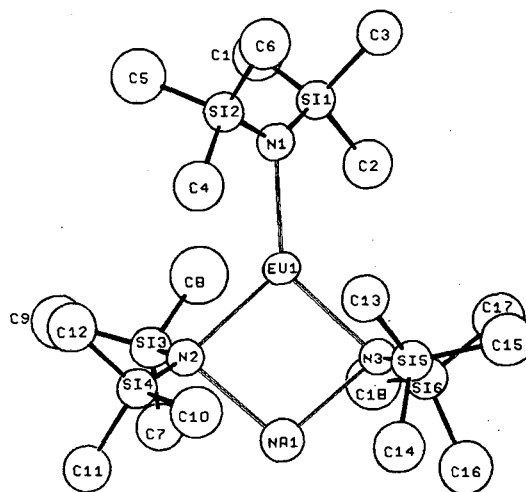


Figure 5-1. ORTEP drawing of $NaEu[(Me_3Si)_2N]_3$ (XBL 8110-7069)

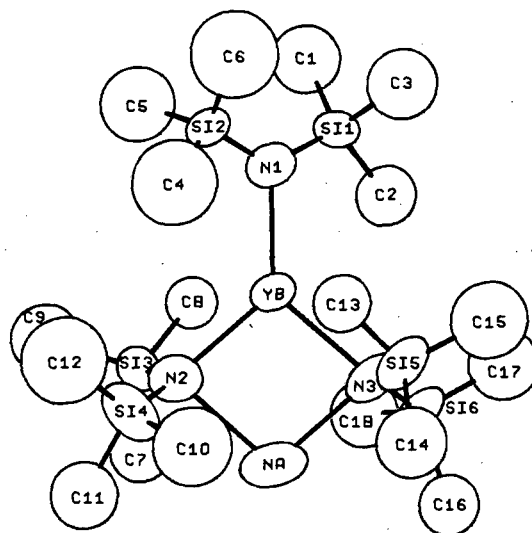


Figure 5-2. ORTEP drawing of $NaYb[(Me_3Si)_2N]_3$ (XBL 823-8228)

6. Bis(pentamethylcyclopentadienyl)ytterbium (II) as a Lewis Acid and Electron-transfer Ligand; Preparation and Crystal Structures of $[\text{Yb}(\text{Me}_5\text{C}_5)_2(\mu\text{-CO})_x\text{Mn}(\text{CO})_{5-x}]_y$ where X and Y Are Two and X Is Three and Y Is Infinite (Publication 17)

J.M. Boncella and R.A. Andersen

The divalent ytterbium metallocene, $(\text{Me}_5\text{C}_5)_2\text{Yb}(\text{OEt}_2)$, reacts with $\text{Mn}_2(\text{CO})_{10}$ to give a compound of composition $(\text{Me}_5\text{C}_5)_2\text{YbMn}(\text{CO})_5$ 1/4 PhMe (see Figure 6-1), which was shown by an x-ray crystallographic study to be composed of a polymeric chain of $[(\text{Me}_5\text{C}_5)_2\text{Yb}(\mu\text{-OC})_3\text{Mn}(\text{CO})_2]$ units with dimeric units $[(\text{Me}_5\text{C}_5)_2\text{Yb}(\mu\text{-OC})_2\text{Mn}(\text{CO})_3]$ packed between the polymeric sheets. The toluene of solvation fills regular spaced voids in the network of dimer and polymer sheets. The space group is $C2/m$ with $a = 18.942(5)$ Å, $b = 32.592(5)$ Å, $c = 19.029(5)$ Å, $\beta = 109.92(2)^\circ$, $V = 11,045(18)$ Å³, and

$Z = 16$. The contact ion-pair complex results from $(\text{Me}_5\text{C}_5)_2\text{Yb}$ acting as an electron-transfer reagent, $(\text{Me}_5\text{C}_5)_2\text{Yb} \rightarrow (\text{Me}_5\text{C}_5)_2\text{Yb}^+ + 1e^-$, and as a Lewis acid by way of $\text{Yb}(\mu\text{-OC})\text{Mn}$ interactions. The solution and solid-state infrared spectra are discussed relative to the alkali-metal analogues. The rhenium carbonyl $\text{Re}_2(\text{CO})_{10}$ behaves similarly.

7. Dibenzouranocene and Related Compounds (Publication 12)

A. Streitwieser, Jr., R.Q. Klutz, K.A. Smith, and W.D. Luke

Bis-benzo[8-annulene]uranium(IV)(dibenzouranocene), 4 in Figure 7-1, and the thorium analog, 5, have been prepared from benzocyclooctatetraene dianion and the metal tetrachlorides. The Diels-Alder product from cyclooctatrienyne and butadiene,

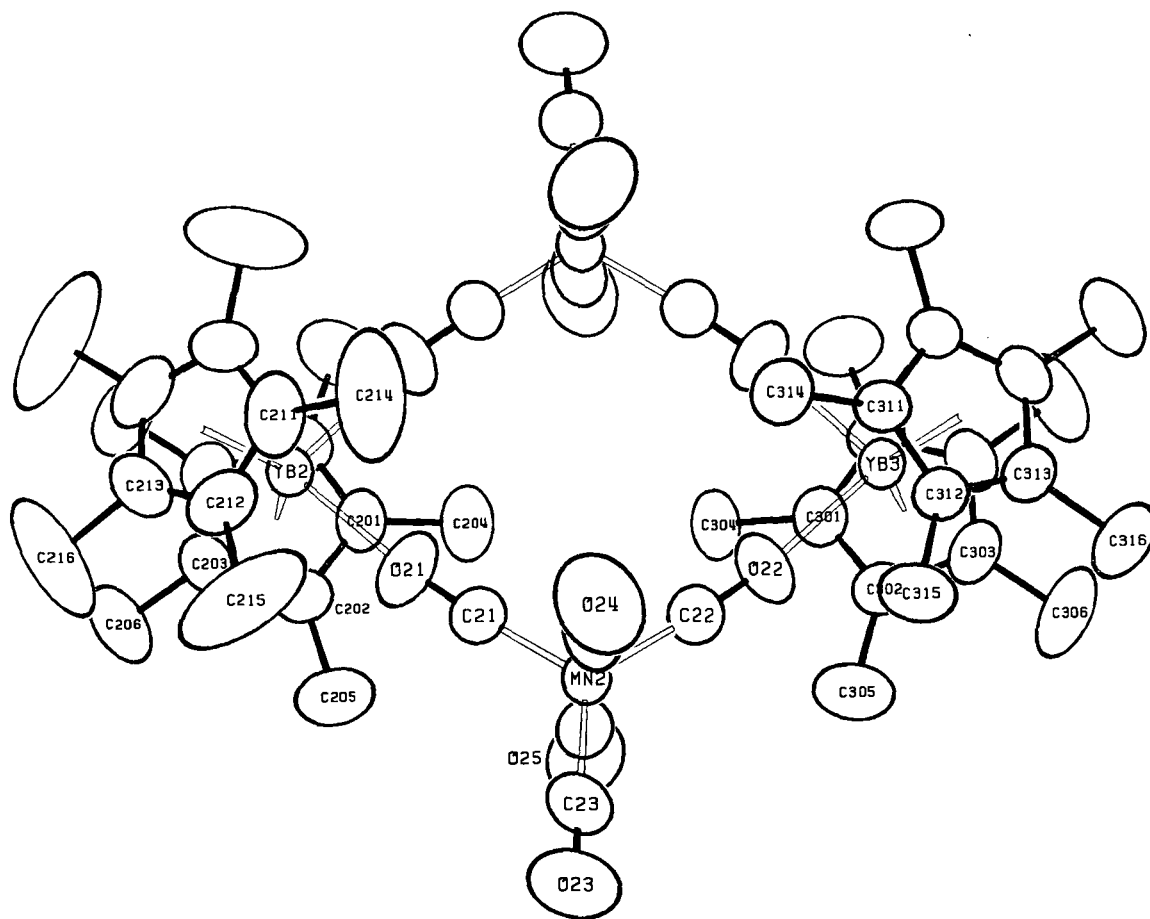


Figure 6-1. ORTEP drawing of $[(\text{Me}_5\text{C}_5)_2\text{Yb}(\mu\text{-OC})_3\text{Mn}(\text{CO})_2]$.

(XBL 826-10530)

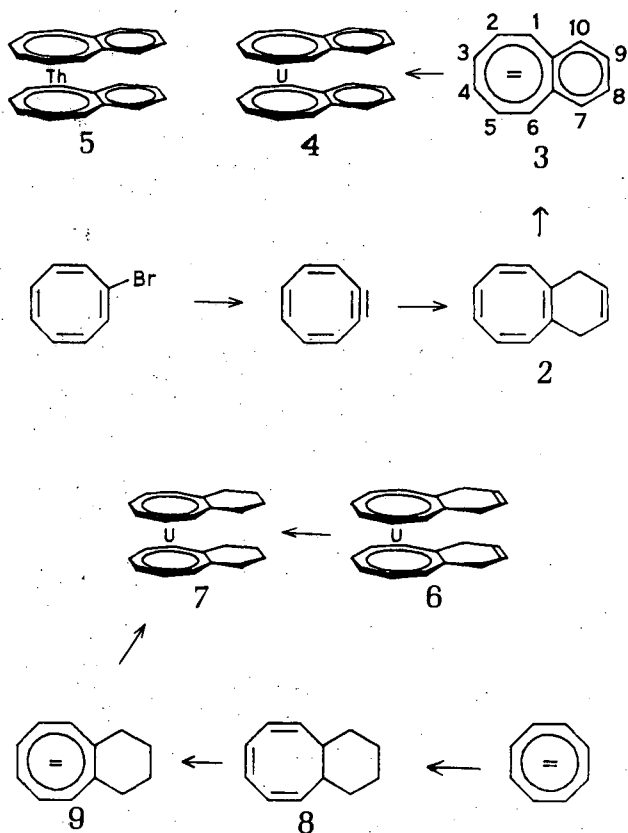


Figure 7-1. Summary of reactions of dibenzouranocene and related compounds. (XBL 8312-2496)

7, 10-dihydrobenzocyclooctatetraene, 2, gave a uranocene derivative, 6, which could not be dehydrogenated to 4. Catalytic hydrogenation, however, did give the uranium derivative, 7, of tetrahydrobenzocyclooctatetraene. The corresponding deuteration gave 70% exo and 30% endo incorporation of deuterium. Reaction of cyclooctatetraene dianion with 1,4-dibromobutane gave cisbicyclo-[6.4.0]dodeca-2,4,6-triene, 8, which on deprotonation with KNH_2/NH_3 and treatment with UCl_4 also gave 7. Analysis of NMR spectra of 4 (see Figure 7-2) indicates a spin-density distribution closely related to that in the radical anion of benzocyclooctatetraene. The ligand-exchange equilibrium between 4 and uranocene has been determined and found to favor the mixed sandwich compound with an equilibrium constant of 7.1.

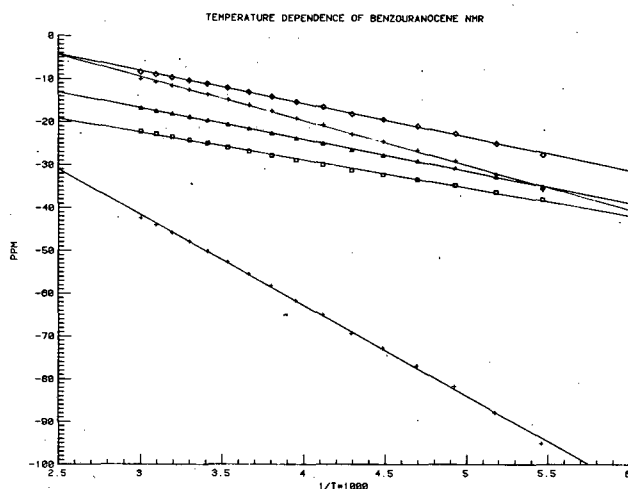


Figure 7-2. Linear temperature dependence ($1/T$) versus chemical shifts (PPM) of dibenzouranocene. (XBL 818-11176)

8. The Synthesis and Characterization of $(\text{UCp}_3)_2$ (Pyrazine) and $[\text{U}(\text{MeCp})_3]_2$ (Pyrazine): π -bridged Dimers of U^{3+} (Publication 1)

C.W. Eigenbrot, Jr. and K.N. Raymond

The title compounds are formed by the reaction of $\text{U}(\text{C}_5\text{H}_5)_3(\text{C}_4\text{H}_8\text{O})$ and $\text{U}(\text{C}_6\text{H}_7)_3(\text{C}_4\text{H}_8\text{O})$ with pyrazine ($\text{C}_4\text{H}_4\text{N}_2$) and are characterized by elemental analysis, mass, IR, ^1H NMR, electronic spectra, and x-ray powder patterns. The $[\text{U}(\text{C}_6\text{H}_7)_3]_2(\text{C}_4\text{H}_4\text{N}_2)$ exhibits anomalous magnetic behavior that remains under investigation.

9. Bis(2-methylimidazolium) Tetrachlorodioxouranium(VI), $(\text{CH}_3\text{C}_3\text{N}_2\text{H}_4^+)_2(\text{UO}_2\text{Cl}_4)^{-2}$ (Publication 5)

A. Zalkin, D. Perry,[†] L. Tsao,[†] and Z. Dechun[‡]

The structure of bis(2-methylimidazolium) tetrachlorodioxouranium(VI) was analyzed by single-crystal x-ray diffraction using molybdenum x-rays. The crystals, which are strongly luminescent,

are monoclinic, space group $P2_1/c$, with cell dimensions (at 23°C) $a = 7.177(2)$ Å, $b = 18.526(4)$ Å, $c = 12.600(3)$ Å, and $\beta = 94.08(2)^\circ$. For $Z = 2$ the calculated density is 2.30 g/cm^3 . For 1501 reflections [$F^2 > \sigma(F^2)$] $R = 0.035$. The structure consists of the packing of columns of $\text{UO}_2\text{Cl}_4^{2-}$ anions and columns of $\text{CH}_3\text{C}_3\text{N}_2\text{H}_4^+$ cations that are parallel to the a axis (see Figure 9-1).

[†]Present address: Earth Sciences Division, Lawrence Berkeley Laboratory, Berkeley, California 94720.

[‡]Present address: East China Engineering Institute, Nanjing, People's Republic of China.

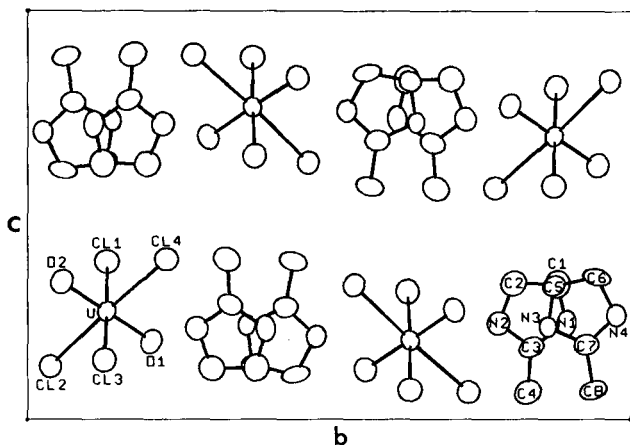


Figure 9-1. ORTEP view of the molecules in a unit cell as viewed down the a axis. (XBL 834-9359)

PHYSICAL AND SPECTROSCOPIC PROPERTIES

10. Uranium Five (U V), the 1S_0 Level and a Parametric Analysis of the $5f^2$ Configuration (Publication 24)

C.H.H. Van Deurzen,[†] K. Rajnak,[‡] and J.G. Conway

The 1S_0 level of the $5f^2$ configuration of U V has been found at $43,613.58 \pm 0.1 \text{ cm}^{-1}$. A parametric fit of the 13 levels of the $5f^2$ configuration gives an rms deviation of 9.8 cm^{-1} with $F^2 = 51,938 \pm 39$, $F^4 = 42,708 \pm 100$, $F^6 = 27,748 \pm 68$, $\alpha = 35.5 \pm 0.4$, $\beta = -664 \pm 25$, $\gamma = 744 \pm 26$, $\zeta = 1968 \pm 2$, $P^2 =$

573 ± 66 , $P^4 = 524 \pm 144$, and $P^6 = 1173 \pm 321$, all in cm^{-1} .

[†]Present address: British Columbia Institute of Technology, Burnaby, V5G 3H2, British Columbia.

[‡]Present address: Department of Physics, Kalamazoo College, Kalamazoo, Michigan 49007.

11. Parametric Analysis of the Energy Levels of U^{4+} in D_2 and Limiting D_2 Sites in Incommensurate ThBr_4 (Publication 11)

P. Delamoye,[†] K. Rajnak,[‡] M. Genet,[†] and N. Edelstein

Below $T_c = 95 \text{ K}$, $\text{U}^{4+}:\text{ThBr}_4$ exists as an incommensurately modulated structure. The U^{4+} ions occupy a range of sites which vary from D_{2d} to a limiting D_2 site. The D_{2d} and limiting D_2 sites have been identified spectroscopically. We report a parametric analysis of the U^{4+} energy levels in both sites. For 26 levels in the D_{2d} site, the rms deviation $\sigma = 36 \text{ cm}^{-1}$, and $F^2 = 42,253 \pm 127$, $F^4 = 40,458 \pm 489$, $F^6 = 25,881 \pm 383$, $\zeta = 1783 \pm 7$, $\alpha = 31 \pm 1$, $\beta = 644 \pm 75$, $\gamma = 1200$, $B_2^2 = -1096 \pm 80$, $B_0^4 = 1316 \pm 146$, $B_4^4 = -2230 \pm 85$, $B_6^6 = -3170 \pm 379$, and $B_6^6 = 246$, all in cm^{-1} . For 38 D_2 levels $\sigma = 39 \text{ cm}^{-1}$, and those parameters which occur in both symmetries are only slightly changed. The additional parameters which occur only in the D_2 symmetry are $B_2^2 = -78 \pm 30$, $B_2^4 = 318 \pm 122$, $B_2^6 = 136 \pm 101$, and $B_6^6 = 123 \pm 125$, all in cm^{-1} . F^2 is 81% of the free-ion value. This decrease in F^2 is more like that found for 3d than for 4f electrons.

[†]Present address: Laboratoire de Radiochimie, Institut de Physique Nucleaire, Universite de Paris-Sud, Orsay, France.

[‡]Present address: Department of Physics, Kalamazoo College, Kalamazoo, Michigan 49007.

12. Site-selective Excitation of U^{4+} Diluted in Incommensurate ThBr_4 (Publication 10)

P. Delamoye,[†] J.C. Krupa,[†] J.G. Conway, and N. Edelstein

Selective-excitation experiments in the visible region are reported for the $\text{U}^{4+}:\text{ThBr}_4$ system. These permit the classification of absorption and emission

lines to the sites found in the incommensurately modulated structure of ThBr_4 . The lines are assigned to a $D_{2d}(\text{B})$ site, a continuous distribution of $D_2(\text{C})$ sites, and to the limiting $D_2(\text{A})$ site. By application of the model of Delamoye and Currat,¹ the energy levels have been mapped as a function of the phase angle ϕ of the distortion (see Figure 12-1). The agreement between the predictions of the model and experiment is very good. It is shown that the incommensurate structure of ThBr_4 must be of higher order than $q_s/c^* = 4/13$ (where q_s is a modulation wave vector and c^* is one of the basis vectors of the reciprocal lattice of the tetragonal unit cell).

[†]Present address: Laboratoire de Radiochimie, Institut de Physique Nucleaire, Universite de Paris-Sud, Orsay, France.

1. Currat, J. Phys. (Paris) Lett. 43, L655 (1982).

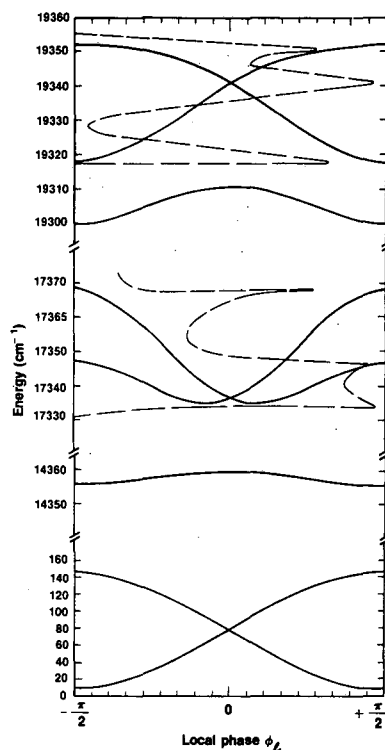


Figure 12-1. Energy levels obtained as a function of ϕ , by fitting the parameters of the Delamoye-Currat model to the measured energies at the A and B sites. The dashed lines represent the profiles of the absorption bands from which the parameters were evaluated. (XBL 837-10528)

13. Anisotropic Magnetic Susceptibility of Single-crystal UCl_4 (Publication 8)

E. Gamp, N. Edelstein, C.K. Malek,[†] S. Hubert,[†] and M. Genet[†]

The anisotropic magnetic susceptibilities χ_{\parallel} and χ_{\perp} of UCl_4 have been measured in single crystals between 1.6 and 350 K (see Figure 13-1). Powder measurements of the average susceptibility were also performed but were found to be unreliable due to orientation effects. The single-crystal results were interpreted in terms of the parametrized crystal field model with the following parameters: $\zeta = 1819 \text{ cm}^{-1}$, $F^2 = 42,632 \text{ cm}^{-1}$, $F^4 = 38,680 \text{ cm}^{-1}$, $F^6 = 23,320 \text{ cm}^{-1}$, $B_0^2 = -1008 \text{ cm}^{-1}$, $B_0^4 = 1730 \text{ cm}^{-1}$, $B_2^4 = -2704 \text{ cm}^{-1}$, $B_0^6 = -2705 \text{ cm}^{-1}$, $B_2^6 = 346 \text{ cm}^{-1}$, $\alpha = 29 \text{ cm}^{-1}$, $\beta = -638 \text{ cm}^{-1}$, and $\gamma = 1617 \text{ cm}^{-1}$. These parameters yield a $\Gamma_4(^3H_4)$ ground state and a paramagnetic first excited state $\Gamma_5(^3H_4)$ at 110 cm^{-1} and are in good agreement with the optical spectrum.

[†]Present address: Laboratoire de Radiochimie, Institut de Physique Nucleaire, Universite de Paris-Sud, Orsay, France.

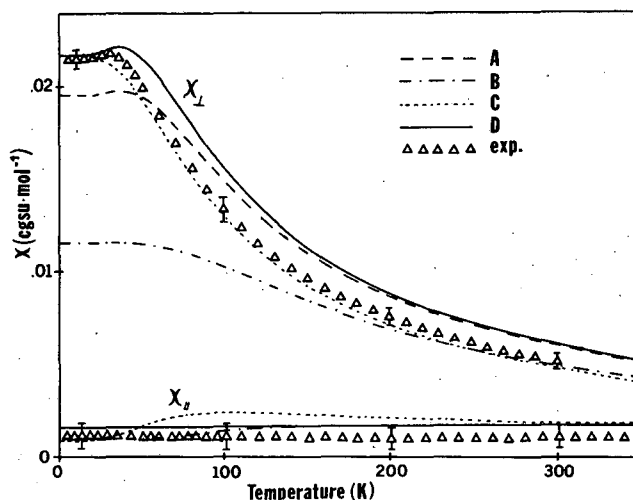


Figure 13-1. Molar single-crystal susceptibility in UCl_4 as a function of temperature. The labels of the calculated curves correspond to various parameter sets. (XBL 834-9169)

14. Optical and Magnetic Properties of Uranium Borohydride and Tetrakis(methylborohydride) (Publication 21)

K. Rajnak,[†] E. Gamp, R. Shinomoto, and N. Edelstein

The $U(BD_4)_4/Hf(BD_4)_4$ optical spectrum reported by Bernstein and Keiderling¹ has been reanalyzed. All 19 allowed transitions have been identified. The crystal field is ~ 2.5 times as strong as that of $U^{4+}/ThBr_4$, but the values of the F^k and ζ parameters are nearly the same. The magnetic susceptibility of the structurally related molecule $U(BH_3CH_3)_4$ has been measured from 2 to 330 K. Using the eigenvectors from the optical analysis, the magnetic data can be fit with an orbital reduction factor $k = 0.85$. For $U(BD_4)_4/Hf(BD_4)_4$, $k = \zeta/\zeta_{\text{free ion}} = 0.91$.

[†]Present address: Department of Physics, Kalamazoo College, Kalamazoo, Michigan 49007.

1. Keiderling, J. Chem. Phys. **59**, 2105 (1973).

15. Analysis of the Optical Spectrum of $Np(BD_4)_4$ Diluted in $Zr(BD_4)_4$ and the Magnetic Properties of $Np(BH_4)_4$ and $Np(BH_3CH_3)_4$ (Publication 22)

K. Rajnak,[†] R.H. Banks,[‡] E. Gamp, and N. Edelstein

The optical spectrum of $Np(BD_4)_4/Zr(BD_4)_4$ is reported and analyzed. The parameter values obtained are consistent with those for $U(BD_4)_4/Hf(BD_4)_4$. A total of 46 levels were fit with $\sigma = 84 \text{ cm}^{-1}$. EPR data on $Np(BD_4)_4/Zr(BD_4)_4$ and $Np(BH_3CH_3)_4/Zr(BH_3CH_3)_4$ and the magnetic susceptibility of $Np(BH_3CH_3)_4$ are reported. They could be fit with the eigenvectors from the optical analysis only by the inclusion of orbital reduction factors $k = 0.885$ for $Np(BD_4)_4$ and 0.862 for $Np(BH_3CH_3)_4$. These values indicate greater covalency for the methylborohydride compound than for the borohydride.

[†]Present address: Department of Physics, Kalamazoo College, Kalamazoo, Michigan 49007.

[‡]Present address: NALCO Chemical Company, Naperville, Illinois 60566.

16. Effects of Small Distortions on the EPR of the Γ_6 State (T_d Symmetry) of $Np(BH_3CH_3)_4$ Diluted in $Zr(BH_3CH_3)_4$ (Publication 23)

E. Gamp and N. Edelstein

The single-crystal and powder EPR spectra of $^{237}\text{Np}(BH_3CH_3)_4$ diluted in $Zr(BH_3CH_3)_4$ are reported and interpreted in terms of an orthorhombic spin Hamiltonian with $g_x = 1.7739(4)$, $g_y = 1.8293(4)$, $g_z = 1.7961(5)$, $A_x = 0.1079(2) \text{ cm}^{-1}$, $A_y = 0.1153(2) \text{ cm}^{-1}$, and $A_z = 0.1135(2) \text{ cm}^{-1}$ (see Figure 16-1). A modified point-charge calculation indicates qualitatively that very small deviations of the site symmetry from T_d are enough to account for the observed splitting of the g values.

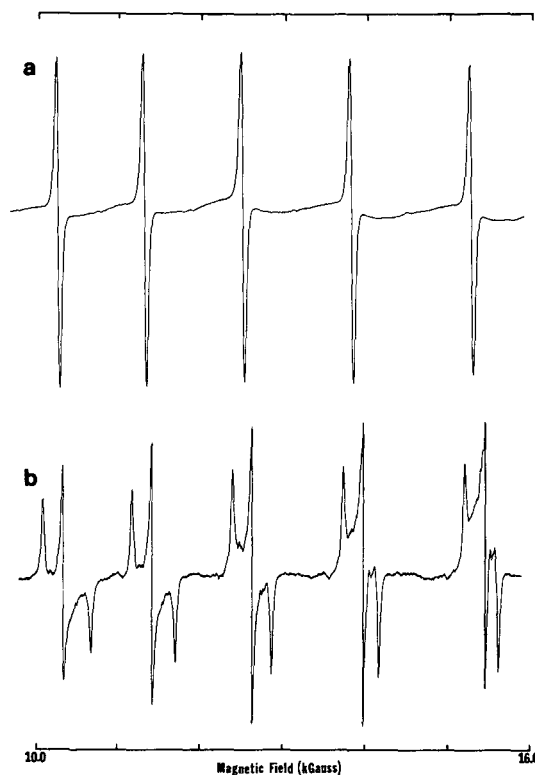


Figure 16-1. a. EPR spectrum of a $\sim 1.5 \times 10^{-3}$ M glassy solution of $^{237}\text{Np}(BH_3CH_3)_4$ in methylcyclohexane at 2 K. b. Powder spectrum of $^{237}\text{Np}(BH_3CH_3)_4$ diluted in $Zr(BH_3CH_3)_4$ at 2 K showing g and A tensor anisotropy.

(XBL 837-10538A)

17. He-I and He-II Photoelectron Studies of Bonding in Metal Silylamido Complexes, $M[N(\text{SiMe}_3)_2]_n$ ($n = 1, 2, \text{ or } 3$) (Publication 6)

J.C. Green,[†] M. Payne,[†] E.A. Seddon,[†] and R.A. Andersen

Gas-phase He-I and He-II photoelectron spectra have been obtained for the following bis(trimethylsilyl)amido-metal complexes: $M[N(\text{SiMe}_3)_2]_n$, where $M = \text{Li or Na}$; $M[N(\text{SiMe}_3)_2]_2$, where $M = \text{Mg or Co}$; and $M[N(\text{SiMe}_3)_2]_3$, where $M = \text{Al, Cr, Ce, Pr, Nd, Eu, Yb, or U}$. Nitrogen lone-pair and metal-nitrogen π -bonding ionization energies show a constant trend throughout the series, increasing with the charge and decreasing with the size of the metal ion. A d band similar to that of $\text{Cr}[N(\text{CHMe}_2)_2]_3$ is detected for $\text{Cr}[N(\text{SiMe}_3)_2]_3$, and a very weak $4f$ band is the first ionization band in the spectrum of $\text{Ce}[N(\text{SiMe}_3)_2]_3$. The $5f$ band of $\text{U}[N(\text{SiMe}_3)_2]_3$ has a full width at half maximum of 1 eV, part of which is due to unresolved spin-orbit coupling.

[†]Present address: Inorganic Chemistry Laboratory, South Parks Road, Oxford OX1 3QR, England.

18. He-I and He-II Photoelectron Spectral Studies of Alkyluranocenes (Publication 13)

J.C. Green,[†] M.P. Payne,[†] and A. Streitwieser, Jr.

Photoelectron spectra of a series of alkyl-substituted uranocenes, obtained with both He-I and He-II radiation, are presented. Intensity measurements confirm an ionization energy ordering $e_{2u} < e_{2g}$ and are consistent with relativistic SCF- $X\alpha$ scattered-wave calculations. Analysis of ionization-energy trends suggests that metal-ring bonding interactions increase in strength with increasing alkylation of the [8]annulene rings.

[†]Present address: Inorganic Chemistry Laboratory, Oxford OX1 3QR, England.

19. Quasi-relativistic SCF- $X\alpha$ Scattered-wave Study of Uranocene, Thorocene, and Cerocene (Publication 19)

N. Rosch[†] and A. Streitwieser, Jr.

Quasi-relativistic SCF- $X\alpha$ scattered-wave calculations are presented for di- π -[8]annulene-uranium(IV) (uranocene), -thorium(IV) (thorocene), and -cerium(IV) (cerocene). Improved agreement over previous nonrelativistic results is found both for optical-absorption spectra and photoelectron spectra. An explanation is presented for the apparent relative success of the previous nonrelativistic calculations. The quasi-relativistic calculations confirm that $f_{\pm 2}$ orbitals of the central metal atom contribute to covalent ring-metal bonding, but emphasize even more than the nonrelativistic treatment the important role of the $6d$ orbitals in such bonding (see Figure 19-1).

[†]Present address: Lehrstuhl für Theoretische Chemie, Technische Universität München, 8046 Garching, West Germany.

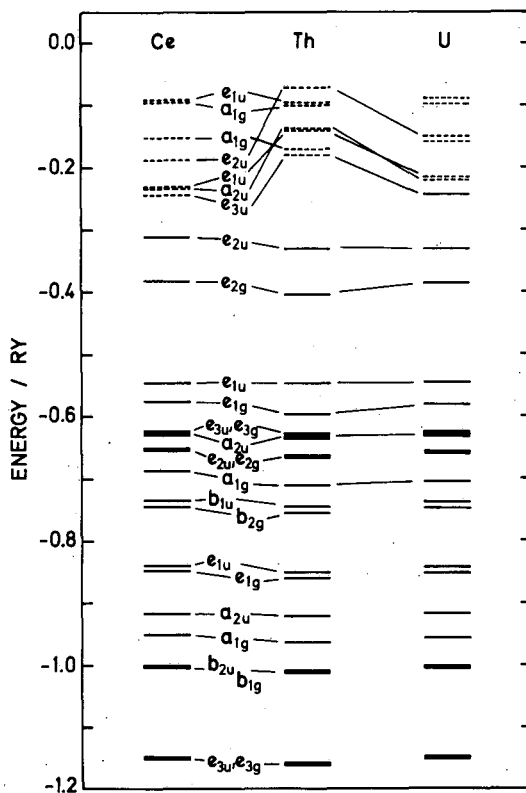


Figure 19-1. Calculated SCF- $X\alpha$ relativistic energy levels for $(\text{C}_8\text{H}_8)_2\text{M}$ for $M = \text{Ce, Th, and U}$. (XBL 8312-2495)

20. Ionization Potential of Neutral Iron, Fe I, by Laser Spectroscopy (Publication 30)[†]

E.F. Worden,[‡] B. Comaskey,[‡] J. Densberger,[‡]
J.A. Paisner,[‡] and J.G. Conway

We have determined the ionization potential of Fe I by three-step laser excitation to produce an autoionizing Rydberg series with high n^* (~ 28 to ~ 52) that converges to the second ionization limit 384.77 cm^{-1} above the ionization potential of neutral Fe. The method used has been described in detail in the literature. The three steps used were laser 1 at 3824.444 \AA ($0-26,140.19 \text{ cm}^{-1}$, $J = 4$ to 3), laser 2 at 5283.621 \AA ($26,140.18-45,061.33 \text{ cm}^{-1}$, $J = 3$ to 3), and laser 3, which scanned from 5310 to 5240 \AA to produce the autoionizing series. The limit $64,122(2) \text{ cm}^{-1}$ found for this series yields an ionization limit of $63,737(2) \text{ cm}^{-1}$ [$7.9024(2)\text{eV}$] for Fe I. This ionization limit is considerably more accurate than current values available in the literature [$63,700(80) \text{ cm}^{-1}$, $63,400 \text{ cm}^{-1}$, and $63,480(500) \text{ cm}^{-1}$]. We intend to observe other series and attempt to further reduce the error limit on the ionization potential. This precise value should be useful to astrophysicists, plasma physicists, and theorists.

[†]This work was performed under the auspices of the U.S. Department of Energy by the Lawrence Livermore National Laboratory under Contract No. W-7405-ENG-48.

[‡]Present address: University of California, Lawrence Livermore National Laboratory, Livermore, California 94550.

1983 PUBLICATIONS AND REPORTS

Refereed Journals

1. Charles W. Eigenbrot, Jr. and Kenneth N. Raymond, "The Synthesis and Characterization of $(\text{UCp}_3)_2(\text{Pyrazine})$ and $[\text{U}(\text{MeCp})_3]_2(\text{Pyrazine})$: μ -bridged Dimers of U^{3+} ," *Polyhedron* **1**, 417 (1982); LBL-13074.
2. Paul E. Riley, Salim F. Haddad, and Kenneth N. Raymond, "Preparation of Praseodymium(III) Chloranilate and the Crystal Structures of $\text{Pr}_2(\text{C}_6\text{Cl}_2\text{O}_4)_3 \cdot 8\text{C}_2\text{H}_5\text{OH}$ and $\text{Na}_3[\text{C}_6\text{H}_2\text{O}(\text{OH})(\text{SO}_3)_2] \cdot \text{H}_2\text{O}$," *Inorg. Chem.* **22**, 3090 (1983); LBL-15002.
3. T.D. Tilley, R.A. Andersen, and A. Zalkin, "Tertiary Phosphine Complexes of the f-block Metals; Preparation of Pentamethylcyclopenta-

dienyl Tertiary Phosphine Complexes of Ytterbium(II and III) and Europium(II). The Crystal Structure of $\text{Yb}(\text{Me}_5\text{C}_5)_2\text{-Cl}(\text{Me}_2\text{PCH}_2\text{PMe}_2)$," *Inorg. Chem.* **22**, 856 (1983); LBL-14367.

4. R.P. Planalp, R.A. Andersen, and A. Zalkin, "Dialkyl Bis[bis(trimethylsilyl)amido] Group IV A Metal Complexes; Preparation of Bridging Carbene Complexes by γ Elimination of Alkane. Crystal Structure of $\{\text{ZrCHSi}(\text{Me}_2)\text{-SiMe}_3[\text{N}(\text{SiMe}_3)_2]\}_2$," *Organometallics* **2**, 16 (1983); LBL-14754.
5. A. Zalkin, D. Perry, L. Tsao, and D. Zhang, "Bis(2-methylimidazolium)tetrachlorodioxouranium(VI), $(\text{CH}_3\text{C}_3\text{N}_2\text{H}_4^+)_2(\text{UO}_2\text{Cl}_4)^{-2}$," *Acta Cryst. C* **39**, 1186 (1983); LBL-15726.
6. J.C. Green, M. Payne, E.A. Seddon, and R.A. Andersen, "He-I and He-II Photoelectron Studies of Bonding in Metal Silylamido-complexes, $\text{M}[\text{N}(\text{SiMe}_3)_2]_n$ ($n = 1, 2, \text{ or } 3$)," *J. Chem. Soc. Dalton Trans.*, 887 (1982).
7. J.C. Krupa, S. Hubert, M. Foyentin, E. Gamp, and N. Edelstein, "Optical Spectroscopy and Electron Paramagnetic Resonance of Pa^{4+} in ThBr_4 and ThCl_4 Crystals," *J. Chem. Phys.* **78**, 2175 (1983); LBL-15084.
8. E. Gamp, N. Edelstein, S. Hubert, M. Genet, and C. Khan Malek, "Anisotropic Magnetic Susceptibility of Single Crystal UCl_4 ," *J. Chem. Phys.* **79**, 2023 (1983); LBL-15873.
9. R. Shinomoto, E. Gamp, N.M. Edelstein, D.H. Templeton, and A. Zalkin, "Syntheses and Crystal Structures of the Tetrakis-(methyltrihydroborato) Compounds of Zirconium(IV), Thorium(IV), Uranium(IV), and Neptunium(IV)," *Inorganic Chem.* **22**, 2351 (1983); LBL-15090.
10. Pierre Delamoye, J.C. Krupa, John G. Conway, and N. Edelstein, "Site-selective Excitation of U^{4+} Diluted in Incommensurate ThBr_4 ," *Phys. Rev. B* **28**, 4913 (1983); LBL-16326.
11. P. Delamoye, K. Rajnak, M. Genet, and N. Edelstein, "Parametric Analysis of the Energy Levels of U^{4+} in D_{2d} and Limiting D_2 Sites in Incommensurate ThBr_4 ," *Phys. Rev. B* **28**, 4923 (1983); LBL-16360.
12. A. Streitwieser, Jr., R.Q. Kluttz, K.A. Smith, and W.D. Luke, "Dibenzouranocene and Related Compounds," *Organometallics* **2**, 1873 (1983), LBL-16567.
13. J.C. Green, M.P. Payne, and A. Streitwieser, Jr., "He-I and He-II Photoelectron Spectral Studies of Alkyluranocenes," *Organometallics* **2**, 1707 (1983).[†]

LBL Reports

14. Paul E. Riley, Kamal Abu-Dari, and Kenneth N. Raymond, "Specific Sequestering Agents for the Actinides. 9. Synthesis of Metal Complexes of 1-hydroxy-2(1H)-pyridinone and the Crystal Structure of Tetrakis(1-hydroxy-2(1H)-pyridinone)aquothorium(IV) Dihydrate," submitted to *Inorg. Chem.*, LBL-15003.[‡]
15. A. Zalkin, D.H. Templeton, R. Kluttz, and A. Streitwieser, Jr., "The Disordered Structure of Dibenzouranocene, $[\text{C}_8\text{H}_6(\text{C}_4\text{H}_4)_2\text{U}]$," LBL-16381.
16. P.G. Edwards, R.A. Andersen, and A. Zalkin, "Tetraalkyl-phosphine Complexes of the f-block Metals; Crystal Structures of $\text{Th}(\text{CH}_2\text{Ph})_4(\text{Me}_2\text{PCH}_2\text{CH}_2\text{PMe}_2)$ and $\text{U}(\text{CH}_2\text{Ph})_3\text{Me}(\text{Me}_2\text{PCH}_2\text{CH}_2\text{PMe}_2)$," LBL-15890.
17. J.M. Boncella and R.A. Andersen, "Bis(pentamethylcyclopentadienyl)ytterbium(II) as a Lewis Acid and Electron-transfer Ligand; Preparation and Crystal Structures of $[\text{Yb}(\text{Me}_5\text{C}_5)_2(\mu\text{-CO})_x\text{Mn}(\text{CO})_{5-x}]_y$ where X and Y are Two and X is Three and Y is Infinite," submitted to *Inorg. Chem.*, LBL-16168.
18. A. Streitwieser, Jr., "Some Recent Advances in Uranocene Chemistry," *Inorg. Chim. Acta*, in press, LBL-16569.
19. N. Rosch and A. Streitwieser, Jr., "Quasi-relativistic SCF- $X\alpha$ Scattered Wave of Uranocene, Thorocene and Cerocene," *J. Am. Chem. Soc.*, in press, LBL-16337.
20. K. Rajnak, E. Gamp, R. Banks, R. Shinomoto, and N. Edelstein, "Optical and Magnetic Properties of Uranium and Neptunium Borohydrides and Tetrakis(methylborohydrides)," *Inorg. Chim. Acta*, in press, LBL-16234.
21. K. Rajnak, E. Gamp, R. Shinomoto, and N. Edelstein, "Optical and Magnetic Properties of Uranium Borohydride and Tetrakis(methylborohydride)," LBL-16460.
22. K. Rajnak, R.H. Banks, E. Gamp, and N. Edelstein, "Analysis of the Optical Spectrum and Electron of $\text{Np}(\text{BD}_4)_4$ Diluted in $\text{Zr}(\text{BD}_4)_4$ and the Magnetic Properties of $\text{Np}(\text{BH}_4)_4$ and $\text{Np}(\text{BH}_3\text{CH}_3)_4$," LBL-16486.
23. E. Gamp and N. Edelstein, "Effects of Small Distortions on the EPR of the Γ_6 State (T_d Symmetry) of $\text{Np}(\text{BH}_3\text{CH}_3)_4$ Diluted in $\text{Zr}(\text{BH}_3\text{CH}_3)_4$," LBL-16484.
24. C.H.H. Van Deurzen, K. Rajnak, and John G. Conway, "Uranium Five (U V), the $^1\text{S}_0$ Level, and a Parametric Analysis of $5f^2$ Configuration," accepted for publication in *J. Opt. Soc. Am. B* 1, (1984), LBL-15924.
25. John G. Conway, Earl F. Worden, James W. Brault, Robert P. Hubbard, and Jeremy J. Wagner, "Classified Line of the First and Second Spectrum of Uranium Between 1817 and 5500 Wave-numbers (5.5 to 1.8 Microns)," accepted by *Atomic Data and Nuclear Data Tables*, LBL-15764.
26. John G. Conway and Earl F. Worden, "The Isotope Shift of Uranium in the Infrared Region Between 1817 and 5598 cm^{-1} ," LBL-15925.
27. T.D. Tilley, R.A. Andersen, and A. Zalkin, "Divalent Lanthanide Chemistry; Preparation and Crystal Structures of Sodium Tris[bis(trimethylsilyl)amido]-Europate(II) and -Ytterbate(II), $\text{NaM}[\text{N}(\text{SiMe}_3)_2]_3$," submitted to *Inorg. Chem.*, LBL-15886.

Other Publications

28. W.T. Carnall and J.G. Conway, "Appendix G, Spectroscopic Studies of the Transplutonium Elements," in *Opportunities and Challenges in Research with Transplutonium Elements*, National Academy Press, Washington, D.C., 1983, p. 287.
29. N. Edelstein, B. Johansson, and J.L. Smith, "Appendix H, Magnetic and Solid State Properties," in *Opportunities and Challenges in Research with Transplutonium Elements*, National Academy Press, Washington, D.C., 1983, p. 299.
30. C.F. Worden, B. Comaskey, J. Danshengen, J. Christensen, J.M. McAfee, J.A. Paisner, and J.G. Conway, "The Ionization Potential of Neutral Iron, Fe I, by Multistep Laser Spectroscopy," submitted to *J. Opt. Soc. Am. B.*, UCRL-89701.[§]
31. D.H. Templeton, "Anomalous Scattering," in *Crystallography in North America*, D. McLachlan and J.P. Glusker, eds., American Crystallographic Association, New York, 1983, p. 268.
32. D.H. Templeton and L.K. Templeton, "Multiple-wavelength Method of Phase Determination," American Crystallographic Association Meeting, Columbia, Missouri, March 14-18, 1983, Abst. L4.^{||}
33. D.H. Templeton and L.K. Templeton, "X-ray Dichroism and Anomalous Scattering in Platinum and Copper Compounds," American Crystallographic Association Meeting, Snowmass, Colorado, August 1-5, 1983, Abst. K2.^{||}

Invited Talks

34. Kenneth N. Raymond, "Coordination Chemistry and Microbial Iron Transport" and "Specific Sequestering Agents for Iron and Actinides," Fourth Rachele Distinguished Lecturer, Long Beach State University, Long Beach, California, March 15-16, 1983.
35. Kenneth N. Raymond, "Specific Sequestering Agents for Iron and the Actinides," Distinguished Scientist Series, University of Arizona, Tucson, Arizona, April 21, 1983; U.S.-Italy Workshop on Environmental Inorganic Chemistry, San Miniato, Italy, June 6-10, 1983; LBL-16410.
36. K.N. Raymond (presenter), G.E. Freeman, and M.J. Kappel, "Actinide-specific Complexing Agents: Their Structural and Solution Chemistry," presented at the First International Conference on the Chemistry and Technology of the Lanthanides and Actinides, Venice, Italy, September 5-10, 1983; LBL-16441.
37. Kenneth N. Raymond, "Synthetic Iron Chelating Agents as Probes of the Iron Coordination Site and Metal Ion Exchange Kinetics of Transferrin and Lactoferrin," First International Conference on Bioinorganic Chemistry, Florence, Italy, June 13-17, 1983.
38. Andrew Streitwieser, Jr., "Some Recent Advances in Uranocene Chemistry," First International Conference on the Chemistry and Technology of Lanthanides and Actinides, Venice, Italy, September 5, 1983.
39. R.A. Andersen, "Organoactinide and Lanthanide Chemistry," Rare-earth Research Conference, Florida State University, April 18, 1983; Gordon Research Conference on Inorganic Chemistry, Wolfeboro, New Hampshire, August 8, 1983.
40. John G. Conway, "Laser Spectroscopy," Department of Physics, Naval Postgraduate School, Monterey, California, August 26, 1983.
41. N. Edelstein, "Optical and Magnetic Properties of Uranium and Neptunium Borohydrides and Tetrakis(methylborohydrides)," First International Conference on the Chemistry and Technology of the Lanthanides and Actinides, Venice, Italy, September 5, 1983.

†Supported in part by MMRD.

‡Supported in part by the National Institute of Health through Grant HL24775.

§Performed under the auspices of the U.S. Department of Energy by Lawrence Livermore National Laboratory under Contract No. W-7405-ENG-48.

¶Supported in part by the National Science Foundation.

Fossil
Energy

A Review of Unsolved Problems of Pressing Importance in Fluid Mechanics Affected Erosion*

Joseph A.C. Humphrey, Investigator

INTRODUCTION

The purpose of this study is to review and assess the role played by fluid mechanics in erosive-wear processes caused by particle impact. In many systems of engineering interest, erosive particles have such short response times that their trajectories are significantly affected by the state of motion of the fluid. Depending on the particular flow configuration, the change in trajectory may or may not be advantageous. This research seeks to establish the most pressing unsolved problems relating to fluid-mechanics-affected erosion with significant impact in the energy field. Attempts will be made to provide guidance for their study and solution.

1. Modeling Solid-fluid Turbulent Flows With Application to Predicting Erosive Wear (Publication 1)[†]

F. Pourahmadi and J.A.C. Humphrey

Numerical modeling of fluid-particulate turbulent-flow transport processes, including erosion, cannot substitute (at least for the present) for good experimentation. Notwithstanding, the calculation approach offers a viable, relatively inexpensive, and complementary alternative for gleaning useful information on the relative dependence of particle transport and erosion on the flow system parameters of relevance. In the present study these parameters include the particle-phase response time, Reynolds number, and concentration; the turbulent characteristics of the fluid phase; and the channel aspect ratio and curvature. This publication summarizes the main results predicted by means of a numerical procedure for the motion of a dilute suspension of solid particles driven by turbulent flow in curved and straight two-dimensional channels. An exposi-

*This work was supported by the Assistant Secretary for Fossil Energy Research, University Coal Research Division, U.S. Department of Energy under Contract No. DE-AC03-76SF00098.

tion of the theoretical development, the numerical model, and its testing and application to these configurations of special engineering interest is provided. A simple model is used to illustrate the prediction of erosive wear.

[†]Numerical calculations for this study were supported by the Office of Naval Research under Contract No. N00014-80-C-0031.

2. Numerical Calculation of Particle Dispersion in a Turbulent Mixing-layer Flow (Publication 2)[†]

R.S. Crowder, J.W. Daily, and J.A.C. Humphrey

Numerical calculations have been performed for two-phase turbulent mixing-layer flows. Eulerian forms of the transport equations were solved allowing two-way coupling between continuous fluid and solid phases. A two-equation $k-\epsilon$ model was used to simulate the turbulent-flow characteristics. Although imperfect, the predictions allow a relative evaluation of the importance of modeling turbulent interactions between phases in intense shear-layer flows. Predictions in air show the extent to which fluid-solid interaction terms affect the flow characteristics because of increased fluid viscosity; the terms are approximately one order of magnitude larger in air at 1200 K than in air at 300 K. Correspondingly, predictions in water show the extent to which a reduction of the pure phase density ratio $\tilde{\rho}_p/\tilde{\rho}_f$ reduces the importance of the same terms. Increasing the particle-phase volume fraction, or decreasing the particle size, leads to increased damping of the fluid-phase turbulent kinetic energy and, as a consequence, of associated turbulent diffusion. For the conditions investigated, the influences of gravity and of slip between phases were found to be negligible. In general, present results are in qualitative agreement with information available for particle-laden turbulent jet flows. Corresponding data for the mixing-layer configuration are lacking and should be obtained.

[†]Financial support for R.S. Crowder was provided by the National Science Foundation under Grant ENG 77-0219.

3. Work in Progress

A major review article is in progress. Findings to date strongly support the need for such a review.

1983 PUBLICATIONS AND REPORTS

Refereed Journals

1. F. Pourahmadi and J.A.C. Humphrey, "Modeling Solid-fluid Turbulent Flows with Application to Predicting Erosive Wear," *Physico-Chemical Hydrodynamics* 4, 191-219 (1983); LBL-15289.[†]

Other Publications

2. R.S. Crowder, J.W. Daily, and J.A.C. Humphrey, "Numerical Calculation of Particle Dispersion in a Turbulent Mixing Layer Flow," to appear in the *Journal of Pipelines*; also accepted for presentation at the ASME 1984 Fluids Engineering Conference, New Orleans, Louisiana.[‡]

[†]Supported partly by the Office of Naval Research.

[‡]Supported partly by the National Science Foundation.

Electrode Surface Chemistry*

Philip N. Ross, Investigator

INTRODUCTION

Commercialization of phosphoric acid fuel-cell technology requires a capital cost reduction and an extension of power section life compared to currently available technology. Significant capital cost reduction can be achieved if an oxygen-reduction catalyst which is catalytically more active than Pt supported on graphitized carbon black can be developed. Towards this end, extensive fundamental studies of Pt electrochemistry are being conducted to learn how Pt activity depends on temperature, acid anion, water concentration, and surface structure (morphology). Surface studies of gas-phase oxygen adsorption by x-ray photoemission spectroscopy (XPS) suggest that modification of the adsorptive properties of Pt by the substitution of ligands to the Pt coordination sphere could result in enhanced Pt catalysts. The objective of the present research is to develop the physical and chemical understanding of oxygen-platinum-ligand interaction necessary for the rational selection of alloying components. Fundamental studies of the alloy-electrolyte interface using modern surface science techniques should provide the means to optimize the alloy ligand or to redirect the search for more active materials along the most rational paths. Alloying may have significant beneficial effects on electrode performance above and beyond effects on the oxygen-reduction kinetics, e.g., reduced Pt dissolution and surface-area loss. These additional alloying effects will also be studied at the atomic level, e.g., surface reconstruction and surface self-diffusion.

1. Recent Improvements in the Utilization of Pt in Phosphoric Acid Fuel Cells (Publication 4)

Philip N. Ross

Since 1977, DOE- and EPRI-funded research programs have concentrated on concepts that may

*This work was supported by the Assistant Secretary for Fossil Energy, Office of Coal Fuel Cells, Advanced Concepts Division of the U.S. Department of Energy under Contract No. DE-AC03-76SF00098, through the Fuel Cell Project Office, NASA Lewis Research Center, Cleveland, Ohio.

reduce the decay rate or may lead to higher catalytic activity than the standard Pt catalyst. The major sources of decay appear to be loss of Pt surface area and corrosion of the carbon support. Corrosion of the support may accelerate the rate of surface-area loss as well as cause "flooding" of the gas pores in the catalyst layer. Recent research has successfully identified a number of carbon-black support materials that have much better corrosion resistance than Vulcan XC-72R, and improvements in air-electrode lifetime appear to be evolving. Our own laboratory has been pursuing concepts to improve the catalytic activity of Pt-based catalysts. We have worked extensively on the crystallite size effect, particularly studies of the morphology of Pt clusters and the relation between surface structure and the kinetics of oxygen reduction. The kinetics do not differ significantly between low-index single-crystal surfaces (e.g., [111] vs [110]), nor between well-annealed surfaces and poorly annealed sputtered surfaces. The crystallite size effect observed with very highly dispersed Pt appears to be an intrinsic property of ensembles of Pt atoms smaller than a characteristic dimension of 2 nm. Photoelectron spectroscopy indicated that these clusters have different electronic states than bulk Pt, perhaps a d^8s^2 electronic configuration rather than d^9s . This suggested that alloying with a constituent that would increase the d-electron density of states would be beneficial. The Engel-Brewer bonding rules indicate the Pt Group IVb intermetallics have strong d-orbital interaction with increased d-electron density around the Pt nucleus relative to pure Pt. Consequently, we have studied a variety of Pt alloy catalysts, particularly Pt with Ti, Zr, Hf, V, Nb, and Ta. Preparation as dispersed bimetallic clusters of uniform composition is a requirement and is very difficult to accomplish in all cases. Pt-Ti and Pt-V are the easiest to prepare as practical catalysts, although from the kinetic studies the best results were obtained with PtTa₃. The optimum concentration of base metal appeared to be 15–20%. On a unit area basis, the Pt-Ti and Pt-Ta catalysts were a factor of 4–5 more active than standard supported Pt catalysts. Pt-Ti catalysts are undergoing fuel-cell evaluation in both DOE- and EPRI-sponsored research. Initial results have indicated a 20–30 mV improvement in air-cathode potential at 200 mA/cm², about what was expected from the results in laboratory-scale experiments. The gain in catalytic activity of the Pt in these new catalysts should lead eventually to a factor of two reduction in catalyst loading at the cathode for the same performance level as the 1977 state of technology.

2. Low-energy Electron-diffraction (LEED) and Auger Electron Spectroscopy (AES) Study of Structural and Chemisorptive Properties of Zr Overlayers on the Pt(001) Surface (Publication 2)

U. Bardi,[†] P.N. Ross, and G. Somorjai

Zirconium overlayers were deposited onto a Pt(100) surface by electron-beam evaporation in UHV, and the composition and structure of the surface were determined by AES and LEED. The overlayers were highly reactive towards oxygen, carbon monoxide, and hydrocarbons, forming oxide or carbide overlayers. Several metastable ordered structures were observed by LEED when oxidized overlayers were thermally annealed in UHV. Protracted annealing at >900 K (see Figure 2-1) resulted in reduction and dissolution of the oxidized overlayer with complete disappearance of zirconium from the surface. Oxygen dosing of annealed surfaces at 25°C caused re-segregation of zirconium to the surface, and the formation of an ordered PtZr_xO_y surface phase which may be a zirconium analogue to the yttria ternary oxide $\text{PtYO}_{3.5}$. This phase was stable in oxygen at 25 – 300°C , but oxygen dosing at above 300°C resulted in precipitation of ZrO_2 islands on top of the Pt(100)–(1 \times 1) substrate.

[†]Present address: Department of Chemistry, University of Florence, Florence, Italy.

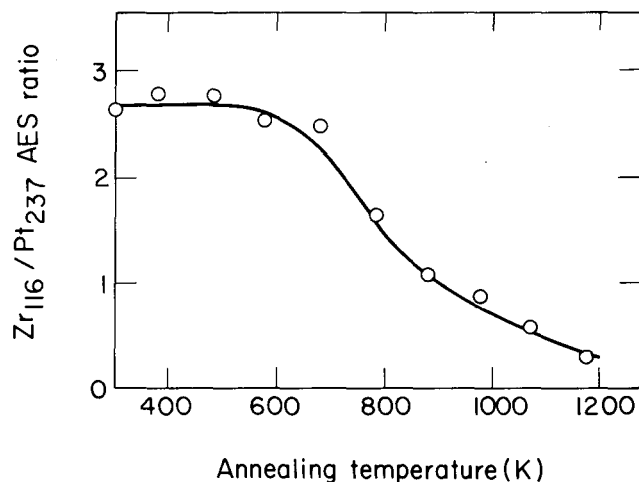


Figure 2-1. Zr(116 eV)/Pt(237 eV) AES ratio for successive annealings at increasing temperature. Initial O(503 eV)/Zr(116 eV) AES ratio = 0.3; final ratio (after annealing at 1200 K) = 2.5. (XBL 8210-4778)

3. Ligand Effects in Chemisorption on Pt₃Ti Surfaces (Publication 3)

U. Bardi,[†] G. Somorjai, and P.N. Ross

The Pt-Ti bimetallic system is interesting for several reasons, but most particularly as an example of an Engel-Brewer type intermetallic. The highly exothermic enthalpy of formation of these alloys has been interpreted in terms of strong bonding interaction of electrons in the d bands of both metals. In principle, such a strong interaction is likely to modify the electronic properties of the metals and cause changes in the chemical properties that are often called ligand effects. Ligand effects have been considered as a possible cause for the increased catalytic activity, compared to pure Pt, of Pt-Ti bimetallic catalysts used for the reduction of oxygen to water in acid fuel cells.

In order to understand the reasons for this enhanced activity, we have undertaken a study of the surface properties of the ordered Pt₃Ti intermetallic compound, which has the most exothermic heat of formation in the Pt-Ti system. In this paper we report the results of a study of carbon monoxide and hydrogen chemisorption, which we used as chemical probes to test the presence of ligand effects. In comparison with pure Pt, the CO thermal desorption spectra (TDS) curve for polycrystalline Pt₃Ti showed two important differences: smaller area, indicating lower total CO coverage, and a shift of the peak toward lower temperature. CO adsorption experiments on Pt₃Ti(100) and (111) single crystals gave single TDS peaks displaced to lower temperatures than for either Pt(100) or (111) surfaces. If we estimate the adsorption energy from the temperature at which the first-order desorption rate is maximum, the two adsorption states on Pt correspond to 32 and 25 kcal/mole, and the state on Pt₃Ti to 21 kcal/mole, at least a 4 kcal/mole decrease in adsorption energy. Also, a very small hydrogen signal, in comparison to a pure Pt surface, was observed from the Pt₃Ti surfaces. This small signal was taken to indicate essentially no chemisorption of hydrogen on these surfaces at room temperature. The suppression of hydrogen chemisorption and the reduced bond energy for adsorbed carbon monoxide appear to be genuine effects of the presence of Ti on the Pt surface.

[†]Present address: Department of Chemistry, University of Florence, Florence, Italy.

4. Structure of the Pt₃Ti(001) Surface by LEED Dynamic-intensity Analysis (Publication 5)[†]

U. Bardi,[‡] M. Maglietta,[‡] M. Torrione,[‡] E. Zanazzi,[‡] and P.N. Ross

Strong modifications to the chemisorptive properties of Pt occur when Ti is incorporated into the surface. In particular, polycrystalline Pt₃Ti and Pt₃Ti(001) and (111) single-crystal surfaces have shown dramatically different adsorptive properties than either pure Pt or Ti surfaces. The strong intermetallic bonding in these compounds may be responsible for these ligand effects. Intermetallic bonding should be very sensitive to the local ordering in these surfaces, so we have undertaken a study of the structure of the Pt₃Ti(001) surface by dynamic LEED analysis. Pt₃Ti has a bulk structure with an fcc lattice of the Cu₃Au type. Surface planes normal to the [001] crystallographic axis can result in two nonequivalent terminations, one (Pt-rich) formed by a plane containing no Ti atoms, the other (Ti-rich) by a plane containing a 1:1 ratio of Pt:Ti atoms. LEED patterns of the clean surface have the (2 × 2) superlattice symmetry expected for a simple bulk truncation, but only a dynamic calculation can distinguish the Pt-rich from the Ti-rich outer surface.

LEED intensities were collected in the 30 to 130 eV range from 14 beams, three at normal incidence. Calculations were performed by multiple scattering theory, in the RFS scheme, using 6 phase shifts. The models considered were: (i) simple bulk truncation, either Pt-rich or Ti-rich; (ii) Ti-rich termination, with a buckling of the first layer with the titanium and platinum atoms of the outermost layer not lying in the same plane; and (iii) simple bulk truncation model, as in (i), with statistic (random) titanium enrichment. Variation of the distance of the surface layer to the first bulk layer, as well as variation of the distance between the first and second bulk layer, is allowed for each model. Based on the beams at normal incidence, the Ti-rich simple truncation model is preferable to the Pt-rich model, but the other models allowing Ti mixing between the first two atomic layers could not be excluded definitively.

[†]In collaboration with the Institute of Chemical Physics, University of Florence, and with funding from the CNR (Italy).

[‡]Present address: Department of Chemistry, University of Florence, Florence, Italy.

5. Work in Progress

These previous studies have clearly shown two important properties of Pt Group IVb intermetallic surfaces: (1) there is a strong ligand effect from the intermetallic bonding in the chemisorption of reducing gases like hydrogen and carbon monoxide; (2) the intermetallic surface is unstable with respect to oxidizing conditions like that of a fuel-cell cathode. Further studies are in progress to determine the composition and structure of the surface formed by electrochemical oxidation using the gas-phase oxidation-formed surfaces as a guide. Also, studies directed at relating the behavior of bulk surfaces to supported bimetallic clusters (the practical catalyst) are under way. These studies will utilize XPS and EXAFS (extended x-ray absorption fine structure) in characterizing changes to the state of the base metal and the coordination about the Pt surface atoms during use as a fuel-cell cathode catalyst.

1983 PUBLICATIONS AND REPORTS

Refereed Journals

1. P.N. Ross and K. Gaugler, "The Observation of Surface Sensitive M_{2,3} Absorption Edge Shifts by REELS," *Surf. Sci.* **122**, L579 (1982); LBL-14579.

LBL Reports

2. U. Bardi, P.N. Ross, and G.A. Somorjai, "LEED and AES Study of Structural and Chemisorptive Properties of Zr Overlayers on the Pt(001) Surface," submitted to *J. Vac. Sci. Tech. A*, LBL-15294.
3. U. Bardi, G.A. Somorjai, and P.N. Ross, "Ligand Effects in Chemisorption on Pt₃Ti Surfaces," *J. Catal.*, in press, LBL-15603.

Invited Talks

4. P.N. Ross, "Recent Improvements in the Utilization of Pt in Phosphoric Acid Fuel Cells," presented at 161st Meeting of the Electrochemical Society, Montreal, Quebec, 1982, LBL-17119.
5. U. Bardi, M. Maglietta, M. Torrione, E. Zanazzi, and P.N. Ross, "Structure of the Pt₃Ti(001)

Surface by LEED Dynamical Intensity Analysis," presented at the 1983 Meeting of the National Group for Structure of Matter, Genoa, Italy, LBL-17120.[†]

[†]In collaboration with the Institute of Chemical Physics, University of Florence, and with funding from the CNR (Italy).

Studies of Materials Erosion in Coal Conversion and Utilization Systems*

Alan V. Levy, Investigator

INTRODUCTION

The mechanisms and rates of surface loss of materials used for the containment of gas and liquid-solid particle flows in coal conversion and utilization systems were investigated in a generic research program. Portions of the operating environments of components where erosion degradation occurs — in coal gasification and liquefaction processes, fluidized-bed combustion, and advanced pulverized-coal boilers — were simulated to investigate the behavior of candidate alloys and protective coatings. Tests were carried out using flat specimens of various engineering materials with varying compositions and morphologies over a range of controlled test conditions. Rates and mechanisms of surface loss were determined, and models governing the degradation were developed. The fluid mechanics of two-phase flows were established for use in conjunction with the models to predict erosion rates in various containment geometries.

1. Elevated Temperature Combined Erosion-corrosion of Metals in Energy Systems (Publication 17)

Elliott Slamovich, Nancy Jee, and Alan Levy

An investigation was made of the effect of erodent particle size and test temperature on the combined erosion-corrosion behavior of a series of steels containing 2-1/4, 5, 9, and 12% chromium. The particle sizes used were 5 μm , 50 μm , and 100 μm , and the test temperatures ranged from 700 to 950°C. The tests were made in the oxygen-rich exhaust gases of a methane-air burner that propelled the particles at the specimens at 15 m/sec for 30 min.

It was determined that corrosion was the dominant mechanism at all test conditions for all alloys.

The erosion process enhanced the growth rate of multi-layered iron oxide and iron-chromium oxide spinel scales and markedly changed the morphology of the scale surfaces and the thickness of the various scale layers. These changes were determined to be affected by the particle size of the erodent, the test temperature, and the chromium content of the alloy.

2. Combined Erosion-corrosion of 9Cr-1Mo Steel at Elevated Temperatures (Publication 19)

Yang-Fa Man and Alan Levy

An investigation was made of the effect of particle velocity and test temperature on the air-solid particle erosion of 9Cr-1Mo steel in a jet-nozzle type of erosion tester. The tests were conducted at 650–900°C at velocities from 10 to 70 m/sec using 130- μm Al_2O_3 particles. It was determined that the rate of metal surface recession increased with the test temperature by different degrees for the different velocities of the particles. The greatest increase occurred for the 70-m/sec velocity. The corrodant scale was an iron-chromium oxide spinel. At all test conditions the dominant mechanism of surface degradation was corrosion. The formation of oxide scales was enhanced by the erosion process. At the highest test velocities and temperatures, there was evidence that the scale surface had been compacted and deformed by the particles striking it.

3. The Effect of Test Variables on the Mechanism of Erosion of Ductile Metal (Publication 12)

Greg Hickey and Alan Levy

The erosion of ductile metals was investigated at low impingement angles and high velocities to determine if the basic mechanism of erosion changed from platelet formation to cutting. The early portion of an erosion curve was also studied using sequential erosion techniques to determine whether the mechanism of erosion changed during the early portion of erosion. It was determined that the platelet mechanism of erosion, i.e., the extrusion and forging of platelets and their removal from the surface, occurred at impingement angles as low as 20° and at velocities as high as 130 m/sec (the maximum speed the equipment used could achieve). It was also

*This work was supported by the U.S. Department of Energy under DOE/FE AA 15 10 10 0, Advanced Research and Technical Development, Fossil Energy Materials Program, Work Breakdown Structure Element LBL-3.5 and under Contract No. DE-AC03-76SF00098.

determined that early in the erosion cycle when the first layer of platelets has covered the eroding surface, a short-duration erosion-rate peak occurs as these first, more vulnerable platelets are removed.

4. Elevated Temperature Erosion of Steels (Publication 20)

Jennifer Patterson and Alan Levy

Several low-chromium-content steels were erosion-tested at elevated temperatures to 800°C using 240- μm SiC particles at a velocity of 30 m/sec and an impingement angle of 30°. Nitrogen was used as the carrier gas to prevent oxidation of the specimens during the tests. It was determined that the 2-1/4Cr-1Mo and 5Cr-1/2Mo steels had erosion rate versus temperature curves shaped the same as those of mild steel and higher chromium-content steels such as 304SS and 310SS. From room temperature to about 400°C, there was little change in the erosion rate with temperature. From 400°C the erosion rates increased rapidly with test temperature. It was determined that the 400°C temperature correlates with the beginning of a rapid decrease in tensile strength of the alloys with test temperature. At elevated temperatures when no corrosion occurred, the impacting particles caused a characteristic pattern of narrow gouges to occur on the eroding metal surface. These gouges are not observed on surfaces eroded at room temperature, or on surfaces eroded at elevated temperatures where corrosion scales can form during combined erosion-corrosion.

5. Erosion of Steel Alloys by Coal-kerosene Slurries (Publication 13)

Greg Hickey and Alan Levy

Further studies of the slurry erosion of a number of commercial steels used in process plants have determined that the most influential property on the erosion resistance of the alloys is the strain-hardening coefficient. Incremental erosion-rate curves were developed for the alloys, and all curves showed that the initial erosion rate after the incubation period was the highest one measured and that the steady-state erosion rate was one-half to one-third of the highest rate. This behavior was related to the effect of surface cold work on the resistance of

the alloy to further erosion. Other properties such as tensile strength, ductility, and hardness did not show any correlation with erosion resistance.

The high initial erosion rate and lower steady-state rate determined to occur in slurry erosion is the opposite of the low initial rate and high steady-state rate observed in gas/solid-particle erosion. The effect of the liquid in the slurry acting as a coolant on the eroding surface is thought to be the reason for the reversal in the shapes of the incremental erosion curves. The same physical erosion mechanism — the formation and removal of platelets — occurs in both liquid and gas/solid-particle erosion of metals.

6. Erosion of Steels in Coal-solvent Slurries (Publication 11)

Nancy Jee and Alan Levy

The slurry erosion rates of several process-plant construction steels were determined at temperatures to 175°C for a series of increasing viscosity and different lubricity solvents and coal particle slurries. Kerosene, creosote oil, and anthracene oil were used with 1200-mesh coal particles at several slurry velocities. It was determined that the erosion rates decreased with increasing viscosities and that differences in the lubricity of the solvents also affected the resultant erosion rates. The erosion rates of different alloys were affected to greater or lesser degrees by the different viscosities. The erosion rates of the alloys generally increased with the temperature of the slurry because the viscosity of the slurries decreased with increasing temperature.

7. The Slurry Erosion of Carburized 8620 Steel (Publication 15)

Johnny Yan and Alan Levy

An investigation was conducted to determine how the tempering of carburized 8620 steel at two different temperatures affected the slurry-erosion behavior of the steels in sand-water slurries of different solids loadings at several slurry velocities. The tempered steels were compared to as-carburized 8620 steel. It was determined that the tempering treatments improved the erosion resistance of the carburized steel. The greater the solids loading of sand in the water, the higher was the erosion rate.

Steady-state erosion rates were reached in the first 10 minutes of testing; these rates did not change as additional erosion time occurred on the specimens, indicating that short-term erosion tests are adequate for determining long-term erosion rates. The erosion resistance of the carburized steels related directly to their tempered hardness. The erosion rates of the specimens increased as the carburized case was penetrated, exposing lower-hardness material.

8. Effect of Various Coals on the Slurry Erosion of Metals (Publication 16)

Nancy Jee and Alan Levy

Several different coals and vacuum bottoms were obtained from Exxon Corporation's EDS coal-liquefaction pilot plant and used to erode 1018 steel by coal-kerosene slurries at room temperature. The particles were received in various sizes from $< 60 \mu\text{m}$ to $> 400 \mu\text{m}$. It was determined that each coal tested has a different erosivity that is primarily a function of particle size and ash content. The larger the particle size and the higher the ash content, the greater was the erosivity of the coal or vacuum bottoms. Illinois No. 6 coal with an average particle size of $74 \mu\text{m}$ caused the 1018 steel to erode at $(13\text{g}/\text{cm}^2) \times 10^{-4}$, while $443\text{-}\mu\text{m}$ diameter particles of the same coal resulted in an erosion rate of $(140\text{g}/\text{cm}^2) \times 10^{-4}$. A low-ash Texas lignite caused an erosion rate of $(14\text{g}/\text{cm}^2) \times 10^{-4}$, while a high-ash version of the same lignite caused the 1018 steel to erode at $(30\text{g}/\text{cm}^2) \times 10^{-4}$.

9. The Role of Turbulence in Two-phase Flow on the Erosivity of Fluid/Solid-particle Jet Streams (Publication 21)

S. Dosanjh and J. Humphrey

An analytical study has been carried out to determine how turbulence in a two-phase flow stream from a jet impingement nozzle affects the velocity, particle trajectories, and local solids loading of the stream as it strikes a flat surface. It is known that turbulent flow fluctuations away from the surface can produce significant deviations in particle trajectories. It was determined that the particles impact on surfaces with particle density distributions, velocities, and impingement angles that are significantly

different than they would be in the absence of turbulence. Predictions for spherical particles in air showed that increasing the particle phase volume fraction or decreasing the particle size increased damping of turbulence in the flow. This in turn reduced the turbulent diffusion (dispersion) of the solid phase. The resulting predicted particle velocities and impingement angles at the instant of impact can be used as inputs to erosive wear prediction models. Using this information with a representative erosion model, it was determined that decreasing the turbulence intensity of the jet flow results in an increase in total surface erosion.

10. Two-phase Turbulent Flow Measurements in a Ninety Degree Bend Using Laser Doppler Velocimetry (Publication 18)

Yannis Kliafas

The mean streamwise and radial velocities and the associated Reynolds-stresses have been measured in a square-sectioned 90° bend of 1.76 radius ratio for two different Reynolds numbers, 2.2×10^5 and 3.47×10^5 using laser Doppler velocimetry. A superposition of stress-driven and pressure-driven radial velocities is observed up to the $\theta = 30^\circ$ station. At 75° the stress-driven secondary flow is overwhelmed by the secondary motion of the first kind.

The mean streamwise and radial velocities and the corresponding turbulence intensities of $50\text{-}\mu\text{m}$ and $100\text{-}\mu\text{m}$ glass spheres were also studied at very dilute suspension flows. The velocity profiles for the gas and the solids were quite flat and crossed over near the outer wall, with the solids having the higher speed. Results of the present study should help enhance the understanding of two-phase flows and assist with the development of erosion models dealing with erosion characteristics inside curved pipes and ducts.

1983 PUBLICATIONS AND REPORTS

Refereed Journals

1. A. Levy and P. Chik, "The Effects of Erodent Composition and Shape on the Erosion of Steel," *Wear* **89**(2), 45 (1983); LBL-13802.
2. T. Foley and A. Levy, "The Erosion of Heat

Treated Steels," *Wear* 91(2), 45 (1983); LBL-13745.

3. J. Patterson and A. Levy, "Methods for Characterization of Erosion by Gas Entrained Solid Particles," *Wear* 91(3), 333 (1983); LBL-15017.
4. F. Pouramadhdi and J. Humphrey, "Modelling Solid-fluid Turbulent Flows with Application to Predicting Erosive Wear," *Physico-Chemical Hydrodynamics* 4(3), 191 (1983); LBL-13808.
5. S.M. Chang, J. Humphrey, and A. Modavi, "Turbulent Flow in a Strongly Curved U-bend and Downstream Tangent of Square Cross-sections," *Physico-Chemical Hydrodynamics* 4(3), 243 (1983).
6. R. Yang and M. Holt, "Boundary Layer Control by Means of Strong Injection," *J. Appl. Mechanics* (1983); LBL-16089.
7. M. Holt and W.S. Yeung, "A Numerical Investigation for Curved Pipe Flow at High Reynolds Numbers," *J. Appl. Mechanics* 105 (1983); LBL-9905.

LBL Reports

8. A. Levy and E. Slamovich, "Combined Corrosion-erosion of Steels in Oxidizing Environments," submitted to *NACE Corrosion* 84, LBL-15657.
9. M. Landkof, D. Boone, R. Gray, A. Levy, and E. Yaniv, "The Effect of Surface Doping on the Oxidation of Chromia Former Alloys," submitted to *NACE Corrosion* 84, LBL-17237.
10. A. Davis, D. Boone, and A. Levy, "Erosion of Ceramic Thermal Barrier Coatings," submitted to *NACE Corrosion* 84, LBL-15667.
11. A. Levy, N. Jee, and P. Yau, "Erosion of Steels in Coal-solvent Slurries," submitted to *NACE Corrosion* 84, LBL-17238.
12. A. Levy, M. Aghazadeh, and G. Hickey, "The Effect of Test Variables on the Platelet Mechanism of Erosion," submitted to *Wear*, LBL-15656.
13. A. Levy and G. Hickey, "Liquid-solid Particle Erosion of Steels," LBL-17239.
14. A. Levy and P. Yau, "Slurry Erosion by Jet Impingement," LBL-15658.
15. J. Yan and A. Levy, "Sand-water Slurry Erosion of Carburized AISI 8620 Steel," submitted to *Wear*, LBL-17241.
16. N. Jee and A. Levy, "The Erosivity of Coal Particles in Coal-solvent Slurries," submitted to *ASTM*, LBL-17242.
17. A. Levy, E. Slamovich, and N. Jee, "Elevated Temperature Combined Erosion-corrosion of

Metals in Energy Systems," submitted to *ICMC*, LBL-17243.

18. Y. Kliafas, "Two Phase Turbulent Flow Measurements in a Ninety Degree Bend using Laser Doppler Anemometry," LBL-17244.
19. Y. Man and A. Levy, "Combined Erosion-corrosion of 9Cr-1Mo Steel at Elevated Temperatures," submitted to *Wear*, LBL-17245.
20. A. Levy and J. Patterson, "Elevated Temperature Erosion of Chromium Containing Steels," submitted to *Wear*, LBL-17246.
21. S. Dosanjh and J. Humphrey, "Erosion by Turbulent, Particle-laden, Fluid Jets: A Numerical Analysis," submitted to *ASME Journal of Fluids Engine*, LBL-17247.

Other Publications

22. T. Foley and A. Levy, "The Effect of Heat Treatment on the Erosion Behavior of Steel," in *Proc. ASME Wear Conf.*, Reston, Virginia, April 1983; LBL-13745.
23. A. Levy, "Erosion Mechanisms in Ductile and Brittle Materials," in *Proc. Erosion by Liquid and Solid Impact Conf.*, Cambridge, England, September 1983; LBL-12015, LBL-15240.
24. A. Levy, "The Erosion of Protective Coatings," in *Proc. Erosion by Liquid and Solid Impact Conf.*, Cambridge, England, September 1983; LBL-15293, LBL-15667.
25. A. Levy, T. Bakker, and E. Sholz, "Erosion of Hard Metals," in *Proc. High-temperature Protective Coatings Conf.*, AIME Annual Meeting, Atlanta, Georgia, March 1983; LBL-15293.

Invited Talks

26. T. Foley and A. Levy, "Effect of Alloy Properties and Microstructure on Erosion," AIME Annual Meeting, Atlanta, Georgia, March 1983.
27. A. Levy and M. Aghazadeh, "Effect of Velocity on Platelet Mechanism of Erosion," AIME Annual Meeting, Atlanta, Georgia, March 1983.
28. A. Levy, E. Sholz, and D. Boone, "The Erosion of CVD Silicon Carbide Coatings," AIME Annual Meeting, Atlanta, Georgia, March 1983.
29. E. Slamovich and A. Levy, "Combined Erosion-corrosion of Metals at Elevated Temperatures," AIME Annual Meeting, Atlanta, Georgia, March 1983.
30. A. Levy, "Combined Erosion-corrosion of Metals," Gordon Research Conference, New London, New Hampshire, July 1983.
31. A. Levy, Y-F. Man, and E. Slamovich, "Combined Erosion-corrosion of Steels," AIME-TMS

- Fall Meeting, Philadelphia, Pennsylvania, October 1983.
32. A. Levy, J. Patterson, and Y-F. Man, "Elevated Temperature Erosion of Alloys," AIME-TMS Fall Meeting, Philadelphia, Pennsylvania, October 1983.
 33. N. Jee and A. Levy, "The Erosivity of Coals in Slurries," AIME-TMS Fall Meeting, Philadelphia, Pennsylvania, October 1983.
 34. A. Levy, P. Yau, and N. Jee, "Coal Slurry Erosion of Piping Steels," AIME-TMS Fall Meeting, Philadelphia, Pennsylvania, October 1983.
 35. A. Levy, J. Patterson, and Y-F. Man, "Elevated Temperature Erosion and Erosion-corrosion of Steels," Electrochemical Society Annual Meeting, Washington, D.C., October 1983.
 36. A. Levy and P. Yau, "Erosion of Steels in Liquid Slurries," American Institute of Chemical Engineers, Diamond Jubilee Meeting, Washington, D.C., November 1983.

Chemistry and Morphology of Coal Liquefaction*

Heinz Heinemann, Investigator, with A.T. Bell, R.H. Fish, and G.A. Somorjai, Investigators

INTRODUCTION

This program is designed to look at the basic chemistry and physics of transformation of coal and coal liquids during processing. It involves investigators of different disciplines and a great variety of instruments which can be brought to play in the different tasks of the project. During the past year, a number of discoveries have been made. (1) It has, for instance, been found that carbon, present as graphite or char, can be reacted with steam in the presence of catalysts at quite low temperatures to produce not only methane and carbon dioxide, as described earlier, but also substantial quantities of ethylene and propylene. This points the way to a potential combination of a gasifier and a synthesis unit operating at very mild conditions. It is now proposed to investigate whether the higher hydrocarbons are primary and methane is a secondary product, to explain the mechanism of reaction, and to investigate potential poisoning phenomena which inhibit continuous operation at steady state. (2) In Fischer-Tropsch chemistry, comparison of fixed-bed and stirred-tank reactors has resulted in some interesting findings. The collection of data on kinetics of the hydrocarbon synthesis over unsupported iron catalysts will be completed, and results will then be represented in the form of rate expressions for each component. (3) The selective hydrogenation of only the nitrogen-containing ring in polynuclear hydrocarbons has now been achieved with heterogenized metallo-organic complexes. It has also been found that the same catalysts permit hydrogen donation from the partially saturated aromatics to hydrogen acceptors. This program will now investigate potential poisons for the reaction and catalyst life and will continue to determine reaction mechanisms. A totally automated, computer-controlled catalytic unit which permits 24 hour per day, 7 day per week

*This work was jointly supported by the Director, Office of Energy Research, Office of Basic Energy Sciences, Chemical Sciences Division and the Assistant Secretary for Fossil Energy, Office of Coal Research, Liquefaction Division of the U.S. Department of Energy under Contract No. DE-AC03-76SF00098, through the University Contracts Management Division of the Pittsburgh Energy Technology Center, Pittsburgh, Pennsylvania.

operation was installed in the first half of 1983. This unit will permit determination of catalyst life and poisoning for this and many other reactions.

1. Selective Synthesis of Gasoline Range Components from Synthesis Gas (Publication 5)

A.T. Bell, with R.A. Dicter, W. Canella, and H. Heinemann

Kinetics of Fischer-Tropsch synthesis over a potassium-promoted fused-iron catalyst were studied as a function of catalyst-reduction conditions. Severe reduction leads to a very active catalyst that deactivates rapidly. Milder reduction conditions give a less active but more stable catalyst. Differences in the order of dependence on H_2 and CO and the fact that activation energies are independent of reduction conditions suggest that different fractions of the surface are brought into an active state.

A study of potential support-metal interaction was undertaken. There are significant differences in the product spectrum between fused Fe_2O_3 and precipitated Fe_2O_3 catalysts. Supported iron on silica, mordenite, Y-zeolite, and ZSM-5 indicated that chain-growth probability is the same for all these supports. The olefin-to-paraffin ratio increases with increasing Al/Si ratio. Dependencies of rates of formation of individual products on H_2 and CO partial pressure are different for each support.

2. Catalyzed Low-temperature Hydrogenation of Coal (Publications 1, 2, 6, and 7)

G.A. Somorjai, with F. Delannay, W.T. Tysoe, and H. Heinemann

The reaction of a KOH-loaded graphite powder with steam at atmospheric pressure in the 700–900 K temperature range proceeds via two successive stages. During Stage I, hydrogen and hydrocarbons are evolved at a high rate, but no CO or CO_2 are produced. This stage ceases after the equivalent of 0.5 molecules of H_2 per potassium molecule in the sample is produced. During Stage II, gasification proceeds catalytically at a much reduced rate with the production of one CO molecule per equivalent H_2 molecule. The absence of CO or CO_2 evolution during Stage I indicates the formation of a stable oxygen-containing compound. This compound may

be decomposed thermally by heating the sample up to 1300 K. CO evolves almost exclusively during this high-temperature treatment. These results suggest a step-reaction mechanism involving the following four steps: (1) the dissociative adsorption of water-forming C-H and C-OH (phenol) groups; (2) the formation of a K-O-C entity (phenolate) from the reaction of KOH with the phenol groups; (3) the decomposition of these K-O-C entities to give CO, K₂O, and perhaps metallic potassium; and (4) the formation of KOH from reaction of K₂O with water. The transition from Stage I to Stage II is due to the consumption of KOH to form the K-O-C species. The rate of the catalytic reaction (Stage II) is controlled by the slowest step (step 3).

When powdered graphite samples loaded with various amounts of KOH are reacted with steam at atmospheric pressure in the 700–900 K temperature range, significant amounts of C_{1–6} hydrocarbons are found in the gaseous products of this reaction. Both the abundance of these hydrocarbons with respect to hydrogen and their relative distribution vary as a function of reaction time, KOH loading, and temperature. A model for their production is proposed according to which C-H groups are stabilized by the formation of a potassium phenolate-type compound at the prismatic edge of graphite. Hydrocarbons would then be produced from the direct hydrogenation of surface carbon atoms. The hydrocarbon distribution shows large deviations from the ideal Schulz-Flory distribution, giving little support to a chain-growth-type mechanism.

Although the reaction described above appears to be limited by stoichiometry, it has recently been found that catalytic amounts of Fe₂O₃ cause the decomposition of the K-O-C entity and permit a truly catalytic reaction to proceed.

3. Chemistry of Coal Solubilization and Liquefaction (Publication 8)

R.H. Fish, with A.D. Thormodsen, G.E. Cremer, and H. Heinemann

Deuterium experiments with quinoline, phenanthridine, and 7,8-benzoquinoline provide evidence for reversibility in the catalytic hydrogenation using Wilkinson's Catalyst of the carbon-nitrogen double bond; stereoselectivity in the reduction of the 3,4-double bond (quinoline and 7,8-benzoquinoline); and exchange (cyclometallation) of the aromatic carbon hydrogens beta (quinoline, phenanthridine) and

gamma (7,8-benzoquinoline) to the nitrogen atom. Reactions are carried out at 100–150°C and 100–200 psig. Steric and electronic effects are important in competitive binding experiments designed to find model coal constituents that inhibit and enhance the rate of hydrogenation of quinoline. (Φ₃P)₃RuHCl is a better catalyst (faster rates) than its rhodium equivalent, (Φ₃P)₃RhCl. Polymer-supported Wilkinson's Catalyst hydrogenates the model coal compounds studied at rates 10–20 times faster than the homogeneous analogue. Catalytic transfer (metal catalyzed) of hydrogen from 9,10-dihydrophenanthridine, 1,2-dihydroquinoline, and 9,10-dihydroacridine to other nitrogen heterocyclic compounds provides information on the plausible mechanisms for similar occurrences in donor-solvent coal liquefaction processes.

1983 PUBLICATIONS AND REPORTS

Refereed Journals

1. D.J. Coates, J.W. Evans, and H. Heinemann, "In Situ Observations of the Gasification of Carbon Catalyzed by Calcium Oxide," *Applied Catalysis* 7, 233-241 (1983); LBL-15521.
2. R. Casanova, A.L. Cabrera, H. Heinemann, and G.A. Somorjai, "Calcium Oxide and Potassium Hydroxide Catalyzed Low Temperature Methane Production from Graphite and Water," *Fuel* 62, 1138-1144 (1983); LBL-15067.
3. Heinz Heinemann, "A Society of Catalytic Chemists and Engineers," in *Heterogeneous Catalysis*, B.H. Davis and W.P. Hettinger, eds., ACS Symposium Series 222, 1983, #36; LBL-10278.
4. David Stern, A.T. Bell, and Heinz Heinemann, "Effects of Mass Transfer on the Performance of Slurry Reactors Used for Fischer-Tropsch Synthesis," *Chem. Eng. Sci.* 38, 4, 597 (1983).

LBL Reports

5. R.A. Dicter and A.T. Bell, "On-line Analysis of Fischer-Tropsch Synthesis Products," accepted by I&E Chem. Fundamentals, LBL-15544.
6. F. Delannay, W.T. Tysoe, H. Heinemann, and G.A. Somorjai, "The Role of KOH in the Low-temperature Gasification of Graphite," accepted for publication in *Carbon*, LBL-16049.
7. F. Delannay, W.T. Tysoe, H. Heinemann, and G.A. Somorjai, "Distribution of Reaction Products in the KOH-initiated Low-temperature

Steam Gasification of Graphite," accepted for publication in Applied Catalysis, LBL-16050.

8. R.H. Fish, A.D. Thormodsen, and H. Heinemann, "A Comparison of Polymer-supported Wilkinson's Catalyst to its Homogeneous Analogue in the Selective Reduction of Polynuclear Heteroaromatic Compounds," submitted to Molecular Catalysis, LBL-16918.

Invited Talks

9. H. Heinemann, "The Philosophy of Industrial Research," Stanford University, Stanford, California, August 1983 (Stanford Industrial Affiliates).

Materials Characterization in Fossil-Fuel Combustion Products*

Donald Boone and Alan Levy, Investigators

INTRODUCTION

The objective of this program is to determine how compositional, structural, and processing factors influence the ability of metallic and ceramic protective coatings on structural metals to resist oxidation, hot corrosion, erosion, and thermal shock in combustion-product environments on the combustion surfaces of heat-insulated engines.

1. Sliding Wear Behavior of Protective Coatings for Diesel Engine Components (Publication 2)

Eric January, Anthony Davis, Donald Boone, and Alan Levy

A series of sliding wear tests was performed using a washer-on-disc specimen configuration at room temperature to determine the nature of the sliding wear behavior of ceramic coating pairs that are candidates for use on the cylinder walls and piston rings of heat-insulated diesel engines. An oscillatory type of motion was used where the sliding action reversed each 90° of rotation. It was determined that the wear rate increased with the contact pressure for unimpregnated Y_2O_3 - ZrO_2 plasma-sprayed ceramic coatings. Impregnating the ceramic with Cr_2O_3 significantly decreased its wear rate. At the lowest contact pressure, 25 psi, the wear debris from the impregnated ceramic coating acted as abrasive, causing a higher-wear, three-body abrasive wear mechanism to occur. At the higher contact pressures of 50 and 100 psi, the wear debris was crushed and acted as a solid film lubricant, eliminating the difference in the wear rates of the ceramic as a function of contact pressure and resulting in lower wear rates at steady-state conditions than were measured for the 25-psi contact pressure. When hard chromium plating was rubbed against the ceramic coating, the wear rates of both the unimpregnated

and impregnated Y_2O_3 - ZrO_2 became the same and were much greater than the low wear rate of the chromium-plated 1018 steel.

2. Erosive Wear of CVD Tungsten/Tungsten Carbide Components (Publication 3)

Greg Hickey and Donald Boone

The erosive wear properties of CM 500 and CM 500L, two ultrafine-grain, tungsten/tungsten carbide, hard (1400–2300 VHN), chemical-vapor-deposited (CVD) coatings were investigated. Their erosive wear resistance was compared to other CVD hard coatings that are candidates for wear surfaces in advanced heat engines. CM 500 has a vapor deposition temperature from 800 to 900°C, whereas the CM 500L is a low-temperature application version that is deposited between 350 and 500°C so that it can be applied to ferrous alloys. Room-temperature erosion tests were conducted using 250–300 μ m SiC erodent particles at impingement angles of $\alpha = 30^\circ$ and 90° with a particle velocity of 30 m/sec. It was determined that the steady-state wear rates for CM 500 were 0.15×10^{-4} and 0.16×10^{-4} g/g for $\alpha = 30^\circ$ and 90° , respectively. These rates compare well with the best silicon carbide CVD coating tested, CM 4000, which was determined to have a steady-state wear rate of 0.15×10^{-4} and 0.17×10^{-4} g/g for $\alpha = 30^\circ$ and 90° , respectively. The CM 500 and CM 500C hard coatings were determined to be erosion-resistant alternatives to CVD silicon carbide for use in slurry pump liners and in other highly erosive environments.

1983 PUBLICATIONS AND REPORTS

Refereed Journals

1. D.H. Boone, R.T. Lambertson, S. Shaffer, and D.E. Peacock, "The Effect of Deposition and Processing Variables on the Oxide Structure of M-Cr-Al Coatings," *Thin Solid Films* 107, 463 (1983).

LBL Reports

2. A. Levy, D. Boone, E. January, and A. Davis, "Sliding Wear of Protective Coatings for Diesel Engine Components," submitted to *Wear*, LBL-17240.


*This work was supported by the Office of Naval Research, Department of Defense, under Government Contract No. N 00014-82-F-0055.

3. G. Hickey, J. Stiglich, D. Boone, and A. Levy, "Erosion Resistance of Conventional and Ultrafine Grain CVD Hard Metal Coatings," LBL-17486.

Invited Talks

4. D. Boone, "Effect of Coating Processing Techniques on Superalloy Properties," 28th International Gas Turbine Conference, Phoenix, Arizona, March 1983.
5. D. Boone and R. Lambertson, "The Effect of Aluminide Processing Variables on the Oxide Structure Using the Deep Etch Technique," International Conference on Metallurgical Coatings, San Diego, California, April 18-22, 1983.
6. D. Boone and J. Stiglich, Jr., "Structure and Erosion Behavior of an Ultrafine Grained SiC," The American Ceramic Society Meeting, Chicago, 1983.
7. D. Boone, "The Protective Oxide Structures of Thermal Spray Applied M-Cr-Al Coatings," presented as a poster at the 10th International Thermal Spraying Conference, Essen, West Germany, May 1983.
8. A. Levy, D. Boone, and A. Davis, "Wear of Protective Coating Systems," AIME-TMS Fall Meeting, Philadelphia, Pennsylvania, October 1983.
9. D. Boone, and R. Streiff, "The Role of Hf and Active Element in Oxidation Resistant Coatings," 164th Meeting of the Electrochemical Society, Washington, D.C., October 1983.
10. D. Boone, R. Streiff, and E. Godlewska, "The Development of Chromium Modified Coatings," 164th Meeting of the Electrochemical Society, Washington, D.C., October 1983.

Energy
Storage
Systems



ELECTROCHEMICAL ENERGY STORAGE

James W. Evans, Rolf H. Muller, John Newman,
Philip N. Ross, and Charles W. Tobias, Investigators

Surface Morphology of Metals in Electrodeposition*

Charles W. Tobias, Investigator

INTRODUCTION

The objective of this project is to gain understanding of the partial processes and their interactions involved in the deposition and dissolution of metals by electrolysis. Of particular interest is the influence of hydrodynamic flow on electrocrystallization and the distribution of charge transfer rates on advancing and receding metal profiles, as determined by the electric and concentration fields in the solution and by the kinetics of the charge transfer reaction. Control of the morphology of metallic deposits has been traditionally affected by addition agents that interfere with the crystallization process. In energy storage applications, however, other means may have to be employed for the control of morphology. Rotating-disk electrodes (RDE) and planar electrodes in channel-type electrolyzers are used for the preparation of metal deposits, over large ranges of solution properties and hydrodynamic conditions, with potentiostatic or galvanostatic control. The genesis of surface textures is studied, using both *in situ* motion picture photography and *post mortem* examination by electron microscopy.

1. The Effect of Hydrodynamic Flow on the Morphology of Electrodeposited Zinc (Publication 3)

James L. Faltemier and Charles W. Tobias

The influence of hydrodynamic flow and other process variables on the macromorphology of zinc

electrodeposited from acid solutions has been investigated under galvanostatic control at an RDE and in three-channel flow cells by using photomacrography, scanning electron microscopy, and *in situ* time-lapse motion picture photography. In addition, variable current-step techniques were employed, and mass-transfer-limiting currents of zinc were determined using an RDE.

Up to approximately 80 mA/cm² in 1M ZnCl₂, zinc forms a striated deposit within 3–15 minutes. Grooves develop parallel to the flow direction: straight in channel cells, spiral-shaped on an RDE. Increasing the flow rate or rpm causes more rapid development of more sharply contoured striations in the flow direction. Macroscopically smooth deposits are always obtained in both laminar and turbulent flow above 100 mA/cm² (see Figure 1-1) or when the current is pulsed. Although they develop sooner near the leading edge, striations form along the entire length of the electrode, up to 30 cm in this study. Time-lapse motion photography reveals detailed morphological sequences without interruption of the electrolysis and without any external handling. Zinc first deposits smoothly on the substrate surface. Then after several minutes protrusions appear randomly on the smooth surface, grow laterally in the flow direction, and join with other protrusions downstream, producing ridges. Substrate material, surface roughness, and variations in pH (in the 2–5 range) are of secondary importance.

The experimental evidence supports the idea that a sharp dependence of nucleation rate, as against rate of crystal growth, on overpotential (or current density) is the principal cause for the development of striations. The nucleation rate of crystals progressively increases as the current density level is raised, dominating any preferential outward growth of crystallites and producing a smooth surface. At the lower current density levels (far below transport-limiting conditions), wakes forming behind the largest crystallites cause improved mass transport because of small decreases in the mass transfer overpotential. As a consequence, current density increases locally in the wakes (see Figure 1-2). Better mass transport and smaller ohmic resistance to the developing ridges support their continued preferen-

*This work was supported by the Assistant Secretary of Conservation and Renewable Energy, Office of Energy Systems Research, Energy Storage Division of the U.S. Department of Energy under Contract No. DE-AC03-76SF00098.

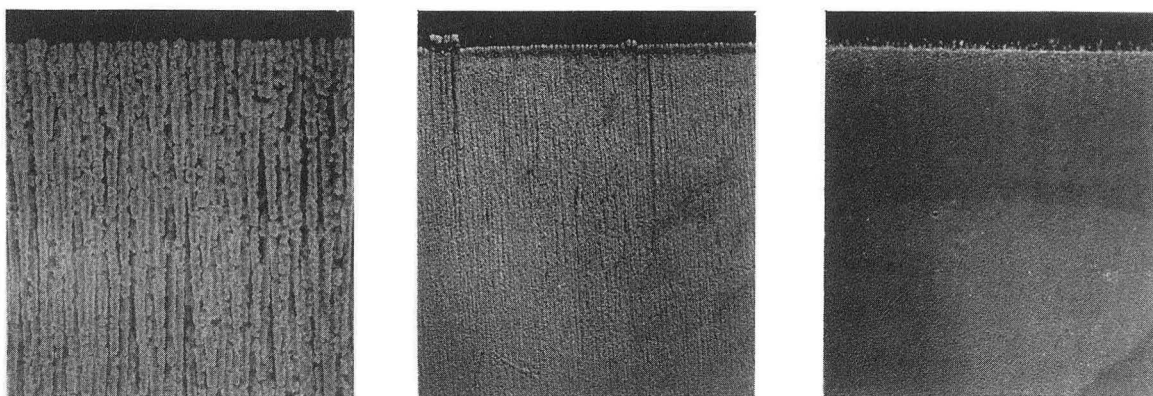


Figure 1-1. Striations in zinc deposits at different flow rates and times. Left: 10 mA/cm² for 90 min; center: 30 mA/cm² for 30 min; right: 100 mA/cm² for 9 min. All samples are in 1M ZnCl₂, pH = 4.6, RE 2300. The average thickness of the metal is 2.56 μm (54 coulombs/cm²) in all three cases. The leading edge is at the top of the picture. Each photo shows an area 3 cm wide. (XBB 831-378)

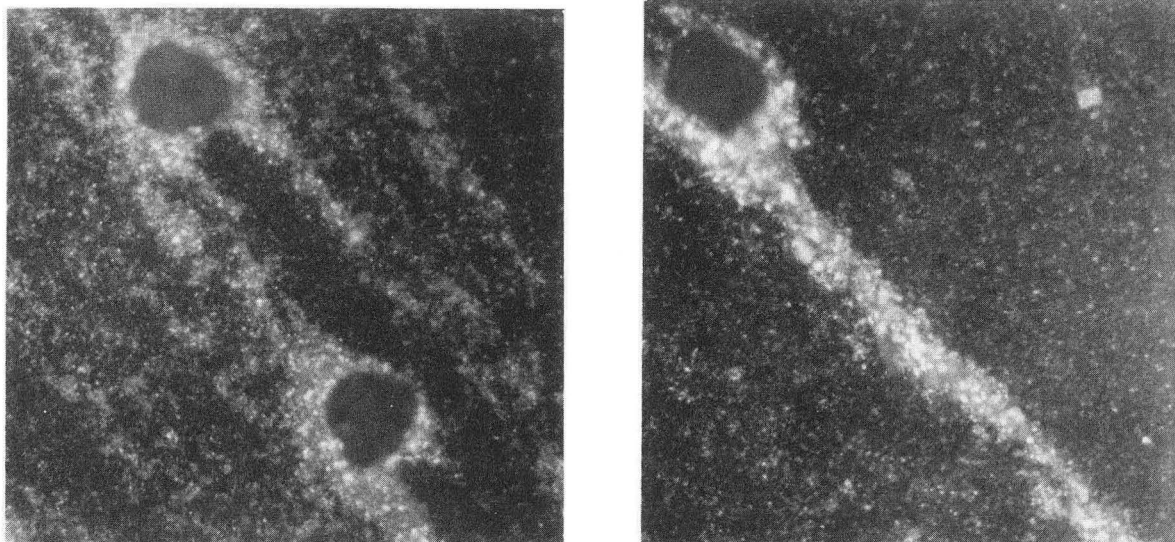


Figure 1-2. Ridge formation in the wake behind a protruding nodule in 1M ZnSO₄, pH = 4.6, 400 rpm. The flow rate is 5 mA/cm² for 25 min. Each photo shows an area 225 μm wide. (XBB 831-371)

tial growth, resulting eventually in fully striated deposits.

2. Work in Progress

Precise measurements are being carried out on the dependence of number density of initial protrusions on various substrates, under potentiostatic and galvanostatic control. *In situ* time-lapse photography is being used to observe the growth of selected sites

with constant or slowly pulsed current. A general finite element code was written for a model, based on potential theory, which includes realistic consideration of mass transfer and charge transfer overpotential. This model was first employed to obtain the potential and current distribution in the vicinity of a dielectric sphere attached to an electrode. The model has been tested successfully in computing the current distribution at the base of a hydrogen bubble attached to an electrode.

Metal Couples in Nonaqueous Electrolytes

Charles W. Tobias, Investigator

INTRODUCTION

The objective of this project is to explore practical alternatives to aqueous or high-temperature molten salt systems for the efficient electrochemical reduction and oxidation of reactive metals. Electrometallurgy of active metals has so far relied entirely on reduction of metals from aqueous electrolytes or from high-temperature molten salts. Recent developments in advanced galvanic cells and projected high-energy rechargeable battery systems involve the use of alkali-metal negatives. To expand the possibilities for application of reactive metals at near-ambient temperatures, new ionizing media must be sought that have high decomposition potentials and are capable of dissolving ionic compounds (or form ionic states by reacting with the solute). The propylene carbonate family of solvents has been shown in this laboratory to allow the reduction of alkali metals at room temperature with reasonably high efficiency. Solvent stability in the presence of reactive metals remains a critical issue, especially in

rechargeable galvanic-cell applications. Current work includes the study of viable reactions for the positive electrode and investigation of the role of co-solvents in improving solubility and conductivity. Under the support of the Office of Basic Energy Sciences, novel solvent purification techniques are being evaluated. A related project under the direction of Rolf H. Muller concerns the chemical nature of surface films on alkali metals in propylene carbonate electrolytes.

1. Work in Progress

Studies by cyclic voltammetry demonstrate that the oxidation of iodide to iodine in propylene carbonate proceeds in two steps: triiodide is formed first; then, at a potential more positive by 440 mV than the first step, oxidation proceeds to iodine. The voltammetric loops were modeled, using diffusional transport theory, and the reversibility of the above reaction was confirmed up to sweep rates of 200 mV/sec. The molar extinction coefficient and wavelengths of maximum absorbance of iodine in propylene carbonate were determined, and estimates were made of the free energy and entropy change of the disproportionation reaction: $2I_2 = I^+ + I_3^-$. The iodine/iodide couple promises to be a viable reaction for the positive electrode in propylene carbonate for electrolysis and galvanic-cell applications.

Engineering Analysis of Electrolytic Gas Evolution

Charles W. Tobias, Investigator

INTRODUCTION

Electrolytic gas evolution is among the most common reaction types in electrolysis and in advanced rechargeable batteries. Modern applications in energy storage and transmission (e.g. hydrogen) require much higher energy efficiency and lower capital cost than have been achieved in gas generating processes in the past. This project is directed toward the quantitative description of partial processes and their interactions involved in the nucleation, coalescence, and detachment of gas bubbles. Of special interest are the effects of individual moving bubbles and of gas-electrolyte emulsions on ohmic cell resistance and on mass transport of charged and uncharged species to and from electrode surfaces. A thorough understanding of the physical processes involved in the liberation and movement of gases at electrodes and in the electrolyte should lead to improved energy efficiency and lower capital costs in process and device technology.

1. Mass Transfer at Gas-evolving Surfaces in Electrolysis (Publication 5)

Dennis W. Dees and Charles W. Tobias

A novel micromosaic electrode was developed to resolve time-dependent mass-transfer distribution in the close vicinity of bubble phenomena. The electrode, prepared on a silicon wafer using integrated circuit manufacturing technology, consists of a 10 by 10 matrix of coplanar, electrically isolated, square platinum segments on 100- μm centers, surrounded by a relatively large buffer segment. A computer-actuated data acquisition and control system was assembled and software was developed to monitor the current to each of the segments and to control the potential of selected segments.

The utility of the electrode in examining interfacial mass-transport phenomena with characteristic lengths as small as 100 μm has been clearly demonstrated. The effect of a single hydrogen bubble disengagement, and of the coalescence of two bubbles, on the limiting current of the reduction of ferric

to ferrous ions was measured using the micromosaic electrode in a horizontal, facing-up orientation (see Figure 1-1). In the absence of gas evolution, large regular fluctuations in the limiting current to the segments with a period of 29 seconds were observed (see Figure 1-2). This periodic behavior is attributed to free convection: a cellular fluid motion moving across the electrode with a velocity of 40 $\mu\text{m}/\text{sec}$. It was found that the mass-transfer enhancement resulting from bubble disengagement is small when compared to that resulting from coalescence. Increases in the mass-transfer rate of more than an order of magnitude over the free-convection-limiting current were observed for the coalescence phenomena.

Two theoretical models were developed to account for the observed effect of a bubble disengagement on the mass-transfer rate to the surface. Numerical solutions of the convective diffusion equation were obtained for the flow generated by an ascending fluid sphere near a horizontal surface and for the flow in the wedge formed by the electrode and the bubble in the region near the collapse of the bubble contact area. The models correctly predict the observed direction of the initial change in the limiting current beneath a separating and ascending bubble.

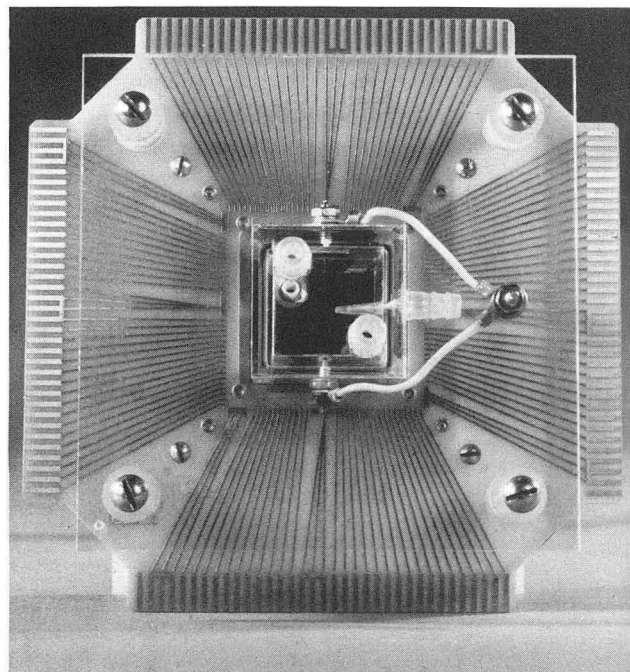


Figure 1-1. Top view of electrolysis cell containing a micromosaic electrode. The 100 electrically isolated platinum surface segments occupy a 1-mm² area in the center of the 5 × 5 cm platinum surface (the dark square facing the viewer). Radial leads provide individual connections to each segment.

(CBB 800-12427)

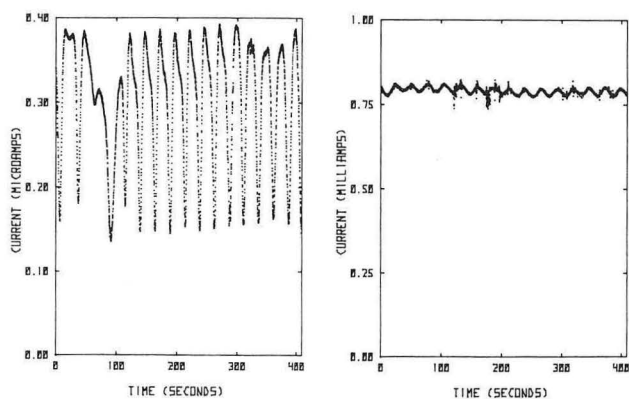


Figure 1-2. Free-convection-limiting current for the reduction of ferric to ferrous sulfate. Left: current to a single segment; right: current to the entire electrode. Note the smaller relative amplitude in the entire-electrode case, resulting from the averaging of fluctuations in mass-transfer rates, which are out of phase but have the same wavelength. (XBL 836-10385)

2. Work in Progress

Growth and disengagement of single bubbles are observed and recorded by high-speed cinematography. Bubble shape and size at disengagement are compared to theoretical predictions, based on our numerical integration of the Laplace-Young equation. These calculations show that the curvature of the electrode surface dramatically affects the maximum size at disengagement. For example, the equilibrium volume at disengagement of a bubble growing on a 63.5- μm -diameter hemispherical cap is only 5% that of a bubble having the same phase angle growing on a planar surface. New specifications have been prepared for the second generation of micromosaic electrodes, incorporating design features that will eliminate attack by corrosion.

1983 PUBLICATIONS AND REPORTS

LBL Reports

1. C.W. Tobias, D. Rajhenbah, and J. Faltemier, "Mass-transfer-limiting Currents of Zinc Deposition in Acidic ZnCl_2 and ZnSO_4 Solutions," LBL-15338.
2. D.S. Fischl (M.S. Thesis), with R.H. Muller and C.W. Tobias, "Effects of Small Flow Obstacles on the Limiting Current and Pressure Drop in a Square Duct," LBL-16422.[†]
3. J.L. Faltemier (Ph.D. Thesis), with C.W. Tobias, "The Effect of Hydrodynamic Flow on

the Morphology of Electrodeposited Zinc," LBL-16485.

4. J. Faltemier, M. Jaksic, C.W. Tobias, and T. Tsuda, "An Inventory of Photographs of Zinc Electrodeposited from Acid Electrolytes," LBL-16601.
5. D.W. Dees (Ph.D. Thesis), with C.W. Tobias, "Mass Transfer at Gas Evolving Surfaces in Electrolysis," LBL-16176.

Other Publications

6. A. Kindler and C.W. Tobias, "The Morphology of Copper Electrodeposition; Powder Deposition," Electrochemical Society Meeting, San Francisco, May 8–13, 1983, Ext. Abstr. 83-1, No. 583, pages 879–80; based on LBL-12838.
7. P.C. Foller, M.L. Goodwin, and C.W. Tobias, "Glassy Carbon Anodes and Air-depolarized Cathodes for the Generation of Ozone," Electrochemical Society Meeting, San Francisco, May 8–13, 1983, Ext. Abstr. 83-1, No. 578.[‡]
8. D.W. Dees and C.W. Tobias, "Development of a Data Acquisition and Control System for the Study of Mass Transfer Phenomena on a Micromosaic Electrode," Electrochemical Society Meeting, San Francisco, May 8–13, 1983, Ext. Abstr. 83-1, No. 469.
9. Process for Producing Ozone (1983): U. S. Patent No. 4,375,395 (with P.C. Foller and M.L. Goodwin).[‡]

Invited Lectures

10. C.W. Tobias (with Douglas Bennion, E.J. Cairns, Karl Kordesch, John Newman, and William Tiedemann, instructors), short course on electrochemical engineering of batteries, Marriott Hotel, Berkeley, California, June 20–24, 1983.
11. C.W. Tobias, "Electrochemical Techniques for the Studies of Mass Transport Phenomena," invited colloquia lectures, The University of Pennsylvania, Philadelphia, October 3, 1983; Carnegie-Mellon University, Pittsburgh, Pennsylvania, October 5, 1983.[†]
12. C.W. Tobias, "Effect of Hydrodynamic Flow on the Morphology of Zinc Deposited from Acid Electrolytes," Workshop on Zinc/Halogen Batteries, under the auspices of LBL and EPRI, Palo Alto, California, November 30–December 2, 1983.

[†]Supported by the Director, Office of Energy Research, Office of Basic Energy Sciences, Materials Sciences Division, U.S. Department of Energy.

[‡]Supported entirely from University funds.

Surface Layers on Battery Materials*

Rolf H. Muller, Investigator

INTRODUCTION

The purpose of this work is to provide direct experimental information about the formation and properties of surface layers on battery-electrode materials. Present studies are concerned with lithium in various ambient-temperature nonaqueous electrolytes. Surface layers which form in these media prevent the spontaneous (corrosion) reaction of the metal with solvents and solutes. However, these surface layers also appear to be the principal reason for the lack of rechargeability of the lithium electrodes, and layers with more desirable properties are being sought. A more broadly based research program, supported by the Office of Basic Energy Sciences, Division of Materials Sciences, DOE, is described in the sections "Electrochemical Phase Boundaries," R.H. Muller, Investigator, and "Electrochemical Processes," C.W. Tobias, Investigator.

1. Ellipsometer Studies of Surface Layers on Lithium (Publication 2)

F. Schwager,[†] Y. Geronov,[‡] and R.H. Muller

The growth of surface layers on lithium in propylene carbonate solutions can be followed by ellipsometry, although the refractive indices of many potential film materials are close to those of the electrolyte. Film thicknesses calculated from ellipsometer measurements increase over periods of several days at open circuit; they are several times larger than those derived from galvanostatic-pulse measurements. Films are found to be inhomogeneous, with properties varying continuously as a function of distance from the substrate. Compact regions are located adjacent to the metal, and porous regions are located adjacent to the solution. Electrode-capacitance measurements are sensitive to the thin

compact region; this region can also be generated by reaction with water vapor. Ellipsometer measurements are primarily affected by the thicker porous region, which may be formed by the precipitations of decomposition products of the solution.

[†]Present address: Mettler Instruments AG, CH-8606 Greifensee, Switzerland.

[‡]Permanent address: Central Laboratory of Electrochemical Power Sources, Bulgarian Academy of Sciences, Sofia, Bulgaria.

2. Effect of Residual Water in Propylene Carbonate on the Nature of Films Formed on Li (Publication 3)

G. Nazri and R.H. Muller

A thin-layer cell with electrode separation of 50 μm has been used to minimize the effect of impurities in the electrolyte on film formation. Trace amounts of water have been removed from propylene carbonate (PC) by Hg-Li amalgam. The resulting solvent interacts differently with film-free lithium than with lithium containing residual water. Analysis of films formed on Li by infrared spectroscopy, x-ray diffraction, and electron spectroscopy for chemical analysis (ESCA) showed formation of polymerized PC as well as Li_2CO_3 in the absence of water. However, films formed on Li in PC containing residual water were composed of lithium oxide.

3. Work in Progress

The morphology of lithium deposited from 1M LiClO_4 in propylene carbonate and in 2-methyl tetrahydrofuran on Li, Cu, and Pt substrates has been found to be very porous (see Figure 3-1). Several inhibitors (Rhodamine 116, Coumarine 30, Ethyl Orange, Azobenzene, EDTA) did not change the morphology or prevent reaction with the solvents. Protective surface layers with improved ionic conductivity are now being formed and characterized.

*This work was supported by the Assistant Secretary of Conservation and Renewable Energy, Office of Energy Systems Research, Energy Storage Division of the U.S. Department of Energy under Contract No. DE-AC03-76SF00098.

1983 PUBLICATIONS AND REPORTS

LBL Reports

1. F. Schwager and R.H. Muller, "Impedance and Ellipsometer Measurements of Lithium Electrodes in Propylene Carbonate Solutions," LBL-13618.
2. F. Schwager, Y. Geronov, and R.H. Muller, "Ellipsometer Studies of Surface Layers on Lithium," submitted to J. Electrochem. Soc., LBL-13557.

Other Publications

3. G. Nazri and R.H. Muller, "Effect of Residual Water in Propylene Carbonate on the Nature of Films Formed on Lithium," Electrochem. Soc. Meeting, Washington, D.C., October 9-14, 1983, Ext. Abstr. 61; LBL-16094.

Invited Talks

4. Rolf H. Muller, "Surface Layers on Battery Materials," Energy Storage Technology Division, DOE, Lead Center Coordination Meeting, Washington, D.C., February 2, 1983.

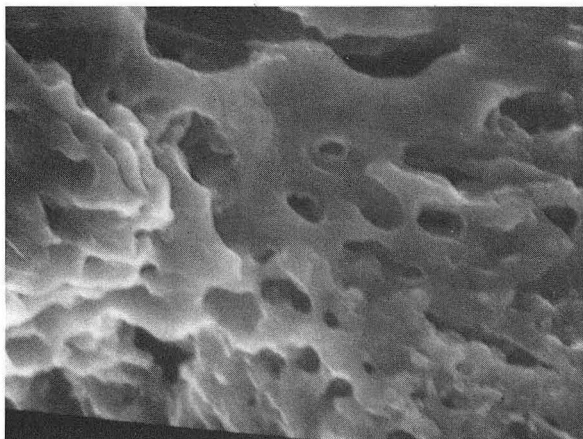
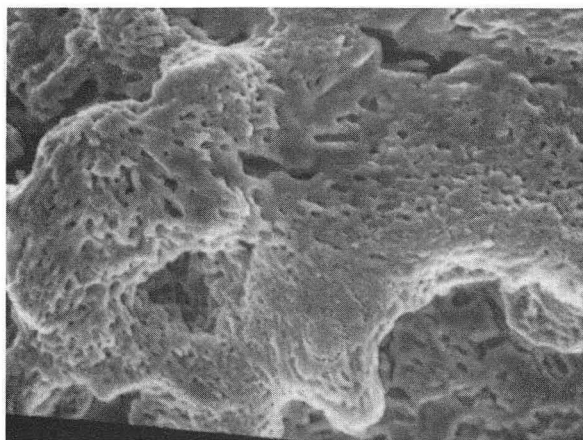


Figure 3-1. Porous micromorphology of lithium deposited from 1M LiClO₄ in propylene carbonate on Cu, as seen by the scanning electron microscope. Upper figure — 1000X magnification. Lower figure — 5000X magnification.

(XBB 839-8204)

Electrode Kinetics and Electrocatalysis*

Philip N. Ross, Investigator

INTRODUCTION

Complex electrochemical reactions in which chemical bonds are broken and/or formed are invariably catalytic, with electrode kinetics varying by many orders of magnitude for different electrode materials. Catalytic electrode materials are essential to technologies like fuel cells, metal-air batteries, electrolyzers, and electro-organic synthesis processes. Bifunctional air electrodes, which both consume and evolve oxygen, are attractive positive electrodes which, when coupled with Fe or Zn negative electrodes, form high-energy-density (150–200 Wh/kg) batteries. Bifunctional air electrodes require the development of catalytic materials that are both active and corrosion-resistant over a demanding range of electrode potentials.

Metal/metal-ion (Me/Me^{Z+}) couples form the largest class of negative-electrode types for batteries. Two further distinctions of Me/Me^{Z+} couples can be made: those where the ionic state (or discharged state) is insoluble (e.g., a metal/metal-oxide couple) and those where the ionic state is solvated (e.g., Zn/Zn^{2+} in acid). The kinetics of Me/Me^{Z+} couples are relatively rapid, but they are not usually controlled by only a charge transfer step. These reactions are often quasi-reversible, in the sense that they proceed at high rate and small overpotential, but they do not follow “ideal” charge transfer rate expressions. Phenomena frequently cited as contributing to the “nonideal” behavior of Me/Me^{Z+} systems are critical nucleation, intermediate or precursor formation, and impurity adsorption. The structural transformations to the metallic surface as a result of cyclic Me^{Z+} formation are not well known, particularly at the atomic scales of structure. Yet these structural transformations may control critical phenomena in Me/Me^{Z+} cyclability.

*This work was supported by the Assistant Secretary of Conservation and Renewable Energy, Office of Energy Systems Research, Energy Storage Division of the U.S. Department of Energy under Contract No. DE-AC03-76SF00098.

1. The Corrosion of Carbon-black Anodes in Alkaline Electrolyte: I. Acetylene Black and the Effect of Cobalt Catalyzation (Publication 6)

Philip N. Ross and Harvey Sokol

Labeling of acetylene black by ^{14}C was used together with mass-spectroscopic analysis of the gas evolved to determine the current efficiencies for oxygen evolution, carbon dissolution, and carbon gasification (to carbon monoxide). The current efficiencies were found to depend dramatically on the potential, temperature, and presence of an evolution catalyst like Co_3O_4 . On uncatalyzed black, three regimes could be distinguished. (1) At potentials below 500 mV vs Hg/HgO and at temperatures below 50°C, carbon dissolution is the primary anodic process. (2) At 500–600 mV and 50°C or lower, carbon dissolution and oxygen evolution occur at equivalent rates. (3) Above ~600 mV or above ~60°C, oxygen evolution and gasification of the carbon to carbon monoxide are the dominant processes. Catalyzation with Co_3O_4 collapsed these regimes so that all three anodic processes were concurrent throughout the potential region of interest, and the overall rate of corrosion increased significantly. In addition, Co_3O_4 catalyzation caused the production of organic products (~5% current efficiency) in a potential region where none is produced from acetylene black alone. The mechanism of action of Co_3O_4 on the acetylene-black corrosion is not yet understood, but it is clear that the selection of carbon materials for bifunctional air electrodes must take the effect into account.

2. Diffusion-controlled Multisweep Cyclic Voltammetry: III. Deposition of Silver on Stationary and Rotating-disk Electrodes (Publication 5)

P.C. Andricacos and P.N. Ross

An experimental study of diffusion-controlled silver electrodeposition has been carried out in order to investigate the applicability of the model (Publications 2 and 3) to reversible metal deposition during multisweep cyclic voltammetry. For a stationary planar electrode (see Figure 2-1), excellent agreement between theory and experiment has been obtained for the position of the cathodic-current maxima on the potential axis as well as for the dependence of their magnitude on parameters such as sweep rate,

3. LEED Analysis of Electrode Surfaces — I. Structural Effects of Potentiodynamic Cycling on Pt Single Crystals (Publication 1)

F.T. Wagner and P.N. Ross

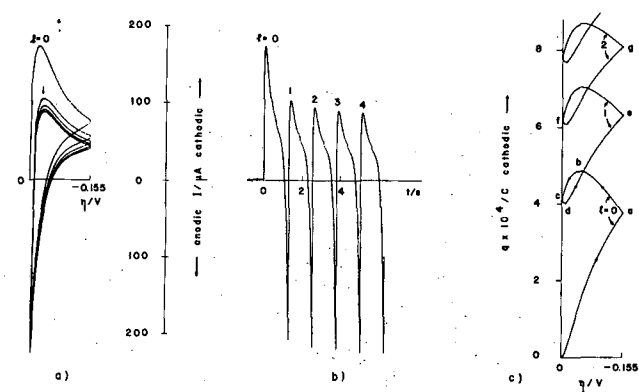


Figure 2-1. Cyclic voltammetry of Ag deposition on a stationary electrode. (a) Multisweep current/potential diagram obtained at 0.050 V/s for a cathodic reversal overpotential of 6 (RT/F) or a $\theta = 6$. (b) Identical to (a) but recorded on a time axis. (c) Charge potential diagram record simultaneously with (a) and (b). (XBL 836-10358)

cathodic-reversal potential, and number of applied sweeps. Anodic currents measured at the foot of the wave deviated from theoretical predictions as a consequence of the small but uncompensated resistance of the electrolyte. In an effort to predict and therefore control the amount of deposit, integral charges associated with each sweep have been measured and successfully correlated with the parameters of the experiment. It has been found that at millimolar concentrations, deposit thicknesses of the order of up to 20 monolayers can be formed with quantitative control. Experiments with a rotating-disk electrode have demonstrated that a periodic-current response is obtained upon multiple sweeping as predicted by theory. First-sweep and periodic currents normalized with respect to the limiting current could be correlated with the dimensionless sweep rate in accordance with the theoretical predictions. Contrary to previous investigations, the diffusion coefficient of the silver ion was determined by limiting-current measurements, and the value thus obtained was subsequently used to successfully correlate stationary-electrode cyclic-voltammetry data. During limiting-current measurements with very slow sweeps, a time-dependent increase in current (above the time-invariant value at fast sweeps) was observed that inhibited the onset of surface roughening. Based on the dimensionless sweep rate, a semi-empirical criterion was developed for the optimal conditions for the potentiodynamic determination of steady-state limiting currents, the use of which may eliminate errors arising from both transient effects and surface-area increase due to roughness.

It is of both technological and fundamental importance to develop an understanding of the changes in the morphology of electrode surfaces when they are subject to various electrochemical treatments. In battery systems, metal electrodes are cycled between oxide states, between the metallic and the oxide states, or between a solvated state and the metallic state. To understand what happens in such systems at the atomic level requires a method of following the changes in the atomic structure of the electrode surface. Low-energy electron diffraction (LEED) is now a well-developed and still-improving method for surface-structure determination that is used in virtually every contemporary study of surfaces in vacuum. It should be possible, under certain conditions, to make definitive structure determinations by LEED analysis of electrode surfaces *ex situ*, thereby considerably advancing the state of understanding the transformations occurring at electrode surfaces. In this report, we review the LEED theory with regard to the determination of the structure of nearly ordered surfaces containing characteristic imperfections and show how the LEED apparatus can be interfaced to an electrochemical cell. The electrode system and effects studied here are the Pt electrode in dilute HF electrolyte and, in particular, the effects of potentiodynamic cycling on the structure of the low-index single-crystal surfaces. A LEED analysis of the (100) surface is presented here. The analysis indicates that cycling can alter the long-range ordering (>10 nm) of the surface, but that local ordering (1.3–1.9 nm) is always preserved. Cycling between the hydrogen-electrosorption region and the edge of the oxygen-electrosorption region (0–0.82 V RHE) caused no discernable change in the Pt(100)-(1 × 1) LEED pattern. However, cycling well into the oxygen-electrosorption region (to 1.58 V RHE) produced LEED patterns characterized by alternate broadened and sharp spots. The breadth of a given spot fluctuated with the energy of the incident electron beam in a manner consistent with the formation of a correlated island-hole structure, with islands and holes monoatomic in height and 5–7 atoms in width. The island-hole structure can reasonably be derived from a place-exchange mechanism of oxide formation with attractive adatom and vacancy interactions.

4. Work in Progress

Preliminary studies of heat-treated furnace blacks have shown that in some cases dramatic reductions in corrosion rate can be accomplished by heat treatment at 2700–2800°C. Transformations to the furnace-black microstructure upon heat treatment are being followed using high-resolution electron microscopy. For some furnace blacks, graphitic layer-plane ordering occurs during heat treatment without the fusion of the prime particles, thus preserving relatively high surface area. However, heat-treated blacks having nominally similar graphitic microstructures appear to show markedly different corrosion behavior. Further studies to relate carbon microstructure to corrosion resistance are in progress.

1983 PUBLICATIONS AND REPORTS

Refereed Journals

1. F.T. Wagner and P.N. Ross, "LEED Analysis of Electrode Surfaces: Structural Effects of Potentiodynamic Cycling on Pt Single Crystals," *J. Electroanal. Chem.* **150**, 141–164 (1983); LBL-14761.
2. P.C. Andricacos and P.N. Ross, "Diffusion Controlled Multisweep Cyclic Voltammetry: I. Reversible Deposition on a Rotating Disk Electrode," *J. Electrochem. Soc.* **130**, 1340–1352 (1983); LBL-14524.
3. P.C. Andricacos and P.N. Ross, "Diffusion Controlled Multisweep Cyclic Voltammetry: II. Reversible Deposition on a Stationary Planar Electrode," *J. Electrochem. Soc.* **130**, 1353–1359 (1983); LBL-14525.
4. F.T. Wagner and P.N. Ross, "The Thickness of Electrolyte Layers on Emerged Pt Electrodes," *J. Electrochem. Soc.* **130**, 1789 (1983).
5. P.E. Andricacos and P.N. Ross, "Diffusion Controlled Multisweep Cyclic Voltammetry: III. Deposition of Silver on Stationary and Rotating Disk Electrodes," submitted to *J. Electrochem. Soc.*, LBL-16734.
6. P.N. Ross and H. Sokol, "Corrosion of Carbon Black Anodes in Alkaline Electrolyte: I. Acetylene Black and the Effect of Cobalt Catalyzation," submitted to *J. Electrochem. Soc.*, LBL-16520.
7. P.N. Ross and F.T. Wagner, "The Application of Surface Physics Techniques to the Study of Electrochemical Systems," in *Advances in Electrochemistry and Electrochemical Engineering*, Vol. XIII, H. Gerischer and C.W. Tobias, Eds., Wiley-Interscience, New York, in press; LBL-16235.
8. P.N. Ross, "Hydrogen," chapter in *Oxidation-Reduction Potentials of Aqueous Solutions: A Selective and Critical Source Book*, A. Bard, J. Jordan, and R. Parsons, Eds., Marcel Dekker, New York, in press.

LBL Reports

Other Publications

Electrical and Electrochemical Behavior of Particulate Electrodes*

James W. Evans, Investigator

INTRODUCTION

Particulate electrodes (for example, fluidized-bed electrodes) have very high surface areas per unit mass of electrode. Mass-transfer rates are also typically high in such electrodes. These effects make particulate electrodes attractive where electrochemical reactions are to be conducted at high space-time yields. In the context of energy storage, this means an electrode with high specific power. A major disadvantage of such electrodes is that their electrical and electrochemical behavior is poorly understood, inhibiting their wider application. This research is an examination of particle and electrolyte transients in particulate electrodes and their variation with position in the electrode. Also of interest are charge transport (electronic conduction) mechanisms within the electrode and the behavior of metals (particularly zinc) when subjected to the fluctuating potentials encountered in a particulate electrode during electro-dissolution or deposition.

Abstracts of published and printed reports describing other elements of the research program are listed under "*In Situ* Investigations of Gas-solid Reactions by Electron Microscopy," James W. Evans, Investigator.

Work in Progress

Potential transients have been measured in fluidized electrodes consisting of copper particles, zinc-coated copper particles, and Sorapec particles (zinc-coated polymer particles under commercial development by Sorapec for battery applications). The transients, after statistical analysis, show distinct differences in behavior that are attributed to the differences in exchange-current density for zinc and copper deposition/dissolution or to the low density (and consequent dynamic behavior) of the Sorapec particles.

1983 PUBLICATIONS AND REPORTS

See "*In Situ* Investigations of Gas-solid Reactions by Electron Microscopy."

*This work was supported by the Assistant Secretary of Conservation and Renewable Energy, Office of Energy Systems Research, Energy Storage Division of the U.S. Department of Energy under Contract No. DE-AC03-76SF00098.

Electrochemical Properties of Solid Electrolytes*

Lutgard C. De Jonghe, Investigator

INTRODUCTION

Sodium-beta aluminas are used as ceramic separators in advanced high-energy-density storage batteries. In such batteries, the semipermeable ceramic membrane separates the molten-sodium negative electrode from the molten sodium polysulfide positive electrode. When the solid electrolyte is in prolonged contact with the electrodes during operation of the cell at 300 to 350°C, degradation phenomena may occur. These degradation phenomena can take different forms. The work in this program is aimed at elucidating the causes of the electrochemical degradation of the electrolyte and formulating recommendations based on a fundamental understanding which, when implemented, should lead to improved performance of the sodium/sulfur battery.

1. Oxygen Interstitial Transport and Chemical Coloration in Sodium-beta Alumina (Publication 4)

Lutgard C. De Jonghe, Andrew Buechele, and Michel Armand

A reaction-rate maximum occurs around 250°C in the bleaching of chemically discolored sodium-beta aluminas, as shown in Figure 1-1. It has been determined that the bleaching rate depends on the diffusion rate of oxygen interstitials in the conduction planes of the sodium-beta alumina. The reaction-rate maximum indicates that an irreversible transition occurs from a high-mobility to a low-mobility oxygen interstitial at around 300°C. This transition is likely due to one in which a free-oxygen interstitial is converted into an interstitial that is trapped by aluminum ions from the adjacent spinel blocks, i.e., a Roth-type defect.

*This work was supported by the Assistant Secretary of Conservation and Renewable Energy, Office of Energy Systems Research, Energy Storage Division of the U.S. Department of Energy under Contract No. DE-AC03-76SF00098. Additional support for this work was received from the Electric Power Research Institute for D. Hitchcock, A. Buechele, L. De Jonghe, and M. Armand.

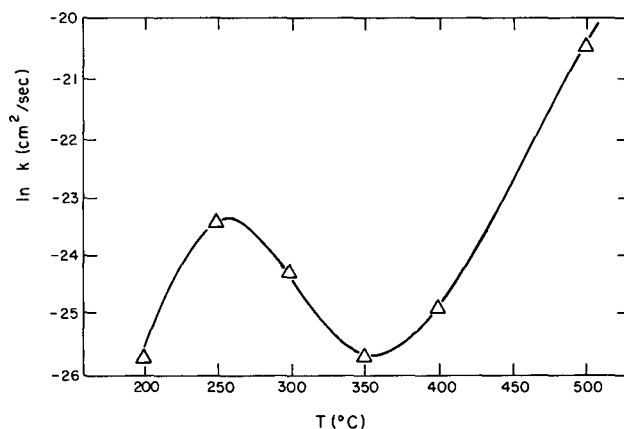


Figure 1-1. Bleaching rate of chemically discolored sodium-beta alumina as a function of temperature. The scaling constant k of the reaction rate is calculated from $dx/dt = k/x$, where x is the bleached layer thickness measured after a time $t = 24$ hr of annealing in air. A bleaching-rate anomaly is observed between 250 and 350°C. (XBL 8211-7361)

2. Fracture Toughness Anisotropy of Sodium-beta Alumina (Publication 6)

D. Hitchcock and Lutgard C. De Jonghe

The fracture toughness was determined for sodium-beta alumina single crystals, using a hardness indent method. For cracks with a habit plane normal to the 00.1 planes, the fracture toughness was about 2 MPa.m^{1/2}, while for cracks running parallel to the 00.1 planes the fracture toughness was only about 0.16 MPa.m^{1/2}. This extreme anisotropy may partly explain the difference between calculated and observed critical-current densities for Mode I failure initiation of polycrystalline solid electrolytes.

3. Solid Electrolyte Degradation: Problems and Solutions (Publication 5)

Lutgard C. De Jonghe

Examination of sodium-beta alumina solid electrolytes after their use in sodium/sulfur cells reveals a variety of progressive changes. These changes can be summarized in four categories: (1) darkening of the solid electrolyte in contact with molten sodium (chemical coloration); (2) sodium precipitation in the interior of the electrolyte (Mode II degradation); (3) rapid or slow crack penetration through the electrolyte, causing partial or total short circuits (Mode I

degradation); and (4) cracking and electrode imprinting on the sulfur side of the electrolyte (sulfur side attack).

Chemical coloration is now fairly well established to be associated with a partial reduction of the electrolyte. The oxygen vacancies that are introduced are compensated for by electrons, thus increasing somewhat the electronic conductivity of the electrolyte over its intrinsic value. This does not affect the Faradic efficiency of the cell in a measurable way. The observation of reduction implies that the oxygen in the electrolyte is mobile to some extent. Estimates of the oxygen-diffusion coefficient based on the coloration and bleaching experiments described above put the oxygen-diffusion coefficient at about 2×10^{-16} cm²/sec at 300°C for an electrolyte with a 1.1- μ m grain size. This movement of the oxygen ions may play some role in slow degradation phenomena.

When an ionic current is passed through the electrolyte, forming sodium metal at the exit surface, no oxygen is provided locally, so that the oxygen chemical potential at the sodium-exit surface drops continuously. Stronger reducing conditions should therefore be expected at the sodium-exit surface during sodium electrolysis. Differences in the intensity of the chemical coloration between sodium-entrance and sodium-exit sides of the electrolyte appear to support this assertion.

Mode II degradation, involving the internal deposition of sodium when a gradient in the ionic/electron transport-number ratio is present, was calculated to be avoidable under normal cell-operating conditions. But Mode II degradation could arise where impurity contamination becomes important or when strong reducing conditions prevail. Such strongly reducing conditions can occur during cell charging at the tip of a sodium-filled crack that has partially penetrated the electrolyte from the negative electrode. It is thus conceivable that this mode of degradation, as well as the intense chemical reducing conditions, leads to slow crack growth. Evidence for slow crack growth has been found in the rate dependence of critical current density thresholds for crack initiation.

Sulfur-side attack is also found frequently in electrolytes that have been used for extended periods in sodium/sulfur cells. Laboratory experiments have confirmed that the polysulfide-discharge composition

is very corrosive, especially if the melt is in equilibrium with solid Na₂S₂. Such conditions can be reached locally at the positive-electrolyte surface during the discharge cycle of the cell. Appropriate cell-operating conditions and good positive-electrode design can minimize this effect.

1983 PUBLICATIONS AND REPORTS

Refereed Journals

1. A.C. Buechele and Lutgard C. De Jonghe, "Degradation of Sodium-beta Alumina: Effect of Microstructure," *J. Electrochem. Soc.* **130**, 1042 (1983); LBL-13188.
2. L.C. De Jonghe, "Degradation Mechanisms of Sodium-beta Aluminas," *J. Electrochem. Soc.* **82** (2), 538 (1982); LBL-14365.
3. L.C. De Jonghe, A. Buechele, and K.H. Yoon, "Grain Boundaries and Solid Electrolyte Degradation," *Advances in Ceramics* **4**, 342 (1983); LBL-14150.

LBL Reports

4. Lutgard C. De Jonghe, Andrew Buechele, and Michel Armand, "Oxygen Interstitial Transport and Chemical Coloration in Sodium-beta Alumina," LBL-15308.
5. Lutgard C. De Jonghe, "Solid Electrolytes: Problems and Solutions," LBL-16716.
6. D. Hitchcock and L.C. De Jonghe, "Fracture Toughness Anisotropy of Sodium-beta Alumina," LBL-16115.

Invited Talks

7. L.C. De Jonghe, "Oxygen Interstitials in Sodium-beta Alumina," Fourth International Congress of Solid State Ionics, Grenoble, France, July 1983.
8. L.C. De Jonghe, "Sodium-beta Alumina Life Limitations," CGE, Paris, France, July 1983.
9. L.C. De Jonghe, "Degradation Mechanisms of Sodium-beta Aluminas," 162nd Meeting, American Electrochemical Society, Detroit, October 1982.

Analysis and Simulation of Electrochemical Systems*

John Newman, Investigator

INTRODUCTION

This program includes the investigation of efficient and economical methods for electrical-energy conversion and storage, development of mathematical models to predict the behavior of electrochemical systems and to identify important process parameters, and experimental verification of the completeness and accuracy of the models. Specific projects include the analysis of the thin-gap flow cell for electrochemical synthesis and energy storage, the mathematical modeling of the Li-Al/FeS battery and the Li-Si/FeS₂ battery, the study of transport processes in sodium polysulfide melts, alternating-voltage measurements on the dissolution of zinc, and the investigation of methods for the design and scale-up of battery systems.

1. Experimental Determination of the Passive-active Transition for Iron in 1M Sulfuric Acid (Publication 1)[†]

Philip P. Russell and John Newman

Current-voltage curves from three rotating iron disks are obtained using a polarization device which permits determination of the transition region between the active and passive states. Diameters of the three electrodes are 0.494, 0.298, and 0.0986 cm, respectively. Results from the smallest electrode have the least amount of ohmic distortion. Trends in the data, which are observed as the electrode size is decreased, form the basis for the conclusions that are drawn from this work. Analysis of these trends indicates that the active-passive transition is characterized by a nearly vertical line on a current vs potential plot. The z-shaped nature of the current-voltage curves, reported by Epelboin *et al.*,¹ is entirely due to the ohmic-potential drop in the solution. Analysis of the data, within the framework of a

*This work was supported by the Assistant Secretary of Conservation and Renewable Energy, Office of Energy Systems Research, Energy Storage Division of the U.S. Department of Energy under Contract No. DE-AC03-76SF00098.

mathematical model presented by Law and Newman,² indicates that the average current density on the active portion of the disk increases as the size of the active area decreases during the passivation process.

[†]This work was supported in part by the Solar Energy Research Institute.

1. I. Epelboin, C. Gabrielli, M. Keddam, J.C. Lestrade, and H. Takenouti, *J. Electrochem. Soc.* **119**, 1632 (1972).

2. C.G. Law and J. Newman, *J. Electrochem. Soc.* **126**, 2150 (1979).

2. Analytic Expression of the Warburg Impedance for a Rotating-disk Electrode (Publication 2)[†]

Bernard Tribollet[‡] and John Newman

In the presence of the convective-flow pattern of the rotating disk, the classical Warburg impedance is modified, particularly at low frequencies. The transformation of Scherson permits the alternating-current impedance problem to be related to the transient flux-step or concentration-step behavior of the same system. Here flux-step results are used to generate low- and high-frequency analytic expressions which overlap at intermediate frequencies.

[†]This work was supported in part by the National Science Foundation through an Exchange Visitor Program with "Centre National de la Recherche Scientifique" No. G050252.

[‡]Present address: Groupe de Recherche No. 4 du CNRS, "Physique des Liquides et Electrochimie," Associé à l'Université Pierre et Marie Curie, 75230 Paris Cedex 05, France.

3. The Modulated Flow at a Rotating-disk Electrode (Publication 3)[†]

Bernard Tribollet[‡] and John Newman

The frequency-response analysis for an electrochemical system (current or potential) to a sinusoidal-speed modulation at a rotating-disk electrode involves three steps. First is the analysis of the corresponding unsteady Navier-Stokes equations, for which the four first terms of the instantaneous velocity expansions are given. The study of the unsteady mass transport is the second problem; its solution is a series expansion in $Sc^{-1/3}$, for which the two first terms are given. Finally, the electrical response of

the electrochemical system is determined. This involves the electrochemical impedance (the diffusion- or convective-Warburg impedance, the charge-transfer resistance, the electrolyte resistance, and the double-layer capacitance). The results are experimentally confirmed, in potentiostatic and galvanostatic regulations, over a wide frequency range ($10^{-2} < p < 5$) for the reduction of $\text{Fe}(\text{CN})_6^{3-}$ to $\text{Fe}(\text{CN})_6^{4-}$ in 1M KCl.

†This work was supported in part by the National Science Foundation through an Exchange Visitor Program with "Centre National de la Recherche Scientifique" No. G050252.

‡Present address: Groupe de Recherche No. 4 du CNRS, "Physique des Liquids et Electrochimie," Associé à l'Université Pierre et Marie Curie, 75230 Paris Cedex 05, France.

4. Current Distribution on a Rotating Disk below the Limiting Current (Publication 4)

John Newman

The distribution of current across the surface of a rotating-disk electrode is calculated for the general case where electrode kinetics, mass-transfer limitations, and ohmic resistance are all significant.

5. The Asymmetric Graetz Problem in Channel Flow (Publication 5)

Victoria Edwards and John Newman

A convenient representation of the solution to the asymmetric Graetz problem in channel flow is presented. The asymmetric Graetz problem in channel flow is similar to the classical Graetz problem of heat or mass transfer to a fluid flowing in a round duct. In the classical problem, the tube wall undergoes a step change in concentration at a given axial position. In the asymmetric Graetz problem, the duct is flat and the concentration step occurs at only one channel wall. It is shown how this solution to the asymmetric Graetz problem may be used in a superposition integral to determine the wall flux in problems where the arbitrary channel-wall concentrations differ on the two walls.

6. Hydrodynamics and Mass Transfer in a Porous-wall Channel (Publication 6)

Philip Lessner and John Newman

The hydrodynamics and mass-transfer equations for a porous-wall flow channel have been solved over a large range of Re and Sc. Journé¹ has analyzed the low-Re, high-Sc case. For the high-Re, high-Sc case, we find that $\frac{\tau_{xy}h^2}{\mu XV_w} = 2.43 \text{ Re}^{0.5}$ and $\nu = 0.8277 \text{ Re}_{0.5} \text{ Sc}_{1/3}$ at the solid wall. The intermediate range is treated by numerical methods.

1. J. Journé, *J. Electrochem. Soc.* **129**, 1727 (1982).

7. Applications of Porous Electrodes to Metal-ion Removal and the Design of Battery Systems (Publication 7)

Gary George Trost

This report first treats the use of porous electrodes as electrochemical reactors for the removal of dilute metal ions. Then a methodology for the scale-up of porous electrodes used in battery applications is given.

The removal of 4 $\mu\text{g}/\text{cc}$ of Pb in 1M sulfuric acid feed streams was investigated in atmospheric and high-pressure flow-through porous reactors. The atmospheric reactor used a reticulated vitreous-carbon bed that had been coated with a mercury film. The best results show a 98% removal of lead from the feed. In the high-pressure experiments, pressures were varied up to 120 bar on electrode beds of copper- or lead-coated spheres. The copper spheres showed high hydrogen-evolution rates that inhibited lead deposition. The use of lead spheres inhibited hydrogen evolution but often resulted in the formation of lead sulfate layers.

Experimental data of one-dimensional porous battery electrodes are combined with a model for the current collector and cell connectors to predict specific energy and maximum specific power for complete battery systems. The discharge behavior of the plate, including electrochemical and grid resistances, is combined with the voltage and weight

penalties of the interconnecting bus and post, positive and negative active material, etc., to give specific results for the lithium-aluminum/iron sulfide battery. The battery can be optimized for maximum energy or power, or a compromise design may be selected.

8. The Transport Properties of Sodium Polysulfide Melts and a Theoretical Comparison of Flow-through and Flow-by Porous Electrodes at the Limiting Current (Publication 8)

Timothy Kent Risch

Two problems of electrochemical interest are addressed. First, the transport properties of sodium polysulfide melts are investigated using two models. A macroscopic model is first proposed which considers the melt to be composed of sodium cations and sulfide anions in a neutral sulfur solvent. The resulting values calculated from experimental data are shown to exhibit unpredictable behavior.

A more sophisticated model is then developed which considers sodium cations and seven different polysulfide anions as the melt components. Predictions of the melt-diffusion coefficient made from this model are shown to lie within the ranges of experimental data for diffusion coefficients in polysulfide melts.

In the second part, a limiting-current model for the potential and concentration distribution for a flow-by porous electrode is developed. For flow-by electrodes, the maximum solution-phase potential drop is shown to depend on one relevant parameter: the product of the electrode width and the reciprocal of the penetration depth. Criteria delineating the optimal electrode configuration are given using this potential difference as a basis for comparison. Design equations are also derived relating fixed and variable costs to electrode design and operating variables. The sum of fixed and variable costs is then optimized for the flow-through and flow-by configurations to give the conditions under which each configuration is preferred.

9. Electrochemical Reaction Engineering (Publication 9)

Gary G. Trost, Victoria Edwards, and John Newman

Although electrochemistry is involved to a significant extent in the present-day industrial economy, engineering design procedures for electrochemical systems have not been developed as thoroughly as for mass-transfer operations such as distillation. Nevertheless, the fundamental laws governing electrochemical systems are known. The purpose of this work is to review the design and analysis of certain electrochemical systems in relation to these fundamental laws.

10. Current Distribution and Cell Design (Publication 10)

John Newman

The motivation and direction for electrochemical engineering are reviewed briefly. The use of computers in the practical development of mathematical models is outlined and illustrated by examples in the design of molten-salt batteries. The use of the Schwarz-Christoffel transformation is detailed for obtaining the primary resistance of a cell for photoelectrochemical energy production.

11. Impedance Model for a Concentrated Solution. Application to the Electrodeposition of Copper in Chloride Solutions (Publication 11)[†]

Bernard Tribollet[‡] and John Newman

From the Stefan-Maxwell equations a model has been developed which describes the distribution of concentration of each species in the solution. This model provides for an arbitrary number of simul-

taneous homogeneous and heterogeneous reactions and is used to treat the steady state and the impedance of an electrochemical interface. As an example, this method is applied to the anodic dissolution of a rotating disk of copper in chloride solutions.

[†]This work was supported in part by the National Science Foundation through an Exchange Visitor Program with "Centre National de la Recherche Scientifique" No. G050252.

[‡]Present address: Groupe de Recherche No. 4 du CNRS, "Physique des Liquides et Electrochimie," Associé à l'Université Pierre et Marie Curie, 75230 Paris Cedex 05, France.

12. Fundamental Mathematical Principles for Electrochemical Engineering (Publication 13)

John Newman

Principles of current distribution are related to fundamental transport equations. These equations include both mass transfer and applications of potential theory, where the potential distribution satisfies Laplace's equation. It is important to include the potential as a variable, because the difference in potential between the electrode and the solution governs which electrochemical reactions will occur. Emphasis is also placed on the mathematical techniques used to treat the effects of convective-mass transfer and ohmic potential simultaneously.

13. Transport Properties in Concentrated Electrolytes (Publication 15)

John Newman

The analysis of mass-transport processes in battery systems requires accurate values of the transport properties of electrolytic solutions. A generally valid theory of mass transport is presented and described.

Mass-transport properties are defined by the theory chosen to describe the flux of mobile species. A consistent set of transport equations has been developed for dilute solutions of electrolytes. This theory breaks down, however, in concentrated solutions. In concentrated-solution theory, the migration and diffusion fluxes are defined with respect to an average velocity of the fluid, and the driving force for these fluxes is the electrochemical potential. Unlike dilute-solution theory, concentrated-solution theory correctly defines the number of transport

properties. The fundamental binary transfer coefficients defined by concentrated-solution theory may be calculated as functions of concentrations from independent measurements of diffusion coefficients, transference numbers, and conductivity.

The measurement of fringe displacements of diffusing solutions in an optical concentration cell is a method of determining diffusion coefficients. This method is described, and results for nitric acid solutions are given.

14. Work in Progress

An alternating-current impedance method is being used to study the anodic electrodisolution of a rotating zinc disk in an acidic chloride medium. Initially, the corrosion process must be characterized by establishing the dc-polarization behavior. A model has been developed to analyze experimentally obtained kinetic data. The model also determines the corrosion potential and current for a wide range of electrolyte compositions. Finally, the ac behavior must be studied. An ac-impedance experimental procedure, applicable over a wide frequency domain, is currently being developed. Information about the capacitive double layer, along with the faradaic electrode reaction, will be obtained and analyzed.

Sodium-sulfur batteries appear to be attractive for both vehicle propulsion and utility load-leveling applications. Since the performance of sodium-sulfur cells is strongly influenced by the diffusion of anions and cations through the sodium polysulfide melt, the optimal design of sulfur electrodes will depend on the availability and accuracy of diffusion-coefficient data for polysulfide melts. The method of restricted diffusion will be used to measure the diffusion coefficient of sodium ions in sodium polysulfide melts.

Channel flow between two parallel planar electrodes is used in many industrial electrochemical processes, such as metal refining, energy storage, and electro-organic synthesis. A mathematical model, useful in the design of such systems, is being developed to calculate the concentration, potential, and current distribution in a thin-gap flow cell. An experimental apparatus has been built to verify the completeness of the model.

The LiAl/FeS and the Li(Si)/FeS₂ batteries appear to be attractive for load-leveling and electric-vehicle applications. A general energy-balance equation has been developed that is useful for estimating the cell thermal characteristics required for the design and thermal management of these and other

batteries. Work is currently in progress to develop a complete model of the thermal and discharge behavior of the Li(Si)/FeS₂ battery.

1983 PUBLICATIONS AND REPORTS

Refereed Journals

1. Philip P. Russell and John Newman, "Experimental Determination of the Passive-active Transition for Iron in 1M Sulfuric Acid," *J. Electrochem. Soc.* **130**, 547 (1983).[†]
2. Bernard Tribollet and John Newman, "Analytic Expression of the Warburg Impedance for a Rotating Disk Electrode," *J. Electrochem. Soc.* **130**, 822 (1983).[‡]
3. Bernard Tribollet and John Newman, "The Modulated Flow at a Rotating Disk Electrode," *J. Electrochem. Soc.* **130**, 2016 (1983).[‡]
4. John Newman, "Current Distribution on a Rotating Disk below the Limiting Current," *Current Contents, Citation Classics Section*, **14**, 24 (November 21, 1983).

LBL Reports

5. Victoria Edwards and John Newman, "The Asymmetric Graetz Problem in Channel Flow," submitted to *Int. J. Heat and Mass Transfer*, LBL-16455.
6. Philip Lessner and John Newman, "Hydrodynamics and Mass Transfer in a Porous-wall Channel," submitted to *J. Electrochem. Soc.*, LBL-16568.
7. Gary George Trost (Ph.D. Thesis), "Applications of Porous Electrodes to Metal-ion Removal and the Design of Battery Systems," LBL-16852.
8. Timothy K. Risch (M.S. Thesis), "The Transport Properties of Sodium Polysulfide Melts and a Theoretical Comparison of Flow-through and Flow-by Porous Electrodes at the Limiting Current," LBL-17160.
9. Gary G. Trost, Victoria Edwards, and John Newman, "Electrochemical Reaction Engineering," in *Chemical Reaction and Reactor*

Engineering, A. Varma and J. Carberry, eds., in press, LBL-15984.

Invited Talks

10. John Newman, "Current Distribution and Cell Design," invited plenary lecture at the Erlangen, Germany, meeting of the International Society of Electrochemistry, September 22, 1983, Ext. Abstr. (P)IV.4.
11. Bernard Tribollet and John Newman, "Impedance Model for a Concentrated Solution. Application to the Electrodeposition of Copper in Chloride Solutions," Washington, D.C. meeting of the Electrochemical Society, October 9-14, 1983, Ext. Abstr. 194.[‡]
12. Philip P. Russell and John Newman, "Electrochemical Oscillations in the Iron-Sulfuric Acid System," The National Association of Corrosion Engineers Corrosion Research Symposium, Anaheim, California, April 18, 1983.[§]
13. John Newman, "Fundamental Mathematical Principles for Electrochemical Engineering," invited review for the Symposium on Inorganic Electrosynthesis and Electrochemical Engineering Principles, Denver meeting of the American Institute of Chemical Engineers, August 29, 1983, submitted to *AICHE Symp. Volume*, LBL-16785.
14. John Newman, onsite review for the Department of Energy of the bench and vehicle test of sodium-sulfur batteries by the Ford Motor Company, Newport Beach, California, July 18 and 19, 1983.
15. John Newman, "Transport Properties in Concentrated Electrolytes," Electric Power Research Institute, Palo Alto, California, November 30, 1983.
16. John Newman, "Current Distribution and Cell Design," lecture for Faculty of Technology, Split, Yugoslavia, September 28, 1983.

[†]This work was supported in part by the Solar Energy Research Institute.

[‡]This work was supported in part by the National Science Foundation through an exchange visitor program with "Centre National de la Recherche Scientifique" No. G050252.

[§]This work was supported in part by the National Science Foundation, Grant No. CPE 82-19827.

Magnetic
Fusion Energy



Structural Materials and Weldments for High-Field Superconducting Magnets*

J.W. Morris, Jr., Investigator

INTRODUCTION

The purpose of this work is the design and laboratory development of improved high-field superconducting magnets. The research is motivated by the need for new alloys having suitable strength and toughness in welded structures in high magnetic fields at 4.2 K to satisfy the structural materials needs for future generations of high-field superconducting magnets. The project has three tasks. The first of these concerns the development of new ultrahigh-strength ferritic alloys and weldments for magnet structural applications. The second concerns the development and testing of new austenitic Fe-Mn alloys that offer high strength and toughness at cryogenic temperatures. The third includes testing and analysis of the mechanical properties of current and potential structural alloys in high magnetic fields.

1. Effects of Magnetic Fields on Martensitic Transformations and Mechanical Properties in Stainless Steel at Low Temperatures (Publication 6)

B. Fultz, G.M. Chang, and J.W. Morris, Jr.

Many important cryogenic structural steels are, or include, a metastable austenite phase that may undergo low-temperature transformation to martensite. This paper briefly reviews the combined effects of magnetic fields and mechanical loading on the transformation, reports initial experiments in a pulsed magnetic field, and describes a new testing facility that has been established to determine mechanical properties at 4 K in fields up to 8 T.

2. The Effects of High Magnetic Fields on the Microstructure and Toughness of Cryogenic 9Ni Steel (Publication 5)

G.O. Fior, B. Fultz, and J.W. Morris, Jr.

Commercial 9Ni steel was heat-treated to produce thermally unstable retained austenite. The transformation of this austenite to martensite at low temperatures was shown to be enhanced in the presence of 17-T magnetic fields. The amount of this transformation was much larger than expected from thermodynamic arguments that have been used to explain the systematics of magnetically induced transformations in Soviet austenitic steels. Although the full explanation of the amount of magnetically induced transformation is yet unclear, this transformation induces changes in Charpy toughness that are consistent with those changes caused by the thermal transformation of austenite alone. The observed reductions in Charpy toughness correlated with an increased amount of quasi-cleavage fracture. The temperature independence of this mechanical effect suggested that the mechanism of quasi-cleavage fracture induced by the transformation of the austenite is temperature independent.

3. The Fatigue-crack Growth Behavior in a Nitrogen-strengthened High-manganese Steel at Cryogenic Temperatures (Publication 1)

R. Ogawa and J.W. Morris, Jr.

The fatigue-crack growth rate (FCGR) of a nitrogen-strengthened high-manganese stainless steel of nominal composition 18Mn/5Ni/16Cr/0.02C/0.22N was determined in the intermediate stress-intensity-factor range (20–70 MPa \sqrt{m}) at 77 K and 4 K. Fractographic investigations were performed on the fracture surfaces. The FCGR at 4 K is very nearly the same as that at 77 K and substantially below the crack-growth rate for AISI 304LN steel. The fracture surfaces of both the high-manganese

*This work was supported by the Director, Office of Energy Research, Office of Fusion Energy, Development and Technology Division of the U.S. Department of Energy under Contract No. DE-AC03-76SF00098.

alloys and the 304LN showed a transgranular failure mode, but the detailed fractographic features varied with temperature and alloy type. The fractography was closely related to changes in the FCGR.

4. Weldability of 2BT-treated 9Ni Steel with Ferritic Filler Metal (Publication 2)

H.J. Kim and J.W. Morris, Jr.

Fracture-toughness tests show that the weldment of 9Ni steel has very high toughness values (300 MPa \sqrt{m}) at 77 K but becomes brittle at 4.2 K. Values of 110, 90, and 145 MPa \sqrt{m} were obtained for the base metal, HAZ, and weld metal, respectively. It has also been determined that the microstructural source of HAZ toughness differs from that of the base metal.

5. Magneto-mechanical Effects in 304L Stainless Steel (Publication 3)

B. Fultz and J.W. Morris, Jr.

Austenitic AISI 304 stainless steels are metastable with respect to the martensite transformation at low temperatures. Previous measurements of cryogenic mechanical properties of 304 stainless steels are discussed with respect to their dependence on microstructural changes induced by the martensite transformation. The martensite transformation is enhanced in the presence of a high magnetic field. New experimental measurements of cryogenic mechanical properties in steady 8-T magnetic fields are described. Effects of magnetic fields on ultimate tensile strengths (and possibly other magneto-mechanical effects in fatigue and toughness) are reported. These results correlate to microstructural changes induced by the martensite transformation. Evidence for existence of a synergetic interaction between plastic deformation and the magnetic field is presented.

6. The Influence of Processing on the Cryogenic Mechanical Properties of High-strength High-manganese Stainless Steel (Publication 4)

R. Ogawa and J.W. Morris, Jr.

A very promising combination of yield strength, fracture toughness, and fatigue resistance at 4 K can

be obtained with modified AISI 205 high-manganese austenitic stainless steel with a nominal composition 18Mn/5Ni/16Cr/0.02C/0.22N. In order to clarify the microstructural sources of toughness and fatigue resistance in this alloy, the influence of processing (hot-rolling conditions and solution-treatment conditions) was investigated. The yield strength at 4 K increased from 1145 MPa to 1290 MPa on decreasing the hot-rolling temperatures (1250–1150°C), while the toughness [$K_{IC}(J)$] at 4 K decreased from 250 MPa to 167 MPa. The strength-toughness combinations were superior to those of 304LN over the whole range tested. The influence of cold rolling (30%) and annealing on the strength and toughness is discussed.

7. Work in Progress

Research in progress in 1984 includes the development of high-strength, high-toughness cryogenic steels from both the ferritic (Fe-Ni) and austenitic (Fe-Mn) steel classes, the welding of these steels, and the investigation of the performance of these steels under the combined influence of low temperature and high magnetic fields.

1983 PUBLICATIONS AND REPORTS

LBL Reports

1. R. Ogawa and J.W. Morris, Jr., "The Fatigue Crack Growth Behavior in a Nitrogen Strengthened High Manganese Steel at Cryogenic Temperatures," Amer. Soc. for Testing Materials, in press, LBL-16024.
2. H. Jin Kim and J.W. Morris, Jr., "Weldability of 2BT-treated 9Ni Steel with Ferritic Filler Metal," LBL-16531.
3. B. Fultz and J.W. Morris, Jr., "Magneto-mechanical Effects in 304L Stainless Steel," in *Advances in Cryogenic Engineering*, in press, LBL-16536.
4. R. Ogawa and J.W. Morris, Jr., "The Influence of Processing on the Cryogenic Mechanical Properties of High Strength High Manganese Stainless Steel," in *Advances in Cryogenic Engineering*, in press, LBL-16528.
5. G.O. Fior, B. Fultz, and J.W. Morris, Jr., "Effects of High Magnetic Fields on the Microstructure and Toughness of Cryogenic 9Ni Steel," in *Ferritic Materials for Nuclear Energy Applications*, J. Davis, Ed., TMS-AIME, Metals Park, Ohio, in press, LBL-16972

Other Publications

6. B. Fultz and J.W. Morris, Jr., "Effects of Magnetic Fields on Martensitic Transformations and Mechanical Properties of Stainless Steels at

Low Temperatures," in *Austenitic Steels at Low Temperature*, R.T. Reed and T. Horiuchi, eds., Plenum Pub. Corp., New York, 1983, LBL-15324.

Health and
Environmental Sciences



Semiconductor Materials and Devices*

Eugene E. Haller, Investigator

INTRODUCTION

The recently achieved ultrahigh purity and crystalline perfection of large germanium single crystals and, to a lesser degree, silicon single crystals have led to the discovery of a large number of novel impurity and defect complexes which exhibit energy levels in the band gap of these semiconductors. Understanding the composition and electronic structure of these novel acceptors and donors through the use of a sensitive far-infrared spectroscopy technique and novel radioactive tracer schemes represents one component of this research effort. Another closely coupled component focuses on the formation of these centers during crystal growth.

Two factors have helped greatly in identifying the composition of these novel acceptors and donors: (1) correlations between concentration and electronic-structure effects of a given center, and (2) control of the materials involved in the crystal growth and purification, such as the crucible material (typically synthetic silica or graphite) and the ambient (typically H_2 , N_2 , or vacuum). One of the major findings is that atomic hydrogen plays an important role in the formation and composition of many of the new impurity complexes. The information gained through this research is of immediate use to LBL's semiconductor radiation-detector program, which originated this research.

The use of ultrapure crystals as starting material for specially doped crystals is studied in connection with the development of sensitive far-infrared photoconductors for low-photon-flux applications in outer space and neutron-transmutation-doped germanium bolometers. The high ratio of intentional-dopant concentrations and residual-impurity concentrations has led to photoconductors with very high responsivity working at close to the photon noise limit.

The close coupling between crystal synthesis and analysis has enabled us to effectively study and use these extremely pure and structurally perfect materials.

*This work was supported in part by the Director's Office of Energy Research, Office of Health and Environmental Research, U.S. Department of Energy, under Contract No. DE-AC03-76SF00098, and in part by NASA Contract No. W-14,606, under interagency agreement with the Department of Energy.

1. Two Novel Acceptors in Ultrapure Germanium: Nature and Interconversion (Publication 1)

E.E. Haller and R.E. McMurray, Jr.

Experimental data from photothermal-ionization spectroscopy (see Figure 1-1) are presented for two shallow acceptors A_4 and $A_{3,5}$ in pure germanium. The two acceptors appear, in concentrations up to $\sim 10^{11}/\text{cm}^3$, exclusively in ultrapure germanium single crystals which have been grown in a pure N_2 ambient from a melt contained in a graphite crucible. The bound excited-state spectra of both acceptors are hydrogenic. The ground state of A_4 is a Γ_8 quadruplet, while the $A_{3,5}$ acceptor exhibits a ground-state manifold consisting of at least two Kramers doublets, one with Γ_6 symmetry and the other with Γ_7 symmetry. The energy splitting between the two doublets is 1.1 meV, and the splitting is symmetric in relation to the position of the A_4 ground state. Complete and reversible interconversion can be induced with appropriate thermal annealing (see Figure 1-2). The experimental results suggest that A_4 and $A_{3,5}$ are two forms of one center. Above 700 K the A_4 concentration decreases irreversibly following an exponential decay. Interconversion can be observed at any point during the irreversible annealing of the center.

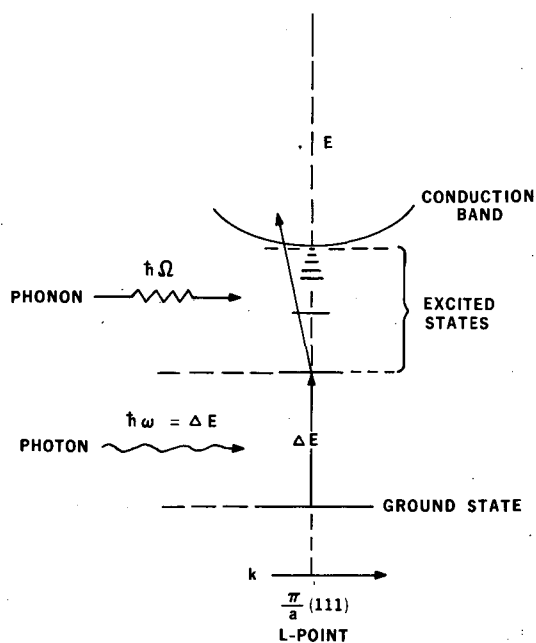


Figure 1-1. Illustration of the two-step process leading to photothermal ionization spectroscopy (PTIS), also called photoelectric spectroscopy. (XBL 7411-8629)

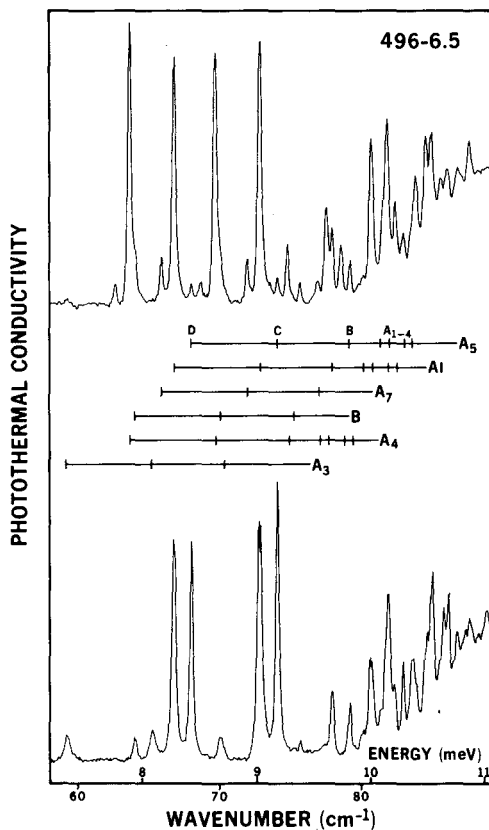


Figure 1-2. Spectra obtained with a Ge sample annealed at room temperature (lower spectrum) and heated to 673 K (upper spectrum). (XBL 828-11319)

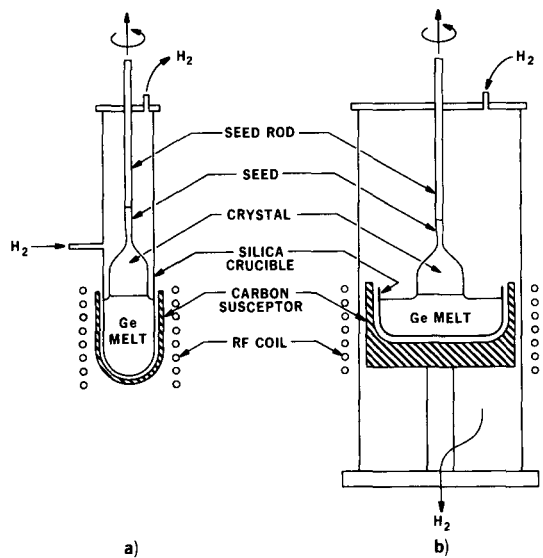


Figure 2-1. Simplified illustrations of crystal-growth designs currently used for high-purity germanium. Design (a) uses an external carbon susceptor and a crucible which closely matches the crystal diameter. The shape of the melt/solid interface is probably dominated by heat radiation from the crystal. Design (b) uses an internal susceptor and a large melt diameter. The shape of the melt/solid interface for this design is probably dominated by heat transport by hydrogen gas convection. (XBL 8210-3055)

2. High-purity Germanium-crystal Growing (Publication 28)

W.L. Hansen and E.E. Haller

The germanium crystals used for the fabrication of nuclear-radiation detectors are required to have a purity and crystalline perfection which is unsurpassed by any other solid material. These crystals should have a net electrically active impurity concentration not greater than $10^{10}/\text{cm}^3$ and should be essentially free of charge-trapping defects.

Such perfect crystals of germanium can be grown only because of the highly favorable chemical and physical properties of this element. (See Figure 2-1 for two crystal-growth designs.) However, ten years of laboratory-scale and commercial experience still have not made the production of such crystals routine. The origin and control of many impurities (see Figure 2-2) and electrically active defect complexes are now fairly well understood, but regular production is often interrupted for long periods for one of

two reasons: (1) the difficulty of achieving the required high purity, or (2) charge trapping in detectors made from crystals seemingly grown under the required conditions.

The compromises involved in the selection of zone-refining and crystal-growth parts and ambients

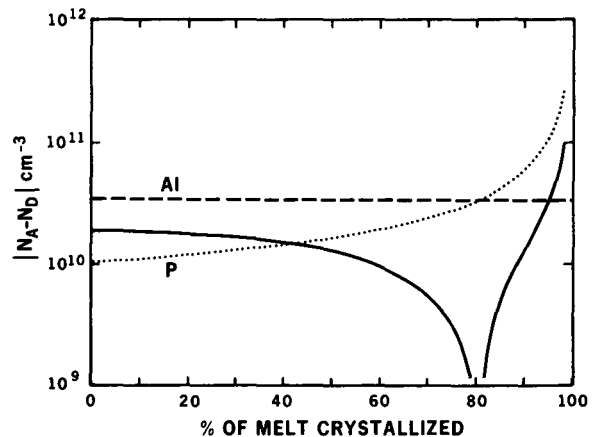


Figure 2-2. The solid line shows a common type of impurity profile for high-purity germanium. This profile results from equal concentrations of Al and P in the melt of $3 \times 10^{10}/\text{cm}^3$. The Al is nonsegregating, and the P has an effective segregation coefficient of 0.3 at our growth rate. (XBL 8210-3056)

are discussed, and the difficulty in controlling the purity of key elements in the process is emphasized. The consequences of growing in a hydrogen ambient are discussed in detail, and it is shown how complexes of neutral defects produce electrically active centers.

3. Performance and Materials Aspects of Ge:Be Photoconductors (Publication 10)

N.M. Haegel, E.E. Haller, and P.N. Luke

Ge:Be photoconductors have been developed for low-photon-background applications in the 30–50 μm wavelength region (see Figure 3-1). These detectors provide higher responsivity and lower noise equivalent power (NEP) than the Ge:Ga detectors currently operating in this wavelength range. Beryllium-doped single crystals were grown by the Czochralski method from a carbon susceptor under a vacuum of $\sim 10^{-6}$ torr. We report an optimum detective quantum efficiency of 46% at a background flux of 1.5×10^8 photons/sec (7×10^{-13} W). Ge:Be-detector performance is strongly influenced by the absolute concentrations and the concentration

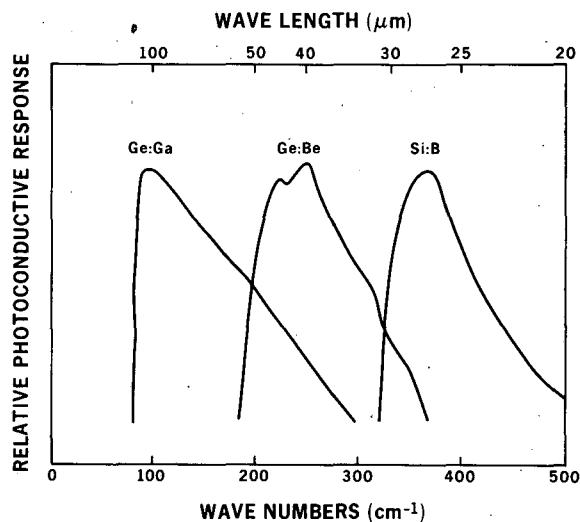


Figure 3-1. Schematic photoconductor power response as a function of photon energy. Ge:Be has a peak response at $\approx 40 \mu\text{m}$. (XBL 832-8251)

ratio of residual shallow donors and shallow acceptors.

4. Neutron-transmutation-doped Germanium Bolometers (Publication 11)

N.P. Palaio, M. Rodder, E.E. Haller, and E. Kreysa†

Six slices of ultrapure germanium were irradiated with thermal-neutron fluences between 7.5×10^{16} and $1.88 \times 10^{18} \text{ cm}^{-2}$. After thermal annealing the resistivity was measured down to low temperatures ($< 4.2 \text{ K}$) and found to follow the relationship $\rho = \rho_0 \exp(\Delta/T)$ in the hopping-conduction regime (see Figure 4-1). Also, several junction field-effect transistors (FETs) were tested for noise performance at room temperature and in an insulating housing in a 4.2-K cryostat. These FETs will be used as first-stage amplifiers for neutron-transmutation-doped germanium bolometers.

†Permanent address: Max-Planck-Institut for Radioastronomy, Bonn, West Germany.

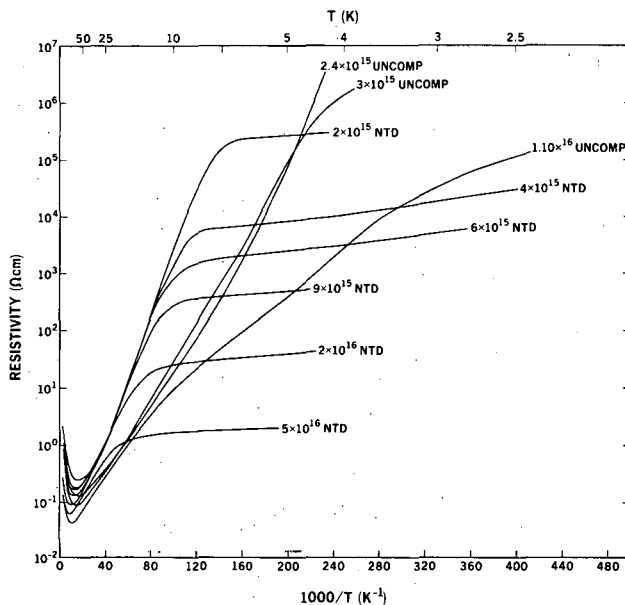


Figure 4-1. Resistivity as a function of $1000/T$ for NTD and uncompensated Ge samples. The numbers preceding NTD and UNCOMP are the gallium-acceptor concentrations in cm^{-3} . (XBL 823-8357)

5. Bulk-acceptor Compensation Produced in p-type Silicon at Near-ambient Temperatures by an H₂O Plasma (Publication 19)

W.L. Hansen, S.J. Pearton, and E.E. Haller

We report the neutralization of the shallow acceptors boron and gallium in p-type silicon to a depth $> 1 \mu\text{m}$ after exposure to an H₂O plasma for 3 hours at temperatures as low as 80°C. The fact that uncompensated n-type silicon is unaffected by the plasma treatment means that donor formation is excluded. Exposure to either O₂ or H₂ plasmas does not lead to acceptor removal. However, sequential treatment in an O₂ plasma followed by an H₂ plasma produces the same effect as treatment in the H₂O plasma, while the inverse sequence has no effect. Our observations can be explained with a model considering rapidly diffusing atomic oxygen and hydrogen which recombine on acceptor sites, forming neutral A⁻OH⁺ complexes. The model shows that acceptor-compensation kinetics is dominated by the diffusion of atomic hydrogen.

1983 PUBLICATIONS AND REPORTS

Refereed Journals

1. E.E. Haller and R.E. McMurray, Jr., "Two Novel Acceptors in Ultrapure Germanium: Nature and Interconversion," Proc. 12th Intl. Conf. on Defects in Semiconductors, 1982, Amsterdam, Physica **116B+C**, 349 (1983); LBL-14227.
2. P.N. Luke, H.M. Steiner, and E.E. Haller, "Direct Detection of VUV Scintillations in Liquid Helium Using Germanium Photodiodes," Appl. Phys. Lett. **41**, 315 (1982); LBL-14356.
3. A.E. Lange, E. Kreysa, S.E. McBride, P.L. Richards, and E.E. Haller, "Improved Fabrication Techniques for Infrared Bolometers," Intl. J. Infrared and Millimeter Waves **4** (5), 689 (1983); LBL-13832.
4. E.J. Pakulis, E.E. Haller, and C.D. Jeffries, "EPR of the Lithium Ion-dangling Bond Complex in Germanium Containing Dislocations," Solid State Comm. **44**, 1209-1211 (1982); LBL-14836.
5. K.P. Doering, N. Haas, E.E. Haller, D. Herlach, W. Jacobs, M. Krauth, H. Orth, J. Rosenkranz, A. Seeger, J. Vetter, K.P. Arnold, T. Aurenz, and H. Bossy, "Muonium in Ultrapure Germanium," Proc. 12th Intl. Conf. on Defects in Semiconductors, 1982, Amsterdam, Physica **116B+C**, 354-360 (1983).
6. P.N. Luke, E.E. Haller, and H.M. Steiner, "Liquid Helium Scintillation Detection with Germanium Photodiodes," IEEE Trans. Nucl. Sci. **NS-30** (1), 429 (1983); LBL-14459.
7. E.E. Haller, R.E. McMurray Jr., L.M. Falicov, N.M. Haegel, and W.L. Hansen, "Three Holes Bound to a Double Acceptor: Be⁺ in Germanium," Phys. Rev. Lett. **31**, 1089 (1983); LBL-15988.
8. G.A. Held, E.E. Haller, and C.D. Jeffries, "Observation of Luminescence from Bound Multiexciton Complexes in Gallium-doped Germanium," Solid State Comm. **47** (6), 459-462 (1983); LBL-15557.
9. J.W. Cross, L.T. Ho, A.K. Ramdas, R. Sauer, and E.E. Haller, "Excitation Spectra of Group II Acceptors in Ge: Ge(Be⁺), Ge(Be⁻), and Ge(Mg⁺)," Phys. Rev. B **28** (12), 6953 (1983).
10. N.M. Haegel, E.E. Haller, and P.N. Luke, "Performance and Materials Aspects of Ge:Be Photoconductors," Int. J. Infrared and Millimeter Waves **4** (6), 945 (1983); LBL-15409.
11. N.P. Palaio, M. Rodder, and E.E. Haller, "Neutron-transmutation-doped Germanium Bolometers," Int. J. Infrared and Millimeter Waves **4** (6), 933 (1983); LBL-15410.
12. S.J. Pearton, J.M. Kahn, and E.E. Haller, "Deep Level Effects in Silicon and Germanium after Plasma Hydrogenation," J. Electronic Materials **12** (6), 1003 (1983); LBL-15920.
13. S.W. Teitsworth, R.M. Westervelt, and E.E. Haller, "Non-linear Oscillations and Chaos in Electrical Breakdown in Ge," Phys. Rev. Lett. **51**, 825 (1983).

LBL Reports

14. J.M. Jaklevic, K-M Yu, M.D. Strathman, and E.E. Haller, "Application of Heavy-ion Backscattering Spectrometry to the Analysis of Semiconductor Materials," submitted to Thin Solid Films, LBL-16191.
15. S.J. Pearton, A.J. Tavendale, J.M. Kahn, and E.E. Haller, "The Nature of the Dominant γ -induced Defects in High-purity Germanium," submitted to Radiation Effects, LBL-15921.
16. S.J. Pearton, J.M. Kahn, W.L. Hansen, and E.E. Haller, "Deuterium in Germanium: Interaction with Point Defects," submitted to J. Appl. Phys., LBL-15944.

17. S.J. Pearton, E.E. Haller, and J.M. Kahn, "Quenched-in Deep Acceptors in Germanium," submitted to *J. Phys. C*, LBL-16198.
18. S.J. Pearton, A.J. Tavendale, J.M. Kahn, and E.E. Haller, "Deep Level Impurities in Germanium and Silicon: Low Temperature Passivation or Removal Techniques," *IEEE Trans. Nucl. Sci. NS-31* (1), (1984), in print; LBL-15943.
19. W.L. Hansen, S.J. Pearton, and E.E. Haller, "Bulk Acceptor Compensation Produced in P-type Silicon at Near Ambient Temperatures by an H₂O Plasma," submitted to *Appl. Phys. Lett.*, LBL-16688.
20. S.J. Pearton, E.E. Haller, and A.G. Elliot, "Hydrogenation of Electron Traps in Bulk GaAs and GaP," *Electron. Lett.*, in print; LBL-16916.
21. W.L. Hansen, S.J. Pearton, and E.E. Haller, "Low-temperature Oxygen Diffusion in Silicon," submitted to *Appl. Phys. Lett.*, LBL-16961.
22. S.J. Pearton, E.E. Haller, and A.G. Elliot, "Nitridization of GaAs Surfaces: Effects on Diode Leakage Currents," submitted to *Appl. Phys. Lett.*, LBL-16915.
23. N.M. Haegel (M.S. Thesis), with E.E. Haller, "Performance and Materials Aspects of Ge:Be and Ge:Ga Photoconductors for Far Infrared Detection," LBL-16694.
24. N.P. Palaio (M.S. Thesis), with E.E. Haller, "Development of Neutron Transmutation-doped Germanium Bolometer Material," LBL-16695.
28. W.L. Hansen and E.E. Haller, "High-purity Germanium Crystal Growing," *Proc. Materials Research Soc. 1982 Annual Meeting, Symposium F*, **16**, Elsevier Science Publishing Co., Inc., New York, 1983, pp. 1-16; LBL-14916.
29. N. Haegel and E.E. Haller, "Ge:Be Photoconductors: Single Crystal Growth and Device Development," *Proc. 7th Intl. Conf. on Infrared and Millimeter Waves, Feb. 14-18, 1983*, Marseilles, France.
30. N. Palaio and E.E. Haller, "Neutron-transmutation-doped Germanium Bolometers," *Proc. 7th Intl. Conf. on Infrared and Millimeter Waves, Feb. 14-18, 1983*, Marseilles, France.
31. H.R. Hueschen, E.E. Haller, and P.L. Richards, "Ge:Ga Photoconductors: Development and Ideal Performance," *Proc. 7th Intl. Conf. on Infrared and Millimeter Waves, Feb. 14-18, 1983*, Marseilles, France.
32. E.E. Haller, N.M. Haegel, R.E. McMurray Jr., and L.M. Falicov, "A⁺ Centers in Beryllium-doped Germanium Single Crystals," *Bull. Am. Phys. Soc. Series II* **28** (3), 411 (1983); LBL-15371.
33. R.E. McMurray Jr. and E.E. Haller, "Interconversion of Two Acceptor Complexes in Ultra-pure Germanium: A_{3,5} → A₄," *Bull. Am. Phys. Soc. Series II* **28** (3), 411 (1983); LBL-15370.
34. N.M. Haegel and E.E. Haller, "Performance and Materials Aspects of Ge:Be Photoconductors," *Bull. Am. Phys. Soc. Series II* **28** (3), 360 (1983); LBL-15365.
35. G.A. Held, E.E. Haller, and C.D. Jeffries, "Observation of Luminescence from Bound Multi-exciton Complexes in Ge:Ga," *Bull. Am. Phys. Soc. Series II* **28** (3), 542 (1983); LBL-15644.
36. J.W. Cross, L.T. Ho, A.K. Ramdas, R. Sauer, and E.E. Haller, "Excitation Spectra of Group II Impurities in Ge: Ge(Mg⁰), Ge(Be⁰) and Ge(Be⁻)," *Bull. Am. Phys. Soc. Series II* **28** (3), 339 (1983).
37. R.M. Westervelt, S.W. Teitsworth, and E.E. Haller, "Non-linear Oscillations and Chaos in Electrical Conduction in Ge," *Bull. Am. Phys. Soc. Series II* **28** (3), 383 (1983).
38. M.R. Hueschen, E.E. Haller, and P.L. Richards, "Ideal Performance of Gallium-doped Germanium Far Infrared Photoconductors," *Bull. Am. Phys. Soc. Series II* **28** (3), 359 (1983).
39. C.W. Clawson, S.S. Rosenblum, K.M. Crowe, E.E. Haller, and J.H. Brewer, "Effects of Electronically Neutral Impurities on Muonium in

Other Publications

25. E.E. Haller, N.P. Palaio, M. Rodder, W.L. Hansen, and E. Kreysa, "NTD Germanium: A Novel Material for Low Temperature Bolometers," *Proc. Fourth Int. Neutron Transmutation Doping Conf. on Semiconductors*, National Bureau of Standards, June 1-3, 1982, Gaithersburg, Maryland; LBL-14649.
26. E. Kreysa and E.E. Haller, "He³ Bolometers for mm and Sub-mm Photometry," *Proc. Second ESO Infrared Workshop, April 20-23, 1982, Garching, West Germany*; A.F.M. Moorwood and K. Kjaer, eds., 1982, pp. 197-204.
27. J.T. Walton, and E.E. Haller, "Silicon Radiation Detectors — Materials and Applications," *Proc. Materials Research Soc. 1982 Annual Meeting, Symposium F*, **16**, Elsevier Science Publishing Co., Inc., New York, 1983, pp. 141-173; LBL-14909.

- Silicon and Germanium," *Proc. Yamada Conference on Muon Spin Rotation, April 18-22, 1983, Shimoda, Japan*; LBL-16944.
40. K.P. Doring, K.P. Arnold, M. Gladisch, N. Haas, E.E. Haller, D. Herlach, W. Jacobs, M. Krause, M. Krauth, H. Orth, and A. Seeger, "Muonium in Ultra-pure and Si-doped Germanium," *Proc. Yamada Conference on Muon Spin Rotation, April 18-22, 1983, Shimoda, Japan*.

Invited Talks

41. E.E. Haller, "The National Center for Advanced Materials," Department of Electrical Engineering and Computer Science Seminar, University of California Berkeley, April 6, 1983.
42. E.E. Haller, "IR Spectroscopy in Ultra-pure Semiconductors," Physics Department, University of California Berkeley, May 12, 1983.
43. E.E. Haller and R.E. McMurray Jr., "Novel Centers in Pure Semiconductors," Solid State Seminar, Physics Department, University of California Berkeley, November 9, 1983.

Work for
Others

NATIONAL AERONAUTICS AND SPACE ADMINISTRATION

Theoretical Studies of Formyl Radical Formation in Selected Combustion Processes*

William A. Lester, Jr., Investigator

INTRODUCTION

It is generally recognized that a better understanding of the mechanisms governing pyrolysis and oxidation is necessary to understand the chemistry of combustion. Although simplified mechanisms can often be devised to describe systems over narrow ranges of experimental conditions, their predictions over extended ranges are frequently deficient. State-to-state and molecular-beam experiments provide one source of valuable mechanistic information. In recent years, theoretical studies have also begun to play an increasingly important role in obtaining a detailed understanding of chemical reactions.

Recent advances in computational techniques of quantum chemistry have rendered quantum-mechanical methods a powerful tool for the study of chemical reactions. Indeed, it is now possible to provide quantitatively accurate descriptions of molecules involving several first-row atoms. Among these advances, two are especially noteworthy. They are the ability to describe accurately (1) electron-correlation effects in molecules and therefore bond formation and bond breaking and (2) potential energy hypersurfaces from computations of the first and second derivatives of the energy with respect to nuclear coordinates.

Such capability has been introduced by us into the computer code HONDO, and successfully used in the study of molecular structures and chemical reactions which play an important role in combustion processes.

In this research effort the same approach is applied to important problems of combustion chem-

istry, now with particular emphasis on emission processes in flames. One intermediate species that can contribute to flame spectra is the formyl (HCO) radical, because it has a low-lying electronically excited state ($A^2\Pi$) that is ~ 27 kcal/mol above the ground (X^2A') state. A research effort was undertaken to theoretically study the reactions that generate HCO radicals.

1. Work in Progress

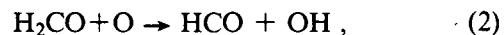
Ab initio Hartree-Fock (HF), multiconfiguration Hartree-Fock (MCHF), and configuration-interaction (CI) calculations have been carried out for the reaction



The reaction coordinate leading to the formation of the ground-state formyl radical $\text{HCO}(X^3A')$ has been fully characterized by determining the structures and energies of reactants, transition state, and products. In the transition state the attaching O atom is nearly collinear with the attacked CH bond.

No transition state could be found with the spin-restricted HF method. While a transition state can be determined with the MCHF method, the MCHF relative energies are in poor agreement with thermochemical data. Energies calculated from extended CI are in semiquantitative agreement with experiment.

The hydrogen-abstraction channel for $\text{O}(^3P) + \text{H}_2\text{CO}$, i.e.,



has also been studied. The same qualitative conclusions hold regarding the adequacy of HF, MCHF, and CI wavefunctions.

Characterization of the electronically excited surface of (1) to form $\text{HCO}(A^2\Pi)$ was attempted but not achieved. The difficulty is associated with this state's being the second one of doublet spin. The computed wavefunction was found to collapse to the ground state.

*This work was supported by the National Aeronautics and Space Administration under Contract No. A 86130B Amd 1.

OFFICE OF NAVAL RESEARCH

Structure and Performance of Al_2O_3 Scales Formed on Aluminides Containing Noble Metal*

Donald Boone and Alan Levy, Investigators

Platinum-modified Alumina Coatings (Publication 1)

Lori Purvis, Donald Boone, and R. Streiff

An investigation was conducted to determine the function of Pt and other noble metals in influencing the formation, adherence, and protectivity of Al_2O_3 -forming coating systems. The effects of Pt level, prealuminizing diffusion treatments, and aluminizing temperature and activity have been determined in establishing a series of archetype structures. Samples with these structures were prepared for hot corrosion testing. Additional samples were analyzed to determine the initial stages of oxide formation, the phases present, and the relationship between the structural features of the oxide and their test behavior.

It was determined that the structures of the so-called "platinum aluminide" coatings vary over a wide range, from single-phase PtAl_2 , through two-phase PtAl_2 and Ni(Pt)Al , to a single-phase NiAl with platinum in solution rather than consisting of a single structural type. An investigation of the

amount of platinum deposited, prealuminizing diffusion treatments, and aluminizing temperature and activity has established the necessary parameters to reproduce the archetypes.

1983 PUBLICATIONS AND REPORTS

Other Publications

1. R. Streiff, L. Purvis, and D. Boone, "Structures of Platinum Modified Aluminide Coatings," Proc. NATO Les Arc's, Paris, June-July 1983.
2. R. Streiff and L. Purvis, "Les Revêtements d'Aluminiures Modifiés par le Platine: Un Nouveau Type de Revêtements Protecteurs Contre la Corrosion," Proc. Société Française de Metallurgie, Paris, France, October 1983.

Invited Talks

3. D. Boone, L. Purvis, and R. Streiff, "The Formation and Structure of Platinum Modified Aluminide Coatings," International Conference of Metallurgical Coatings, San Diego, California, April 1983.
4. D. Boone, D.E. Peacock, and B.R. Rose, "Hot Corrosion Resistance of Modified Aluminide Coatings," International Conference of Metallurgical Coatings, San Diego, California, April 1983.

*This work was supported by the Assistant Secretary for Fossil Energy, Office of Coal Research, Heat Engines and Heat Recovery Division of the U.S. Department of Energy under Contract No. DE-AC03-76SF00098, through the Battelle Memorial Institute, Pacific Northwest Laboratories, Richland, Washington.

Quantum Monte Carlo for Molecular Studies*

William A. Lester, Jr., Investigator

INTRODUCTION

We are pursuing the use of the quantum Monte Carlo (QMC) method for the computation of the binding energy and other molecular properties. This approach, borrowed from statistical mechanics and currently in great favor in particle theory, allows one to calculate essentially exact quantum-mechanical expectation values. Recasting the Schrödinger equation into a diffusion-type equation enables a stochastic solution by a simulation of the appropriate diffusion process.

1. Work in Progress

Current work includes exploration of the following directions: (1) Development of adaptive or self-

improving Monte Carlo schemes. The goal is to feed knowledge gained from a simulation back into an improved importance function. Such an algorithm should iteratively correct a starting function to reduce the variance and even correct the nodes. (2) Use of "differential" methods to obtain potential surfaces. In order to obtain a potential curve or surface one must, in principle, recalculate the Born-Oppenheimer energy at different geometries. However, a separate statistical error is associated with each calculation, making differences (slopes) even more uncertain. By using the same random numbers to calculate the energy at nearby geometries, the errors become correlated. Thus a much more accurate relative energy may be obtained. (3) Reduction of statistical variance through such techniques as correlated sampling and control variates. The statistical error bars in QMC remain the largest obstacle to practical calculation of chemical accuracy. If these errors can be reduced without increasing the sample space (and hence the computer time), QMC will truly have come of age.

*This work was supported by the Office of Naval Research under Contract No. N00014-83-F-0101.

Electron-Phonon Coupling and the Properties of Thin Films and Inhomogeneous Superconductors*

Vladimir Z. Kresin, Investigator

INTRODUCTION

Several interrelated problems connected with the properties of superconductors and thin films have been studied.

1. Josephson Tunneling and the Proximity Effect (Publication 1)

Vladimir Z. Kresin

Josephson junctions containing one or two proximity systems (e.g., S_α - M_β - S_γ or S_α - M_β - I - M_γ - S_β , where $M_{\beta(\gamma)}$ is a normal metal or superconductor) were studied. An analysis of the thickness and temperature dependences of the maximum dc Josephson current I_M was carried out. The curvature of the function $I_M(L_\beta)$ was found to depend strongly on the ratio of energy gaps $\epsilon_\gamma/\epsilon_\alpha$ and on the temperature. The analysis was based on the thermodynamics Green's-function method, and the effect of strong coupling was also taken into account. If the proximity system contains two superconductors S_α and S_β , then it appears that the electron-phonon interaction described by the constant λ_β contributes noticeably even if $T > T_{C\beta}$.

2. Interaction and Transport Properties of Interface States (Publication 2)

Vladimir Z. Kresin

In oxides that coat metals, localized states exist that hybridize strongly with conduction electrons to form interface states (IS). This hybridization yields several qualitative and quantitative new effects typical for oxide-coated metals. The Hamiltonians for these new effects describe the enhanced coupling of

IS phonons, strengthened and weakened superconducting interactions of IS, and additional resonant tunnel channels via IS in qualitative agreement with experiments.

3. Coexistence of Phonon and Nonphonon Mechanisms of Superconductivity and a Method of Their Separation (Publication 3)

Vladimir Z. Kresin

The problem of the coexistence of phonon and nonphonon mechanisms in superconductivity is discussed. A method that allows one to separate their contributions is proposed. The method is based on the analysis of tunneling data and the temperature dependence of electronic-heat capacity.

4. Work in Progress

The behavior of the critical temperature and the energy gap of proximity systems is being investigated.

1983 PUBLICATIONS AND REPORTS

Refereed Journals

1. V.Z. Kresin, "Josephson Tunneling and the Proximity Effect," *Phys. Rev. B* **28**, 1294 (1983); LBL-15770.

LBL Reports

2. V.Z. Kresin and J. Halbritter, "On the Interaction and Transport Properties of Interface States," submitted to *Solid State Communications*, LBL-16957.
3. V.Z. Kresin, "Coexistence of Phonon and Nonphonon Mechanisms of Superconductivity and a Method of Their Separation," submitted to *Phys. Rev. Lett.*, LBL-16816.

Other Publications

4. V.Z. Kresin, "Josephson Current in Proximity Junction," *IEEE Trans. on Magnetics* **MAG-19** (3), (1983); LBL-15647.
5. V.Z. Kresin, "Josephson Tunneling and Proximity Effect," *Bull. Am. Phys. Soc.* **2**, (1983); LBL-17164A.

*This work was supported by the Office of Naval Research under Contract No. N00014-82-F-0103.

6. V.Z. Kresin, H. Gutfreund, and W.A. Little, "Dependence of T_c on the Phonon Spectrum of a Superconductor," Bull. Am. Phys. Soc. 2, (1983); LBL-17163A.
7. W.A. Little, H. Gutfreund, and V.Z. Kresin, "Superconductivity in the Strong Coupling Limit," Bull. Am. Phys. Soc. 2, (1983).

ELECTRIC POWER RESEARCH INSTITUTE

Inhibitive Salts for Reducing High-Temperature Oxidation and Spallation*

John Stringer, Acting Investigator†

INTRODUCTION

It has been known for many years that the addition of reactive elements such as yttrium, cerium, lanthanum, or hafnium to heat-resisting alloys forming Cr_2O_3 or Al_2O_3 protective oxides could have a number of beneficial effects. Most notably, the scale adhesion is considerably improved. More recently, it has been shown that fine dispersions of the oxides of the reactive elements within the alloy have virtually the same effect. However, treatments which appear to be superficial can also be beneficial. These include ion implantation of the reactive element, and the use of an aqueous solution of a water-soluble salt of the reactive element, or of a solgel containing the element. From the point of view of elucidating the

mechanism of the "reactive-element effect," these superficial techniques are particularly interesting, since several aspects of the currently most successful model imply that the reactive element is present within the alloy. No systematic study of these techniques has been made, however: they have been used only as means of enhancing the oxidation resistance of already resistant materials.

1. Work in Progress

Preliminary studies using Co/15Cr and Co/25Cr alloys have shown that the aqueous-solution technique can indeed improve scale adhesion on the higher chromium alloy. But unlike the reactive element or oxide addition to the alloy itself, the aqueous solution treatments have little or no effect on the lower chromium alloy. Furthermore, the quantity of salt required on the surface to induce a beneficial effect is relatively large. This may imply that a different mechanism is responsible. Ion-implantation studies on the same two alloys will begin shortly.

* This work was supported by the Electric Power Research Institute under Contract No. RP 2261-1, through an agreement with the Director, Office of Energy Research, U. S. Department of Energy under Contract No. DE-AC03-76SF00098.

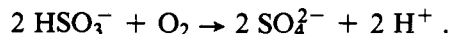
†Dr. Stringer is affiliated with the Electric Power Research Institute, Palo Alto, California. He is continuing the research program started by the late Dr. D.P. Whittle.

Reaction Mechanism of the Oxidation of Bisulfite Ion by Oxygen*

Robert E. Connick, Investigator

INTRODUCTION

Bisulfite ion in aqueous solution is oxidized by oxygen according to the reaction



This reaction is of importance in flue-gas desulfurization schemes making use of aqueous scrubbers and in the atmospheric oxidation of sulfur dioxide on suspended particles coated with an aqueous film. The understanding and control of the rate of reaction is an important objective. Although the kinetics of the reaction has been studied for more than 80 years, there is no agreement on the rate law or the mechanism. Because the reaction is a chain reaction, it is very sensitive to small amounts of a great variety of chemicals. The present research is aimed at elucidating the mechanism of the reaction and the catalytic and inhibitory effect on the rate of a variety of chemicals.

1. Work in Progress[†]

Robert E. Connick and Paul Chieng

In order to eliminate the problems of mass transfer of oxygen gas into the solution when two phases are present, the reaction rate of bisulfite is measured in an enclosed aqueous phase by following

the disappearance of dissolved oxygen with an oxygen meter and/or the appearance of hydrogen ions with a pH meter. Kinetic studies have been made on the dependence of the rate on the concentrations of O_2 , HSO_3^- , H^+ , Fe^{3+} , Fe^{2+} , Mn^{2+} , Co^{2+} , Ni^{2+} , Cr^{3+} , Sn^{2+} , H_3AsO_3 , Zn^{2+} , Ag^+ , $\text{S}_2\text{O}_3^{2-}$, EDTA, CH_3OH , $\text{C}_2\text{H}_5\text{OH}$, isopropyl alcohol, and various combinations of these species. Because the rate law of a chain reaction (long chain) can be expressed as

$$\text{Rate} = \left(\frac{\text{rate initiation}}{\text{rate termination}} \right)^{\frac{1}{n}} \text{rate propagation,}$$

where n is a small whole number, studies are under way to determine whether the effect of each added reagent is exerted through the initiation, termination, or propagation step. Although definite mechanisms cannot yet be written, it is known that at a pH below 5.5 the first product is a peroxysulfite ion which decomposes to sulfate and hydrogen ions by a first-order process with a lifetime of the order of a minute at room temperature. This result greatly limits the number of chain mechanisms that need to be considered.

[†]Supported in part by the Office of Coal Research, Advanced Environmental Control Division of the U.S. Department of Energy, Morgantown Energy Technology Center, Morgantown, West Virginia.

1983 PUBLICATIONS AND REPORTS

Invited Talks

See talks listed under "Formation of Oxyacids of Sulfur from SO_2 ," Robert E. Connick, Investigator.

*This work was supported by the Electric Power Research Institute, Palo Alto, California.

Appendices

APPENDIX A

MATERIALS AND MOLECULAR RESEARCH DIVISION PERSONNEL

1983 Scientific Staff

<u>Investigators</u>	<u>Postdoctoral and Other Scientists</u>	<u>Graduate Students</u>
Neil Bartlett	J. Huston B. Desbat M. Dove G-X. Feng M. Motoyama T. Richardson A. Tressaud W. Totsch J. Verniolle A. Waterfeld	K. Kourtakis J. Koukouvetakis T. Mallouk B. McQuillan J. Nitschke F. Okino G. Rosenthal
Alexis Bell		R. Dictor T. Frederick R. Hicks D. Jordan M. Reichmann J. Rieck R. Underwood P. Winslow G. Yokomizo
Robert Bergman	J. Hayes W. Hersh J. Stryker T. Wenzel	P. Becker T. Bischoff J. Bonfiglio H. Bryndza J. Buchanan P. Comita J. Doney T. Gilbert N. Jacobsen L. Newman C. Nitsche R. Periana-Pillai M. Seidler P. Seidler P. Stoutland M. Wax W. Weiner G. Yang

Investigators	Postdoctoral and Other Scientists	Graduate Students
Robert Bragg	D. Baker L. Henry K. Kawamura B. Mehrotra	J. Hoyt J. Johnson M. Tidjani
Leo Brewer	D. Davis R. McCurdy C.B. Meyer G. Rosenblatt	J. Bularzik E. Faizi J. Gibson S. Hahn K. Krushwitz R. McCurdy R. Stimach
John Clarke	D. Abraham M. Devoret C. Urbina	E. Ganz C. Hilbert H. Mamin J. Martinis R. Miracky J. Pelz D. Seligson F. Wellstood
Marvin Cohen	S. Froyen S. Louie W. Maysenholder S. Richardson D. Vanderbilt	C. Chan K. Chang M-Y. Chou M. Hybertsen P. Lam Z. Levine J. Northrup
Robert Connick	C. Chieng K. Krushwitz W. Tini K. Ward	D. Horner M. Wagner
Didier de Fontaine	A. Forouhi O. Lyon T. Mohri J-P. Simon W. Teitler	B. Clark E. Colas R. Haag K. Krishnan J. Kulik M-O. Lafon R. Pro H-C. Tsai

Investigators

Lutgard De Jonghe

Norman Edelstein

R. Andersen
N. Bartlett
S. Brown
J. Conway
K. Raymond
G. Seaborg
A. Streitwieser
D. Templeton
A. Zalkin

Postdoctoral
and Other Scientists

M. Armand
M. Chang
M. Rahaman
J. Sasaki
H. Schmid

K. Abu-Dari
H-D. Amberger
S. Bachrach
J. Bucher
G. Chapuis
S. Davis
P. Delamoye
P. Edwards
J-R. Hamon
C. Hawkins
T. Hayhurst
F. Jensen
R. Klutz
J. Koningstein
J. Krupa
W. Muller
C. Ng
C. Orvig
K. Rajnak
J. Reynolds
G. Shalimoff
L. Templeton
H-K. Wang
G. Wong
D. Zhang
D. Zhu

Graduate Students

C. Balfe
Y. Boiteux
M. Chang
J-C. Chen
M. Herrera
D. Hitchcock
S. Kikugawa
Y. Kim
N. Naito
D. Olson
G. Raj
E. Reiner
M. Weiser
S. Wu

N. Abraham
J. Arenivar
S. Barclay
P. Becker
J. Boncella
B. Borgias
J. Brennan
T. Chung
M. Derzon
S. Fletcher
G. Freeman
B. Gilbert
G. Girolami
R. Glazer
M. Halpern
T. Henly
S. Kinsley
R. Kulawiec
L. Loomis
R. Moore
V. Pecoraro
E. Peltzer
R. Planalp
J. Rigsbee
R. Roemmele
N. Rutherford
R. Scarrow
P. Sasse
R. Shinomoto
K. Smith
P. Smith
T. Tufano
S. Un
G. Williams

Investigators	Postdoctoral and Other Scientists	Graduate Students
Anthony Evans	R. Cannon B. Dalgleish W. Kriven J. Lamon D. Marshall M. Omori	W. Blumenthal L. Cheng H. Choy G. Crumley M. Drory K. Faber Y. Fu S. Inoue S. Johnson D. Johnson-Walls R-L. Loh K. Louie M-C. Lu E. Luh J. Maasberg J. Marion C. Ostertag C. Rossington W. Shubin M. Thouless H-C. Tsai
James Evans	D. Coates Y. Nakano D. Rieck	M. Hall T. Huh H-C. Lee C. Palmer M. Rau K. Spring
Leo Falicov		M. Robbins R. Victora
Iain Finnie	N. Mawsouf M. Weiss K. Youssefi	S. Chavez J. Dydo A. McGee K. Pool S. Soemantri K. Youssefi
Andreas Glaeser		J-C. Chen
Eugene Haller	S. Pearton	

Investigators

Ronald Gronsky

Charles Harris

Heinz Heinemann

Dennis Hess

Joseph Humphrey

Carson Jeffries

Postdoctoral
and Other Scientists

B. Bitin
E. Boden
A. Goldberg
M. Kawazoe
K. Kemmochi
J. Liang
E. Lodge
A. Nakamura
M. O'Keefe
J. Penisson
P. Rez
K. Sakamoto
Y. Shudo
J. Steeds
L. Tanner
I. Uchiumi
R. Wallace
H. Watanabe

J. Morgan
D. Waldeck

P. Zollinger

Graduate Students

L. Andersen
C. Clark
P. DeRoo
J. Howe
E. Kamenetzky
R. Kilass
M. Kundmann
J. Mazur
M. McCormack
J. Rose
N. Takaliashi
E. Thomann
B. Tracy

M. Alivasatos
M. Berg
J. Brown
S. George
G. Goncher
A. Harris
C. Parsons

C. Blair
C. Tang
A. Wakita

S. Donsanjh

P. Bryant
G. Held
J. Perez
J. Testa

<u>Investigators</u>	<u>Postdoctoral and Other Scientists</u>	<u>Graduate Students</u>
Harold Johnston	R. Carlson A. Young	J. Hebel S. Solomon D. Swanson
William Jolly	C. Eyermann	M. Ajmani D. Beach
Yuan Lee	R. Buss P. Felder J-M. Mesdagh D. Normand H. Schmidt J. VanDenBiesen	R. Brudzynski S. Bustamente L. Butler R. Continetti M. Covinsky J. Frey S. Huang D. Krajnovich T. Minton D. Neumark M. Okumura R. Page J. Reutt G. Robinson A-M. Schmoltnner P. Schulz M. Valentine M. Vernon P. Weiss A. Wodtke L. Yeh
William A. Lester, Jr.	S. Alexander J. Burnet M. Dupuis K. Jolls V. Kresin P. Reynolds S. Rothstein	R. Barnett C. Dateo R. Grimes Y. Huang B. Ruf B. Wells

Investigators	Postdoctoral and Other Scientists	Graduate Students
Alan Levy	D. Boone A. Al-Borno W. Coons T. Foley R. Glardon M. Holt J. Humphrey Y-F. Man P. Turi W. Worrell	M. Arnal E. Ettehadieh H. Frank K. Johnson I. Kliafas
S. Louie	S. Froyen D. Vanderbilt	C-T. Chan S. Fahy M. Hybertsen J-Q. Wang
Richard Marrus	J-P. Briand A. Chetoui H. Gould J. Leavitt M. Mittleman M. Prior H. Shugart	P. Drell C. Munger C. Tanner
William Miller	C. Cerjan L. Hubbard R. Jaquet E. Pollak S. Shi	D. Ali T. Carrington P. Dardi S. Gray S. Schwartz J. Tromp
C. Bradley Moore	L. Aljibury C. Chi-Ke S. Filseth D. Guyer C. Kahler K. Katagiri A. Kung W. Lawrence D. Nesbitt P. Ogilby	A. Abbate D. Bamford D. Darwin M. Foltz J. Frisoli W. Green, Jr. F. Hovis A. Langford W. Natzle H. Petek W. Polik J. Wong L. Young

Investigators	Postdoctoral and Other Scientists	Graduate Students
John W. Morris, Jr.	D. Dionisios H-J. Kim R. Kopa H. Lee R. Ogawa J. Sanchez M-C. Shin Y. Tomota	J. Chan G-M. Chang C. Chu K. Davis I. Dazo D. Dietderich R. Emigh D. Fior-Zurlo D. Frear B. Fultz M. Hong P. Johnson-Walls H-J. Kim Y-H. Kim H-L. Lin K. Sakai S. Shaffer Y-C. Shih H-K. Shin M. Strum L. Summers D. Tribula I-W. Wu K. Xue
Earl Muetterties	R. Feltham D. Heinekey J. Kouba J. Stein M. Tachikawa	J. Bleeke R. Burch H. Choi W. Cwirla T. Gentle V. Grassian D. Klarup R. Lum Y. Otonari G. Schmidt K. Shanahan S. Slater R. Wexler
Rolf Muller	J. Farmer W. Giba G. Nazri D. Rajhenbah	D. Barkey D. Dees J. Dukovic J. Faltemier R. Gyory R. Hyman P. Johnson S. Mayer J. Stoughton G. Whitney

Investigators

John Newman

Donald Olander

Joseph Pask

Norman Phillips

Alexander Pines

Postdoctoral
and Other Scientists

M. Balooch
R. Kohli
A. Machiels
H. Ohashi
D. Winterbauer
S. Yagnik

P. Spencer
A. Tomsia

E. Hornung
K. Matho

A. Garroway
R. Goldberg
H. Fujiwara
M. Munowitz
U. Nitsan

Graduate Students

M. Berg
D. Bernardi
V. Edwards
A. Hauser
N. Matlosz
M. Orazem
T. Risch
S. Thompson
G. Trost

J. Abrefah
M. Derzon
D. Dooley
P. Goubeault
L. Hansson
K. Kim
G. Mitchem
M. Moalem
D. Sherman
A. Suchy
F. Tehranian
S. Yagnik

K. Wada

C. Lisse
M. Mayberry
J. Van Curen

A. Bielecki
J. Baum
H. Cho
G. Davenport III
G. Drobny
R. Eckman
J. Garbow
M. Gochin
J. Millar
B. Oh
E. Schneider
D. Shykind
A. Thayer
R. Tycko
D. Zax

Investigators	Postdoctoral and Other Scientists	Graduate Students
Kenneth Pitzer	K. Balasubramanian S-W. Wang	R. Neisler
John Prausnitz		F. Anderson A. Harvey E. Larsen W. Whiting J. Wong
Paul Richards	A. Smith	G. Bernstein J. Bonomo W. Challenger S. Chiang M. Engelhardt M. Fischer M. Hueschen A. Lange S. McBride W. McGrath D. Nolte P. Thiel G. Tobin J-Q. Wang
Robert Ritchie	N. Croft D. Sarma S. Suresh	V. Dutta T. George S. Ivy K. Johnston T. Lin R. Pendse J-L. Tzou E. Zaiken
Philip Ross	P. Andricacos D. Dahlgren G. Derry J. Thonstad F. Wagner J. Willsau	
Richard Saykally		D-H. Gwo D. Hovde D. Ray R. Robinson S. Strahan

Investigators	Postdoctoral and Other Scientists	Graduate Students
Henry Schaefer III	J. Bicerano J. Breulet J. Goddard R. Pitzer A. Schier H. Sokol M. Vincent Y. Yamaguchi	M. Colvin G. Fitzgerald D. Fox J. Gaw R. Grev M. Hoffman T. Lee G. Raine R. Remington
Alan Searcy	D. Beruto D. Chung S. Louie D. Meschi Z. Munir A. Stacy E. Thomsen	J. Farnsworth A. Hegedus M. Kim E. Opila T. Reis
Y. Ron Shen	T. Rasing S. Shen L. Shi G-Z. Yang P. Ye H. Zhu	G. Boyd M-M. Cheung S. Durbin T. Heinz H. Hsiung J. Hunt H. Tom X-D. Zhu
David Shirley	U. Becker P. Dabbousi W. Heppler Z. Hussain G. Kaindl G. Kalkowski G. Lui G. Truesdale	A. Baca C. Bahr J. Barton R. Davis T. Ferrett P. Heimann L. Klebanoff P. Kobrin D. Lindle C. Parks J. Pollard S. Robey A. Schach von Wittenau M. Schulz L. Terminello J. Tobin C. Truesdale

Investigators	Postdoctoral and Other Scientists	Graduate Students
Gabor Somorjai	M. Asscher P. Davies F. Delannay G. Ertl M. Farias S. Ferrer P. Garcia M. Khan M. Kudo M. Langell R-F. Lin M. Salmeron C. Sanchez K. Sieber N. Spencer J. Turner W. Tysoe M. Van Hove K. Zhen	B. Bent E. Benjamin G. Blackman J. Carrazza J. Crowell E. Garfunkel A. Gellman D. Godbey W. Guthrie M. Hendewerk M. Hilton D. Kelly B. Koel M. Levin T. Lin M. Logan C. Mate B. Naasz D. Ogletree M. Quinlan J. Twiford R. Yeates G. Yee F. Zaera
Angelica Stacy		R. Patterson J. Platenak J. Womack H. zur Loye
John Stringer	H. Akuezue I. Cornet S. Smith R. Streiff M. Lee	S-H. Choi P. Hou J-Y. Lee F. Yang

Investigators

Gareth Thomas

Charles Tobias

K. Peter Vollhardt

**Postdoctoral
and Other Scientists**

J. Davey
M. Hall
T. Harvey
R. Hoel
N. Kim
J. Koo
C. Kung
J. Leteurtre
R. Mishra
G. Monks
M-H. Oh
J. Penisson
J. Rayment
W. Saleksy
M. Sarikaya
J. Steeds
W. Stobbs
M. von Heimendahl
C. Warble
C-K. Wu
J. Yan
A-J. Yan

P. Cettou

H. Mesdagh
D. Van Horn

Graduate Students

J. Ahn
T. Dinger
B. Demczyk
L. Fell
J-S. Gau
H-M. Ho
K. Krishnan
C. Kwok
S. Miyasato
A. Nakagawa
M. Ohmura
S. Ong
L. Rabenberg
R. Ramesh
J. Ruchlewicz
M. Sung
H. Tokushige
J. Wasynczuk
X-F. Wu
Y-S. Yoon

P. Andersen
R. Anderson
S. Elliott
D. Fischl
K. Hanson
W. Hui
R. Hyman
R. McIntosh
L. McVay
T. Tsuda
M. Verbrugge
B. Wines

R. Colborn
J. Drage
J. King
J. Tane
M. Tilset
E. Walborsky
T. Weidman

Investigators	Postdoctoral and Other Scientists	Graduate Students
Jack Washburn	R. Hagstrom G. Hirsch C. Lampert D. Sadana Y. Wang	R. Caron J. Ding M. Hong C. Jou H. Ling P. Ling W-L. Lo D. Lopes T. Mowles T. Sands D. Sipes T-H. Wei N-R. Wu Y-J. Wu A. Yu T. Zee
Kenneth Westmacott	P. Boss G. Colville U. Dahmen J. Davey P. Ferguson R. Gleyvold M. Hall G. Monks J. Pennison J. Steeds R. Schonbucher G. Szaloky M. Von Heimendahl	S. Puranikmath L. Wu
Peter Yu		C. Collins J. Weiner

Support Staff

Division Administrative Staff

C. Peterson — Assistant Division Head, Administration
K. McArthur — Assistant Division Administrator

Administration

M. Janzen
L. Irvin
S. Jones

Personnel

M. Montgomery
P. Palidini
M. Bowman
I. Gosiengfiao
C. Berke

Purchasing

S. Stewart
C. Sterling
P. Ogden
C. Boris

Technical Editing

R. Albert
J. Knight

Special Projects

E. Skrydlinski

Travel

S. Quarello

Administrative/Secretarial Staff

R. Arcol
M. Atkinson
C. Baker
K. Bean
K. Becker
H. Benson
C. Bilorusky
G. Brazil
K. Brusse
D. Carmichael
J. Denney
S. Ewing
M. Gabbay
S. Gangwer
M. Gill

C. Gliebe
C. Gloria
D. Israel
R. Jones
A. Kahn
M. Knight
S. Mikesell
N. Miller
M. Moore
B. Moriguchi
V. Narasimhan
M. Noyd
A. Ozturkmen
M. Penton
L. Pham

M. Rector
J. Reed
M. Rutan
G. Sharp
J. Shull
J. Smith
N. Su
S. Thur
N. Weightman
S. Wilde
J. Wortendyke
C. Yoder
S. Young
B. Zambrano

Technical Staff

W. Toutolmin — Technical Coordinator

D. Ackland
T. Bakker
G. Baum
G. Blowers
H. Bowman, Jr.
H. Brendel
J. Brown
T. Bruemmer
R. Brusasco
M. Cima
B. Clark
A. Davis
I. Dazo
R. Dick
D. Dietderich
M. Eberhard
L. Fell
K. Franck
L. Galovich
K. Gaugler
J. Glazer
R. Gray

A. Gronsky
R. Hinds
G. Hirsch
J. Holthuis
J. Jacobsen
M. Jayko
L. Johnson
D. Jurica
B. Kan
J. Kelsey
H. Kerkoff
R. Kopa
D. Krieger
M. Kujala
F. Lam
R. Lambertson
E. (Fong) Mah
R. Mah
D. Marinaro
J. Martinis
S. Mathews
R. McCurdy

J. Patterson
H. Riebe
K. Sakai
E. Scholz
J. Severns
W. Shubin
E. Slamovich
S. Smit
H. Sokol
N. Somorjai
R. Stimach
A. Suchy
G. Tong
J. Twiford
K. Wada
F. Watanabe
M. Wall
H. Weeks
W. Wong
P. Yau
A. Yu
C. Ze

APPENDIX B

MATERIALS AND MOLECULAR RESEARCH DIVISION COMMITTEES

DIVISIONAL COUNCIL

A. Bell
M. Cohen
N. Edelstein
H. Heinemann
H. Johnston*
C. Bradley Moore
J. Morris, Jr.

DIVISIONAL RESEARCH STAFF COMMITTEE

N. Edelstein
L. Falicov
R. Muller*
K. Westmacott

ELECTRON MICROSCOPE USERS COMMITTEE

R. Gronsky
J. Morris, Jr.
P. Ross*
K. Westmacott

EQUIPMENT REVIEW COMMITTEE

J. Clarke
A. Evans
N. Phillips
R. Muller*

TECHNICAL STAFF AND SHARED FACILITIES COMMITTEE

L. De Jonghe*
R. Gronsky
J. Morris, Jr.
P. Ross
G. Somorjai

MMRD Building 62 Building
Manager: D. Meschi
(Alternate: C. Peterson)

*Chairman

PERFORMANCE APPRAISAL COMMITTEES

Administrative Staff Committee

K. McArthur*
R. Muller
C. Peterson

Scientific Staff Committee

N. Edelstein
L. Falicov
R. Muller*
K. Westmacott

Technical Staff Committee

L. De Jonghe*
R. Gronsky
J. Morris, Jr.
P. Ross
G. Somorjai

SAFETY AND LABORATORY STANDARDS COMMITTEE

D. Ackland	K. McArthur
G. Baum	D. Meschi*
M. Cima	R. Muller
K. Franck	C. Peterson
B. Fultz	H. Riebe
T. Gentle	J. Severns
W. Hemphill	E. Slamovich
T. Hickcock	S. Smith
J. Holthuis	C. Sterling
L. Irvin	S. Stewart
L. Johnson	L. Summers
D. Krieger	W. Toutolmin
E. (Fong) Mah	W. Wong

MMRD Building 72 Building
Manager: K. Westmacott
(Alternate: D. Ackland)

APPENDIX C

LIST OF DIVISIONAL SEMINARS

Surface Science and Catalysis Seminars

<u>Date</u>	<u>Speaker and Affiliation</u>	<u>Seminar Title</u>
1-10-83	Prof. M.S. Wrighten Massachusetts Institute of Technology	Inorganic Photochemistry at Interfaces
1-13-83	Prof. R. Haydock University of Oregon	Mobility of Bonds Near a Metal Surface
1-19-83	Prof. R. Madix Stanford University	Reactive Scattering and Reactive Interme- diates on Single Crystal Metal Surfaces
1-21-83	Dr. C.B. Duke Xerox Corporation	Semiconductor Interface Structure: Sur- face Chemistry for Microelectronics
1-27-83	Prof. F.E. Massoth University of Utah	Catalytic Functionalities on Support CoMo Catalysts
1-28-83	Dr. A. Heller Bell Laboratories	Catalysts and Junctions in Hydrogen- generating Photoelectrochemical Cells
2-1-83	Prof. T. Marks Northwestern University	Design of Molecular and Macromolecular Metals
2-9-83	Prof. Xie Xi-De Fudan University, Shanghai	Surface Science Research in the People's Republic of China
2-10-83	Dr. S.T. Picraux Sandia Laboratory	Ion Implantation and Pulsed Heating of Metals
2-17-83	Prof. J.H. Lunsford Texas A & M University	Methanol Synthesis Over Supported Palladium
2-24-83	Dr. D.W. Goodman Sandia Laboratory	Catalytic Reactions Over Chemically Modi- fied Surfaces
3-3-83	Dr. W.P. Ellis Los Alamos National Laboratory	Laser-surface Interactions on Group VA Semimetals
3-10-83	Dr. S. Butter Air Products and Chemicals, Inc.	Selectivity in Heterogeneous and Homogene- ous Catalysis
3-18-83	Dr. J. Gland Exxon Research and Engineering	Carbon Monoxide Oxidation on the Pt(321) Surface: Evidence for Selective Reac- tion of Terrace Oxygen
3-29-83	Prof. Y. Nihel University of Tokyo	The Photoelectron Diffraction as a Tool for Characterization of Solid Surfaces
4-1-83	Dr. C. Mims Exxon Research and Engineering	Alkali-catalyzed Carbon Gasification

<u>Date</u>	<u>Speaker and Affiliation</u>	<u>Seminar Title</u>
4-7-83	Dr. M. Cardillo Bell Laboratories	The Pervasive Role of Steps in Chemical Desorption from Single Crystals
4-14-83	Prof. A. Brenner Wayne State University	Catalytic Activity of Supported Metals and Complexes
4-21-83	Dr. J. Stoehr Exxon Research and Engineering	Surface Crystallography by Means of SEXAFS and NEXAFS
4-28-83	Prof. D. Lichtenberger University of Arizona	High-resolution Photoelectron Spectroscopy of Small Molecules on Metals and Compounds
5-5-83	Dr. G.N. Derry MMRD/LBL	High-coverage States of Oxygen Adsorbed on Pt(100) and Pt(111) Surfaces
5-10-83	Dr. D. Klimesch General Motors Research	Nitrogen Oxide Pollution in the Troposphere
5-12-83	Dr. L.L. Hegedus W.R. Grace Company	Solid-state Electrocatalytic Reactions
5-19-83	Dr. G.G. Kleiman Georgia Institute of Technology	X-ray Excited Auger Studies of Metals and Alloys
5-20-83	Prof. K. Oura Osaka University	Metal-induced Superstructures on Si(111) Surfaces Studied by ISS and LEED/CMTA
5-25-83	Dr. J. Harris KFA-Jülich, West Germany	Physisorption Interaction of He and H ₂ with Metal Surfaces: Some Consequences for Atom Scattering and Sticking
6-2-83	Prof. Y.W. Chung Northwestern University	Mechanism of Strong Metal-support Interaction in Ni/TiO ₂
6-7-83	Dr. H. Niehus KFA-Jülich, West Germany	Low Energy Ion Scattering for the Determination of the Atomic Positions of Surface Atoms
6-9-83	Prof. L. Guzzi Worcester Polytechnic Institute	Catalytic and Surface Study on RuFe Films and on Supported FeRu Catalysts
6-16-83	Dr. Eric Derouane Mobil Research and Development Corp.	Structural Characterization of Zeolites: High-resolution Magic Angle Spinning Solid State Si ²⁹ and Al ²⁷ NMR Spectroscopy (work performed at University of Namur, Belgium).
6-27-83	Dr. S.P. Tear York University, United Kingdom	The Development of a Computer-controlled Low-energy Electron Diffractometer
6-30-83	Dr. Miguel Salmeron Autonomous University, Madrid, Spain	Core and Valence Band Energy Shifts in Small Two-dimensional Islands of Gold Deposited on Pt(100): The Effect of Step-edge Surface and Bulk Atoms

<u>Date</u>	<u>Speaker and Affiliation</u>	<u>Seminar Title</u>
7-7-83	Dr. R.A. van Santen Shell Oil Company	Quantum Chemistry of Chemisorption to Transition Metal Surfaces
7-8-83	Dr. J.P. Biberian Marseille, France	Adsorption of Cl on Si(111) and Etching of Silicon by Cl: Effect of Electron Bombardment
7-14-83	Dr. Troy W. Barbee, Jr. Stanford University	Physical Vapor Deposition: A Moving Interface Problem
7-18-83	Dr. D. Bartomoef French Catalysis Institute	Conjugate Acid-base Sites in Zeolites
7-21-83	Dr. C. Warble CSIRO, Melbourne, Australia	The Crystal Surface — A Defect Interface: Exploration with the TEM
7-26-83	Dr. R.F. Willis Cambridge University	Surface Structural Phase Transformations and Surface Solutions
8-8-83	Prof. C. Kemball University of Edinburgh	Mechanistic Studies of Hydrocarbon Reac- tions on Metal Catalysts
8-11-83	Dr. R. Baird Ford Motor Company	Surface Composition, Surface Crystallo- graphy and Electronic Structure of α -Cu-Al Alloys
8-16-83	Prof. G. Comsa KFA-Jülich, West Germany	Kinetics of CO/Pt Interaction Studies by He-beam Scattering
8-29-83	Dr. J.R. Anderson University of Melbourne, Australia	Recent Developments in Hydrocarbon Synthesis over ZSM-5 Zeolites
9-1-83	Dr. J. Hrbek Exxon Research and Engineering	Methanol Interaction on Clean and Modified Ruthenium Surfaces
9-8-83	Prof. J.C. Hemminger University of California Irvine	Raman Spectroscopy of Charge Transfer in Chemisorption Bonding: Tetracyano- ethylene Adsorption on Ni(111)
9-15-83	Dr. L. Batra IBM, San Jose	Surface Structure Determination Using Helium Diffraction
9-22-83	Dr. R. Fish University of California Berkeley	A Comparison of Homogeneous and Polymer- supported Catalysts for the Selective Reduction of Polynuclear Heteroaromatic Compounds
9-28-83	Dr. J.L. Margitfalvi Central Research Institute for Chemistry, Hungarian Academy of Sciences, Budapest, Hungary	Surface Carbon Formed under the Condition of Dehydrocyclization

<u>Date</u>	<u>Speaker and Affiliation</u>	<u>Seminar Title</u>
9-29-83	Prof. A.T. Bell Department of Chemical Engineering, University of California Berkeley	The Chemistry and Structure of Carbon Formed During Fischer-Tropsch Synthesis
10-5-83	Prof. H. Vahrenkamp University of Freiburg, West Germany	Some Reactions of Organo-transition Metal Clusters
10-6-83	Prof. P. Biloen University of Pittsburgh	The "Isotope Advantage" in Transient Kinetic Measurements; Principles and Applications in Catalysis
10-13-83	Dr. C. Campbell Los Alamos National Laboratory	Surface Science Studies and Heterogeneous Catalysis: Ethylene Epoxidation over Silver
10-14-83	Dr. N. Avery CSIRO, Melbourne, Australia	On the Relationship Between Bonding Configuration and Reactivity of Mole- cules on Metal Surfaces
10-20-83	Dr. A. Gavezzotti University of Milan, Italy	Generation of Trial Structures and Evaluation of Formation Energy for Layers of Molecules: A Packing Energy Approach to Chemisorption
10-26-83	Dr. Jean Gobet Clarkson College and EPFI, Switzerland	Preparation and Adsorption Properties of Organosilyle Layers Chemisorbed on Silica Surfaces
10-27-83	Dr. Edith Flanigen Union Carbide	Molecular Sieve Materials
10-31-83	Dr. H.J. Schoennagel Mobil Research and Development Corp.	Rejuvenation Chemistry of Reforming Catalysts
11-3-83	Dr. J.W. Gadzuk National Bureau of Standards	Non-adiabatic Effects in Elementary Sur- face Reactions: State-to-state Mole- cular Beam Experiments as a Probe
11-10-83	Dr. S.W. Wang Lawrence Berkeley Laboratory	The Shape Stability of Very Large and Very Small Clusters
11-11-83	Prof. B.W. Wojciechowski Queen's University, Kingston, Ontario	An Experimental and Theoretical Approach to the Study of the F-T Synthesis
11-17-83	Prof. M. Dignam University of Toronto	Infrared Vibrational Spectroscopy of Adsorbed Species
11-18-83	Prof. S.C. Fain University of Washington	Physics in Flatland; Molecules on Graphite
11-28-83	Prof. M. Simonetta University of Milan, Italy	A Pseudopotential Approach to the Chemi- sorption Problem

<u>Date</u>	<u>Speaker and Affiliation</u>	<u>Seminar Title</u>
12-1-83	Prof. M.G. Lagally University of Wisconsin	LEED Analysis of Finite-size Effects on Surfaces and Adsorbed Layers
12-9-83	Dr. F. Hoffmann Exxon Research and Engineering	Vibrational Spectroscopy of CO Bond Weakening on Potassium-promoted Pu(001) Studied by EELS, TIMS, LEED, and Work Function Measurements

Reaction Dynamics Seminars

1-24-83	Prof. E. Pollak Chemical Physics Department, Weizmann Institute of Science, Rehovot, Israel	Vibrationally Adiabatic Molecules
3-21-83	Dr. C. Freeman Department of Physical and Inorganic Chemistry, University of Western Australia	Laboratory Studies of Gaseous Ion-molecule Processes
3-21-83	Prof. R. Wyatt Department of Chemistry, University of Texas	Dynamics of the F + H ₂ Reaction: A Few New Angles
3-24-83	Dr. R. Campargue Laboratoire des Jets Moleculaires, Centre d'Etudes Nucleaires de Saclay, France	Free Jets and Molecular Beams from Heated Sources
5-2-83	Dr. R. B. Walker Los Alamos National Laboratory	What do Reactive Resonances Look Like in Laboratory Angular Distributions?
5-12-83	Prof. R. Bernheim Department of Chemistry, Pennsylvania State University, Philadelphia	Pulsed Optical Double Resonance Studies of Rydberg States of Li ₂
7-14-83	Dr. G. Mainfray Service de Physique des Atomes et des Surfaces, Centre d'Etudes Nucleaires de Saclay, France	Multiply Charged Ions Induced by Multiphoton Absorption
7-15-83	Prof. S. Mukamel Department of Chemistry, University of Rochester	Mode Coupling Approach to Spectroscopy of Super-cooled Molecules
8-8-83	Dr. L.F. Phillips Department of Chemistry, University of Canterbury, Christchurch, New Zealand	Excimer Laser Studies of Atom-radical Reactions

<u>Date</u>	<u>Speaker and Affiliation</u>	<u>Seminar Title</u>
8-9-83	Dr. H-H. Limback Institut für Physikalische Chemie, Universität Freiburg, West Germany	Liquid and Solid State NMR Studies of Kinetic Isotope Effects and Tunneling and Multiple Proton Transfer Reactions
10-27-83	Prof. M. Baer Soreq Nuclear Research Center, Yavne, Israel	Reactive Scattering Collisions Within the Infinite Order Sudden Approximation

Other Seminars Hosted

1-20-83	Prof. K.E. Heusler Corrosion Department, Technical University, Clausthal, West Germany	Uniform and Nonuniform Dissolution of Oxide Films
1-25-83	Dr. M. O'Halloran Department of Physics, Stanford University	Photodissociation of ICN, C ₂ CN, and BrCN
1-25-83	Dr. R. Vasudev Department of Chemistry, Stanford University	Photodissociation Dynamics of HONDO
3-16-83	Dr. M. Mehring University of Stuttgart, West Germany	PEIERLS Transition in Polyacetylene
3-18-83	Prof. B. Kastening Institute of Physical Chemistry, University of Hamburg, West Germany	Electrochemical Polarization of Suspensions and their Use for Metal Etching Processes
3-18-83	Prof. P.A. Throver Pennsylvania State University	Electron Microscopic Characterization of Carbon Fibers
3-27-83	Dr. P. Soukiassian Institut de Recherche Fondamentale, C.E.N./Saclay, France	UPS and ELS Studies of the Electronic Properties of the Adsorption of Cesium on Transition Metals
3-30-83	Dr. M. Goldman C.E.A. Service de Resonance Magnetique, Gif-sur-Yvette, France	Principles of Production and the Study of Nuclear Magnetic Ordering
4-6-83	Prof. H-D. Amberger Institut für Anorganische und Angewandte Chemie, Universität Hamburg, West Germany	The Electronic Structure of Organometallic Complexes of the f Elements

<u>Date</u>	<u>Speaker and Affiliation</u>	<u>Seminar Title</u>
4-13-83	Dr. M.R. De Agudelo Center of Investigation and Development, Department of Petroleum, INTEVEP, Caracas, Venezuela	Applied Catalysis
4-15-83	Dr. J. Schaeffer Monsanto Corporation, St. Louis, Missouri	Applications of High Resolution NMR and Cross-polarization in Biological Molecules
4-15-83	Dr. H.W. Spiess University of Mainz, West Germany	Deuteron NMR Studies of the Structure and Dynamics in Solid Polymers, Liquid Crystalline Polymers, and Polymer Model Membranes
6-2-83	Drs. G. Levy and C. Dumoulin SPECNET — Syracuse University	Workshop on Laboratory Data Processing and NMR
6-7-83	Prof. V. Vitek University of Pennsylvania	Atomic Structure of Grain Boundaries in Metals
6-10-83	Dr. A Parr Physics Division, National Bureau of Standards	Resonance Phenomena in Molecular Photoionization
6-13-83	Mr. B. Wells Physical Chemistry Laboratory, Oxford University, England	<i>Ab Initio</i> Methods for the Determination of Intermolecular Forces
6-15-83	Dr. P. Delamoye Institut de Physique Nucleaire, Laboratoire de Radiochimie, Université de Paris-Sud, Orsay, France	Parametric Analysis of the Energy Level of U^{4+} in D_2d and Limiting D_2 Sites in Incommensurate $ThBr_4$
6-16-83	Dr. R. Wind Technische Hogeschool Delft, The Netherlands	Applications of Dynamic Nuclear Polari- zation in NMR Solid State Research
6-28-83	Dr. J. Virlet C.E.N./Saclay, France	Spin Thermodynamics in the Presence of Multiple Pulse Techniques
7-26-83	Prof. H. King Department of Chemistry, State University of New York, Buffalo, New York	Rydberg Excited States of Molecules
7-26-83	Prof. A. Marchand University of Bordeaux and Centre de Recherche Paul Pascal	Carbon Research at Centre de Recherche Paul Pascal
7-28-83	Prof. Y. Hishiyama Mushashi Insitute of Technology	Thermoelectric Power of Heat Treated Glassy Carbon
8-5-83	Prof. S. Bell Department of Chemistry, Dundee University, Scotland	<i>Ab Initio</i> Studies of the Dundee Group

<u>Date</u>	<u>Speaker and Affiliation</u>	<u>Seminar Title</u>
8-12-83	Prof. Dr. D. Quitmann Physics Department, Freie Universität Berlin, West Germany	Binary Dynamics and Association in Liquid Alloys
8-15-83	Dr. G. Kastner Akademie der Wissenschaften, West Germany	The Systematic Many-beam Case — An Analytical Approach
8-29-83	Dr. M. Mehring University of Stuttgart, West Germany	Solitons and Polyacetylene
9-15-83	Dr. V. Lupei Central Institute for Physics, Institute for Physics and Technology of Radiation Devices, Bucharest, Romania	Magnetic and Optical Studies of Uranium in Solids and Liquids
10-18-83	Dr. L.S. Singer Union Carbide Corporation, Parma Technical Center	Carbon and Graphite — Materials of the 21st Century
10-27-83	Dr. M. Baer Soreq Nuclear Research Center, Yavne, Israel	Coupled-states and Infinite-order Sudden Studies of F + F ₂ Reactive Scattering
11-30-83	Dr. D. Hildenbrand SRI International, Menlo Park, California	Thermochemical Studies of Actinide Compounds
12-14-83	Prof. J.A. Koningstein Carleton University, Ottawa, Ontario	Laser Raman Studies of Rare Earth Compounds

APPENDIX D

INDEX OF INVESTIGATORS

Andersen, Richard A.	231	Miller, William H.	167, 187
Bartlett, Neil	217, 231	Moore, C. Bradley	151
Bell, Alexis T.	199, 210, 256	Morris, John W., Jr.	39, 279
Bergman, Robert G.	220	Muetterties, Earl L.	214
Boone, Donald H.	259, 290	Muller, Rolf H.	112, 122, 261, 266
Bragg, Robert H.	69	Newman, John	211, 261, 274
Brewer, Leo	115	Olander, Donald R.	118
Clarke, John	97	Pask, Joseph A.	55
Cohen, Marvin L.	105	Phillips, Norman E.	109
Connick, Robert E.	197, 295	Pines, Alexander	137
Conway, John G.	231	Pitzer, Kenneth S.	154
de Fontaine, Didier	36	Prausnitz, John M.	226
De Jonghe, Lutgard C.	66, 272	Raymond, Kenneth N.	231
Edelstein, Norman M.	231	Richards, Paul L.	82
Evans, Anthony G.	44, 51, 79	Ritchie, Robert O.	7, 49
Evans, James W.	31, 261, 271	Ross, Philip N.	247, 261, 268
Falicov, Leo	102	Saykally, Richard J.	163
Finnie, Iain	77	Schaefer, Henry F., III	164, 167, 185
Fish, Richard H.	210, 256	Seaborg, Glenn T.	231
Glaeser, Andreas	75	Searcy, Alan W.	58
Gronsky, Ronald	1, 21, 64	Shen, Yuen-Ron	87
Haller, Eugene E.	84, 92, 102, 283	Shirley, David A.	171
Harris, Charles B.	148	Somorjai, Gabor A.	32, 125, 143, 199 210, 248, 256
Heinemann, Heinz	32, 33, 210, 256	Streitwieser, Andrew, Jr.	231
Hess, Dennis W.	121	Stringer, John	73, 294
Humphrey, Joseph A.C.	245, 253	Templeton, David H.	231
Jeffries, Carson D.	91	Thomas, Gareth	5, 21
Jolly, William L.	206	Tobias, Charles W.	112, 261, 263, 264
Johnson, Harold S.	145	Vollhardt, K. Peter	203
Kresin, Vladimir Z.	160, 292	Washburn, Jack	3, 25, 62
Lee, Yuan T.	88, 174, 179	Westmacott, Kenneth H.	17, 21
Lester, William A., Jr.	158, 289, 291	Yu, Peter Y.	95
Levy, Alan V.	251, 259, 290	Zalkin, Alan	231

This report was done with support from the Department of Energy. Any conclusions or opinions expressed in this report represent solely those of the author(s) and not necessarily those of The Regents of the University of California, the Lawrence Berkeley Laboratory or the Department of Energy.

Reference to a company or product name does not imply approval or recommendation of the product by the University of California or the U.S. Department of Energy to the exclusion of others that may be suitable.

TECHNICAL INFORMATION DEPARTMENT
LAWRENCE BERKELEY LABORATORY
UNIVERSITY OF CALIFORNIA
BERKELEY, CALIFORNIA 94720